—Plenary Paper—

Trace Gas Budgets of High Arctic Permafrost Regions

Torben R. Christensen
Dept. of Physical Geography and Ecosystem Analyses, Lund, Sweden, and Abisko Scientific Research Station, Abisko, Sweden
Thomas Friborg
Institute of Geography, Copenhagen University, Øster Voldgade 10, DK-1350 Copenhagen K, Denmark
Margareta Johansson
Dept. of Physical Geography and Ecosystem Analyses, Lund, Sweden, and Abisko Scientific Research Station, Abisko, Sweden

Abstract

Trace gas fluxes in tundra regions have attracted substantial attention in recent years because of the large quantity of carbon stored in tundra soils and the associated feedbacks to climate change. Major international assessments (e.g., ACIA, IPCC) have not been able to come up with a conclusive answer as to trace gas budgets of the Arctic. Here we find that the Circumpolar North is roughly in balance with respect to carbon dioxide exchanges, with some regions showing signs of current losses and others showing sings of current carbon sinks. Taking into account methane emissions over a decadal timescale, however, the Circumpolar North is considered a current source of radiative forcing. Whether this source functioning will continue or increase into the future is uncertain and depends on the fate of permafrost, soil moisture, and surface hydrology.

Keywords: Arctic tundra; carbon dioxide (CO_2); methane (CH_4); permafrost regions; trace gas flux.

Introduction

Arctic terrestrial ecosystems have attracted major attention in the context of global carbon cycling in recent years (ACIA 2005, Millenium Ecosystem Assessment 2005, McGuire et al. 2007). A reason for this is that Arctic terrestrial ecosystems store a significant proportion of the global stock of soil organic carbon (C). In the arctic tundra proper, some 121-191 Gt of C are stored, or approximately 12-16% of the estimated world total (McKane et al. 1997, Tarnocai et al. 2003). Arctic permafrost regions are predicted to undergo significant changes due to anthropogenic climate impacts (Kittel et al. 2000, IPCC 2001, Wookey 2002, ACIA 2005, Lawrence and Slater 2005). These changes and the feedbacks they engender could change the climatic conditions that have allowed the development of such large soil C stocks in the Arctic (Gorham 1991, Shaver et al. 1992, McKane et al. 1997, Hobbie et al. 2000). Extensive regions of the High Arctic that lack substantial C stocks and currently have very limited rates of atmospheric exchange could develop dynamic C cycles. Climate driven changes in plant community structure, specifically shifts from herbaceous and cryptogamous dominance to systems dominated by ericaceous and woody species, are also likely to change ecosystem C dynamics and balance.

Arctic soils are often wet and, when waterlogged, become anoxic. Anoxic soils often accumulate C in the form of peat (Gorham 1991, Clymo et al. 1998) and release methane (CH_4), a radiatively important trace gas (Matthews and Fung 1987, Joabsson and Christensen 2001, Öquist and Svensson 2002). Methane flux is rarely a quantitatively important component in the ecosystem C balance but it can play a disproportionately important role in terms of greenhouse gas forcing (gram for gram methane in the atmosphere has 23 times the radiative forcing potential of CO_2).

Permafrost environments are very dynamic with respect to trace gas exchanges and there are important interactions between permafrost dynamics and, in particular methane emissions both in terrestrial (Christensen et al. 2004) and thaw lake ecosystems (Walter et al. 2006). Here we briefly review the current state of budgets for the northern permafrost regions with respect to observational data on seasonal and annual CO_2 and CH_4 fluxes.

Mechanisms

Processes controlling trace gas budgets in arctic ecosystems vary across a continuum of space (plot to region) and time (minutes to decades), and varying classes of biological complexity (e.g. from individual species, through trophic interactions, to whole ecosystems). Thus, determining an accurate C budget for the Arctic requires an extensive and sustained observational capacity, which incorporates measurements and instrumentation that are sensitive to processes influencing C uptake, storage and loss. The latter is arguably the greatest source of current scientific uncertainty due to significant uncertainties remaining in the mechanistic understanding of processes controlling C losses, whereas accurate scaling across space and time is perhaps more constrained by logistical and funding limitations. Here, we discuss the importance of several crucial processes controlling C uptake, loss and storage in arctic tundra. Factors that are important for scaling process studies across space and time are considered below.

There are a finite number of basic processes involved in controlling CO_2 exchange. Net ecosystem production (NEP) of organic carbon is the net product of two independent processes that drive the uptake and release of C; gross primary production (GPP) and respiration (both autotrophic and heterotrophic, CO_2 as well as CH_4; Fig. 1). The net

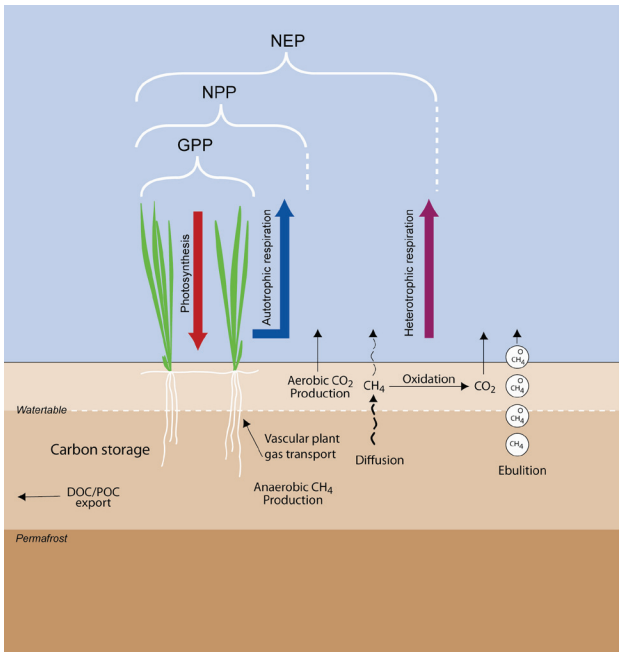

Figure 1. Schematic diagram of the processes governing the net balance of CO_2 and CH_4 fluxes in typical permafrost regions.

annual C budget of a given ecosystem is also affected by export of dissolved and particulate organic C in ground and streamwater flows (Michaelson et al. 1998, Tipping et al. 1999, Cole et al. 2002, Judd and Kling 2002), which are relatively unknown for the Arctic. In addition to the capacity for C transport in Arctic soils and streams (Kling et al. 1991, Judd and Kling 2002) there are minor releases of volatile organic compounds (Kesselmaier et al. 2002) contributing to a full C budget. The net annual C balance or budget is, hence, the result of both independent and coupled (e.g., Boone et al. 1998, Högberg et al. 2001) processes that often respond differentially to the same abiotic forcing factors which makes interpretation and prediction of their quantitative impact a major challenge.

The net emission of CH_4 from a given ecosystem is also the result of a complex set of independent processes that regulate production, oxidation and transport (Fig. 1). Controls on these processes include soil temperature, plant species composition (and functional type), and factors that influence the redox potential (Eh) of the soil environment (e.g. the position of the water table) (Moore and Knowles 1989, Christensen 1993, Funk et al. 1994, Yavitt et al. 1997, Bellisario et al. 1999, Christensen et al. 1999, 2000, Joabsson and Christensen 2001, Öquist and Svensson 2002, Sjögersten and Wookey 2002, Blodau and Moore 2003, Ström et al. 2005). Also, as is the case for CO_2 exchange, the temporal dynamics of net CH_4 fluxes between a given landscape and the atmosphere can be highly variable due to contrasting processes controlling exchange at different times of the year. Permafrost dynamics impact all these factors (Fig. 1) in arctic, subarctic and some boreal ecosystems. Thus, changes in the permafrost regime (Christensen et al. 2004, Lawrence and Slater 2005, Walter et al. 2006) will have fundamental consequences for CO_2 and CH_4 fluxes in the Arctic.

Seasonal Flux Dynamics

Figure 2 illustrates critical components controlling the seasonal dynamics of C exchange in a simplified arctic tundra ecosystem. Within the four seasons (I-IV in Figure 2) there are important, and at times very different, processes acting which are resulting in the net effect of the individual seasons on the annual budget. Critical facets of early-season conditions - such as a substantial C loss during spring melt and early summer due to release of trapped CO_2, and possibly a hindered onset of photosynthesis due to dry early summer conditions - can seriously affect the annual budget.

In midsummer again water deficit can be important as a limiting factor for photosynthesis, while a very warm summer has the potential to stimulate respiration (including root respiration) more than photosynthesis (in particular in dry years) so these effects together can be very important for the annual budget (Crawford et al. 1993, Marchand et al. 2005, Kwon et al. 2006). In the third season, a mild autumn followed by the delayed appearance of a consistent snowcover could be critical for processes involved in C fluxes. Usually photosynthesis will decline regardless of warm "Indian" summer conditions that will stimulate respiration for as long as the soils remain unfrozen (or contain free water). So a mild autumn may also be a very important triggering factor for C losses on an annual basis (Jackovitz-Korchinsky et al. in prep.). The critical factors for determining the annual carbon budget of a simplified arctic tundra are summarized in Table 1, which includes examples of factors that can affect seasonal processes (δa, δb, δc, δd) occurring in season I (spring), II (summer), III (autumn) and IV (winter) and, therefore estimation of annual budgets. The annual budget can then be summarised as Equation 1 (below) where k is a site specific productivity factor and δ represents seasonal factors that indicate the positive or negative effects that each season is having on the net annual balance.

$$C_{annual} = k * (\delta a + \delta b + \delta c + \delta d) \quad (1)$$

Importantly, there may be several complications associated with this very simplified model. For example, an early freeze-up in season III, which would tend to increase net C uptake in a given year through preventing respiratory C losses in a lengthy autumn, may act very differently during the subsequent year depending upon whether or not the soil is underlain by permafrost. In a permafrost free setting, where there are still unfrozen conditions and substantial microbial activity beneath the freezing front, there is the chance for a substantial winter-time build-up of CO_2 below the frozen ice and soil layer, which in turn may affect the δa in the subsequent year through a substantial and potentially pulsed release of trapped CO_2. In continuous permafrost this hand-over effect from one year to the next may be less apparent.

Nonetheless, Equation 1 may be useful for comparing annual budgets between ecosystems, studies and sites to determine factors controlling not only intra-site inter-annual variability but also for comparing why different sites appear with different annual budgets. The discussion on estimates of annual fluxes below rationalizes why such differences in annual budgets can be found both within and between sites.

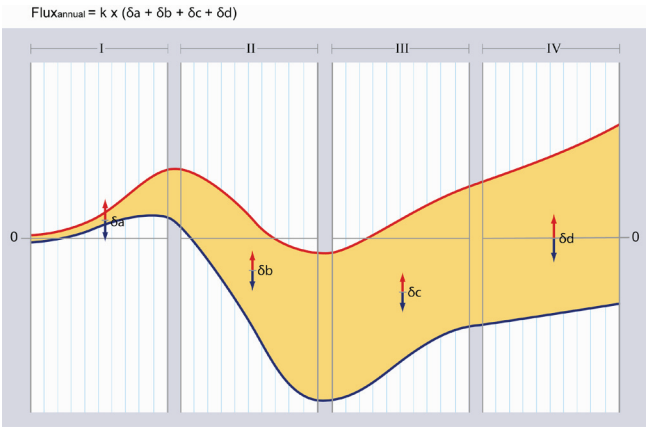

Figure 2. Conceptual model for the seasonal dynamics of accumulated carbon exchange with the atmosphere in a tundra ecosystem. The four different seasons determining the annual balance are indicated starting with the Spring (I) defined as the time from snowmelt until the carbon balance turns negative. The reverse point defines the end of the following period defined as Summer (II). Autumn is from the turning point of the carbon balance to the onset of permanent snowcover (III) and winter is the permanent snow covered period (IV). Examples of critical parameters for the annual total budget outcome in these individual parts of the season are shown in table inserted below.

Table 1. Examples of requirements for δx (Fig. 2) to be:

	Positive	Negative
δa	Short (little snow); Soil moisture limitation; Lots of trapped CO_2	Long and cold; Little trapped CO_2
δb	Short and warm. Moisture limitations on GPP; Insect outbreaks	Long and cold. No moisture deficit for GPP
δc	Long and dry	Short; Early freeze-up
δd	(snowcover) long	(snowcover) short

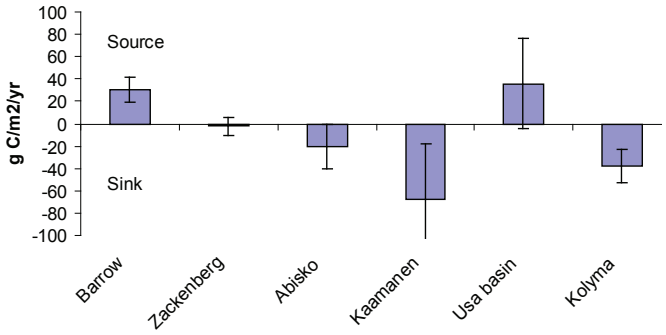

Figure 3. A compilation of annual C budgets based on measurements at sites ranging from Alaska over Greenland, northern Scandinavia and north-eastern European Russia to NE Siberia. (Data from Oechel et al. 2000, Nordstroem et al. 2001, Soegaard et al. 2000, Christensen et al. 2000, Aurila et al. 2004, Jackovitz-Korchinsky et al. in prep, Heikkinen et al. 2003 and Corradi et al. 2005.)

Trace Gas Budgets

Annual estimates

Due to the natural interannual variability determined by the factors discussed above it is extremely difficult to ascertain the C budget status of any tundra ecosystem from single year or even 2-3 year studies. The degree of variability between years is generally quite high. The longest series of annual C balance estimates for tundra ecosystems is from N Alaska, where chamber flux measurements in the 1970's and 1980's, and eddy correlation measurements in more recent years, have indicated a shift from sink to source by the early 1990's, after which there was a tendency for the system to tend towards sink status despite remaining a net source (Oechel et al. 2001). Regardless of these rather dramatic fluctuations in annual budgets over decadal time scales, tundra sites in northern Alaska have also shown relatively stable summertime uptake rates of 40 to 70 g C m^{-2} $season^{-1}$ (Spring to Fall) in recent years (Kwon et al. 2006), emphasising the importance of the shoulder season for determining the variability between years.

Other sites where full annual budgets have been monitored include Stordalen in northern Sweden (Jackovitz-Korchinsky et al. in prep.) and Kaamanen in northern Finland (Aurela et al. 2002, 2004). From NE Greenland there are several years of full seasonal flux observations available both from wet tundra fen and dry heath sites and annual budgets have been estimated at an overall balance close to zero (Soegaard et al. 2000, Nordstroem et al. 2001, Groendahl et al. 2006). In Siberia an annual sink estimate of 38 g C m^{-2} $year^{-1}$ was measured in tussock tundra in NE Siberia (Corradi et al. 2005).

The status of C exchange in the Circumpolar North based on the few actually observed annual C budgets indicate that Arctic terrestrial ecosystems are functioning with significant spatial and temporal heterogeneity with some regions being sources of carbon to the atmosphere (mostly dry and mesic ecosystems) and some regions sinks (mostly wet tundra) (Fig. 3).

From the available circumpolar data it is very difficult to provide a straight answer to the question of whether the Arctic tundra is a source or a sink of atmospheric carbon. There was a time in the 1990s where there was a tendency for the studies and sites that represented the larger areas of tundra to show source activity (northern Alaska and European Russia, Figure 3) but this pattern has changed since the vast NE Siberian tundra became represented by Corradi et al.'s (2005) study (Fig. 3). Taking into account the error bars also shown in Figure 3 it is impossible, given the currently available measured annual carbon budgets, to say for certain that the overall carbon balance of the Circumpolar North should be different from equilibrium.

Greenhouse gas budgeting

Few of the annual budgets referred to above include observations of CH_4 emissions. Where such combined measurements are available on an annual basis, i.e. at Stordalen (Sweden), Kaamanen (Finland) and Kolyma (NE Siberia), the contribution of CH_4 to the actual net annual carbon exchanges (NEP, Figure 2) amounts to 10-25% of the heterotrophic respiration (Jackovitz-Korchinsky et al. in prep, Corradi et al. 2005).

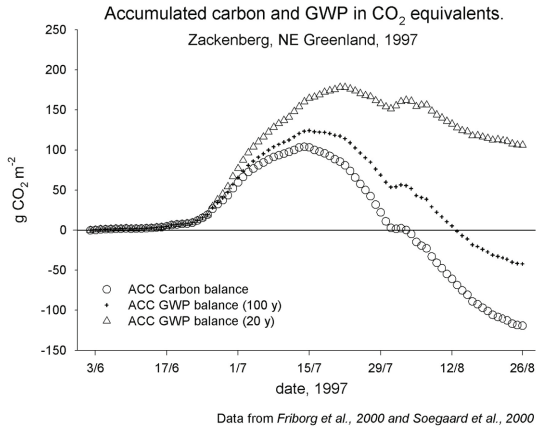

Figure 4. An accumulated greenhouse gas budget (CO_2 and CH_4 as CO_2 equivalents) for a northern wet tundra site versus one of CO_2 only (from ACIA, 2005 based on data in Soegaard et al. 2000 and Friborg et al. 2000).

Since CH_4 is a greenhouse gas with a radiative forcing potential 23 times greater (expressed as gram per gram) than that of CO_2 (in a 100 yr time perspective), the emissions of methane from wet tundra ecosystems, in particular, must be taken into account in any attempt to document the radiative forcing capacity of arctic landscapes (Johansson et al. 2006). For tundra ecosystems where a third commonly studied greenhouse gas, nitrous oxide (N_2O), is assumed to be rarely exchanged with the atmosphere due to nutrient limitations, estimates of total greenhouse gas fluxes are usually confined to the combined effects of CO_2 and CH_4 exchange. Here a complicating factor is time. Most tundra ecosystems have accumulated carbon over many thousands of years. Over such a period the accumulated and reduced radiative forcing potential of CO_2 uptake is a stronger factor than that of accumulated CH_4 emissions (Frolking et al. 2006). However, in most greenhouse gas budgets, focus is generally directed to the immediate emissions and possible changes that may occur and what impact these will have on climate as this responds to change over the coming decades. Over decadal time scales, most wet tundra CH_4 emissions will be a stronger greenhouse forcing factor acting on climate than the CO_2 uptake. Typical calculations of such a total GHG budget may look like that illustrated in Figure 4, which has been derived for the Zackenberg eddy tower site in NE Greenland by applying two typical CH_4 greenhouse warming potentials of 63 for a 20 yr time perspective and 23 for a 100 yr time perspective respectively (Friborg et al. 2004, ACIA 2005).

Many dry/mesic tundra ecosystems have minimal CH_4 emissions, if any, and CO_2 budgets are balanced around zero or are actual sources of C to the atmosphere, However, we conclude that arctic tundra regions should currently be considered a net contributor to greenhouse warming because wet tundra ecosystems are likely to be sources of climate warming over the next few decades due to strong CH_4 emissions. Whether this source functioning will continue into the future without acclimation is uncertain. In all likelihood, this may depend on the response of permafrost that appears to be warming, soil moisture status that appears to be variable with moisture levels increasing in some regions and drying in other regions. A further factor is the future state and carbon fixing potential of the High Arctic.

Current research infrastructure, monitoring and international and scientific coordination will not be sufficient to answer such questions. To further understand the significance of arctic environmental change for global greenhouse warming potential, new and concerted efforts need to be sustained to investigate further and adequately measure processes modulating C flux in arctic tundra and how C fluxes in arctic landscapes vary across multiple scales of space and time.

Conclusions

Throughout the Holocene, most tundra in the Arctic has been a net sink for carbon due to low rates of decomposition and loss relative to rates of uptake. Based on the few observed annual carbon budgets in the Circumpolar North, the current status of carbon exchanges indicates that Arctic terrestrial ecosystems are dynamic and heterogeneous, with some regions being sources of carbon to the atmosphere (mostly dry and mesic ecosystems) and some regions being sinks (mostly wet tundra). If the measurements from sites in N America and North Eurasia are assumed representative for these vast regions, then source and sink areas are roughly balanced.

Current global and regional climate modeling of predicted future states of arctic precipitation dynamics and hydrological balance are highly uncertain (ACIA, 2005). The models must be better parameterized and validated in order to constrain predictions of future soil hydrological states that will determine the magnitude and of C efflux from arctic tundra and the dynamics and the composition (CO_2, CH_4, VOCs etc.) of that exchange (Sitch et al. 2007).

Many dry/mesic tundra ecosystems have minor CH_4 emissions if any, and CO_2 budgets are balanced around zero or are actual sources. However, wet tundra ecosystems are likely to enhance radiative forcing over decadal time scales through the emission of CH_4. As such, arctic tundra and small lake regions should be concluded to currently be acting as a source of greenhouse warming. Whether this source functioning will continue or increase into the future is uncertain and will depend on the fate of permafrost, soil moisture and surface hydrology and the future state of ecosystem structure and function in the high arctic. To decrease uncertainty and improve our fundamental understanding of carbon balance at high northern latitudes new novel and concerted research and monitoring efforts need to focus over decadal time scales.

Acknowledgments

This paper forms the foundation for an updated presentation at NICOP 2008 representing an extract from a larger review under preparation in an IASC supported process (the FATE group and a continued follow-up from a 2003 workshop at Skogar, Iceland) that has involved contributions from a range of people in addition to the current authors including: C. E. Tweedie, P. M. Crill, J. A. Gamon, L. Groendahl, J. Gudmundsson, Y. Harazono, F. Huemmrich, C. Lloyd, P. J. Martikainen, W.C. Oechel, H. Oskarsson, N. Panikov and P.A. Wookey.

References

ACIA, 2005. *Arctic Climate Impact Assessment.* Cambridge University Press. 1042 pp.

Aurela, M., Laurila, T. & Tuovinen, J.P. 2002. Annual CO2 balance of a subarctic fen in northern Europe: Importance of the wintertime efflux. *Journal of Geophysical Research-Atmospheres* 107: art-4607.

Aurela M, Laurila T. & Tuovinen, J.P. 2004. The timing of snow melt controls the annual CO2 balance in a subarctic fen. *Geophysical Research Letters* 31.

Bellisario L.M., Bubier J.L., Moore, T.R. & Chanton, J.P. 1999. Controls on CH4 emissions from a northern peatland. *Global Biogeochemical Cycles* 13: 81-91.

Blodau, C. & Moore, T.R. 2003. Experimental response of peatland carbon dynamics to water table fluctuation. Aquatic Sciences 65: 47-62.

Boone, R.D., Nadelhoffer, K.J., Canary, J.D. & Kaye, J.P. 1998. Roots exert a strong influence on the temperature sensitivity of soil respiration. *Nature* 396: 570-572.

Christensen, T.R. 1993. Methane emission from Arctic tundra. *Biogeochemistry* 21:117-139.

Christensen, T.R., Jonasson, S., Callaghan, T.V., Havström, M. & Livens, F.R. 1999. Carbon Cycling and Methane Exchange in Eurasian Tundra Ecosystems. *Ambio* 28: 239-244.

Christensen, T.R., Friborg, T., Sommerkorn,M., Kaplan, J., Illeris, L., Soegaard, H., Nordstroem, C. & Jonasson, S. 2000. Trace gas exchange in a high-arctic valley 1. Variations in CO2 and CH4 flux between tundra vegetation types. *Global Biogeochemical Cycles* 14, 701-713.

Christensen, T.R., Johansson, T., Malmer, N., Åkerman, J., Friborg, T., Crill, P., Mastepanov, M. & Svensson, B. 2004. Thawing sub-arctic permafrost: Effects on vegetation and methane emissions, *Geophysical Research Letters* 31: L04501, doi:10.1029/2003GL018680.

Clymo, R..S., Turunen, J. & Tolonen, K. 1998. Carbon accumulation in peatlands. *Oikos* 81: 368-388.

Cole L., Bardgett, R.D., Ineson, P. & Adamson J.K. 2002. Relationships between echytraeid worms (Oligochaeta), climate change, and the release of dissolved organic carbon from blanket peat in northern England. *Soil Biology and Biochemistry* 34: 599-607.

Corradi, C., Kolle, O., Walter, K., Zimov, S.A. & Schulze, E.D. 2005. Carbon dioxide and methane exchange of a north-east Siberian tussock tundra. *Global Change Biology* 11: 1910-1925.

Crawford, R.M.M., Chapman, H.M., Abbott, R.J. & Balfour, J. 1993. Potential impact of climatic warming on arctic vegetation. *Flora* 188 (4): 367-381.

Friborg, T., Christensen, T.R., Hansen, B.U., Nordstroem, C. & Soegaard, H. 2000. Trace gas exchange in a high-arctic valley 2. Landscape CH4 fluxes measured and modeled using eddy correlation data. *Global Biogeochemical Cycles* 14: 715-723.

Friborg, T., Soegaard, H., Christensen, T.R., Lloyd, C.R. & Panikov, N.S. 2003. Siberian Wetlands: Where a sink is a source. *Geophysical Research Letters* 30: 2129.

Frolking, S., Roulet, N. & Fuglestvedt, J. 2006. The impact of a northern peatland on the earth's radiative budget: sustained methane emission versus sustained carbon sequestration. *Journal of Geophysical Research-Biogeochemistry* 111: G01008, doi:10.1029/2005JG000091.

Funk, D.W., Pullman, E.R., Peterson, K.M., Crill, P.M. & Billings WD. 1994. Influence of water-table on carbon dioxide, carbon monoxide, and methane fluxes from taiga bog microcosms. *Global Biogeochemical Cycles* 8: 271-278.

Gorham, E. 1991. Northern peatlands: role in the carbon cycle and probable responses to climatic warming. *Ecological Applications* 1: 182-195.

Groendahl, L., Friborg, T. & Soegaard, H. 2006. Temperature and snow-melt controls on interannual variability in carbon exchange in high Arctic. Theoretical and Applied Climatology, doi: 10.1007/s00704-005-0228-y.

Heikkinen, J. E. P., Virtanen, P. T, Huttunen, J. T., Elsakov, V. & Martikainen, P. J. 2004. Carbon balance in East European tundra. *Global Biogeochemical Cycles* 18: 10.1029/2003GB002054.

Hobbie, S.E., Schimel, J.P., Trumbore, S.E. & Randerson, J.P. 2000. Control over carbon storage and turnover in high-latitude soils. *Global Change Biology* 6 (Suppl. 1): 196-210.

Högberg, P., Nordgren, A., Buchmann, N., Taylor, A.F.S, Ekblad, A., Högberg, M.N., Nyberg, G., Ottosson-Lofvenius, M. & Read, D.J. 2001. Large-scale forest girdling shows that current photosynthesis drives soil respiration. *Nature* 411: 789-792.

IPCC 2001. *Climate Change 2001: Synthesis Report.* A Contribution of Working Groups I, II and III to the Third Assessment Report of the Intergovernmental Panel on Climate Change. Watson, R.T. and the Core Writing Team (eds.). Cambridge, U.K., and New York: Cambridge University Press, 398 pp.

Joabsson, A. & Christensen, T.R. 2001. Methane emissions from wetlands and their relationship with vascular plants: an Arctic example. *Global Change Biology* 7 (8): 919-932.

Johansson, T., Malmer, N., Crill, P.M., Mastepanov, M. & Christensen, T.R. 2006. Decadal vegetation changes in a northern peatland, greenhouse gas fluxes and net radiative forcing. *Global Change Biology* 12: 2352–2369.

Judd, K.E. & Kling, G.W. 2002. Production and export of dissolved C in arctic tundra mesocosms: the roles of vegetation and water flow. *Biogeochemistry* 60(3): 213-234.

Kesselmeier, J. et al. 2002. Volatile organic compound emissions in relation to plant carbon fixation and the terrestrial carbon budget. *Global Biogeochemical Cycles* 16: 1–9.

Kittel, T.G.F., Steffen, W.L. & Chapin, F.S. III. 2000. Global and regional modelling of Arctic boreal vegetation distribution and its sensitivity to altered forcing. *Global Change Biology* 6: 1-18.

Kling, G.W., Kipphut, G.W. & Miller, M.C. 1991. Arctic Lakes and streams as gas conduits to the atmosphere: implications for tundra carbon budgets. *Science* 251(4991): 298-301.

Kwon, H.-J., Oechel, W. C., Zulueta, R. C. & Hastings, S.J. 2006. Effects of climate variability on carbon sequestration among adjacent wet sedge tundra and moist tussock tundra ecosystems. *Journal of Geophysical Research* 111, G03014, doi:10.1029/2005JG000036.

Lawrence, D.M. & Slater, A.G. 2005. A projection of severe near-surface permafrost degradation during the 21st century. *Geophysical Research Letters* 32 (24): Art. No. L24401.

Marchand, F.L., Mertens, S., Kockelbergh, F., Beyens, L. & Nijs, I. 2005. Performance of High Arctic tundra plants improved during but deteriorated after exposure to a simulated extreme temperature event. *Global Change Biology* 11 (12): 2078-2089.

Matthews, E. & Fung, I. 1987. Methane emission from natural wetlands: Global distribution, area, and environmental characteristics of sources. *Global Biogeochemical Cycles* 1: 61-86.

McGuire, A.D., Chapin, F.S. III, Wirth, C., Apps, M., Bhatti, J., Callaghan, Y., Christensen, T.R., Clein, J.S., Fukuda, M., Maximov, T., Onuchin, A., Shvidenko, A. & Vaganov, E. 2007. Responses of high latitude ecosystems to global change: Potential consequences for the climate system. In: *Terrestrial Ecosystems in a Changing World.* Edited by Canadell, J.G., Pataki, D.E. & Pitelka, L.F.), pp. 297-310. The IGBP Series, Springer-Verlag, Berlin Heidelberg.

McKane, R.B., Rastetter, E.B., Shaver, G.R., Nadelhoffer, K.J., Giblin, A.E., Laundre, J.A. & Chapin, F.S. III. 1997. Reconstruction and analysis of historical changes in carbon storage in arctic tundra. *Ecology* 78: 1188-1198.

Michaelson, G.J., Ping, C.L., Kling, G.W, & Hobbie, J.E. 1998. The character and bioactivity of dissolved organic matter at thaw and in the spring runoff waters of the arctic tundra north slope, Alaska. *Journal of Geophysical Research* – Atmospheres 103 (D22): 28939-28946.

Millenium Ecosystem Assessment. 2005. *Ecosystems and human well-being: Current state and trends*. Findings of the Condition and Trends Working Group. Millennium Ecosystem Assessment Series. Island Press, Washington.

Moore, T.R. & Knowles, R. 1989. The influence of water-table levels on methane and carbon dioxide emissions from peatland soils. *Canadian Journal of Soil Science* 69: 33-38.

Nordstroem, C., Soegaard, H., Christensen, T.R., Friborg, T. & Hansen, B.U. 2001. Seasonal carbon dioxide balance and respiration of a high- arctic fen ecosystem in NE-Greenland. *Theoretical and Applied Climatology* 70: 149-166.

Oechel, W.C., Vourlitis, G.L., Hastings, S.J., Zulueta, R.C., Hinzman, L. & Kane, D. 2000. Acclimation of ecosystem CO2 exchange in the Alaskan Arctic in response to decadal climate warming. *Nature* 406: 978-981.

Öquist, M.G. & Svensson, B.H. 2002. Vascular plants as regulators of methane emissions from a subarctic mire ecosystem. *Journal of Geophysical Research* 107: (D21). 4580, doi:10.1029/2001JD001030.

Shaver, G.R., Billings, W.D., Chapin, F.S., Giblin, A.E., Nadelhoffer, K.J., Oechel, W.C. & Rastetter, E.B. 1992. Global change and the carbon balance of arctic ecosystems. *BioScience* 42: 433-441.

Sitch, S, McGuire, A.D., Kimball, J., Gedney, N., Gamon, J., Emgstrom, R, Wolf, A., Zhuang, Q. & Clein, J. 2007. Assessing the circumpolar carbon balance of arctic tundra with remote sensing and process-based modeling approaches. *Ecological Applications* 17: 213–234.

Sjögersten, S. & Wookey, P.A. 2002. Spatio-temporal variability and environmental controls of methane fluxes at the forest-tundra ecotone in the Fennoscandian mountains. *Global Change Biology* 8: 885-894.

Soegaard, H., Nordstroem, C., Friborg, T., Hansen, B.U., Christensen, T.R. & Bay, C. 2000. Trace gas exchange in a high-arctic valley 3. Integrating and scaling CO2 fluxes from canopy to landscape using flux data, footprint modeling, and remote sensing. *Global Biogeochemical Cycles* 14: 725-744.

Ström, L., Mastepanov, M. & Christensen, T.R. 2005. Species-specific effects of vascular plants on carbon turnover and methane emissions from wetlands. *Biogeochemistry* 75: 65-82.

Tarnocai, C., Kimble, J. & Broll, G. 2003. Determing carbon stocks in Cryosols using the Northern and Mid Latitudes Soil Database. In: *Permafrost.* Edited by Phillips, M., Springman, S.M. & Arenson, L.U. Proceedings of the Eighth International Conference on Permafrost, 21-25, Zurich Switzerland. (Vol. 2, p. 1129-1134). Lisse, The Netherlands: Sets & Zeitlinger B.V.

Tipping, E., Woof, C., Rigg, E, Harrison, A.F., Ineson, P., Taylor, K., Benham, D., Poskitt, J., Rowland, A.P., Bol, R. & Harkness, D.D. 1999. Climatic influences on the leaching of dissolved organic matter from upland UK moorland soils, investigated by a field manipulation experiment. *Environment International* 25: 83-95.

Walter, K.M., Zimov, S.A, Chanton, J.P., Verbyla, D. & Chapin, F.S. 2006. Methane bubbling from Siberian thaw lakes as a positive feedback to climate warming. *Nature* 443, 71–75.

Wookey, P.A. 2002. Tundra. *Encyclopedia of Global Environmental Change*. Vol. 2: *The Earth system – biological and ecological dimensions of global environmental change,* edited by H.A. Mooney and J. Canadell. London: Wiley, pp. 593-602.

Yavitt, J.B., Williams, C.J. & Wieder, R.K. 1997. Production of methane and carbon dioxide in peatland ecosystems across north America: Effects of temperature, aeration, and organic chemistry of peat. *Journal of Geomicrobiology* 14: 299-316.

Interannual Variations in Active Layer Thickness in Svalbard

Hanne H. Christiansen
The University Centre in Svalbard, UNIS, P.O. Box 156, 9171 Longyearbyen, Norway,
Ole Humlum
Institute of Geoscience, University of Oslo, P.O. Box 1041 Blindern, 0316 Oslo, Norway
The University Centre in Svalbard, UNIS, P.O. Box 156, 9171 Longyearbyen, Norway

Abstract

Long-term monitoring of active layer thickness and top permafrost thermal state has been ongoing since the year 2000 in the UNISCALM site on a loess-covered terrace in Adventdalen, central Svalbard. The site has proved to be excellent for studying the effects of meteorological variables such as air temperature and cloud cover on active layer thickness. The active layer thickness varied from 74 to 105 cm in the UNISCALM site since 2000. This fairly-large interannual active layer thickness variation reflects extremely shallow thaw in 2005. The top permafrost is warm, and no two-sided freezing occurs. This makes the site susceptible to the meteorological variations with MAAT variations, with MAAT variations between -1.7ºC and -6.1ºC recorded over the 2000 to 2007 monitoring period.

Keywords: active layer; CALM; interannual variations; monitoring, permafrost temperature; Svalbard.

Introduction

Svalbard is located in a high arctic maritime setting, exposed to significant interannual meteorological variations similar in magnitude to modeled climatic changes during the 21st century. Permafrost is classified as continuous (Humlum et al. 2003), and several characteristic periglacial landforms, such as rock glaciers, ice-wedges, and pingos, all show widespread permafrost existence. The mean annual air temperature (MAAT) at sea level has varied, however, between -1.7ºC and -6.1ºC in the period 2000–2006, measured at the official meteorological station at Longyearbyen airport (www.met.no).

MAAT for the year 2006 was 4.4ºC above the average for the entire period of meteorological measurements in Svalbard, but the warming mainly occurred in winter, with the summer average temperature 6.3ºC (June, July, and August) closer to the average of 4.4ºC (1912–2007 summers), but still warmer than ever recorded before. The 2007 summer temperature was higher still, at 6.4ºC. As ground thaw progression measurements exist since 2000, we can study how much and how quickly the active layer responded to the recent warm years.

Circumpolar Active Layer Monitoring (CALM) network sites exist in Svalbard, mainly along the west coast (Brown et al. 2000). The UNISCALM site, located in the most continental central part of Svalbard, is probed regularly during the thawing season from May to September to follow the thaw progression. Inside the UNISCALM site, active layer and top permafrost temperatures are measured directly in the sediment. This combination of measurements enables a good understanding of how the active layer has responded to recent meteorological variations.

The UNISCALM site

Adventdalen is one of several large valleys that dissect the mountainous landscape in central Svalbard. The UNISCALM site is located at 10 m a.s.l. in the central lower part of Adventdalen at 78º12′N, 15º45′, on a Late Holocene loess-covered terrace. The upper 1.3 m of sediment consists of horizontally layered silt-dominated sediments (Christiansen et al. in prep).

UNISCALM extends over a 100 x 100 m grid, with 10 m grid size spacing. It was established in mid-summer of 2000. It is being measured by physical probing of all 121 grid points from 8 to 15 times during the thawing season from May–September each year to follow the seasonal thaw progression and record the active layer thickness (ALT). As the grid was established in July 2000, only four measurements were carried out that year. The location of the grid is marked by small wooden pegs extending 5 cm above ground. The repetitive seasonal measurements are taking place in the same hole each summer to follow thaw progression in each grid point. Each year the location of the probe hole is moved slightly from the year before, to avoid measuring into earlier years' sites. Three persons have done the measurements in the eight-year period, usually by only one person during each season.

To investigate spatial variability within the UNISCALM site over the eight-year period, a normalized variability index (Iv) was calculated for each grid node (Hinkel & Nelson 2003) for the ALT measurements in late summer. If Iv varies only slightly between years, the interannual node variability (INV) is small (Hinkel & Nelsen 2003), indicating a high degree of consistency in thaw depths over the eight-year period. If Iv varies much between years, local factors may have a large influence on ALT.

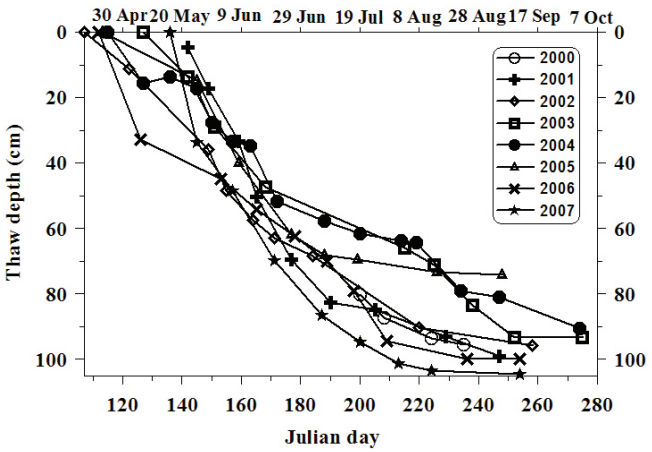

Figure 1. Thaw progression in the UNISCALM site calculated as the average from all 121 grid points at each date.

Active layer temperatures have been measured at the centre on the UNISCALM grid since it was established in summer 2000. Data are obtained by miniature dataloggers of the Tinytag type, with external sensors inserted horizontally directly into the ground at 0, 10, 20, 50, and 110 cm depths in the active layer and one was placed vertically into the top permafrost by drilling. Air temperature at 20 cm above ground is also measured by a Tinytag datalogger with an external sensor, also located at the site of the ground thermal profile, but built into a well-ventilated cairn of rocks. The resolution of the Tinytags is ±0.1ºC and the recording interval is one hour. Snow depths are measured manually on a regular basis during winters at the site of the active layer ground temperature profile.

Meteorology

The nearest official meteorological station to the UNISCALM site is the Longyearbyen airport, 9 km to the west, at the mouth of Adventdalen. It is situated at 28 m a.s.l. but closer to the sea than UNISCALM. This station has operated since 1975, but older data exist from nearby stations, and a homogenized data series exists for the entire period since the first meteorological records in 1912 (Førland et al. 1997).

Mean annual air temperatures (MAAT) has varied from -12ºC to -1.7ºC in the 1912–2006 recording period (www.met.no), partly because of warming since the Little Ice Age, but also because of large interannual temperature variations, which are natural in the maritime setting of Svalbard. The average MAAT for the entire period of measurements is -6.1ºC (www.met.no). The interannual variations are largest during winter, while summer temperatures vary significantly less. This causes a somewhat reduced meteorological influence on ALT, as summer temperatures typically exert large meteorological control.

The annual precipitation varies from 100–200 mm (www.met.no). It is evenly distributed throughout the year, but shows large interannual variation. During the winter, most precipitation falls as snow. Wind activity causes exposed areas at the UNISCALM site in the flat valley bottom to have only a shallow snow cover. This allows good energy exchange between atmosphere and ground.

Table 1. UNISCALM data and statistics based on data from the Longyearbyen airport meteorological station.

	2000	2001	2002	2003	2004	2005	2006	2007
Active layer (cm)	95	99.	96	93	91	74	100	105
Max (cm)	110	119	108	108	107	92	116	121
Min (cm)	81	83	83	70	70	51	85	90
TDD thaw start	12 Jun	8 June	25 May	1 June	21 May	28 May	8 April	9 May
TDD thaw end	22 Aug	4 Sep	15 Sep	9 Sep	30 Sep	5 Sep	11 Sep	11 Sep
TDD at thaw end	391	544	609	546	567	600	708	620
TDD total	560	643	680	576	581	637	749	687
TDD % at thaw end	70 %	85 %	90 %	95 %	98 %	94 %	95 %	90 %
Rain (mm)	43.5	40.6	40.6	26.4	69.9	40.4	63.1	31.2
Cloud cover (%)	68.4	73.6	75.4	77.2	76.0	77.9	74.3	70.1
Wind speed (m/s)	4.1	4.3	3.9	3.7	4.1	4.8	4.5	4.3

Results

Thaw progression

Thawing degree-days (TDD) start when continuous positive air temperatures start in the spring. TDD thaw end is the date of the UNISCALM active layer measurement. TDD to thaw end is the amount of TDD during the recorded active layer thawing period, calculated from average daily temperature values. TDD total is for the entire year from the beginning of continuous daily positive air temperatures to the last day of the year. TDD at thaw end is the % TDD recorded at the time when the active layer measurement was done. Rain is the amount of precipitation falling during the month of June, July and August. Cloud cover (% of the sky with cloud cover) and wind speed are the means for the TDD thawing period. In 2007 TDD total and TDD at thaw end could not be calculated as the year was not over at the time of paper submission.

The average ALT recorded in the UNISCALM site was 94 cm for the 2000–2007 period with large interannual variations; the minimum was 74 cm in 2005, while 105 cm was the maximum in 2007. Thawing started as early as the end of April (2002 and 2006), and as late as end of May 2001 and 2007 (Fig. 1 and Table 1). The largest interannual variation in thaw progression occurred in the uppermost 40

cm (Fig. 1). These large differences are mainly controlled by the timing of snowmelt. No thawing is recorded until the surface is snow-free. In a year with very early thaw, such as in 2006 when continuous positive air temperatures were recorded from April 8 with a few subsequent short cold periods, thawing was very early. In contrast, in 2005 thawing was very slow for the first month because of a more protracted snowmelt period. The 50 cm thaw depth was reached in the same period June 4–19 in all years. Below this depth, some interannual variation exists, but with maximum thaw depths reaching 90–100 cm in most years. In 2005 the active layer, however, only reached down to 74 cm as late as September 5. In 2000, the active layer was already 95 cm by August 22. There is generally a correlation between the ALT and the TDD at the time of the active layer recording, but 2005 was clearly anomalous (Fig. 2).

Summer air temperatures (June, July, and August) exhibited less variability than other months, in the entire study period. The coldest summer was 2000, and the warmest summer was 2007. The active layer was 4.7 cm thicker in 2007 than in 2006, although the summer air temperature was only 0.1ºC higher in 2007, and TDD at the end of thaw (Table 1) was higher in 2006 than in 2007, because thawing had already started by April of 2006. The low correlation between ALT and summer air temperature (Fig. 2) largely reflects the influence of the anomalous years in 2000 and 2005. This means that something other than air temperature can have significant influence on ALT in some years. The difference cannot be explained by bad timing of the active layer measurements, as 94% of the annual TTD (Table 1) had occurred at the time of active layer recording in 2005. Only 70% of the annual TDD had occurred in 2000 at the time of active layer recording, so most likely the active layer was somewhat deeper this year, which most likely would locate it closer to most of the other years. In all other years, the ALT was recorded when around 85–98% of the TDD had occurred, indicating that normally the active layer develops in early to mid September.

Precipitation in the form of rain could affect ground thawing. Although there is rather large interannual variation in the amount of summer rain in the study period (Table 1), there is no correlation between the amounts of summer rain and the active layer depths (Fig. 2). Actually, the 2007 summer with only 31.3 mm rain had the deepest thaw of 104.6 cm.

The mean cloud cover in the entire thaw season varied on average from 68–78% and had the best correlation with ALT. ALT decreased when the cloud cover increased (Fig. 2). This indicates that increasing amounts of direct radiation increase thawing in this valley-bottom site. Increasing mean wind speeds over the summer generally increase the ALT, but again this correlation becomes low when including the year 2005.

Spatial variation

The UNISCALM site has a characteristic spatial thaw pattern (Fig. 3) with the deepest active layer in the southern and northeastern part, while the northwestern corner consistently had the thinnest active layer. The maximum grid node point ALT was as deep as 92–121 cm (Table 1)—all in the southern part of the grid during the 2000–2007 period (Fig. 3). The spatial thaw pattern is reproduced in all years except in 2005, where thawing in the southern part was particularly shallow: only 60–70 cm in several areas consisting of more points. The entire southern part of the grid had shallower thaw in 2005 than in all other years. This year, thawing was thinnest in the southern part of the grid, while it was deeper and not far from the depths recorded in the other years in the northern part of the grid.

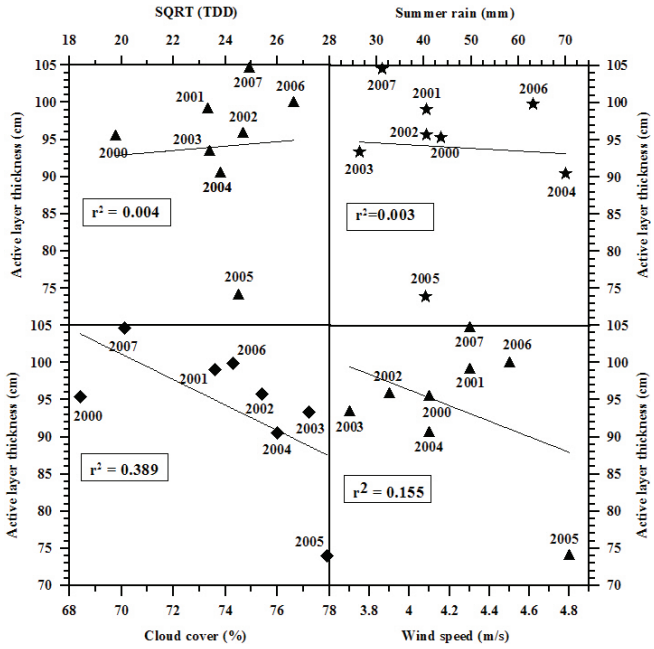

Figure 2. UNISCALM active layer thickness correlated to meteorological parameters in the 2000–2007 period. Correlations include data from all years 2000–2007.

The average interannual grid node variability (INV) is 18.5% for the entire site, with a maximum of 46% and a minimum of 3.3% for the individual grid nodes. The areas with high INV (Fig. 4) are exactly the areas with relatively shallow thaw in summer 2005. Otherwise, the INV values are fairly low, showing little interannual thaw variability and a generally consistent thaw pattern.

Temperature in the active layer

Active layer and top permafrost thermal monitoring was continuous, except for two summer breaks in the ground surface temperature in the summers of 2001 and 2004. Data from a borehole 100 m away, also on the loess-covered terrace, were used to substitute the missing values in 2004, while data from another flat ground surface site 2.5 km further up the Adventdalen were used in the 2001 period. The air temperature recording was first established in October 2000, so data from the Adventdalen site was also used in the first months.

The annual ground temperature distribution is presented from September 1–August 31 in the following year for all

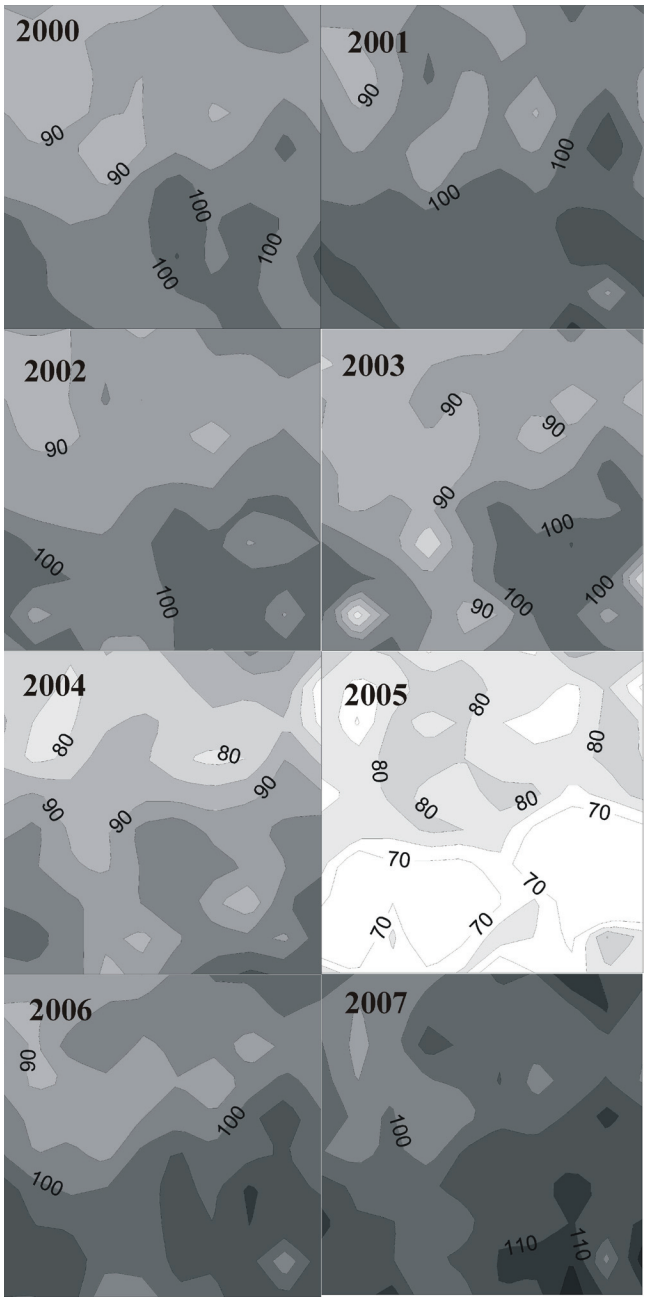

Figure 3. Spatial distribution of the active layer thickness in the UNISCALM site, mapped using the kriging interpolation method (Golden Software, 2002), and a grid spacing of 11 m, based on the 10 m grid node measurements. N is towards the top.

years (Fig. 5). There is large interannual variation especially in the winter ground temperatures, while the summer temperatures have much less variation between the years, as for the air temperature conditions. The thermal conditions in the summer of 2005 are not significantly different from the other summers (Fig. 4). The phase change during freezing in autumn occurs mainly from the top down, so that the zero curtain is much shorter in the top than at the bottom of the active layer. The difference is up to 2 months before the bottom of the active layer is completely frozen and further cooling can occur. It is mainly the top 70–50 cm of the active

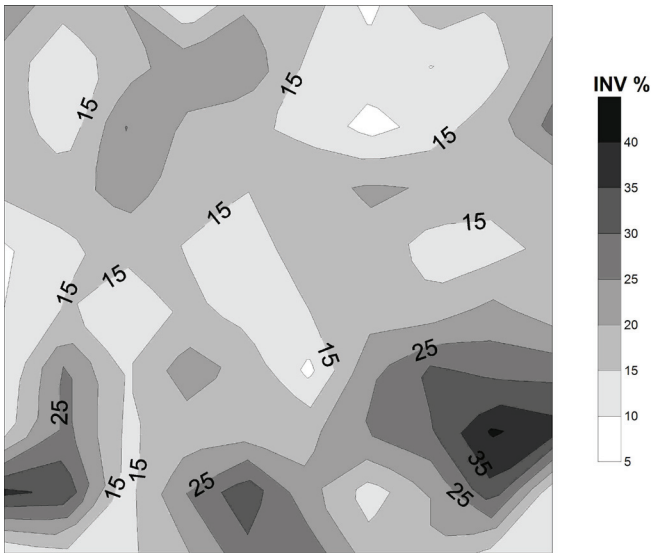

Figure 4. Interannual grid node variability (INV) for the period from 2000–2007. The mean for the entire grid is 18.5%. Based on the kriging interpolation method (Golden Software, 2002), with a grid spacing of 11 m of the 10 m grid node measurements.

layer that experiences significant cooling with temperatures below -10ºC, whereas the lower part of the active layer and top permafrost, especially in the last two years, have not reached temperatures below -10ºC. Also, in the last 3 winters, relatively longer periods of warming of the ground have occurred with ground temperatures as high as -4ºC in almost the entire active layer (Fig. 5).

Figure 3. Spatial distribution of the active layer thickness in the UNISCALM site, mapped using the kriging interpolation method (Golden Software, 2002), and a grid spacing of 11 m, based on the 10 m grid node measurements. N is towards the top.

MAAT varied from -6.2°C to -3.2°C in the study period, while MAGST varied from -5.7°C to -2.2°C and MAGT at 110 cm, in the top permafrost, varied from -5.8°C to -3.6°C (Fig. 6).

Thus, the largest annual variation was at the ground surface, and it occurred in just three consecutive years. The highest mean annual ground temperature was found at 10 cm depth in three of the seven years; thus the theoretical ground temperature profile (Smith & Riseborough 2002) did not occur in all years. There is very large interannual variation in the mean annual ground temperature conditions.

The almost vegetation-free UNISCALM site at the exposed valley-bottom terrace has a generally thin snow cover from late September or October to April or May, with a maximum of 20–30 cm snow depth. Despite the shallow snow, annual surface offsets (Smith & Riseborough 2002) from 2.0–0.4ºC occurred. The n-factor (Carlson 1952) varied from 0.57–0.93 despite the shallow snow cover. The annual thermal offsets (Smith & Riseborough 2002) varied from 2.0–0.1 ºC.

Annual ALT was calculated from the interpolated ground thermal data by locating the lowest position of the 0ºC isotherm in Figure 5. This shows active layer values from 98–105 cm, which is comparable to the UNISCALM-

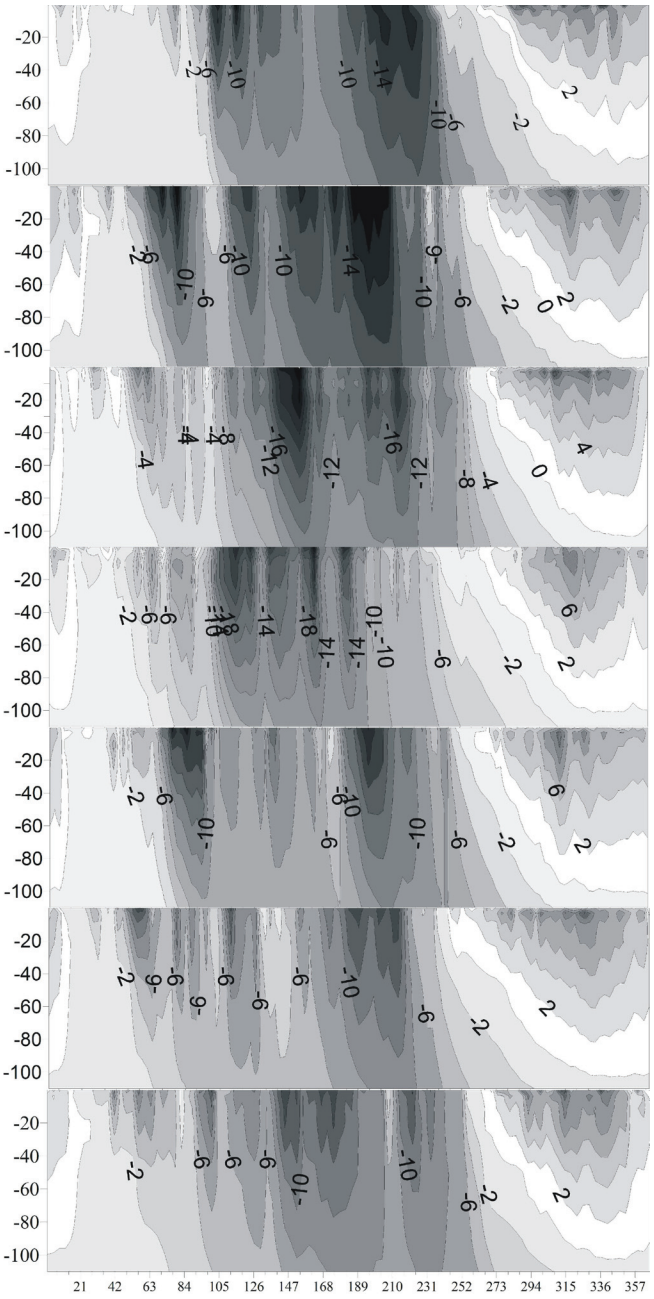

Figure 5. Active layer and top permafrost temperatures in the UNISCALM site measured by miniature loggers with temperature sensors at 0, 10, 20, 50, and 110 cm depths. The annual ground temperature distribution is presented from September 1–August 31 in the following year, and the units on the x-axis are therefore days after September 1. The upper plot is 2000–2001, while the lowermost is 2006–2007.

measured average values, but with less interannual variation. This is especially true in 2005 when the calculated active layer was 102 cm, and thus not as shallow as the clear minimum in the UNISCALM data. The timing of the calculated active layer is much earlier than the measured values in UNISCALM—up to 2 months, but typically one to four weeks.

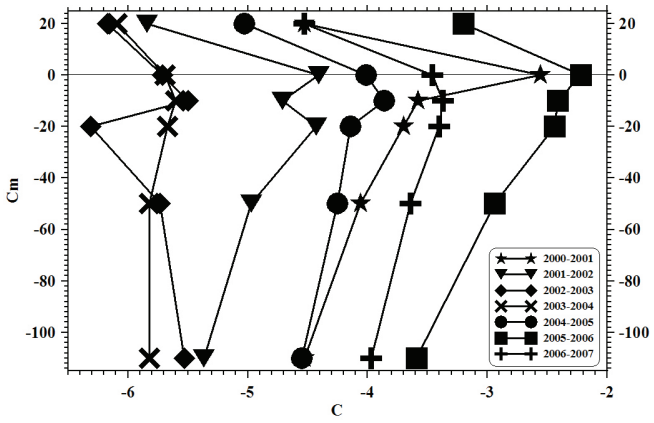

Figure 6. Annual mean temperature distribution from 20 cm above ground down through the active layer and into the top permafrost in the UNISCALM site. Data is from Tinytag miniature dataloggers.

Discussion and Conclusions

In the fine-grained UNISCALM loess site in the Adventdalen valley bottom setting, the active layer varied from 0.74–1.04 m in the 2000–2007 period. Fourteen km further into Adventdalen on the exposed Janssonhaugen sandstone bedrock hill, the active layer varied from 1.5–1.8 m in the 2000–2006 period (Harris et al. submitted).

Sediments are often assumed to experience less interannual active layer variation due to the effect of ice-rich conditions in the transient layer between the active layer and permafrost top (Shur et al. 2005). The active layer monitoring data from bedrock and sediment in Adventdalen, however, show variation of the same size. Therefore the transient layer is presumably not ice-rich in the UNISCALM site, enabling large interannual fluctuations in ALT.

The recorded 30 cm interannual ALT variation in the UNISCALM seems to be mainly controlled by meteorological conditions. However, there is not only a simple correlation between TDD and ALT, but most likely also the cloud cover influences ALT, as this parameter has the highest correlation with ALT for the entire 2000–2007 study period (Fig 3). Thus direct solar radiation seems to affect ALT at this site. This seems most likely due to the relatively low water vapor and dust content in the High Arctic atmosphere in combination with a dark-colored sediment surface with very little vegetation, which will have a low albedo. This combination promotes ground heating during direct radiation in summer. Also the water content in the site is fairly low during most of the summer, as only a little summer rain falls, as stressed by the missing correlation between summer rain and ALT. Finally the UNISCALM site is dry due to the local topography, without drainage from surrounding areas, which further supports it being most likely relatively ice-poor in the top permafrost. Water contents of only 10–18% of the dry soil weights were measured in summer 200 0, with the largest values down through the active layer (Oht 2002).

It is mainly the relatively shallow thaw depths from the end of the 2005 summer that cause large INV in the southern

end of the UNISCALM site. We do not think that these values represent bad probing, as the thaw progression curve is consistent through the summer with no significant jumps. Comparing the calculated active layer depth of 102 cm from the temperature profile in the middle of the UNISCALM site to the entire UNISCALM average ALT of 74 cm, and studying the typical annual distribution of ALT in the entire UNISCALM site in 2005, show that the southern part experienced significantly reduced thawing this summer.

In the UNISCALM site, the ALT is largely controlled by the air temperature and radiation, with the warmest conditions occurring in the last two warm years. ALT increased 21 cm from 2005–2007 according to the average UNISCALM data (Fig. 4), but only 3 cm according to the ground thermal data (Fig. 5). This large difference between the two methods must lead to precautions when interpreting the direct effect of climatic variations on the ALT.

The significant surface offsets existing every year of the study period show that the winter influence of even a shallow snow cover of 20–30 cm significantly reduces the ground cooling. Also, there is a clear thermal offset causing the top permafrost in the UNISCALM site to be a relatively warm, 0 to -2ºC, during summer with no significant two-sided freezing in autumn. These conditions and the generally low assumed ice content in the top permafrost make the UNISCALM site very susceptible to meteorological variations, as it has experienced in the last 8-year period. This first overall data analysis from the UNISCALM site shows that this site is a good monitoring site for recording the response of climatic variations to the state of the top permafrost and active layer, but also that several factors affect the atmosphere and ground interaction in the maritime Svalbard setting, such as the Adventdalen site.

The UNISCALM site experienced much larger interannual variations than what is recorded in another flat High Arctic sediment CALM site, the ZEROCALM-1 site in northeast Greenland (Christiansen 2004). This is most likely due to the much-more maritime setting of Svalbard compared to the Zackenberg area in northeast Greenland.

Acknowledgments

Several persons have been our field assistants during the UNISCALM measurements. We extend our thanks to all of them for patiently writing down numbers. A special thanks to Sigurd D. Nerhus, who conducted the UNISCALM measurements in 2006 and 2007. The University Centre in Svalbard, UNIS, is thanked for providing funding for the equipment used to operate the UNISCALM site. The measurements from 2007 are part of the International Polar Year project "Permafrost Observatory Project: A Contribution to the Thermal State of Permafrost in Norway and Svalbard," supported by the Research Council of Norway, grant no. 176033/S30. Thanks to the two anonymous reviewers and the review editor for constructive comments. Thanks to our colleague Doug Benn for improving the English of the paper.

References

Brown, J. Hinkel, K.M. & Nelson, F.E. 2000. The Circumpolar Active Layer Monitoring (CALM) Program: Research Designs and Initial Results. *Polar Geography* 24: 165-258.

Carlson, H. 1952. *Calculation of Depth of Thaw in Frozen Ground.* Frost Actions in Soils: A Symposium. Washington DC: Highway Research Board Special Report 2, National Research Council, 192-223.

Christiansen, H.H. 2004. Meteorological Control on Interannual Spatial and Temporal Variations in Snow Cover and Ground Thawing in Two Northeast Greenlandic Circumpolar-Active-Layer-Monitoring (CALM) Sites. *Permafrost and Periglacial Processes* 15: 155-169.

Christiansen, H.H., Hormes, A. & Snowball. I. (in prep.) High resolution Late Holocene loess record with syngenetic ice-wedges in Adventdalen, Svalbard. *The Holocene.*

Førland, E.J., Hanssen-Bauer, I. & Nordli, P.Ø. 1997. *Climate statistics and long-term series of temperature and precipitation at Svalbard and Jan Mayen.* DNMI Klima rapport 21/97, 72 pp.

Harris, C., Arenson, L.U. Christiansen, H.H., Etzelmüller, B., Frauenfelder, R., Gruber, S., Haeberli, W., Hauck, C., Hölzle, M., Humlum, O., Isaksen, K., Kääb A., Lehning, M. Lütschg, M.A., Matsuoka, N., Murton, J., Nötzli, J., Phillips, M., Ross, N., Seppälä, M., Springman, S. & Vonder Mühll, D (submitted). Permafrost and climate in Europe: Geomorphological impacts, hazard assessment and geotechnical response. *Earth Science Reviews*.

Hinkel, K.M. & Nelson, F.E. 2003. Spatial and temporal patterns of active layer thickness at Circumpolar Active Layer Monitoring (CALM) sites in northern Alaska, 1995–2000. *Journal of Geophysical Research* 108: D2:ALT 9: 1-13.

Humlum, O., Instanes, A. & Sollid, J.L. 2003. Permafrost in Svalbard: A review of research history, climatic background and engineering challenges. *Polar Research* 22: 191-215.

Oht, M. 2002. *Impact of meteorological factors and local conditions on active layer depth and temperature, Adventdalen Area in central Spitsbergen, Svalbard.* Unpublished M.Sc. thesis, 77 pp.

Shur, Y., Hinkel, K.M. & Nelson, F.E. 2005. The transient layer: Implications for geocryology and climate-change science. *Permafrost and Periglacial Processes* 16: 5-17.

Smith M.W. & Riseborough, D.W. 2002. Climate and the limits of permafrost: a zonal analysis. *Permafrost and Periglacial Processes* 13: 1-15.

Experimental Study of the Self-Preservation Effect of Gas Hydrates in Frozen Sediments

E.M. Chuvilin
Department of Geocryology, Geological Faculty, Moscow State University, Russia
O.M. Guryeva
Department of Geocryology, Geological Faculty, Moscow State University, Russia

Abstract

Gases released from shallow frozen sediments may include methane from the dissociation of relict gas hydrate maintained by self-preservation. A series of experiments to substantiate this possibility were conducted. This research involved artificial formation of methane hydrate in frozen sediments, including samples recovered from gas shows in permafrost horizons, and studying the effect of self-preservation of gas hydrates in frozen soil samples at decreased pressure. The experiments show that self-preservation of gas hydrates in frozen sediments is enhanced by low formation temperatures, high ice content, and low sediment gas permeability.

Keywords: dissociation; gas hydrate; self-preservation.

Introduction

The presence of gas hydrate in permafrost has been confirmed by hydrate found in core samples and by indirect evidence in various regions of the world (e.g., Canadian Arctic, Alaska, and northern Siberia). Hydrate-containing samples have been recovered from permafrost and subpermafrost layers in the Mackenzie Delta (Dallimore & Collett 1995, Dallimore et al. 1999). In addition, there is evidence that self-preservation of relict methane hydrate, made possible by the continual frozen nature of the sediment, occurred in the upper permafrost layers (Dallimore et al. 1996).

Numerous hydrate shows were also indirectly found in Russia above a depth of 200 m in northwest Siberia and other regions containing permafrost (Are 1998, Chuvilin et al. 1998, Skorobogatov et al. 1998, Yakushev & Chuvilin 2000). These "relict" gas hydrates may have formed during glacial periods. Subsequently, glacial retreat induced metastable preservation of the hydrate by self-preservation (Ershov et al. 1991, Stern et al. 2001, Istomin et al. 2006).

Gas hydrate self-preservation phenomenon can be defined as a very slow decomposition of gas hydrates when the external pressure drops below a three-phase equilibrium pressure of the gas-ice-hydrate system at sub-zero (below -3 to -2°C) temperature as a result of thin ice film emergence on the gas hydrate surface (Istomin et al. 2006).

This effect was initially discovered and described in detail between 1986 and 1992, by researches from Canada (Ottawa National R&D Center) and Russia (VNIIGAZ and Moscow State University) (Davidson et al. 1986, Handa 1988, Ershov et al. 1989, 1991). The term "gas hydrate self-preservation" was introduced by Russian researches after several laboratory experiments revealed that gas hydrate decomposition came to a virtual halt when hydrate particles became covered by a thin ice shell at the initial decomposition stage.

Japanese scientists from Hokkaido Institute (HNIRI) studied methane hydrate decomposition kinetics and the self-preservation effect using X-ray diffraction. They showed that at temperatures above -84°C there are two stages in methane hydrate dissociation. Initially, hydrate dissociates rapidly (during first 10 minutes) then the rate of hydrate decomposition abruptly decreases due to the formation of an ice film on the surface of hydrate. The slow rate of decomposition is controlled by the conditions of methane diffusion through the pores or boundary of ice crystals (Takeya et al. 2002).

Research on the kinetics of gas hydrate decomposition at temperatures below 0°C revealed irregularly low rates of methane hydrate dissociation at temperatures between -31°C and -2°C, which was termed "anomalous preservation" of gas hydrates (Stern et al. 2001).

German scientists studied anomalous preservation of CH_4 and CO_2 hydrates and structural transformation of ice at low temperatures using neutronography and scanning electron microscopy (Kuhs et al. 2004). They determined that the lower temperature boundary of methane hydrate self-preservation occurs at -33°C; at temperatures below this threshold the ice structure does not inhibit gas diffusion, while gas diffusion becomes hindered as the ice structure changes at -33°C.

Using field data from gas shows in shallow permafrost and laboratory research of gas hydrate behavior at negative temperatures, we can identify the so-called metastable zone of gas hydrates. This zone is located above the stability zone of gas hydrates where the temperature conditions are favorable for the self-preservation effect (Fig. 1).

These self-preserved shallow-depth gas hydrates are presently under non-equilibrium conditions and pose a serious geological hazard to drilling exploration in these regions. The dissociation of shallow metastable methane hydrate may also contribute to global warming by adding significant amounts of methane, a greenhouse gas, to the atmosphere.

Since relict gas hydrates are poorly understood, experimental research on the self-preservation effect of

gas hydrates in frozen sediments under non-equilibrium conditions is of significant importance.

Methods

Experiments on the self-preservation of gas hydrate in frozen sediments under non-equilibrium conditions were conducted on natural samples from Vorkuta, Russia, located 160 km beyond the Arctic Circle. Cores were collected from permafrost horizons exhibiting gas release at the Yamburg gas field (dust sand, depth: 63 m) and the Bovanenkovo gas field (light loam, depth: 65 m) (Table 1). The initial sediment water contents ranged from 10 to 20%.

The experimental technique is based on physical modeling of water phase transitions and frozen methane hydrate-saturated samples in pressure chambers (Chuvilin & Kozlova 2005a). Methane (99.98% pure) was used to form hydrate at temperatures between ~0.5 and 2.0°C in two partially water saturated 9-cm long sediment samples with 4.6 cm and 6.8 cm diameters. The pressure chambers were filled to 6-7 MPa. After hydrate formation stopped, the pressure chamber containing the test sample was cooled to -8°C freezing any remaining free water and pushing the hydrate deeper into the stability field. The experimental technique is described in detail in Chuvilin et al. (2003).

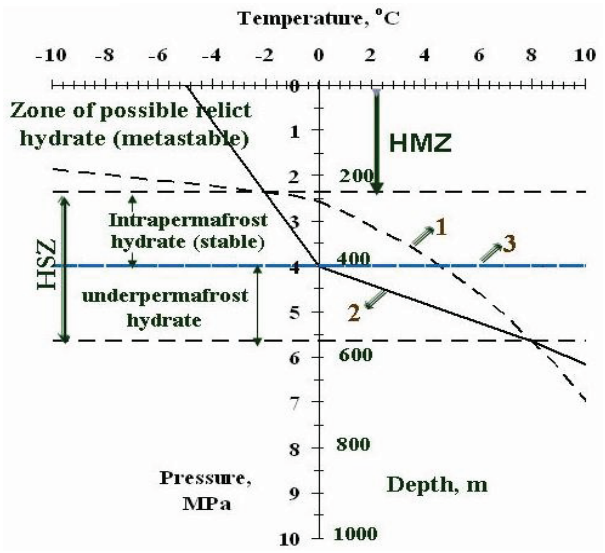

Figure 1. Conditions of gas hydrate occurrence in permafrost environments. **1** - Equilibrium curve of methane-hydrate stability in water-gas medium; **2** – Ground temperature profile; **3** - Permafrost boundary; **HSZ** - Hydrate stability zone; **HMZ** – Hydrate metastability zone.

The hydrate content and hydrate coefficient (share of water which has transformed in hydrate) were determined from changes in thermobaric conditions incorporating compressibility according to Mendeleyev-Clapeyron equation:

$$m_G = \frac{P_i \cdot V \cdot M}{R \cdot T_i \cdot z},$$

where P_i is pressure at a point in time i (MPa); V is free volume of the pressure chamber (cm^3); M is molar mass of gas (g/mol); R is absolute gas constant (N·m/K ·mol); T_i is temperature at a point in time i (K); z is gas compressibility.

After chamber pressure was vented to atmosphere, the chamber was opened in a cold room at -8°C. Detailed petrophysical analyses were performed on the frozen hydrate within 30 minutes of it being taken out of the chamber. Petrophysical analyses included macro- and micromorphological observations, calculation of water content, density, gas and hydrate content, porosity, hydrate coefficient, degrees of hydrate, and ice pore saturation. Gas content was measured by thawing in a solution of NaCl. Quantification of methane hydrate dissociation assumed a hydrate number of 5.9.

Remaining frozen hydrate-bearing sediment samples were stored on weighing devices for extended periods of time at freezing temperatures. Sublimation of the ice was reduced by a thin ice coating on the samples. Samples were monitored for over a month, during which time volumetric hydrate content Hv (Hv =VH·100% /Vsamp where VH is volume of hydrate, Vsamp is volume of the sample), hydrate saturation Sh (Sh = Hv /ϕ, % where Hv is volumetric hydrate content, and ϕ is sample porosity); ice saturation Si (Si = Iv /ϕ, % where Iv is volumetric ice content) and hydrate coefficient K_h (share of pore water which has transformed in hydrate) were calculated.

Experimental Results

In general, the test samples were characterized by homogeneous sediment structure and uniform distribution of hydrate and ice in the pore space resulting from an initial uniform water distribution (Chuvilin & Kozlova 2005b). The samples were also characterized by massive cryohydrates.

Table 1. Characteristics of soils.

Type of sediment	Particle size distribution, %			Particle density, ρ_s, g/cm^3	Plastic limit, W_p, %	Liquid limit, W_l, %	Salinity, %
	1-0.05 mm	0.05-0.001mm	<0.001 mm				
Silty sand	84	14	2	2.65	-	-	0.089
Sandy loam	41.8	53.7	4.5	2.68	11	15	0.075
Light loam	63.5	25.5	11.0	2.7	20	33	0.693

Table 2. Properties of frozen hydrate-saturated sediment samples.

Parameters	Silty sand		Silty sand		Sandy loam		Light loam	
	$p>p_{eq}$	$p<p_{eq}$	$p>p_{eq}$	$p<p_{eq}$	$p>p_{eq}$	$p<p_{eq}$	$p>p_{eq}$	$p<p_{eq}$
Gravimetric water content (W_g, %)	14		18		18		20	
density (ρ, g/cm^3)	1.76		1.63		1.68		1.82	
Porosity (ϕ)	0.41		0.44		0.47		0.43	
Hydrate coefficient (K_h)	-	0.68	0.74	0.66	0.30	0.23	0.12	0.11
Hydrate pore saturation (S_h, %)	-	45	50	42	23	15	11	10
Ice pore saturation (S_i, %)	-	15	8	15	20	28	67	68
Volumetric hydrate-content (H_v, %)	-	18	22	20	11	7	5	4

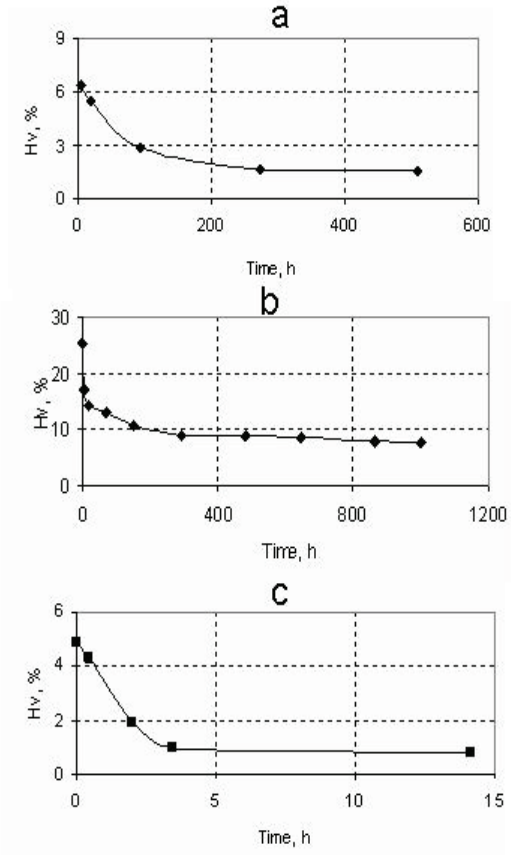

Figure 2. Methane hydrate dissociation kinetics in hydrate saturated frozen sediment after release of pressure to 0.1 MPa (atmospheric pressure).

a - sandy loam (W_g = 18%, t = -7.0°C);

b - silty sand (W_g = 18%, t = -6.5°C);

c - light loam (W_g = 20%,t = -5.0°C).

The sample properties are presented in Table 2. The porosity of the artificially hydrate-saturated sediment samples ranged from 0.41 to 0.47. The proportion of water incorporated into hydrate (K_h) in the silty sand sample (W_g=18%) (under equilibrium condition prior to pressure release) was 0.74, with a hydrate pore saturation (S_h) of 50%. 30-minutes after pressure release K_h and S_h decreased to 0.66 and 42% respectively. The light loam sample (W_g = 20%) had a K_h of 0.12 and S_h of 11% under equilibrium conditions. These values decreased to 0.11 and 10% respectively after pressure release. Thus, hydrate distribution in the finer-grained sediments was more dispersed and the pore saturation was lower. After pressure release, there is an intense decomposition of pore-space hydrate, followed by a more gradual decomposition (Fig. 2).

Our experimental data show that self-preservation reduces decomposition of pore-space hydrate in all samples. The self-preservation effect forms a thin ice film around particles of dissociating gas hydrate at temperatures below 0°C. As a result of this effect, hydrate can remain in a metastable condition for a long time.

As hydrate saturation decreases, ice content (S_i) increases (Fig. 3). At the beginning of the experiment (before gas release) hydrate saturation was 50%, and ice saturation was 8% in the silty sand sample. After 845 hours, gas hydrate saturation decreased to 13%, and ice saturation increased to 43%.

Self-preservation of gas hydrate in frozen sediment depends on many factors such as thermobaric conditions, hydrate and ice saturation, gas permeability, structure of organic-mineral skeleton of sediment, pore water salinity, and structure of hydrate, including micromorphology.

Ice formed during freezing of residual pore water which has not transformed into hydrate plays a special role in the self-preservation of gas hydrates. Occurrence of this ice promotes gas hydrate stability in a porous medium. As a rule, samples of frozen hydrate with greater ice content after pressure release are more prone to self-preservation. The presence of clay particles increases gas hydrate dispersion and reduces, but does not eliminate, the self-preservation

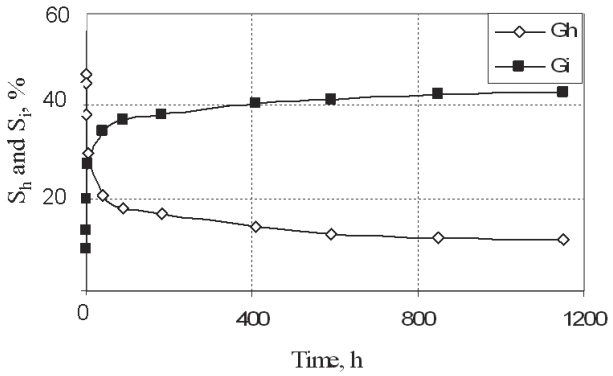

Figure 3. Change in methane hydrate saturation (S_h) and ice saturation (S_i) in hydrate-saturated silty sand (W_g=18%, t = -6.5 °C) after pressure release to 0.1 MPa.

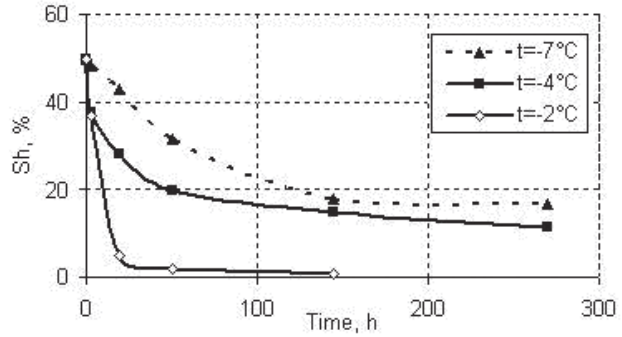

Figure 4. Methane hydrate dissociation kinetics in artificially hydrate-saturated frozen silty sand (W_g=14%) after pressure release to 0.1 MPa.

effect even in loamy deposits. Presence of salt in hydrate containing sediments also reduces the self-preservation effect. Thus, in light loam the intensive reduction of hydrate content after pressure release can be connected with the higher salinity (to compare to other samples) (Table 1, Fig. 2).

Results of experiments on sand and loam samples show that the intensity of pore gas hydrate dissociation sharply decreases with lower temperatures. In the silty sand sample (W_g=14%, initially about 45% hydrate saturation at all temperatures) hydrate saturation after pressure release decreased to 5% at -2°C in 20 hours, 28% at -4°C, and 43% at -7°C (Fig. 4). After 150 hours at -2°C, little hydrate remained, however, at -4°C and -7°C decomposition was sharply decreased.

Pore-hydrate dissociation practically ceases at lower temperatures. Because experimental temperatures compare favorably to natural temperatures (-5°C to -7°C) for permafrost sediments at the Yamburg and Bovanenkovo gas fields, it is possible for *in situ* gas hydrate to remain in a metastable condition for long periods of time.

In addition, the weight of overburden and high ice content of sediments provide additional stability to the metastable hydrate.

Conclusions

Experiments were conducted on kinetics of gas hydrate dissociation. Our experiments conducted on core samples confirm the self-preservation of natural pore-space gas hydrates. The conditions promoting self-preservation of natural gas hydrates are: low temperature, high ice content, low gas permeability, and overburden pressure. However, increased sediment temperature and pore water salinity, and gas hydrate dispersion in fine-grained sediment reduce the self-preservation effect.

Acknowledgments

This research was funded by the Russian Foundation Basic Research Program No 05-05-39019 and 06-05-91573. We thank the anonymous referees for various suggestions to improve the manuscript.

References

Are, F.E. 1998. Problem of deep-earth gases emission to the atmosphere. *Cryosphere of the Earth* II:42-50 (in Russian).

Chuvilin, E.M., Yakushev, V.S. & Perlova, E.V. 1998. Gas and gas hydrates in the permafrost of Bovanenkovo gas field, Yamal Peninsula, West Siberia. *Polarforschung 68* (erschienen 2000): 215-219.

Chuvilin, E.M., Kozlova, E.V., Makhonina, N.A. & Yakushev V.S. 2003. Experimental investigation of gas hydrate and ice formation in methane-saturated sediments. *Proceedings of the 8th International Conference on Permafrost, Zurich, Switzerland:* 145-150.

Chuvilin, E.M. & Kozlova, E.V. 2005a. Research of formation of frozen gas hydrate-saturated sediment. *Earth Cryosphere Journal*, 9:73-80 (in Russian).

Chuvilin, E.M. & Kozlova E.V. 2005b. Experimental estimation of hydrate-containing sediments stability. *Proceedings of the 5th International Conference on Gas Hydrates. Thermodynamic Aspects, v.5, Trondheim, Norway*: 1562-1567.

Dallimore, S.R. & Collett, T.S. 1995. Intrapermafrost gas hydrates from a deep core hole in the Mackenzie Delta, Northwest Territories, Canada. *Geology* 23: 527-530.

Dallimore, S.R., Chuvilin, E.M., Yakushev, V.S. Grechischev, S.E., Ponomarev, V. & Pavlov A. 1996. Field and laboratory characterization of intrapermafrost gas hydrates, Mackenzie Delta, N.W.T., Canada. *Proceedings of the 2nd International Conference on Natural Gas Hydrates, Toulouse, France*: 525-531.

Dallimore, S.R., Uchida, T. & Collett T.S. 1999. Summary. In: S.R. Dallimore, T.Uchida, T.S. Collett (eds), *Scientific results from JAPEX/JNOC/GSC Mallik 2L-38 Gas Hydrate Research Well, Mackenzie Delta, Nothwest Territories, Canada*. Geological Survey of Canada, Bulletin 544:1-17.

Davidson, D.W., Garg, S.K., Gough, S.R., Handa, Y.P., Ratcliffe, C.I., Ripmeester, J.A., Tse, J.S. & Lawson W.F. 1986. Laboratory analysis of a naturally occurring gas hydrate from sediment of the Gulf of Mexico. *Geochimica et Cosmochimica Acta* 50: 619-623.

Ershov, E.D., Lebedenko, Yu.P., Chuvilin, E.M., Istomin, V.A. & Yakushev, V.A. 1989. Problems of hydrate formation in the permafrost. *Permafrost exploring, MSU*: 50-63 (in Russian).

Ershov, E.D., Lebedenko, Yu.P., Chuvilin, E.M., Istomin, V.A. & Yakushev V.A. 1991. Peculiarity of gas hydrates existence in the permafrost. *Reports of Academy of Sciences USSR* 321: 788-791 (in Russian).

Istomin, V.A., Yakushev, V.S. Mokhonina, N.A., Kwon, V.G. & Chuvilin, E.M. 2006. Self-preservation phenomenon of gas hydrate. *Gas industry of Russia* Digest 4: 16-27.

Kuhs, W.S., Genov, G., Staykova, D.K. & Hansen, T. 2004. Ice perfection and onset of anomalous preservation of gas hydrates. *Physical Chemistry and Chemical Physics* 6: 1-6.

Skorobogatov, V.A., Yakushev, V.S. & Chuvilin, E.M. 1998. Sources of natural gas within permafrost North-West Siberia. *Proceedings of the 7th International Permafrost Conference, Yellowknife, Canada*: 1001-1007.

Stern, L.A, Circone, S., Kirby, S.H. & Durham, W.B. 2001. Anomalous Preservation of Pure Methane hydrate at 1 atm. *Journal of Physical Chemistry* 105: 1756-1762.

Takeya, S., Ebinuma, T., Uchida, T., Nagao, J. & Narita, H. 2002. Self-preservation effect and dissociation rates of CH_4 hydrate. *Journal of Crystal Growth:* 237-239, Part 1: 379-382.

Yakushev, V.S. & Chuvilin, E.M. 2000. Natural gas and hydrate accumulation within permafrost in Russia. *Cold Regions Science and Technology* 31:189-197.

Effects of Recent Climate Change on High Mountains of Western North America

John J. Clague
Simon Fraser University

Abstract

Pronounced step-wise atmospheric warming during the 20th century reduced ice cover in mountains by 25–50 percent. Net changes in average annual and mean summer temperatures responsible for this remarkable deglacierization are less than 2°C, a small fraction of the warming that occurred at the end of the Pleistocene. Yet the effects of these changes on mountain landscapes have been profound. Alpine permafrost, which expanded during the Little Ice Age, now appears to be thinning and disappearing in many areas. Loss of alpine permafrost and glacier downwasting appear to be partly responsible for accelerated mass wasting and catastrophic rock-slope failures in high mountains. New lakes appeared during the Little Ice Age when glaciers advanced across streams and rivers and blocked drainage. Most of these lakes drained one or more times during the 20th century, producing catastrophic floods orders of magnitude larger than normal nival or rainfall floods. In some instances, lakes have appeared upvalley of former, drained ones as glaciers have continued to retreat under a warming climate. Lakes also formed behind Little Ice Age end moraines when glaciers retreated in the early 20th century. Moraine dams are vulnerable to failure because they are steep-sided and consist of loose sediment. Outburst floods from lakes dammed by glaciers and moraines erode, transport, and deposit huge amounts of sediment over distances tens of kilometers. They broaden flood plains, destroy pre-flood channels, and create a new braided planform. The changes can persist for decades after the flood.

Keywords: climate change; deglacierization; jökulhlaup; landslides; Little Ice Age; permafrost thaw.

Introduction

Alpine glaciers in the Northern Hemisphere achieved their greatest extent of the Holocene during the "Little Ice Age" (AD 1200–1900; Holzhauser 1985, Grove 1988, Wiles et al. 1999, Luckman 2000, Luckman & Villalba 2001). Although Earth's climate was highly variable during this period, alpine glaciers grew episodically but progressively larger, culminating with the maximum advances of the Little Ice Age in the late 17th to mid 19th centuries.

Climate variability during the Little Ice Age (Moberg et al. 2005) probably was caused by a combination of forcing mechanisms (Mann et al. 1998). Explosive volcanism has contributed to Northern Hemisphere temperature changes during the past 600 years (Bradley & Jones 1993, Briffa et al. 1998), and some glacier advances coincided with intervals of elevated volcanic aerosols in the atmosphere (Porter 1986). Some researchers have argued that solar activity influenced the climate of the past millennium (Lean et al. 1995, Crowley & Kim 1996, Crowley 2000); indeed, periods of late-Little Ice Age moraine formation generally coincide with solar minima (Lawrence 1950, Wiles et al. 2004, Luckman & Wilson 2005). In addition, ocean-atmosphere interactions influenced atmospheric circulation and thus glacier behavior during the past millennium (Hendy et al. 2002, Nesje & Dahl 2003, Lewis & Smith 2004, Mann et al. 2005). Ruddiman (2003) suggested that widespread farm abandonment during the Black Death plagues and attendant reforestation may explain the cool phases of the Little Ice Age by changing concentrations of atmospheric carbon dioxide and methane.

The Little Ice Age ended about 100 years ago when climate around the world began to warm. Glaciers in most mountain ranges in the Northern Hemisphere, including those in western North America, receded during the first two decades of the 20th century. Some glaciers advanced in the 1920s but underwent rapid and extensive recession over the next three decades. Most glaciers advanced small distances between the 1950s and early 1980s but since then have retreated. Today most glaciers are 25% to 50% smaller than at the end of the Little Ice Age.

Net changes in average annual and mean summer temperatures responsible for glacier and climate change during and following the Little Ice Age are less than 2°C (Mann et al. 1998). This amount is a small fraction of the total warming that occurred during the demise of Northern Hemisphere ice sheets at the end of the Pleistocene. Corresponding changes in mean and seasonal precipitation in most areas also are relatively small. Yet these changes have had significant effects on high mountain environments and on rivers flowing from these mountains. This paper summarizes and discusses these effects.

Permafrost Thaw and Deglacierization

An increase in large landslides in northern British Columbia during the 20th century (Geertsema et al. 2006) may be related to warming or thaw of alpine permafrost and deglacierization. Permafrost expanded in high mountains during the Little Ice Age but now appears to be thinning and disappearing there (Zhang et al. 2006). Alpine permafrost has a complex and patchy distribution that is controlled mainly by altitude, material properties, snow cover, and topography. A rough estimate can be made of changes in the extent of permafrost in high mountains of North America using independently determined temperature changes, bearing in mind that permafrost distribution is affected by more than

Figure 1. Landslide deposit on Black Rapids Glacier, Alaska. The rock avalanche was triggered by a large earthquake in November 2002, but loss of glacier ice on the source slope may have contributed to the failure. The landslide scarp is indicated by an arrow.

just temperature. Using a range of mean annual temperature of 2°C on timescales of decades and an adiabatic lapse rate of 4°C/km–6°C/km, the limit of permafrost shifted vertically 300–500 m during the Little Ice Age. The average rise in the limit of alpine permafrost in the 20th century, during which climate warmed 0.6°C–0.8°C, may have been 100–200 m. These values may not seem significant, but even greater reductions in permafrost can be expected through the remainder of this century. Even 20th century warming and loss of permafrost have been implicated by recent instability of slopes in some mountain ranges (Watanabe et al. 2000, Gruber et al. 2004). Further, permafrost warming alone, without thaw, may increase the likelihood that rock slopes will fail (Davies et al. 2001, Harris et al. 2001). Sediments may mobilize as debris flows when their interstitial ice thaws (e.g., Bovis & Jakob 2000), and masses of rock may fail, generating rockslides and rock avalanches when ice within the fractures undergoes repeated thawing and freezing.

Another consequence of increased thaw of permafrost in high mountains is that many active rock glaciers will cease moving. Evidence has been reported that formerly active rock glaciers became less active or even fossil landforms in the 20th century (McCarroll et al. 2001, Baroni et al. 2004).

Glacier downwasting and retreat appear to be partly responsible for some catastrophic rock-slope failures in high mountains (Evans & Clague 1994, Evans & Clague 1999, Holm et al. 2004). Many marginally stable slopes that were buttressed by glacier ice during the Little Ice Age failed after they became deglaciated in the 20th century (Fig. 1). A factor that possibly has contributed to such failures is steepening of rock slopes by cirque and valley glaciers during the Little Ice Age.

These effects are most pronounced in mountain ranges with the largest ice cover, because it is there that ice losses in the 20th century have been greatest. An extreme example is Glacier Bay, which until the end of the 18th century was covered by glacier ice. Since then, Glacier Bay has become deglaciated with the loss of over 1000 km^2 of ice in 200 years. This amount of ice lost is so great that the land is rising due to isostatic rebound (Larson et al. 2005).

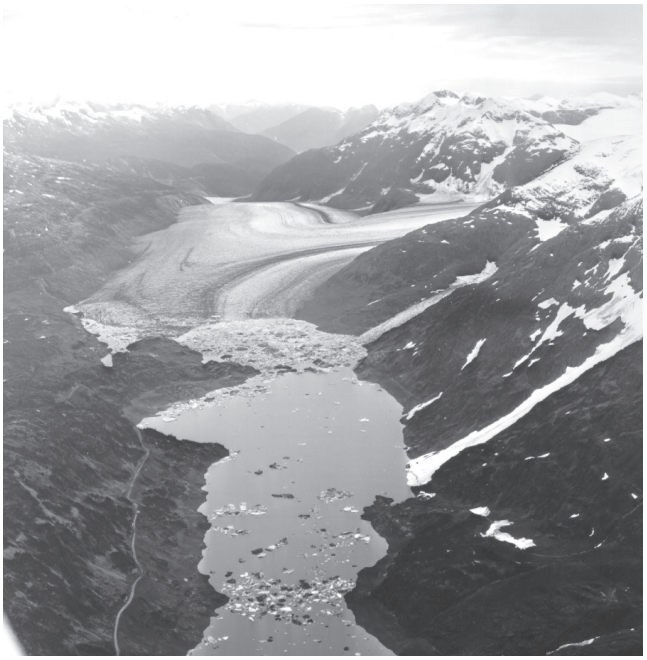

Figure 2. Summit Lake, located in the northern Coast Mountains of British Columbia. The lake is impounded by Salmon Glacier (background) and has drained and refilled more than 40 times over the past 47 years.

Outburst Floods

New lakes appeared in the mountains of western North America when glaciers advanced across streams and blocked drainage during the Little Ice Age (Fig. 2). The histories of these lakes are poorly known except in the 20th century when most of them drained one or more times, producing catastrophic floods (jökulhlaups) orders of magnitude larger than normal nival or rainfall floods (Fig. 3, Costa & Schuster 1988, Clague & Evans 1994, and references therein). These floods have occurred during a period of warming climate due to progressive wastage of the glacier dam and the formation of subglacial, supraglacial, or ice-marginal channels. Lakes may also form during rapid glacier advances ("surges").

New lakes also formed behind Little Ice Age end moraines as glaciers retreated in the late 19th and early 20th century (Fig. 4; Costa & Schuster 1988, O'Connor & Costa 1993, Clague & Evans 1994, Clague & Evans 2000). Moraine dams are vulnerable to failure because they are steep-sided and consist of loose sediment. Irreversible rapid incision of the dam may be caused by a large overflow triggered by an ice avalanche or rockfall. Other failure mechanisms include earthquakes, slow thaw of ice within the moraine, and removal ("piping") of fine sediment from the moraine. "Outburst floods" from lakes dammed by glaciers and moraines erode, transport, and deposit huge amounts of sediment over distances tens of kilometers (Fig. 5).

Outburst floods from glacier- and moraine-dammed lakes display an exponential increase in discharge, followed by a gradual or abrupt decrease to background levels as the water supply is exhausted. Peak discharges are controlled by lake volume, dam height and width, the material properties of the

Figure 3. Jökulhlaup caused by the sudden drainage of Summit Lake, north of Hyder, Alaska.

dam, failure mechanism, and downstream topography and sediment availability. Floods from glacier-dammed lakes tend to have lower peak discharges than those from moraine-dammed lakes of similar size. This is because enlargement of tunnels within ice is a slower process than overtopping and incision of sediment dams.

Floods resulting from failures of glacier and moraine dams may transform into debris flows as they travel down steep valleys. Such flows can only form and be sustained on slopes greater than 10°–15°, and only where there is an abundant supply of sediment in the valley below the dam. Entrainment of sediment and woody plant debris by floodwaters may cause peak discharge to increase down valley, which has important implications for hazard appraisal.

Outburst floods from lakes dammed by moraines and glaciers commonly alter river flood plains tens of kilometers from the flood source (Fig. 5). The floodwaters erode, transport, and deposit huge amounts of sediment. They commonly broaden flood plains, destroy pre-flood channels, and create a new multi-channel, braided planform. The changes can persist for decades after the flood, although rivers quickly reestablish their pre-flood grades by incising the flood deposits.

Climate is an important determinant of the stability of moraine and glacier dams. Most moraine-dammed lakes formed in the last century as glaciers retreated from bulky end moraines constructed during the Little Ice Age. The lakes soon began to fail as climate warmed. With continued warming and glacier retreat, the supply of moraine-dammed lakes susceptible to failure will be exhausted, and the threat they pose will diminish (Clague & Evans 2000). Glacier-dammed lakes typically have gone through a period of cyclic or sporadic outburst activity, lasting up to several decades, since climate began to warm in the late nineteenth century. The cycle of outburst of floods from any one lake ended when the glacier dam weakened to the point that it could no longer trap water behind it. However, with continued glacier retreat, the locus of outburst activity may, in some cases, shift up-glacier to sites where new lakes develop in areas that are becoming deglaciated (Geertsema & Clague 2005).

Figure 4. Moraine-dammed lake in the Bishop River watershed, southern Coast Mountains, British Columbia.

Figure 5. Flood-devastated west fork of Nostetuko River valley, British Columbia. The photograph was taken in 1998, one year after an outburst flood from moraine-dammed Queen Bess Lake.

Changes to Streams

Fluctuations of glacier margins on timescales of decades and centuries can mobilize sequestered glaciogenic sediment. During glacier advance, initial incision due to increased competence of meltwater streams is quickly followed by aggradation as sediment supply increases (Maizels 1979). Sediment stored within and beneath glaciers is delivered at an increasing rate to fluvial systems as glaciers advance (Karlén 1976, Maizels 1979, Leonard 1986, Leonard 1997, Karlén & Matthews 1992, Lamoureux 2000). Similarly, subglacial erosion increases during glacier advance, and meltwater may carry more sediment into river valleys than at times when glaciers are more restricted. Paraglacial sediment pulses may propagate rapidly downstream in narrow mountain valleys when glaciers advance to maximum positions and,

subsequently, as they begin to retreat. Glacier retreat typically exposes large areas of unstable, poorly vegetated sediment that is easily transferred to the fluvial system, causing valley-wide aggradation and complex changes in channel planform (Church 1983, Desloges & Church 1987, Gottesfeld & Johnson-Gottesfeld 1990, Brooks 1994, Ashmore & Church 2001, Clague et al. 2003, Wilkie 2006).

Increased glacial erosion and sediment production during glacier advance, coupled with climatically induced changes in discharge and sediment yield, can cause rivers to aggrade their beds. Sediment delivery to streams in the Coast Mountains of British Columbia, for example, increased during the Little Ice Age, and the streams responded by aggrading their channels and braiding over distances up to tens of kilometers down valley from glaciers (Church 1983, Gottesfeld & Johnson-Gottesfeld 1990, Wilkie 2006). Subsequently, during the 20th century, the streams incised their Little Ice Age deposits and reestablished single-thread channels characteristic of periods of lower sediment flux.

Conclusion

Climate warming during the 20th century and the first decade of the present century has caused changes in the pace of geomorphic processes in mountains in western North America and elsewhere. Rapid, large-scale deglacierization and thaw of alpine permafrost have increased the incidence of landslides and debris flows in mountains. Lakes that formed against retreating glaciers and end moraines have drained suddenly, catastrophically altering valley bottoms far downstream. Changes in sediment delivery to streams have altered local base level and channel planform in mountain valleys. If the forecasts of climate modelers are correct, loss of glacier ice and alpine permafrost will continue and perhaps accelerate through the remainder of this century.

References

Ashmore, P. & Church, M. 2001. *The Impact of Climate Change on Rivers and River Processes in Canada*. Geological Survey of Canada Bulletin 555, 58 pp.

Baroni, C., Carton, A. & Seppi, R. 2004. Distribution of behaviour of rock glaciers in the Adamello-Presanella Massif (Italian Alps). *Permafrost and Periglacial Processes* 15: 243-259.

Bovis, M.J. & Jakob, M. 2000. The July 29, 1998, debris flow and landslide dam at Capricorn Creek, Mount Meager volcanic complex, southern Coast Mountains, British Columbia. *Canadian Journal of Earth Sciences* 37: 1321-1334.

Bradley, R.S. & Jones, P.D. 1993. 'Little Ice Age' summer temperature variations: their nature and relevance to recent global warming trends. *The Holocene* 3: 367-376.

Briffa, K.R., Jones, P.D., Schweingruber, F.H. & Osborn, T.J. 1998. Influence of volcanic eruptions on Northern Hemisphere summer temperature over the last 600 years. *Nature* 393: 450-455.

Brooks, G.R. 1994. The fluvial reworking of late Pleistocene drift, Squamish River drainage basin, southwest British Columbia. *Géographie physique et Quaternaire* 48: 51-68.

Church, M. 1983. Pattern of instability in a wandering gravel bed channel. In: J.D. Collinson & J. Lewin (eds.), *Modern and Ancient Fluvial Systems*. International Association of Sedimentologists Special Publication 6: 169-180.

Clague, J.J. & Evans, S.G. 1994. *Formation and Failure of Natural Dams in the Canadian Cordillera*. Geological Survey of Canada Bulletin 464, 35 pp.

Clague, J.J. & Evans, S.G. 2000. A review of catastrophic drainage of moraine-dammed lakes in British Columbia. *Quaternary Science Reviews* 19: 1763-1783.

Clague, J.J., Turner, R.J.W. & Reyes, A. 2003. Record of recent river channel instability, Cheakamus Valley, British Columbia. *Geomorphology* 53: 317-332.

Costa, J.E. & Schuster, R.L. 1988. The formation and failure of natural dams. *Geological Society of America Bulletin* 100: 1054-1068.

Crowley, T.J. 2000. Causes of climate change over the past 1000 years. *Science* 289: 270-277.

Crowley, T.J. & Kim, K.-Y. 1996. Comparison of proxy records of climate change and solar forcing. *Geophysical Research Letters* 23: 359-362.

Davies, M.C.R., Hamza, O. & Harris, C. 2001. The effect of rise in mean annual temperature on the stability of rock slopes containing ice-filled discontinuities. *Permafrost and Periglacial Processes* 12: 137-144.

Desloges, J.R. & Church, M. 1987. Channel and floodplain facies in a wandering gravel-bed river. In: F.G. Ethridge & R.M. Flores (eds.), *Recent Developments in Fluvial Sedimentology*. Society of Economic Paleontologists and Mineralogists, Special Publication 39: 99-109.

Evans, S.G. & Clague, J.J. 1994. Recent climatic change and catastrophic geomorphic processes in mountain environments. *Geomorphology* 10: 107-128.

Evans, S.G. & Clague, J.J. 1999. Rock avalanches on glaciers in the Coast and St. Elias Mountains, British Columbia. *Proceedings of the 13th Annual Vancouver Geotechnical Conference, Vancouver, BC*. Richmond, BC: BiTech Publishers, 115-123.

Geertsema, M. & Clague, J.J. 2005. Jökulhlaups at Tulsequah Glacier, northwestern British Columbia, Canada. *The Holocene* 15: 310-316.

Geertsema, M., Clague, J.J., Schwab, J.W. & Evans, S.G. 2006. An overview of recent large catastrophic landslides in northern British Columbia. *Engineering Geology* 83: 120-143.

Gottesfeld, A.S. & Johnson-Gottesfeld, L.M. 1990. Floodplain dynamics of a wandering river, dendrochronology of the Morice River, British Columbia, Canada. *Geomorphology* 3: 159-179.

Grove, J.M. 1988. *The Little Ice Age*. London: Methuen Press, 498 pp.

Gruber, S., Hoelzle, M. & Haeberli, W. 2004. Permafrost thaw and destabilization of alpine rock walls in the hot summer of 2003. *Geophysical Research Letters* 31(13): 4 pp.

Harris, C., Davies, M.C.R. & Etzelmuller, B. 2001. The assessment of potential geotechnical hazards associated with mountain permafrost in a warming global climate. *Permafrost and Periglacial Processes* 12: 145-156.

Hendy, E.J., Gagan, M.K., Alibert, C.A., McCulloch, M.T., Lough, J.M. & Isdale, P.J. 2002. Abrupt decrease in tropical Pacific sea surface salinity at the end of Little Ice Age. *Science* 295: 1511-1514.

Holm, K., Bovis, M. & Jakob, M. 2004. The landslide response of alpine basins to post-Little Ice Age glacial thinning and retreat in southwestern British Columbia. *Geomorphology* 57: 201-216.

Holzhauser, H. 1985. Neue Ergebnisse zur Gletscher- und Klimageschichte des Spätmittelalters und der Neuzeit. *Geographica Helvetica* 40: 168-185.

Karlén, W. 1976. Lacustrine sediments and tree limit variations as evidence of Holocene climatic variations in Lappland, northern Sweden. *Geografiska Annaler* 58: 1-34.

Karlén, W. & Matthews, J.A. 1992. Reconstructing Holocene glacier variations from glacial lake sediments: Studies from Nordvestlandet and Jostedalsbreen-Jotunheimen, southern Norway. *Geografiska Annaler* 74: 327-348.

Lamoureux, S. 2000. Five centuries of interannual sediment yield and rainfall-induced erosion in the Canadian High Arctic recorded in lacustrine varves. *Water Resources Research* 36: 309-318.

Larson, C.F., Motyka, R.J., Freymueller, J.T., Echelmeyer, K.A. & Ivins, E.R. 2005. Rapid viscoelastic uplift in Southeast Alaska caused by post-Little Ice Age glacial retreat. *Earth and Planetary Science Newletters* 237: 548-560.

Lawrence, D.B. 1950. Glacier fluctuations for six centuries in southeastern Alaska and its relation to solar activity. *Geographical Review* 40: 191-222.

Lean, J., Beer, J. & Bradley, R. 1995. Reconstruction of solar irradiance since 1610: implications for climate change. *Geophysical Research Letters* 22: 3195-3198.

Leonard, E.M. 1986. Varve studies at Hector Lake, Alberta, Canada, and the relationship between glacial activity and sedimentation. *Quaternary Research* 25: 199-214.

Leonard, E.M. 1997. The relationship between glacial activity and sediment production: evidence from a 4450-year varve record of neoglacial sedimentation in Hector Lake, Alberta, Canada. *Journal of Palaeolimnology* 17: 319-330.

Lewis, D. & Smith, D. 2004. Dendrochronological mass balance reconstruction, Strathcona Provincial Park, Vancouver Island, British Columbia, Canada. *Arctic, Antarctic, and Alpine Research* 36: 598-606.

Luckman, B.H. 2000. Little Ice Age in the Canadian Rockies. *Geomorphology* 32: 357-384.

Luckman, B.H. & Villalba, R. 2001. Assessing the synchroneity of glacier fluctuations in the western Cordillera of the Americas during the last millennium. In: V. Markgraf (ed.), *Interhemispheric Climate Linkages*. New York: Academic Press, 119-140.

Luckman, B.H. & Wilson, R.J.S. 2005. Summer temperatures in the Canadian Rockies during the last millennium; a revised record. *Climate Dynamics* 24: 131-144.

Maizels, J.K. 1979. Proglacial aggradation and changes in braided channel patterns during a period of glacier advance: an Alpine example. *Geografiska Annaler* 61: 87-101.

Mann, M.E., Bradley, R.S. & Hughes, M.K. 1998. Global-scale temperature patterns and climate forcing over the past six centuries. *Nature* 392: 779-787.

Mann, M.E., Cane, M.A., Zebiak, S.E. & Clement, A. 2005. Volcanic and solar forcing of the tropical Pacific over the past 1000 years. *Journal of Climate* 18: 447-456.

McCarroll, D., Shakesby, R.A. & Matthews, J.A. 2001. Enhanced rockfall activity during the Little Ice Age; further lichenometric evidence from a Norwegian talus. *Permafrost and Periglacial Processes* 12: 157-164.

Moberg, A., Sonechkin, D.M., Holmgren, K., Datsenko, N.M. & Karlén, W. 2005. Highly variable northern hemisphere temperatures reconstructed from low- and high-resolution proxy data. *Nature* 433: 613-617.

Nesje, A. & Dahl, S.O. 2003. The 'Little Ice Age' – only temperature? *The Holocene* 13: 139-145.

O'Connor, J.E. & Costa, J.E. 1993. Geologic and hydrologic hazards in glacierized basins in North America resulting from 19th and 20th century global warming. *Natural Hazards* 8: 121-140.

Porter, S.C. 1986. Pattern and forcing of Northern Hemisphere glacier variations during the last millennium. *Quaternary Research* 26: 27-48.

Ruddiman, W.F. 2003. The anthropogenic greenhouse era began thousands of years ago. *Climatic Change* 61: 261-293.

Watanabe, T., Nakamura, N. & Khanal, N.R. 2000. Mountain hazards in the Kanchanjunga area, eastern Nepal; landslides developed on lateral moraines. *Jounal of Nepal Geological Society* 22: 525-532.

Wiles, G.C., Barclay, D.J. & Calkin, P.E. 1999. Tree-ring dated 'Little Ice Age' histories of maritime glaciers from western Prince William Sound, Alaska. *The Holocene* 9: 163-173.

Wiles, G.C., D'Arrigo, R.D., Villalba, R., Calkin, P.E. & Barclay, D.J. 2004. Century-scale solar variability and Alaskan temperature change over the past millennium. *Geophysical Research Letters* 31: L15203.

Wilkie, K.M.K. 2006. *Fluvial Response to Late Holocene Glacier Fluctuations in the Nostetuko River Valley, Southern Coast Mountains, British Columbia*. M.Sc. Thesis, Simon Fraser University, Burnaby, BC, 84 pp.

Zhang, Y., Chen, W. & Riseborough, D.W. 2006. Temporal and spatial changes of permafrost in Canada since the end of the Little Ice Age. *Journal of Geophysical Research* 111, D22: 14 pp.

A Model of Permafrost Distribution and Disturbance Sensitivity for Denali National Park, Using Soil-Ecological Site Inventory Information

Mark H. Clark
USDA-Natural Resources Conservation Service, Palmer, Alaska, USA

Abstract

A soil-ecological site survey of Denali National Park and Preserve (Denali) completed in 2004 by the Natural Resources Conservation Service is used to provide a map of Gelisols, soils with permafrost within 2 m of the surface, and their sensitivity to disturbance. Three sensitivity classes are assigned, based on similarities in the degree and rapidity of change to soil properties and plant communities following disturbance, as well as return interval to the pre-disturbance condition. The model aggregates ecological sites into groups with similar plant community structure and species richness, two elements useful in evaluating wildlife habitat. Dynamic soil properties, such as thickness of organic mat, depth to water table, and permafrost, may also be estimated for the various ecological states identified for each sensitivity class. This information is useful for estimating transient carbon budgets in soils and hydrologic functions, as well as indicating soils that are likely to be impacted by climate change. Gelisols considered highly sensitive to disturbance comprise 118,185 ha, or about 4% of Denali. Moderately sensitive Gelisols comprise 445,192 ha, or 18% of Denali. Gelisols considered low in sensitivity include 391,760 ha, or about 16% of Denali.

Keywords: ecological site inventory; Gelisols; permafrost; soil survey.

Introduction

The northern region of Denali includes areas lying north of the Alaska Range summit. This represents a subset of the Polar Domain described by Bailey (1994) and lies within the zone of discontinuous permafrost (Péwé 1975). The "Interior" climate of the northern part of Denali is continental, with long cold winters and short warm summers, relatively low precipitation, with a significant moisture deficit during the growing season (Patric & Black 1965).

Gelisols, soils with permafrost within 2 m of the surface (Soil Survey Staff 2006), are widely distributed within the northern part of Denali and generally absent in the remainder of the Denali south of the Alaska Range summit (Fig. 1). Gelisols are common to gently sloping, infrequently flooded surfaces throughout the boreal forest biome and lower elevations of the alpine life zone (Fig. 1) Gelisols are defined as having permafrost. However, extensive areas alternate between a poorly-drained, ice-rich condition, and a well-drained, permafrost-free state due to disturbance such as fire and post-disturbance plant succession. In this application, the definition of Gelisols includes those soils that have permafrost within 2 m of the soil surface under potential natural vegetation. Soils that are permafrost-free, with early to mid-succession communities and soil morphological properties that suggest that permafrost is present under potential native vegetation, are also considered Gelisols.

Variable rates of thaw, recession of water tables, and return intervals to the pre-burn condition are common to Gelisols following disturbance (Dyrness 1982). These differences are documented in the Ecological Site or Landtype (Bailey 1994) descriptions for each Gelisol soil component provided in the soil-ecological site survey of Denali National Park and Preserve (Denali) (Clark & Duffy 2004). The purpose of this poster is to provide a distribution map of Gelisols in Denali and present a model of sensitivity of Gelisols to disturbance based on ecological Landtypes.

Methods

The sensitivity of Gelisols to disturbance and lowering or loss of permafrost is modeled using a two-step process. The first step includes deriving a map of the distribution of Gelisols in Denali. This is accomplished using the soil-ecological survey database (Clark & Duffy 2004) to develop criteria and the spatial data to illustrate the map and provide associated statistics. Map units consisting of at least 15% Gelisols are aggregated into a map for consideration in the development of the disturbances sensitivity model (Fig. 1). The second step includes assigning map units into three sensitivity classes based on similar response to disturbance as defined in the ecological landtype descriptions. Significant soil properties associated with each disturbance class are then derived from the ecological landtype database.

Both static and dynamic site and soil properties are determined as useful to the model. Soil texture and overall thickness of the surface mineral layer are important static soil properties useful in determining sensitivity. A soil's ability to conduct heat increases as particle sizes increase (Jury et al. 1991). Soils with a low sand and rock fragment content conduct heat less effectively than soils with high sand or rock fragment content. Soils with high silt content have lower thermal conductivity and are most likely to experience a slower rate of permafrost recession and more rapid return to pre-burn condition than coarse textured soils. Soils with high sand and rock fragment content are less likely to have the potential for permafrost, because the high thermal conductivity promotes summer warming and prevents frost from persisting through the summer months. Dynamic soil and site properties for each ecological landtype are useful

to document transitional states between the non-permafrost and permafrost condition and provide a time-line for change between each pathway element. Dynamic soil properties important to the model include organic mat thickness, depth to permafrost, and depth to water table perched above the permafrost.

Fire is the only major disturbance factor available for use in the criteria. Anthropogenic disturbance in Denali is minimal, and flooding and landslide activity is primarily limited to soils other than Gelisols. The criteria assumes that a level of fire intensity common to the boreal biome and alpine life zone has occurred, including a mosaic pattern of scorched and unburned ground, and only partial incineration of the surface organic mat where burned. Fire disturbance is infrequent on soils with permafrost within the alpine life zone. The assignment of sensitivity classes to Gelisols within the alpine life zone are based on similar soils from within the boreal biome. Criteria used to assign three categories of sensitivity are outlined below.

Gelisols that are highly sensitive to disturbance, are rarely or non-flooded, and have a surface mineral soil layer consisting of 50 to 100 cm of silt loam, or stratified fine sand and silt with few rock fragments over sandy and gravelly alluvium with variable rock fragment content. Soil properties and plant communities associated with this sensitivity class are represented by ecological landtype Loamy Frozen Terraces-131B_104 (Clark & Duffy 2004). Thermal conductivity properties of the silt or stratified surface mineral soil layer are relatively low ranging, from about 0.25 to 1.4 cal $cm^{-1}s^{-1}$ $^{o}C^{-1}$ (Jury 1991). However, the thin nature of the surface mantle does not significantly retard surface warming following disturbance, and subsequent recession of permafrost is relatively fast. The high thermal conductivity of the underlying sand and gravel is estimated at 4.5 cal $cm^{-1}s^{-1}$ $^{o}C^{-1}$ (Jury 1991), and the porous nature of these coarse texture materials likely contributes to rapid warming and recession of permafrost in these soils. Landforms associated with the highly sensitive class include stream terraces, alluvial fans, and high positions on flood plains (Fig. 2). Climax plant communities from this class include shrub birch (*Betula glandulosa*)-bog blueberry (*Vaccinium uliginosum*)/moss scrub within the alpine life zone; and black spruce (*Picea mariana*)-tamarack (*Larix laricina*)/Labrador tea (*Ledum groenlandicum*) woodland within the boreal biome. Soils included in this class include Typic Historthels, Ruptic-Histic Aquiturbels, Fluvaquentic Historthels, and Typic Aquiturbels subgroups of US Soil Taxonomy (Soil Survey Staff 2004).

Gelisols that are moderately sensitive to disturbance are loamy throughout the soil profile, with 15 to 40% rock fragments in the upper 100 cm of soil. Soil properties and plant communities associated with this sensitivity class are represented by ecological landtype Gravelly Frozen Slopes, M135A_180 (Clark & Duffy 2004). These soils have intermediate levels of thermal conductivity related to the moderate level of rock fragments and loamy soil matrix, which overall exchange heat at a slower rate than soils of the first class. Landforms associated with this sensitivity class include till plains, all positions on glaciated low mountains, and on lower mountain slopes of non-glaciated mountains (Fig. 3). This class mostly consists of gelisols within the alpine life zone, commonly with a climax plant community of shrub birch-mixed ericaceous shrub/sedge (*Carex spp*.) scrub. Soils in this sensitivity class include Typic Historthels and Glacic Folistels subgroups of US Soil Taxonomy (Soil Survey Staff 2004).

Soils with permafrost that are considered to have a low sensitivity to disturbance (Fig. 4) are rock-free with silt or stratified fine sand and silt textures over 100 cm thick and have soils with near-surface water tables associated with cottongrass (*Eriophorum spp.*) tussock late succession communities. Soil properties and plant communities associated with this sensitivity class are represented by ecological landtype: Loamy Frozen Slopes, Wet-131B_402 (Clark & Duffy 2004). This group has soil texture of silt loam, loam, or stratified loamy surface layers with relatively low thermal conductivity properties ranging from 0.25 to 1.4 cal $cm^{-1}s^{-1}$ $^{o}C^{-1}$ (Jury 1991). Landforms associated with the low sensitivity class include loess covered plains, hills, and stream terraces (Fig. 4). Climax plant communities include black spruce-tamarack/tussock cottongrass woodland within the boreal biome and tussock cottongrass/mixed ericaceous shrub meadow in the alpine life zone. Soils in this sensitivity class include Typic Histoturbels, Typic Historthels, and Typic Umbrothels subgroups of US Soil Taxonomy (Soil Survey Staff 2004).

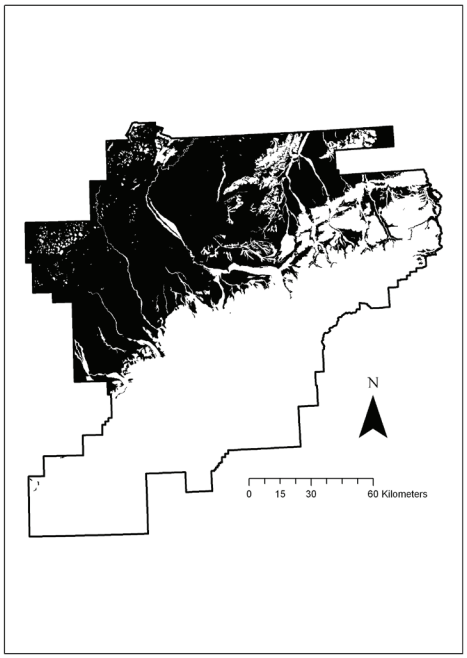

Figure 1. Distribution of soil map units consisting of at least 15% Gelisols in Denali.

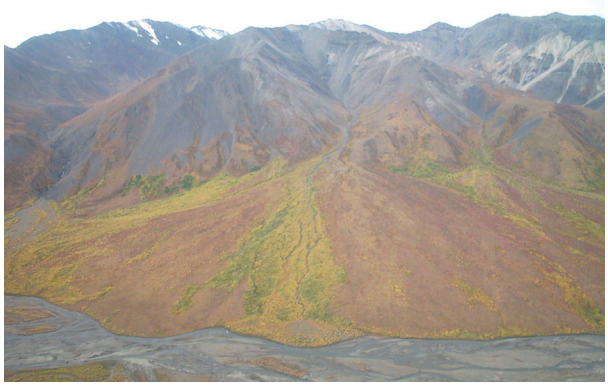

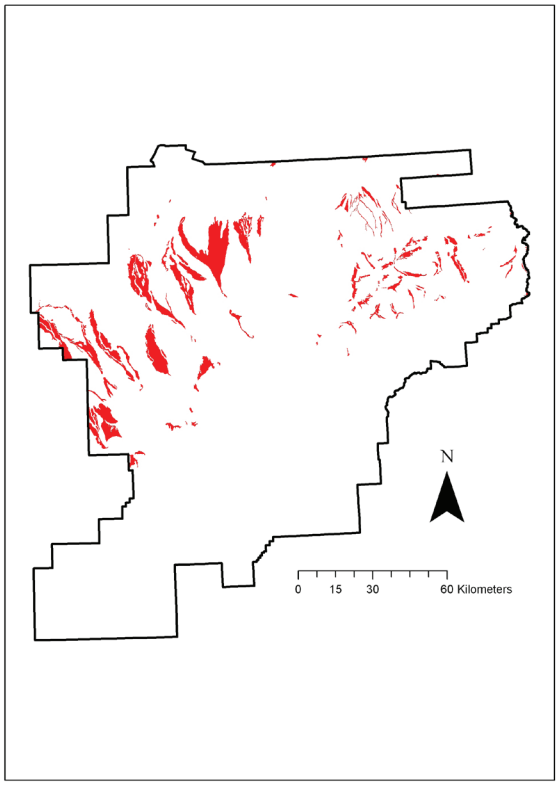

Figure 2. Upper: Alluvial fan with Gelisols illustrated in the foreground with shrub birch-bog blueberry/moss scrub typical of a Gelisol sensitive to disturbance. Lower: Gelisols highly sensitive to disturbance or temperature change are represented in black and total 118,185 ha, or about 4% of Denali.

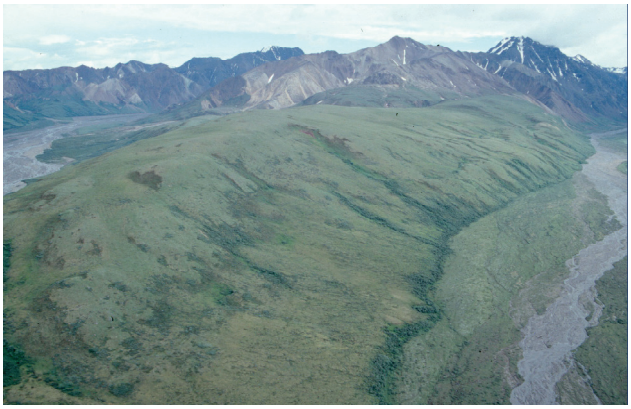

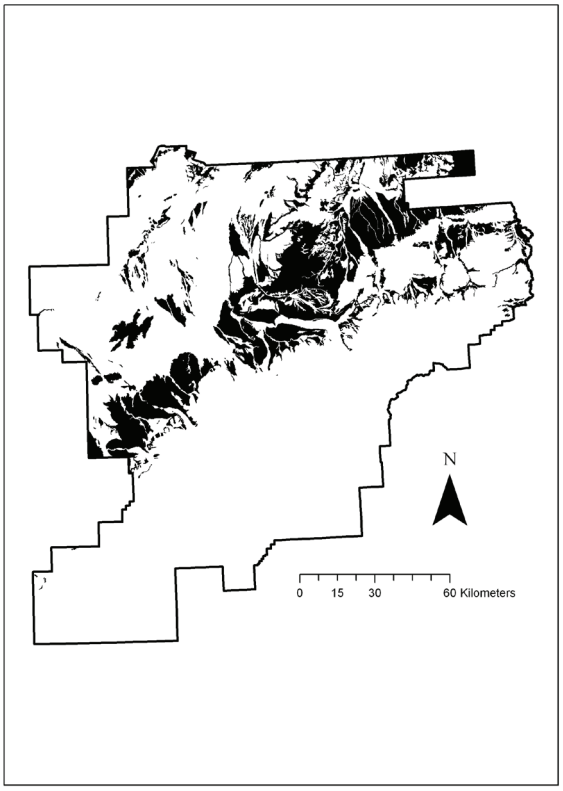

Figure 3. Upper: Glaciated mountains with shrub birch-mixed ericaceous shrub/sedge scrub illustrated in the light tonal areas of the foreground. Soils are primarily Gelisols that are moderately sensitive to disturbance. Lower: Gelisols moderately sensitive to disturbance are represented in black and total 445,192 ha, or 18% of Denali.

Results

Distribution of soil map units with Gelisols in Denali is provided in Figure 1. This illustrates map units containing soil components with permafrost that comprise 15% or more of the map unit. The total distribution of map units that meet these criteria encompasses 931,000 ha, or about 38% of the park. Soil map units with Gelisols highly sensitive to disturbance or temperature change are represented in black, and total 118,185 ha, or about 4%, of Denali (Fig. 2). The high thermal conductivity property of soils is considered an important factor in the high sensitivity of these soils to change following disturbance Permafrost is observed to drop rapidly to below 200 cm of the ground surface within one to three years following fire in this class. Return to the pre-burn condition in the black spruce type in Interior Alaska is suggested as 50 to 70 years Foote (1976) and Viereck (1973). However, based on tree core observations in Denali, a return interval of 100 to 150 years is estimated for this sensitivity category. Gelisols within the boreal biome that are included within this class have a single climax and two distinctive transitional plant communities, suggesting that significant changes in dynamic soil properties following disturbance are associated with a diverse array of wildlife habitat types, especially within the boreal biome.

Soil map units with Gelisols moderately sensitive to

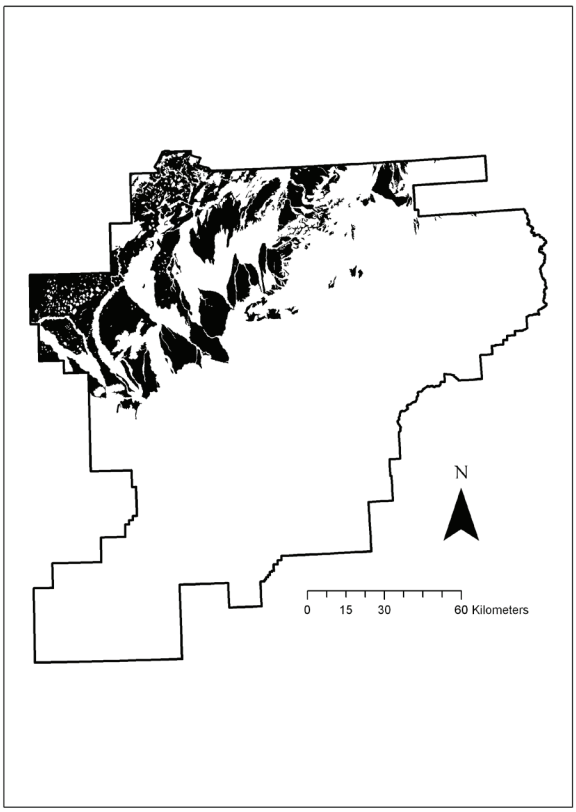

Figure 4. Upper: An extensive loess plain with black spruce/ericaceous shrub woodland and Gelisols with low sensitivity to disturbance. Lower: Gelisols with low sensitivity to disturbance are represented in black and total 391,760 ha or about 16% of Denali.

disturbance or temperature change are represented in black in Figure 5 and total 445,192 ha, or 18% of Denali. The moderate thermal conductivity property of soils is considered an important factor of change in this class. Loss of permafrost to depths below 200 cm is observed at three to five years following fire, and is significantly longer than that observed for the previous class. However, the return to the pre-burn condition is similar to that of the highly sensitive soils: about 130 years. A single climax plant community consisting of shrub birch-mixed ericaceous shrub/sedge scrub has been identified, suggesting a moderately low level of diversity in terms of habitat types.

Soil map units with Gelisols that have low sensitivity to disturbance are represented in black in Figure 7 and total 391,760 ha, or about 16% of Denali. The relatively low thermal conductivity property of soils is attributed to the minimal change on these soils following disturbance. Gelisols within this sensitivity class are observed to experience only slight lowering in depth to permafrost, rarely exceeding 200 cm depth unless associated with localized massive ice degradation. Site and soil characteristics typically return to the pre-burned condition within 25 years, based on tree core observations. Several ecological landtypes are included in this sensitivity class, each with unique climax vegetation and seral communities. Black spruce woodlands with various understory including ericaceous shrub, cottongrass tussock are common late succession communities within the boreal biome and tussock cottongrass/mixed ericaceous shrub meadow in the alpine life zone. Several community types are identified for this sensitivity class. However, most types are similar in terms of species composition, with only subtle differences apparent between succession states.

References

Bailey, R.G., P.E. Avers, T. King & W.H. McNab (eds.), 1994. *Ecoregions and Subregions of the United States* (map). 1:7,500,000. USDA Forest Service. Washington, DC. With supplementary table of map unit descriptions, compiled and edited by W.H. McNab and R.G. Bailey.

Clark, M.H. & Duffy, M. 2004. *Soil Survey of Denali National Park and Preserve Area, Alaska.* Available on Web Soil Survey. http://websoilsurvey.nrcs.usda.gov/app/WebSoilSurvey.aspx.

Dyrness, C.T. 1982. *Control of depth to permafrost and soil temperature by the forest floor in black spruce/feathermoss communities.* U.S. Department of Agriculture, Forest Service. Research Note PNW-396.

Foote, M.J. 1976. *Classification, description, and dynamics of plant communities following fire in the taiga of Interior Alaska.* Fire effects study. U. S. Department of Agriculture, Forest Service, Institute of Northern Forestry. Final report. BLM contract No. 53500-ct2-224.

Viereck, L.A. 1973. Wildfire in the taiga of Alaska. *Quaternary Research* 3(3): 465-495.

Jury, W.A.;. Gardner, W.R & Gardner, W.H. 1991. *Soil Physics*. New York, NY: John Wiley and Sons, Inc.

Patric & Black. 1965.

Péwé, T.L. 1975. *Quaternary geology of Alaska.* Geologic Survey Professional Paper 835. Washington, DC: U.S. Govt. Printing Office.

Soil Survey Staff. 2004. *Keys to Soil Taxonomy*. 10th ed. U.S. Department of Agriculture, Natural Resources Conservation Service.

A Multi-Disciplinary Approach to Assess the Impact of Global Climate Change on Infrastructure in Cold Regions

Jim Clarke
BP Exploration, Sunbury, UK
Clark Fenton
Imperial College, London, UK
Antonio Gens
Universitat Politècnica de Catalunya, Barcelona, Spain
Richard Jardine, Chris Martin, David Nethercot
Imperial College, London, UK
Satoshi Nishimura
Port and Airport Research Institute, Yokosuka, Japan, formerly Imperial College, London, UK
Sebastia Olivella
Universitat Politècnica de Catalunya, Barcelona, Spain
Catherine Reifen, Paul Rutter, Fleur Strasser, Ralf Toumi
Imperial College, London, UK

Abstract

Imperial College London is researching with BP some potential impacts of future climate change. BP has a significant number of facilities in cold high-latitude regions, where global climate models predict significant rises in air and ground surface temperature. This could impact on the state and extent of permafrost, potentially posing risks to facilities, infrastructure, and operations (ACIA 2005). The paper reviews the research, focusing on an exemplar study region in eastern Siberia. The key elements included: (1) Developing an approach to provide a best estimate of future climate change. (2) An engineering geological appraisal of the ground conditions in the study region. (3) Performing a parametric study of geothermal conditions in the study region using finite element thermal analyses. (4) Developing a Thermal-Hydraulic-Mechanical modeling approach for assessment of climate change impact on specific engineering facilities. (5) Developing a methodology for incorporating potential climate change considerations into engineering decision-making and design.

Keywords: climate change; engineering adaptation; engineering geology; GCM modeling; Siberia; thermal modeling.

Introduction

This paper describes research by Imperial College London commissioned by BP Research. The objective was to provide BP with a process for assessing the likely effects of climate change on the integrity of its engineered facilities. The original brief was to:

- Describe the potential impact of changes in local climatic conditions on BP's current operations between now and the 2050s.
- Determine the potential vulnerability of new projects should existing design parameters remain unchanged.
- Provide a process to evaluate BP's exposure to damaging or beneficial effects of climate variability.
- Provide guidelines for the design of structures and infrastructure that anticipate potential future climactic changes in the region of interest.

A generic process has been developed to assess the potential exposure of future projects to climate change, but it became clear during the early parts of study that the outputs of General Circulation Models (GCM) used to predict climate change are not easily converted into data that can be used for engineering design. It was therefore decided to focus particular attention on the possible engineering consequences of air warming on the temperature profiles of frozen ground, the potential effects of permafrost thawing, and the difficulties of operating facilities in permafrost areas. This required the development of new modeling techniques for the assessment of climate change-induced effects on pipelines, foundations, and slopes in regions of existing permafrost.

An area of eastern Siberia was chosen as a relevant example, in order to validate the process,and to demonstrate the potential importance of climate change to BP operations.

Climate Modeling as a Geotechnical Input

The climate data used in this study is based on the predictions of seventeen coupled Atmosphere Ocean General Circulation Models (AOGCM) included in the IPCC Fourth Assessment Report (IPCC 2007), whose data is available from the Coupled Model Intercomparison Project (see URL: https://esg.llnl.gov:8443). These models were chosen because they have provided climate predictions under the conditions of the SRES A2 emissions scenario (Nakicenovic et al. 2000) adopted in this study, which is a standard

pessimistic projection of greenhouse gas emission.

Coupled AOGCMs are the most sophisticated tools available for modeling current and future climate. All models used in this study have produced simulations of 20th Century climate that have been validated against appropriate contemporary observations. Climate models perform better at large spatial scales (such as global mean predictions), than at regional or local level, but there is nevertheless reasonably good agreement between modeled and observed temperature trends in Siberia and other cold regions. Careful statistical assessments indicate that the most reliable predictions are made by averaging the results of all available models to form a multi-model ensemble mean.

The multi-model ensemble mean air temperature (defined as the temperature at 2 m above the ground surface) was compared with the corresponding European Centre for Medium-Range Weather Forecasts 40 Year Re-analysis (ERA-40) observational dataset (Simmons & Gibson 2000) for each study area over the 1958–1998 period. Corrections were applied to the entire 1940–2059 time-series based on the difference between modeled and observed 40–year monthly mean temperature from 1958–1998, in an attempt to eliminate model bias as far as possible. The same process was applied to the corresponding multi-model mean time-series for snow depth. Each model time-series was then considered to correspond to the relevant 2.5° x 2.5° ERA-40 grid cell, which is equivalent to an area of approximately 150 km (east-west) by 280 km (north-south) in the study region. In all cases, the processed time-series represents a significantly larger area than would ideally be required for the thermal ground modeling, but further improvements in resolution would require better coverage of local station data than is currently available. An example of the model output is included in Figure 4, along with the predictions for changes in the ground thermal regime discussed below.

Height corrections were applied to produce both air temperature and snow depth time-series for different elevations. Temperature was adjusted based on mean monthly lapse rates derived from linear regression of the corresponding ERA-40 temperature, available for six elevations between 0 and 3000 m above sea level (m a.s.l.). Snow depth was adjusted in the accumulation phase based on a simple model describing orographic enhancement of precipitation (Roe et al. 2002), for which mean slope and wind speed data were taken from ERA-40. In the melting phase, snow depth was adjusted based on a combination of air temperature and solar radiation (Cazorzi & Fontana 1996), the former being dependent on the height correction applied to the temperature time-series. The final predicted mean monthly time-series were validated against local data and appear to be consistent with conditions in the study areas.

Project Geotechnical Strategy

The strategy developed for assessing the impact of climate change in cold regions has involved geotechnical research and development in four main areas:

1. Assessing the regional engineering geology and geomorphology of the study region, including identification of potential geohazards.
2. Reviews of present conventional frozen ground engineering practice.
3. Developing rigorous geothermal analytical tools and applying these on a regional basis.
4. Exploring and developing the potential of THM modeling in cold region engineering applications.

This work has led to a practical process for assessing geotechnical impact of climate change in cold regions that involves a hierarchy of risk assessment activities. The level of sophistication adopted for the risk assessment reflects the severity of potential adverse effects to BP's infrastructure and operations. The consequence assessment is carried out at a regional scale and incorporates consideration of the local ground conditions (identification of geohazards), the climate modeling outputs (sensitivity of hazard to climate change) and the inventory of BP's infrastructure (exposure and vulnerability).

The following three-level approach is recommended:

- Low-consequence hazards addressed through check-lists combined with simple accepted empirical methods.
- Intermediate-level cases to be tackled through regional (or site-specific) uncoupled geothermal modeling predictions combined with well-established conventional geocryological engineering approaches.
- Potentially high-consequence hazards to be addressed by advanced site-specific THM modeling.

The results obtained from any one of these approaches should confirm or challenge the initial assessment and could lead to a higher level of investigation.

Engineering Geology and Geomorphology

A region of eastern Siberia around Lake Baikal (Fig. 1) was chosen as the main focus for investigating the geotechnical impacts of climate change in an area of variable permafrost. The local geological, geographical, and climatic setting was assessed through an extensive review of published data, including geological and geocryological maps, consulting reports as well as interviews with local and international specialists. A brief reconnaissance field trip was also undertaken. The work was limited by the remote, undeveloped nature of the region. The data availability to western parties was also limited by a combination of material sensitivity, geographic location of resources, and translation requirements. A good data set is crucial to the recommended process and, to progress this study, the current assessment was augmented by reference to data from analogous geological and geocryological settings around the world.

Data requirements

The inputs needed to assess the geotechnical impact of climate change on permafrost are driven by the requirements of the geothermal modeling analyses discussed below. The key data requirements are:

- Comprehensive local climate records.
- Geographical and geomorphological information.

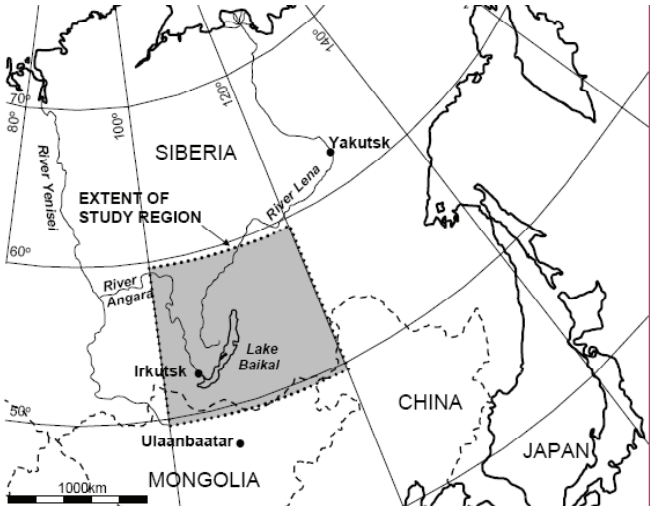

Figure 1. Study region and vicinity map.

- Surface and deeper geology.
- Geocryology, including ground thermal regime and geothermal material properties.
- Land use and forest fire records.
- Inventory of relevant infrastructure.

Regional setting of study area

Ground conditions vary considerably over the area selected for detailed study, which is outlined in Figure 1 and measures approximately 1300 km east-west and 1100 km north-south. The topography ranges from high-relief mountains (Baikal, Patoma, and Khamar Daban ranges) to low-lying fluvial plains towards Mongolia and along the Angara River valley. The geology varies from relatively flat-lying undisturbed sedimentary rocks of the Siberian platform, to much older highly deformed and metamorphosed rocks along the active Baikal rift zone. The significant variation in relief has a profound effect on the observed climatic conditions, the vegetation, drainage characteristics, and hence the permafrost distribution within the region, which varies from being absent to continuous.

Geomorphological units and expected ground conditions

In order to assess the ground conditions across the study region, five geomorphological units were defined, which encompass broadly similar physical characteristics, as shown in Figure 2.

Once these geomorphological units were defined, five "exemplar" study areas were selected (Fig. 2), which provided representative settings for the associated climate modeling, geothermal ground modeling and engineering geological terrain analysis.

Remote sensing data (Shuttle Radar Topography Mission [SRTM] topographic survey data) was used to produce a Digital Elevation Model (DEM), allowing detailed assessment of elevation, slope angle, slope aspect, and drainage characteristics within each study area. This terrain analysis could be further enhanced in future applications by incorporating higher resolution datasets.

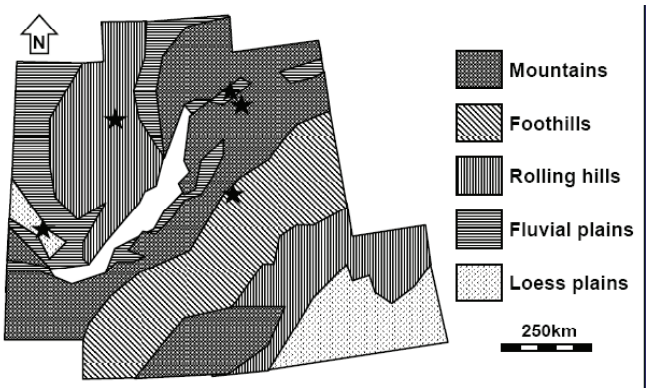

Figure 2. Classification into five geomorphological units. Black stars show location of "exemplar" study areas.

Geological, geocryological, and geotechnical characteristics were interpreted for each study area, based on literature review and field reconnaissance, assigning data where necessary from other global analogues. The latter included representative vegetation and ground void ratio profiles for each study area, which provided best-estimate, lower-bound, and upper-bound parameters for geothermal numerical modeling in each setting.

Although this investigation has included a thorough review of all of the readily available data, there is significant uncertainty associated with the age, provenance, and hence accuracy of some of the available information. The current review is considered adequate for a preliminary research study, which could be compared with the feasibility or possibly appraisal stage of a large civil engineering project. However, detailed site-specific information and further analysis would be essential before progressing to any preliminary design stage.

Geocryological Engineering

Civil engineering activity in the North American cold regions prompted rapid development from the 1960s of specialist geotechnical tools, analyses and practices, as detailed in Andersland & Ladyanyi (2004), for example. Similar work was undertaken from an earlier date in the Former Soviet Union, although much of the output was published in Russian and is less well known in the West. The paradigms, practices, and design codes applied in North America and the Former Soviet Union are substantially different.

Some of the practical geocryological engineering topics that are important to the proposed risk assessment and design processes are highlighted below.

Geocryological analysis: elements, options, and strategy

Geocryological engineering analysis involves many elements; the relative significance of which depends on the nature of the engineering problem of interest. For example, thermal (T), hydraulic (H), and potentially chemical (C) elements are more important than the mechanical (M) element in water discharge or contaminant transport problems. However, it is essential to address the mechanical element

when assessing the viability, stability, and serviceability of facilities, pipelines and slopes.

Checklists, definitions, and indices

The essential precursor for all rational geocryological analyses is the information gathering and data access. Geothermal modeling is only possible when adequate climate, geology, and ground temperature data exist, including the local air-to-ground temperature conversion factors, which are influenced by local vegetation, soil types, topography, and weather patterns.

Ground behaviour associated with thermal regime changes

Engineering activities and climate change trends are both likely to modify the ground's thermal regime. Significant deterioration of the engineering properties of frozen soil is expected as temperatures increase, potentially leading to difficulties with embedded structural elements such as foundations and pipelines. Potentially severe phenomena may be encountered in soils or rocks that become unstable as they thaw. It is also well known that frozen soils show very strongly time-dependent behaviour: creep movements can be large in the field and field strengths may be far lower than are seen in laboratory loading tests.

Furthermore, the thawing of frozen open ground can lead to substantial settlements and large transient pore-water pressures. In cold regions, slope stability is dominated by thermal effects. Slopes sited in permafrost areas experience annual cycles of thawing and freezing in their active layers, experiencing seasonal downslope creep. Large-scale instabilities can also occur as a result of changes in ground surface conditions or sub-surface hydrology.

Construction itself may generate more significant thermal changes in foundation soils and rocks than those expected from climate change alone. Insulation elements, air ducts, or active cooling systems are often designed and installed to improve foundation behaviour, and these could be required more extensively to cope with climate change.

A key issue in pipeline engineering is the effect on the ground thermal regime of heat flow to or from the pipeline and its products. Thawing induced by running warm oil in pipelines buried in frozen ground can induce melting, settlement, strength loss, and even floatation. Elevated sections may be utilised, but these require piled foundations that can cope with the possible geotechnical consequences of climate change. On the other hand, ice migration and growth caused by running chilled gas in buried unfrozen ground can cause serious differential heave in pipelines installed in discontinuous permafrost regions. It is therefore vital to consider all potential damage processes within the risk assessment process.

Thermal Modeling and Permafrost Mapping

In order to make reasonable assessments of how slopes, foundations and pipelines may respond to climate change, it is necessary to be able to reliably predict how ground temperatures and properties will react over tens of metres of depth. GCM models incorporate sophisticated formulations that address temperature variations within the atmosphere and oceans, and offer projections as to how the climate may change in the future. However, the near-surface temperature of the ground is usually considered in a simplistic manner, for example, by assuming a constant ratio between air and ground temperature changes, and little attention is given to what may happen at greater depths. The GCMs therefore fail to predict the considerable time lag between climate change and ground response, potentially resulting in gross overestimates of the depth of permafrost melting expected by any given date, the degree of ground warming, and, therefore, of permafrost degradation and infrastructure distress.

Simple models have been proposed to relate air and ground temperatures; however, the Authors' work has shown that the thermal conductivity is complex and non-linear in permafrost, and a fundamental analytical treatment is necessary to predict the variations with time of the thermal regime, extending tens of metres beneath the ground surface. A fundamentally formulated regional approach has been developed for the present study. A new Finite Element Code (FEM FATALE, Nishimura 2007a) was written to perform rigorous thermal analyses efficiently for multiple vertical profiles. The code can also be applied to any other specific site, for which detailed information is available.

The model is based on non-linear heat conduction theory, with material properties that effectively vary with unfrozen water content and hence temperature. The thermal properties of water, ice, and the soil minerals are fixed, and the global properties at any point in the ground profile depend on the ground's porosity profile (which is input on the basis of the engineering geology assessment described above) and a specific function that relates the degree of ice saturation to temperature. The code also incorporates latent heat effects. The effects of the seasonally-variable snowcover are modeled explicitly. The surface energy transfer is modeled using the n-factor approach (Lunardini 1978), making careful distinctions between summer values and times when the ground is snow-covered, when n is taken as unity. These purely thermal regional analyses do not consider pore fluid migration or ground deformations; these features are covered by the more sophisticated, fully-coupled THM approach reported later.

The purely thermal approach has been applied on a regional basis by considering multiple analyses of the development of permafrost in the circum-Baikal region, covering the period 1940 to 2059. Climate predictions have been applied to stereotypical ground profiles that were selected to encompass the range of geological/geotechnical conditions that might reasonably be expected within the five geomorphological units in the study region. An extensive parametric study has been performed with FEM FATALE to produce time-series predictions for ground temperature and ice content profiles from ground level to 100 m depth, considering the effects of different surface elevations, porosity profiles, snow cover, and natural geothermal gradients; the output data providing the basis of a large-scale risk assessment process for climate change-induced hazards. Examples of some predictions are shown in Figures 3 and 4; substantial warming and thawing is indicated over the next 50 years within

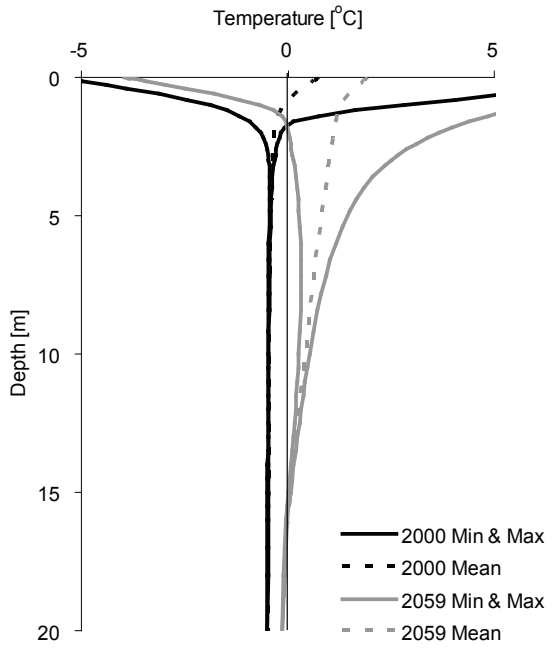

Figure 3. Example of simulated geothermal curves: case of stratigraphy with 1 m colluvial soil (assumed porosity, ∅ = 0.4) and 9 m weathered rock (∅ reducing from 0.4 to 0.04 with depth) overlying base rock (∅ = 0.04) in the rolling hills study area, 643 m a.s.l. (assuming air-surface thawing index, $n_t = 0.6$).

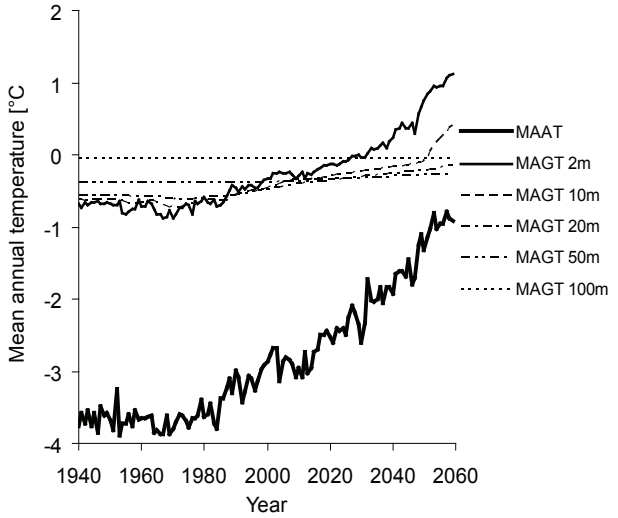

Figure 4. Predicted time-series of temperature at different depths, for example shown in Figure 3.

the top 20 m that would have a considerable negative impact on foundations, pipelines, and slopes.

In addition, a new method has been developed for correlating, synthesising, and presenting the time-dependent evolution of geocryological conditions in a series of layered maps. The approach interfaces data from DEM and GCM sources with the FEM FATALE thermal analyses. The approach has been used to successfully predict, from first principles (i.e., "Type A" prediction, Lambe 1973), the current and historical extent of permafrost in each geological study area, and can be used to produce maps of future distribution of permafrost and its thermal characteristics. Engineering geocryological analyses may be performed based on these data to predict the geotechnical impact for a particular facility or area.

Fully-Coupled Finite Element Analysis

In cases where the consequences of the expected ground temperature changes are sufficiently significant, more rigorous THM analyses of the interconnected thermal (T), hydraulic (H) and mechanical (M) processes may be deemed necessary. THM analyses incorporate predictions for ground movements, soil stresses, and changes in state, along with possible ground failure and soil-structure interaction. While THM models offer potentially powerful tools for assessing climate change impact, they are rarely conducted in practice: their complexity, incompletely developed formulation, and long computational run times limit their current appeal. Assessing, developing, and demonstrating THM applications in cold region geotechnical engineering was an important aspect of the present study, even though THM analyses are likely to be reserved for high-consequence cases.

THM-analysis has been developed intensively for high-temperature problems, particularly related to nuclear waste disposal. However, its application to frozen soils has concentrated on frost heave, and its potential use in permafrost problems has only been noted recently. The group collaborated with colleagues at UPC Barcelona for this purpose, running and developing with them their sophisticated THM programme CODE-BRIGHT (Olivella et al. 1996, Gens 2008). The main aims of the THM component of the study, and the achievements made, were:

- An assessment of the difficulties in applying THM-analysis to permafrost problems. Potential problems have been identified and solutions found that will enable a wider range of applications.
- Developing a robust overall THM modeling framework capable of embracing future sub-model developments. The formulation requires additional features that are important in ice-rich permafrost, including the development of large creep strains under load and the potential for extreme pore pressure generation during thawing.
- A new framework of describing stresses in frozen soils. This development has opened a way for recently developed soil model elaborations to be directly applied in frozen ground modeling.
- Successful back analyses of practical pipeline frost heave problems, which demonstrate the potential for THM analysis in cold region engineering applications.

Freezing ground water migration problems such as frost heaving around chilled pipelines can be simulated with reasonable accuracy by the CODE-BRIGHT model in its current state; the case study outlined below is provided as an illustration. THM analyses undertaken with the code for this project provide good predictions of the frost heave measured in a carefully controlled, long-term field test involving chilled gas running in a frost susceptible unfrozen silty soil (Slusarchuk et al. 1978). Figure

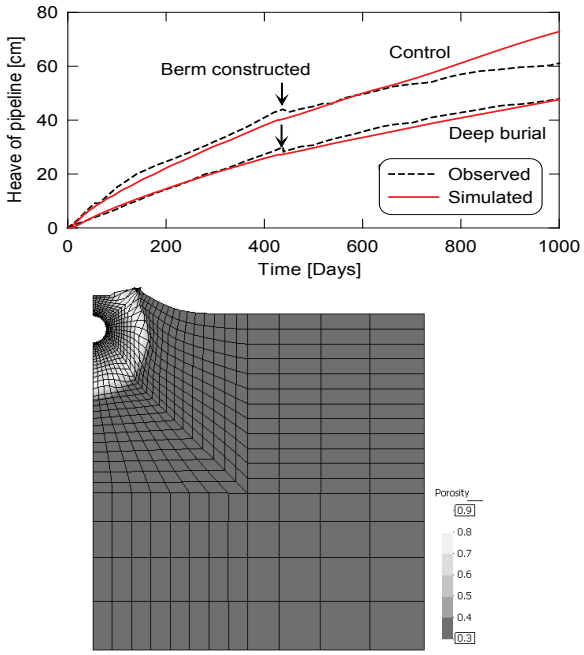

Figure 5. Top: Comparison between observed and measured heave of pipeline buried at two different depths. Bottom: Deformed mesh showing simulated pipeline heave and porosity contours in "Control" case at day 1000.

5 shows the generally good agreement between the observed and simulated heave of pipelines buried at two different depths; 'Control' and 'Deep burial' (Nishimura 2007b).

The THM model's fully-coupled treatment allows far more generalised situations to be considered than conventional engineering geocryological methods. Three-dimensional soil-structure interaction in discontinuous permafrost can be considered, in principle, without many additional modifications.

Conclusions

- A multi-disciplinary approach has been developed to assess the impact of climate change on infrastructure; this has been applied in an exemplar cold region of eastern Siberia.
- The effect of air temperature change on ground temperature profiles has been identified as being of critical significance to facilities and ground conditions in areas of variable or discontinuous permafrost.
- An integrated regional assessment approach has been developed that combines climate modeling data, engineering geology assessments, remote sensing data, and geocryological engineering methodologies to produce regional ground condition predictions.
- More advanced fully-coupled THM approaches have also been explored for site-specific application in critical cases. Key development targets have been identified for future THM modeling research.
- The research predicts that climate change will have a considerable impact on ground conditions in the study region over the next 50 years. However, the effects will be less severe than might be anticipated from studies that do not model the ground response with the same level of sophistication.

Acknowledgments

The Authors thank BP for their permission to publish and acknowledge the modeling groups for providing their data for analysis, PCMDI for collecting and archiving model output, and the JSC/CLIVAR Working Group on Coupled Modeling for organizing model data analysis activity. The multi-model data archive is supported by the Office of Science, U.S. Department of Energy. ERA-40 data have been obtained from the ECMWF data server. We would also like to acknowledge assistance from Arup Geotechnics London with the SRTM processing and terrain analysis.

References

ACIA. 2005. *Arctic Climate Impact Assessment*. Cambridge University Press, 1042 pp.

Andersland, O.B. & Ladanyi, B. 2004. *Frozen Ground Engineering*, John Wiley & Sons, 384 pp.

Cazorzi, F. & Fontana, G.D. 1996. Snowmelt modeling by combining air temperature and a distributed radiation index, *Journal of Hydrology* 181: 169-187.

Intergovernmental Panel on Climate Change. 2007. *Climate Change 2007: The Scientific Basis*. Contribution of Working Group I to the Fourth Assessment Report of the Intergovernmental Panel on Climate Change. Cambridge, UK: Cambridge University Press,

Gens, A. 2008. *Soil-environment interactions in geotechnical engineering*. Rankine Lecture. Presented 21 March 2007. *Geotechnique* (in press).

Lambe, T.W. 1973. Predictions in soil engineering. *Geotechnique* (23)2: 149-202.

Lunardini, V.J. 1978. Theory of n-factors and correlation of data. *Proceedings of the Third International Conference on Permafrost, Edmonton, Alberta*: 41-46.

Nakicenovic, N. et al. 2000. *Special Report on Emissions Scenarios: A Special Report of Working Group III of the Intergovernmental Panel on Climate Change*. Cambridge, UK: Cambridge University Press.

Nishimura, S. 2007a. *Assessment and prediction of circum-Baikal permafrost development over period 1940-2059*. Imperial College Internal Report.

Nishimura, S. 2007b. *THM-Coupled Finite Element Analysis of Soil Freezing: Formulation and Application*. Imperial College Internal Report.

Olivella, S., Gens, A., Carrera, J. & Alonso, E.E. 1996. Numerical formulation for a simulator (CODE_BRIGHT) for the coupled analysis of saline media. *Engineering Computations* 13(7): 87-112.

Roe, G.H. et al. 2002. Effects of orographic precipitation variations on the concavity of steady-state river profiles. *Geology* 30(2): 143-146.

Simmons, A.J. & Gibson, J.K. 2000. *The ERA-40 Project Plan*. ERA-40 Project Report Series No. 1. Reading, UK: ECMWF, Shinfield Park, 63 pp.

Slusarchuk, W.A., Clark, J.I., Nixon, J.F., Morgenstern, N.R. & Gaskin, P.N. 1978. Field test results of a chilled pipeline buried in unfrozen ground. *Proceedings of the Third Intl. Conf. on Permafrost, Edmonton, Alberta*: 878-883.

Freezeback of an Anthropogenic Talik Within Tailings at Nanisivik Mine, Canada

Geoff Claypool, P.Eng.
BGC Engineering Inc.
James W. Cassie, P.Eng.
BGC Engineering Inc.
Robert Carreau
Breakwater Resources Ltd.

Abstract

Following 26 years of successful mining, the tailings facility at the Nanisivik Mine site was reclaimed between 2004 and 2005. The objective of the reclamation plan for the tailings facility was to use the cold environmental conditions to encapsulate the tailings in permafrost, thereby limiting the potential for negative environmental impacts over the long term. During reclamation planning, a talik was identified within the tailings deposit. The talik was studied in detail due to its unknown effect on the stability of the adjacent tailings retention dike and the effect of freezeback on surface water quality, and to assess the time required for freezeback to occur. This paper summarizes the studies undertaken to characterize the talik and assess freezeback, ,and includes performance monitoring undertaken to date.

Keywords: cryoconcentration; freezeback; Nanisivik; pingo; tailings; talik.

Introduction

Nanisivik Mine is located at the northern end of Baffin Island in the Territory of Nunavut in the Canadian Arctic. The mine operated from 1976 to 2002, during which time sulphide ore was mined to produce lead and zinc concentrates. The tailings generated during the mining process were initially deposited directly into West Twin Lake (WTL). However, as additional mining reserves were identified, the West Twin Lake reached its storage capacity, and it became necessary to identify further storage options to keep the mine in production. Construction of a frozen tailings retention dike permitted the continued use of the West Twin Lake area until closure of the mine in 2002. During tailings deposition in the West Twin Disposal Area (WTDA), a partial water cover was maintained over most of the tailings. In areas where the tailings were aerially exposed, or where only a thin water cover was maintained, permafrost aggraded into the tailings. In areas where a deeper water cover was maintained, the tailings remained in a thawed state. As such, a talik, a zone of thawed materials surrounded by permafrost, formed within the tailings deposit.

Between 2002 and 2004, development of the Final Closure and Reclamation Plan (FCRP) for the West Twin Disposal Area was undertaken. This included characterization and delineation of the talik and an assessment of the potential effects of freezeback of the talik anticipated during closure. The talik delineation and characterization program was undertaken by conducting a detailed geotechnical drilling investigation which included installation of several types of monitoring instrumentation. Freezeback assessment of the talik included geothermal modeling to predict the rate of talik freezeback and assessing the potential for pingo growth, frost-heave and generation of high pore pressures within the center of the talik and its effect on the stability of the adjacent dike.

Figure 1. Regional location map – Nanisivik Mine.

Between 2004 and 2005, the reclamation plan for the West Twin Disposal Area was implemented. The partial water cover was removed from the tailings pond and a permafrost aggradation cover was constructed over the tailings to promote the freezeback of the talik. Additional instrumentation was installed after construction of the cover to monitor ground temperatures, pore pressures, and water quality in the talik during freezeback. This paper provides a summary of the talik characterization and assessment work that was completed and a summary of the monitoring data collected during the initial years of talik freezeback.

Background

Location and climate

The Nanisivik Mine Site is located on the northern end of Baffin Island in the Canadian Arctic, as shown on Figure 1.

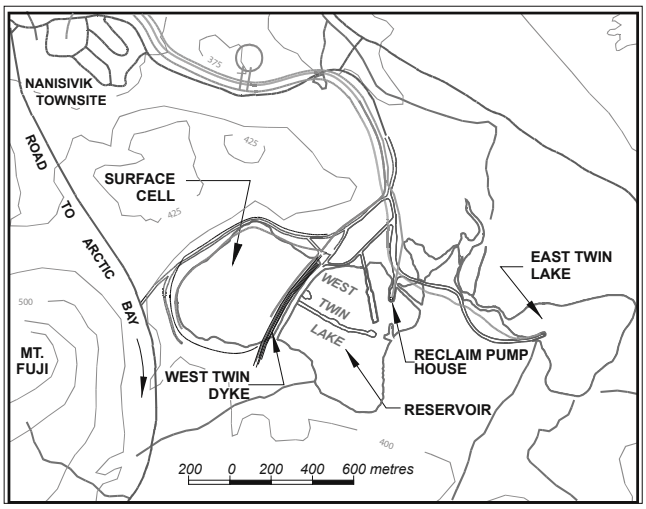

Figure 2. West Twin Disposal Area.

Based on the available climate record from the Nanisivik airport (1971–2006) the mean annual air temperature (MAAT) is approximately -14.8°C and the mean annual precipitation is 282 mm/yr.

Permafrost

Nanisivik is located in the region of continuous permafrost. Permafrost has been observed to extend to a depth of at least 430 m, as observed in a borehole drilled from the underground workings. Ground conditions in the area have been characterized by NRC (1995) as having the potential for medium amounts of ground ice (as high as 20%) and mean annual ground temperatures colder than -10°C. This has been verified by ground temperature measurements at various locations around the mine site as cold as -13°C at depth. The depth of the active layer in natural ground has been observed to average between 1 m to 2 m below ground surface.

Tailings deposition practices

Tailings were initially deposited sub-aqueously into WTL beginning in 1977. Based on the known mine reserves at the time, WTL had sufficient tailings storage capacity for the life of the mine. Mine reserves, however, continued to expand each year and by the mid 1980s, it was apparent that continued production would exceed the storage capacity of WTL. In 1988, an approval was received from the Northwest Territories Water Board to begin surface deposition of tailings at Nanisivik. To accommodate this, WTL was divided into two sections using an earthen dike, as shown on Figure 2. The dike was constructed using a north/south trending causeway that was developed by beaching of tailings in the lake as a foundation. The eastern portion of the lake, the Reservoir, retained its original lake level and was used as a stand-by when surface disposal was not practical (i.e. during annual dike construction periods). The western part of the lake, the Surface Cell, became the main deposition area for the tailings and accommodated sub-aerial tailings.

On-land deposition of tailings in the Surface Cell commenced on August 27, 1990. Tailings discharge in the Surface Cell continued throughout the 1990s, permitted by annual raises of the West Twin Dike in 2 m increments. Tailings continued to be discharged mainly from the northwest corner of the Surface Cell with a deeper section of the pond in the southeast corner for water reclamation and mineral processing purposes. In total, it is estimated that 6.5 million m^3 of tailings were deposited into the Surface Cell between 1978 and 2002.

It should be noted that tailings were deposited sub-aqueously into the area later known as the Reservoir between 1976 and 1990. The discharge of tailings generally took place near the current location of the West Twin Dike resulting in the aggradation of the tailings deposit in a southeasterly direction into the Reservoir. Tailings deposition along an east-west trending line from the centrer of the West Twin Dike resulted in exposure of a tailings causeway in the Reservoir by 1988. This causeway eventually became the foundation for the east/west arm of the Test Cell Dike. Tailings deposition along a northwest-southeast trending line resulted in a second tailings causeway near the reclaim water pumphouse, which was exposed by 1992. This causeway eventually became the foundation for the north/south arm of the Test Cell Dike. The Test Cell Dike was constructed in 2000 and 2001, increasing the storage capacity of the Test Cell thereby allowing for the additional placement of tailings into the Test Cell. Deposition of tailings at the base of the West Twin Dike in 2000 resulted in aerial exposure of tailings in the Reservoir and Test Cell. In total, it is estimated that 3.5 million m^3 of tailings have been deposited into the Reservoir and Test Cell since 1978.

Talik Characterization and Delineation

Geotechnical drilling investigation

In 2002 and 2003, a total of 44 boreholes were drilled in the Surface Cell, Test Cell Dike, and at the base of the West Twin Dike. The drilling was completed using a diamond drill coring rig and chilled brine was used as a drilling fluid to enable core recovery of frozen tailings. The following points summarize the significant observations recorded during the geotechnical drilling investigation:

- The maximum thickness of tailings contained within the Surface Cell was approximately 34 m.
- The maximum thickness of tailings contained within the Test Cell was 20 m.
- During the drilling investigation, thawed tailings were encountered in both the Surface Cell and Test Cell.
- Artesian pore pressures were encountered in the Surface Cell talik.
- The frozen tailings were generally observed to be ice-poor. However, some ice lenses were observed in the frozen tailings. It was unclear if the ice formed in-situ or was encapsulated during deposition.

Select samples collected during the drilling process were forwarded for geotechnical testing. The following points summarize the geotechnical characteristics of the tailings:

- The grain size distribution was variable ranging from 95% sand-sized particles to 95% silt-sized particles.
- Specific gravity ranged from 3.9 to 4.5.
- The tailings generally had a saturation value of greater than 90%.
- The frozen bulk density of the tailings ranged from 2100 to 3500 kg/m^3, with the lowest values associated with samples containing visible ground ice.
- The thermal conductivity of the tailings was measured to be approximately 1.9 W/(m·°C) at room temperature and 3.2 W/(m °C) at -15°C.

A number of monitoring instruments were installed during the geotechnical investigation to further characterize the subsurface conditions. Thermistors and thermocouples were installed to assess geothermal conditions and vibrating wire piezometers were installed to monitor pore pressures within the thawed tailings. Monitoring wells were also installed to assess the pore water quality in the taliks.

Geothermal monitoring data indicated near 0°C temperatures within the talik. Ground temperatures within the thawed zones were observed to be as cool as -0.2°C, indicating freezing point depression. Piezometers installed in the Surface Cell talik indicated artesian pore pressures 3 m to 4 m above ground surface.

The results of the geotechnical investigation and the available historical information on tailings deposition was used to estimate the size of the Surface Cell and Test Cell taliks. Based on the analysis, it was estimated that the Surface Cell and Test Cell taliks contained approximately 2,000,000 m^3 and 1,000,000 m^3 of thawed tailings, respectively, which was approximately 30% of the tailings contained within the facility.

Technical Analyses

Due to the unknown effect of the freezeback of the taliks on the stability of the West Twin Dike, the surface of the reclamation covers or the water quality of the entire system, a number of technical analyses were undertaken. The following sections summarize the objectives and results of each analysis.

Geothermal modeling

Geothermal modeling of the Surface Cell talik was completed to predict the rate of permafrost aggradation into the talik. The results of the modeling were to be used to direct future monitoring efforts and to estimate the time required to achieve various benchmarks during closure.

The geothermal modeling was completed using the commercially available software Temp/W produced by GeoSlope International. The model was calibrated using the geothermal data collected in an area of recently deposited tailings, and by comparing the predicted freezeback thermal regime to the observed freezeback thermal regime over a one year period.

Once the model was calibrated, several analyses were conducted to assess the variability and sensitivity of the results to initial thermal conditions, global warming, snow cover, and the placement of the shale as a cover material. Additionally, an envelope of freezeback times was developed, based on the results of the parametric analyses.

The following is a list of the principal conclusions derived from the geothermal analysis of the Surface Cell talik:

1. There is minimal sensitivity in the predicted depth of permafrost aggradation of the various parameters in the initial 5 years.
2. Permafrost aggradation reaches a depth of 17 m (the base of the West Twin dike) between 7 and 8 years after the initial winter following completion of reclamation activities.
3. Permafrost aggradation reaches an elevation of 365 m, a depth of approximately 23 m, between 13 and 15 years after the initial winter.
4. Depending on the modeled scenario, permafrost aggradation reaches an elevation of 353 m, a depth of approximately 35 m, between 27 and 32 years after the initial winter.
5. The results were not sensitive to assumed global warming values.

Effect of high pore pressures on dike stability

The effect of high pore pressures in the Surface Cell talik on the stability of the West Twin dike were assessed due to the artesian piezometric conditions encountered during the geotechnical investigation.

The artesian pore pressures are thought to be attributed to the process of pore water expulsion that occurs during freezing of saturated soils. McRoberts and Morgenstern (1975) attributes the pore water expulsion process to the fact that when the ice-water interface progresses through a freezing saturated soil, water may be expelled from the ice interface, depending upon soil type and stress level. If no drainage of the excess pore pressures is permitted, then the system is considered closed. If drainage is allowed, the system is considered open.

Useful information can be found on the topic of pore pressures generated by pore water expulsion through the study of pingos. Pingos are intrapermafrost ice-cored hills, typically conical in shape, that grow and persist only in a permafrost environment (Mackay 1998). Many pingos form in the bottoms of old lakes that drained rapidly. They form in response to the development of excessive pore water pressures and differential permafrost thickness. Mackay et al. (1972) suggests that pore pressures generated by pore water expulsion in growing pingos can exceed 80% of the total overburden pressure, even beneath permafrost 40 m thick. Additionally, Mackay (1978) notes that pressure transducers installed in one sub-pingo water lens measured a hydrostatic head of 22 m above lake bottom.

Due to the fact that no evidence of hydraulic connectivity between the Surface Cell talik and the Reservoir was defined during the geotechnical investigation, the Surface Cell talik is considered to be a closed system. As such, the pore pressures within the Surface Cell talik are expected to continue to rise

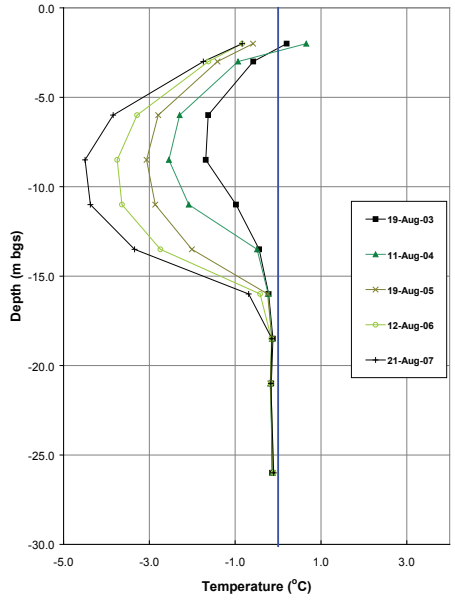

Figure 3. Geothermal monitoring data from edge of Surface Cell talik (BGC03-09).

as freezeback of the talik progresses. Conversely, due to the presence of a hydraulic connection between the Test Cell alik and the Reservoir, the Test Cell talik is considered an open system. However, the flow path is lengthened by the permafrost aggradation which has occurred beneath the Test Cell Dike. As such, the pore pressures within the Test Cell talik may continue to rise as freezeback progresses, however at a much slower rate than they are anticipated to increase in the Surface Cell talik.

Since the West Twin Dike would remain in place during closure, it was important to determine the effect of the high pore pressures on the long term stability of the dike. As such, a stability analysis was completed assuming a portion of the talik extended beneath the base of the dike, which was considered a conservative assumption. A variety of pore pressure conditions were applied to the thawed zone and the effect of these pore pressures on the stability of the dike were noted. The analysis suggested that pore pressures corresponding to 12 m of artesian head would be required to reduce the Factor of Safety against sliding to 1.0. However it should be noted that the results were sensitive to the configuration of the talik. For example, if the pore pressures were confined deeper beneath the base of the dike, it was found that higher pore pressures could be experienced without affecting the stability of the dike.

Pingo growth potential

The potential for pingo growth was assessed due to the potential deformation it could cause to the physical integrity, and the overall effectiveness, of the surface reclamation cover.

Based on the extensive research by Mackay and others, there are several occurrences required to initiate the growth of a pingo, as summarized below from Mackay (1998):

1. A lake, sufficiently deep to form an underlying talik, must drain, allowing permafrost to aggrade into the underlying talik.

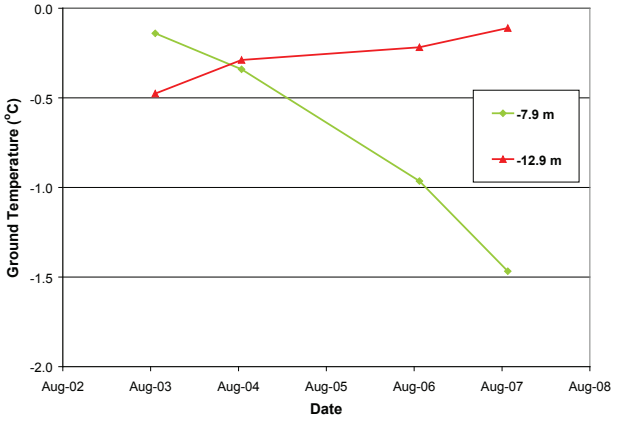

Figure 4. Geothermal data from center of Surface Cell talik (BGC03-10).

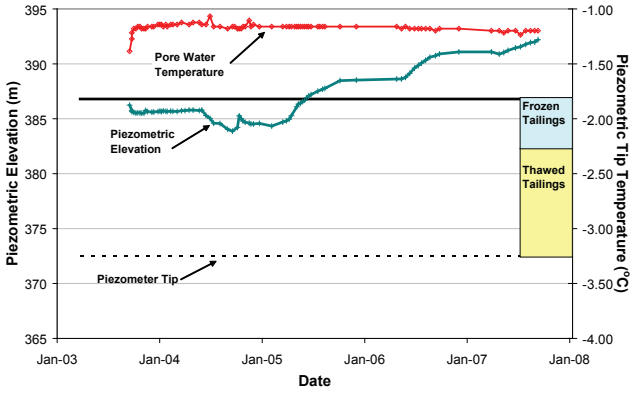

Figure 5. Piezometric monitoring data from Surface Cell (BGC03-35).

2. If there is at least one large and relatively deep residual pond without any permafrost directly beneath it, then expelled pore water can discharge into the unfrozen basin that underlies the residual pond and a pingo is unlikely to grow.

3. If at least one residual pond of sufficient size and critical depth exists so that the bottom sediments gradually freeze downward, the pressure exerted by the groundwater flow from the large lake bottom area of aggrading permafrost acts like an hydraulic jack (Gasanov 1978) on the much smaller area of the frozen bottom of the residual pond to dome it up and so to initiate pingo growth.

As can be inferred from the research, pingo formation results from a very delicate balance of gradual permafrost aggradation, pore water expulsion, and resultant overburden heaving, in combination with the differential in-situ conditions from the residual pond area to the perimeter lake bottom area. For the case of drained lakes that do not lead to the formation of a pingo, the expelled pore water must either report to the surficial pond (through some vertically oriented talik) or a cryopeg must form at depth below the frozen lake bottom.

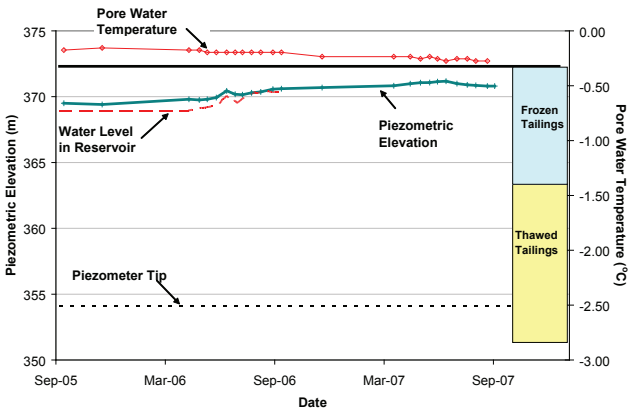

Figure 6. Piezometric monitoring data from Test Cell talik.

In comparison to the pingos formed in the Mackenzie Delta area, the following differences are suggested with respect to the Surface Cell and Test Cell taliks:

1. The remnant pond on the surface of the tailings has been completely removed and the cover has been sufficiently graded such that no residual pond can be formed.
2. Since the pond was completely removed, permafrost aggradation has been quite rapid, as inferred from the geothermal monitoring data collected to date. Due to the rapid aggradation of permafrost, and the high specific gravity of the tailings, the overburden pressure acting on top of the talik was expected to increase soon after completion of the cover.
3. Since there is no remnant pond, there is limited differential in the permafrost aggradation conditions from the previously existing pond area to the surrounding tailings surface.

As a result, instead of a pingo forming, it was considered more likely that a cryopeg would form at depth in the Surface Cell. Based on the monitoring data collected to date, this appears to be the case as no surficial indications of pingo growth have been observed while the pore pressures within the talik continue to increase.

Hydraulic fracturing

Hydraulic fractures occur in frozen ground whenever the fluid pressure exceeds the tensile strength of the enclosing frozen material plus the least compressive principal total stress (Mackay 1998). Hydraulic fractures are of significance significant with respect to reclamation of the WTDA because they could result in the release of pore water from the taliks at surface.

Hydraulic fracturing was thought to be possible in two scenarios during freezeback of the taliks. One area is a hydraulic fracture propagating vertically from the talik to the surface of the Surface Cell. The second is at the base of the West Twin Dike where the fracture could propagate upwards from the talik near the foundation of the dike to surface. Since the freezeback of the top 4 to 5 m of tailings was expected to occur rapidly during the first winter, the water pressure would have to exceed 110 kPa to 135 kPa (the approximate overburden pressure) plus the tensile strength of the frozen tailings for the first scenario to occur. Additionally, the overburden pressure in the area of the talik that underlies the dike is estimated to be approximately 400 kPa. For hydraulic fracture propagation to be initiated, this overburden pressure plus the tensile strength of the frozen tailings must be exceeded.

Table 1. Water quality testing Surface Cell talik.

Instrument	Year	pH	*Total Zinc Concentration*
BGC05-11	2005	10.9	*0.01*
	2006	11.3	*0.08*
	2007	10.5	*0.09*
BGC05-12	2005	10.3	*0.54*
	2006	10.3	*0.29*
	2007	*9.7*	*0.17*

Considering the rapid permafrost aggradation rate into the talik, it was considered unlikely that extremely high pore pressures would develop during the initial freezing period. By the time the pore pressures increased to the values required for fracturing, a frozen layer of sufficient thickness, and of significant frozen density, would likely be in place. Therefore, it was considered unlikely that hydraulic fracturing would occur.

To date, no observations of hydraulic fracturing have been noted. Although, the pore pressures have been observed to be somewhat cyclical potentially indicating that the pore pressures are relieved by some means, at certain times of the year.

Talik Freezeback Monitoring

Instrumentation and monitoring program

After completion of the reclamation covers, an additional twenty instruments were installed to monitor the freezeback of the talik. Thermistors were installed to monitor ground temperatures, vibrating wire piezometers were installed to monitor pore pressures within the talik, and monitoring wells were installed to monitor changes in pore water quality within the talik.

The instrumentation has been monitored regularly since installation. Monitoring is undertaken by site staff on a bi-weekly basis from May through October, and two to three additional times throughout the winter months.

Geothermal monitoring

The thermistors in the Surface Cell monitored since 2003 provide an excellent record of freezeback of the talik. The data from one instrument, BGC03-09, is provided in Figure 3.

Only the data from mid-August of each year is illustrated to provide a clear indication of progression of the freezing front into the talik. As can be seen, the -1°C isotherm has progressed from approximately 11 m below ground surface (bgs) in 2003 to approximately 16 m bgs in 2007. This compares favorably with the predictions made during the geothermal modeling analysis which was predicted for this location. Additional geothermal monitoring data is presented in Figure 4.

The data on Figure 4 is derived from thermistor BGC03-10 which was installed near the center of the talik. As can be seen, nodes within 10 m of the surface are cooling with time, as expected. However, nodes below 10 m have experienced a small degree of warming over the monitoring period. This suggests that heat flow from the surrounding tailings, which are actively freezing, is towards the centrecenter of the talik.

Piezometric monitoring

The piezometers in the Surface Cell monitored since 2003 provide an excellent record of pore pressure in response to freezeback of the talik. The data from one instrument, BGC03-35, is provided in Figure 5.

As can be seen, the pore pressures were not artesian when monitoring began in 2003. This was due to the proximity of the instrument to the former location of the retained pond that used to be contained in the Surface Cell. As the water was removed form the Surface Cell during reclamation activities, the pore pressures in this part of the talik initially reduced. During the first winter after the pond was removed, the pore pressures began to rise in response to freezeback of the talik. This rise in pore pressures suggests that that the system is closed and that pore pressures are not being relieved. Additionally, the vibrating wire piezometers are equipped with a thermistor node at the tip of the instrument. The data collected from this thermistor node suggests the pore water temperature is approximately -1.2°C, indicating a freezing point depression of at least this amount in the centrer of the talik. In contrast, piezometric monitoring data from the Test Cell talik is provided on Figure 6.

As can be seen, the pore pressures in the Test Cell talik are not artesian and tend to mirror the water level in the nearby Reservoir. This suggests hydraulic connectivity between the Test Cell talik and the Reservoir, as was anticipated. Also of note, the pore water temperature measured in the Test Cell talik was approximately -0.2°C, indicating only a slight amount of freezing point depression.

Pore-water quality monitoring

Water samples have been collected from the Surface Cell and Test Cell taliks once a year since completion of the surface reclamation covers in 2005. The data is summarized in Table 1.

The main conclusion drawn from the data is that metals concentrations are highest in the centrer of the talik (BGC05-12) compared to the edge of the talik (BGC05-11). Since the degree of freezing point depression is related to solute concentration, the data suggests that a higher degree of freezing point depression can be expected in the centrer of the talik. This is verified by the monitoring data reviewed earlier which suggested a freezing point depression of at least -1.5°C near the centrer of the talik, compared to -0.2°C along the edge of the talik.

Summary

The freezeback of the tailings at the Nanisivik Mine is a unique process which required detailed study, assessment, and ongoing monitoring to understand the significance with respect to reclamation and long term environmental impacts. Monitoring undertaken to date has supported the conclusions of many of the technical studies undertaken during the development of the reclamation plan.

Acknowledgments

The authors would like to acknowledge Breakwater Resources Ltd. for their permission to publish this paper. We would also like to acknowledge site staff for their meticulous efforts in collecting the monitoring data under challenging conditions.

References

Gasanov, S. 1978. Cyrolithogenesis as an independent hydrothermal type of sedimentary process. *Proceedings 3rd International Conference on Permafrost, Part 1: English translations of twenty-six of the Soviet papers*. National Research Council of Canada, Ottawa, Ontario, NRCC 18119: 225-244.

Mackay, J.R., Rampton, V.N. & Fyles, J.G. 1972. Relic Pleistocene permafrost, western Arctic, Canada. *Science* 176: 1321-1323.

Mackay, J.R. 1978. Sub-Pingo Water Lenses, Tuktoyaktuk Peninsula, Northwest Territories. *Canadian Journal of Earth Sciences* 15: 1219-1227.

Mackay, J.R. 1998. Pingo Growth and Collapse, Tuktoyaktuk Peninsula Area, Western Arctic Coast, Canada: A Long Term Field Study. *Geographie Physique et Quaternaire* 52: 271-323.

McRoberts, E.C. & Morgenstern, N.R. 1975. Pore Water Expulsion during Freezing. *Canadian Geotechnical Journal* 12: 130 - 139.

Natural Resources Canada (NRC) 1995. Canada – Permafrost 1995. *The National Atlas of Canada, 5th Edition.* Published by the National Atlas Information Service, Canada Centre for Mapping, Geomatics Canada and the Terrain Sciences Division, Geological Survey of Canada, Natural Resources Canada 1995.

Geologic Controls on the Occurrence of Permafrost-Associated Natural Gas Hydrates

Timothy S. Collett
U.S. Geological Survey, Denver, Colorado, USA

Abstract

With an increasing number of highly successful gas hydrate field studies, significant progress has been made in addressing some of the key issues on the formation, occurrence, and stability of gas hydrates in nature. The concept of a gas hydrate geologic system as a subcomponent of a conventional oil and gas petroleum system is gaining acceptance. The primary goal of this report is to compare and contrast several permafrost-related gas hydrate systems in order to better understand the geologic controls on the formation and occurrence of gas hydrates. This report focuses on the results of the recently completed BP Exploration Mount Elbert project, which successfully cored, logged, and tested a gas hydrate accumulation on the North Slope of Alaska in the spring of 2007. The Mount Elbert Test, along with the Canadian Mallik 2002 project, have for the first time allowed the rational assessment of the physical response of permafrost-associated gas hydrate occurrences to production.

Keywords: Alaska; Arctic; Canada; gas hydrate; resources.

Introduction

Gas hydrates are naturally occurring 'ice-like' combinations of natural gas and water that have the potential to provide an immense resource of natural gas from the world's oceans and polar regions. Gas hydrates are known to be widespread in permafrost regions and beneath the sea in sediments of outer continental margins. The amount of natural gas contained in the world's gas hydrate accumulations is enormous, but these estimates are speculative and range over three orders-of-magnitude, from about 2,800 to 8,000,000 trillion cubic meters of gas. Milkov et al. (2003) recently reported that the volume of gas trapped in global gas hydrate accumulations was actually in the range of 3,000 to 5,000 trillion cubic meters, which is 1/7 to 1/4 of some of the more widely cited estimates. By comparison, conventional natural gas accumulations (reserves and technically recoverable undiscovered resources) for the world are estimated at approximately 440 trillion cubic meters as reported by Ahlbrandt (2002). Despite the enormous range in reported gas hydrate volumetric estimates, even the lowest reported estimates seem to indicate that gas hydrates are a much greater resource of natural gas than conventional accumulations. However, it is important to note that none of these assessments has predicted how much gas could actually be produced from the world's gas hydrate accumulations.

Arctic Gas Hydrate Accumulations

Gas hydrate in onshore arctic environments is typically closely associated with permafrost. It is generally believed that thermal conditions conducive to the formation of permafrost and gas hydrate have persisted in the Arctic since the end of the Pliocene (about 1.88 Ma). Maps of present day permafrost reveal that about 20 percent of the land area of the northern hemisphere is underlain by permafrost (Fig. 1). Geologic studies (Molochushkin 1978) and thermal modeling of subsea conditions (Osterkamp & Fei 1993) also indicate that permafrost and gas hydrate may exist within the continental shelf of the Arctic Ocean. Subaerial emergence of portions of the Arctic continental shelf to current water depths of 120 m (Bard & Fairbanks 1990), during repeated Pleistocene glaciations, subjected the exposed shelf to temperature conditions favorable to the formation of permafrost and gas hydrate. Thus, it is speculated that 'relic' permafrost and gas hydrate may exist on the continental shelf of the Arctic Ocean to present water depths of 120 m. In practical terms, onshore and nearshore gas hydrate can only exist in close association with permafrost, therefore, the map in Figure 1 that depicts the distribution of onshore continuous permafrost and the potential extent of "relic" sub-sea permafrost also depicts the potential limit of onshore and nearshore gas hydrate.

This paper deals with the assessment of the geologic factors that control the occurrence of gas hydrates. This assessment will be conducted mainly though the examination of several relatively well-characterized gas hydrate accumulations in northern Canada and the United States.

Mackenzie Delta, Canada – Mallik gas hydrate accumulation

Assessment of gas hydrate occurrences in the Mackenzie Delta-Beaufort Sea area have been made mainly on the basis of data obtained during the course of hydrocarbon exploration conducted over the past three decades (Dallimore et al. 1999). Prior to the more recently completed Mallik gas hydrate research drilling programs (Dallimore & Collett 1995, 2005, Dallimore et al. 1999), the most extensively studied gas hydrate occurrences in the Mackenzie Delta-Beaufort Sea region were those drilled in the onshore Mallik L-38 and Ivik J-26 wells (Bily & Dick 1974) and those in the offshore Nerlerk M-98, Koakoak O-22, Ukalerk C-50, and Kopanoar M-13 wells (Weaver & Stewart 1982). On

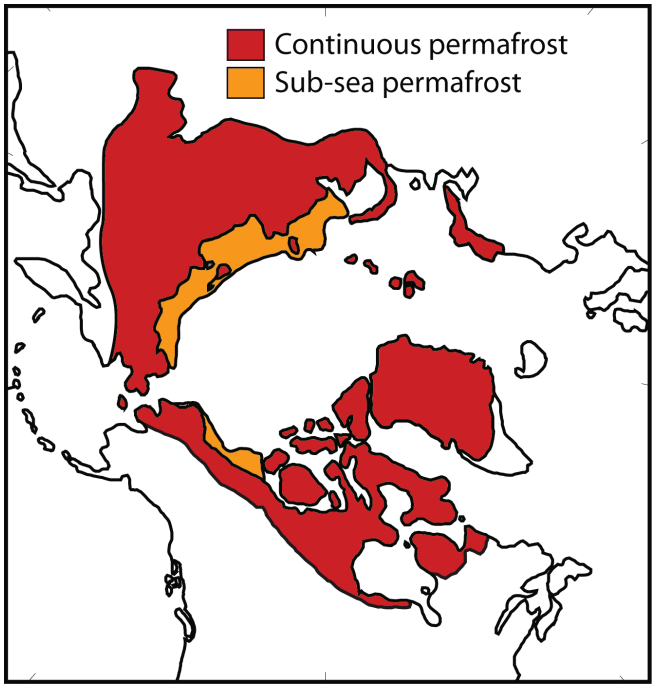

Figure 1. Distribution of permafrost in the Northern Hemisphere.

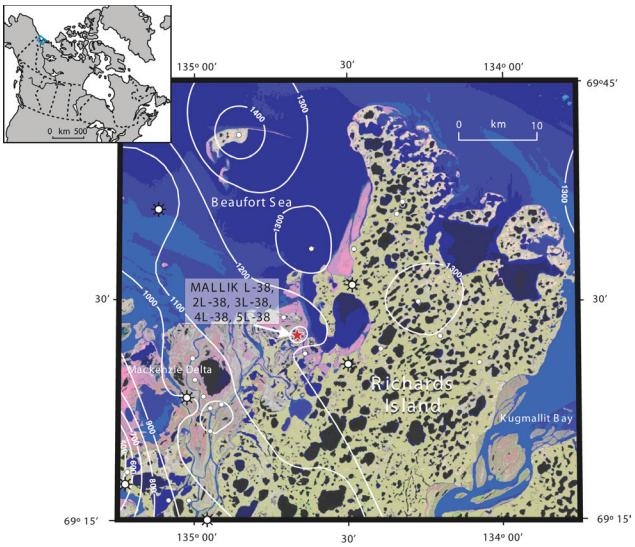

Figure 2. Location of the JAPEX/JNOC/GSC et al. Mallik 3L-38, 4L-38, and 5L-38 gas hydrate production research wells, Mackenzie Delta, Northwest Territories. Base map is a false-color mosaic constructed from a Landsat V image taken July 8, 2002. Contours indicate depth to the base of the gas hydrate stability zone in meters. Symbols include small circles as well locations, larger circles with ticks are wells containing gas hydrate (Dallimore & Collett 2005)

the basis of open-hole well log evaluation, it is estimated that Mallik L-38 encountered about 100 m of gas-hydrate-bearing sandstone, and Ivik J-26 penetrated about 25 m of gas hydrate. Analyses of open-hole well logs and mud-gas logs indicate that the offshore Nerlerk M-98 well penetrated about 170 m of gas-hydrate-bearing sediments, while the Koakoak O-22, Ukalerk C-50, and Kopanoar M-13 wells drilled approximately 40 m, 100 m, and 250 m of gas hydrate respectively. In all four cases, the well-log inferred gas hydrate occurs in fine-grained sandstone rock units.

During a permafrost-coring program in the Taglu area on Richards Island in the outer Mackenzie Delta, ice-bearing cores containing visible gas hydrate and possible pore-space gas hydrate were recovered (Dallimore & Collett 1995). The visible gas hydrate occurred at a depth of about 330 to 335 m and appeared as thin ice-like layers that released methane upon recovery.

Estimates of the amount of gas in the gas hydrate accumulations of the Mackenzie Delta-Beaufort Sea region vary from 9.3 to 27 trillion cubic meters (Smith & Judge 1995, Majorowicz & Osadetz 1999, 2001); however, these estimates are generally poorly constrained. A more detailed study by Osadetz and Chen (2005) resulted in an estimate that is within the same bounds given by Majorowicz and Osadetz (2001) and range between 1.0 to 10 trillion cubic meters of gas within the permafrost associated gas hydrate accumulations of the Beaufort Sea-Mackenzie Delta region.

The JAPEX/JNOC/GSC Mallik 2L-38 gas hydrate research well, drilled in 1998 near the site of the Mallik L-38 well (Fig. 2), included extensive scientific studies designed to investigate the occurrence of in situ natural gas hydrate in the Mallik field area (Dallimore et al. 1999). Approximately 37 m of core were recovered from the gas hydrate interval (878–944 m) in the Mallik 2L-38 well. Pore-space gas hydrate and several forms of visible gas hydrate were observed in a variety of unconsolidated sands and gravels interbedded with non-hydrate bearing silts. The cored and downhole logged gas hydrate occurrences in the Mallik 2L-38 well exhibit both high electrical resistivities and rapid acoustic velocities. In total, the gas hydrate-bearing strata was approximately 150 m thick within the depth interval from 889 to 1101 m.

Because of the success of the 1998 Mallik 2L-38 gas hydrate research well program, the Mallik site has been elevated as an important gas hydrate production test site with the execution of two additional gas hydrate production research programs: (1) The Mallik 2002 Gas Hydrate Production Research Well Program, and (2) 2006–2008 JOGMEC/NRCan Mallik Gas Hydrate Production Research Program.

In June of 2005, the partners in the Mallik 2002 Gas Hydrate Production Research Well Program publicly released the results of the first modern, fully integrated field study and production test of a natural gas hydrate accumulation (Dallimore & Collett 2005). From December 25, 2001 through March 15, 2002 the Mallik 2002 Gas Hydrate Production Research Well Program drilled three wells (the JAPEX/JNOC/GSC et al. Mallik 3L-38 and 4L-38 observation wells and Mallik 5L-38 gas hydrate production test well) in the Mallik Gas Hydrate Field on Richard's Island in the Mackenzie Delta, Northwest Territories, Canada.

The Mallik 5L-38 well cored and recovered gas hydrates and associated sediments from an interval between 880-1150 m depth (Fig. 3). These cores were the subject of intensive examination by members of the Mallik research

team. Detailed information on the geology, geochemistry, geotechnical, and microbiological properties of gas hydrate bearing sediments was complemented by an extensive research geophysics program, which included both surface seismic surveys and downhole logging studies. Downhole measurements allowed for direct estimates of in situ permeability, gas hydrate content, and investigations of the occurrence of natural fractures.

Rather than carry out long term production testing during the Mallik 2002 effort, a decision was made to conduct carefully controlled production experiments. The response of gas hydrates to heating and depressurization was evaluated with careful attention to accurately measure both input conditions and reservoir responses. The overall goal was to combine the science and production program to allow for calibration and refinement of reservoir simulation models capable of predicting long-term reservoir response. Pressure draw down experiments were designed to study the response of gas hydrate to a reduction in formation pressure conditions. The results of three short duration gas hydrate tests demonstrate that gas can be produced from gas hydrates with different concentrations and characteristics, exclusively through pressure stimulation. The data supports the interpretation that the gas hydrates are much more permeable and conducive to flow from pressure stimulation than previously thought. Thermal stimulation experiments were designed to destabilize gas hydrates by using circulated hot water to increase the in situ temperature. A five-day experiment was undertaken within a 17-m-thick section of highly concentrated gas-hydrate-bearing strata. Gas was continuously produced throughout the test at varying rates with maximum flow rate reaching 1500 cubic meters per day. The total volume of gas produced was small, reflecting that the test was a controlled production experiment rather than a long duration well test.

The Mallik 2002 production research well program proved for the first time that gas production from gas hydrates is technically feasible. The Mallik 2002 thermal and depressurization production data have allowed the calibration of several reservoir models used to simulate the thermal and depressurization tests. Part of the calibration process has been the recognition that gas hydrate deposits are much more permeable than previously thought. The Mallik data allowed for the rational assessment of the production response of a gas hydrate accumulation if the various tests were extended far into the future. These studies show that among the possible techniques for production of natural gas from in situ gas hydrates, depressurization will produce more gas than just heating the formation. However, the combination of heating and depressurizing the gas hydrate at the same time will produce the greatest amount of gas. Project-supported gas hydrate computer production simulations, including those performed by Lawrence Berkeley National Laboratory, have shown that under certain geologic conditions gas can be produced from gas hydrates at very high rates, exceeding several million cubic feet of gas per day.

The following discussion dealing with the 2006–2008

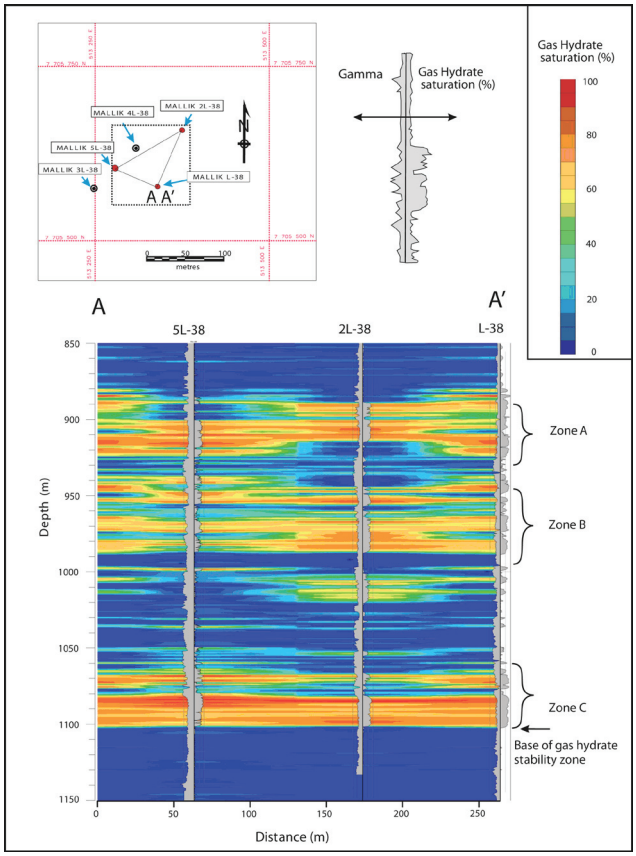

Figure 3. Fence diagram showing well-log-derived gas hydrate concentrations and natural gamma-ray logs for Imperial Oil Ltd. Mallik L-38, JAPEX/JNOC/GSC Mallik 2L-38, and JAPEX/JNOC/GSC et al. Mallik 5L-38 wells. The well locations are shown on the location map (Dallimore & Collett 2005).

JOGMEC/NRCan Mallik Gas Hydrate Production Research Program has been taken almost entirely from a news article appearing in the Spring/Summer 2007, U.S. Department of Energy, Office of Fossil Energy, National Energy Technology Laboratory, Fire in the Ice, Methane hydrate newsletter (available at http://www.netl.doe.gov/tech nologies/oilgas/publications/Hydrates/Newsletter/HMNewsSpringSummer07optmiized.pdf; viewed August 16, 2007). The 2006–2008 JOGMEC/NRCan Mallik Gas Hydrate Production Research Program is being conducted to mainly monitor long term production behavior of gas hydrates. The Japan Oil, Gas, and Metals National Corporation (JOGMEC) and NRCan are leading this research program. Aurora College/Aurora Research Institute is acting as the operator for the field program. The primary objective of the winter 2007 field activities was to install equipment and instruments to allow for long term production testing of several gas hydrate intervals during the winter of 2007–2008. Drilling rigs were used to re-enter and deepen the Mallik 2L-38 and Mallik 3L-38 wells (Fig. 3). Each well was also logged with various tools to establish formation properties prior to testing. After completing operations in the Mallik 2L-38 and 3L-38 wells, a short pressure draw down production test was conducted to evaluate equipment

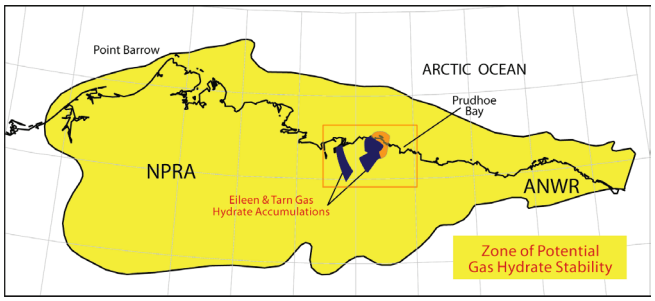

Figure 4. Map of the Alaska North Slope gas hydrate stability zone. Also shown is the location of the Eileen and Tarn gas hydrate accumulations (Collett 1993).

performance and short term producibility of the gas-hydrate-bearing section. A 12-m-thick gas hydrate interval near the base of the gas hydrate stability zone was tested for 60 hours. The test results were described as 'encouraging', documenting "robust" gas flow rates. Important observations were also made in terms of produced water and the sediment response to production. The JOGMEC/NRCan Mallik gas hydrate production research program is currently planning operations for the 2007–2008 winter program.

North Slope, Alaska, USA – Eileen gas hydrate accumulation

On the North Slope, the subsurface temperature data, needed to assess the distribution of the gas hydrate stability zone, comes from high-resolution, equilibrated well-bore surveys in 46 wells and from well log estimates of the base of ice-bearing permafrost in 102 other wells (Collett 1993). The methane-hydrate stability zone in northern Alaska, as mapped in Figure 4, covers most of the North Slope. The offshore extent of the gas-hydrate stability zone is not well established; however, 'relic' permafrost is known to exist on the Beaufort Sea continental shelf to a present water depth of 90 m (Osterkamp & Fei 1993).

Before the recently completed coring and downhole logging operations in the BP Exploration (Alaska) Mount Elbert well in Milne Point, the only direct confirmation of gas hydrate on the North Slope was obtained in 1972 with data from the Northwest Eileen State-2 well located in the northwest part of the Prudhoe Bay Field. Studies of pressurized core samples, downhole logs, and the results of formation production testing have confirmed the occurrence of three gas-hydrate-bearing stratigraphic units in the Northwest Eileen State-2 well (Collett 1993). Gas hydrates are also inferred to occur in an additional 50 exploratory and production wells in northern Alaska based on downhole log responses calibrated to the known gas hydrate occurrences in the Northwest Eileen State-2 well. Many of these wells have multiple gas-hydrate-bearing units, with individual occurrences ranging from 3- to 30-m-thick. Most of the well-log inferred gas hydrates occur in six laterally continuous sandstone and conglomerate units; all are geographically restricted to the area overlying the eastern part of the Kuparuk River Field and the western part of the Prudhoe Bay Field

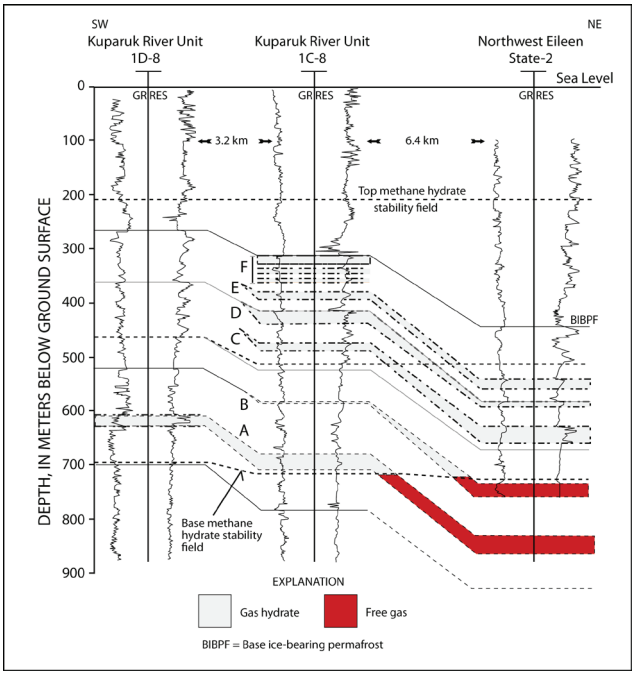

Figure 5. Cross section showing the lateral and vertical extent of gas hydrates and underlying free-gas occurrences in the Prudhoe Bay-Kuparuk River area in northern Alaska. See Figure 6 for location of cross section. The gas-hydrate-bearing units are identified with the reference letters A through F (Collett 1993).

(Figs. 5, 6). The six gas-hydrate-bearing sedimentary units have each been assigned a reference letter, Units A through F, with Unit A being the stratigraphically deepest (Fig. 5). Three-dimensional seismic surveys and downhole logs from wells in the western part of the Prudhoe Bay Field indicate the presence of several large free-gas accumulations trapped stratigraphically down-dip below four of the log-inferred gas hydrate units (Figs. 5, 6 Units A through D). The total mapped area of all six gas hydrate occurrences is about 1643 km^2; the areal extent of the individual units ranges from 3 to 404 km^2. The volume of gas within the gas hydrates of the Prudhoe Bay-Kuparuk River area, which has come to be known as the Eileen Gas Hydrate Accumulation, is estimated to be about 1.0 to 1.2 trillion cubic meters, or about twice the volume of known conventional gas in the Prudhoe Bay Field (Collett 1993).

The 1995 National Oil and Gas Resource Assessment, conducted by the U.S. Geological Survey, focused on assessing the undiscovered conventional and unconventional resources of crude oil and natural gas in the United States. This assessment included for the first time a systematic resource appraisal of the *in-place* natural gas hydrate resources of the United States onshore and offshore regions (Collett 1995). The onshore portion of the assessment dealt with most of northern Alaska, in which it was estimated that there may be as much as 590 trillion cubic feet of in-place gas trapped in gas hydrates.

Under the Methane Hydrate Research and Development Act of 2000 (renewed in 2005), the U.S. Department of Energy (DOE) funds laboratory and field research on both

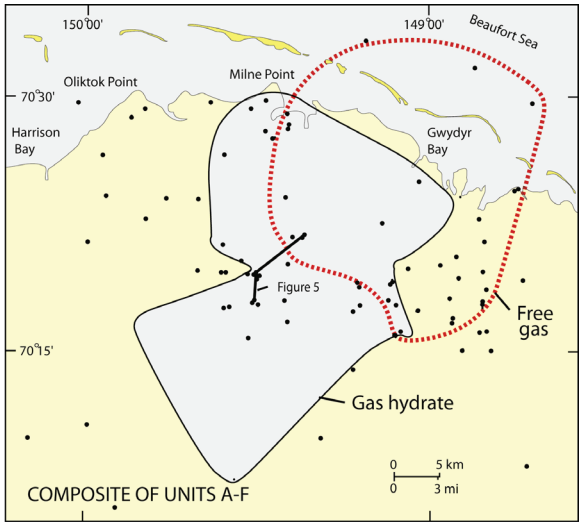

Figure 6. Composite map of all six gas-hydrate/free-gas units (Units A-F) from the Prudhoe Bay-Kuparuk River area in northern Alaska. Also shown is the location of the cross section in Figure 5 (Collett 1993).

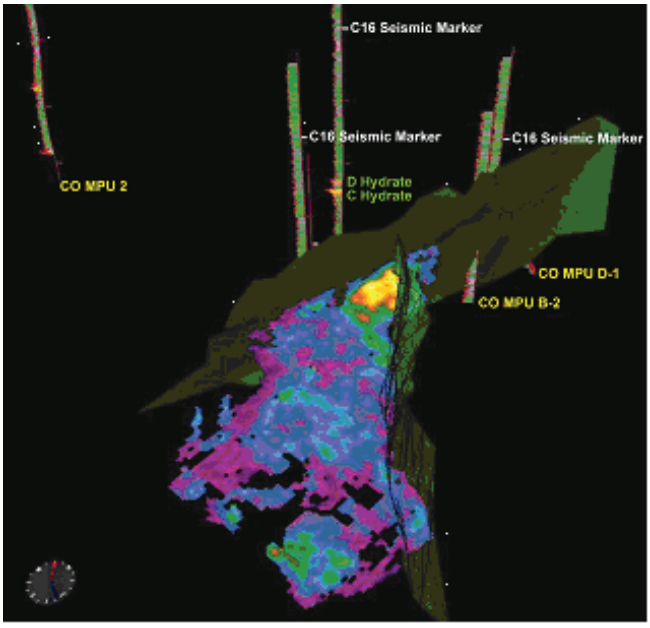

Figure 7. Three-dimensional seismic amplitude map of the Mount Elbert gas hydrate prospect within a three-way fault-bounded closure. Also shown is the location of nearby well locations.

Arctic and marine gas hydrates. Among the current Arctic studies, BP Exploration (Alaska), Inc. and the DOE have undertaken a project to characterize, quantify, and determine the commercial viability of gas hydrates and associated free gas resources in the Prudhoe Bay, Kuparuk River, and Milne Point field areas on the Alaska North Slope. Ultimately, this project could determine if gas hydrates can become a part of the Alaska North Slope gas-resource portfolio.

The following discussion dealing with the BP Exploration (Alaska) Inc. (BPXA) Mount Elbert Gas Hydrate Stratigraphic Test Well has been taken almost entirely from a news article appearing in the Winter 2007, U.S. Department of Energy, Office of Fossil Energy, National Energy Technology Laboratory, Fire in the Ice, Methane hydrate newsletter (available at http://www.netl.doe.gov /technologies/oilgas/publications/Hydrates/Newsletter/HMNewsWinter07.pdf; viewed August 16, 2007). On February 18, 2007, a team of scientists concluded an extensive data collection program in the Mount Elbert Gas Hydrate Stratigraphic Test Well drilled in the Milne Point area on the Alaska North Slope; it yielded one of the most comprehensive datasets yet compiled on naturally-occurring gas hydrates. This project began in earnest in 2002, following BPXA's response to a DOE request for proposals to evaluate the gas hydrate resources on the North Slope. Over the following three years, the project team conducted regional geological, engineering, and production modeling studies through collaborations with the University of Alaska (Fairbanks), the University of Arizona, and Ryder-Scott Company. In 2005, extensive analysis of BPXA's proprietary 3-D seismic data and integration of that data with existing well log data (enabled by collaborations with the U.S. Geological Survey, the Bureau of Land Management, and Interpretation Services, Inc.), resulted in the identification of more than a dozen discrete and mapable gas hydrate accumulations within the Milne Point area. Because the most favorable of those targets was a previously undrilled, fault-bounded accumulation (Fig. 7), BPXA and the DOE decided to drill a vertical stratigraphic test well at that location (named the 'Mount Elbert' prospect) to acquire critical reservoir data needed to develop a longer-term production testing program.

The Mount Elbert gas hydrate stratigraphic test well was designed as a 22-day program with the planned acquisition of cores, well-logs, and downhole production test data. A surface hole was first drilled and cased to a depth of 595 m. The well was then continuously cored to a depth of 760 m with chilled oil-based drilling fluid using the wireline-retrievable coring system. This core system delivered 85% recovery through 154 m of gas hydrate and water-bearing sandstone and shale. The coring team processed these cores on site and collected subsamples for analyses of pore water geochemistry, microbiology, gas chemistry, petrophysical properties, and thermal and physical properties. Core samples were also stored in liquid nitrogen or transferred to pressure vessels for future study of the preserved gas hydrates. After coring, the well was reamed and deepened to a depth of 915 m, and the well was surveyed with a research-level wireline logging program including magnetic resonance and dipole acoustic logging, resistivity scanning, borehole electrical imaging, and advanced geochemistry logging. Following logging, Schlumberger Modular Dynamic Testing (MDT) was conducted at four open-hole stations in two sandstone reservoirs. Each test consisted of flow and shut-in periods of varying lengths, with one lasting for more than 13 hours. Gas was produced from the gas hydrates in each of the tests.

Gas hydrates were expected and found in two stratigraphic

sections. An upper zone, (Unit D) contained ~14 m of gas hydrate-bearing reservoir-quality sandstone. A lower zone, (Unit C), contained ~16 m of gas hydrate-bearing reservoir. Both zones displayed gas hydrate saturations that varied with reservoir quality as expected, with typical values between 60% and 75%. Presently, the project research partners are in the process of fully analyzing and integrating all the data collected from the Mount Elbert test well, including re-calibration of the initial geological and seismic models for the site.

Conclusion

Despite the apparent obstacles to the development of gas hydrate resources, it is important to remember that extraordinary technological developments in the petroleum industry—three-dimensional seismic techniques, secondary recovery methods, and horizontal drilling, for example—have allowed the extraction of resources once thought to be unavailable. Natural gas hydrates may also become economically extractable. On-shore Canada and Alaska are proven exploration targets for gas hydrates. The first commercial production of gas hydrates is likely to occur in either northern Alaska or Canada, where gas from gas hydrates will either support local oil and gas field operations or be available for commercial sale, if and when suitable gas pipelines are constructed. It is important to highlight that on the North Slope of Alaska, critical drilling and transportation infrastructure exists, which will allow gas hydrate prospects to be drilled and produced from existing installations.

Acknowledgments

This contribution was partially funded by both the U.S. Department of Energy (under the Interagency Agreement No. DE-AI21-92MC29214) and the U.S. Bureau of Land Management (under the Interagency Agreement No. LAI -02-0015).

References

Ahlbrandt, T.S. 2002. Future petroleum energy resources of the world. *International Geology Review* 44(12): 1092-1104.

Bard, H.B. & Fairbanks, R.G. 1990. U-Th ages obtained by mass spectrometry in corals from Barbados, sea level during the past 130,000 years. *Nature* 346: 456-458.

Bily, C. & Dick, J.W.L. 1974. Natural occurring gas hydrates in the Mackenzie Delta, Northwest Territories. *Bulletin of Canadian Petroleum Geology* 22/3: 340-352.

Collett, T.S. 1993. Natural gas hydrates of the Prudhoe Bay and Kuparuk River area, North Slope, Alaska. *American Association of Petroleum Geologists Bulletin* 77/5: 793-812.

Collett, T.S. 1995. Gas hydrate resources of the United States. In: D.L. Gautier, G.L. Dolton, K.I. Takahashi & K.L. Varnes (eds.), *1995 National Assessment of United States Oil and Gas Resources* on CD-ROM: U.S. Geological Survey Digital Data Series 30, CD-ROM.

Dallimore, S.R. & Collett, T.S. 1995. Intrapermafrost gas hydrates from a deep core hole in the Mackenzie Delta, Northwest Territories, Canada. *Geology* 23: 527-530.

Dallimore, S.R. & Collett, T.S. (eds.) 2005. *Scientific Results from the Mallik 2002 Gas Hydrate Production Research Well Program, Mackenzie Delta, Northwest Territories, Canada.* Geological Survey of Canada Bulletin 585, two CD-Rom set.

Dallimore, S.R., Uchida, T. & Collett, T.S. 1999. Scientific *Results from JAPEX/JNOC/GSC Mallik 2L-38 Gas Hydrate Research Well, Mackenzie Delta, Northwest Territories, Canada.* Geological Survey of Canada Bulletin 544, 403 pp.

Majorowicz, J.A. & Osadetz, K.G. 1999. *Basic Geological and Geophysical Controls Bearing on Gas Hydrate Distribution and Volumes in Canada.* Geological Survey of Canada Open-File Report, 35 pp.

Majorowicz, J.A. & Osadetz, K.G. 2001. Gas hydrate distribution and volume in Canada. *American Association of Petroleum Geologists Bulletin* 85/7: 1211-1230.

Milkov, A.V., Claypool, G.E., Lee, Y-J., Xu, W., Dickens, G.R., Borowski, W.S. & the Ocean Drilling Program Leg 204 Scientific Party. 2003. In situ methane concentrations at Hydrate Ridge, offshore Oregon: New constraints on the global gas hydrate inventory from active margins. *Geology* 31(10): 833-836.

Molochushkin, E.N. 1978. The effect of thermal abrasion on the temperature of the permafrost in the coastal zone of the Laptev Sea. *Proceedings of the Second International Conference on Permafrost, Takutsk, USSR, July 13-28, 1973.* Washington D.C.: National Academy of Sciences, 90-93.

Osadetz, K.G. & Chen, Z. 2005. A re-examination of Beaufort Sea – Mackenzie Delta Basin gas hydrate resource potential using a petroleum system approach. *Proceedings of the Fifth International Conference on Gas Hydrates, Trondheim, Norway, June 13-16, 2005*, 11 pp.

Osterkamp, T.E. & Fei, T. 1993. Potential occurrence of permafrost and gas hydrates in the continental shelf near Lonely, Alaska. *Proceedings of the Sixth International Conference on Permafrost, Beijing, China, July 5-9, 1993* Washington, D.C.: National Academy of Sciences, 500-505.

Smith, S.L. & Judge, A.S. 1995. Estimates of methane hydrate volumes in the Beaufort-Mackenzie region, Northwest Territories: Geological Survey of Canada, *Current Research 1995-B*: 81-88.

Weaver, J.S. & Stewart, J.M. 1982. In situ hydrates under the Beaufort shelf. In: M.H. French,. (ed.), *Proceedings of the Fourth Canadian Permafrost Conference, 1981*. National Research Council of Canada, The Roger J.E. Brown Memorial Volume: 312-319.

Laboratory Simulations of Martian Debris Flows

François Costard
UMR 8148 IDES Interactions et Dynamique des Environnements de Surface, Université Paris-Sud 11, 91405 Orsay France
Emeric Védie, Marianne Font, Jean-Louis Lagarde
UMR CNRS 6143 «M2C» Université de Caen, 2-4, rue des Tilleuls, 14 032 CAEN Cedex, France

Abstract

Small gullies observed on Mars could be formed by groundwater seepage from underground aquifers or may result from the melting of near-surface ground ice at high obliquity. To test these different hypotheses, a laboratory simulation has been performed. An experimental slope was designed to simulate debris flows over sand dunes with various slope angles, different granulometry, and permafrost characteristics. Preliminary results suggest that the typical morphology of gullies observed on Mars can be best explained by the formation of linear debris flows related to the melting of near-surface ground ice with silty materials. This physical modeling highlights the role of the active layer during debris flow formation.

Keywords: debris flows; gullies; Mars; physical modeling.

Introduction

The recent discovery of groundwater seepage and surface runoff on Mars suggests the local occurrence of subsurface liquid water at mid and high latitudes during recent periods. They have been proposed to result from subsurface seepage of water (Malin & Edgett 2000), brines (Andersen et al. 2002), near-surface ice melting at recent periods of high obliquity (Costard et al. 2002), snowmelt in more recent periods (Christensen 2003), geothermal heating (Mellon & Phillips 2001), or liquid CO_2 breakout (Musselwhite et al. 2001). Among this large variety of surface runoff features, an unusual example of debris flows over sand dunes retains our attention. These debris flows are characterized by (1) their localisation over sand dunes, (2) a typical morphology with long and narrow channels, and (3) the development of networks made of long, parallel down-dip flows (Fig. 1). The exact process of their formation still remains speculative. This study focuses on the formation of that typical morphology by means of various laboratory simulations within a cold room. According to these experiments, we discuss the possibility of explaining these gullies over sand dunes as a consequence of surface and near-surface melt of volatile-rich material. In this study, we describe how the depth of the active layer helps us to understand better the formation of Martian linear gullies observed in the Russell Crater. Such interpretation has important consequences in terms of recent climate change on Mars. We show that the characteristics of these typical linear Martian gullies are consistent with some external processes triggered by seasonal melting at high obliquity.

Gullies on Mars

Morphological characteristics

The observation of small gullies on Mars was one of the more unexpected discoveries of the Mars Observer Camera (MOC) aboard the Mars Global Surveyor spacecraft (Malin & Edgett 2000). *Debris flow* is the term used by Malin and Edgett (2000) to describe a downslope flow of debris mixed with a significant amount of water within the walls of impact craters. They mostly occur in a latitudinal band higher than 30°, with preferential pole-facing gullies in the southern mid-latitudes (Balme et al. 2006). A large majority are sited on the inner walls of impact craters and are occasionally found on central peaks of impact craters (Balme et al. 2006). They often become narrower and shallower downslope, are often slightly sinuous, and sometimes display complex morphologies such as levees, tributaries and streamlining around obstacles.

The upper part of most debris flows has a steeper slope that is dissected by channels, often sinuous, whereas thick accumulations of debris cover the bases of escarpments. The upper part of the slopes (mostly south-facing slopes in the Southern Hemisphere) exhibits alcoves. They are also characterized by their distinct V-shaped channels with well-defined levees. Individual channels exhibit low sinuosity and deep erosion down to the fans that bury the lower parts of the crater walls.

Most of the gullies observed on Mars are preferentially located at latitude higher than 30°. Therefore, they are located in regions where the Martian permafrost is supposed to contain ground ice in the near subsurface (Mellon & Phillips 2001).

Perched aquifer

Various mechanisms have been proposed for the formation of gullies by water. According to Malin and Edgett (2000), debris flows would result from springs fed by shallow aquifers. Water usually emerges from the lower part of the slope producing springs. According to that hypothesis, however, under hydrostatic pressure, springs may occur in the upper part of hills or slopes. The sources of this water can freeze on the surface. When the hydrostatic pressure oversteps the lithostatic pressure, the discharge can occur. The main problem is the difficulty for a shallow aquifer

Figure 1. Linear gullies over sand dune in the inner part of the Russell Crater on Mars. One can note the presence of sinuosity near the crest rim. HIRISE image PSP_002904_1255 (25 cm/pixel). Width of the image: 5 km. Light from the left. Credit: NASA/JPL/University of Arizona.

Figure 2. Close-up over the terminal part of gullies on the megadune. HIRISE image PSP_002904_1255 (25 cm/pixel). Width of the image: 1 km. Light from the left. Credit: NASA/JPL/University of Arizona.

to survive in equilibrium at such shallow depths under the cold ambient conditions. One possibility is to suppose a concentration of brines within the aquifer (Mellon et al. 2001).

CO_2 frost cover

Current seasonal defrosting has been proposed to explain gullies on hill slopes (Bridges et al. 2001) or over dunes (Reiss & Jaumann 2002). Recent HIRISE images clearly show a blanketing of CO_2 frost covering the south flank of dunes. Dark spots observed on the top of the dunes are attributed to the sublimation of CO_2 (Mangold et al. 2003). The possibility of snowmelt is not excluded (Lee et al. 2001; Christensen 2003).

Ice-rich deposit and obliquity scenario

This ground ice may represent one source of liquid water for the debris flows. However, this conclusion is contradictory with the usual consideration that liquid water cannot exist at the surface because of the low pressure and temperatures. This implies either that the ice-water is not pure or that climatic conditions were warmer in the recent past.

Ice-water doped with salts or CO_2 clathrates has been reported in different ways (Hoffman 2000, Ishii & Sasaki 2004). At least, it could explain gullies of the south polar regions, at 70°S, where temperatures are very cold; that is, 190 K of mean annual temperatures. According to terrestrial analogs in periglacial regions, Costard et al. (2002) have discussed the possibility of explaining some of these landforms by debris flows only due to surface and near-surface (<10 m) melt of volatile-rich material at high obliquities. Recent climatic changes may be possible considering the large pseudo-cyclic variations of the obliquity of the planet (Laskar et al. 2004). Variations of the orbital parameters are probably required to generate a subsurface melting of the supposed ice-rich permafrost or seasonal frost in these regions, thus allowing other processes to occur such as transient melting of ice-water (Costard et al. 2002).

Terrestrial analogs

On Earth, debris flows occur in periglacial environments when soils begin to be heavily saturated with water after the melting of the snow cover and/or the ground ice (Coussot et al. 1998). The initiation process of flow is still not fully understood. This initiation can be either due to water saturation by a peak intensity of rainfall events or to a rapid snowmelt (or melting of ground ice) with subsequent saturation or to a seismic event. Field observations indicate that snow cover plays an important role in the dynamic of debris flows. The duration of these debris flows is extremely variable and may occur as single or multiple waves. The deposition occurs along the narrow channel in levees of very coarse materials with boulders.

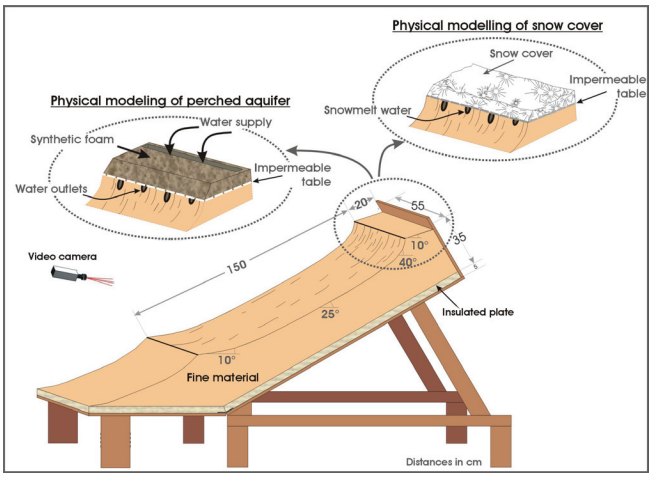

Figure 3. Global overview of the experimental setup and experimental configurations for two types of water supply (perched aquifer and snow cover).

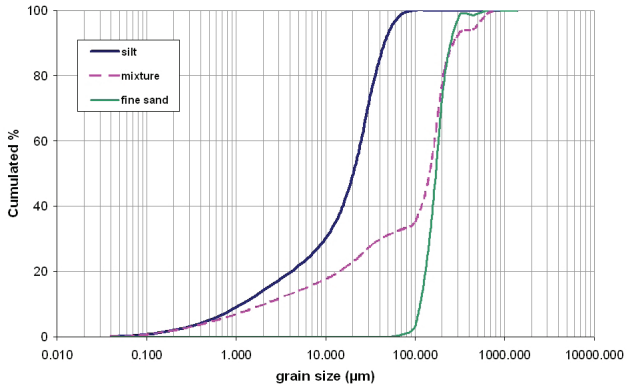

Figure 4. Grain size distribution of materials used for the experiment.

Gullies Over Sand Dunes

Russell Crater, a 200 km large crater located at 55°S and 347°W, exhibits various dune fields. One of them is relatively high (500 m) and covered by relatively low albedo volcanic sands. The SW flank of the megadune exhibits a few hundred long and narrow linear gullies, first discovered by Mangold et al. (2003). Gullies are about 2.5 km in length, and their mean slope is 10°. They start from regularly spaced small alcoves just under the crest of the dune, which is the steepest part of the dune (Fig. 1). Individual gullies exhibit linear and narrow channels with a loose pattern of connections.

Levees are observed on both sides of these channels as continuous and narrow ridges. These levees characterize a flow with a yield strength (Coussot et al. 1998) that corresponds to the minimal shear strength before flow. They are typically associated with flows containing 50% to 90% solid particles (silt to pebble size).

Relatively small distal-lobes are found lower down at the end of the channels at the foot of hill slopes. But gullies without terminal deposits are especially visible on the flank of dunes in the Russell Crater (Fig. 2). From a high-resolution HIRISE image (Fig. 2), most of the terminal deposits do not exhibit terminal lobes, but rather a concentration of small pits of unknown origin (thermokarst process ?).

These dune gullies present sinuosity and connections with a geometry that allows the calculation of flow properties, like the velocity and the viscosity (Mangold et al. 2003). The exact process of their formation over sand dunes, however, still remains speculative.

Terrestrial analogs for these typical linear gullies are unknown, justifying the use of laboratory experiments to try to understand the processes and conditions of the formation of these gullies.

Laboratory Simulations

Many factors work simultaneously in the triggering of debris flow, and their interdependence makes their analysis very difficult. High-resolution images are not completely appropriate in assessing the main parameters affecting the dynamic of debris flow. Laboratory simulation studies provide an opportunity for more detailed monitoring than can be done from imagery. The purpose of the study is to test qualitatively the influence of different parameters on the formation of linear gullies.

Methodology

Physical modeling has been developed in order to simulate the development of some typical gullies observed over Martian sand dunes in the Russell Crater. The major purpose of the experiment was to examine the respective effects of slope angle, material, and permafrost. To simulate a periglacial environment, these experiments require a cold room wide enough to receive an experimental slope (Fig. 3). We used the facility at the University of Caen/CNRS, France in a laboratory dedicated to physical modeling in geomorphology (Font et al. 2006).

Experimental setup

Our small-scale experiment was composed of a rectangular box of 2.5 m by 0.55 m wide and 0.50 m depth in which reconstituted debris from fine sand or silt materials was saturated with water (Figs. 3, 5). Morphologies are tested, with a median slope gradient of 15°, whereas the top and bottom slope gradients are constant (8° and 50° respectively). In order to simulate the periglacial environment, the slope was frozen from the surface, and permafrost was created at depth (0.50 m) with a temperature of -10°C.

The experiment procedure allowed the simulation of natural water supply for the debris flow formation. Two types of water supply were tested (Fig. 3):

1. To simulate perched aquifer, solid and porous synthetic foam was placed on the top of the rim crest. Then during thawing, a controlled water supply was injected into the foam.

2. Inflowing snowmelt water during thawing was simulated using fine particles of ice (<1 mm) covering all of the upper part of the slope.

Figure 5. Close-up of the apparatus used in the physical modeling of debris flows.

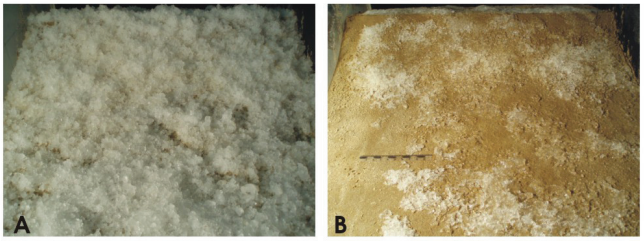

Figure 6. Experimental slope before (A) and after (B) snowmelt. In the laboratory simulation, the snow blanket is covering all of the slope. In that typical situation, no debris flows are observed probably because the snow blanket has a too wide-spread effect during the melting.

Ice-rich permafrost and control of the active layer

For each experiment, the material was initially saturated just before freezing. The thermal stability of the experiment was controlled by using 10 thermocouples at various depths. After freezing, the surface of the frozen soil is then progressively (and naturally) warmed to induce a controlled active layer formation. Thawing of the upper few mm of permafrost was done with an average air temperature of 18°C, giving rise to an active layer of 1 mm to 1 cm thick. Figures 3 and 5 outline the experiment.

Here, we assumed that liquid water was stable on the surface of Mars. The Martian gravity was not taken into account, and we assumed that the scale effect was not a limited factor. Our cold room is not a climatic chamber, so we do not control the atmospheric pressure and the thermodynamic aspect of the debris flow process. Here, the objective was mainly to simulate linear gullies as those observed on Mars in order to evaluate the respective influence of different parameters in terms of the efficiency of different parameters on the formation of these typical linear gullies.

Results

We carried out 42 experiments over two years. Data from a few tens of experimental gullies formation are presented here. They attest to the efficiency of periglacial processes

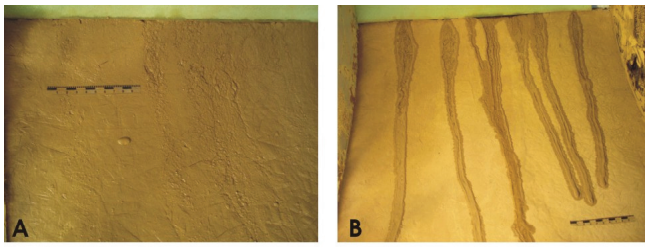

Figure 7. Effect of active layer thickness in a permafrost environment. A: diffused flow on surface with an active layer up to 10 mm. B: localized debris flows with an active layer of 1 mm thick. A relatively thin active layer strongly favors the formation of long and narrow linear gullies like those observed on Mars. Here, narrow gullies are preferentially formed by the water supply in the debris from the progressive thawing of the ice-rich permafrost, which occurs along a significant length of the flow.

that control both erosion and changes in gully morphology: (1) near-surface permafrost leads to a rather low sinuosity of the channel; (2) effects of silty material lead to increase the length/width ratio of the channel.

Blanket of snow or effect of the active layer?

From the experiment, the melting of the snow and the interstitial ice leads to the saturation level being reached within the layer of weathered debris. The decrease of the shear strength of the debris by water saturation is probably responsible for repeated debris flow episodes. According to the Christensen hypothesis (2003), gullies were created by trickling water from melting snowpacks, not by underground springs or pressurized flows. We did several simulations with a blanket of snow on the slope. The subsequent melting of snow deposits all over the slope has no effect on gully formation (Fig. 6B). However, underground springs or pressurized flows (either by a simulated perched aquifer or by inflowing snowmelt water from the rim crest, Fig. 3), both induced the melting of near-surface permafrost and the subsequent formation of linear gullies (Fig. 7B). To obtain such linear gullies, we need a clean pulse of water; the melting of the blanket of snow has a too wide-spread effect to trigger this kind of pulse.

Longitudinal variation and width/length ratio of gullies

According to Johnson (1970), debris flow deposits exhibit a variation of their morphologies in agreement with successive waves of debris. A plan view of the experiment (Fig. 8) shows the supposed waves and deposits formed by successive waves of debris. Figure 9 shows a comparative study between a terminal lobe from our laboratory simulation and a high-resolution image of the terminal lobe of two gullies on the megadune.

From various experiments with both silt and fine sand frozen material, carried out with the same volume of water supply and similar active layer thickness, it appears that silt material strongly favours the total length of debris flows (Table 1). The implication for Mars is to suppose that Martian dunes in the Russell Crater are made of silty materials. This interpretation is in agreement with the low

Figure 8. Narrow gullies with lateral levees and relatively small terminal lobes. The morphological characteristics of these gullies on sand are similar to those found on Mars in the Russell Crater. On the top: sinuous channels on the rim crest (like those observed on Mars). In the middle: connections between gullies and variation of their growth by successive wave of debris due to several pulses of water from the rim crest. The analogy with Figures 1 and 2 is striking.

Table 1. Morphological properties of experimental debris flows obtained by the thaw of the ice-rich permafrost (protocol using synthetic foam).

Material	Lenght/width	% of length incised	% of levees
Sand	23	34	26
Sand/silt mixture	41	34	48
Silt	86	32	66

albedo, which should be volcanic sands. The composition of these debris flows over sand dunes supposes finer particles than usual terrestrial debris flows (Mangold et al. 2003). In our experiment, the existence of linear gullies implies the incorporation of meltwater in the debris. This is only possible if thawing of the ground occurs along a significant length of the flow.

Levees and channel connections

Figure 9 shows a comparative study between a terminal lobe from our laboratory simulation and a high-resolution image of the terminal lobe of two gullies on the megadune.

The morphological change of the levees (Fig. 10) is related to the variation of velocities which results from the small change in slope gradient. This observation is in agreement both with characteristics of Martian gullies (Mangold et al. 2003) and rheological properties of terrestrial debris flows (Johnson & Rodine 1984).

Conclusion

Laboratory experiments have been undertaken to explore processes involved in gully formation over a sand dune in the

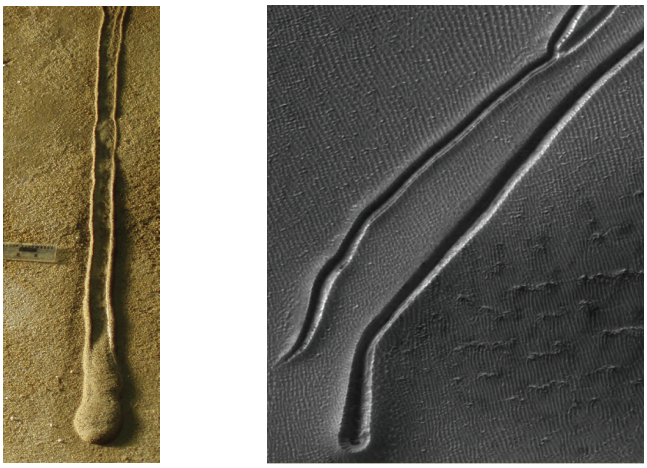

Figure 9. Comparative study of the development of lateral levees and terminal lobe between our experiment (left) and on Mars (right: HIRISE image PSP_002904_1255 (25 cm/pixel). Width of the image: 500 m. Light from the left. Credit: NASA/JPL/University of Arizona.

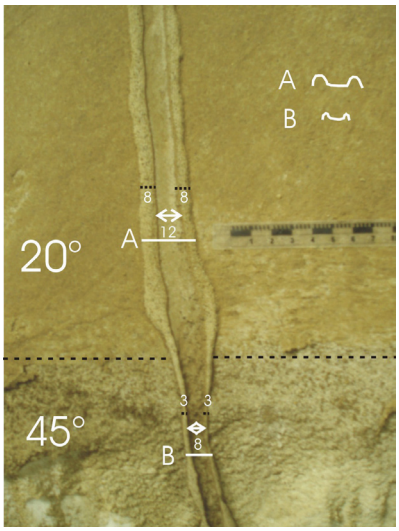

Figure 10. Variations of levees width in relation to slope angle. As on Martian gullies, levees are larger on the lowest slope. Laboratory simulation with fine sand.

Russell Crater. Debris flows over dunes involve either water formation from external processes (Mangold et al. 2003) or subsurface aquifers. The comparison between Martian and laboratory simulations leads to the conclusion that a periglacial environment could explain many of the described features in the Russell Crater. More than 40 laboratory simulations have been proposed in order to understand the formation of gullies over sand dunes on Mars. We used various materials (sand, silt), different slope angles, and different depths of active layers.

Our experiments suggest that the morphology of gullies found on Mars implies the presence of ice-rich permafrost with a relatively thin active layer. In any case (whatever the origin of the water—melting of snow, perched aquifer, or melting of permafrost), the active layer, together with the permafrost, controls the typical morphology of these linear gullies

The best analogy was observed with experimental permafrost made of silty materials with a very thin active layer (higher length/width ratio and percent of total length limited by levees: Table 1).

This preliminary work shows that a periglacial environment and the presence of near-surface permafrost could explain the formation of the Martian gullies. This hypothesis is consistent with some external process triggered by seasonal melting at high obliquity.

In the near future, we plan to test other debris flow formations with lower slope angle in agreement with both slopes from Russell Crater and Martian gravity.

Acknowledgments

This program is supported by "Programme Reliefs de la Terre" INSU, CNRS, France, and GDR mutations polaires: société et environnement.

References

Balme, M, Mangold, N., Baratoux, D., Costard, F., Gosselin, M., Masson, Ph., Pinet, P. & Neukum, V. 2006. Orientation and distribution of recent gullies in the southern hemisphere of Mars: Observations from HRSC/MEx and MOC/MGS data, 111, E05001.

Christensen, P.R. 2003. Formation of recent Martian gullies through melting of extensive snow deposits. *Nature* 163(8), Feb. 22: 116.

Costard, F., Forget, F., Mangold, N. & Peulvast, J.-P. 2002. Formation of recent Martian debris flows by melting of near-surface ground ice at high obliquity. *Science* 295: 110-113.

Coussot, P., Laigle, D., Arattano, M., Deganutti, A. & Marchi, L. 1998. Direct determination of rheological characteristics of debris flow. *J. Hydraul. Eng.* 124: 865-868.

Font, M., Lagarde, J.-L., Amorese, D., Coutard, J.-P., Dubois, A., Guillemet, G., Ozouf, J.-C. & Védie, E. 2006. Physical modelling of fault scarp degradation under freeze/thaw cycles. *Earth Surf. Process. Landforms* 31(14): 1731-1745. doi:10.1002/esp.1371.

Johnson, A.M. 1970. *Physical Processes in Geology*. New York: W.H. Freeman, 576 pp.

Johnson, A.M. & Rodine, J.R. 1984. *Debris flow.* In: D. Brundsen & D.B. Prior (eds.), *Slope Instability*. New York: John Wiley, 257-361.

Hoffman, N. 2000. White Mars: A new model for Mars' surface and atmosphere based on CO_2. *Icarus* 146: 326342.

Laskar, J., Correia, A., Gastineau, M., Joutel, F., Levrard, B. & Robutel, P. 2004. Long term evolution and chaotic diffusion of the insolation quantities of Mars. *Icarus* 170: 343-364.

Lee, P., Cokell, C.S., Marinova, M., McKay, C.P. & Rice, J.W. Jr. 2001. Snow and ice melt flow features on Devon Island, Nunavut, Arctic Canada as possible analogs for recent flow features on Mars (abstract 1809). *Lunar. Planet. Sci. Conf. 32th.*

Ishii, T. & Sasaki, S. 2004. Formation of recent Martian gullies by avalanches of CO_2 frost. *Lunar Planet. Sci. Conf., 35th*, #1556.

Malin, M.C. & Edgett, K.S. 2000. Evidence for recent groundwater seepage and surface runoff on Mars, *Scienc*e 288: 2330-2335.

Mangold, N., Costard, F. & Forget, F. 2003. Debris flows over sand dunes on Mars: Evidence for liquid water, *J. Geophys. Re*s. 108.

Mellon, M.T. & Jakosky, B.M. 1993. Geographic variations in the thermal and diffusive stability of ground ice on Mars. *J. Geophys. Res.* 98: 3345-3364.

Mellon, M.T. & Phillips, R.J. 2001. Recent gullies on Mars and the source of liquid water. *J. Geophys. Res.* 106: 23165-23180.

Musselwhite, D.S., Swindle, T.D. & Lunine, J.I. 2001. Liquid CO_2 breakout and the formation of recent small gullies on Mars. *Geophysical Research Letter*s 28(7): 1283-1286.

Piqueux, S., Byrne, S. & Richardson, M.I. 2003. Sublimation of Mars' southern seasonal CO_2 ice cap and the formation of spiders, *Journal of Geophysical Research* 108(3).

Reiss, D. & Jaumann R. 2002. Spring defrosting in the Russell Crater dune field—Recent surface runoff within the last Martian year. (abstract 2013). *Lunar Planet. Sci. Conf. 33th.*

Schorghofer, N. & Edgett, K.S. 2006. Seasonal surface frost at low latitudes on Mars. 11 *Icarus* 180: 321-334.

Stewart, S.T. & Nimmo, F. 2002. Surface runoff features on Mars: Testing the carbon 14 dioxide formation hypothesis. *J. Geophys. Res.* 107(E9): 5069.

Treiman, A.H. 2003. Geologic settings of Martian gullies: Implications for their origin. *J. Geophys. Res.* 108(E4): 8031.

Modeling the Erosion of Ice-Rich Deposits Along the Yukon Coastal Plain

Nicole J. Couture
Geography Department, McGill University, Montreal, Canada
Md. Azharul Hoque
Geography Department, McGill University, Montreal, Canada
Wayne H. Pollard
Geography Department, McGill University, Montreal, Canada

Abstract

The Yukon Coastal Plain is an area of ice-rich deposits along the Canadian Beaufort Sea and has been identified as highly vulnerable to the effects of sea-level rise and climate warming. Erosion is a function of the composition and morphology of coastal features, as well as wave energy. This paper outlines a simple model that considers these factors. Variations in ground ice contents and onshore and nearshore morphology are examined, as is their effect on the coastal dynamics of the region. Ice volumes are variable, ranging 52% to 84% by volume. A wave climate for the region is hindcast from historical climate records with offshore significant wave heights averaging between 0.32 and 0.45 m. Modeled wave energy shows that cross-shore energy is up to four times greater than longshore. Net longshore sediment transport is westward at all sites although the magnitude varies. Potential erosion is appraised.

Keywords: Beaufort Sea; coastal erosion; erosion model; ground ice; wave climate; Yukon Coastal Plain.

Introduction

Climate changes in the Arctic will have profound impacts on the permafrost coastline of Canada's Beaufort Sea. In addition to warmer air and sea temperatures, changes are expected in several other primary environmental forcings on permafrost coastal systems such as relative sea level (RSL), storminess, and the duration and extent of the open water season. The Yukon Coastal Plain is considered to be in a submergent area (Forbes 1980), with current rates of RSL rise estimated to be approximately 3.5mm/a (Manson et al. 2002). These increases in sea level will be magnified by oceanic thermal expansion which will contribute to the region's sensitivity to erosion (Shaw et al. 1998). Lambert (1995) suggested an increase in the frequency of storms under a warming climate and Solomon et al. (1994) have shown that there is a strong correlation between storm intensity and coastal erosion along the Beaufort Sea. The coast of the Beaufort Sea is micro-tidal with astronomical tide heights less than 0.5 m, so waves play a strong role in coastal change. This is particularly true during the open water season, when sea ice does not dampen wave development. Impacts of climate change along the Yukon Coastal Plain go beyond a physical response. The oil and gas industry are concerned about the effect of shoreline changes on infrastructure and exploration activities. Erosion and changes in the nearshore ecology also have the potential to directly affect local communities since hunting, fishing, and trapping are economic and cultural mainstays for many aboriginal communities along the coast. Numerous historical and archeological sites in the region have already been destroyed by erosion and a number of others are threatened.

The goal of this paper is to outline a simple erosion model to predict how ice-rich coastlines along the Beaufort Sea will respond to changes in climate. A wave climate is hindcast-based on historical climate data and is then used to calculate the potential wave energy available for erosion and sediment transport. The properties of the coastal bluffs are considered in determining spatial variability in erosion potential. The future susceptibility of the different coastline types is considered, based on predicted changes in environmental forcings for the region.

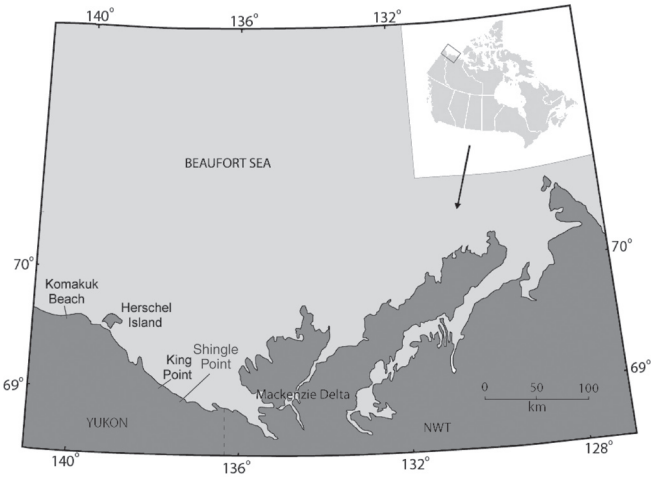

Figure 1. Location map showing the study region and sites along Canada's Yukon Coastal Plain.

Study Area

Canada's Yukon Coastal Plain, located along the Beaufort Sea west of the Mackenzie Delta (Fig. 1), is a lowland of dissected and hilly tundra about 250 km long and 10–30 km wide. Offshore, the continental shelf slopes gently to the shelf break located at about 80 m water depth (Hill et al. 1991). The shelf is relatively narrow, ranging from 40 km wide and sites in the western area to over 150 km wide at the Mackenzie

Delta. This region is classified as having a low arctic climate, with a mean annual temperature of -11°C and mean annual precipitation between 200 and 300 mm. The coastal plain is largely an erosion surface cut into Tertiary sandstone and shale. Most of it was covered by a lobe of the Laurentide ice sheet known as the Buckland Glaciation in the early Wisconsin, as well as by a later stillstand or re-advance known as the Sabine Phase. Surficial deposits reflect this history, with the coast east of Herschel Island being covered by glacial outwash plains and fans, moraines, and fine-grained lacustrine sediment. Moraines make up ice-pushed ridges or else blanket rolling to hummocky topography likely resulting from thermokarst activity (Rampton 1982). West of Herschel Island, the plain was unaffected by the Buckland Glaciation and is made up of coastal lagoons, coalesced deltas, and alluvial fans (Rampton 1982). Most of the flat or gently sloping landscape is covered by organic deposits and peat beds are common, particularly in lacustrine basins (Rampton 1982). Beaches along the coast are generally narrow and are backed by coastal bluffs that can be up to 90 m high. Permafrost along the Yukon coast is continuous and reaches depths of approximately 300 m (Smith & Burgess 2000). The ice content of these soils is high due to the presence of pore ice and thin ice lenses, abundant ice wedges, and beds of massive ice. Subsea ice-bonded permafrost is present below the Beaufort Sea in water depths up to 100 m (Mackay 1972, Dallimore et al. 1988, Dyke 1991). Three sites along the coastal plain were selected for study: Komakuk Beach, King Point, and Shingle Point.

Methods

Coastal composition and morphology

The presence of ground ice in coastal soils constrains the sediment content and influences the coast's susceptibility to erosion. To assess ice content along the Yukon Coastal Plain, a morphological model was developed based on a method first presented by Pollard & Couture (1999). The model calculates the total volume of ground ice for different terrain units along the coast by determining how much of each different type of ground ice is contained within that segment. Three types of ground ice are considered in the calculations: 1) pore ice and thin lenses of segregated ice, 2) wedge ice, and 3) beds of massive ice. As part of the Arctic Coastal Dynamics (ACD) project, a detailed segmentation of the Canadian Beaufort Sea coastline was conducted based on predominant landforms, surficial materials, permafrost conditions, and coastal processes. This initial segmentation was then refined using direct field observations, as well as data from Rampton (1982), Wolfe et al. (2001), and Harper et al. (1985). The percentage of ice content for each type of ground ice was first established, then the volume of each ice type in a terrain unit is determined. Finally, the percentages of total ice content by volume for each terrain unit are calculated.

Wave hindcasting

Meteorological data was obtained from Environment Canada weather observing stations at Komakuk Beach and Shingle Point and from a Campbell Scientific automatic weather station set up at King Point in 2004. Average hourly wind speed and direction were considered for the open water period for the years 2004–2006. The open water period is based on normals of median sea-ice concentration data from the Canadian Ice Service for the period 1971–2000. For the Yukon coast, ice concentrations fall below 5/10 during the last week of June, and open water lasts until the first week of October. Data from the King Point observing station was first adjusted to the 10 m level. Wind speed measurements from the three overland stations were then converted to overwater values to account for differences in roughness between the two surfaces, using commonly used empirical coefficients (Resio & Vincent 1977, cited in Kamphuis). The wind data were then used to model deepwater waves, following the JONSWAP method:

$$H_s = \frac{\lambda u^2}{g} \quad (1)$$

where H_s = significant wave height for a fully developed sea (m), λ = dimensionless coefficient (approximately equal to 0.243), u = wind speed (m/s), and g = gravitational acceleration (9.8 m/s^2).

In the above calculations, shoreline orientation at each site was accounted for, and only offshore winds were considered to be capable of wave generation; winds blowing from a landward direction were set to 0. The waves are not considered to be fetch-limited, so the values are for a fully developed sea. Although only local winds are used to derive the offshore wave climates characteristics, the JONSWAP method considers the entire wave spectrum, so low frequency swell waves, which may be generated a great distance from the area of interest, are included in the calculated outputs. Nevertheless, swell waves are rare in the study region and are low when they are seen (Forbes 1997).

Wave energy and material transport

As waves approach shore, the bottom of the wave begins to interact with the seabed and shoaling begins. The wave is slowed, the wavelength becomes shorter, successive waves begin to pile up, and the heights of the waves increase until they steepen to the point that they break on the shore. The energy they contain is thereby liberated to effect sediment transport and erosion. If a wave approaches the shore at an angle, the portion of the wave closer to shore will slow first, while the deeper portion remains unaffected. As a result, the wave is refracted, or bent, so that the wave crest more closely parallels the shore. Standard equations based on linear wave theory were used to convert the deepwater waves to nearshore ones and determine the height of the breaking wave. Wave energy was then calculated based on the following equation:

$$E = \frac{\rho g H_b^2}{8} \quad (2)$$

where E = energy per area (N/m^2), ρ = density of seawater (1025 kg/m^3), g is as noted above, and H_b = breaking wave height.

The energy term was separated into its component vectors to give longshore and cross-shore values. Sediment transport in the longshore direction is given by the CERC expression (Kamphuis 2000):

$$Q = 330 H_b^{5/2} \sin 2\alpha_b \quad (3)$$

where Q = volume of transported material (m^3/h) and α_b = the incident angle of breaking wave.

Results

Wind data for the three-year period under consideration are shown in Figure 2. The importance of using site- specific wind data has been noted by earlier studies (Pinchin &and Nairn 1987), and is highlighted here by the differences between the stations examined. The coastal plain is narrowest in the west, and at Komakuk Beach, the close proximity of the British Mountains contribute to channeling the winds in an east-west direction. Offshore waves were hindcast from these winds producing average significant wave heights ranging up to approximately 0.5 m. Details of the significant wave heights for the three sites are given in Table 1.

The breaking wave heights are used to generate wave energy for each modeled wave, which is then broken down into a crossshore component (X) and a longshore one (Y) (Table 2). The proportion of energy going into each component is dependent on the incident angle of the nearshore wave which is, in turn, a factor of the original wind direction and the degree of wave refraction that occurs. This angle also governs which direction the longshore current will take (overall east or west, in the cases examined here). Net annual longshore energy is obtained by subtracting the total longshore in one direction from the total in the opposite direction. Using Equation 3, the potential net volume of sediment transported by the longshore wave energy can be calculated for the three-year period examined (Table 3). Although these calculations indicate potential transport of several thousands of cubic metres of sediment, the amount transported at Shingle Point is nevertheless not considered to be significant, if one considers that the uncertainty of the method is on the order of 10–-20%.

In order to assess how this potential sediment transport might affect coastal retreat at the study sites, the actual volume of material in the bluff needs to be considered. At Komakuk Beach, coastal bluffs are approximately 3 m high and consist of fine-grained lacustrine material. Ground ice comprises 61% by volume of the coastline. At King Point, cliffs up to 30 m high are made up of morainic material. The presence of beds of massive ice contributes to a very high ice content of 84%. At Shingle Point, the 10 m high bluffs are also morainic in origin, but their ice content is only 52%.

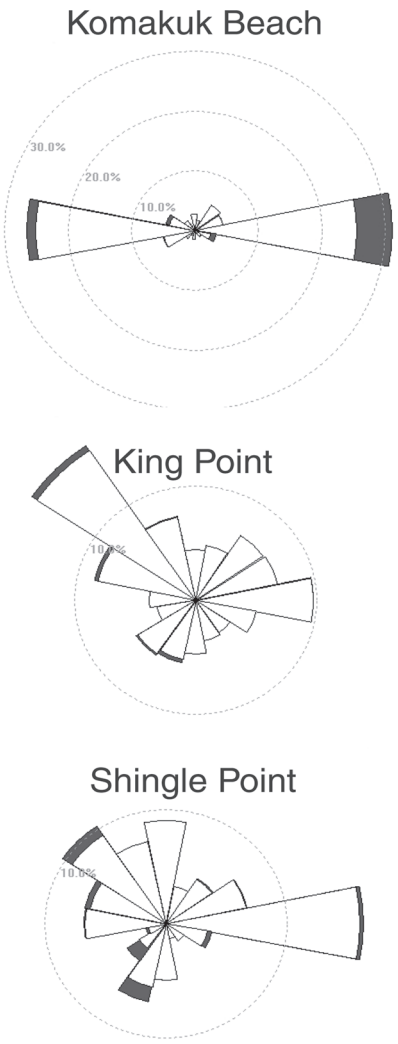

Figure 2. Wind roses showing frequency and magnitude of winds. Shaded areas indicate winds in excess of 37 km/hr, a common criteria for storm winds.

Figure 3 provides an indication of how these values compare to other sites along the Yukon coast.

Based on cliff heights and the percentage of ice they contain, the volume of sediment for a section of the coast extending 1 m inland can be calculated for each segment of coastline under study:

$$V = lh(1 - PIV) \quad (4)$$

where V = volume of sediment in a homogeneous coastline segment based on ACD project criteria (m^3),
l = length of the coastline segment (m),
h = height of the coastal bluff, and
PIV = percentage of ice from all sources of ground ice.

Entire segments of coastline are used to account for the fact that not all sediment being transported alongshore at any one point is necessarily sediment eroded from the coastline at that particular point. Rather, some of it has been supplied from further up the coast and is simply in transit. It

Table 2. Cross shore (X) and longshore (Y) components of modeled wave energy.

Site	Total X (N/m^2)	Total Y (N/m^2)	Eastward Y* (N/m^2)	Westward Y* (N/m^2)	Ratio X/Y
Komakuk	15.7×10^5	5.2×10^5	0.7×10^5	4.6×10^5	3.0
King Pt.	13.4	3.4×10^5	1.3×10^5	2.1×10^5	4.0
Shingle Pt.	16.0	4.5×10^5	2.2×10^5	2.2×10^5	3.6

* These represent only general direction of Y component. Actual movement of material is parallel to the shore at each site.

Table 3. Modeled longshore sediment transport for 2004–06.

Site	Q (m^3)
Komakuk	3.2×10^5 towards the west
King Pt.	0.5×10^5 towards the west
Shingle Pt.	0.1×10^5 towards the west (not significant)

Table 4. Volume of sediments and erosion rates for the different coastline segments in this study.

Site	Segment length (m)	Volume of sediments (m^3)	Annual sediment transport (m^3)	Potential retreat (m/yr)
Komakuk	6020	0.70×10^4	10.6×10^4	15.1
King Pt.	2990	1.43×10^4	1.8×10^4	1.3
Shingle Pt	8850	4.23×10^4	0.3×10^4	0

is therefore more realistic to integrate erosion over a longer length of homogeneous coastline. Total sediment transport for the 3-year period of study was averaged to arrive at a potential annual rate of transport. Assuming that this volume of sediment is being removed from the segment of coastline under consideration, then based on the volume of the sediments in the segment, a potential rate of annual coastline retreat is calculated (Table 4).

Discussion and Conclusions

This study examines nearshore wave energy generated through hindcasting. Previous studies have modeled potential erosion through wave climate analysis (Solomon et al. 1994, Hequette & Barnes 1990), but used offshore waves only so the results cannot be directly compared. Different techniques for nearshore wave transformation produce varying results (Pinchin & Nairn 1987) and the results of this study will need to be validated using measured nearshore waves. Previous work usually considers only storm winds and waves in their evaluation of erosion. We chose to examine all waves because several processes unique to arctic coasts can provide material for erosion between storms. Figure 4 shows two types of failures along coastal bluffs—retrogressive thaw slumps and block failures—that are common in ice-rich environments such as the Yukon Coastal Plain. In both cases, material is available close to the waterline and so is potentially subject to erosion by even moderate wave action. The erosion of the sediment from such failures may not result in any immediate retreat in the shoreline position, but once that material is removed, the toe of the bluff is not longer protected from direct wave action and subsequent shoreline retreat can proceed more rapidly. This study only examines three years of data and so does not necessarily reflect the

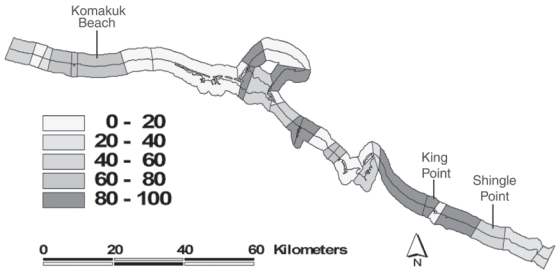

Figure 3. Ground ice volumes (by percentage) for different terrain units along the Yukon Coastal Plain.

longer term retreat rates resulting from these types of slopes failures

The modeled results can be considered acceptable given that the annual erosion rates are of the same order of magnitude as measured rates for the region (e.g., Harper 1990, Solomon 2005). Although the rate for Komakuk Beach shown here is higher than ones reported in earlier studies (0.76 m/a in Forbes 1997), this may be due to the fact that, rather than contributing to active erosion, the majority of the wave energy is devoted to transporting the high sediment loads being input from two rivers to the east of the site..

The simple erosion model in this study provides a first approximation of the influence of wave energy on coastal retreat rates. However, this model can only hope to explain some of the lower- level coastal landscape features. Coastal dynamics are extremely complex and are also influenced by currents, wave refraction around major features such as Herschel Island, river inputs of sediment, shoreface profiles, and ice-push events. The larger landscape structures like spits and barrier islands are likely controlled by major storm events. This is underscored by the fact that even though sediment transport at Shingle Point is shown to be not significant, a major spit does exist at this site. Improvements to the model presented here can be made by extending the length of the data set (preferably to at least 15 years), by validating the hindcast wave climate, and by incorporating grain size into the sediment transport equation since the one used for this study assumes that all transported material is sand. Fetch length was considered to be unlimited as soon as ice concentrations fell below 5/10, but its variability with time and direction should be part of future work. An examination of crossshore sediment transport is also planned. 4a) Ab) Episodic events such as these deliver sediments to the beach that can be subsequently removed by even moderate wave activity. The model could be used to examine future erosion rates, but several factors would need to be considered including changes to sea ice extent.

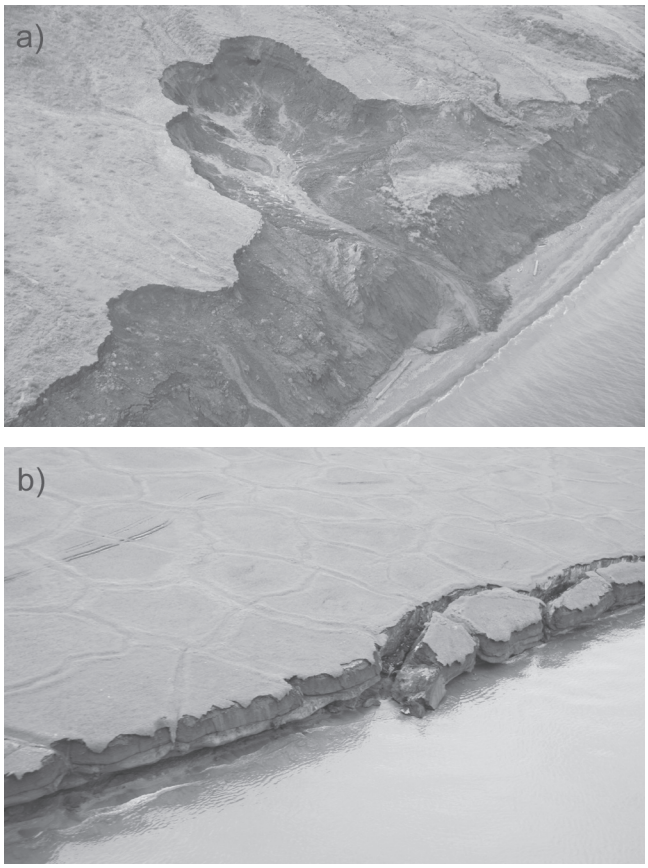

Figure 4. a) A retrogressive thaw slump near King Point and b) a block failure near Komakuk Beach. . Episodic events such as these deliver sediments to the beach that can be subsequently removed by even moderate wave activity.

Acknowledgments

Financial assistance was provided by ArcticNet NCE (1.2, 1.2 and 2.4), the Natural Science and Engineering Research Council of Canada, and Fond québécois de la recherche sur la nature et les technologies. Fieldwork was made possible by the Polar Continental Shelf Project and the Northern Scientific Training Program. We would also like to thank the Alfred Wegener Institute for Polar and Marine Science (Potsdam), Herschel Island Territorial Park, Ivvavik National Park, the Aurora Research Institute, S. Solomon, H. Lantuit, G. DePascale, T. Haltigin, and D. Leitch. Comments by S. Ogorodov and an anonymous reviewer are very much appreciated.

References

Dallimore, S.R., Kurfurst, J.J. & Hunter, J.A.M. 1988. Geotechnical and geothermal conditions of near-shore sediments, southern Beaufort Sea, Northwest Territories, Canada. *Proceedings of Fifth International Permafrost Conference*, *Trondheim, Norway*: 127-131.

Dyke, L.D. 1991. Temperature changes and thaw of permafrost adjacent to Richards Island, Mackenzie Delta, N.W.T. *Canadian Journal of Earth Sciences* 28: 1834-1842.

Forbes, D.L. 1980. *Late Quaternary sea level in the Beaufort Sea.* GSC Paper 80 (1B), 75-87.

Forbes, D.L. 1997. *Coastal erosion and nearshore profile variability in the southern Beaufort Sea, Ivvavik National Park, Yukon Territory.* Geological Survey of Canada, Open File 3531, 28 pp.

Harper, J.R., Reimer, P.D., & Collins, A.D. 1985. *Canadian Beaufort Sea physical shore zone analysis*. Geological Survey of Canada, Open File Report 1689, 105 pp.

Héquette, A. & Barnes, P.W. 1990. Coastal retreat and shoreface profile variations in the Canadian Beaufort Sea. *Marine Geology* 91: 113-132.

Hill, P.R., Blasco, S.M., Harper, J.R. & Fissel, D.B. 1991. Sedimentation on the Canadian Beaufort Shelf. *Continental Shelf Research* 11: 821-842.

Kamphuis, J.W. 2000. *Introduction to Coastal Engineering and Management*. Singpore: World Scientific Publishing, 437 pp.

Lambert, S.J. 1995. The effect of enhanced greenhouse warming on winter cyclone frequencies and strengths. *Journal of Climate* 8: 1447-1452.

Mackay, J.R., 1972. The world of underground ice. *Annals of the American Association of Geographers* 62: 1-22.

Manson, G.K., Solomon, S.M. & MacDonald, A. 2002. Describing Beaufort Sea coastal climate variability. *Reports on Polar and Marine Research* 413: 31-33.

Pinchin, B.M. & Nairn, R.B. 1987. *Beaufort Sea coastal sediment study: evaluation of inshore wave climate and coastal sediment transport techniques at King Point, Yukon*. Toronto, Ontario: Keith Philpott Consulting Limited.

Pollard, W.H. & Couture, N.J. 1999. *The use of morphological methods to estimate ground ice volumes along the Canadian Beaufort Sea coast.* Report for the Geological Survey of Canada (Atlantic), 30 pp.

Rampton, V.N. 1982. *Quaternary Geology of the Yukon Coastal Plain*. Geological Survey of Canada Bulletin 317, 49 pp.

Shaw, J., Taylor, R.B., Forbes, D.L., Ruz, M.-H. & Solomon, S. 1998. *Sensitivity of the coasts of Canada to sea-level rise.* Geological Survey of Canada Bulletin 505, 79 pp.

Smith, S., & Burgess, M. 2000. *Ground temperature database for northern Canada*. Geological Survey of Canada, Open File 3954, 28 pp.

Solomon, S.M., Forbes, D.L. & Keirstead, B. 1994. *Coastal impacts of climate change: Beaufort Sea erosion study*. Geological Survey of Canada, Open-File 2890. Solomon, S.M. 2005. Spatial and temporal variability of shoreline change in the Beaufort-Mackenzie region, Northwest Territories, Canada. *Geo-Marine Letters* 25: 127-137.

Wolfe, S. A., Kotler, E. & Dallimore, S. R. 2001. *Surficial characteristics and the distribution of thaw landforms (1970–1999), Shingle Point to Kay Point, Yukon Territory*. Geological Survey of Canada, Open File 4115, 18 pp.

Dynamics of Patterned Ground Evolution

James G.A. Croll
University College London, London, England WC1 E 6BT

Abstract

New dynamic mechanisms for the formation of a number of different forms of patterned ground are postulated to result from alternations of solar energy reaching the ground surface. Extensions of the thermo-mechanical processes widely believed to power the growth of ice wedge polygons are suggested to contribute to the dynamic evolution of many patterned ground features, such as sorted and unsorted stone circles, polygons, nets, stripes and steps. hummocks, frost mounds, palsas, and pingos. For each, fluctuations in solar energy at various temporal scales are argued to provide at least part of the dynamic driving force in what might be referred to as thermo-mechanical ratchet processes. While these ratchet models appear to be supported by past field observation, new field data are clearly needed if they are to be adequately assessed as to whether they might better explain the formation of many forms of patterned ground.

Keywords: contraction; cracking; expansion; patterned ground; periglacial morphologies; ratchet; thermal loading.

Introduction

Many forms of patterned ground within periglacial environments have been the subject of long-standing fascination. From the formation of geometrically patterned ground, to the sometimes distinctive mounds developing out of otherwise flat areas of permafrost, to the hummocks and other regular geometric patterns observed over ground subject to seasonal freeze-thaw cycles, much has been written as to their possible causes. Understanding of the processes responsible for their initiation and growth is of significance in relation to the interpretation of past climatic conditions through the observation of the relic geomorphic features remaining long after previous permafrost has receded. It is therefore not surprising that the processes which might have been responsible for the growth of these various forms of patterned ground have occupied considerable research attention. In many cases there is widespread agreement on the processes involved in these formations while in others there remains considerable uncertainty.

This paper approaches the subject of the mechanical causes of these various features from a somewhat different perspective. It postulates dynamic mechanisms that are in some form the result of alternations of solar energy reaching the ground surface. It suggests that these alternations of solar energy produce warming periods when the frost layer, or permafrost where it is present, is subject to horizontal compressive forces arising from the restrained, lateral, thermal expansion. During subsequent cooling, tension forces will accompany the restrained thermal contraction. Because of differential mechanical properties exhibited by ice and ice-rich ground at high and low temperatures, or under compression and tension, certain forms of deformation will accumulate to form morphological features through processes that might be generically referred to as thermal ratchets. Of particular interest here is how these processes might be at work in the development of patterned ground and as such is intended to complement earlier work dealing with the development of various forms of surface mound (Croll 2004, 2007b).

Ice wedges and ice wedge polygons are widely accepted to be the result of a form of this thermo-mechanical ratchet process. This was recognised by Lachenbruch (1964) and further elaborated from the field observations of Mackay (1974, 2000) and Mackay & Burn (2002). In this model of the formation of ice wedges and ice wedge polygons, the thermal ratchet process relies upon the cyclic compressive and tensile energies being dissipated through two very different processes. During seasonal warming, the compression phase, the release of stored energy is through an outward shoving of ground material, particularly within the active layer, giving rise to upward shearing and folding into the typical forms of rampart either side of the ice wedge. During seasonal cooling, the tensile phase, the dissipation of energy is the result of brittle tensile fracture, preferentially accumulating in the growing ice wedge. Over many such cycles the outward and upward movement of permafrost and active layer material compensates the growth in volume of the peripheral ice wedges. Yet surprisingly, the elegant logic of this seasonally driven thermal ratchet model process has not been transferred into efforts to better understand other periglacial phenomena occurring at possibly different spatial and temporal scales. As the following suggests, a related from of thermal ratchet model may also be responsible for the development of some of the many patterned ground features so eloquently described by Washburn (1979).

Stone Circles and Polygons

While reasons have in the past been proposed for the horizontal movements needed to form such curious features as the sorted stone circles of Figure 1(a), or polygons of Figure 1(b), etc, none of them appear to be entirely convincing or able to account for all such features. Encouraged by field measurements showing clear patterns of outward radial movements of the surface materials, from the centres of well formed stone circles (see e.g., Hallet et al. 1986), there have

been many attempts to explain the formation of stone circles in terms of the development of convection motions within the active layer. Indeed, during the 1980s the convective cell model seems to have become the dominant explanation for the growth of stone circles (Gleason et al. 1986, Ray et al. 1983).

There are, however, fundamental problems with these models based as they are upon density differences largely resulting from variations in moisture content of the soil. First, the forces required to not just power the outward radial surface motion of the fines, but also shift the considerable weight of the border stones to allow the surface layers to be subducted beneath, would seem to be very much higher than any generated by the relatively small changes in soil density,and this does not even include the very considerable forces needed to visco-plastically distort the soil layers. Just as the density differences due to thermal gradients were held to be insufficient to drive a convection cell at the scale required for stone circles (Morgenstern 1932), it would appear that the forces due to density differences are also inadequate. Even the measurements of outward deformations of the soil surface do not appear to support the hypothesis of buoyancy driven convection. Accurate readings taken in western Spitzbergen clearly show radial deformation rates increasing away from the centre of the monitored stone circles (see Fig. 5, Hallet et al. 1986). Were the driving mechanism to be convection, very simple considerations of mass conservation would predict that the outward deformation rates would decrease with radial distance form the centres.

There appear to be similar problems with some of the more recent hypotheses for the development of stone circles and ice wedge polygons, even though results from computer generated models appear to support them (Kessler et al. 2003, Plug et al. 2002). Space does not allow fuller discussion. While it is likely that no single explanation will be able to account for all motions involved in the formation of periglacial morphologies, the following would appear a feasible explanation for at least some of the features outlined in classic texts such as Washburn (1979) and French (1996).

Role of thermal ratchetting

To illustrate how thermal-mechanical ratchet processes could be at work in the horizontal motions of both top soil and stones, consider a typical stone lying at surface level a distance h from the centre of a stone circle having radius r that is in the process of forming, as depicted in Figure 2. Here "circle" will be assumed to cover the case where the circular diameters are such that they would overlap were it not for the development of interacting polygons, nets, etc. Putting aside for the moment the question of what governs the characteristic dimensions of the stone circles, of current concern is the process that continues to drive the outward movement of the stones and surface material once the basic geometric patterns have been defined. In early autumn the seasonally unfrozen ground will start to refreeze. Initially this surface freezing and thawing would be governed by

Figure 1 (a). Examples of sorted stone circles.

Figure 1 (b). Examples of stone polygons.

circadian periodicities, for which the temperatures would follow a pattern similar to that shown in Figure 2(a). Each night the typical stone will be locked into the downwardly propagating freezing layer as suggested at time (1) in Figure 2(b). With the frozen layer being grounded within the stone boundary rampart, a drop in surface temperatures will develop tensile stresses in the frozen surface layer, as a result of the constrained contraction – time (2). Desiccation and even discrete cracks, associated with the development of the tensile stress, will attract moisture that at the low temperatures will turn to ice – time (3) in a similar way to ice wedge polygons. When temperatures begin to increase towards morning, the frozen ground will start to develop compressive stress as a consequence of the restraint to the expansion that would otherwise occur. Because the frozen layer of soil is likely to have fairly high compressive strength the overall radial forces being developed will be in certain ground conditions sufficiently high to dislodge the stone and cause it to move outward – time (4). At least in early autumn and spring the nocturnal frozen layer will completely thaw during the high diurnal warmth, leaving the stone and adjacent soil permanently moved out a small distance, δu, as shown at time (5). And so the process will continue with the radial distances moved increasing as the circadian fluctuations in temperature are increased.

To provide an indication of the levels of radial deformation and force developed during a typical circadian period, consider a nocturnally frozen layer of thickness 10 mm, having a coefficient of linear thermal expansion $\alpha = 50\text{x}10^{-6}/°\text{C}$, subject to an increase in temperature $\Delta T = 10°\text{C}$ during

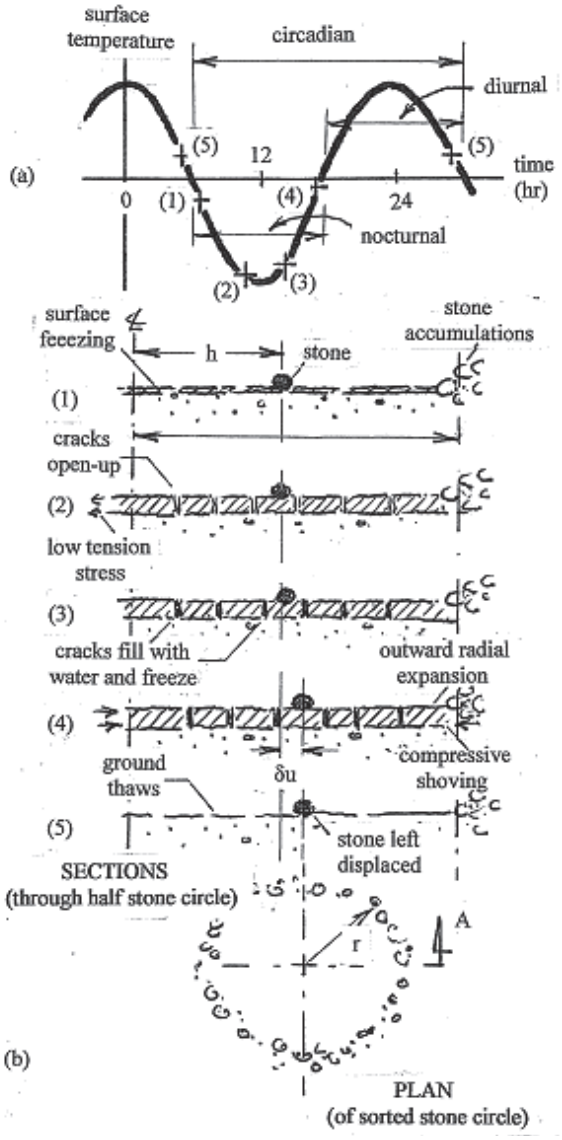

Figure 2. Schematic representation of (a) typical autumnal circadian thermal cycle acting on a stone circle, showing (b) typical half cross sections taken at times indicated.

the diurnal warming and prior to any melting. If there were no radial restraint, the outward radial deformation of a stone at a distance of, say, h = 1500 mm from the circle centre, would be $\delta u = \alpha\, \Delta T\, h$ = 1.3 mm/d. These rates of outward deformation are consistent with those recorded by Hallet et al. (1986). In that they are predicted to increase linearly with the distance from the centre of the stone circle, the deformation profiles are, in contrast with those predicted from the convection cell model, also in accord with those recorded by Hallet et al. (1986). If the outward radial deformation was to be fully restrained by the stone boundary, the radial stress σ_r developed in the frozen soil, assumed to have a modulus of elasticity E = 1 GPa, would be $\sigma_r = \alpha\, \Delta T\, E$ = 0.5 MPa. With the frozen layer of thickness 10 mm, a single stone of diameter 50 mm would attract a radial force of 250 N, or nearly 60 lbf, enough to dislodge even the most recalcitrant of stones. While it is difficult to conceive of soil convection developing force levels of this magnitude, the above scoping calculations suggest that a combination of thermal expansion and contraction is well capable of providing the driving force for the development of stone circles.

Even when the frozen layer ceases to completely thaw and starts to propagate downward, there may be short, daily or possibly longer, timescales over which a surface melt allows the stone to be ratcheted out a little further in much the same way as that described above. Under these circumstances the mechanism discussed in Figure 2 would operate in the diurnally thawed layer above the seasonal, downwardly-propagating frozen layer. Longer period thermal cycles could also be operating in the seasonally frozen ground in much the same way as they do in the growth of ice wedge polygons. As discussed below, these longer-term thermal cycles could play an important part in the determination of the characteristic dimensions of the rock or stone circles.

Controls of characteristic dimensions

While the above appears to provide a very plausible mechanism for driving the development of stone circles, it does not directly explain the mechanics whereby the stone circles are formed in the first instance and what it is that determines for a particular set of circumstances the characteristic radii for the rock circles, polygons, etc. In a given location and within a particular set of thermal climatic conditions, the characteristic dimensions of any stone circles appear to be fairly robust. If the forcing mechanism derives from a ratchet process driven by fluctuations in thermal loading, like that described above, then the nature of the mechanics involved but at longer timescales could also determine the characteristic dimensions that can be achieved. There are a number of mechanical processes that could be controlling these characteristic dimensions.

At annual timescales the depth of the thermal wave would determine not just the thickness of the frozen ground but also the depth and the spacing of any cracks connecting up to form crack-wedge polygons. This form of tensile energy relief could influence the typical dimensions of the eventual stone polygons, in much the same way as they control the characteristic dimensions of the ice wedge polygons within the deeper permafrost.

Another potentially controlling factor could be the shear capacity between the frozen layer and the underlying unfrozen ground. For a given set of ground conditions, the total shear capacity resisting an outward radial expansion would increase linearly with increasing radius of the stone circle. For a given range of thermal loading, which for a fully restrained expansion would control the maximum compressive force developed, the radius of accumulating stones would be increased until such time as the thermally dependent compressive force just equilibrates the shear resistance inhibiting radial movement. The most extreme thermal loading could be controlled by relatively short term thermal cycles, with moderately large temperature fluctuations but for which the frozen ground might be

expected to retain high stiffness, or it could be the longer-term, annual seasonal, thermal cycles involving much larger average temperature fluctuations but for which the visco-plastic response would imply that the frozen ground has a lower effective stiffness to thermal straining. Whichever exerts the most extreme compressive loading will control, for a given set of prevailing underlying shear strength properties, the maximum or characteristic radius of the stone circle – or polygon where these start to overlap. The stone ramparts could be caused by shoving actions similar to the processes responsible for the formation of ramparts at the edges of expanding lake ice (Gilbert 1890, Hobbs 1911, Scott 1927).

Another possible mechanical condition that could control the characteristic radii would be the development of a form of upheaval buckling of the frozen layer, similar to the process recently described for the possible formation of pingos (Croll 2004, 2007a,b). Depending upon the thickness of the frozen layer and the thermal compression developed when during the spring its average temperature is increased, it is possible that the characteristic radius could be controlled by thermal uplift buckling. While such an upward doming would likely be recovered when the frozen ground thaws, the sloping sides and the surface melt in spring prior to this recovery might also contribute to the outward movement of any surface material to the lower edges of the buckled dome.

Development of differential frost heave

Once sorting of the type described above has taken place, there will be spatial inhomogeneity in the thermal conductivity of the surface layers. Peripheral stone or rock mounds with air voids will be likely to have a lower than average thermal conductivity with the result that downward growth of the circadian, seasonal or other periodicity growth of the frozen layer will be retarded around the periphery. The more rapid downward propagation over the central regions would induce greater rates of frost heave in these areas. If sufficiently large, this form of differential frost heave could elevate the central regions sufficiently that gravity might also lead to larger stones and rocks being moved towards the outer periphery. Even if the slopes are not sufficient to induce purely gravity-related sliding of the larger particles, a form of Moseley-Davidson thermal ratchet, similar to that described by Croll (2006) and believed to be the cause of insolation creep (Moseley 1855, Davison 1888), could be operating. However, on this basis the differential frost heave would be the result of the sorting not its cause.

Sorting through erosion

The thermal ratchet model described above would also account for the finer soil particles also being gradually shoved out to form peripheral edge ramparts, like those shown in Figure 1. Why these fines do not remain could be accounted for by subsequent differential surface erosion. Surface runoff from the elevated edge ramparts and selective erosion of the fines within these peripheral accumulations would wash back into the lower central regions of the circle/polygon. In certain circumstances it is likely that summer surface water or wind action could see the accumulated finer soil at the outer edges being eroded back to fill the fissures and pores left by the melting of ice from the previous winter's cracking action. This additional form of mass movement would accentuate the process of soil sorting whereby the centres of the circle are gradually colonised by finer particles and the outer edges by those of larger dimension.

High-centred stone circles

It is interesting to speculate as to why in seemingly more restrictive circumstances the larger stones accumulate not at the outer boundaries but at the centres of the graded stone circles, polygons, etc. It seems plausible, as suggested by Washburn (1979), that these stone accumulations may be an advanced form of the stone polygon. The corner nodes of the polygonal array may eventually attract, through a process similar to that described above, the accumulations previously occurring at the edges of the polygon. These nodes would then become the centres of arrays of essentially high-centred triangles, the triangular array representing the congugate of the original polygonal array. High-centred, sorted, or unsorted circles may either be the result of collapse of the underlying ice wedges at the boundaries, or in active permafrost be the result of a compression failure at the centre of the circle. Such failures might involve a process of upheaval buckling similar to that described recently in relation to the development of hummocks, frost mounds, palsas, and pingos (Croll 2007a,b).

Other Permafrost Features

Descriptions of many periglacial geomorphic features are consistent with the role of thermal ratchet processes like those described above being ubiquitous. Stone nets, stripes, and steps appear to be driven by mechanisms similar to those described above, but with the intervention of gravity the geometric patterns become orientationally distorted. Stone pavements and string bogs appear to have many features in common with the process described above for the formation ice wedge polygons. High-centred polygons seem to share a close resemblance to and possible similarity in origin to the pingo. As observed by Washburn (1979, p. 135) "some ice-wedge polygons enclose small pingo-like ice cored mounds."

Mention should also be made of frost-creep in the context of ratchetting processes. In this case the ratchet mechanism within currently accepted models is somewhat different, and thought to involve a combination of frost-heave occurring normal to the slope, followed by a thaw that results in a stone or other object settling vertically under the action of gravity. The result is a gradual downward motion accompanying each freeze-thaw cycle. Space does not permit consideration of the extent to which those phenomena, explained in terms of solifluction and gelifluction, might also have contributions from the thermo-mechanical ratchet processes outlined above.

In all of these surface motions, it is possible to construct models that could be complementing the processes currently considered to provide the driving force.

Some Closing Remarks

One of the purposes of this paper has been to suggest a form of dynamic mechanisms that may be contributing to the initiation and development of various forms of patterned ground. Thermo-mechanical ratchet processes, derived from fluctuations in the levels of solar radiation reaching the earth's surface, are suggested to contribute to the formation of rather more periglacial processes than currently accepted. The dynamic mechanism for the formation of various forms of patterned ground is postulated to result from alternations of solar energy reaching the ground surface. Extensions of the thermo-mechanical processes widely believed to power the growth of ice wedge polygons have been postulated to contribute to the dynamic evolution of many patterned ground features, such as sorted and unsorted stone circles, polygons, nets, stripes, and steps. Simple calculations have demonstrated that outward radial displacements of the frozen surface soil are consistent with previous field measurements. They also show that the levels of force generated when the expansions are restrained are large enough to account for the outward shoving of the stone ramparts.

Similar processes have recently been discussed (Croll 2007a,b) for the development of hummocks, frost mounds, palsas, and pingos. For each, fluctuations in solar energy at various temporal scales are argued to provide at least part of the dynamic driving forces in what might be referred to as thermo-mechanical ratchet processes.

While these ratchet models appear to be supported by past field observation, new field data are clearly needed if they are to be adequately assessed as to whether they might better explain the formation of many forms of patterned ground. Field tests would need to be devised that would allow, for example, the radial displacement rates to be correlated with the thermal conditions and especially temperature alternations. To be adequate, these measure-ments would need to be recorded continuously over full circadian cycles at the times of the year when motions are at their greatest. They would need to monitor variations in both the thickness and temperature gradients through the thickness of the frozen layer at circadian and other periodicities. If such data are to be adequately interpreted, it will be important to measure the site-specific coefficient of thermal expansion, modulus of elasticity, and other thermo-mechanical properties of the frozen soil.

As is becoming clear in evidence from recent planetary probes, many of the surface features being observed on the other planets and their satellites (see e.g., Kuzmin 2002, Yoshikawa 2002) would appear to have close relationships with similar features on Earth. Improved understanding of the mechanics responsible for developing these features will be essential if these observations are to allow better understanding the origins of the solar system, including a more complete appreciation of the nature and influences of present and past climatic conditions.

It is also becoming clear that closely related morphological features exist at very small scale in the behaviour of asphalt (Croll 2005a, 2006, 2007c). In these analogous cases similar forms of thermo-mechanical ratchet processes would appear to be responsible. Again, better understanding of the mechanics will be essential if future design and maintenance strategies can be expected to reduce the currently high maintenance costs for asphalt pavements. To capture all these phenomena, account must be taken of the relationships linking the thermal periodicities and the spatial scales.

Fluctuations in levels of solar energy and the operation of various forms of thermo-mechanical ratchet process seem to be rather more common in the shaping of environments, including periglacial environments, than is currently recognised. This paper represents a small start towards suggesting for patterned ground a new classification based upon the form of the thermo-mechanical ratchet processes that might be at work in their formation.

Acknowledgments

Financial support to cover attendance at the 2008 NIPC has been provided by a fellowship from the Leverhulme Foundation, whose support is gratefully acknowledged. Being relatively new to this fascinating field, I have relied heavily upon the excellent descriptions in books by French (1996) and Washburn (1979) and the impressive series of papers by Mackay. I have also benefited from private correspondence with Professors Mackay and Burn, whose efforts to correct many misunderstandings and provide references that might put me on a more correct path are gratefully acknowledged. In preparing this revised version of the original paper, I have also benefited from the comments of two anonymous referees, whose perceptive and helpful comments I hope to have at least partially addressed.

References

Croll, J.G.A. 2004. An Alternative Model for "Pingo" Formation in Permafrost Regions. *Proceedings of 21st International Congress of Theoretical and Applied Mechanics*, *August, 2004*, *ICTAM-04, Warsaw*:15-21.

Croll, J.G.A. 2005a. Thermal buckling of pavement slabs. *Proceedings of the Institution of Civil Engineers 2005, Transportation Vol. 158 (May)*: 115-126.

Croll, J.G.A. 2005b. *Pulsatile motion of solids.* Internal report. University College London.

Croll, J.G.A. 2006. From asphalt to the arctic: new insights into thermo-mechanical ratchetting processes. Presented at *Third International Conference on Computational Mechanics*, *Lisbon, Portugal, 5–8 June, 2006*.

Croll, J.G.A. 2007a. Thermal ratchet uplift buckling and periglacial morphologies. Presented at *International Conference Cryogenic Resources of Polar Regions*, *Salekhard City, Russia, 17–22 June, 2007.*

Croll, J.G.A. 2007b. Mechanics of thermal ratchet uplift buckling in periglacial morphologies, *Proceedings of the SEMC Conference*, *Cape Town, South Africa, September, 2007*.

Croll, J.G.A. 2007c. Thermal ratchetting in the blister buckling of asphalt pavements. *International Journal of Pavement Engineering* (in press).

Davison, C. 1888. Note on the movement of scree material. *Quarterly Journal of the Geol Soc*. (4): 232-238.

French, H.M. 1996. *The Periglacial Environment*, second edition. Addison Wesley Longman Ltd

Gilbert, G.K. 1890. *Lake Bonneville.* U.S. Geological Survey Monograph 1, 1890, 438pp.

Gleason, K.J., Krantz, W.B., Caine, N., George, J.H. & Gunn, R.D. 1986. Geometric aspects of sorted patterned ground in recurrently frozen soil. *Science* 232: 216-220.

Hallet, B. & Prestrud, S. 1986. Dynamics of periglacial stone circles in western Spitsbergen. *Quarternary Research* 26: 81-99.

Hobbs, W.H. 1911. Requisite conditions for the formation of ice ramparts. *Journal of Geology* 19: 157-160.

Kessler, M.A. & Werner, B.T. 2003. Self-organisation of sorted patterned ground. Science 299: 380-383.

Kuzmin, R.O., Ershow, E.D., Komarow, I.A., Kozlov, A.H. & Isaev, V.S. 2000. The comparative morphometric analysis of polygonal terrain on Mars and the Earth high latitude areas, *Lunar and Planetary Science* 33: 2000.

Lachenbruch, A.H. 1962. Mechanics of thermal contraction cracks and ice-wedge polygons in permafrost. *Geological Society of America*, Special paper 70, 69 pp.

Mackay, J.R. 1974. Ice-wedge cracks, Garry Island, NWT. *Journal of Earth Science* 11: 1366-1383.

Mackay, J.R. 2000. Thermally induced movements in ice-wedge polygons, Western Arctic coast: A long term study. *Geographie physique et Quarternaire* 54: 41-68.

Mackay, J.R. & Burn, C.R. 2002. The first 20 years (1978-79 to 1998-99) of ice-wedge growth at the Illisarvik experimental drained lake site, western Arctic coast, Canada. *Canadian Journal of Earth Sciences* 39(1): 95-111 and (39)11: 1657-1674.

Moseley, H. 1855. Descent of a solid body on an inclined plane when subject to alternations in temperature, *Proceedings of the Royal Society VII*, *April, 1855*: 341.

Plug, L.J. & Werner, B.T. 2002. Non-linear dynamics of ice-wedge networks. *Nature* 417: 929-933.

Scott, I.D. 1927. Ice-push on lake shores*, Michigan Academy of Science, Arts, and Letters* 7: 107-123.

Strathan, I. 1977. *Earth Surface Sediment Transport*. Clarendon Press.

Washburn, A.L. 1979. *Geocryology: A Survey of Periglacial Processes and Environments*, Second edition. London, England: Edward Arnold Ltd.

Yoshikawa, K. 2000. Contraction cracking and ice-wedge polygons in Mars. *Second International Conference on Mars Polar Science and Exploration*, *August, 2000*: 186-187.

Legacy and Accomplishments of Frozen Ground Engineering Studies in Alaska 60 Years Ago

Margaret Cysewski
University of Alaska Fairbanks, Department of Civil and Environmental Engineering, Fairbanks, Alaska, USA
Yuri Shur
University of Alaska Fairbanks, Department of Civil and Environmental Engineering, Fairbanks, Alaska, USA

Abstract

One of the most extensive frozen ground engineering studies in the world was started in Alaska in 1945. It was led by the U.S. Army Corps of Engineers and has remained the most ambitious project in frozen ground engineering research. The name of the project was "Investigation of airfield construction in arctic and subarctic regions." This paper presents a review of some parts of this project, which paved the way for numerous further studies.

Keywords: aerial photographs interpretation; foundations design and construction; n-factor; permafrost; thermal conductivity.

Introduction

One of the most extensive frozen ground engineering research programs was conducted 60 years ago in Alaska. It was led by the St. Paul District of the U.S. Army Corps of Engineers and was a most ambitious project in frozen ground engineering research. The purpose of the program was "to determine design methods and procedures to be used in military construction in arctic and subarctic regions" (U.S. Army 1950). This goal was achieved, and results of the studies were widely used in military manuals for arctic and subarctic construction. The results have also contributed to contemporary knowledge on permafrost, and some of these became a starting point for numerous later studies.

The program integrated direct frozen ground engineering with supplementary studies. The direct frozen ground engineering studies consisted of the construction of sections of runways, with different types of embankments, insulation, and surfaces, and buildings with different types of foundations. These construction sections were conducted at Fairbanks Research Area with "the purpose of providing an opportunity to observe various types of structures erected on permafrost under conditions that would be known and recorded from the beginning to the conclusions of operations" (U.S. Army 1950). The study also included the monitoring of existing runways and buildings, and their impact on permafrost. These existing facilities were at the Northway Airfield, Eielson Air Force Base (near Fairbanks), and Ladd Air Force Base (Fort Wainwright).

The supplementary studies included development of methods for aerial photographic reconnaissance in permafrost regions, applicability of geophysical methods to permafrost investigations, thermal properties of frozen and unfrozen soils, and literature research.

In this paper, we describe the most notable studies and their results, which were presented in 1950 within the comprehensive report (U.S. Army 1950) by the Corps of Engineers and in several reports on the supplementary studies.

Design and Construction Studies at Fairbanks Research Area

Numerous experiments were conducted at the Fairbanks Research Area. They included the evaluation of terrain modifications (Area No. 1), different types of runways (Area No. 2), and different building foundations (Area No. 3) in the permafrost region.

Area No. 1 included three 61 m by 61 m sections of different surface conditions. Section A was an undisturbed area with natural vegetation. In Section B, trees and bushes were removed, but the surface vegetation cover was left. In Section C, all vegetation was removed with the top 40 cm of soil. Then another 10 m by 30 m section, Section D, had all the vegetation removed with the top 30 cm of soil. This section was then backfilled with sand to the original ground line and paved with 15 cm of concrete. Then the section was divided in three equal sections where two were colored white and black, and the third was left its natural gray color.

Monitoring of permafrost conditions in Area No. 1 included observations of the ground temperature to a depth of 10 m, the supra-permafrost ground water level, the vertical movement of the soil surface, probing to the permafrost table, and testing of the soil moisture content and density.

The report presents mean monthly soil temperature data for Sections A, B, and C from July 1946 to November 1948, and the positions of the permafrost table in 1947 and 1948. The studies in Area No. 1 are well-known from Linell (1973), who presented 17 years of observations of the positions of the permafrost table in Sections A, B, and C. Recent positions of the permafrost table are evaluated by Douglas et al. (in these proceedings).

The soil temperature data for Section D covered only one year of observations. At the end of summer 1948, the depth to the permafrost table under each part of Section D was about 2.5 m. The authors of the report concluded that "concrete surface color whether black, gray or white under the test conditions has no appreciable effect on depth of

thaw" (U.S. Army 1950). It seems to us that the period of observation was too short for such conclusion.

Area No. 2 included 26 runway test sections of approximately 250 m by 60 m each. The natural vegetation was removed from the site, and the upper soil was stripped to various depths from 0.3 m to 1.2 m. The thicknesses of embankment of test sections varied from 0.6 m to 3.6 m, with 1.2 m thickness for most sections. Two sections had gravel surfaces, while the others had asphalt or concrete surfaces. Some sections were insulated with 7.5 cm and 15 cm thick foamglas, 15 cm and 30 cm thick cell concrete, and 15 cm thick compacted moss. Fifteen sections were not insulated.

The data presented in the report on ground temperatures and soil freezing and thawing in the runway test sections cover only one year of monitoring and are of very limited value. However, one conclusion is worth mentioning: it was found that "the ground temperature below the insulation is cooler in summer and warmer in winter than if the insulation were not present. The net effect is that the mean annual ground temperature is about the same, whether or not insulation is used" (U.S. Army 1950). This conclusion has not appealed to many arctic engineers, and thermal insulation is still often considered as a trusted measure of permafrost protection under roads and airfields in any permafrost area. Nidowicz and Shur (1998) analyzed data presented in several works from Alaska, Canada, and Russia which also show that thermal insulation has either no effect or increases the mean annual soil temperature. Thermal insulation is effective in areas of cold permafrost because it decreases the depth of seasonal thawing and protects upper ice-rich permafrost, while at the same time, the increase in permafrost temperature does not impact the integrity of structures in these areas. In the discontinuous permafrost zone, thermal insulation does not protect permafrost from degradation. The permafrost protective effect of thermal insulation in any permafrost area is greatly increased with the addition of a soil cooling system, such as heat pipes or ventilated ducts. These cooling systems make the soil colder under thermal insulation in the winter, and thermal insulation decreases heat flow into the soil in the summer.

Eleven buildings were built in 1946–1947 in Area No. 3 to study the stability of different types of foundations. Five of them were built on gravel pads where the thickness ranged from 0.6 m to 1.8 m, with concrete or insulated wood floors placed on the ground. Two buildings had 60 cm high crawl spaces, where one of them had wood skirting. One building had an open crawl space that was 1.2 m high.

Building No. 11 was constructed on a gravel pad of 1.5 m thickness. It was based on a 48 cm thick concrete slab containing a layer of continuous hollow tile that was open to air on both sides. Ventilation of the foundation was not sufficient, and the permafrost thawed to a depth of 3.2 m under the center of the building in 1948. The monitoring data of the settlement of building corners in 1948 to 1964 were presented by Linell and Lobacz (1980). The maximum thaw settlement from 1948 to 1964 reached 75 cm. The buildings, also, were left unheated from 1957 to 1964 which did not stop the thaw settlement during this period.

Building No. 10 was built on piles with an open crawl space of 1.2 m. One pile at the southwest corner did not refreeze and frost jacked 18 cm during 1947–1957. Posts supporting two porches were installed in the active layer and frost jacked 40 cm in the same period (Linell & Lobacz 1980).

During initial observations covered by the report, it was found that seasonal vertical movement depends on the thickness of the gravel pads for buildings with floors placed on the ground. Movement was less than 2 cm for Building No. 4 constructed on a 1.8 m thick pad and more than 12 cm movement for Building No. 8 which was constructed on the natural surface. Data show this dependence greatly decreases when the thickness of the pad reaches 1.2 m.

Lobacz and Quinn (1966) analyzed the performance of buildings from their construction in 1946 until 1954, and found that the gravel pads did not protect the buildings from permafrost degradation and had "appreciable amounts of vertical settlement" (Lobacz & Quinn 1966). The thermal insulation of the floors slightly improved the foundations' integrity. They also found that buildings on piles with open crawl spaces performed well when "piles are firmly bonded in permafrost" (Lobacz & Quinn 1966).

The special project on the Navy monotube test piling was not successful. A steel pile of 18 m length and another steel pile of 12 m length were installed by steam thawing of the permafrost during November 13–20, 1947. The loading was concluded on December 12, 1947. It is possible that the method of pile installation was chosen because of the contemporary belief that "Piles cannot be driven into permafrost by the usual methods. It is therefore necessary to resort to a preliminary thawing of the ground by steam points" (Muller 1947). But the same source warned that "at a depth of 5 or 6 meters below the permafrost table the freezing of a pile to permafrost takes about a month and a half to 2 months. Only after that time can the pile be loaded with the calculated weight of the projected structure" (Muller 1947). Both statements do not specify the permafrost conditions for which they are applicable. At the test site, freezeback did not occur, and the piles experienced rapidly accelerating settlement, even after a part of the load was taken away.

The permafrost temperature at the site was close to 0°C, and only lack of experience can explain the chosen method of pile installation in warm permafrost and the pile loading shortly after the pile's installation. Even six months later, in June 1948, soil temperature was above 0°C throughout the length of both piles (U.S. Army 1950). The experiment did produce one interesting result, where thermistors were installed in the pipes attached to the piles showed an increase in soil temperature during the settlement of the piles.

The full history of the Fairbanks Research Area was recently briefly described by Henry and Bjella (2006).

N-Factor

One of the long-lasting results of the studies at the Fairbanks Research Area is the way of correlating air and

surface temperatures. "Since air temperatures are generally available and surface temperatures are not, a study has been made of data from Fairbanks, Alaska to determine the relation between a thawing or freezing index calculated from air temperature and indexes calculated from the temperatures of different types of surfaces with the thermocouples so installed that they were partially embedded in the surfaces" (U.S. Army 1950, Carlson 1952). As a result of the Corps of Engineers studies, the correlation factor, which is now known as the n-factor, was proposed to evaluate a surface thawing or freezing index from the known air thawing of freezing index. With time, the n-factor approach became a very powerful tool in arctic engineering and permafrost studies.

The set of data for the correlation factors (n-factors) for different types of surfaces was developed on the basis of surface temperature measurements at the Fairbanks Research Area and air temperature measurements at the Weeks Airfield in 1947 and 1948. The correlation factors founded in the study were later included in countless works. We highly value this part of the study, as well, because it had a great impact on the development of engineering methods of the evaluation of soil freezing and thawing and permafrost methodology. We should observe that the air and surface temperature measurements were taken at two separate sites, which could have compromised the data, especially for winter conditions. The Fairbanks Research Area is on a gentle south-facing slope, and the Weeks Airfield was located on the flat surface of a low terrace of the Chena River. The distance between sites was 5 km, and the difference in elevation was about 10 m. This elevation difference in Fairbanks, which is famous for winter inversions, can partly explain why the winter n-factors for concrete and asphalt surfaces without snow were as low as 0.7. We also suspect that the snow was not completely plowed from the thermistor locations to protect them from damage.

Permafrost Existence and Thermal Offset

In the Russian book, *General Permafrost Studies,* by Sumgin et al (1940), the authors of the report identified the following equation as "a definite contribution" which describes "the conditions necessary for the existence of permafrost" (Main Report 1950):

$$k_f T_f \tau_f > k_u T_u \tau_u, \quad (1)$$

f = factors in the equation during freezing
u = factors during thawing
k = coefficient of thermal conductivity
T = average temperature of the ground at depth h
τ = time during freezing or thawing.

The equation (1) was found by Krylov (1934) from the Stephan equation for soil freezing and thawing, with an assumption that permafrost exists if freezing is greater than thawing.

$$\sqrt{\frac{2k_f(T-T_f)\tau_f}{L}} > \sqrt{\frac{2k_u(T-T_f)\tau_u}{L}} \quad (2)$$

At sites where the bottom of the active layer merges with the permafrost table, the depth of the seasonal freezing is equal to the depth of the active layer defined by seasonal thawing. Kudriavtsev (1954) named the freezing associated with the left part of the equation (1) as the potential freezing. The authors of the comprehensive report finally presented the equation (3) in the following form (U.S. Army 1950, Carlson 1952):

$$\frac{k_f}{k_u} > \frac{I}{F} \quad (3)$$

I = thawing index at the soil surface,
F = freezing index at the soil surface.

The authors of the report noticed that the ratio in the left part of equation (3) is greater than one, if the thermal conductivity of soil in the frozen state is greater than its thermal conductivity in the unfrozen state. They concluded that "permafrost can exist even though the thawing index is greater than the freezing index" (U.S. Army 1950).

The greater the thermal conductivity of the frozen soil than the unfrozen soil also leads to the decrease of the soil mean temperature at the bottom of the active layer in comparison with the temperature at the soil surface. Kudriavtsev (1954) used the Russian term *temperaturnaya sdvizhka* to describe this effect. Burn (1988) and, Romanovskiy & Osterkamp (1995) use the term *thermal offset*, and Shur & Jorgenson (2007) literally translated the Russian term as *the thermal shift*. Kersten (see below) showed that the thermal conductivity of coarse well-drained soils in the frozen state can be smaller than their thermal conductivity in the thawed state. In this case, the disparity (3) should be rewritten as

$$\frac{k_f}{k_u} < \frac{I}{F} \quad (4)$$

From (4) we can conclude that permafrost can be absent even though the freezing index of the soil surface is greater than the thawing index. In this case, the thermal offset (thermal shift) has the opposite sign. To be consistent, we should consider the negative thermal offset (which is usually referred to as the thermal offset) and the positive thermal offset.

Thermal Properties of Frozen and Unfrozen Soils

The Corps of Engineers contracted the research of the thermal properties of soil, with objectives "to determine under varying conditions of temperature, moisture, bulk density, and composition the thermal properties of representative soils and organic material from Alaska" (Kersten 1949). The study was conducted at the Oak Street Laboratories of

the Engineering Experimental Station of the University of Minnesota. Miles S. Kersten, Associate Professor of Civil Engineering, was in immediate charge of the investigation. Procedures and results were presented in a report (Kersten 1949) and numerous publications since then.

Soils from Alaska included Chena River gravel, sand, silty clay loam, silt loam, and peat from Fairbanks; sand and silt loam from Northway; and clay from Healy. To cover a wider range of soil properties, some soils from other regions were also studied.

Soil was placed in a hollow cylinder for thermal conductivity tests. Boundary conditions at the inside face of a hollow soil cylinder were kept at a constant heat flow. Constant temperature was the boundary condition on the outside face. Temperature was measured at two points in the inside face and two points at the outside face. To evaluate the coefficient of thermal conductivity the following equation was used:

$$q = \frac{\frac{k(A_2 - A_1)}{\ln(A_2 / A_1)}(T_1 - T_2)}{r_2 - r_1} \quad (5)$$

where:
q = measured rate of heat flow,
k = coefficient of thermal conductivity,
A_2 = area of outside face of soil cylinder,
A_1 = area of inside face of soil cylinder,
T_1 = temperature at inside face,
T_2 = temperature at outside face,
r_2 = outside radius,
r_1 = inside radius.

This equation can be transformed into the commonly used equation, written for one unit of length:

$$q = \frac{2\pi k(T_1 - T_2)}{\ln(r_2 / r_1)} \quad (6)$$

The equations define steady-state heat flow between two cylindrical surfaces having constant temperatures consequently T_1 and T_2. This is not the case for the test conditions dealing with a composed hollow cylinder with prescribed heat flux at one surface and prescribed temperature at the other. To satisfy the boundary conditions expected in equations (5) and (6), the heat flow (voltage and amperage of the heater) at the inner face was manually adjusted to reach the desired temperature at this face of the hollow cylinder filled with soil. Measurements were taken when temperature variations were less than 1% during a five-hour period.

The thermal conductivity of soils was studied using a wide range of soil densities and water contents at average temperatures of 70, 40, 25, and 20°F. The temperature difference between sides of the soil cylinder was 10°F. This means that for the average temperature of 25°F, it was 30°F on the hot face of the soil cylinder and 20°F on the cold face.

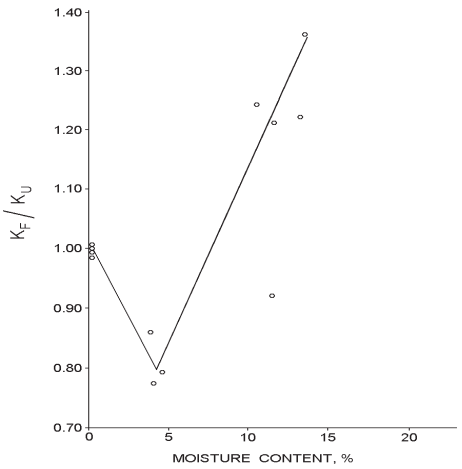

Figure 1. Ratio of soil thermal conductivity in frozen state to thermal conductivity in unfrozen state (from Kersten 1949).

After the tests, the moisture content of sandy soils at the cold side of the specimens was greater by a few percentages than on the warm side, and some mass transfer occurred during the tests. This could be driven by extremely high temperature gradients which were about 6°C over 5 cm.

Experimental data show that over a wide range of soil moisture content, the ratio of soil thermal conductivity in a frozen state is greater than the thermal conductivity of the same soil in an unfrozen state. This is because the thermal conductivity of ice is four times greater than the thermal conductivity of water. This rule is practically always applicable to fine soils. Kersten also found that, at low water content, the thermal conductivity of unfrozen soil is greater than the thermal conductivity of frozen soil, and the ratio k_f/k_{un} is less than one (Fig. 1). This was because of the separation of soil particles and the disturbance of thermal contacts between particles by ice during freezing, and an increase in soil porosity (Gavriliev 2004). It is a very rare situation for fine soils, but it is a common one for well-drained coarse soils.

Thermal conductivity of a few soils were compared (Kersten 1949) with limited data obtained by the Corps of Engineers New England Division, Boston, by a different method on the same soils. Values found by the University of Minnesota are less than those of the Boston study, but the difference does not exceed 10%.

Kersten did not test the frozen soils in their natural state. Soils from Alaska were remolded, and different water contents were assigned that were limited by saturation. In natural conditions, permafrost soils often have water content sufficiently greater than soils studied by Kersten. This limitation was later overcome by Slusarchuk and Watson (1975). Extensive research of thermal conductivity of surface covers was done by Gavriliev (2004).

Aerial Photo Interpretation for Permafrost Identification

As a part of the research, the U.S. Army Corps of Engineers funded and provided field support of the studies

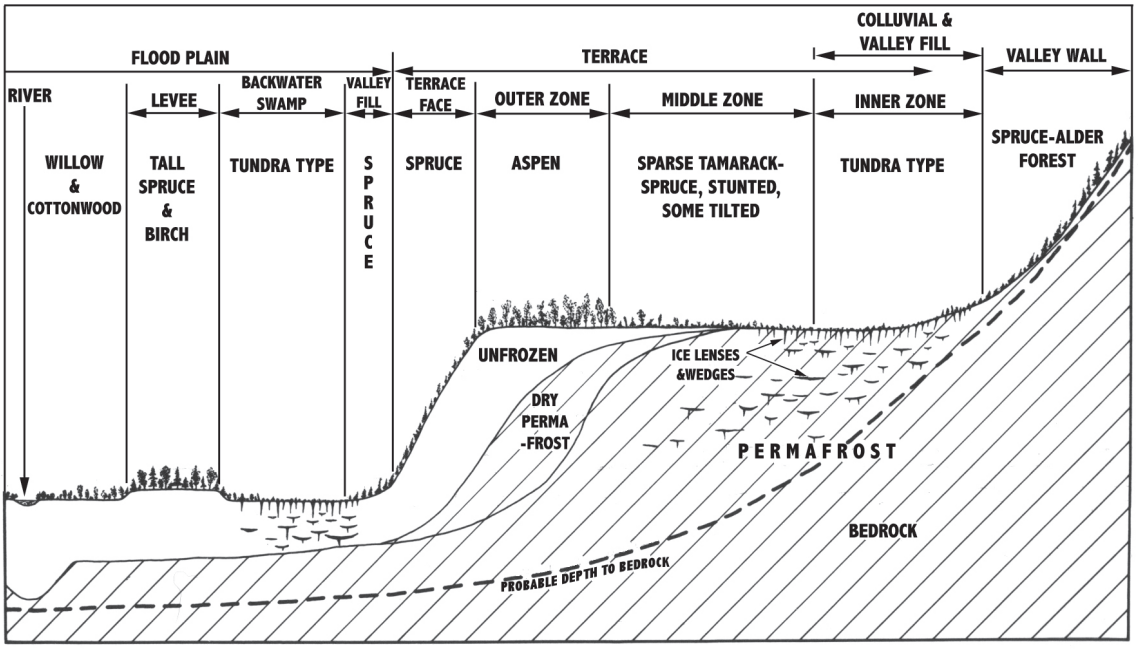

Figure 2. Possibly the first permafrost-relief-vegetation sequence (from Frost 1950).

by Purdue University. The purpose was to evaluate soils and permafrost conditions in Alaska by means of aerial photographs. Colonel Yoder, one of the leaders of the project, described expectations in the following words: "In relatively undeveloped regions, such as in the Territory of Alaska, aerial photographs can be used to great advantage in locating airports, highways, railroads, bases, etc. In a few hours' time, a general engineering soil map can be produced which will show the good, poor, and intermediate soil areas evaluated on the basis of anticipated performance of engineering structure. Thus, the poor soil areas can be eliminated almost entirely by study of the aerial photographs, and the field investigation can be concentrated on those areas best suited to construction" (Frost 1950).

Scientists from Purdue University spent five summers in Alaska, gathering information which helped to develop techniques of aerial photograph interpretation. Field work was conducted in Interior Alaska, Seward Peninsula, Yukon-Kuskokwim Delta, Arctic Slope, and Arctic Coastal Plain. "When possible, such studies were made by 'on the spot' sampling with the aerial photographs in hand" (Frost 1950). As a result of the field studies and analysis of the field data, aerial photo patterns related to permafrost conditions were developed. They include vegetation, topography, drainage, erosion, and some direct indicators of permafrost conditions. With the information from the aerial photographs and ground reconnaissance, engineering soils maps can be made for finding suitable construction sites. These maps can shorten the preliminary investigation and eliminate the need for costly, extensive preliminary drilling (Frost 1950). This work became widely known from the extensive paper presented by R.E. Frost in a symposium, *Frost Action in Soils,* and published in the proceedings of this symposium (Frost 1952).

The report compiled by Frost (1950) for the Corps of Engineers consists of several examples of aerial photographs and descriptions of land forms and vegetation in relation to permafrost in Alaska. Figure 2, from the report, presents the typical profile through a river valley in the discontinuous permafrost zone showing patterns of permafrost existence and absence in relation to relief and vegetation. It is possible that this figure is the first permafrost profile of such kind in permafrost literature.

Frost's report outlines a comprehensive approach to applications of aerial photography to permafrost studies. It stimulated similar studies in Russia (Protas'eva 1967) and Canada (Brown 1964, 1966). It was also the first step in the series of studies which led to the effective application of terrain unit analysis to permafrost investigations for the Trans-Alaska Pipeline. Kreig and Rigert (1982) improved and effectively applied aerial photo interpretation and application of the terrain analysis to geotechnical investigations for the pipeline, with the acknowledgement Frost's report. Roger Brown (1970) in his book, *Permafrost in Canada*, also acknowledged the pioneering studies by Purdue University in Alaska and later in Canada, which "justified the belief in the applicability of airphoto interpretation methods for preliminary site surveys in permafrost areas" (Brown 1970). The method, which was initially solicited for engineering investigations for airfields in the Arctic, finally became an interdisciplinary tool of arctic and subarctic scientific studies and applied investigations of different scales and for multiple purposes.

Stoeckeler, who worked with the Purdue University team, studied a relationship between permafrost and vegetation. He found that vegetation is not a good indicator of permafrost presence in areas where the permafrost table is lower. "The presence of the permafrost table at a depth of 6 feet or more from the ground surface has little or no deleterious effect on

tree growth, with the possible exception to deep rooted trees like balsam poplar, cottonwood, and jack pine. Therefore, vegetation alone can be employed only as an indicator of soil conditions to a relatively shallow depth" (Stoeckeler 1949). This message, from 1949, still remains relevant to permafrost and many other studies in the discontinuous permafrost zone.

Conclusions

In the 1940s, the St. Paul District of the U.S. Army Corps of Engineers carried out pioneering research. This paved the way for future intensive research of frozen ground engineering in Alaska, as well as around the world.

Investigations by the Minnesota and Purdue Universities were funded by the Corps of Engineers for specific engineering tasks, as parts of the project. Their immense impact on permafrost studies over the last 60 years proved that there is nothing more valuable than good science.

Acknowledgments

We wish to thank Jerry Brown, Hugh French, and Mikhail Kanevskiy for helpful discussions and advice.

This work was supported by the Alaska EPSCoR, (NSF award 0701898 and NSF grant ARC 0454939). Any opinions and findings expressed in this material are those of the authors and do necessarily effect the views of the NSF.

References

Brown, R.J.E. 1964. *Permafrost Investigations on the Mackenzie Highway in Alberta and Mackenzie District*. Ottawa: National Research Council of Canada, Division of Building Research, 36 pp.

Brown, R.J.E. 1966. Influence of vegetation on permafrost. *Proceedings of the Permafrost International Conference, Lafayette, Indiana, November 11–15, 1963:* 20-25.

Brown, R.J.E. 1970. *Permafrost in Canada.* Toronto: University of Toronto Press, 234 pp.

Burn, C.R. & Smith, C.A.S. 1988. Observations of the thermal offset at several sites near Mayo, Yukon Territory, Canada. *Arctic* 41(2): 99-104.

Frost, R.E. 1950. *Evaluation of soils and permafrost conditions in the Territory of Alaska by means of aerial photographs.* USA: U.S. Army: 110 pp.

Frost, R.E. 1952. Interpretation of permafrost features from airphotos. *Frost Action in Soils: A Symposium, Highway Research Board Special Report No. 2*. Washington, DC: National Research Council, 223-246.

Gavriliev, R.I. 2004. Thermal properties of soils and surface covers. In: D.C. Esch (ed.), *Thermal Analysis, Construction, and Monitoring Methods for Frozen Ground.* Reston: American Society of Civil Engineers, 277-294.

Henry, K.S & Bjella, K. 2006. History of the Fairbanks permafrost experiment station, Alaska. *Proceedings of the 13th International Symposium on Cold Regions Engineering 2006: Current Practices in Cold Regions Engineering, Orono, Maine, July 23–26, 2006:* 11 pp.

Kersten, M.S. 1949. *Final report laboratory research for determination of the thermal properties of soils.* St Paul, MN: University of Minnesota, 227 pp.

Kreig, R.A. & Reger, R.D. 1982. *Air-photo analysis and summary of landform soil properties along the route of the Trans-Alaska Pipeline System*. Fairbanks: Alaska Division of Geological & Geophysical Surveys, 149 pp.

Krylov, M.M. 1934. The thermal analysis of soil freezing. *Engineering bulletin* 10: 53-59 (in Russian).

Linell, K.A. 1973. Long-term effects of vegetation cover on permafrost stability in an area of discontinuous permafrost. *Proceeding of the Second International Conference on Permafrost, Yakutsk, U.S.S.R., July, 13–28, 1973*: 688-693.

Linell, K.A. & Lobacz, E.F. (eds.). 1980. *Design and construction of foundations in areas of deep seasonal frost and permafrost*, *CRREL Special Report 80-34*. Hanover: U.S. Army Cold Regions Research and Engineering Laboratory, 310 pp.

Lobacz, E.F. & Quinn, W.F. 1966. Thermal regime beneath buildings constructed on permafrost. *Proceedings of the Permafrost International Conference, Lafayette, Indiana, November 11–15, 1963:* 247-252.

Muller, S.W. 1947. *Permafrost or Permanently Frozen Ground and Related Engineering Problems.* Ann Arbor: J.W. Edwards, 230pp.

Nidowicz, B. & Shur, Y. 1998. Pavement thermal impact on discontinuous permafrost. *Proceedings of 9th International Conference on Cold Regions Engineering: Cold Regions Impact on Civil Works, Duluth, Minnesota*, *September 27–30, 1998*: 34-45.

Protas'yeva, I.V. 1967. *Aeromethods in Geocryology*. Moscow:,Nauka, 196 pp (in Russian).

Romanovsky, V.E. & Osterkamp, T.E. 1995. Interannual variations of the thermal regime of the active layer and near-surface permafrost in Northern Alaska. *Permafrost and Periglacial Processes* 6(4): 313-335.

Shur, Y.L. & Jorgenson M.T. 2007. Patterns of permafrost formation and degradation in relation to climate and ecosystems. *Permafrost and Periglacial Processes* 11(1): 7-19.

Slusarchuk, W.A. & Watson, G.H. 1975. Thermal conductivity of some ice-rich permafrost soils. *Canadian Geotechnical Journal* 12: 413-424.

Stoeckeler, E.G. 1948. *Identification and evaluation of Alaskan vegetation from airphotos with reference to soil, moisture and permafrost conditions: A preliminary paper*. St. Paul: U.S. Army, 103 pp.

Sumgin, M.I., Kachurin, S.P., Tolstikhin, N.I. & Tumel', V.F. 1940. *General permafrost science*. Moscow: U.S.S.R. Academy of Sciences, Moscow-Leningrad, 340 pp.

United States Army, Corps of Engineers, St. Paul District 1950. Main Report and Appendix III, *Comprehensive report, investigation of military construction in arctic and subarctic region: 1945–1948*. USA: U.S. Army, 68 pp. & 22 pp.

High-Resolution Surface and Subsurface Survey of a Non-Sorted Circle System

Ronald Daanen
Geophysical Institute, University of Alaska Fairbanks, Fairbanks, Alaska
Vladimir Romanovsky
Geophysical Institute, University of Alaska Fairbanks, Fairbanks, Alaska
Donald (Skip) Walker
Department of Biology and Wildlife, University of Alaska Fairbanks, Fairbanks, Alaska
Mike LaDouceur
Geophysical Institute, University of Alaska Fairbanks, Fairbanks, Alaska

Abstract

Non-sorted circle patterned ground features are abundant in the Arctic tundra. These features show large variability in active layer depth in summer and heave in winter. There is a lot of research devoted to measuring active layer depth, yet little is known about small-scale variability of the active layer in patterned ground systems. The active layer is sometimes used as an indicator of a warming climate which is not always correct. The active layer depth varies from year to year as it freezes and thaws. It also expands and shrinks as it accumulates ice and loses ice. We have conducted two surveys, one in the spring of 2007 and one in the summer of 2007. The surveys were taken from the Biocomplexity research site near Franklin Bluffs, North Slope Alaska. We were able to reference the surveys points to a deep well located near the site that is used for deep-permafrost temperature sampling. The well is 60 m deep and, therefore, permanently anchored in the permafrost. The surface elevation is recorded in a 25 cm dense grid over an area of 10 by 10 m. The plot contains approximately 20 non-sorted circles. The average surface elevation in winter was 85 cm below the reference point, and in the summer it was 97 cm below the reference point. This means that there was a 12 cm surface elevation difference. We suggest multiple mechanisms that could explain this amount of heave. Current active layer development shows a decreasing trend (smaller active layers over time) with long-term observations near our site, in contrast to the annual average soil temperatures that are increasing. Reasons for a decreasing trend may include a lack of a warming trend in summer, changes in thermal conditions, and greening of the Arctic, which may lead to increased transpiration rates and absorption of incoming shortwave radiation. Long-term observation of surface movement in this grid will reveal more detailed information on the behavior of ice accumulation in the active layer.

Keywords: active layer; non-sorted circles; permafrost; snow; soil; survey.

Introduction

During the annual cycle, arctic soils form an active layer in the summer that refreezes during the fall and winter. In this paper, we present a high-resolution elevation dataset of a non-sorted circle system on continuous permafrost near Franklin Bluffs, Alaska. Non-sorted circles are defined as "semi barren areas in the tundra that lack a border of stones" (Washburn 1956). The non-sorted circle system is defined here as interacting areas of vegetated and semi-barren surfaces. The system can be as small as a single non-sorted circle with its surrounding vegetation. This vegetation zone can be anywhere from 10 cm to 10 m. The vegetated surface is generally underlain by a well-developed, organic layer several centimeters thick.

Besides these data we also provided information on the soil climate (soil temperature and moisture content) at the time the survey was done, as well as historical climate variation from the area, to put the elevation data from the survey in perspective.

The survey helped our understanding of the processes of frost heave and thaw settlement. Frost heave and thaw settlement (consolidation) is scale dependent and can be viewed as one-dimensional on a landscape scale (Brown et al. 2000, Hinkel & Nelson 2003). The Circumpolar Active Layer Monitoring (CALM) sites are treated as a landscape scale measurement, where it takes many measurements to determine the average active layer depth for a region, to eliminate any local heterogeneity. On a smaller scale, however, it is a three-dimensional process. Small heterogeneities in topography, vegetation, and organic layer thickness, are observed at a typical plot scale of a 100 m^2. Micro climate at the soil surface generated by vegetation and micro relief has a strong effect on the soil surface energy balance. Soil climate, driving freezing and thawing processes, depends on: the micro climate above the soil, soil properties, wetness, and permafrost conditions below the active layer. Frost heave, driving freezing and thawing processes, causes the soil surface to move up and down within the season and between annual cycles. This aspect of movement of the soil surface is also called ice segregation and thaw settlement. These two processes are not monitored in the CALM sites and it is therefore not possible to monitor the loss and gain of ground ice within and between the annual cycles. This loss or gain of ground ice has only a limited effect on the active layer depth, due

Figure 1. Ice lens formation in silty clay loam.

to the limited amount of soil present in the ice rich transient layer (Pullman et al. 2007, Shur & Jorgenson 2007).

The annual soil surface movement is driven by frost heave or frost action, where the strongest movement is expected in frost susceptible soils. During freezing these soils accumulate ice in the form of lenses that form perpendicular to the temperature gradient (Cheng 1983, Kokelj & Burn 2005, Kokelj et al. 2007, Mackay 1983). This is also called secondary frost heave (Miller 1980). This process drives an expansion of the soil which exceeds the difference in density between water and ice. For secondary frost heave to take place water needs to flow to the freezing front, driven by cryostatic suction, to make this expansion possible (Daanen et al. 2007). The source of this water is still not resolved in the literature. Many models require an unlimited water supply to be able to generate the amount of frost heave observed. In a laboratory setup it was found that even without adding water to a frost susceptible soil during one dimensional freezing it was possible to generate heave beyond the expansion of water alone (Daanen unpublished data). This process can be explained as drying of the soil between the ice lenses (Daanen et al. 2007). The dry soil occupies a volume and in addition the ice occupies a volume.

The interannual soil movement is caused by segregated ice at the bottom of the active layer, which can cause thaw settlement (Pullman et al. 2007). Slow refreezing at the bottom of the active layer in the fall generally causes larger ice lenses compared to the upper active layer, where freezing is faster. Formation and loss of this ice depends on many of the same energy balance processes as mentioned above but in addition, it depends on variations in hydrological conditions between years (Kokelj & Burn 2005).

Soil surface movement is generally hard to detect due to a lack of a proper reference point in the tundra. Romanovsky (Walker et al. 2004) and Washburn (Washburn 1997) have used permafrost anchors as a reference point to measure the difference between frost heave in non-sorted circles and vegetated tundra. This method is good when the anchors are deep enough to prevent them from heaving out of the ground on a longer time span. Satellite observations through interferometry would be an option when data is available during a small window in the fall before freezing and spring if the signal is not distorted by the snowpack. Differences between seasons may be too small to detect. Global Positioning System (GPS) equipment could be used to identify the movement of the soil surface; however accuracy of the equipment in elevation differences is a concern (Berthling et al. 2003).

Methods

For this study we used a deep borehole casing as a reference point to survey our site with a total station, at a resolution of 25 cm. The borehole is 60 m deep (with at least 59 m anchored in permafrost) located near Franklin Bluffs along the Dalton Highway, Alaska. The site was part of a biocomplexity study "Biocomplexity associated with biogeochemical cycles in arctic frost-boil ecosystems," which ended in 2006 (Walker et al. 2004). The site can be described as "mesic" or "zonal" and therefore a good representation of the regions in terms of vegetation and soil climate conditions (Walker et al. 2004). The annual average air temperature in the region is -11.3°C. The silty clay loam soils at the site are frost susceptible and generate a lot of segregated ice lenses during freezing (Fig. 1).

These soils are capable of forming and sustaining non-sorted circles, for a more detailed description of the internal workings of these system we refer to Daanen et al. (2007). These non-sorted circles provide a heterogeneous soil and soil surface that causes a large spatial variability in the active layer depth and frost heave level (Kade et al. 2006, Walker et al. 2004). Due to the scale of the non-sorted circles we chose to survey our plot with a resolution of 25 cm to capture the smaller nuances of relief between the non-sorted circles and the surrounding tundra.

We surveyed the site with a Leica TPS400 series total station using the deep permafrost borehole as a reference point (±0.03 m). The first survey was done in the April of 2007 well before the onset of snowmelt. The second survey was done in August of 2007 near the point of maximum thaw depth. In addition to the soil surface survey we also measured the snow depth in winter and the thaw depth in the summer. Measurements of the air temperature, soil temperature, and soil moisture are collected at the site using a datalogger and presented later in the results section.

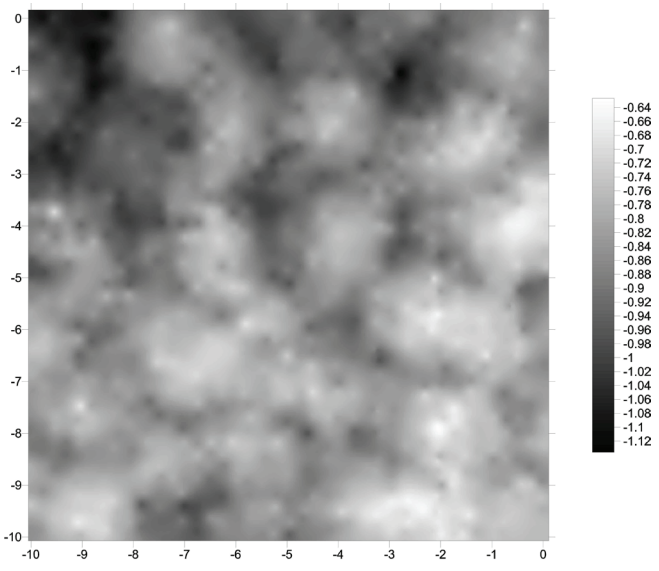

Figure 2. Elevation of the grid in winter relative to the fixed well casing (units are meters), April 26, 2007.

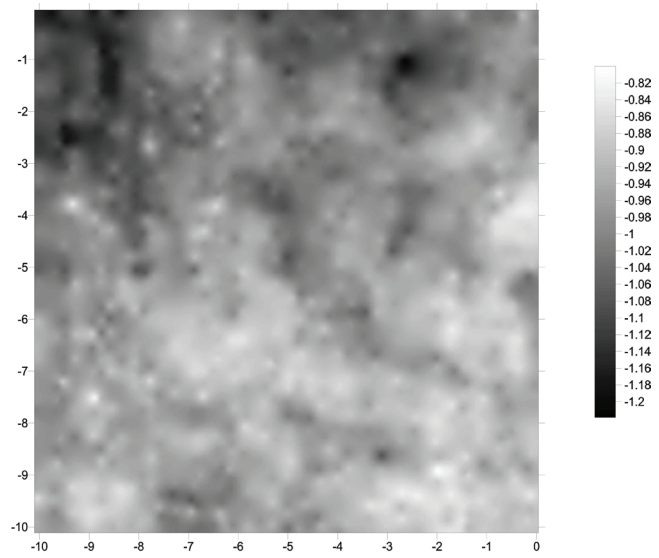

Figure 3. Elevation of the grid in summer August 27, 2007, relative to the fixed well casing (units are meters).

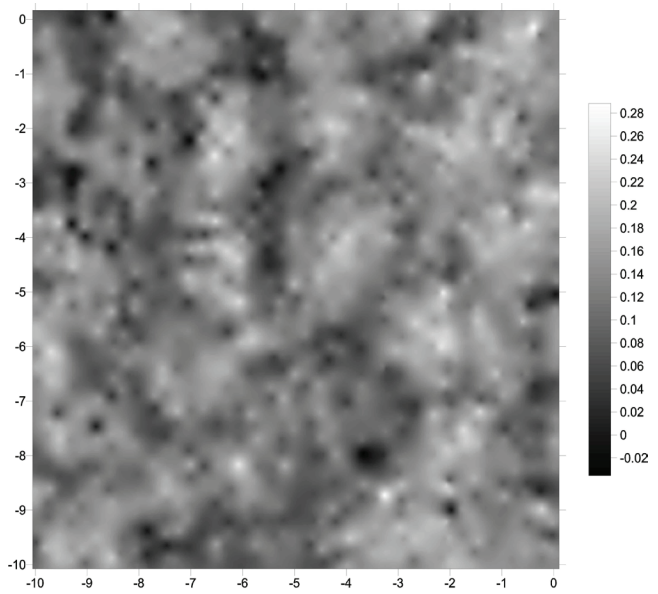

Figure 4. Elevation differences between summer and winter for the Franklin Bluffs site (units are meters). This plot represents frost heave.

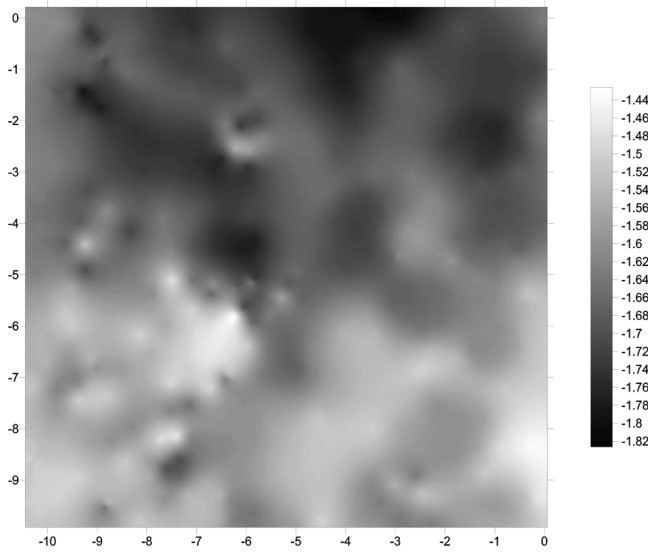

Figure 5. Permafrost table elevation for the site relative to the well casing on August 28, 2007 (units are meters)

Results

The spatial distribution of surface elevation in winter and summer is shown in Figure 2 and 3, respectively.

The winter results show a clear distribution of non-sorted circles in the lighter areas where the surface is raised above the inter circle areas (approximately 25 non-sorted circles within the domain of 10 x 10 m). Compared with Figure 3 the non-sorted circles are more visible due to increased frost heave in the circles. From Figure 3 the elevations still show the non-sorted circles, which implies that the elevation gain during freezing is not all lost during the summer thaw. Also visible from both illustrations is the gentle slope from upper left to lower right or from northwest to southeast.

We found that there was on average a 12 cm elevation difference between the summer and winter conditions. The scales on Figures 2 and 3 have an offset; for the lowest point 8 cm and the highest point 18 cm relative to the well casing.

The elevation difference for each observation point between the two data sets is given in Figure 4. Areas with the greatest difference are shown in the lighter shades. The non-sorted circles are also distinctly visible as areas with the greatest amount of annual frost heave.

The permafrost table elevation map is given in Figure 5.

The active layer depth is the difference between the surface elevation in summer and the permafrost table. A map of this depth is given in Figure 6. The average depth measured in the grid was 65.9 cm with a standard deviation of 7.8 cm. This depth is on track with active layer depths measured

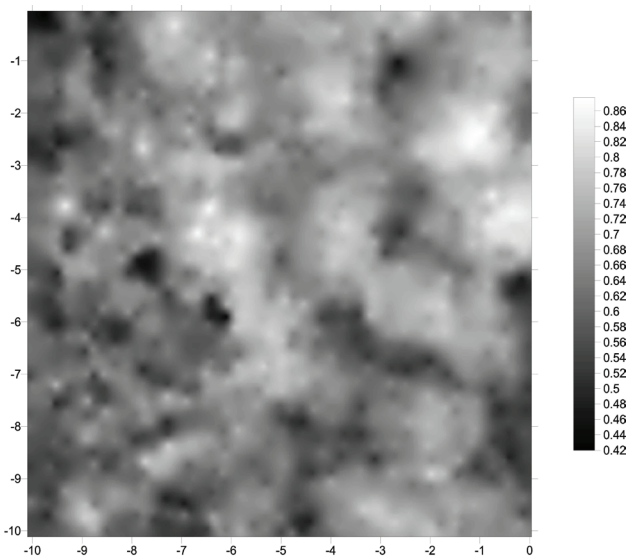

Figure 6. Active layer depth generated from the difference between the surface elevation and the permafrost table elevation (units are meters).

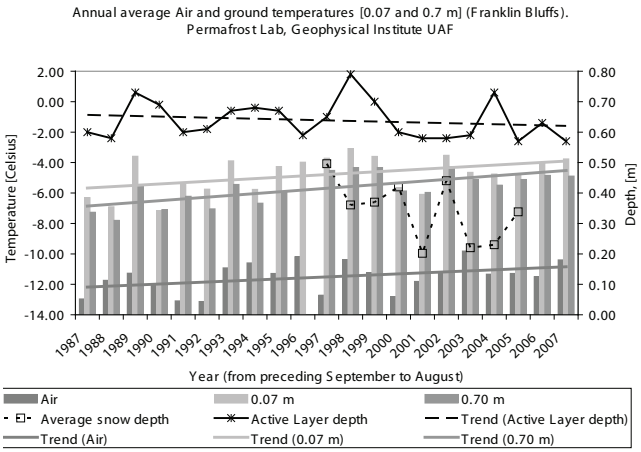

Figure 7. Long-term trends in active layer depth, air temperature, soil temperature (0.0 and 0.7 m), and snow depth near Franklin Bluffs, Alaska, from 1987–2007.

over a long period for the area as part of the long-term permafrost observation network (Fig. 7). Figure 7 also shows the trends in air and soil temperature over the past 20 years near Franklin Bluffs, Alaska. Over that period following the trend lines the annual average air temperature increased by 1.334°C, the soil at 0.07 m increased by 1.774°C, the soil at 0.7 m increased 2.34°C and the active layer depth decreased 0.036 m. Observed surface and permafrost temperatures north of our field site shows an even stronger warming trend then shown here (Romanovsky et al. 2008).

The active layer depth at the Franklin Bluffs site is measured by the permafrost laboratory at the Geophysical Institute as part of the long-term permafrost observation network. These measurements are taken in a larger 100 by 100 m grid surrounding the deep permafrost temperature well. The average thaw depth measured for long-term observations for Franklin Bluffs was 57.1 cm for August 28, 2007. The standard deviation for the larger grid was 10.4 cm.

To compare current soil conditions to recent years, we present daily air and soil temperature data in Figure 8. These data show that the winter was cooler then previous winters, and the summer was warmer than previous summers. Soil moisture data from the same period is given in Figure 9.

These soil moisture data suggest that the active layer was drying over the period presented here. This may lead to decreased frost heave during next season.

Discussion

The observed movement of the soil surface resulted in an average 12 cm of annual heave. These 12 cm cannot be explained by expansion due to phase change alone, because there is a limited amount of water in the active layer. The mineral soils have approximately 40% moisture by volume that would only result in 3 cm of heave during refreezing of the active layer. In non-frost-susceptible soils a similar amount of heave was observed in Canada (Mackay & Burn 2002). In our site, the soils are frost susceptible and water can move during freezing. However there are no obvious other large water reservoirs in the area that are close enough to make a difference to the amount of heave. The small slope to the site would drain the water just as fast as it would add water to the site. Our hypothesis is that there is additional water contained inside the soil profile, like water stored in small surface depressions and thick organic layers (inter circle area). It was observed during our spring measurements that there was no ice in the depressions where there is normally water in summer. Part of this water could have been absorbed by the freezing mineral soil, which is cooling more rapidly than the organic soils in between the non-sorted circles (Daanen et al. 2007). Additional heave can be attributed to drying of the soil as it freezes water from the soil segregates and forms ice lenses while the soil dries out. Air would replace water in the pore spaces and increase the volume of the soil column and the soil skeleton supports the overburden. Evidence was found that larger cracks within the active layer are ice free (Romanovsky pers. com.). A last reason for the low elevation of the soil surface could be attributed to the dry soil conditions during the summer survey see Figure 9. There are clay minerals in the soil profile that may have the potential to shrink as the soil dries. It has to be noted that the inter circle areas did not shrink significantly (Fig. 3).

The average active layer depths within the surveyed grid are 65.9 cm and the average active layer depth in the larger long-term grid is 57.1 cm. The difference can be explained by a difference in drainage, the surveyed grid is better drained due to small relief compared to the larger grid sampled. The draining of water would result in less ice buildup in the active layer and therefore less energy required for thawing the profile. Improved drainage also affects the vegetation at the site, which tends to have less moss than the wet vegetation plot down slope of the surveyed grid.

The active layer depth compared with other sites along

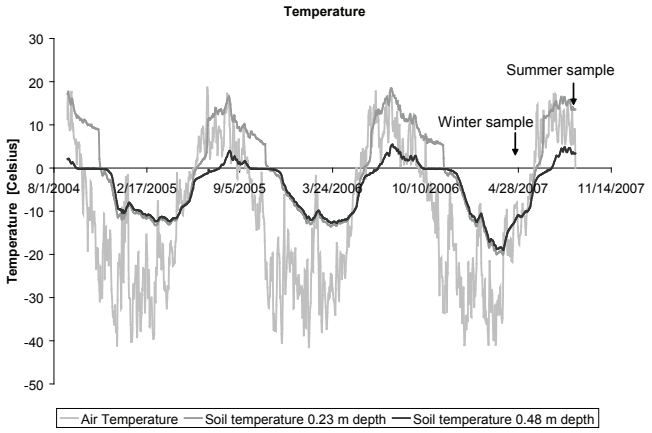

Figure 8. Air and soil temperature near the surveyed grid.

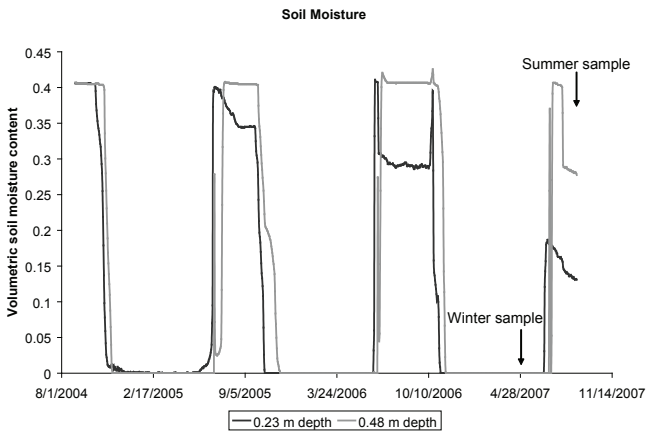

Figure 9. Soil moisture near the surveyed grid.

the Dalton Highway shows no trend that can be related to soil climate (Romanovsky et al. 2008). This is caused by differences in vegetation, with a much more developed vegetated/organic mat in the south compared to the vegetated/organic mat in the north.

The active layer depth over time shows a slight decreasing trend even though the soil temperature shows a trend toward warmer conditions (Fig. 7). There are many reasons to explain the trend. The summer air temperature did not increase. Average annual temperatures from the more recent period do not show a major trend toward warming conditions. The winter of 2006/2007 was colder (Fig. 8) than normal due to less snow compared with normal conditions, the snow data are not in the graph due to malfunction of the probe. The colder soils take longer to warm up and thaw. The dry conditions over the summer months had a reducing effect on the thermal conductivity of the organic layer. Another reason for a limited active layer depth could be loss of segregated ice near the bottom of the active layer. The potential loss of segregated ground ice is what we will measure during future surveys when we compare different years. The last reason is related to long-term observations of "greening" in the Arctic (Jia et al. 2003). Increased vegetation or Leaf Area Index (LAI) may be responsible for increased insulation (boundary layer), shading or transpiration at the site during the summer which leads to shallower thaw depths, even though the average annual temperatures have increased. Cooler conditions due to increased evapotranspiration have been observed on Banks Island where a constant wind made soils of southwest facing slopes cooler in summer (French 2007). In our situation an increase in LAI leads to increased radiation adsorption which causes increased transpiration rates. The spatial distribution of the vegetation in the non-sorted circle system shows that vegetated surfaces have shallower thaw depth.

Results from the survey also show the large variability in heave and thaw in a relatively small area of 10 x 10 m. Driven by increased insulation of the vegetation and underlying organic mat the energy flux through the surface is greatly reduced (Daanen et al. 2007). The heterogeneity on the soil surface causes temperature differences in the soil during freezing. This leads to cryostatic suction toward cooler areas where ice accumulates as the water freezes. Cryoturbation in the non-sorted circles reduces vegetation succession which keeps the non-sorted circles semi-barren and poorly insulated.

Conclusions

A high-resolution elevation survey of a non-sorted circle ecosystem near Franklin Bluffs, Alaska, shows substantial soil surface movement. The average elevation difference between summer and winter sampling is 12 cm. This heave cannot be explained with expansion of water due to phase change. Other explanations for the large difference are additional water from organic material froze as ice lenses in the mineral soil, ice lens formation in conjunction with soil freeze drying, and soil shrinkage due to dry conditions in summer.

The long-term active layer observations do not show a clear trend with average air and soil temperatures in our records. Some reasons suggested here are that the summer is not warming enough to affect the active layer, and the increased greening of the Arctic may lead to increased transpiration by the vegetation. More data is needed to identify a set of reasons that can fully explain the variability and behavior of the active layer system.

Heterogeneity of the soil surface vegetation causes heterogeneity in soil surface movement (frost heave) due to preferential ice accumulation in the semi-barren areas called non-sorted circles. The same vegetation pattern also causes preferential active layer development and thaw settlement.

Acknowledgments

This research was funded by the Polar Earth Science Program, Office of Polar Programs, National Science Foundation Grant No. ARC-0612533, OPP-0120736 ARC-0632400, and ARC-0520578.

References

Berthling, I., Etzelmuller, B., Eiken, T. & Sollid, J.L. 2003. The rock glaciers on Prins Karls Forland: corrections of surface displacement rates. *Permafrost and Periglacial Processes* 14: 291-293.

Brown, J., Nelson, F.E. & Hinkel, K.M. 2000. The circumpolar active layer monitoring (CALM) program research designs and initial results. *Polar Geography* 3: 165-258.

Cheng, G. 1983. The mechanism of repeated-segregation for the formation of thick layered ground ice. *Cold Regions Science and Technology* 8: 57-66.

Daanen, R.P., Misra, D. & Epstein, H.E. 2007. Active-layer hydrology in non-sorted circle ecosystems of the arctic tundra. *Vadose Zone Journal (accepted)*.

French, H.M. 2007. *The Periglacial Environment*. West Sussex, Chichester: Wiley.

Hinkel, K.M. & Nelson F.E. 2003. Spatial and temporal patterns of active layer thickness at Circumpolar Active Layer Monitoring (CALM) sites in northern Alaska, 1995-2000. *Journal of Geophysical Research-Atmospheres* 108 (D2).

Jia, G.S.J., Epstein, H.E. & Walker, D.A. 2003. Greening of arctic Alaska, 1981-2001. *Geophysical Research Letters* 30(20).

Kade, A., Romanovsky, V.E. & Walker, D.A. 2006. The n-factor of nonsorted circles along a climate gradient in Arctic Alaska. *Permafrost and Periglacial Processes* 17(4): 279-289.

Kokelj, S.V. & Burn, C.R. 2005. Near-surface ground ice in sediments of the Mackenzie Delta, Northwest Territories, Canada. *Permafrost and Periglacial Processes* 16(3): 291-303.

Kokelj, S.V., Burn, C.R. & Tarnocai, C. The structure and dynamics of earth hummocks in the subarctic forest near Inuvik, Northwest Territories, Canada. *Arctic Antarctic and Alpine Research* 39(1): 99-109.

Mackay, J.R. 1983. Downward water movement into frozen ground, western arctic coast, Canada. *Canadian Journal of Earth Sciences* 20: 120-134.

Mackay, J.R. & Burn, C.R. 2002. The first 20 years (1978-1979 to 1998-1999) of active-layer development, Illisarvik experimental drained lake site, western Arctic coast, Canada. *Canadian Journal of Earth Sciences* 39(11): 1657-1674.

Miller, R.D. 1980. *Freezing phenomena in Soil. Applications of Soil Physics*. New York: Academic Press, 254-299.

Pullman, E.R., Jorgenson, J.C. & Shur, Y. 2007 Thaw Settlement in Soils of the Arctic Coastal Plain, Alaska, *Arctic, Antarctic, and Alpine Research* 39(3): 468-476.

Romanovsky, V.E., Marchenko, S., Daanen, R.P., Sergeev, D.O. & Walker, D.A. 2008. Soil climate and frost heave along the Permafrost/Ecological North American Arctic Transect. *Proceedings of the Ninth International Conference on Permafrost*, *Fairbanks, Alaska, June 29–July 3, 2008* (this proceedings).

Shur, Y.L. & Jorgenson, M.T. 2007. Patterns of permafrost formation and degradation in relation to climate and ecosystems, *Permafrost and Periglacial Processes* 18(1): 7-19.

Walker, D.A., Epstein, H.E., Gould, W.A., Kelley, A.M., Kade, A.N., Knudson, J.A., Krantz, W.B. Michaleson, G., Peterson, R.A., Ping, C.L., Raynolds, M.A., Romanovsky, V.E. & Shur, Y. 2004. Frost-boil ecosystems: complex interactions between landforms, soils, vegetation, and climate. *Permafrost and Periglacial Processes* 15: 171-188.

Washburn, A.L. 1956. Classification of patterned ground and review of suggested origins. *Geological Society of America Bulletin* 67: 823-866.

Washburn, A.L. 1997. *Plugs and Plug Circles; a Basic Form of Patterned Ground, Cornwallis Island, Arctic Canada; Origin and Implications*. Seattle, WA, United States (USA): University of Washington, Quaternary Research Center.

Effect of Adsorbed Cations on Unfrozen Water in Silty Soil as Determined Using the NMR Method

Margaret M. Darrow
University of Alaska Fairbanks
Scott L. Huang
University of Alaska Fairbanks
Satoshi Akagawa
Hokkaido University
Go Iwahana
Hokkaido University

Abstract

To investigate adsorbed cations effects on the unfrozen water in frozen soil, laboratory experiments were conducted on Hanover silt. Monovalent and divalent cation treatments were prepared by exchanging the soil's adsorbed cations in saturated salt solutions. Laboratory experiments included measuring unfrozen water content with pulse NMR, T2 relaxation time, ζ-potential, and specific surface area. T2 relaxation time provides insight into unfrozen water changes during freezing. As the soil temperature decreases from -0.2°C to -2°C, the T2 net magnetization signal strength decreases rapidly, and subsequently levels off for temperatures colder than -2°C. This may indicate a reduction in the mobility of unfrozen water, as it is restricted under the influence of surface potential. Monovalent cation-treated samples have shorter T2 relaxation times than divalent cation-treated samples, suggesting less mobility of unfrozen water in monovalent-saturated soil. The monovalent cation-treated samples also demonstrated greater ζ-potentials, resulting in thicker unfrozen water films.

Keywords: cation; frozen soil; mobility; NMR; T2; unfrozen water; ζ-potential.

Introduction

The presence of unfrozen water in frozen soil is an integral part of frost heave theory, permafrost studies, and frozen ground engineering. Since unfrozen water was first identified by Bouyoucos (1917, 1920), numerous different methods have been used to measure it. Tice et al. (1978, 1982) presented the nuclear magnetic resonance (NMR) method as a viable technique to measure the unfrozen water content. While the NMR method has been used by these and other researchers to quantify unfrozen water, no reference has been made to spin-spin relaxation measurements (T2) or their meaning as related to the behavior of unfrozen water in frozen soil.

As part of a larger research project, we investigated the unfrozen water content using the NMR method, ζ-potential, and other chemical and mineralogical properties of natural soil and its associated cation-treated samples. In this paper, we present NMR free-induction decay (FID) data and spin-spin relaxation (T2) data for a silty soil, and investigate the effects of cation treatments upon T2 relaxation time and ζ-potential.

Methods

Soil preparation

Hanover silt loam (HS) was sieved following the procedure implemented by Rieke et al. (1983), and all organic matter was removed from the original soil sample. This sieved soil is referred to as the "Baseline" (BSLN) sample. The results of a semi-quantitative x-ray diffraction (XRD) analysis indicated that the HS BSLN sample contained illite/mica, kaolinite, chlorite, and interlayered smectite, as well as other non-clay mineral species. The total percentage of phyllosilicates in the HS BSLN sample was 20.8%. In order to investigate the effects of surface chemistry on the unfrozen water content, cation treatments were applied to the BSLN soil. Four different salts, magnesium chloride ($MgCl_2$), calcium chloride ($CaCl_2$), sodium chloride (NaCl), and potassium chloride (KCl), were used for the various treatments. For a complete description of the cation treatment preparations, see Darrow (2007).

ζ-potential measurements

In certain clay minerals, the negative potential at the Stern layer is manifested as the ζ-potential, which can be quantified by placing a dilute soil suspension into an electric field. The negatively-charged soil particles will migrate toward the positive pole, while the remaining cation swarm in the fluid will migrate toward the negative pole. The ζ-potential is the negative potential formed at the shearing surface of the soil particle (Greenland & Hayes 1978). The ζ-potential depends on the type of cations adsorbed within the Stern layer. Thus, changing the adsorbed cations on the mineral surface affects the measured ζ-potential and the overall double layer thickness.

The ζ-potential of the HS BSLN and cation treatments was determined using a Zeta-Meter. To begin the sample preparation, 0.5 g of each sample was placed into a

scintillation vial, to which distilled, deionized water was added. After the soil was completely saturated, the vial was shaken vigorously in order to suspend most of the soil particles. A small portion of the suspension was taken from the vial and mixed with additional distilled, deionized water to create a dilute suspension for ζ-potential measurements. The amount of suspension removed and diluted was not exact; instead, these samples were prepared "by eye," having the concentration necessary to provide adequate particle tracking under the Zeta-Meter microscope (Zeta-Meter Inc. 1975). The dilute suspension was poured into the Zeta-Meter's electrophoresis cell, and the time necessary for each of 50 soil particles to travel 120 μm at room temperature was recorded. The dilute suspension was replaced after 15 to 25 particles were tracked. This ensured that the heat added by the Zeta-Meter components had a minimal effect on the ζ-potential measurements. Once all 50 particles were tracked, the time measurements and charts available in the Zeta-Meter manual (1975) were used to calculate the ζ-potential of the soil particles.

As a fine-grained soil may contain several different types of clay minerals, its measured ζ-potential will form a wide particle-charge distribution curve, demonstrating the range of the ζ-potential for all clay minerals present (Riddick 1968). The median ζ-potential value for each bulk soil sample was calculated from the particle-charge distribution curve, using a procedure outlined by Riddick (1968).

Unfrozen water measurements using NMR

FID and T2 measurements were made using a pulse NMR. NMR measurements were made at the following temperatures: -0.2°C, -0.5°C, -1°C, -2°C, -3°C, -4°C, -5°C, -7.5°C, -10°C, -15°C, and -20°C. After these measurements were completed, the sample was warmed to above freezing, and FID and T2 measurements were made at 10°C. The moisture content of the soil was determined at the above-freezing temperature, and the unfrozen water content, w_U, at each sub-freezing temperature was calculated by:

$$w_U = \frac{w_{10^o C} \cdot x_T}{x_{10^o C}} \quad (1)$$

where w_{10^oC} is the measured gravimetric water content at 10°C, x_{10^oC} is the NMR signal amplitude at 10°C, and x_T is the NMR signal amplitude at the corresponding sub-freezing temperature. All w_U values presented here are gravimetric water contents, and NMR signals used in these calculations represent FID peak times. Likewise, T2 net magnetization signal strength amplitudes presented are the peak values measured for each temperature.

Results

ζ-potential measurements

Figure 1 contains the ζ-potential particle-charge distribution curves for the HS BSLN sample and corresponding cation treatments, and the median ζ-potential values for the five HS samples are summarized in Table 1. The range for the Na^+ sample is larger than the other samples, resulting in a wider curve. The median ζ-potential values for the monovalent cation-treated samples are greater (i.e., more negative) than the divalent cation-treated and BSLN samples.

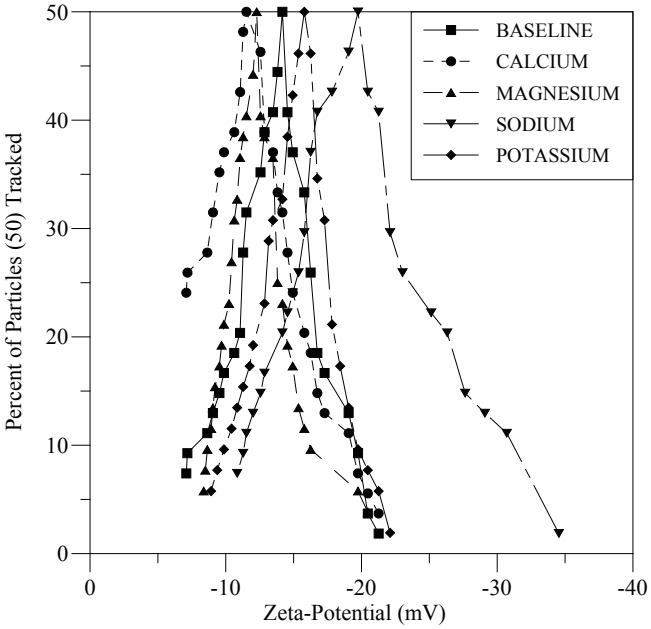

Figure 1. ζ-potential particle-charge distribution curves for the HS BSLN sample and corresponding cation treatments.

Table 1. Summary of ζ-potential median values for HS BSLN and corresponding cation treatments.

Sample	ζ-potential median values (mV)
BSLN	-14.17
Ca^{2+}	-11.76
Mg^{2+}	-12.28
Na^+	-19.74
K^+	-15.79

Unfrozen water measurements

The w_U data for HS BSLN sample and corresponding cation treatments calculated using the FID peak times are presented in Figure 2. The K^+-treated sample has the highest w_U at a given temperature, followed by the Na^+-treated sample. The w_U of the three remaining samples are very close to one another over the range of temperatures measured. The overall trend is similar for each sample, with the w_U steadily decreasing in an exponential fashion with decreasing temperature.

A plot of T2 net magnetization signal strength versus temperature for the HS samples is shown in Figure 3. The trends in these data are noticeably different from those in Figure 2. For each sample, the T2 signal strength decreases rapidly from -0.2°C to -2°C. There is little change in the T2 signal strength at temperatures colder than -2°C until -20°C, at which point the T2 signal strength drops close to 0 for all samples. This noticeable break at -2°C suggests a difference in the behavior of the unfrozen water at this temperature.

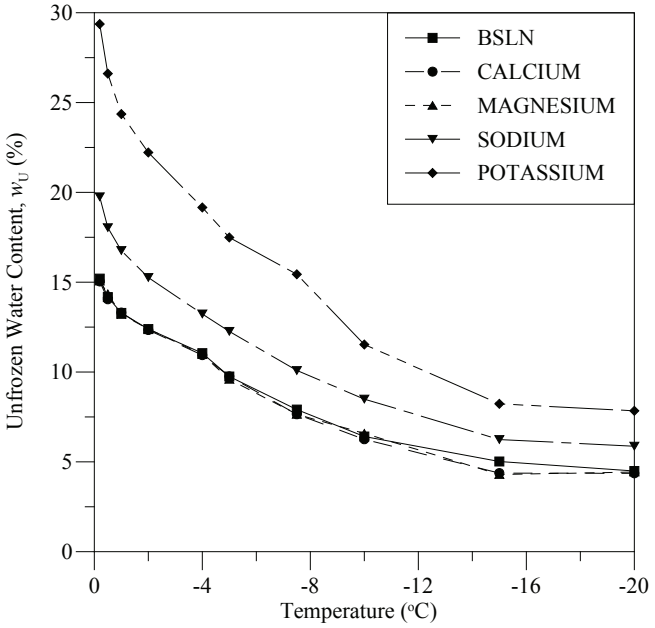

Figure 2. Unfrozen water content, w_U, versus temperature for HS BSLN and corresponding cation treatments.

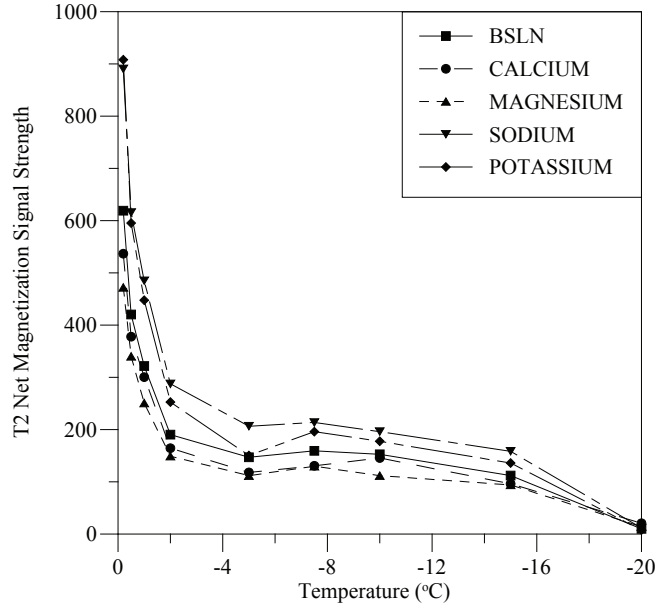

Figure 3. T2 net magnetization signal strength versus temperature for HS BSLN and corresponding cation treatments.

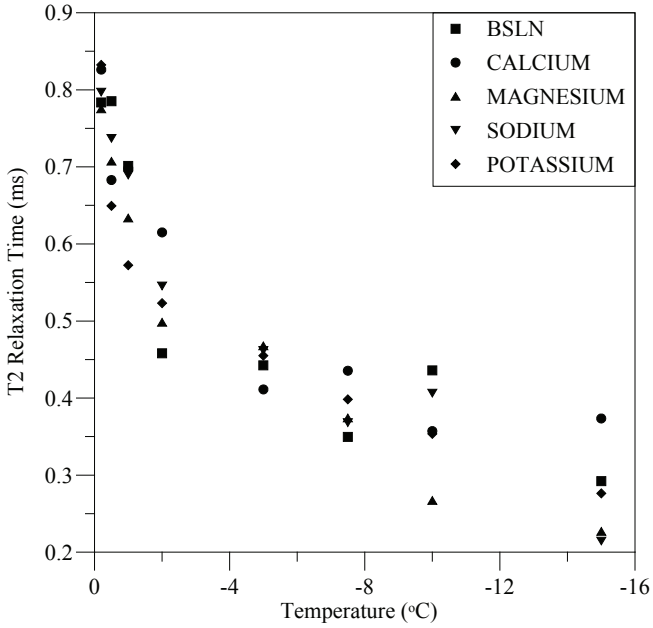

Figure 4. T2 relaxation time versus temperature for HS BSLN and corresponding cation treatments.

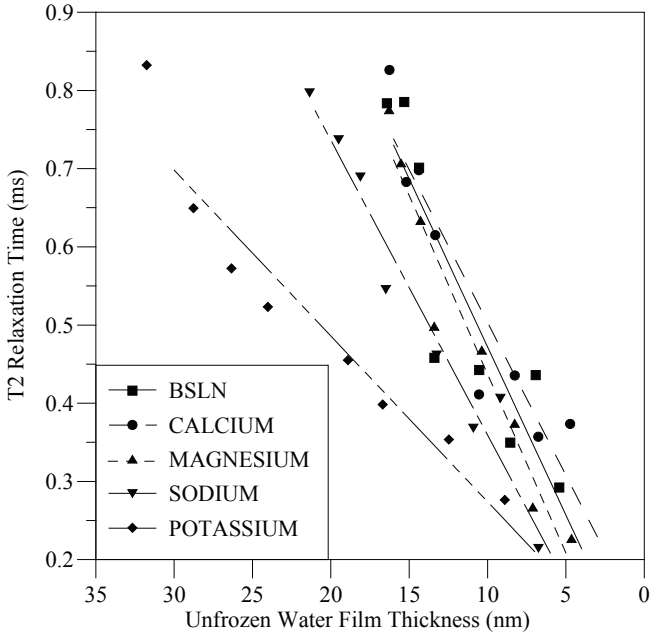

Figure 5. T2 relaxation time versus calculated unfrozen water film thickness for HS BSLN and corresponding cation treatments. Linear trend lines are shown for each data set.

The raw T2 signal data was processed to yield T2 relaxation times, which are presented in Figure 4. While these data demonstrate more scatter than those in the previous figures, T2 relaxation time also decreases in an exponential fashion with decreasing temperature. Although not shown in Figure 4, T2 relaxation times were also calculated for each sample at 10°C. These times ranged from 1.69 ms to 2.59 ms, with the monovalent cation-treated samples demonstrating the shorter times.

The thickness of the unfrozen water film in each sample was calculated at each temperature using the w_U data presented in Figure 2, the measured HS specific surface area of 9.25 m^2/g, and water densities for each sub-freezing temperature interpolated from published data (Hodgman 1956). The calculated thicknesses are plotted against T2 relaxation times for each corresponding temperature, as shown in Figure 5. For all samples, T2 relaxation time decreases with decreasing unfrozen water thickness in a linear fashion. This is indicated by the best-fit linear trend lines, with coefficients of determination (r^2) ranging from 0.81 to 0.96.

Discussion

While NMR FID signal strength data is a useful means of quantifying the unfrozen water content in a frozen soil, T2 data may yield important information about unfrozen water mobility.

Kojima and Nakagami (2002) used the magnetic resonance imaging (MRI) technique to investigate water mobility in the gel-layer of a drug. They found that the T2 relaxation time of the outer portion of the gel-layer was close to that of free water. However, in the inner portion of the gel-layer, the T2 relaxation time progressively decreased, suggesting that the water mobility around the core interface became highly restricted.

Similar interpretations can be made from the data presented here. In Figure 3, the rapid decrease in T2 net magnetization signal strength from -0.2°C to -2°C may indicate the freezing of water within the soil pores and capillaries, and some reduction in the thickness of the unfrozen water layers around individual soil particles. In Figure 5, for any given unfrozen water thickness, the monovalent cation-treated samples have shorter T2 relaxation times than the divalent cation-treated and BSLN samples. This suggests less mobility of unfrozen water in the monovalent cation-treated samples than in the divalent cation-treated samples. The monovalent cation-treated samples also demonstrated the greatest ζ-potentials of the sample group, resulting in their thicker unfrozen water films.

T2 relaxation times within water "layers" around the soil particles were calculated by taking the difference of the T2 signal strength at two sequential temperature readings. Unfrozen water "layers" with smaller numeric values are closer to the soil particle surface. These results, presented in Figure 6, demonstrate scatter because of the calculation method and variations within the data; however, generally T2 relaxation time decreases exponentially with decreasing distance to the soil particle surface.

Conclusions

The NMR method is a useful means for quantifying the unfrozen water content of a frozen soil through FID signal strength data. The results presented here indicate that T2 net magnetization signal strength and resulting T2 relaxation time provide insight into the mobility of unfrozen water. The rapid decrease in the T2 signal strength from -0.2°C to -2°C and the subsequent leveling off of the signal for temperatures colder than -2°C indicate a reduction in the mobility of the unfrozen water, as the unfrozen water becomes more restricted by the proximity of the soil particles' surfaces.

T2 relaxation time decreases linearly with the decreasing thickness of unfrozen water films. Soil saturated with monovalent cations demonstrates shorter T2 relaxation times than that saturated with divalent cations. The monovalent cation-treated soil also demonstrates greater ζ-potential, resulting in thicker unfrozen water films. Thus, the predominantly adsorbed soil cations strongly affect T2 relaxation time and the mobility of unfrozen water. T2 relaxation time decreases exponentially with decreasing unfrozen water "layers"; however, the effect of cation treatments on the water "layers" is not well-defined for this soil.

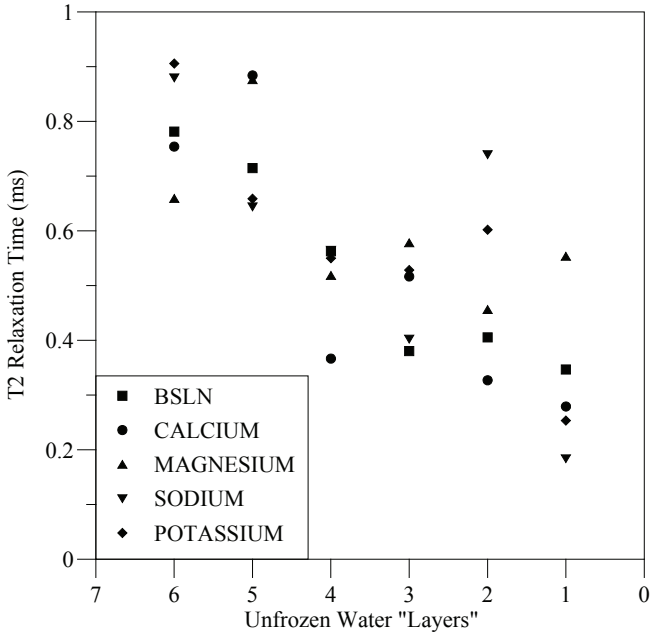

Figure 6. T2 relaxation time versus unfrozen water "layers." Each "layer" represents the difference in T2 signal strength at two sequential temperature readings. Unfrozen water "layers" with smaller numeric values are closer to the soil particle surface.

Acknowledgments

The authors would like to thank the National Science Foundation for providing financial support to the first author for her doctoral studies.

References

Bouyoucos, G. 1917. *Classification and Measurement of the Different Forms of Water in the Soil by Means of the Dilatometer Method*, Technical Bulletin 36, Michigan: Michigan Agricultural College Experiment Station.

Bouyoucos, G. 1920. A new classification of the soil moisture. *Soil Science* 11 (1): 33-47.

Darrow, M.M. 2007. *Experimental Study of Adsorbed Cation Effects on the Frost Susceptibility of Natural Soils*. Ph.D. thesis. Fairbanks: University of Alaska Fairbanks, 257 pp.

Greenland, D.J. & Hayes, M.H.B. (eds.) 1978. *The Chemistry of Soil Constituents*. New York: John Wiley & Sons.

Hodgman, C.D. (ed.) 1956. *Handbook of Chemistry and Physics*. Cleveland: Chemical Rubber Publishing, Co.

Kojima, M. & Nakagami, H. 2002. Investigation of water mobility and diffusivity in hydrating micronized low-substituted hydroxypropyl cellulose, hydroxypropylmethyl cellulose, and hydroxypropyl cellulose matrix tablets by magnetic resonance

imaging (MRI). *Chem. Pharm. Bull.* 50(12): 1621-1624.

Riddick, T.M. 1968. *Control of Colloid Stability through Zeta Potentia*. New York: Zeta-Meter, Inc.

Rieke, R.D., Vinson, T.S. & Mageau, D.W. 1983. The role of specific surface area and related index properties in the frost heave susceptibility of soils. *Proceedings, Permafrost: Fourth International Conference, Fairbanks, Alaska, July 17-22, 1983*: 1066-1071.

Tice, A.R., Burrous, C.M. & Anderson, D.M. 1978. Determination of unfrozen water in frozen soil by pulsed nuclear magnetic resonance. *Proceedings, Third International Conference on Permafrost, Edmonton, Alberta, July 10-13, 1978*: 149-155.

Tice, A.R., Oliphant, J.L., Nakano, Y. & Jenkins, T.F. 1982. *Relationship between the Ice and Unfrozen Water Phases in Frozen Soil as Determined by Pulsed Nuclear Magnetic Resonance and Physical Desorption Data*, Hanover: CRREL Report 82-15.

Zeta-Meter, Inc. 1975. *Zeta-Meter Manual*. New York: Zeta-Meter, Inc.

Changes in Active Layer Thickness and Seasonal Fluxes of Dissolved Organic Carbon as a Possible Baseline for Permafrost Monitoring

S.P. Davydov
Northeast Science Station Pacific Institute of Geography, Far-Eastern Branch of Russian Academy of Sciences, Cherskii, Republic Sakha (Yakutia), Russia
D.G. Fyodorov-Davydov
Institute of Physicochemical and Biological Problems in Soil Science of RAS, Pushchino, Moscow Region, Russia
J.C Neff
Geological Sciences and Environmental Studies, University of Colorado at Boulder, Boulder, CO 80309, USA
N.I. Shiklomanov
Department of Geography, University of Delaware, Newark, DE 19716, USA
A.I Davydova
E-mail: sdavydov@cher.sakha.ru

Abstract

This study investigates the relationship between changes in active layer thickness (ALT) above permafrost and the discharge of dissolved organic carbon (DOC) in streams of the Kolyma Lowland, northeastern Siberia. The results of observations indicate that the increase in ALT began in northern taiga landscapes in 2001–2005 and 2007. The contribution of melted ice from the thawed permafrost layer to the regional runoff is estimated to be 5–10% of the annual precipitation. The Kolyma Lowland is underlain by ice- and organic-rich Pleistocene deposits (Yedoma or Ice Complex). The observed increase in ALT results in involvement of ancient DOC in a contemporary biochemical cycle. This phenomenon is reflected by the structure and age of the DOC in streams in the fall. The observed effect of the increase in ALT on DOC potentially allows the use of radiocarbon dating for the integrative assessment of permafrost conditions over large territory.

Keywords: ALT monitoring; DOC; transitional layer; Yedoma.

Introduction

During the last decade, a great amount of research has underlined an increase of Siberian river discharge into the Arctic Ocean (Peterson et al. 2002, McCleland et al. 2004). This process has many sources, and permafrost thawing is among them. This study investigates the proposal to examine dissolved organic carbon (DOC) in seasonal streams for permafrost monitoring of the Arctic ecosystem.

The Kolyma Lowland occupies the northeast of the vast Siberian Coastal Plains. The region is characterized predominantly by continental climate (Table 1). The greatest positive changes of the study area occurred during recent years.

The lowland is wholly underlain by continuous permafrost that is the most ancient underground ice formation of Eurasia since the Pliocene Age. The total thickness of frozen sediments is 500–650 m with a mean temperature of permafrost from -3° to -11°C (Fyodorov-Davydov & Davydov 2006). Northern ecosystems of the Kolyma Lowland are underlain by ice-rich loess sediments with high organic content are called the Yedoma Suite or Ice Complex in Russia. Yedoma deposits are mid to Late Pleistocene continental loamy sediment with ice wedges. The total ice content in yedoma (sedimentary soil and ice wedges combined) is on average 75% (Gasanov 1971, Kholodov et al. 2003). The mean organic content in these sediments is estimated to be from 5–12 kg/m3 (Kholodov et al. 2003) to 21 kg/m3 (Zimov et al. 2006, Zimov et al. 2006a).

Table 1 Meteorological characteristic* of the study area.

	Period	aver	max	min
Mean Annual temperature, °C	1980 –2007	-10.8	-7.6 (2007)	-13.2
Mean summer temperature, °C	1980 –2007	10.7	14.9 (2007)	8.3
Mean sum positive summer temperature, °C	1980 –2007	993.6	1371.3 (2007)	670.7
Mean Annual precipitation, mm	1980 –2007	224.0	322.1 (2006)	146.1

*data of meteorological station "Cherskii."

The upper layer (0.1–2.0 m) of yedoma was thawed during the climatic optimum of the Holocene (6.3–9.6 thousand years ago for northeast Siberia). The consequent refreezing resulted in formation of a secondary frozen layer, called the transitional Layer (TL) (Shur 1988). This layer forms a boundary between the active and older permafrost layers of a yedoma.

Methods

Monitoring of changes in active layer thickness

The North-East Science Station (NESS) has carried out

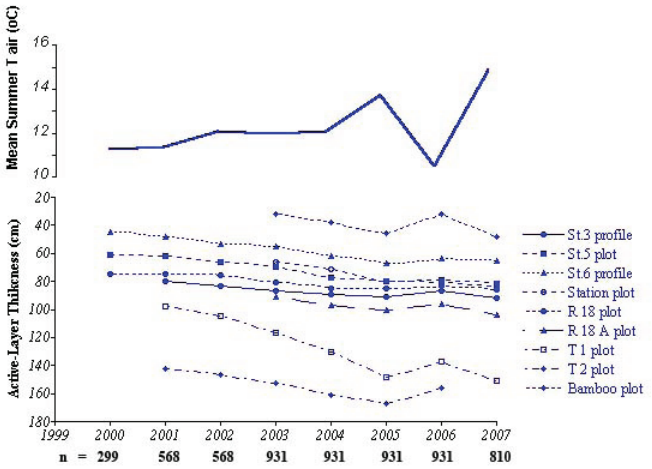

Figure 1. Annual dynamics of active layer thickness in different sites of the upland landscape of the Kolyma lowland; *n* – numbers of observation points on each year.

research of seasonal changes in ALT for more than 20 years. Since 1996, this study has been extended by participation in the network of the Circumpolar Active Layer Monitoring (CALM) Project. Sediments of the upper part of the permafrost and soils of the watershed area, both upland and lowland streams, have loamy and loamy sandy grading of soils. Therefore, measurements of seasonal changes in ALT were made by steel probes with length more than the maximum depth of the active layer. This method has an accuracy of 1–2 cm. We also used thermologgers, which were installed in thermometric boreholes.

Long-term observations for seasonal changes of ALT were made on 9 sites (Fig. 1). Each of 7 plots has 121 data points and different grids for measurements: one plot, 10 x 10 m; five plots, 1 x 1 m; and one plot, 0.5 x 0.5 m. Two profiles have 64 data points.

ALT monitoring started in all sites after the melting of snow cover. Observations were made once in 2 weeks (for profiles) or once in the beginning of every month (for plots) during the warm season. Every year the maximum of ALT was determined in the beginning of soil freezing in all points for each site.

Determination of volumetric soil moisture content

We used two methods for determination of volumetric soil moisture content in transitional horizon soils and permafrost of watersheds: (1) direct measurement of volumetric soil moisture content of undisturbed drilling soil sample; and (2) calculating the method by the N.A. Tsytovich equation (Gasanov 1971).

$$V_i = \frac{\gamma}{\Delta_i} * \frac{W_s - W_{ms}}{1 + W_s} \quad (1)$$

where

V_i = volumetric soil moisture content, %;

W_s = the gravimetric water content of frozen soil in % of soil dry weight,

W_{ms} = quantity of unfrozen water in % soil dry weight; mean content for sediments of the transitional horizon and yedoma is 2% unfrozen water for study area.

γ = density of the frozen soil of undisturbed structure, g/cm^3; mean density for sediments of the transitional horizon and yedoma 1.8 g/cm^3 for study area.

Δ_I = ice density, g/cm^3

Figure 2. Some types of cryogenetic textures of transitional layer.

Calculation of contribution of the release water partitioning by percentage of summer precipitation

For calculations of percentage of the release water partitioning of total summer precipitation we used the equation

$$P_{ALT}(\%) = \frac{\Delta_{ALT} * 0.3}{S_\Sigma} * 100\% \quad (2)$$

where

P_{ALT} = percentage of the release water partitioning of total summer precipitation, %;

Δ_{ALT} = annual gradient of thawing ALT, mm;

0.3 = mean part of the volumetric soil moisture content for transitional horizon of study area;

S_Σ = total summer precipitation, mm.

Results and Discussion

Changes in active layer thickness and hydrologic regime

Observational studies of active layer monitoring sites are characterized by different variants of the larch taiga landscapes and dispose at some watersheds of upland streams. Their active layer is characterized mainly by the soil cover of loamy cryohydromorphic soils (Cryozems and Gleyzems). Cryozems occupy more than 80% of soils (Fyodorov-Davydov & Davydov 2006). We used various methods of observation for ALT (profiles and plots) at Circumpolar Active Layer Monitoring (CALM) and North-East Science Station (NESS) sites from upland landscapes.

The observed increase in ALT is characteristic for all sites in 2001–2005. The correlation between ALT and mean summer temperatures reaches 0.96, and the maximal observed increase in ALT reaches 40% from long-term mean on some sites, which suggests that the increase in annual thawing has resulted from the abnormally high summer temperatures (Fig. 1).

The TL is characterized by very ice-rich cryogenetic textures that presented a predominance of lens-wicker, ataxitic, and lens-layered cryotextures (Fig. 2). Measurements

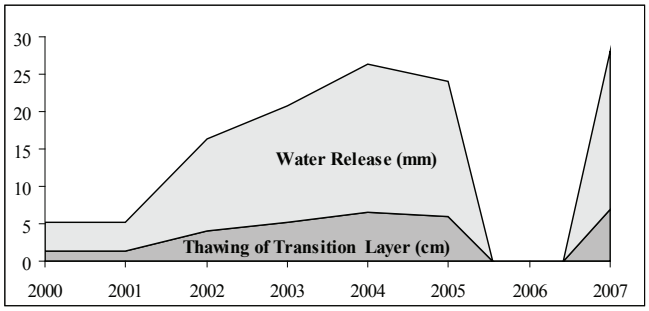

Figure 3. The relationship between thawing of the transitional layer and water release from melting permafrost.

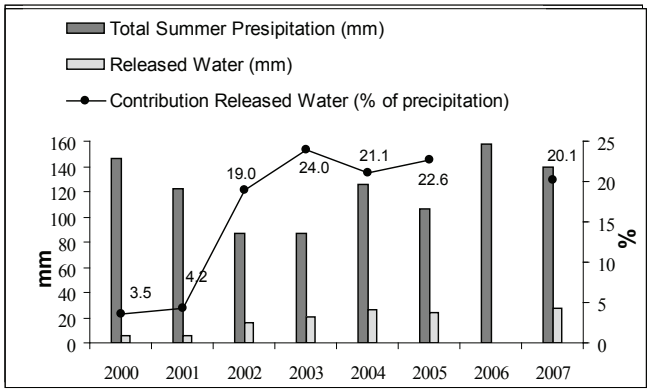

Figure 4. The contribution of the total annual water flux from the degrading transitional layer, estimated by percentage of summer precipitation.

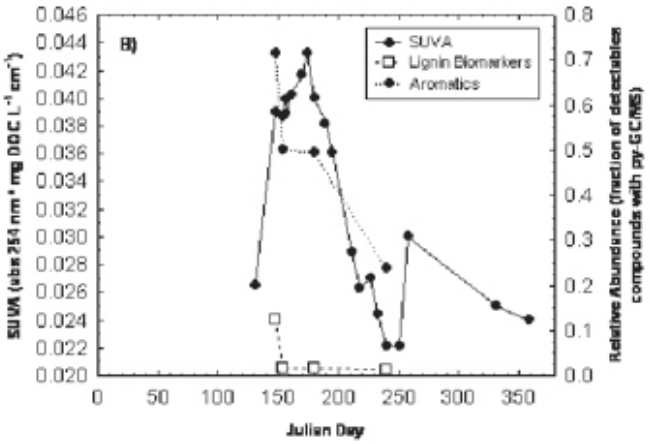

Figure 5a. Seasonal changes for lignin biomarkers, aromatics, and SUVA values (specific ultraviolet absorbance at 254 nm) for DOC (Neff et al. 2006).

of volumetric soil moisture content (10 cm above frozen horizon) indicate that the mean moisture content is 25% for the AL (n=128) and 55% for the TL and upper permafrost horizons (n=104) in a 10 cm layer lower depth of seasonal melting. Observations of soil moisture content were conducted at the end of the thawing season or at the beginning of winter for landscapes of watershed. We used direct or calculation methods for estimation of volumetric soil moisture. To preliminarily evaluate the release of water from the thawing of the upper permafrost, we considered the difference in volumetric water content between active and underlying transitional layers. The 30% difference translates to a 3 mm thick layer of water for each cm of thawed soil (Fig. 3). Due to moisture saturation characteristic of low-lying surfaces, wetlands were not considered for analysis.

The observed increase in ALT results in degradation of the TL. In 2003–2005 and 2007 at several sites, the transient horizon has degraded completely, causing thawing of deeper, perennially frozen layers. In 2006 the mean temperature decreased, and the summer precipitation abnormally increased, perhaps stimulated by the ice cover reduction at the East-Siberian Sea in last years. In this season the ALT decreased and there was a pause in the annual degradation of the TL. The release water and DOC fluxes stopped from the older permafrost layer. In 2007 the mean summer temperature vastly increased. That initiated thawing of the horizon, which was frozen in the previous season, and re-thawing of the TL with the formation of a new portion of release water (Fig. 3).

When the upper horizon of permafrost is thawing, a saturated layer is formed, and its water takes part in the seasonal hydrological cycle. Processes of transpiration have little influence on the release water fluxes from the permafrost, since plants vegetation of watershed landscapes in the middle of August–beginning of September basically has finished. In the same period, water migration in the upper soil horizon does not occur for the absence of soil freezing.

The contribution of the released water to the regional water runoff is estimated as 5–10% of the 280 mm of mean annual precipitation and reaches 20% of mean summer precipitation (Fig. 4).

Age and structure of dissolved organic carbon

A relatively thin layer of earth materials between the ground surface and the top of the permafrost undergoes an annual cycle of freezing and thawing (active layer) and is an important component of the Arctic ecosystem. A systematic and widespread increase in the thickness of the active layer could lead to changes in the biochemical cycle of high latitudes. Moreover, the TL and the yedoma contain a high level of dissolved organic carbon (DOC) held by frozen sediments and ice wedges. The significant increase of thawing leads to the involvement of buried, dissolved organic matter in the contemporary carbon biogeochemical cycle.

Strong seasonal trends in carbon age and chemical composition of DOC during the seasonal thawing were shown by Neff et al. (2006). Concentrations of lignin and aromatics of DOC in runoff of upland streams are decreasing from spring to fall (Fig. 5a), while relative DOC age is increasing (Fig. 5b). However, such trends are not evident in lowland streams located in the Kolyma flood plain, underlain by relatively young Holocene permafrost (Fig. 5b). The seasonal increase of DOC radiocarbon age can indicate the involvement of ancient carbon in contemporary hydrobiochemical cycles. A high water flux from the thawed horizon provides an effective vehicle for DOC to reach

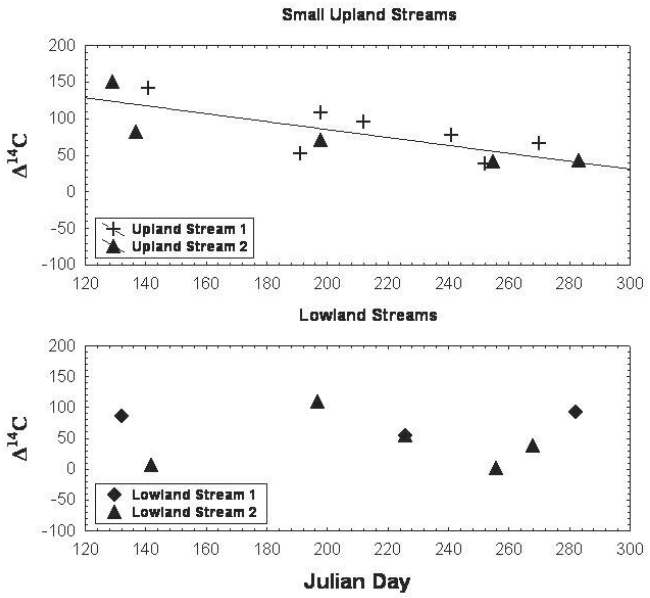

Figure 5b. Small upland streams – seasonal changes in the Δ14C content and the Δ14C of DOC. Lowland streams that drain seasonally flooded, modern permafrost – seasonal distribution of the Δ14C of DOC (Neff et al. 2006)

streams. However, the limited biochemical data (one, 2003 year) does not allow us to reach a definite conclusion about carbon release and migration due to an increase in annual thaw propagation. It is probable that the part of seasonally-released DOC, which remains in soil, migrates upward through the soil profile due to freezing and influences the age and structure of the DOC during consecutive thawing seasons.

Chemical composition and age of DOC can be measured in autumn, at the end of thawing season, when the ALT is maximal.

Conclusions

The results of observations suggest a progressive increase in active layer thickness in the Kolyma Lowland.

The observed changes in active layer thickness result in metachronous degradation of the ice- and organic-rich transitional layer.

The total annual water flux from the degrading transient layer can reach 20% of the total summer precipitation during dry and warm thawing seasons.

The seasonal dynamic of DOC composition and age suggests the involvement of ancient carbon previously stored in the upland (yedoma) sediments in contemporary hydrobiochemical cycles.

The relationship between degradation of the transient layer and DOC age and chemical composition can potentially allow the use of these characteristics for the integrative assessment of permafrost condition over a large territory at the end of the warm season.

Acknowledgments

Support was provided by CALM II project (NSF OPP 0352958), NSF RAISE projects, and the Russian Academy of Science.

References

Fyodorov-Davydov, D.G. & Davydov S.P. 2006 Seasonal thawing of soils on the north of the Kolyma Lowland. *Soil Processes and Spatio-Temporal Organization of Soils*. Moscow: Nauka, 455-471 (in Russian).

Gasanov, S.S. 1971. Volume ice content of frozen sediments. *Periglacial processes* 38: 167-180 (in Russian).

Kholodov, A.L., Rivkina, E.M., Gilichinsky, D.A. Fyodorov-Davydov, D.G., Gubin, S.V., Sorokovikov, V.A., Ostroumov, V.E. & Maksimovich, S.V. 2003. Estimation of the organic carbon input into Arctic Ocean due to erosion of the East-Siberian seashore. *Kriosphera Zemli* 7(3): 3-12 (in Russian).

McClelland, J.W., Holmes, R.M., & Peterson, B.J. 2004. Increasing river discharge in the Eurasian Arctic: Consideration of dams, permafrost thaw, and fire as potential agents of change. *J. Geophysical Research-Atmospheres* 109.

Neff, J.C., Finlay, J.C., Zimov, S.A., Davydov, S.P., Carrasco, J.J., Schuur, E.A.G. & Davydova A.I. 2006. Seasonal changes in the age and structure of dissolved organic carbon in Siberian Rivers and streams. *Geophysical Research Letters* 33(23).

Peterson, B.J., Holmes, R.M., McClelland, J.W., Vorosmarty, C.J., Lammers, R.B., Shiklomanov, A.I., Shiklomanov, I.A. & Rahmstorf, S. 2002. Increasing river discharge to the Arctic Ocean. *Science* 298(5601): 2171-2173.

Shur, Y.L. 1988 The upper horizon of permafrost soil. *Proceedings of the Fifth International Conference on Permafrost, Norway*: 867–871.

Zimov, S.A., Schuur, E.A.G. & Chapin, F.S. 2006. Permafrost and the global carbon budget. *Science* 312: 1612-1613.

Zimov, S.A., Davydov, S.P., Zimova, G.M., Davydova, A.I., Schuur, E.A.G., Dutta, K. & Chapin, F.S. 2006a. Permafrost carbon: Stock and decomposability of a globally significant carbon pool. *Geophysical Research Letters* 33.

Geophysical Mapping of Ground Ice in the Western Canadian Arctic

Gregory P. De Pascale
William Lettis & Associates, Inc., Walnut Creek, California, USA
Wayne H. Pollard
McGill University, Montreal, Quebec, Canada

Abstract

Warming in the Arctic is occurring sooner and more rapidly than was initially expected and is predicted to increase with time. The nature and distribution of ground ice is one of the most unpredictable geological variables in near-surface materials characterized by continuous permafrost. It is also the main reason permafrost is considered vulnerable to climate warming. In this study, coordinated measurements by two complementary geophysical tools—capacitive-coupled resistivity (CCR) and ground penetrating radar (GPR)—were used to map ground ice and cryostratigraphy at King Point and Richards Island in the western Canadian Arctic. Validation of geophysical interpretations was accomplished using adjacent natural exposures. The synergenistic benefits of using these two geophysical tools permitted accurate mapping of various types of ground ice including massive ice, and wedge ice, and detection of the top of the massive ice bodies.

Keywords: climate change; ground ice; ground penetrating radar; massive ice; resistivity.

Introduction and Significance of Ground Ice

The primary goals of this paper are (1) to characterize ground ice conditions at two ice-rich sites in the Western Canadian Arctic, and (2) to demonstrate the complementary nature of GPR and CCR data in the analysis of ground ice in continuous permafrost. The nature and distribution of ground ice is one of the most unpredictable geological variables in surficial sedimentary deposits characterized by continuous permafrost (Pollard & French 1980). Volumetric ground ice contents can range from <10% in relatively dry permafrost to >90% in ice-rich permafrost containing massive ice (Mackay & Dallimore 1992). Massive ground ice is defined as ice greater than 1 m thick with a gravimetric water content exceeding 250% on a dry weight basis (Permafrost Subcommittee 1988). Ice content patterns are often related to soil texture and depositional and freezing histories. In this classification, ground ice occurrence ranges from disseminated ice crystals in a soil matrix (pore ice) to discrete V-shaped linear networks of vertically foliated ice (wedge ice) to thick (10–20 m), horizontally continuous layered bodies of nearly pure segregated ice that often extends for several km^2. The significance of ground ice pertains to its geomorphic and geologic role in landscape development and geotechnical characteristics. The former includes various processes and landforms associated with either ground ice aggradation, like frost heave or the formation of ice-cored landforms, or with ground ice degradation, particularly thermokarst and associated ground ice subsidence. Ultimately, ground ice is a hazard for northern development, and disturbance of sites with ground ice present can cause thermokarst and disturbance of wildlife habitat, and create concerns with traditional land uses.

For this study, we selected two sites in the Western Canadian Arctic: King Point on the Yukon coast and a site on Northern Richards Island in the Mackenzie Delta Region of the Northwest Territories (Fig. 1).

The King Point site was selected because ground ice conditions have been well documented (Pollard & Dallimore 1988) and is known for having different types of ground ice present and visible in a large retrogressive thaw slump. Previous ground ice research in this area involves a series of cryostratigraphic studies based on detailed examination of ground ice exposures along the Yukon coast (Harry et al. 1988, Pollard & Dallimore 1988). In each case, massive ice interpreted as intra-sedimental ice was documented between 3–5 m below the surface. This research also describes a widespread thaw unconformity, which in some cases truncates massive ice (Harry et al. 1988) and the burial and preservation of surface snow patches (Pollard & Dallimore 1988). In each case, these studies provide compelling evidence of extensive massive ice and a previous deep thaw event that lead to truncation of Pleistocene ice wedges. The retrogressive thaw slump at King Point permitted direct validation of geophysical data (Fig. 2).

The Richards Island site was selected because of the presence of a large retrogressive thaw slump that is approximately 250 m long and 5 to 10 m high (Fig. 3).

This slump is unreported in the literature and appears to have formed sometime between 2005 and 2006. Again, the access to this site permitted direct comparison of the geophysical data with the stratigraphy in the natural exposure.

Methods and Data Acquisition

In this study, two geophysical tools, capacitive-coupled resistivity (CCR) and ground penetrating radar (GPR), were used to map ground ice occurrence at two sites that have not previously been investigated. Fieldwork was conducted in March 2005 and March 2006 using geophysical techniques. Winter fieldwork permitted smooth survey lines due to snow cover and noise-free datasets because during winter the active

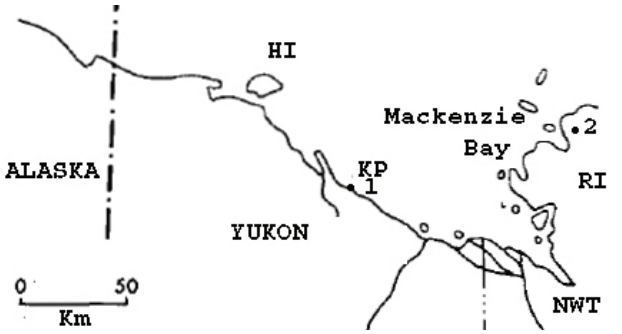

Figure 1. Map of two study sites with 1) King Point and 2) Ground Ice slump on Richards Island. HI is Hershel Island, RI is Richards Island.

Figure 2. Oblique air photo showing the King Point site. Note the coalescing coastal landslides and the small ice wedge melt ponds and polygonal ground in the foreground.

layer is frozen. Ground resistivity and radar techniques give valuable information about subsurface conditions based on different electromagnetic properties of sediments. Electrical resistivity determines the subsurface resistivity distribution from induced current measurements made at the ground surface. From these measurements, the specific resistivity of subsurface materials can be determined. The resistivity of a material can be calculated using Ohm's law: $R = V/I$ (resistance = voltage/current).

For geoelectrical measurements of ground resistivity, Ohm's Law is used in its differential vector form: $\rho = E/J$, where ρ is resistivity, E is electric field, and J is current density. By measuring an electric field at a known current, it is possible to calculate the resistance of the total volume of material between the transmitter and receiver to the depth of detection limit of the transmitter signal (Loke & Barker 1996). Resistivity techniques work well in regions of permafrost because there is a marked increase in electrical resistivity of water that occurs at the phase change from liquid to solid water (Hoekstra et al. 1975, Wolfe et al. 1996, Calvert et al. 2001, Calvert 2002, Hauck 2002, Hauck et al. 2003 De Pascale et al., in press). In permafrost regions resistivity will vary directly as a function of the ice content and type; for example, sediments with low ice contents are generally conductive and typically have low resistivity values. Massive ice will generally have higher resistivity values than pore ice. Sediments with high ice content will generally have resistivities higher than sediments without ground ice present, but lower resistivities than sediments containing massive ice.

Capacitive-coupled resistivity (CCR) surveys are a recent advancement in electrical resistivity mapping. Other workers have used Direct Current (DC) resistivity with success for mapping permafrost and ground ice (Kneisel et al. 2000, Hauck & Kneisel 2006), although this techniques is not as effective in cold continuous permafrost. For a detailed review of the theory behind capacitive-coupled resistivity, see Timofeev et al. (1994). As with DC resistivity, CCR uses two dipoles. In principal, current is applied to the ground by a transmitter via capacitive-coupling and the resulting potential is measured at the receiver dipole. Two previous studies using CCR techniques in permafrost were not able to distinguish between massive ice and glaciofluvial sediment with ice contents >30% (Wolfe et al. 1996), but Calvert (2002) noted that two-dimensional resistivity measurements were acquired relatively quickly in areas of ground ice. In another recent study, different resistivity techniques are compared in an area of mountain permafrost in the Swiss Alps (Hauck & Kneisel 2006). In that environment, permafrost conditions are very different from the Mackenzie Delta region; for example, mid-latitude alpine permafrost is much warmer and wetter (higher liquid water content), and contains little ground ice (extensive massive ice is largely absent), and bedrock plays an important control on landscape development. These differences limit the applicability of comparing the geophysical results between these two permafrost regions. The only study to combine CCR and GPR data in continuous permafrost regions (De Pascale et al., in press), was also the first occasion where methodology for CCR data acquisition was discussed.

Ground penetrating radar (GPR) is another geophysical tool that has been used increasingly over the last 30 years for a wide range of subsurface mapping applications. By transmitting an electromagnetic pulse into the ground and recording the travel time of reflections caused by contrasts in dielectric properties, GPR measurements are used to characterize the structure and stratigraphy of near-surface geology. Previous studies have used GPR to study permafrost (Doolittle et al. 1990, Hinkelet et al. 2001, Moorman 1994, 1995, Arcone et al. 1998, Moorman et al. 2003) and massive ground ice (Dallimore & Davis 1987, Dallimore et al. 1992, Robinson 1994). These studies have shown that GPR data reliably indicate contacts between ice and frozen sediments, ice and solid rock, and frozen and thawed regions. The only study to-date that has integrated GPR and CCR techniques to map massive ice in permafrost was De Pascale et al., in press.

In this study, geophysical surveys were conducted in March 2005 and March 2006 with air temperatures between -15ºC and -40ºC, and the ground surface was covered by wind-crusted snow. Ground resistivity was measured using a Geometrics OhmMapper TR1 system, with operating frequencies in the range of 8 to 32 kHz using a dipole-dipole transmitter and receiver. Current is run along the transmitter's

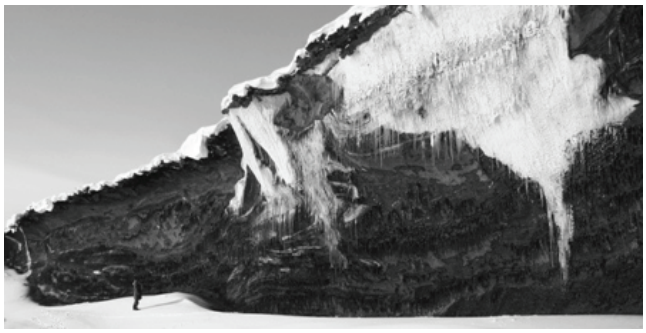

Figure 3. Photo showing the retrogressive thaw slump on Richards Island. Note person for scale and exposed white ice wedges.

dipole cables with the dipoles acting as one plate of a capacitor and the ground as the other. The resulting voltage, measured at the receiver dipole, is proportional to the ground resistivity between the two dipoles and the initial current emitted from the transmitter. The apparent resistivities are calculated from the measured resistances using the geometric factor, which corresponds to the distance between the transmitter and receiver. Multiple passes are made along each survey line to gather data over a range of n-spacings, which is the ratio of the distance between the transmitter and receiver and the dipole spacing, permitting resistivity measurements of the materials at several depths. By increasing the distance between the transmitter and receiver, a larger survey line is created, giving a greater depth of investigation. In this study, the initial n-spacing was used for two passes at each site in order to ensure data reliability and measurement consistency. The GPR system used was a MALA controller with RTA antennas operating at 50 MHz and 250 MHz. The controller triggers pulses of energy that are transmitted into the surface by the antenna which acts as a band-pass filter, emitting sine waves with the center frequency determined by the antenna. Since penetration depth of a GPR signal depends on the antenna frequency and the electromagnetic properties of the subsurface materials, the frozen ice-rich nature of our sites was favorable for penetration depths on the order of ~15 m at the frequencies used. Due to the lack of topography at the sites, static corrections were unnecessary. Sediment and ice were sampled from Richards Island for petrographic and geochemical analysis, and the results from these data are forthcoming.

Data processing

The CCR data were reduced using the DataMap 2000 software (Geometrics 2001), while inversions were completed using the two-dimensional inversion software RES2DINV (Loke & Barke 1996). These CCR data were transferred to RES2DINV, where filtering techniques such as despiking were employed to remove outliers and smooth the datasets with a 3-point running average. Data were plotted in a pseudo-section, where the depth scale is calculated as a function of the separation between the dipoles. A pseudo-section is a geometrical view of the measured apparent resistivity dataset, whereas the inversion model shows the true resistivity for each model block, which is calculated independent of the resistivities of the surrounding model blocks. Interpretations of the CCR models were constrained by other subsurface information available at each of the sites, including the natural exposures in the retrogressive thaw slumps and ice wedge troughs. GPR data were processed using the ReflexW software package. Processing involves time-zero surface correction and horizontal filtering of the direct coupling wave. This processing is standard for GPR data and removes system noise that could mask real data. Because of the frozen nature of the field sites, penetration depth estimates assumed a dielectric constant of 6 (v = 0.12 m/ns) for frozen sediments and a dielectric constant of 3 (v = 0.16 m/ns) of ground ice. Generally we used an average of v = 0.14 m/ns due to the varied nature of these sites.

Results

At King Point we conducted a 225 m 2-D transect parallel and approximately 5–10 m from the Yukon coast. This survey intersected several ice wedge troughs that were visible on the surface. The setting varied from ice wedge terrain, as detected by low-center polygons on the surface, to terrain with massive ice exposed in a large retrogressive thaw slump (Fig. 4).

On Richards Island we surveyed a 250 m long 2-D transect parallel and above a retrogressive thaw slump. In the exposure, ice wedges, massive ice, and stratigraphic relationships were logged using digital cameras to map site conditions during the survey for geophysical validation (Fig. 5).

King Point results

Based on our surveys we were able to map out ground ice distribution at the site. The CCR data detected wedge ice (2500 to 500 Ohm.m), massive ice (5000–10000 Ohm.m) and variations in the depth to top of massive ice. The depth of the top of massive ice is extremely variable, which is expressed as a wavy, however continuous surface and varies between 3.5 to 7 m below ground surface. The RMS value for this site was 17.4%, which is a suitable error considering the variance in resistivities of these materials. With the GPR data, we were able to show strong reflectors at two levels, with the upper reflections being mainly horizontal to wavy and extending to a depth of ~50 ns, and the lower interface appearing at ~100 ns and exhibiting more variations in topography.

Stratigraphic information from adjacent coastal exposures and retrogressive slump were used to help guide the interpretation. The region between the two areas of high reflections contains semi-horizontal structures. These areas correspond to regions of massive ice occurrence. Estimated depths were calculated using a velocity of 0.14 m/ns assuming a combination of frozen sediments and areas of massive ice. Using these depths, the upper reflections extend to ~3.5 m, and the tops of the lower reflections are at ~7 m. The semi-

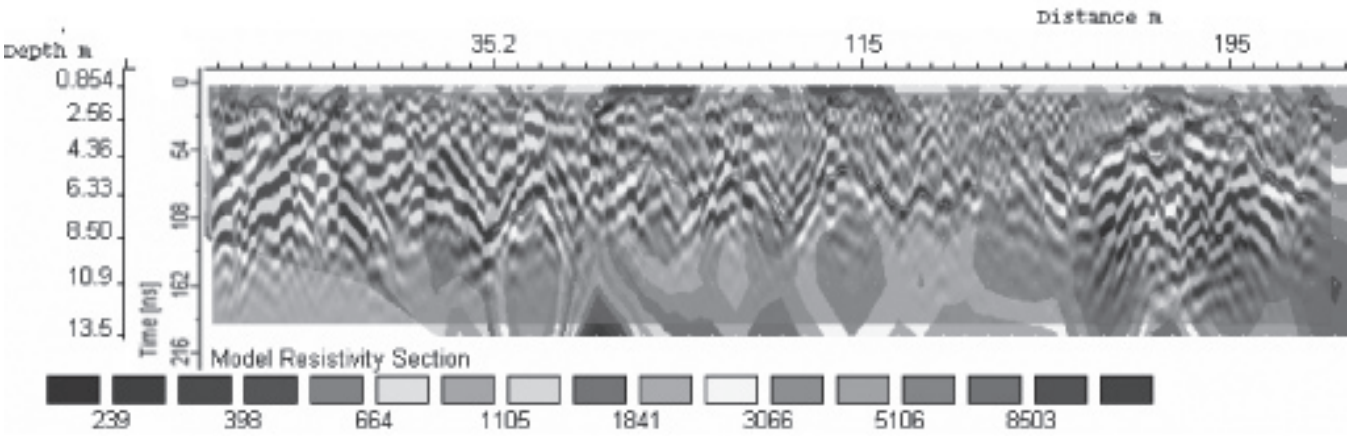

Figure 4. Combined CCR and GPR (50 MHz) data for the King's Point study site. A west-to-east transect with higher zones of resistivities (shown in red) corresponding with massive ground ice distribution and the dark brown which corresponds with wedge ice. Note the prominent reflector in pink that corresponds with the yellow increase in resistivity values and ground ice content (found between 3 and 6 m below ground surface). The increase in resistivity values east of station 160 corresponds with the transition between polygonal ground (wedge ice) and massive ice with no surface expression.

horizontal structures at approximately 3.5 m corresponds to the depth in the CCR data where resistivity levels become much larger below 3.5 m; this is the contact between frozen sediments to ice-rich frozen sediments. This could possibly be the maximum depth of the frozen Hypsithermal active layer, as noted in other sites in the Western Arctic (De Pascale et al., in press). Data with both systems were difficult to resolve below 13 m at this site. Wedge ice was detected between stations 35 and 150, and expressed as oval-shaped zones of higher resistivities with zones of lower resistivities between these zones of wedge ice. East of station 160, there is a transition from an area with ice wedges to massive ice, and there is a marked increase in resistivity values at this contact. The GPR data shows a decrease in signal attenuation east of station 160, which is consistent with massive ground ice occurrence due to a decrease in electrical conductivity.

Richards Island results

As with the King Point surveys, we were able to map the ground ice distribution at this site. The CCR data detected wedge ice (2,600 to 5,000 Ohm.m), massive ice (10,000 to 60,000 Ohm.m), and depth to the top of the massive ice. The RMS value for this site is 16.1%. The depth to the top of the massive ice varies from 7 to 8 m below ground surface. With the GPR data, we were able to detect strong reflectors at two levels, with the upper reflectors being subhorizontal to wavy and continuous for up to 60 m over a ~200 m section of the transect. The upper interface was ~100 ns and the lower interface appearing at ~225 ns. The upper interface corresponds with the top of the massive ice, while the lower interface is beyond the depth of the exposure. This reflector could be the base of the massive ice. Using these depths, the upper reflections extend from 6 to 8 m below the ground surface, while the lower reflector was at ~16 m. There was good agreement between the geophysical data and exposure adjacent to the transect, which permitted direct validation to the geophysical results. From the geophysical data, the contrast between pore-ice- rich sediments and the underlying massive ice was easily obtained. The lithologies of the materials under the major GPR reflector would be difficult to interpret without the CCR data, which demonstrated large variations in resistivity. However, this dielectric contrast between the massive ice and overlying sediments caused a strong reflector to be present in the GPR data. This contact was detected with both systems and showed 2 to 3 m of hummocky subsurface topography. The location of the ice wedges was easily detected due to geometry and increase in resistivity values, and from ice wedge troughs on the surface. Overall, the amount of massive ice found at this site permitted deeper investigations than at the Kings Point site.

Conclusions

Massive ground ice, wedge ice, ice-rich sediments, the active layer, a thaw unconformity corresponding to the hypsithermal paleo-active layer, as well as basic stratigraphic relationships found in the surrounding sediments were mapped. The two-dimensional geometry of ice bodies was obtained using these two geophysical techniques. Massive ice was consistently found at depths greater than 4 m, a depth corresponding with the Hypsithermal thaw unconformity, although modern wedge ice is often encountered at depths less than 2 m. It was found that that the hummocky surface of the massive ice body and the top of ice wedges were variable at both locations. This was possibly due to differential melting during the hypsithermal, prior to re-aggredation of permafrost within this section. A number of authors (e.g., Burn 1997, French 1998) describe the hypsithermal as a well-developed, shallow thaw unconformity in permafrost exposures in numerous locations throughout the western Canadian Arctic that appears between 2–3 m below the ground surface as an abrupt change in ice content, ice chemistry, soil colour,

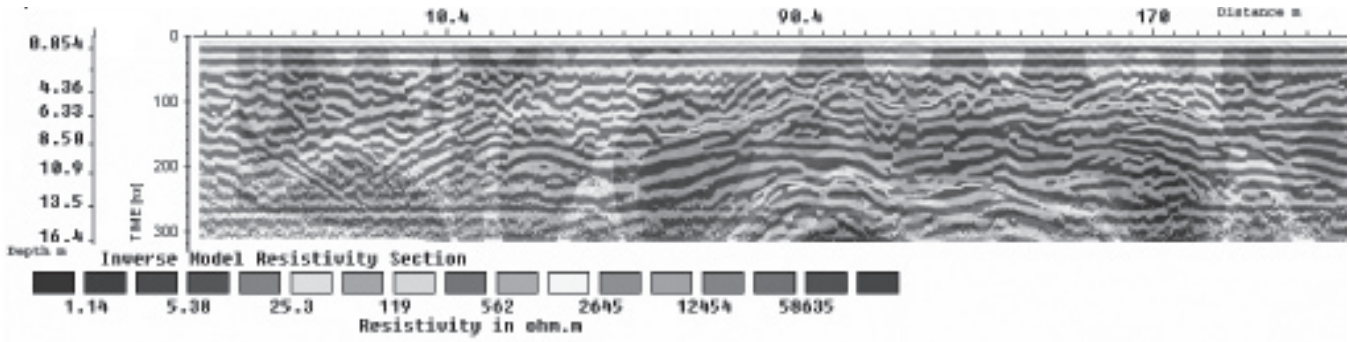

Figure 5. Combined CCR and GPR (50 MHz) data for the Richards Island site in a west-to-east transect. Higher zones of resistivities (shown in red) correspond with massive ground ice distribution. Note the anticline at station 90 m at a depth of approximately 14, and how there is a reduction in resistivities that corresponds with anticline structures found at depth. Green picks outline top and base of massive ice body. Note the wedge ice at stations 10 and 20 at depths near the surface and below 6 m.

organic content, and cryostructure. Examination of the King Point exposure revealed a number of these features, as well as several truncated ice-wedge tops (Harry et al. 1985) at a depth of ~2.5–3.0 m. The strong reflector at between 3 to 5 m depths seen in both the GPR and CCR data is interpreted as this transition. Dating of organic material (French 1998) from the overlying thawed zone from other sites confirms that this unconformity is related to an early Holocene warm interval referred to as the Hypsithermal (8.0–9.0 ka BP), when active layers were 2–2.5 times deeper than present. Another important finding is the large variation in resistivity values, almost a magnitude in the case of this study, for similar types of ground ice found in different settings. Coastal ground ice exposures have lower resistivity values than those found inland, and this is most likely due to the higher levels of cations present in the system from proximity to saline coastal conditions. The overall reduction in depth of investigation between our coastal site (King Point) and our inland site (Richards Island), suggests that the influence of coastal cations reduces the electrical resistivity values for all materials at a site. Because of this, more work needs to be undertaken to better understand the resistivity "signatures" of continuous permafrost.

Fieldwork on ground ice characterization at Richards Island in the Mackenzie Delta and King Point on the Yukon Coast, utilizing non-invasive geophysical methods like CCR and GPR, provided an opportunity to assess the synergistic benefits of using two complementary geophysical systems. Our results support previous research showing that, individually, CCR and GPR are useful tools for obtaining general subsurface information in permafrost (e.g., Calvert 2002, Dallimore & Davis 1987, Arcone et al. 1998, Moorman et al. 2003, De Pascale et al., in press), and clearly show the added value that results by combining their outputs. This study, based on the examination of sites at King Point and Richards Island, together with De Pascale et al. (in press), which focuses on massive ice in coarse-grained sediments, illustrates the enhanced benefit of integrating two complimentary geophysical techniques. These techniques detect and map the distribution of permafrost materials and structures containing ground ice, and if GPR is properly constrained using CCR data, a more accurate estimate of depth is possible. There was excellent agreement between these two systems that permit accurate mapping of ground ice locations. To our knowledge this is the first report of the young retrogressive thaw slump on Richards Island. Future work with these techniques can help us to better understand complex ground ice settings where various different ground ice are present, without damaging the natural environment using these non-destructive methods. To date our research has used observed cryostratigraphic relationships (nature sections or boreholes) and surface geomorphic expression (ice wedges polygons) to constrain our interpretation of subsurface permafrost conditions. Like any form of remote sensing, confidence levels increase when ground truthing confirms interpretations based on proxy data. For example, given the range of resistive values we have observed for massive ice, we are reasonably confident that in areas of deep continuous permafrost, where surface geomorphology does not indicate any unusual hydrologic phenomenon (e.g., saline ground water), we can detect the location, extent, and thickness of a massive ice unit. We are also confident that the distinct pattern of reflection together with resistivity can detect ice wedges, even relict ice wedges beneath a thaw unconformity. Ultimately, with the appropriate configuration (antenna frequency, spacing, …) of equipment, the combination of GPR and CCR is an effective and non-invasive technique to detect and map ground ice.

Acknowledgments

Funding for this research was provided by a NSERC Discovery Grant, ArcticNet, the Canadian Space Agency, and a PERD/DIAND financial agreement managed by R. Gowan with McGill University (W. Pollard). Field support for this research was provided by the Aurora Research Institute (ARI) in Inuvik and was conducted under NWT research License numbers 13560 and 13753 and Inuvialuit Land Administration (ILA) License number 03TIN055. The authors would like to thank an anonymous reviewer for the

very helpful comments and suggestions. G.P.D would like to thank the professional development program William Lettis & Associates for supporting this work.

References

Arcone, S.A., Lawson, D.E., Delaney, A.J., Strasser, J.C. & Strasser, J.D. 1998. Ground penetrating radar reflection profiling of groundwater and bedrock in an area of discontinuous permafrost. *Geophysics 63*: 1573-1584.

Burn, C. 1997. Cryostratigraphy, paleogreography and climate change during the early Holocene warm interval, western Arctic coast. *Canadian Journal of Earth Sciences* 34, 912-925.

Calvert, H.T. 2002. Capactive-coupled resistivity survey of ice-bearing sediments, Mackenzie Delta, Canada. *Society of Exploration Geophysicists, 72nd annual meeting, Salt Lake City, UT, Oct. 2002*. Society of Exploration Geophysicists, Tulsa, OK, USA.

Calvert, H.T., Dallimore, S.R. & Hunter, J.A. 2001. Application of Geophysical Techniques For Mapping of Ice-Bearing Sediments, Mackenzie Delta, Western Arctic, Canada. *Conference on the Geophysical Detection of Subsurface Water on Mars,* 674 pp.

De Pascale, G.P., Williams, K.W., Pollard, W.H. In Press. Geophysical mapping of ground ice using a combination of capacitive coupled resistivity and ground penetrating radar, NWT, Canada. *Journal of Geophysical Research – Earth Surface.*

Doolittle, J.A., Hardisky, M.A. & Gross, M.F. 1990. A ground penetrating radar study of active layer thicknesses in areas of moist sedge and wet sedge tundra near Bethel, Alaska, USA. *Arctic and Alpine Research 22:* 175-182.

French, H.M. 1998. An appraisal of cryostratigraphy in North-West Arctic Canada. *Permafrost and Periglacial Processes* 9: 297-312.

Harry, D.G., French, H.M. & Pollard, W.H. 1985. Ice wedges and permafrost conditions near King Point, Beaufort Sea Coast. *Current Research, Part E, Geological Survey of Canada, Paper 85-1A,* 111-116.

Harry, D.G., French, H.M. & Pollard, W.H. 1988. Massive ground ice and ice-cored terrain near Sabine Point, Yukon Coastal Plain. *Canadian Journal of Earth Sciences* 25: 1846-1856.

Hauck, C. 2002. Frozen ground monitoring using DC resistivity tomography. *Geophysical Research Letters 29(*21): 2016.

Hauck, C. & Kneisel, C. 2003. Application of a capacitively coupled resistivity system for mountain permafrost studies and implications for the interpretation of resistivity values. *Proceedings of the Eighth International Conference on Permafrost, Zurich 2003*: 55-56.

Hauck, C. & Kneisel, C. 2006. Application of capacitively-coupled and DC electrical resistivity imaging for mountain permafrost studies. *Permafrost and Periglacial Processes* 17: 169-177.

Hauck, C., Muhll, D.V. & Maurer, H. 2003. Using DC resistivity tomography to detect and characterize mountain permafrost. *Geophysical Prospecting 51*: 273-284.

Hoekstra, P., Sellmann, P.V. & Delaney, A. 1975. Ground and airborne resistivity surveys of permafrost near Fairbanks, Alaska. *Geophysics* 40: 641-656.

Kneisel, C., Hauck, C. & Vonder Mühll, D. 2000. Permafrost below the timberline confirmed and characterized by geoelectrical resistivity measurements, Bever Valley, Eastern Swiss Alps. *Permafrost and Periglacial Processes* 11: 295-304.

Loke, M.H. & Barker, R. 1996. Rapid least-squares inversion of apparent resistivity pseudo-sections using a quasi-Newton method. *Geophysical Prospecting* 44: 131-152.

Mackay, J.R. 1972. The world of underground ice. *Annals of the Association of American Geographers* 62: 1-22.

Mackay, J.R. & Dallimore, S.R. 1992. Massive ice of the Tuktoyaktuk area, western Arctic coast, Canada. *Canadian Journal of Earth Sciences* 29: 1235-1249.

Moorman, B.J., Robinson, S.D. & Burgess, M.M. 2003. Imaging periglacial conditions with ground-penetrating radar. *Permafrost and Periglacial Processes 14:* 319-329.

Permafrost Subcommittee, Associate Committee on Geotechnical Research. 1988. *Glossary of Permafrost and Related Ground-Ice Terms*. National Research Council of Canada. Technical Mem. No. 142, 156 pp.

Pollard, W.H. & Dallimore, S.R. 1988. Petrographic characteristics of massive ground ice, Yukon Coastal Plain, Canada. *Proceedings of the Fifth International Conference on Permafrost, VI, Trondheim, Norway, Tapir Publishers,* 224-229.

Pollard, W.H. & French, H.M. 1980. A first approximation of the volume of ground ice, Richard Island, Pleistocene Mackenzie delta, NWT. *Canadian Geotechnical Journal* 17: 509-516.

Robinson, S.D. 1994. Geophysical studies of massive ground ice, Fosheim Peninsula, Ellesmere Island, Northwest Territories. *Current Research 1994-B, Geol. Surv. Can.*, Ottawa, Ont.: *11-18.*

Timofeev, V.M., Rodozinski, A.W., Hunter, J.A. & Douma, M. 1994. A new ground resistivity method for engineering and environmental geophysics, *Proceedings of the Symposium on the Application of Geophysics to Engineering and Environmental Problems, EEGS*: 701-715.

Wolfe, S.A., Burgess, M.M., Douma, M., Hyde, C. & Robinson, S.D. 1996. Geological and Geophysical Investigations of the Canamera Carat Lake Esker- Delta Complex, Slave Geological Province, NWT. *Geol. Surv. Can.,* Ottawa, Ont., 38 pp.

Recent Interannual Variations of Rock Glacier Creep in the European Alps

Reynald Delaloye, Eric Perruchoud
Department of Geosciences, Geography, University of Fribourg, Switzerland
Michael Avian, Viktor Kaufmann
Institute of Remote Sensing and Photogrammetry, Graz University of Technology, Austria
Xavier Bodin
Institute of Alpine Geography, Joseph Fourier University, Grenoble, France
Helmut Hausmann
Institute of Geodesy and Geophysics, Vienna University of Technology, Austria
Atsushi Ikeda
Graduate School of Life and Environmental Sciences, University of Tsukuba, Japan
Andreas Kääb
Department of Geosciences, University of Oslo, Norway
Andreas Kellerer-Pirklbauer
Institute of Geography and Regional Science, University of Graz, Austria
Karl Krainer
Institute of Geology and Paleontology, University of Innsbruck, Austria
Christophe Lambiel
Institute of Geography, University of Lausanne, Switzerland
Dragan Mihajlovic, Benno Staub
Institute of Geography, University of Bern, Switzerland
Isabelle Roer
Department of Geography, University of Zurich, Switzerland
Emmanuel Thibert
Cemagref, Grenoble, France

Abstract

Recent interannual variations of rock glacier surface motion are compared for 16 landforms monitored for a few years in various parts of the European Alps. Large fluctuations have been observed particularly since 2002. Most investigated rock glaciers have shown a similar behavior whatever their location in the Alpine arc, their size, or their velocity. The observed interannual variations appear to be primarily related to external climatic factors rather than to internal characteristics. They are mostly well correlated with mean annual ground surface temperature shifts with a delay of a few months, reflecting the thermal wave propagation deeper into permafrost. Seasonal factors may also play a significant role: a lower intensity of winter ground freezing and/or a larger winter snow accumulation appear to facilitate a higher rate of rock glacier surface motion.

Keywords: creep; European Alps; interannual variations, rock glaciers; surface motion.

Introduction

Rock glaciers act as sediment conveyors in cold periglacial mountain environments. Where a rock glacier is perched on a steep valley side, it may be the source of slope instability processes (mainly rock falls and debris flows). Any change in the rate of permafrost creep may modify the delivery of loose materials at the rock glacier snout and affect the frequency, the magnitude, and even the type of related slope instabilities (e.g., Roer et al. 2008). In this context, and paying regard to the ongoing climate warming trend, there is an increasing request in the densely inhabited European Alps for precise and up-to-date data documenting the evolution of the high-altitude permafrost environment. In addition to the assessment of longer term (decadal to pluri-decadal) changes affecting rock glacier dynamics, which can be precisely determined by airborne photogrammetric analysis (Kääb et al. 2003), documentation of the short-term (interannual and even seasonal) variations is needed. Two decades after the pioneer work on the Gruben rock glacier (Haeberli 1985), the systematic survey of annual velocities was reinitiated a few years ago by several research teams by means of terrestrial measurements. This paper provides a first comparison of time series that have been measured since 1999/2000 or later on a sample of 16 rock glaciers located in six regions of the Alpine arc.

Background

Mostly located in the lower half of the mountain discontinuous permafrost belt, Alpine rock glaciers are rather warm. They may move relatively fast and are highly sensitive to small temperature changes (Kääb et al. 2007).

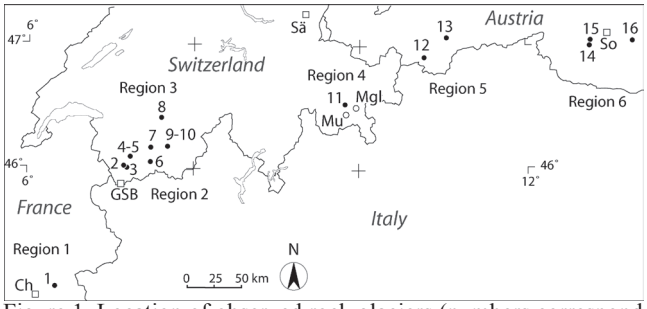

Figure 1. Location of observed rock glaciers (numbers correspond to Table 1). Other cited rock glaciers : Mu: Murtèl; Mgl : Muragl. Regions: 1. southwestern Alps (France), 2. western Swiss Alps (Valais), 3. northwestern Swiss Alps (Bernese Alps), 4. eastern Swiss Alps (Upper Engadine), 5. western Austrian Alps, 6. central Austrian Alps. Weather stations : Ch: St.-Christophe-en-Oisans; GSB : Grand-St-Bernard; Sä : Säntis; So : Sonnblick.

Three types of temporal variability in surface motion are superimposed on a secular time scale in response to ground surface temperature variations (e.g., Kääb et al. 2007, Perruchoud & Delaloye 2007): a decadal to pluri-decadal trend, interannual variations, and a seasonal rhythm. Non-thermally induced changes in rock glacier dynamics (e.g., topography effect) may also influence the creep rate particularly at longer time scales, whereas the infiltration of snowmelt water (Ikeda et al. 2008) and the influence of subpermafrost groundwater (Haeberli 1985, Krainer & Mostler 2006) are also advanced as controlling factors at shorter time intervals. The early measurements on the Gruben rock glacier already indicated that strong short-term velocity variations occur where the permafrost base is above bedrock, and that these variations can be different in lower and upper rock glacier parts (Haeberli 1985).

Studies carried out in various parts of the Alps (e.g., Roer et al. 2005, Kääb et al. 2007, Kaufmann et al. 2007) have shown that the motion of alpine rock glaciers has drastically accelerated since the 1980s, probably in response to an increase in permafrost temperature consecutive to warmer air temperatures. For the past 15 years or so, however, no clear further warming trend has been visible in the borehole temperatures time series on the Murtèl rock glacier in the eastern Swiss Alps (Vonder Mühll et al. 2007).

Seasonal variations have been reported for several rock glaciers (Haeberli 1985, Kääb et al. 2003, Hausmann et al. 2007a, Perruchoud & Delaloye 2007), whereas almost constant annual velocities have also been observed (Krainer & Mostler 2006), particularly where permafrost is reaching into bedrock as on the Murtèl rock glacier (Haeberli et al. 1998). Where existing, seasonal fluctuations can be large, reaching up to 50 % from the annual mean. They occur every year more or less at the same time but are not fully synchronous for all rock glaciers. Highest velocities are reached in most cases between summer and early winter, whereas the lowest values are usually observed in spring or early summer. The seasonal increase in velocity can be rapid and connected to the snowmelt process (Perruchoud & Delaloye 2007) or slower and delayed (Kääb et al. 2007). On the Muragl rock glacier (eastern Swiss Alps), the annual amplitude of the seasonal rhythm varies significantly, the winter/spring decrease being reduced by warmer winter ground surface temperature (Kääb et al. 2007).

Interannual Velocity Survey and Dataset

Interannual velocities are surveyed by terrestrial measurements (geodetics or real-time kinematic GPS) with accuracy in the mm to cm range. The annual campaign at each rock glacier is carried out as closely as possible on the same date - ideally by late summer - in order to avoid an effect of potentially strong seasonal variations on the reliability of the data. Ten to more than 100 marked points, covering part or the whole of the rock glacier or disposed along longitudinal and/or transversal profiles, are surveyed. The compared value is then the mean horizontal velocity for all moving points with uninterrupted series. This value is considered to be a proxy for the activity of a whole rock glacier, keeping in mind that local differences in flow rates and amplitudes of annual changes are probable.

The 16 observed rock glaciers (Fig. 1) are located in six distinct regions and are briefly described hereafter and in Table 1. There is a distance of 600 km between Laurichard (southwest) and Dösen (east) rock glaciers.

Region 1: Southwestern Alps (France)

Laurichard is a tongue-shaped rock glacier which displays longitudinal furrows in its steepest part and transversal ridges near the edge. Surface velocities have been measured since 1983 (Francou & Reynaud 1992) along a 420 m long longitudinal profile of 17 painted blocks. Mean horizontal velocity over the 1983–2007 period is 0.75 ma^{-1}.

Region 2: Western Swiss Alps (Valais)

Mille is a rock glacier looking inactive on morphological criteria (Delaloye 2004), however moving slowly in its steeper lower half (0.02 to 0.05 ma^{-1}).

Aget-Rogneux is a low active back creeping push-moraine located in the Little Ice Age forefield of a small vanished glacier (Lambiel & Delaloye 2004).

Mont-Gelé B and C are two coalescent small rock glaciers. Whereas Mont-Gelé B is moving faster, the deformation of Mont-Gelé C is much reduced despite an apparently higher ice content (Lambiel & Delaloye 2004).

Tsarmine is a tongue-shaped, currently very active rock glacier ending at the top of a steep gully and providing large amounts of loose materials. Local disturbances of the block surface point to a recent drastic acceleration of the rock glacier movement (Lambiel et al. 2008).

The Becs-de-Bosson rock glacier is an active feature consisting of two adjacent lobes. There is no permafrost—and no creep—in the rooting zone of the rock glacier due to the former development of a local glacier during the Little Ice Age. Significant seasonal variations are observed on the whole rock glacier (Perruchoud & Delaloye 2007).

HuHH1 and HuHH3 are two adjacent multilobate rock glaciers situated below cirques. Both landforms are of similar size and showed maximum horizontal velocities up to 4 ma^{-1} in 2003/04 (Roer 2007).

Region 3: Northwestern Swiss Alps (Bernese Alps)

Furggentälti is a small, tongue-shaped rock glacier with annual surface displacement currently 5 to 10 times larger than during the period 1960–1974 (Mihajlovic et al. 2008). Seasonal fluctuations were observed in 1998/99.

Table 1. Alpine rock glaciers with annual surface velocity survey.

N°	Name	Coordinates	Elevation m a.s.l.	Area km^2	Aspect	Available data	Mean horizontal velocity (2003/04) ma^{-1}	Relative drop (2004-2006) %
1	Laurichard	45°01'N, 06°24'E	2424-2644	0.08	N	1999-...	1.03	-40
2	Mille	46°01'N, 07°12'E	2340-2430	0.02	NE	2003-...	0.05	-61
3	Aget-Rogneux	46°01'N, 07°14'E	2810-2890	0.03	SE	2001-...	0.20	-50
4	Mont-Gelé B	46°06'N, 07°17'E	2600-2740	0.02	NE	2000-...	1.20	-81
5	Mont-Gelé C	46°06'N, 07°17'E	2620-2820	0.05	N	2000-...	0.22	-42
6	Tsarmine	46°03'N, 07°30'E	2480-2650	0.04	W	2004-...	-	-
7	Becs-de-Bosson/Réchy	46°10'N, 07°31'E	2610-2850	0.10	NW	2001-…	0.97	-36
8	Furggentälti/Gemmi	46°24'N, 07°38'E	2450-2650	0.03	N	1994-...	3.08	-52
9	HuHH1	46°11'N, 07°43'E	2630-2780	0.04	NNW	2001-2005	1.26	-
10	HuHH3	46°11'N, 07°43'E	2515-2650	0.05	NW	2002-...	1.78	-52
11	Büz North (Trais Fluors)	46°32'N, 09°49'E	2775-2840	0.02	NE	1998-2005	0.74	-
12	Ölgrube	46°54'N, 10°45'E	2380-2810	0.21	W	2000-2005	1.50	-
13	Reichenkar	47°03'N, 11°02'E	2310-2750	0.27	NE	1998-2006	3.15	-9
14	Weissenkar	46°57'N, 12°45'E	2610-2720	0.15	W	1999-...	0.08	-41
15	Hinteres Langtalkar	46°59'N, 12°46'E	2455-2700	0.15	NW	1999-...		
	(upper part)		>2655	0.06			0.18	-28
	(lower part)		<2655	0.09			2.22	-21
16	Dösen	46°59'N, 13°17'E	2340-2650	0.19	W	1995-...	0.26	-19

Region 4: Eastern Swiss Alps (Upper Engadine)

The Büz North (Trais Fluors) pebbly rock glacier comprises two superimposed lobes, 70 and 90 m long. At the beginning of the survey in 1998, no pronounced morphological expression of flow was noticed. However, the movement turned out to be in the order of 1 ma^{-1} and more (Ikeda et al. 2008, Kääb et al. 2007).

Region 5: Western Austrian Alps

Ölgrube rock glacier consists of two lobes of varying activity. Maximum annual velocities (1.5 ma^{-1}) occur in the central lower part. Seasonal variations were observed with a velocity decrease of about 50% during winter 2003 (Krainer & Mostler 2006, Hausmann et al. 2007a).

Reichenkar is a 1400 m long, very active tongue-shaped rock glacier. Highest velocity (up to 3 ma^{-1}) occurred in 2003/04. No seasonal variation was noticed in 2002 and 2003 (Krainer & Mostler 2006, Hausmann et al. 2007a, b).

Region 6: Central Austrian Alps

Weissenkar is a slowly moving, tongue-shaped rock glacier consisting of an upper lobe overriding a lower one, and characterized by well developed furrows and ridges at the entire lower half. Weissenkar rock glacier moves on average 0.02 to 0.11 ma^{-1} (Kaufmann et al. 2006).

Hinteres Langtalkar houses a highly active, tongue-shaped rock glacier advanced over a prominent terrain ridge into steeper terrain most likely in 1994 (Avian et al. 2005). Several transverse crevasses have developed since (e.g., Roer et al. 2008). The current movement pattern differentiates a faster lower part and a substantially slower upper part.

Dösen is a tongue-shaped rock glacier. Displacement measurements started in 1995—including photogrammetric work of the preceding period until 1954—revealing mean velocity rates of 0.13–0.37 ma^{-1} (Kaufmann et al. 2007).

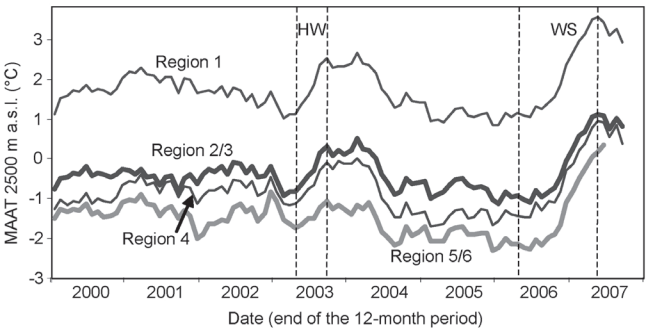

Figure 2. Mean annual air temperature (12-month running mean) standardized at 2500 m a.s.l. (gradient: -0.56°C/100 m). HW: heat wave 2003; WS: warm swell 2006/07. Region 1: St. Christophe, 1570 m a.s.l. (Météo-France). Region 2/3: Grand-St-Bernard, 2472 m a.s.l. (MeteoSwiss). Region 4: Säntis, 2490 m a.s.l. (MeteoSwiss). Region 5/6: Sonnblick, 3105 m a.s.l. (ZAMG –Central Institute for Meteorology and Geodynamics).

MAAT and MAGST in 2000–2007

Air temperature

The 1987–2007 mean annual air temperature (MAAT) in the Alps was on average 1°C to 2°C warmer than during the preceding decades. Since 2000, two extreme, warm climatic events affected the Alpine region: the heat wave of summer 2003 and the 2006/07 warm swell, namely 15 months of quasi continuous, large, positive temperature anomaly between April 2006 and June 2007 (except August 2006). The 2003 heat wave induced a rapid warming of MAAT towards values exceeding those of earlier and later years (except in the Austrian Alps), and the 2006/07 event resulted in an exceptionally high MAAT, which exceeded everywhere the 2003 value by 0.5°C to 1.5°C (Fig. 2).

Ground surface temperature

There are no boreholes on the 16 observed rock glaciers, except a shallow one (6 m) at Trais Fluors. Ground surface temperature is nevertheless monitored on several of them. Variations of the mean annual ground surface temperature (MAGST)

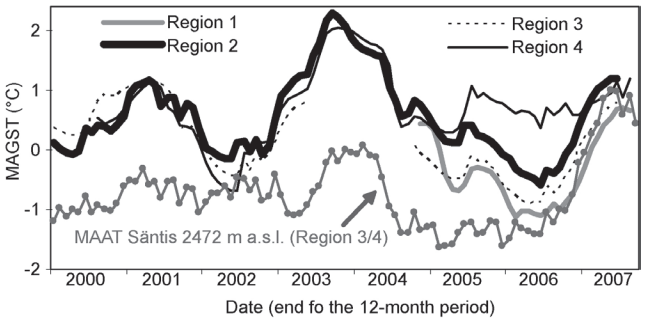

Figure 3. Interregional comparison of MAGST behavior in the western and central Alps (12-month running mean). Region 1: Laurichard rock glacier (average of 2 sites of measurement). Region 2: Becs-de-Bosson/ Réchy (2). Region 3: Furggentälti/ Gemmi (1). Region 4: Trais Fluors (1).

are used as a proxy for the permafrost thermal regime at shallow depth, even if the intensity of the winter cooling and summer warming (freezing and thawing index) should not be neglected. The snow cover buffers the ground-atmosphere heat exchanges for a long part of year, varying annual snow cover conditions alter the behavior of MAGST in comparison with MAAT: both are not evolving in a parallel way (Fig. 3). Despite the effect of snow, a homogeneous MAGST behavior is observed at the regional scale (e.g., Delaloye & Monbaron 2003). The larger variations of MAGST are also similar at the interregional scale in the Alps with, however, some differences in 2005–2006—colder values in the western regions 1–3 (Fig. 3). Three periods of warmer MAGST occurred in 2001, 2003/04 and 2007, with the 2003/04 event as the warmest.

Both 2003 and 2006/07 warm climatic events did not affect MAGST in the same way. In 2003 a strong MAGST increase already had occurred during the winter due to earlier snow insulation (e.g., Vonder Mühll et al. 2007); a second phase of warming succeeded in summer and was caused by the heat wave. An extremely high MAGST value was reached by the end of 2003. In 2006/07, the situation was the reverse. Later and lesser snowfalls in early winter favoured the cooling of the ground surface in spite of the persistence of mild air temperature. The extremely high MAAT was strongly attenuated in MAGST.

Results

Despite variable size, morphology, complexity of flow field, mean annual velocity, seasonal rhythm, etc., the compared rock glaciers have shown a rather homogeneous and synchronous behavior (Fig. 4). Three phases of higher creep rate can be quoted in 2000/01, 2003/04, and 2006/07. They all followed immediately a period of warmer MAGST.

Every rock glacier reached an absolute or relative maximal creep rate in 2003/04 before a drastic drop occurred for most of them between 2004 and 2006 (up to -81%, Table. 1). The drop was generally stronger to the west (Regions 1–3) than to the east (Regions 5–6). Stationary or slightly increased velocities were observed everywhere in 2006/07.

The situation in 2000/01 was more contrasted. A peak rate of deformation occurred in Region 4 and was also almost reached in Region 1. Relative maxima are reported from Regions 3 and 6 (no data in Region 2) whereas no maximum is documented in Region 5. Neighboring regions did not display similar behavior in rock glacier movement.

Discussion

Neglecting small differences in interannual variations that may be due to either internal and topographical characteristics of the rock glaciers or to the variability of the seasonal rhythm or to a shift in the measurement date, the rather homogeneous behavior of Alpine rock glaciers allows us to state that: (1) the driving processes are likely to be the same for all observed rock glaciers; (2) there should be a common climatic control of the permafrost creep rate; (3) a dominant effect of active layer solifluction or surface boulder creep can be excluded, as corroborated, for instance, by borehole deformation measurements on the Trais Fluors rock glacier (Ikeda et al. 2008).

As the interannual changes of surface motion appear to be mostly correlated to the evolution of the MAGST with a delay of a few months (Fig. 4) - the warmer the MAGST, the larger the velocity, - one can infer that they should be caused by a thermally induced process. The delay being not long enough for the surface thermal signal to penetrate deeply into permafrost, interannual changes would thus be primarily caused by shifts in the deformation rate of shallow permafrost layers mostly located—if existing—above the shear horizon.

Higher creep rates should also be caused by the development of a thick winter snow cover, which during early summer provides more meltwater to penetrate into a warm rock glacier system. This process is evoked by Ikeda et al. (2008) to explain the high activity of the Trais Fluors rock glacier in 2001. In that region, the snow cover in winter 2000/01 was much deeper than for both the previous and the following winters. The unusually high amount of meltwater in early summer 2001 is advanced as a factor which facilitated permafrost creep. A similar situation occurred in the Laurichard area in the French Alps. The snow accumulation (2.42 m we) recorded that winter on the Sarennes glacier at a distance of 24 km was 0.65 m we above the 1984–2007 mean and the only value exceeding 2 m we since 1995 (Fig. 5). Among the six regions defined in this study, both Laurichard and Trais Fluors regions are the most exposed to southerly precipitations, a situation which prevailed in winter 2000/01.

Changing interannual creep rates may finally be related to the intensity of winter ground freezing. Where data is available, the maximal activity of rock glaciers appears to be linked to lower freezing index values. In the western and eastern Swiss Alps, the highest annual velocities occurred after the warmest winters on the ground surface, in 2001 and 2003 (Fig. 6). On the Muragl rock glacier, close to Trais Fluors, seasonal velocity surveys carried out between 1998 and 2003 (Kääb et al. 2007) showed that, contrary to other winters, the velocity of the rock glacier did not decrease during winter 2000/01. The higher annual velocity was caused by the absence of a winter deceleration.

Conclusions and Perspectives

Rapid and slow rock glaciers have shown mostly a similar kind of annual velocity variations in the whole arc of the

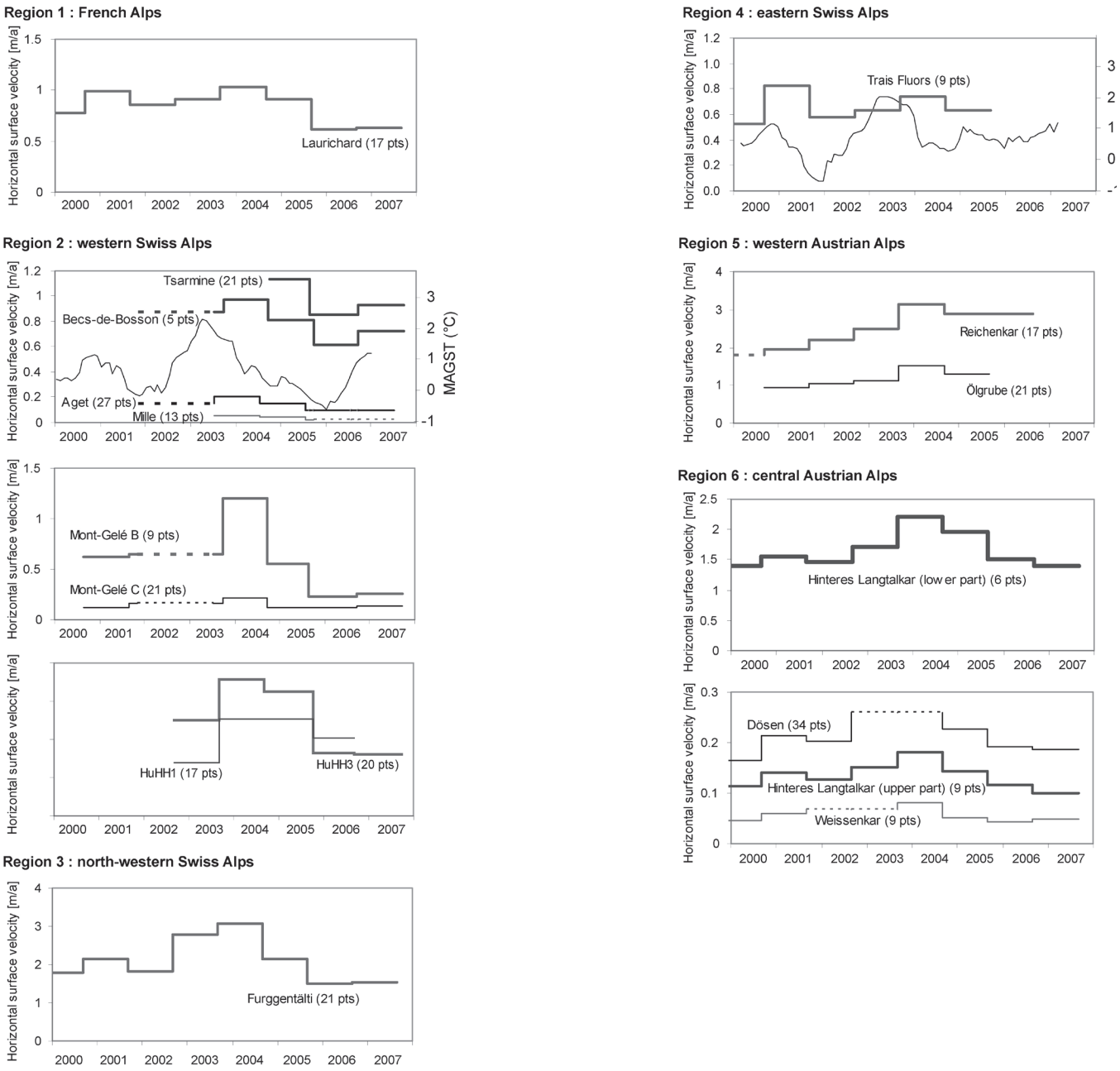

Figure 4. Annual horizontal velocities of alpine rock glaciers. The velocity scale is not identical on every graph. Dotted lines indicate a 2-year interval of measurement. Mean annual ground surface temperature (MAGST) at Becs-de-Bosson and Trais Fluors rock glaciers are inserted in the respective chart with date corresponding to the median of the 12-month period.

European Alps since 2000. Interannual variations of rock glacier dynamics appear so far—with probably a few exceptions—to be primarily related to external climatic factors rather than to the internal characteristics of the rock glaciers. They are mostly well related to shifts in mean annual ground surface temperature with a few months of time lag reflecting the delay in propagation of corresponding anomalies deeper into permafrost. Seasonal factors may also play an important role. A lower intensity of winter ground freezing and/or a larger amount of winter (October–May) snowfall facilitate a higher rate of annual rock glaciers surface motion.

The set of 16 rock glaciers is representative of six alpine regions. It establishes a pioneer network for the observation of short-term variations of rock glacier activity. The first synthetic results strongly encourage the continuation of the monitoring effort and the extension of the network to further regions, particularly in the southern Alps for which such data is still mostly lacking. The availability of uninterrupted series, complemented by ground surface temperature and snow data acquired on the rock glaciers or in their close vicinity, will serve a more precise identification and quantification of the factors driving the short-term behavior of permafrost creep rate in temperate mountain areas.

Acknowledgments

Special thanks are due to both reviewers and to the reviewer editor for their comments, and to all involved in the field survey campaigns for their inestimable contribution.

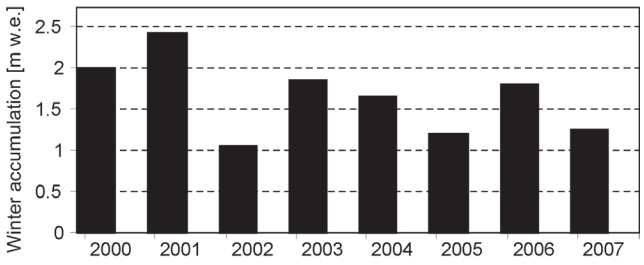

Figure 5. Winter snow precipitations (cumulative amount from October to April in meters of water equivalent, m we) recorded at Sarennes Glacier (French Alps).

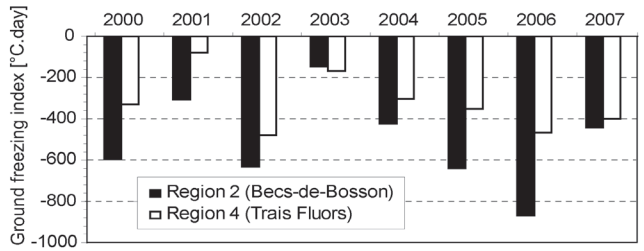

Figure 6. Interregional comparison of ground freezing index in the Swiss Alps.

References

Avian, M., Kaufmann, V. & Lieb, G.K. 2005. Recent and Holocene dynamics of a rock glacier system – the example of Langtalkar (Central Alps, Austria). *Norwegian Journal of Geography* 5: 149-156.

Delaloye, R. & Monbaron, M. 2003. Snow effects on recent shifts (1998-2002) in mean annual ground surface temperature at alpine permafrost sites in the western Swiss Alps. *Eighth Conference on Permafrost, Zurich 2003, Extended Abstracts*: 23-24.

Delaloye, R. 2004. *Contribution à l'étude du pergélisol de montagne en zone marginale*. Ph.D. Thesis, University of Fribourg, Switzerland, *GeoFocus* 10.

Francou, B. & Reynaud, L. 1992. 10 years of surficial velocities on a rock glacier (Laurichard, French Alps). *Permafrost and Periglacial Processes* 3: 209-213.

Haeberli, W. 1985. Creep of mountain permafrost: internal structure and flow of Alpine rock glaciers. *Mitteilung VAW/ETH Zurich* 74.

Haeberli, W., Hoelzle, M., Kääb, A., Keller, F., Vonder Mühll, D. & Wagner, S. 1998. Ten years after drilling through the permafrost of the active rock glacier Murtèl, eastern Swiss Alps: answered questions and new perspectives. *Proceedings of the Seventh International Conference on Permafrost, Yellowknife,* Nordicana 57: 403-410.

Hausmann, H., Krainer, K., Brückl, E. & Mostler, W. 2007a. Creep of Two Alpine Rock Glaciers – Observation and Modelling (Ötztal- and Stubai Alps, Austria). *Grazer Schriften der Geographie und Raumforschung* 43: 145-150.

Hausmann, H., Krainer, K., Brückl, E. & Mostler, W. 2007b. Internal Structure and Ice Content of Reichenkar Rock Glacier (Stubai Alps, Austria) Assessed by Geophysical Investigations. *Permafrost and Periglacial Processes* 18: 351-367.

Ikeda, A., Matsuoka, N. & Kääb, A. 2008. Fast deformation of perennially frozen debris in a warm rock-glacier in the Swiss Alps: an effect of liquid water. *Journal of Geophysical Research* (in press).

Kääb, A., Kaufmann, V., Ladstädter, R. & Eiken, T. 2003. Rock glacier dynamics: implications from high-resolution measurements of surface velocity fields. *Proceedings of the Eighth International Conference on Permafrost, Zurich,* Balkema : 501-506.

Kääb, A., Frauenfelder, R. & Roer, I. 2007. On the response of rockglacier creep to surface temperature increases. *Global and Planetary Change* 56(1-2): 172-187.

Kaufmann, V., Ladstädter, R. & Lieb, G.K. 2006. Quantitative assessment of the creep process of Weissenkar rock glacier (Central Alps, Austria). *Proceedings of the Eighth High Mountain Remote Sensing and Cartography Symposium, La Paz, Bolivia, March 20-27, 2004*: 77-86.

Kaufmann, V., Ladstädter, R. & Kienast, G. 2007. 10 years of monitoring of the Doesen rock glacier (Ankogel group, Austria) - A review of the research activities for the time period 1995-2005. *Proceedings of the Fifth Mountain Cartography Workshop, Bohinj, Slovenia, March 29–April 1, 2006*: 129–144.

Krainer, K. & Mostler, W. 2006. Flow velocities of active rock glaciers in the Austrian Alps. *Geografiska Annaler, Series A: Physical Geography* 88(4): 267–280.

Lambiel C. & Delaloye R. 2004. Contribution of real-time kinematic GPS in the study of creeping mountain permafrost: examples from the Western Swiss Alps. *Permafrost and Periglacial Processes* 15: 229-241.

Lambiel, C., Delaloye, R., Strozzi, T., Lugon, R. & Raetzo, H. 2008. ERS InSAR for detecting the rock glacier activity. *Proceedings of the Ninth International Conference on Permafrost, Fairbanks, Alaska, June 29–July 3, 2008* (this proceedings).

Mihajlovic, D., Staub, B., Nussbaum, A., Krummenacher, B. & Kienholz, H. 2008. Twenty years of permafrost research on the Furggentälti rock glacier, Western Alps, Switzerland. *Proceedings of the Ninth International Conference on Permafrost, Fairbanks, Alaska, June 29–July 3, 2008* (this proceedings).

Roer, I. 2007. Rockglacier kinematics in a high mountain geosystem. *Bonner Geographische Abhandlungen* 117.

Roer, I., Kääb, A. & Dikau, R. 2005. Rockglacier acceleration in the Turtmann valley (Swiss Alps) - probable controls. *Norwegian Journal of Geography* 59(2): 157–163.

Roer, I., Haeberli, W., Avian, M., Kaufmann, V., Delaloye, R., Lambiel, C. & Kääb, A. 2008. Observations and considerations on collapsing active rockglaciers in the Alps. *Proceedings of the Ninth International Conference on Permafrost, Fairbanks, June 29–July 3, 2008* (this proceedings).

Perruchoud, E. & Delaloye, R. 2007. Short-term changes in surface velocities on the Becs-de-Bosson rock glacier (western Swiss Alps). *Grazer Schriften der Geographie und Raumforschung* 43: 131-136.

Vonder Muehll, D., Noeztli, J., Roer, I., Makowski, K. & Delaloye, R. (eds). 2007. *Permafrost in Switzerland.* PERMOS Reports 4 & 5 (2002/03 & 2003/04). Swiss Acad. of Sciences.

Ground-Based LIDAR Data on Permafrost-Related Rockfall Activity in the Mont Blanc Massif

Philip Deline, Stéphane Jaillet, Antoine Rabatel, Ludovic Ravanel
EDYTEM Lab, Université de Savoie, CNRS, Le Bourget-du-Lac, France

Abstract

It is hypothesized that climatic warming since 1980 increases rock wall instability in high mountains due to permafrost degradation. This is supported by the observation of ice in several rockfall scars. Due to a lack of systematic observations, magnitude and frequency of high mountain rock failures remain poorly known. As part of the French-Italian *PERMAdataROC* project, we apply ground-based LIDAR to monitor instability on representative permafrost-affected rock walls (3000 to 4650 m a.s.l.) in the Mont Blanc massif. Initial results indicate that rockfall activity probably relates to different conditions at the 3 reported sites. The Piliers de Frêney and Grand Pilier d'Angle, both above 4000 m, are virtually stable (0 m³ of rockfalls) and indicate conservation of permafrost at high altitudes even on south-facing rock walls. With a probably critical state of permafrost, Tour Ronde E-Face and Arête Freshfield NE-Face (3460–3792 m) released ca. 1000 m³ of rockfall from 2005–2007. On Les Drus (2700–3700 m a.s.l.), 560 m³ of rockfalls were observed; we argue that these occur due to slope readjustment to the 2005 rock avalanche and are not directly linked to permafrost degradation.

Keywords: LIDAR; Mont Blanc massif; *PERMAdataROC* project; permafrost; rockfall; terrestrial laser scanning.

Introduction

Recently, large rock and rock/ice avalanches have occurred in high mountain areas worldwide (*e.g.,* Kolka-Karmadon, Caucasus 2002, Huggel et al. 2005). In the Alps, Brenva Glacier (1997), Punta Thurwieser (2004), the west face of Les Drus (2005), and the east face of Monte Rosa (2006, 2007) are the most recent examples (Deline 2001, Noetzli et al. 2003, Fischer et al. 2006, Ravanel 2006). In addition, innumerable smaller rockfalls detached from steep rock walls during the hot summer of 2003 (Gruber et al. 2004). The hypothesis that the increase of high mountain rock wall instability relates to permafrost changes gains force (Haeberli et al. 1997, Gruber & Haeberli 2007) from the fact that (1) ice was observed in many starting zones; (2) the mean annual air temperature in the Alps has increased more than 1°C during the 20th Century; and (3) the warming trend has accelerated since 1980.

However, frequency and volume of instability events in high mountains are still poorly known because of the lack of systematic observations, and ongoing permafrost changes in rock walls remain poorly understood due to the difficulties in carrying on in situ measurements. So far, permafrost studies are mainly based on modeling, with a few existing instrumented sites.

The PERMAdataROC project

The *PERMAdataROC* project aims at studying the relation between permafrost degradation and high mountain rock wall instability in two west Alpine areas, the Mont Blanc massif and the Matterhorn, based on the interface of three research assignments (Ravanel & Deline 2006).

The first assignment deals with the collection, maintenance and analysis of recent rockfall/rock avalanches in the Mont Blanc massif in a data base, based on (1) systematic survey of slope instability events (localisation, exposition, time, meteorological conditions, snow conditions, estimated volume, path) carried out by local, trained people (mountain guides, rescue people, hut keepers) in collaboration with the researchers; (2) digitalisation of the events in a GIS; and (3) analysis of the topographical, geological and climatic parameters of the affected rock walls. This data base is complemented by past events that are documented by newspapers, hut, and guide books, as well as previous studies and guide interviews.

The second research assignment deals with measuring and the thermal regime in rock walls. The instrumentation (thermistors at 5, 10, 30, and 55 cm depth) and measurement of relevant properties (albedo, irradiation, thermical conductivity) of rock wall superficial layer and surface at the selected study sites, combined with high altitude climatic data recorded by a movable automatic weather station, will contribute to validate the models of temperature distribution and variations.

The third research assignment is provided by the monitoring of the instability of representative rock walls, by (1) frequently repeated surveys with long-range ground-based LIDAR (LIght Detection And Ranging) and terrestrial photogrammetry, and (2) the installation of a geophone network in one of the study sites to determine the frequency and volume of rockfalls, considering variable parameters (altitude, aspect, slope angle, lithology, fracturing, shadow effect, height drop).

Italian (CNR-IRPI Torino, ARPA Valle d'Aosta and FMS Courmayeur) and French (EDYTEM Lab) partners are involved in the *PERMAdataROC* project, with collaboration with the GGG of University of Zürich.

Here we present initial results of the monitoring of the

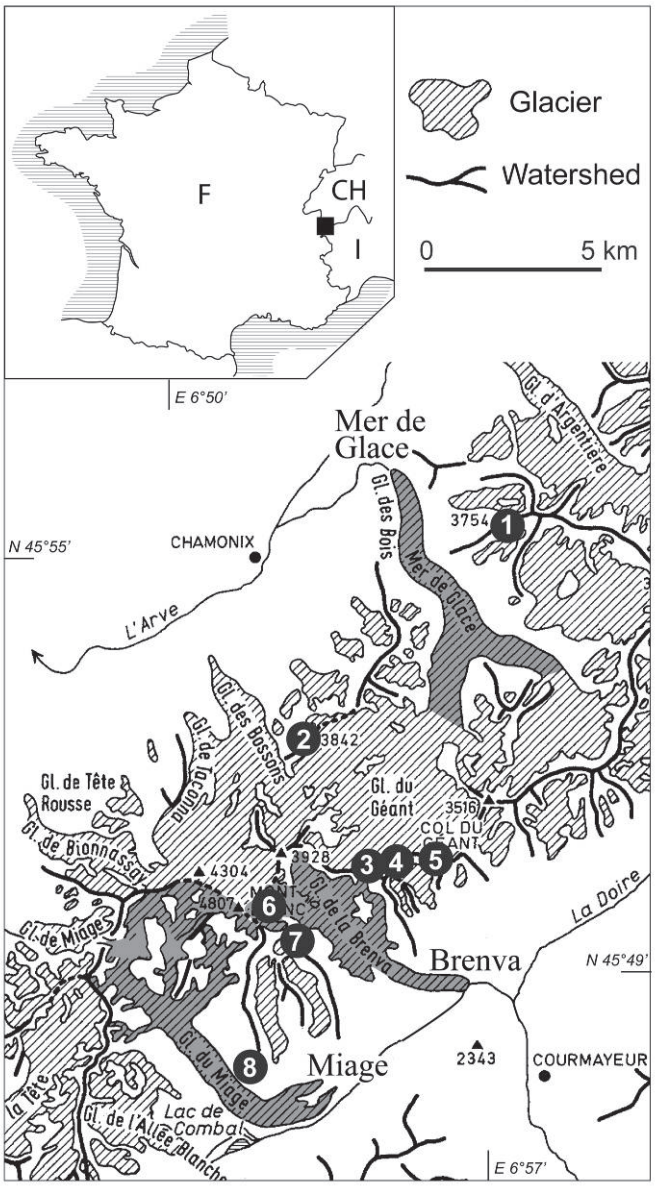

Figure 1. Location map of GB-LIDAR surveyed sites in the Mont Blanc massif within the framework of the *PERMAdataROC* project. 1: Drus; 2: Aiguille du Midi; 3: Tour Ronde-Arête Freshfield; 4: Aiguilles d'Entrèves; 5: Grand Flambeau; 6: Piliers du Frêney-Grand Pilier d'Angle; 7: Aiguilles Blanches de Peuterey; 8: Vallon du Miage. Largest glaciers are highlighted. This paper presents initial results from sites 1, 3, and 6.

instability of rock walls at three sites in the Mont Blanc massif since 2005.

Study Area

The Mont Blanc massif covers an area of approximately 350 km², 40% of which is glacierized. It reaches its highest point at 4808 m a.s.l., but many of its granitic, fractured faces, peaks, and aiguilles stand well above 3000 m. The water divide between Rhône and Pô basins is a 35 km long crest line which always exceeds 3300 m and is often higher than 4000 m. Being one of the most active uplift spots in the Alps (>1.5 mm.an^{-1}), the massif is not only characterized by very high, but also steep faces and rock walls.

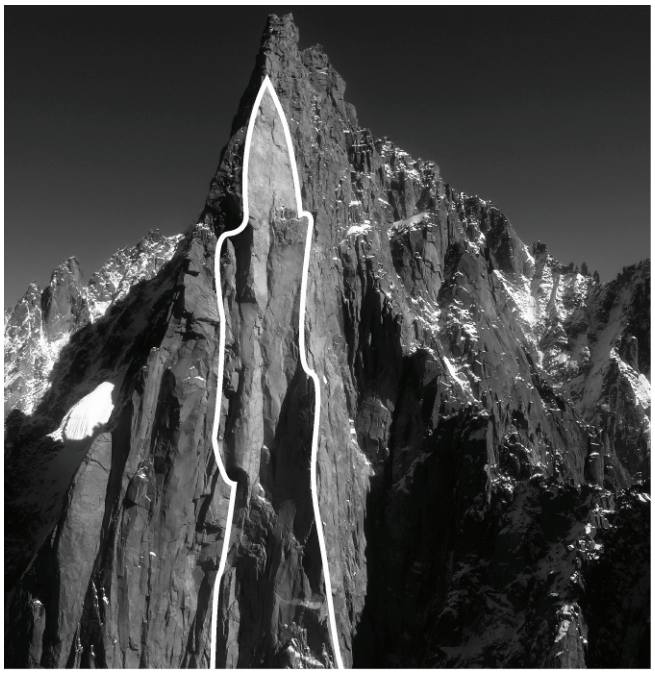

Figure 2. Upper part of the west face of Les Drus. The upper part of the 2005 rock avalanche scar is delimited by the white line. To survey the face, the ground-based LIDAR is set up on Les Flammes de Pierre (crest on bottom right).

Seven study sites from 3000 to 4650 m with different aspects were selected in the Mont Blanc massif within the *PERMAdataROC* project (Fig. 1): the west face of Les Drus, a >70° rock wall between 2700 and 3700 m affected by a series of rockfalls since 1950 with increasing magnitude until June 2005, when collapse of the Pilier Bonatti generated a rock avalanche of >250,000 m^3 (Fig. 2) (Ravanel 2006); the surveyed area at Les Drus is between 3000 and 3700 m; the Piton Central of the Aiguille du Midi (3770–3842 m) which towers above the cable car station, with all aspects; the east face of the Tour Ronde, and the NE-facing Arête Freshfield which develops at the south (3460–3792 m), where rockfalls have been active for several years; the west face of the Aiguilles d'Entrèves (3490–3591 m); the Grand Flambeau (3410–3561 m), close to the Helbronner cable car station, with all aspects; the east-facing Piliers de Frêney (4000–4650 m) and the south face of the Grand Pilier d'Angle (4050–4308 m), on the south side of Mont Blanc summit, and the NW face of the Aiguille Blanche Nord de Peuterey (4000–4103 m). These high elevation sites are complemented by a low-elevation control site (2200–2700 m) without permafrost, on the SW-facing side of the Vallon du Miage.

Methods

Since June 2005, ground-based LIDAR measurements are realised seasonally (summer/autumn) or annually at the eight sites in the Mont Blanc massif, using helicopter or cable cars

for access. Data are processed for calculating high-resolution (centimeter-scale) triangulated irregular networks (TIN). Volumetric changes, extracted on the rock faces by comparing the successive TINs, represent the fallen rocks between the measurement periods (Ravanel & Deline 2006).

LIDAR survey

LIDAR measurements are performed using an Optech® ILRIS 3D ground-based LIDAR. This laserscanner works at distances of up to 800 m if surface reflectivity and visibility are good. The angle of view is 40°×40°, and the sampling rate reaches a maximum frequency of 2000 points per second. At a distance of 100 m, the laser beam diameter is about 30 mm (perpendicular shot), and the accuracy on a flat surface is about 3–5 mm. The LIDAR point to point distances on the rock walls we are surveying range between 61 mm and 246 mm (in 2006 and 2007), on the closest and farthest areas, respectively.

Data processing

Data processing (Rabatel et al., submitted) is realised using InnovMetric PolyWorks® software, with (1) alignment of individual point clouds using the IMAlign module: they are merged with a rototranslation matrix into a unique local reference system, after cleaning individual scans from outliers (Fig.3); and (2) creation of the TIN using the IMMerge module.

The computation of the fallen rock volume in a rock wall between two successive field work campaigns is achieved with the PolyWorks® IMInspect module, which compares two point clouds and quantifies the thickness changes. A reference plan is built, and the volume between the surface topography and this plan is computed for each date.

Error estimation

The total uncertainty can be estimated by the quadratic sum of the different independent errors in the processing. (1) LIDAR error is 3–5 mm at 100 m (manufacturer data). (2) TIN is interpolated from existing points of the global point cloud (set of 3D images). To merge it into a unified polygonal mesh, most parameter values are calculated using input point cloud values. Due to the average mesh used, the TIN construction error is ca. 7 cm. (3) To be compared, diachronous TINs have to be very overlapped. But because of very large TINs, there is a TIN overlapping error, which is 5 cm as measured by Polyworks. This yields an overall uncertainty of 9 cm, which is reduced by directly comparing the point clouds.

Mask effect

Masks result from (1) the topography of the rock wall (roofs, ledges, corners, spurs); (2) the common scarcity of sites to set up the LIDAR (e.g., for the west face of Les Drus, there is only one possible on Les Flammes de Pierre: Fig. 2); and (3) the snow cover, whose extension differs each year. Masks could represent an important part of the surface surveyed, and appear as holes in the TINs. This is particularly the case if there are no multiple viewing angles (Les Drus), or if the snow-ice cover is important (Peuterey).

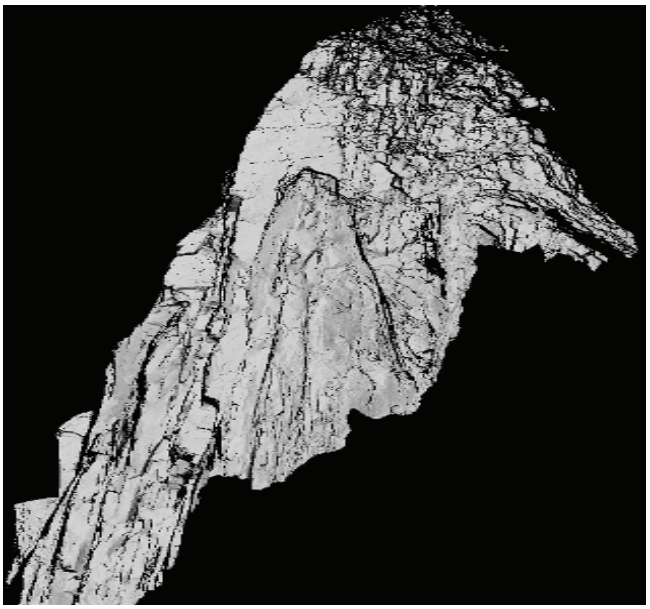

Figure 3. Point clouds of the west face of Les Drus derived from LIDAR surveys (left: October 2005; right: October 2006). The height of the 2005 rock avalanche scar here represented is 500 m.

The Polyworks® IMEdit module allows to reduce their extension. The hole area is first selected. A tool allows the holes to fill automatically using irregular triangles. Only the maximum distance between the vertices of a triangle has to be specified. The longer this distance, the greater resulting size of the plugged hole.

Results

We present initial results from three of the seven high-elevation selected sites in the Mont Blanc massif: (1) the west face of Les Drus; (2) the east face of the Tour Ronde and the NW side of the Arête Freshfield; and (3) the Piliers de Frêney and the south face of the Grand Pilier d'Angle (Table 1).

West face of Les Drus

Comparison of October 2005 and October 2006 TINs reveals a detachment from the 2005 rock avalanche scar of height rock elements of a volume ≥1 m³: five boulders are ≤6 m³, and three are larger. At about 3600 m a.s.l., a notch of 29×10×1.8 m (426 m³) is present on the 2006 TIN; the rocks reached the small debris-covered glacier of Les Drus, at the foot of the west face. Lower on the rock wall, two elements of 19 and 84 m³ also collapsed in this one-year period. In total, 546 m³ of rock were released in the surveyed area between October 2005 and October 2006.

The third survey, carried out at the end of September 2007, shows reduced rockfall activity over the period extending from October 2006 to September 2007: only one small rockfall occurred (22 m³), out of the 2005 scar.

Table 1. Rockfall data from LIDAR surveys (2005–2007).

Site	Period of measurement (d/m/y)	Surface of surveyed area by LIDAR (m^2)	Volume of rockfalls (m^3)		Mean rock wall retreat rate in surveyed area (mm a^{-1})	Extreme distance of point to point on rock wall (mm)
			Total	2 main		
Drus (W face)	11/10/2005–11/10/2006	70,500	546	426 + 84	7.7	Not calculated
	12/10/2006–24/09/2007		22	-	0.3	71–208
Piliers de Frêney - Grand Pilier d'Angle (S face)	14/07/2005–10/10/2005	115,600	0	0	0.0	Not calculated
	11/10/2005–30/06/2006		0	0	0.0	Not calculated
	01/07/2006–13/10/2006		0	0	0.0	61–246
	14/10/2006–12/10/2007		0	0	0.0	61–246
Tour Ronde (E face) – Arête Freshfield (NE face)	13/07/2005–18/07/2006	67,400	536	382 + 154	8.4	Not calculated
	19/07/2006–12/10/2006		0	0	0.0	75–207
	13/10/2006–12/10/2007		448	448	6.6	75–207

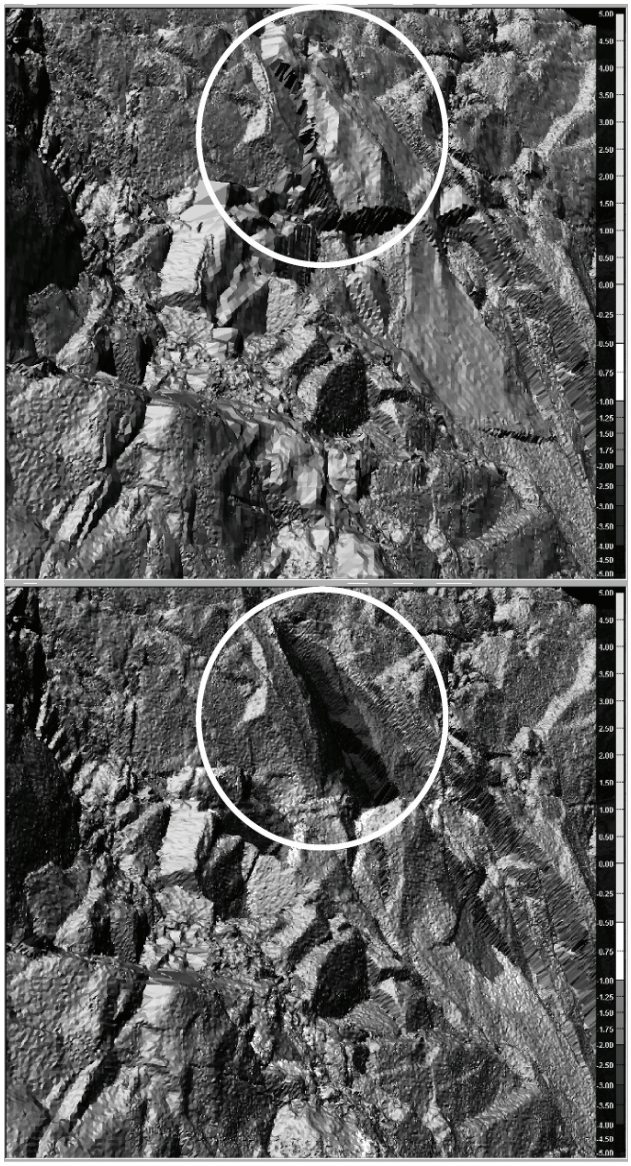

Figure 4. East face of the Tour Ronde TIN (detail). The view focuses on the area affected by the main rockfall between July 2005 (top box) and July 2006 (bottom box). Dimensions of the main scar (visible in bottom box circle) are 17.5×7.8×4.3 m, with a volume of 382 m^3 (image size: ca. 45 m × 45 m).

East face of La Tour Ronde-NE face of Arête Freshfield

At the Tour Ronde, the evolution of the surface topography of the east face between July 2005 and July 2006 shows two main rockfall events, with a volume of 382 m^3 (Fig. 4) and 154 m^3 (main scar sizes are 17.5×7.8×4.3 m and 15.1×9.3×1.4 m, respectively). The total volume of these two rockfall reaches 536 m^3.

The comparison of LIDAR measurements for the second period, between July 2006 and October 2006, shows no significant change during the 2006 summer.

During the third, and last, period of survey, no change was observed on the east face of Tour Ronde. On the other hand, at least two rockfalls occurred on the NE side of the Arête Freshfield, involving a set of large boulders (total volume: 448 m^3) which detached from a small area where bedrock is highly dislocated.

Piliers de Frêney-south face of Grand Pilier d'Angle

Five successive LIDAR surveys performed since July 2005 display no change on the rock walls during a period of 27 months, including 3 summers. Mask effects are important, due to the rough topography of the area (large pillars separated by deep couloirs) and the unique site available to set up the ground-based LIDAR. Thus, only a part of this area is surveyed, but no significant rockfall was observed over the 115,000 m^2 it represents.

Discussion and Conclusions

Results indicate that rockfall activity probably relates to different conditions at the three sites.

On the west face of Les Drus, the rockfalls which occurred probably represent slope readjustment after the large rock avalanche of 2005 and are not directly related to permafrost degradation. For example, the detachment of 84 m^3 between October 2005 and October 2006 is due to the fall of an individualized, hanging, and poorly-rooted slice. Moreover, the small pieces of rock (<1 m^3) identified between 2005 and 2006 were probably destabilized during the fall of the largest element (426 m^3). Lastly, no rockfall occurred into the 2005 scar between 2006 and 2007: this suggests that the mesoscale slope readjustment in the scar is now achieved.

But it is noteable that a new permafrost active layer forms in the 2005 rock avalanche scar.

On the other hand, on the east face of La Tour Ronde and on the NE side of the Arête Freshfield, the rockfalls (2005–2006: 536 m^3; 2006–2007: 448 m^3) probably result from permafrost degradation. This is suggested both by (1) the high rock fall activity during recent years: the normal route to the summit of Tour Ronde is not used when snow cover has melted; and (2) the modeling of the surface temperature of rock walls in alpine areas with similar weather conditions. For instance, mean annual surface temperatures range between -2°C and -4°C at Junfraujoch at 3500–3750 m a.s.l. for E/NE aspect (Gruber et al. 2004: Fig. 2), without taking into account the local topography of the rock faces.

Contrary to the two others sites, the area of the Piliers de Frêney and the south face of the Grand Pilier d'Angle show stable conditions. The results suggest that no or very occasional degradation of the permafrost occurs at very high altitude (>4000 m), including south-facing rock walls like the Grand Pilier d'Angle. Several large grey scars at the foot of the Piliers de Frêney and the nearby Piliers du Brouillard and Mont Maudit, which clearly contrast to the reddish surrounding granite, indicate that rockfalls and rock avalanches have occurred at elevations greater than 4000 m; but preliminary studies (Böhlert et al. 2008) suggest that these grey scars could have formed before 1,500 yr BP, during previous Holocene cold periods.

Given that high-alpine rock walls are a poorly known system, the introduced methodology shows a great potential to reveal quantitative data on geomorphological processes in permafrost-affected rock walls

Acknowledgments

The paper benefited from critical comments by the two anonymous referees, one of them also improving the English. Thanks to all partners of the *PERMAdataROC* project. The European Union (FEDER), the Town Council of Chamonix, and the Conseil Général de la Haute-Savoie are acknowledged for funding. This paper is part of the Interreg IIIA France-Italy # 196 *PERMAdataROC* project.

References

Deline, P. 2001. Recent Brenva rock avalanches (Valley of Aosta): new chapter in an old story? *Supplemento Geografia Fisica e Dinamica Quaternaria* 5: 55-63.

Böhlert, R., Gruber, S., Egli, M., Maisch, M., Brandová, D., Haeberli, W., Ivy-Ochs, S., Kubik, P.W. & Deline, P. 2008. Comparison of exposures ages and spectral properties of rock surfaces in steep, high Alpine rock walls—a field study at Aiguille du Midi, France. *Proceedings of the Ninth International Conference on Permafrost, Fairbanks, Alaska, June 29–July3, 2008* (this proceedings).

Fischer, L., Kääb, A., Huggel, C. & Noetzli, J. 2006. Geology, glacier retreat and permafrost degradation as controlling factor of slope instabilities in a high-mountain rock wall: the Monte Rosa east face. *Natural Hazards and Earth System Sciences* 6: 761-772.

Gruber, S. & Haeberli, W. 2007. Permafrost in steep bedrock slopes and its temperature-related destabilization following climate change. *Journal of Geophysical Research* 112:F02S18, doi: 10.1029/2006JF000547.

Gruber, S., Hoelzle, M. & Haeberli, W. 2004. Permafrost thaw and destabilization of Alpine rock walls in the hot summer of 2003. *Geophysical Research Letters* 31, L13504, doi: 10.1029/2004GL020051.

Haeberli, W., Wegmann, M. & Vonder Mühll, D. 1997. Slope stability problems related to glacier shrinkage and permafrost degradation in the Alps. *Eclogae Geologicae Helvetiae* 90: 407-414.

Huggel, C. Zgraggen-Oswald, S., Haeberli, W., Kääb, A., Polkvoj, A., Galushkin, I. & Evans, S.G. 2006. The 2002 rock/ice avalanche at Kolka/Karmadon, Russian Caucasus: assessment of extraordinary avalanche formation and mobility, and application of QuickBird satellite imagery. *Natural Hazards and Earth System Sciences* 5: 173-187.

Noetzli, J., Hoelzle, M. & Haeberli, W. 2003. Mountain permafrost and recent Alpine rock fall events: a GIS-based approach to determine critical factors. *Proceedings of the 8thInternational Conference on Permafrost, Zürich, Switzerland, August, 2003*: 827-832.

Rabatel, A., Deline, P., Jaillet, S. & Ravanel, L., submitted. Rock falls in high-alpine rockwalls quantified by terrestrial LIDAR measurements. A case study in the Mont Blanc area. *Geophysical Research Letters*.

Ravanel, L. 2006. *Contribution à l'étude des écroulements dans les parois à permafrost de la haute montagne alpine. L'exemple du Petit Dru (massif du Mont Blanc) depuis la fin du Petit Age Glaciaire)*. MSc thesis, Université de Savoie, 116 pp.

Ravanel, L. & Deline, P. 2006. Nouvelles méthodes d'étude de l'évolution des parois rocheuses de haute montagne: application au cas des Drus. *Actes du Colloque Géologie et risques naturels: la gestion des risques au Pays du Mont-Blanc, Sallanches, France, November 18, 2006*: 48-53.

Use of Ground-Penetrating Radar to Characterize Cryogenic Macrostructures in Southern New Jersey, USA

Mark Demitroff
Department of Geography, University of Delaware, Newark, DE USA
James A. Doolittle
National Soil Survey Center, USDA-NRCS, Newtown Square, PA, USA
Frederick E. Nelson
Department of Geography, University of Delaware, Newark, DE, USA

Abstract

The Pine Barrens of southern New Jersey has a well-documented periglacial legacy, evidenced by traces of relict frost fissures and related deformational structures. This study measures the potential of three-dimensional ground-penetrating radar (3D GPR) techniques to detect and identify subsurface cryogenic macrostructures investigated previously in the region, including deformed wedges, sediment-filled pots, and frost-fissure casts. Radar images are especially useful where infill is sandy, and the host sediments are indurated. Although geometric relations between cryostructures are more subtle than in the few contemporary permafrost environments where 3D GPR has been employed and interpretation is more difficult, the ability of 3D GPR to detect networks of fossil features warrants further investigation. The methodology complements traditional field observation and appears to have considerable potential as a tool for detecting and analyzing networks of relict subsurface permafrost features.

Keywords: cryostructures; ground-penetrating radar; New Jersey Pine Barrens; permafrost; remote sensing; thermokarst.

Introduction

The Pine Barrens of southern New Jersey is a highly weathered landscape lying 50 to 150 km beyond the maximum extent of late Pleistocene ice sheets. Its regolith repeatedly experienced cold, dry, and windy conditions during the late Pleistocene, leaving behind a long-debated fossil signature of climate change (Wolfe 1953, Newell & Wyckoff 1992, Demitroff 2007). Permafrost was present in at least three intervals during the last 200,000 years (French et al. 2007). Various periglacial geomorphic processes operated intermittently in the region, including thermal-contraction cracking, desiccation, and thermokarst displacement.

Alternating cold and warmer intervals created a complex suite of distinctive soil phenomena in southern New Jersey (French & Demitroff 2003, French et al. 2003, 2005), including sand-wedge casts, "soil wedges," and thermokarst features. We refer to these features collectively as cryogenic macrostructures (Huijzer 1993). Recent investigations (French & Demitroff 2001, French et al. 2003, 2005) indicate that the coarse-textured soils, sparse vegetation, and thin snow cover of the region during cold intervals favored deep frost penetration. Gravel-rich hilltops and proximal slopes composed of near-surface gravelly colluvium are the best locations to observe macrostructures, because the features are best preserved in such topographic situations. This study evaluates the ability of ground-penetrating radar (GPR) to image cryogenic macrostructures on both two-dimensional (2D) radar records and three-dimensional (3D) pseudo-images.

Frost-Fissure Casts

Sand-wedge casts

Ice wedges are commonplace in contemporary Arctic landscapes. This was not the case in Pleistocene New Jersey. Moisture was minimal when thermal-contraction cracking occurred in the Pine Barrens, so open fissures were mostly filled with wind-blown sands instead of ice. Primary mineral-filled frost cracks are called *sand wedges* (Murton et al. 2000). Pine Barrens sand wedges were epigenetic. They are found just below the uppermost 0.5 to 1.0 m of the soil surface, range in depth from 1.5 to 3.0 m, and average from 20 to 40 cm in width. Two distinct types of sand-wedge-cast forms are recognized in southern New Jersey, "older" (Fig. 1A) and "younger" (Fig. 1B), based on luminescence ages (French et al. 2003). Both exhibit variable spacing (10 to 40 m apart), although smaller sand-wedge casts can grade toward closer spacing.

Older sand-wedge casts typically extend 2–3 m below the surface and are found in higher landscape positions. They contain slightly indurated, fine loess-like to medium sand laminae that stand in sharp contrast to the indurated enclosing matrix, which is interpreted as a fragipan. Small amounts of near-vertically oriented gravels are present towards wedge tops. Luminescence dates indicate that these structures are Early Wisconsinan (Oxygen Isotope Stage 4 [OIS-4]), Illinoisan (OIS-6), or even older structures. Younger sand wedges are 1 to 2 m in depth and can be located across various landscape elevations. They are filled with coarse, loosely packed sand grains that that have been less abraded by wind than those found in older macrostructures. Infill is massive, and lacks the vertical foliation common to older

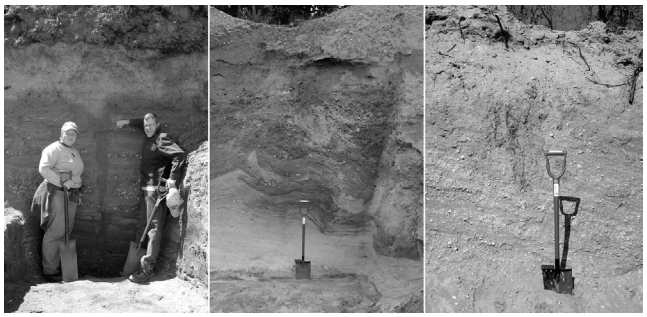

Figure 1. Examples of frost-fissure cast forms at study sites. (A) Older sand-wedge cast, Dorchester. (B) Younger sand-wedge cast, Unexpected 1. (C) "Soil wedge," Unexpected 1.

sand-wedge casts. Luminescence dating indicates that they formed during the Late Wisconsinan (OIS-2).

Soil wedges

In addition to sand-wedge casts, smaller, more closely spaced (2 to 6 m) wedge casts (Fig. 1C) have been described in the Pine Barrens (French et al. 2003). These structures are shallower in depth (<1.5 m) and often narrower in width than sand wedges. Due to their superposition on older features, these structures may be of similar age or possibly younger than the late Wisconsinan sand-wedge casts (OIS-2). Little is known of the dynamics of these features, which have been termed *soil wedges* by Romanovskij (1985). They appear to be artifacts of a dry, cold period at the end of the late Wisconsinan. Active soil wedges have been described from Siberia, but are uncommon under current climatic conditions. Their origin is attributed to cryodesiccation in a seasonally frozen soil layer. Permafrost need not be present for such wedges to form (Jahn 1975, French & Demitroff 2001).

Thermokarst-Modified Wedges

Deformed wedges

Downslope from salients and relict plateaus, the fragipan, which preserves the wedge features, dissipates and the moisture gradient increases. Accompanying this change is modification of upland sand wedges into deformed, furrow-like structures (Fig. 2A) up to 3 m by 3 m. These features are created through deformation of the original macrostructures by thaw erosion, gullying, cryoturbation, and slumping (French et al. 2005). The modifications occurred during periods of climatic amelioration and permafrost degradation, approximately 30 ka (French et al. 2007).

Sediment-filled pots

Associated features known as sediment-filled pots (Fig. 2B) occur at the intersection of deformed wedges. These kettle-like features appear as large elongated to bulbous shaped structures up to 3 to 5 m wide, extend 3 to 4 m below the surface, and extend horizontally up to a few meters in distance. Sediment-filled pots are complex vessels of sands, and silty-to-clayey-to-gravelly diamict.

Figure 2. Examples of thermokarst-modified wedges at study sites. (A) Modified sand wedge, Unexpected 2 (B) sediment-filled pot, Unexpected 2.

Locations and Methods

Study sites

Sites investigated in this study are located in two commercial sand and gravel operations in southern New Jersey where various cryogenic macrostructures have been identified. The sites are referred to as the Dorchester (39.29013°N, 74.95023°W) and the Unexpected (originally named Brimfield Crossing) (39.56707°N, 74.91448°W) sites. The Dorchester site is in an area of Aura sandy loam, with 0 to 2 percent slopes. The Unexpected site is located in an area of Downer loamy sand, with 0 to 5 percent slopes. The very deep, well-drained Aura and Downer soils were formed in unconsolidated alluvial sediments on the Outer Coastal Plain's Bridgeton Formation. Aura soils are moderately deep (50 to 100 cm) to fragipan. Aura is a member of the coarse-loamy, siliceous, semiactive, mesic Typic Fragiudults family. Downer is a member of the coarse-loamy, siliceous, semiactive, mesic Typic Hapludults family. At the Unexpected site, the upper 25 to 50 cm surface materials had been removed in preparation for mining. A very dense and compact B horizon is also present at the latter site.

Field methods

Survey grids were established at each site. At the Dorchester site, a 2.5 × 2.5 m grid was established immediately behind an excavation wall that contained an older sand-wedge cast. Traverse-line spacing was 25 cm. Two grids were established at the Unexpected site. A 20 × 15 m grid was established near an excavation wall containing deformed wedges, soil wedges, and sediment-filled pots. A 20 × 13 m grid was established near an excavation wall that contained younger sand-wedge casts and soil wedges. For each of these grids, the traverse line spacing was 50 cm.

All grids were established across recently cleared, accessible, and level areas adjacent to excavation walls. For each grid, two parallel axis lines were laid out and spaced either 2.5 m (Dorchester) or 20 m (Unexpected) apart. Along these two parallel axes, survey flags were inserted into the ground at a spacing of 25 cm (Dorchester) or 50 cm (Unexpected), and a reference line was extended between matching survey flags on opposing sides of the grid using

a graduated rope. GPR traverses were conducted along this reference line (the X-axis). A 400 MHz antenna was pulled along the graduated rope, which was stretched across the soil surface, and, as it passed each 50 cm (Dorchester) or 100 cm (Unexpected) graduation, a mark was impressed on the radar record. Following completion of a transect, the reference line was moved to the next pair of survey flags to repeat the process.

The radar unit is the TerraSIRch Subsurface Interface Radar (SIR) System-3000, manufactured by Geophysical Survey Systems, Inc. (GSSI; Salem, New Hampshire, USA). The system consists of a digital control unit (DC-3000) with keypad, SVGA video screen, and connector panel, weighs about 4.1 kg (9 lbs), and is backpack portable. The system requires two people to operate.

The *RADAN for Windows* (version 5.0) software program developed by GSSI was used to process the radar records. Processing included: setting the initial pulse to time zero, color table and transformation selection, marker editing, distance normalization, range gain adjustments, high-pass filtering, and migration. The Super 3D QuickDraw program developed by GSSI was used to construct 3D pseudo-image of the radar records.

Calibration

Ground-penetrating radar is a time-scaled system measuring the time required for electromagnetic energy to travel from the antenna to an interface (e.g., soil horizon, stratigraphic layer) and back. To convert the travel time into a depth scale, either the velocity of pulse propagation or the depth to a reflector must be known. The relationships among depth (D), two-way pulse travel time (T), and velocity of propagation (v) are described in the following equation (Daniels 2004):

$$v = 2D/T \quad (1)$$

The velocity of propagation is principally affected by the relative dielectric permittivity (ε_r) of the profiled material (s) according to the equation (Daniels 2004):

$$\varepsilon_r = (C/v)^2 \quad (2)$$

where C is the velocity of propagation in a vacuum (0.298 m ns^{-1}). Velocity is expressed in meters per nanosecond (m ns^{-1}). In soils, the amount and physical state (temperature dependence) of water have the greatest effect on ε_r and v. The velocity of propagation through the upper part of the soil profile at each grid site was based on the measured depth and the two-way pulse travel time to a known buried reflector, and using equation (1). At the Unexpected Site, the estimated velocity of propagation was 0.119 m ns$^{-1,}$ and the relative dielectric permittivity was 6.3 m ns^{-1}. At the Dorchester Site, the estimated velocity of propagation was 0.136 m ns$^{-1,}$ and the relative dielectric permittivity was 4.8. Daniels (2004) has detailed GPR processing techniques for those who wish to go beyond the scope of this paper.

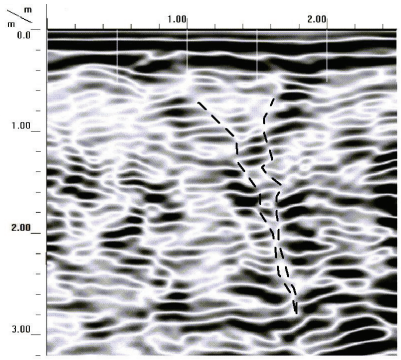

Figure 3. An older sand-wedge cast is faintly expressed in this radar record from the Dorchester site.

Results

Dorchester site

The radar record in Figure 3 was obtained immediately behind an excavation wall in which a well-documented sand-wedge cast (French & Demitroff 2001, French et al. 2003) was exposed. The depth and distance scales are expressed in meters, with depth based on an estimated velocity of propagation of 0.136 m ns^{-1}. A majority of the radar reflections are of moderate to high signal amplitude (darker images) and appear nearly level to slightly inclined. These characteristics are considered typical of fluvial to marine-marginal Coastal Plain sediments. However, these reflectors are not laterally continuous, but appear segmented, with noticeable breaks appearing on the radar record. On radar records, segmentation can be caused by truncation of layers, lateral gradation in the degree of contrast between reflectors, and/or superposition and cancellation of reflected signals.

A sand-wedge cast can be identified on this radar record between the 1.0 and 1.6 m marks at the surface (Fig. 3). Segmented lines highlight the inferred boundary of this sand wedge. The fissure is most clearly expressed in the upper meter of the radar record, where the loosely cemented, smaller grain-sized infill contrasts with the encircling very hard, indurated, and coarser sandy-gravelly matrix. Sand wedges display a wide variety of geometric forms and structures. They may consist of massive or highly stratified materials, have sharp and planar to diffuse and irregular boundaries, and can be wedge-shaped and tapered to irregular, or bulbous (Murton et al. 2000). The morphological characteristics of older sand-wedge casts, in particular, do not favor radar interpretations, owing to their, narrow width and indurated infill. Below depths of about 1 meter, the thin width, tortuous vertical descent, and variable physical properties of the wedge casts contribute to poor, ambiguous boundary expression with the host materials.

In Figure 4 an exposed sand-wedge cast is located on the wall of the excavated pit. All radar traverses were conducted parallel to the X-axis (right foreground). Radar traces were sampled more continuously along this axis, and reflectors are more strongly represented, with little distortion, along it. Along the Y-axis, however, data were not recorded continuously but were instead interpolated over a 25 cm

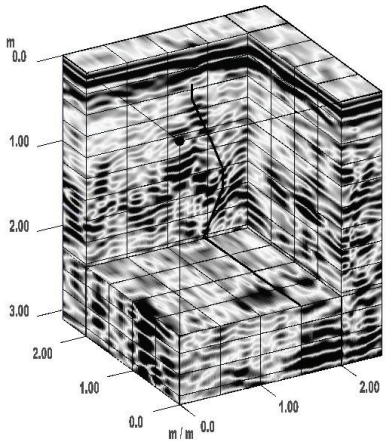

Figure 4. A 3D pseudo-image cube of the Dorchester grid area, with a 2.0 by 2.0 by 2.3 m inset removed.

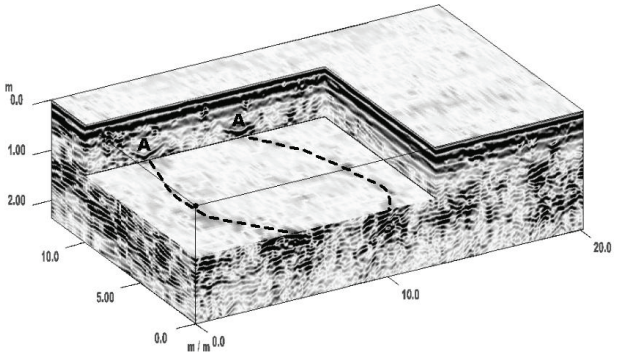

Figure 5. A 3D pseudo-image cube of the Unexpected grid area has subsurface furrows. In this image, a 12.0 m× 10.0 m× 1.0 m inset has been removed.

interval (the distance between radar traverses). As a result, some subsurface information was lost during interpolation, and features appear smudged, less resolved, and more generalized along the Y-axis.

In Figure 4, a bold dashed line emphasizes the inferred centerline of the ancient sand-wedge cast on the back wall and base of the cutout section. The wedge is more evident on the back wall of the cutout. Along its base, only a very weakly expressed and ambiguous trace of very low signal amplitudes (white color) marks the inferred location of the wedge. This frost crack, while evident, was not clearly expressed on either the 2D radar records or the 3D pseudo images prepared from data collected with the 400 MHz antenna. Interpretations are ambiguous and, without knowledge of its location, the fissure may have been missed using GPR. Older sand-wedge casts often defy visual detection as well, requiring careful site preparation and prior familiarity with feature identification. Wedge borders are often faint, with little contrast between infill and enclosing sediments. Wedge outlines may not be fully apparent until hours after excavation. Upon exposure to air, the loose sandy infill dries more rapidly than denser enclosing sediments, creating visible differences in tonal contrast.

Unexpected site

At the Unexpected site, two small grids were established near areas of known cryogenic macrostructures. One grid was established near an area underlain by younger sand-wedge casts and soil wedges that were traced backward and downslope along an excavation wall. Figure 5 is a 3D pseudo-image of the 20 m × 13 m grid area. In this image, the excavation wall parallels the X-axis (right foreground). A 12.0 m × 10.0 m × 1.0 m inset has been removed. All radar traverses were conducted parallel to the X-axis.

The grid was established across an area recently cleared of forest vegetation. In Figure 5, the occasional, high-amplitude, hyperbolic reflections apparent in the upper 70 cm of the image may represent larger tree roots. In general, subsurface reflectors apparent in this pseudo-image suggest the dominance of linear, level to slightly inclined interfaces. These reflectors are presumed to represent the boundaries of contrasting stratigraphic layers within the fluvial sediments.

Along the back wall of the cutout, two perceptible, high-amplitude concavities with downturned reflection patterns are apparent at depths ranging from 70 to 100 cm ("A" in Fig. 5). These features probably represent a continuation of the younger sand-wedge casts clearly visible in the front-wall exposure. Though discontinuous, faint, and somewhat ambiguous, these structures appear to form lineations that extend across the base of the cutout. These lines appear to represent the traces of wedges running parallel to the slope. Beneath the traces are areas with more complex reflector patterns on the front wall of the diagram (right foreground). This plot represents a front-to-back view of a transitional zone, in which sediments that formerly contained little ice (foreground) grade into those that were once ice-rich (30 m beyond the study plot)(Demitroff 2007).

Thermokarst involutions observed by French & Demitroff (2001) and French et al. (2005) were just 30 m downslope from the back of this study plot. Fissures, marked in bold dashed lines on Figure 5, are oriented directly toward these deformed sediments. Recent excavations in this vicinity revealed a younger sand-wedge cast (Fig. 1B) superimposed upon a load-deformed portion of an involution (Demitroff 2007). The underlying thermokarst-affected layer appears to have been deformed by thawing of an ice-rich wedge aligned with the slope-oriented fissures demarcated on the radar image. Older frost cracks appear to have been modified along a moisture gradient. Forms are modified gradually along such gradients, from sand wedges to deformed wedges to thermokarst involutions. Younger sand-wedge casts and soil wedges are little deformed, because thermokarst appears not to have developed during late Wisconsinan (OIS-2) warming (French et al. 2007). Although linkages may be extrapolated from the radar image, their true relationships will soon be revealed as the intervening 30 m of forest is removed and quarrying continues. In the Pine Barrens, younger wedge structures commonly form within earlier cryogenic macrostructures, as these are the most likely locations for

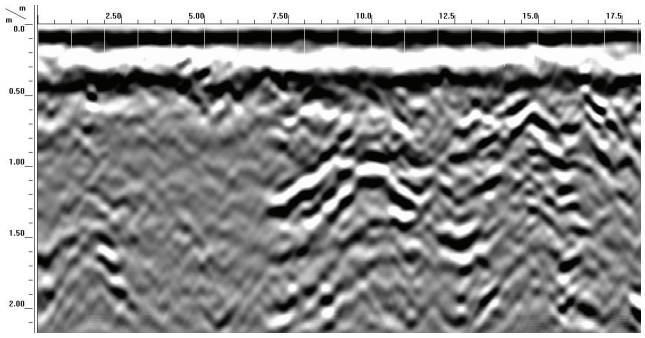

Figure 6. The radar record from the Line Y =10 m at the second Unexpected site.

stress to be relieved during episodes of cracking.

At the Unexpected site, a second grid was established near an exposure containing soil wedges, modified sand wedges, and sediment-filled pots. An 18 m section of a radar record from this site is shown in Figure 6. The number, intensity, and geometry of subsurface reflectors vary across this radar record. The left part of this diagram is comparatively devoid of high-amplitude reflectors, and may be underlain by more homogenous and less anisotropic materials. The right part of this diagram contains multiple, irregularly shaped and sized reflectors, which form a distinct zone about 10 m wide. However, most individual reflectors within this zone are less than 2 to 3 m wide.

The number and complexity of reflectors confound individual interpretations. It is assumed that this portion of the radar record consists of multiple strongly deformed layers and inclusions of soil materials that vary in grain-size distribution, moisture content, and/or density. This portion of the radar record is believed to represent a complex of cryogenic macrostructures. The difficulty in using a planar view is the diverse orientations of many wedge-like features. If viewed from an oblique angle, the radar image may be difficult to interpret. In some cases, the upper portion of a wedge may be perpendicular to the ground, and the lower portion sharply angled.

Figure 7 is a 3D pseudo image of a 20 m × 15 m survey area at Unexpected. In Figure 7, all radar traverses were conducted parallel to the X-axis (right foreground). The base of the cutout contains a diversity of both linear and curved features that vary in width and are not evenly distributed beneath the grid area. Linear features were interpreted as representing deformed wedge furrows (Fig. 2A). Large circular-to-elongate patterns evident on the base of the cutout are interpreted as sediment-filled pots (Fig. 2B).

Figure 8 documents the excavation wall when it had progressed midway across the former GPR grid site. Several well-defined deformed wedges (1st, 2nd and 5th arrows, left to right) and sediment-filled pots (3rd and 4th arrows) are exposed in the pit wall (Fig. 8). Dark patches mark their presence along the diagonal line. The fifth feature is just outside the study bounds. These features support earlier GPR interpretations. The loose, light-colored, aeolian structure-fill markedly contrasts with the indurated, orange/red-colored host materials. Here, the macrostructures are infilled with fine to medium sand with some sandy gravel diamict. Their loosely packed materials contrast with the indurated enclosing matrix of sands and gravel (French et al. 2003). The indurated layers helped to preserve these features as permafrost thawed (French et al. 2005).

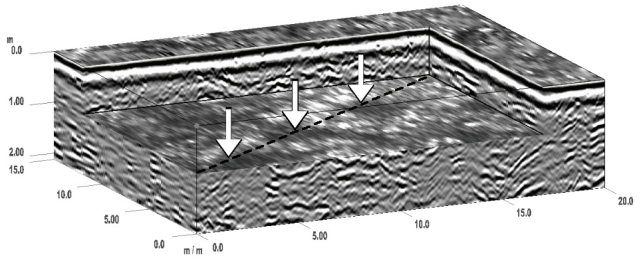

Figure 7. A 3D GPR pseudo-image from the grid site. In this image of the 20 m x 15 m survey area, a 17 m x 12 m x 0.95 m volume has been removed. The dashed diagonal line indicates the location of the wall section of Figure 8 when the photo was taken. Three white arrows mark the location of sand-filled cryogenic macrostructures marked by the inner arrows on Figure 8.

Figure 8. The second Unexpected site with half the soil diagonally removed by excavation. Arrows indicate the locations of larger (eolian) sand-filled cryogenic macrostructures. Smaller periglacial structures occupy the intervening space.

Conclusions

GPR has been used extensively in glacial and periglacial environments (Munroe et al. 2007, Woodward & Burke 2007), where ground ice provides sharp radar reflection contrast with other frozen sediments. Near Barrow, polygonal ice -wedge networks provided impressive geometric patterns in 3D radar images (Munroe et al. 2007). This study indicates that not all paleoperiglacial landscapes are so amenable to ground-penetrating radar application. Relict macrostructures are problematic: (1) primary and secondary fill often provides little contrast with host sediments; (2) subsequent, often polycyclic, modification creates complex, indistinct boundaries; (3) many relict structures are smaller than their Arctic counterparts; and, at least in the Pine Barrens, (4) complete geometric expression of frost-crack polygons is absent. Although rarely observed in plain view, deformed wedge/furrows may form incomplete polygons or lineations parallel to the slope gradient. The absence of well-defined polygons in the uplands indicates that conditions were marginal for their development (French et al. 2003).

Ground-penetrating radar can be used to help locate and characterize various buried cryogenic macrostructures. Uplands of the Pine Barrens are a protean landscape, an

epigenetic tableau that was repeatedly subjected to the waxing and waning of ice-marginal periglacial conditions. The broad suite of composite cold-climate structures present can be baffling, even with careful field scrutiny by experts. In the absence of heavy excavation equipment, the well-developed dense fragipan of the Pine Barrens drastically limits a three-dimensional perspective of cryogenic macrostructures. In lieu of arduous quarrying, radar records are a useful tool for use in identifying the presence, size, and directional trend of generic structures. However, only careful excavation can reveal a structure's origins with certainty.

The study areas have favorable soil properties (i.e., low in clay, soluble salt, and moisture content) for the use of GPR. The features under investigation often lack sufficient contrast and/or have geometrical forms that limit the amount of energy that is reflected back to the radar antenna. Owing to the limited size and complexity of many cryogenic macrostructures in southern New Jersey, some of these features are more difficult to recognize than in other regions such as in Wisconsin (Doolittle, unpubl.).

In southern New Jersey, older sand-wedge casts are narrow and indurated, making detection by GPR alone difficult. Delineation is often problematic even under visual scrutiny in pit sections. The steep inclination and tortuous nature of the wedges produces weak, nearly indistinguishable reflections that are difficult to trace laterally in plan view and preclude recognition of the full extent of their traces. Narrow wedges can be indistinguishable on radar records. Wider deformed sand wedges and related thermokarst features are much more amenable to interpretation. These structures are more nearly linear and are often slope-aligned, producing recognizable GPR images. Boundaries between cryogenic macrostructures and host sediments can be complicated where sloughing of sediments and reworking from the sides has occurred through thaw erosion, gullying, and slumping, especially with deformed wedges and sediment-filled pots. Intricate arrangements of segmented, inclined, or contorted subsurface reflectors, separated by abrupt vertical fissures, may serve to identify these features on radar records.

Acknowledgments

Students from the University of Delaware Geography and Geology Field Geomorphology course in Spring 2006 provided field assistance. Aggregate extraction operations access was kindly provided through Dave Hergert (Mays Landing Sand and Gravel) and another operator who wishes to remain unacknowledged. MD thanks both for long-term support of his field investigations. Manufacturers' names are provided for specific information, and use does not constitute endorsement.

References

Daniels, D.J. 2004. *Ground Penetrating Radar*, 2nd Edition. London, UK: The Institute of Electrical Engineers, 726 pp.

Demitroff, M.N. 2007. *Pine Barrens Wetlands: Geographical Reflections of South Jersey's Periglacial Legacy*. Masters Thesis. University of Delaware, Newark, DE, 224 pp.

French, H.M. & Demitroff, M. 2001. Cold-climate origin of the enclosed depressions and wetlands ('spungs') of the Pine Barrens, southern New Jersey, USA. *Permafrost and Periglacial Processes* 12: 337-350.

French, H.M. & Demitroff, M. 2003. Late-Pleistocene periglacial phenomena in the Pine Barrens of southern New Jersey: GANJ Field Excursion Guide, October 11, 2003. In: M.J. Hozik & M.J. Mihalasky (eds.), *Field Guide and Proceedings, 20th Annual Meeting of the Geological Association of New Jersey, October 10-11, 2003*: 117-142.

French, H.M., Demitroff, M. & Forman, S.L. 2003. Evidence for Late-Pleistocene permafrost in the New Jersey Pine Barrens (Latitude 39°N) Eastern USA. *Permafrost and Periglacial Processes* 14: 259-274.

French, H.M., Demitroff M. & Forman, S.L. 2005. Evidence for Late-Pleistocene thermokarst in the New Jersey Pine Barrens (Latitude 39°N) Eastern USA. *Permafrost and Periglacial Processes*. 16: 173-186.

French, H.M., Demitroff M., Forman, S.L. & Newell, W.L. 2007. A chronology of Late Pleistocene permafrost events in southern New Jersey, Eastern USA. *Permafrost and Periglacial Processes* 18: 49-59.

Huijzer, A.S. 1993. *Cryogenic Microfabrics and Macrostructures: Interrelations, Processes, and Paleoenvironmental Significance*. Ph.D. dissertation, Vrije Universiteit, Amsterdam, 245 pp.

Jahn, A. 1975. *Problems of the Periglacial Zone* (*Zagadnienia strefy peryglacjalnej*). Translated from Polish. Warszawa, POL: Polish Scientific Publishers, 223 pp.

Munroe, J.S., Doolittle, J.A., Kanevskiy, M.Z., Hinkel, K.M., Nelson, F.E., Jones, B.M., Shur, Y. & Kimble, J.M. 2007. Application of ground-penetrating radar imagery for three-dimensional visualization of near-surface structures in ice-rich permafrost, Barrow, Alaska. *Permafrost and Periglacial Processes* 18: 309-321.

Murton, J. B., Worsley, P. & Gozdzik, J. 2000. Sand veins and wedges in cold aeolian environments. *Quaternary Science Reviews* 19: 899-922.

Newell, W.L. & Wyckoff, J.S. 1992. Paleohydrology of four watersheds in the New Jersey Coastal Plain. In: G.S. Gohn (ed.), *Proceedings of the 1988 U.S. Geological Survey Workshop on the Geology and Geohydrology of the Atlantic Coastal Plain*. United States Geological Survey, Circular 1059, 23-28.

Romanovskij, N.N. 1985. Distribution of recently active ice and soil wedges in the USSR. In: M Church & O. Slaymaker (eds.). *Field and Theory: Lectures in Geocryology*. Vancouver, BC: University of British Columbia Press, 154-165.

Wolfe, P.E. 1953. Periglacial frost-thaw basins in New Jersey. *Journal of Geology* 61: 133-141.

Woodward, J. & Burke, M.J. 2007. Applications of ground-penetrating radar to glacial and frozen materials. *Journal of Environmental and Engineering Geophysics* 12(1): 69-86.

Tomodensitometric Analysis of Basal Ice

Matthew Dillon, Daniel Fortier, Mikhail Kanevskiy, Yuri Shur
University of Alaska Fairbanks, Institute of Northern Engineering, Fairbanks, Alaska, U.S.A.

Abstract

Basal ice of contemporary glaciers was studied in an attempt to find convincing evidence of a genesis of buried glacial ice in permafrost. As a part of this study, tomodensitometric scans of basal ice from the Matanuska Glacier in Alaska were made using a micro-computed tomographic scanner. Scans are an excellent complement to field studies of cryostructures because of the level of detail obtained regarding the ice distribution. Two- and three-dimensional models were generated from the scans and were used to study patterns of ice distribution, the volume of ice, sediment, and gas inclusions.

Keywords: basal ice; buried glacial ice; computed tomography; cryostructure; Matanuska Glacier; x-ray.

Introduction

X-ray computed tomography, also known as tomodensitometry, has been widely used in two- and three-dimensional (3-D) visualization of the internal structures of various materials since its inception (Ambrose & Hounsfield 1973). Tomodensitometry is a computer-controlled x-ray photography procedure. By taking a single x-ray photo from multiple angles, a 3-D interpolation of the interior of the sample can be revealed. Tomodensitometry usage is expected to undergo sustained growth due to the relatively low cost of scanner apparatus, the non-destructive aspect of its application, the clear penetration of x-rays into samples, and the high resolution imaging potential related to advances in computing power. One of the immediately recognizable benefits of tomodensitometry is that it is a non-destructive technique. Non-biological objects, such as soils, remain structurally unaffected by x-ray radiation.

In soil sciences, tomodensitometry has been used in multiple ways. Porosity has been calculated by separating phase components post-scanning by Alshibli et al. (2006) and Rachman et al. (2005). By various methods, many typical soil index properties have been determined, such as bulk density distribution, water content distribution, and mineral type distribution (Phogat et al. 1991, Macedo et al. 1998, Rogasik et al. 1999, Pralle et al. 2001, Pedrotti et al. 2004). Computer simulations using real-world geometries of soils for determination of hydraulic conductivity have been performed by Fourie et al. (2007) and Bastardie et al. (2003).

In fresh-water ice studies, tomodensitometry has been used to characterize air inclusions in river ice to aid in synthetic aperture radar interpretation of river ice (Gherboudj et al. 2007).

In permafrost studies, Torrance et al. (in press) used tomodensitometry to study the pattern of ice lenses in soil. Calmels et al. (2004, 2008) used tomodensitometry to image faulted ice and sediment layers in palsas, to infer direction of soil freezing and to provide volumetric content of ice, gas, and sediment components. The thresholding technique used to determine the volumetric contents and the error associated with it has not, however, been specified.

This paper presents some results of tomodensitometric studies of basal ice of glaciers. To the best of our knowledge, this is the first time that this technique has been used to study the structure of basal ice of glaciers. Basal glacier ice is formed at the bed of glaciers due to several processes, such as entrainment and incorporation of sediments by overriding ice, regelation, glacio-hydrologic supercooling, glaciotectonics, basal freeze-on, ice segregation, and downward propagation of cold temperatures in the sediment at the glacier bed (Sharp et al. 1994, Knight 1998, Lawson et al. 1998). We want to develop a classification of basal ice cryostructures for permafrost studies to identify and to distinguish basal glacier ice buried in the permafrost from other types of massive ice (e.g., massive segregated ice and injection ice); however, this paper only addresses the application of tomodensitometry to basal ice analysis. It is focused mainly on the technical aspects of 2-D and 3-D imaging of the samples in order to extract key parameters such as basal ice structure and the volumetric contents of its phase components.

Methods

Sampling

Field work was conducted at the Matanuska Glacier, Alaska (61°46′11″N, 147°44′3″W). We logged, sketched, and photographed the cryofacies and cryostuctures of several basal ice exposures. The description of the basal ice cryostratigraphy is beyond the scope of this paper, and those results will be presented elsewhere. Cores were retrieved from the exposures using a CRREL-SIPRE corer barrel. The cores were covered in plastic wrap and aluminum foil and brought back frozen to the laboratory.

In the lab, cores approximately 50 mm in diameter and 50 mm tall were extracted from the large-barrel cores to accommodate the maximum sample size that the scanning equipment can accept. These smaller cores were wrapped in plastic wrap to prevent sublimation, as well as in cellulose insulation, encased in a hollow plastic container, and kept in a freezer at -10°C

Tomodensitometry

The scans were acquired with a Skyscan 1172™ scanner, equipped with a rotating scan platform, a stationary camera, and an x-ray source. The scans were commenced in a cold room environment at -6°C. In order to ensure adequate "penetration" of the x-rays through dense materials, the scans were performed at 80 kV and 100 µA, the highest voltage and current permitted by the system. An exposure time of 1264 ms, a rotation step of 0.3°, and a scanning domain of 360° were experimentally determined to maximize scan quality. The camera's pixel size was 34.46 µm.

Image processing methods

The scanner results are a "stack" of grayscale images that represent the total volume for the sample. Reference volumes 27.57 mm high by 27.57 mm wide by 13.71 mm deep were selected from each scanned core for streamlined analysis. The resized samples had a pixel size of 68.93 µm. Each image is 400 pixels by 400 pixels and 1 pixel thick. One unit pixel in the image is also called a voxel for 3-dimensional image data. Each voxel is assigned a grayscale value based on its density relative to that of gas—low density values are black pixels with a grayscale value of 0; high density values are white pixels with a grayscale value of 255. All the shades of gray vary linearly between grayscale values of 0 and 255. The Mathworks MATLAB R2007a™ Image Processing Toolbox software was used to process the volume's grayscale values that are obtained from the scanner.

The samples contain three components: gas, ice, and sediment. These components were separated in the scans using a thresholding technique which reassigns a range of grayscale values to white, while everything outside of this range is black. Threshold values were determined from the grayscale histogram on scans of ice made of de-aired and de-ionized water (Fig. 1a). By determining the minima of the gray values on the histogram (Fig. 1c), the limits of thresholding can be applied at these points for a binary image (Fig. 1b). For this study, ice was found to generally range between 10 and 48 in grayscale values, based on several scans of pure ice. Therefore gas was defined as 0–9, ice as 10–48, and sediment as 49–255 grayscale values. The threshold values were applied to the raw scan images (Fig. 2a) to create component reduced images (Fig. 2b).

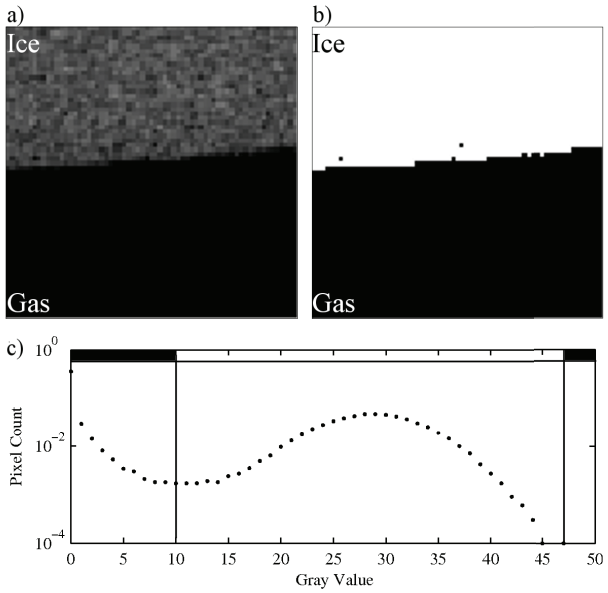

Figure 1. Scan images of an ice cube edge made of de-aired and de-ionized water. a) Cross sectional scan image of ice and gas before thresholding (varying gray values represents ice, black is gas). b) Cross sectional scan image of ice and gas after applying threshold limits at 10 and 48. c) Histogram of grayscale values for the cross section, threshold limits of 10 and 48 define grayscale values for ice.

Volumetric content profiles of gas, ice, and sediment were generated in an iterative process by thresholding each individual slice. Microvariations with height were derived by obtaining a content profile for a cryostructure. The volumetric contents for each component were then calculated using

$$\%Volume_{component} = \frac{\Sigma Voxels_{x-y}}{\Sigma Voxels_{0-255}} \quad (1)$$

where x and y are the range of grayscale values for the component (0–9 for gas, 10–48 for ice, 49–255 for sediment).

We created 3-dimensional models in MATLAB from the 2-dimensional cross section images (Fig. 3). To smooth the data for enhanced processing, and to attempt to account for the partial volume effect (the probability that more than one phase can exist in a single voxel), cross sectional images were eroded and dilated with a kernel of 1 pixel in 2-D (Fourie 2007). The models were created using the "isosurface" function, which creates a three-dimensional contour line representing an area of constant density.

Volumetric component content profiles for two samples are presented in Figure 4. A set of profiles for each component was generated for each sample by determining the percent area occupied by each component in each cross sectional image. By calculating the average for each component profile in each sample, an approximation of the sample's typical component contents was determined. The standard error, σ_{mean}, was calculated by using the standard error of the mean method

$$\sigma_{mean} = \frac{\sigma}{\sqrt{n}} \quad (2)$$

where σ is the standard deviation of the profile, and n is the number slices in the profile.

Results

Many samples with different cryostructures were sampled and scanned, but for the sake of illustration, only one cryostructure will be presented. This type of cryostructure is called *suspended-intergranular* (Fortier et al., in submission) which defines a cryostructure with the sediments located between ice crystals. Two samples (I and II) of this basal

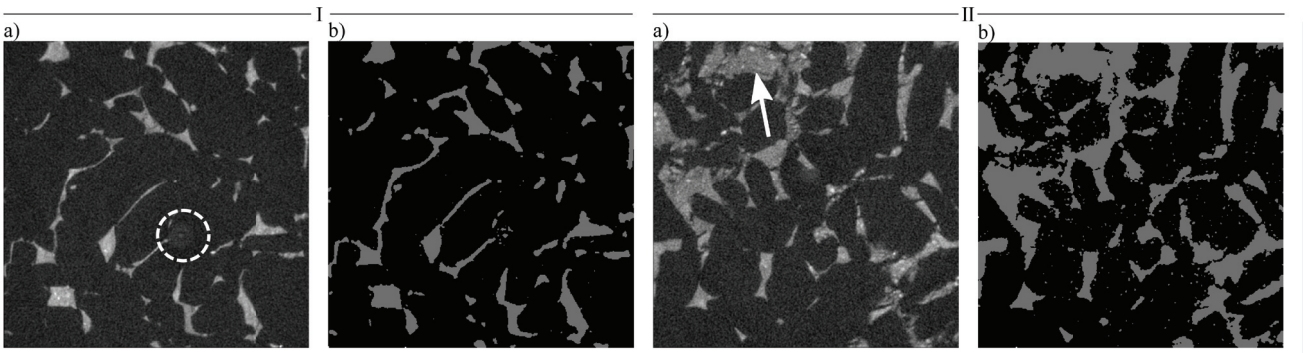

Figure 2. Cross sections from 2 scans of basal glacier ice. a) Raw scans of suspended-interganular cryostructure. Coarser and denser mineral grains are observable (arrow). A ring artifact (circle) is observable on both scans; b) processed images after thresholding showing the three phase components (air is not visible in images at this scale).

ice are presented in Figure 2. Both samples are very ice-rich with volumetric amount of ice 86% for sample I and 66% for sample II.

Figure 2a for both samples shows a raw scan image of the suspended-intergranular cryostructure. In the upper left corner of Figure 2a for sample II, the various mineral grains (see arrow) in the sediment may be observed due to the varying densities as reflected in the grayscale. A ring artifact (circle) is observable on the raw scans, as well (Fig. 2a, sample I).

After applying the threshold values, the complexity of the scan image may be decreased by reducing it into its 3 phases for structural analysis. Figure 2b for both samples shows the results of thresholding. The grey, black, and white represent the sediment, ice, and gas, respectively. Gas bubbles (white) are hardly visible due to their small size and low concentration. The ring artifact has been suppressed by the thresholding technique in Figure 2b.

Figure 3 is a series of 3-D models of the samples with the suspended intergranular cryostructure presented in Figure 2. Figure 3a models the ice, sediment, and gas components together. Figure 3b models the ice component only and shows the ice-rich nature of the samples. Figure 3c models the sediment component only and shows that the sediments are located in between the sub-rounded grains of ice (or ice crystal aggregates).

By applying Equation (1) to each cross section, volumetric profiles for the samples were produced (Fig. 4). The total volume of each phase is given for each cross section (because each cross section has a thickness of 1 voxel) taken along the x-y plane and plotted against the vertical location. The profile for the ice (Fig. 4a) shows a 10% decrease and a 20% increase in ice content from the bottom to the top of samples I and II, respectively, while the sediment (Fig. 4b) shows a 10% increase and a decrease of 20% in samples I and II, respectively. The gas (Fig 4c) remains close to constant (0.10–0.20% and 0.25–0.55%, I and II, respectively) in content which indicates a fairly uniform distribution in the samples. By applying Equation 1 to the entire reference volume, the total volumetric content for each phase was determined (Table 1).

Table 1. Average volume per component and associated error.

	Component Volume (%)		
	Ice	Gas	Sediment
Suspended Intergranular I	85.50±0.16	0.16±0.01	14.34±0.16
Suspended Intergranular II	66.05±0.38	0.38±0.01	33.58±0.39

Discussion

Settings should be consistent, because scan results are highly dependent on the scanner settings. Appropriate settings for voltage, current, pixel size, and exposure time must be determined via calibration with a known substance, such as pure ice.

Ice scans, however, require a sub-freezing temperature-controlled environment to avoid thawing of the sample during testing. Under these conditions, detailed testing and evaluation of an individual sample can be repeated. This is a challenging operation because temperatures colder than -6°C often resulted in mechanical problems in the scanner apparatus, such as the sample stage freezing in place instead of rotating, and the sample door freezing open.

By using a computational software package, such as MATLAB™, quantification of the phase components is a powerful alternative to traditional destructive lab techniques, such as oven drying of samples.

Thresholding effects

Determination of appropriate levels for thresholding is the most critical aspect to this study, as well as the most difficult. Under- and over-estimation of a component can occur if the selected threshold range is too small. While calibration with ice serves as a good reference point, it is not perfect. Scan output data is based on the attenuation of x-rays through a sample; however, the attenuation is not only dependent on the material it is passing through, but on the surrounding materials at any given point, as well. The results of overestimating the selection are exemplified by the slight difference in the boundaries between the ice and sediments in Figure 2b.

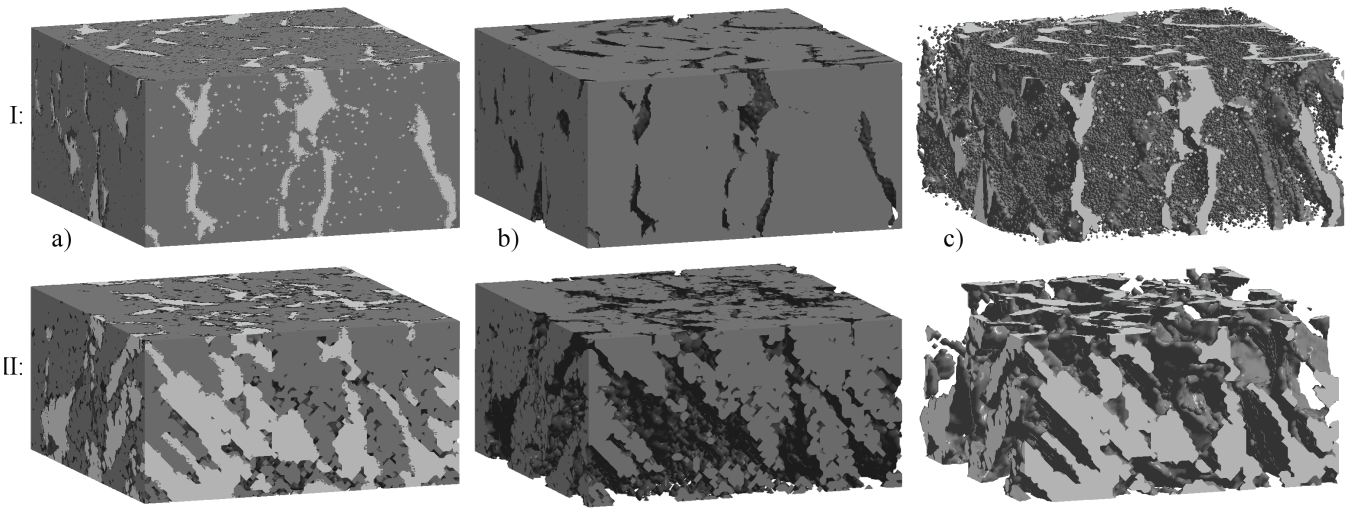

Figure 3. Three-dimensional images created for samples I and II. a) Combined ice and sediment, b) ice component, c) sediment component. Volume dimensions: 25.57 mm by 27.57 mm by 13.71 mm. It is important to note that the 3-D renderings have lighting effects on them. This creates the shading observable on the models which make it possible to distinguish depth in the image.

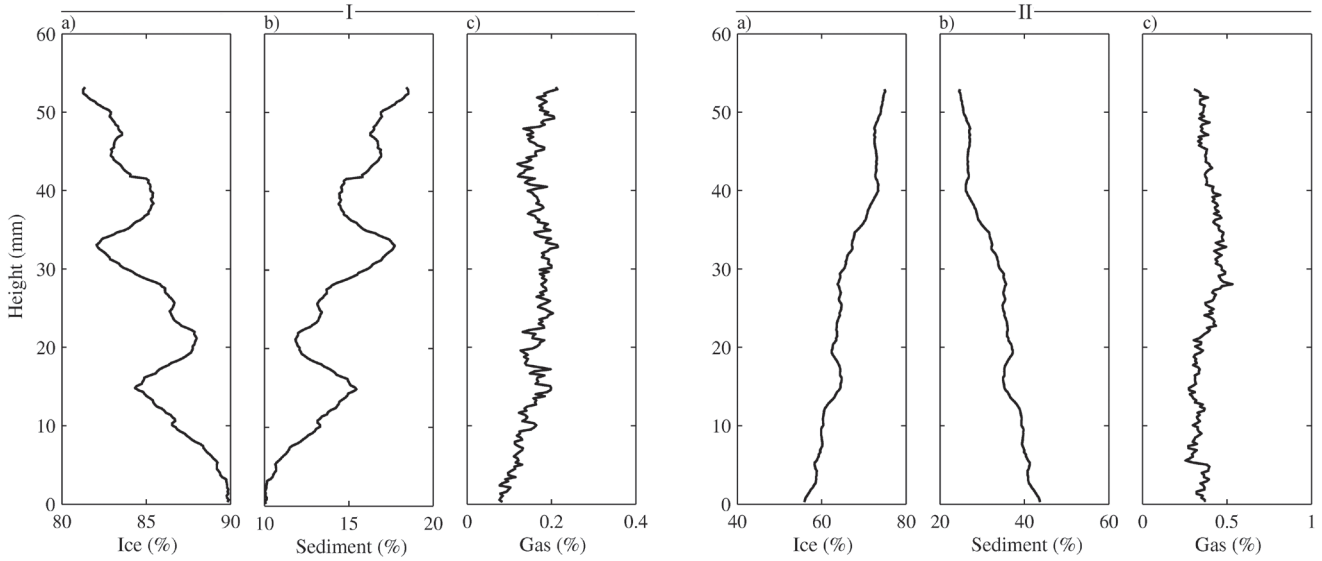

Figure 4. Volumetric content of ice, soil, and gas phases in samples I and II with suspended-intergranular cryostructure.

Cryostructure visualization and phase component quantification

Traditionally, cryostructures are evaluated and classified via visual inspection, typically from cores of frozen soil. When viewing an exposure, the investigator is usually limited to a 2-D view of the cryostructure. The scanner results can be viewed in 2-D "slices," which allow for an in-depth comparison with detailed exposure descriptions from the field.

After applying the limits of thresholding to the cross sections, it became easier to focus on the general structures and patterns in each sample. However, identification of mineral grains is not possible anymore because the thresholding lumps the full range of mineral densities together. A solution to this would be to apply more threshold limits in a series of steps, to show varying degrees of mineral density, however, this study focused on the cryostructure of the sample, so this was not performed. Thus, a side-by-side analysis of the raw scans images and the images with thresholding in 2-D is very beneficial. For instance, Figure 5 shows well the presence of sand grains in the sediments which can not be observed on a processed image. On the other hand, visualization of gas bubble distribution in a section is better realized with a processed scan signal.

Visualization of cryostructures was greatly aided by utilizing both cross sectional images, and 3-dimensional isosurfaces. Three-dimensional spatial relationship between the phase components is a great advantage of tomodensitrometry, because of the ease of generating 3-dimensional models. Gas bubble distribution in ice has traditionally been a very difficult subject to study, because of the inherent problems and time requirements related to generating thin sections

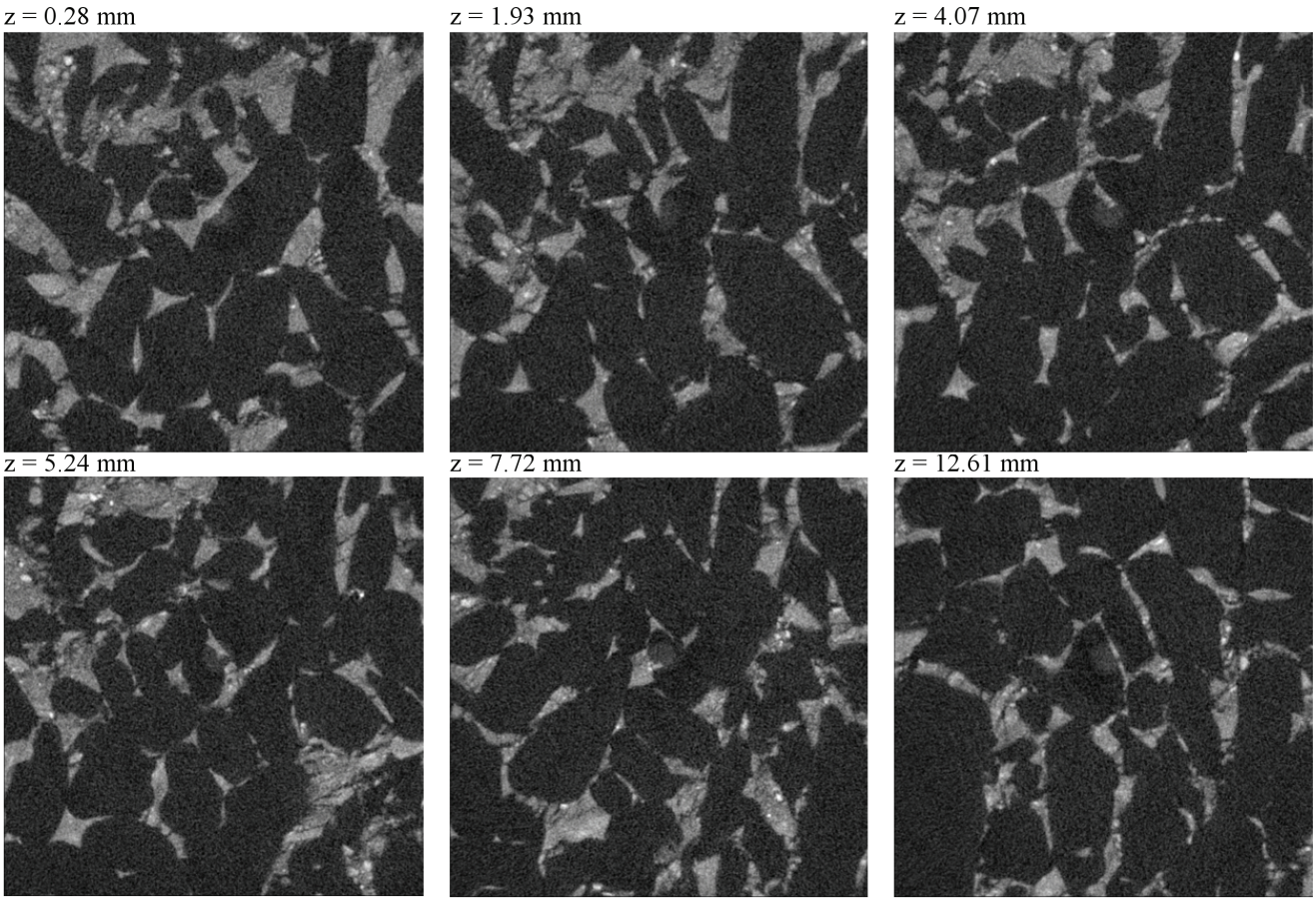

Figure 5. Sequence of cross sectional height for sample II with suspended-intergranular cryostructure. Dark areas are less dense materials such as gas and ice, while light areas are denser, such as different minerals in the sediments. All image dimensions are 27.57 mm by 27.57 mm. The position of a cross section in the sample is denoted by the "z" measured from the bottom of the sample.

(Gherboudj et al. 2007). The cross sectional images show the spatial distribution of components against each other. By comparing cross sections throughout an entire sample (Fig. 5), evaluation of structure and phase component variation along the sample's height is possible.

Understanding how components relate and are distributed in a volume is easily aided by the isosurfaces. These are models of the boundary between one component, and the rest of the sample. These models can "strip away" all of the other components in a sample, and isolate one to have a better representation of its 3-D structure. In Figure 3b, for instance, it can be observed that the samples are mainly composed of ice, which is typical of a suspended cryostructure. The ice content and its geometry typically vary between two samples. In Figure 3c, it can be observed that the sediment particles are located at the junction and in-between the ice grains. This is easier to see than in the 2-D scans. By analyzing a large number of samples, statistics can be derived to obtain a range of values for a given cryostructure type.

The determination of the individual components relies on the output from the thresholding of the original scan data. Once the components have been divided, the calculation of their volumetric content are found using Equation 1.

Traditionally, in the lab, methods for the calculation of volumetric ice content for frozen soil cores requires measurements of the bulk volume of a core, then oven drying the sample, determining the gravimetric water content, and determining, finally, the volumetric ice content. By utilizing the methods presented, all of the intermediate steps may be bypassed, and, the original specimen is completely preserved.

Conclusions

X-ray computed tomography can become a powerful complementary method to traditional field observations and laboratory work. Cross sectional images generated from scans may be viewed as raw images and as images with thresholding. Raw cross sections have the advantage of showing a complete picture of any plane in the sample. Cross sections that have thresholding allow for more direct interpretation of structure in the sample, which aids in cryostructure classification. Three-dimensional models reveal variations of cryostructures in three-dimensions, a key element for generating a new classification. In terms of cryostructure classification, this would be one more method in the field of cryostratigraphy.

Tomodensitometry has applications in many other cold

region studies, such as evaluation of cryostructures in permafrost, and evaluation of river ice, icings, glaciers, and sea ice. Besides being an important tool for research, the practical applications for determining component contents is important in many frozen ground engineering design considerations.

Acknowledgments

We would like to thank the UAF Research Center's Undergraduate Research Symposium and Flint Hills Resources for providing funds to M.D. for this study and Alaska EPSCoR for providing support for technical training. The authors are appreciative of the support received by Skyscan, Inc. This work was supported by the USA National Science Foundation by grants EPS-0346770 to D.F. and M.K., and ARC-0454939 to M.D. and Y.S. Any opinions and findings expressed in this material are those of the authors and do not necessarily reflect the views of the funding agencies. The authors are especially thankful for the constructive comments and advice offered by the reviewer.

References

Alshibli, K.A., Alramahi, B.A. & Attia, A.M. 2006. Assesment of spatial distribution of porosity in synthetic quartz cores using microfocus computed tomography. *Particulate Science and Technology* 24: 369-380.

Ambrose, J. & Hounsfield, G. 1973. Computerized transverse axial tomography. *British Institute of Radiology* 46: 148-149.

Bastardie, F., Capowiez, Y., de Dreuzy, J.R. & Cluzeau, D. 2003. X-ray tomographic and hydraulic characterization of burrowing by three earthworm species in repacked soil cores. *Applied Soil Ecology* 24: 3-16.

Calmels, F. & Allard, M. 2004. Ice segregation and gas distribution in permafrost using tomodensitometric analysis. *Permafrost and Periglacial Processes* 15: 367-378.

Calmels, F. & Allard, M. 2008. Segregated ice structures in various heaved permafrost landforms through CT scan. *Earth Surface Processes and Landforms* 33: 209-225.

Fourie, W., Said, R., Young, P. & Barnes, D.L. 2007. The simulation of pore scale fluid flow with real world geometries obtained from x-ray computed tomography. *Proceedings of the COMSOL Conference, October 4–6, 2007.*

Gherboudj, I., Bernier, M., Hicks, F. & Leconte, R. 2007. Physical characterization of air inclusions in river ice. *Cold Regions Science and Technology* 49: 179-194.

Knight, P.G. 1998. The basal ice layers of glaciers and ice sheets. *Quaternary Science Reviews* 16: 975-993.

Lawson, D.E., Strasser, J.C., Evenson, E.B., Alley, R.B., Larson, G.J. & Arcone, S.A. 1998. Glaciohydraulic supercooling: a freeze-on mechanism to create stratified, debris-rich basal ice: I. Field evidence. *Journal of Glaciology* 44: 547-567.

Macedo, A., Crestana, S. & Vaz, C.M.P. 1998. X-ray microtomography to investigate thin layers of soil clod. *Soil & Tillage Research* 49: 249-253.

Pedrotti, A., Pauletto, E.A., Crestna, S., Holanda, F.S.R., Cruvinel, P.E. & Vaz, C.M.P. 2005. *Soil & Tillage Research* 80: 115-123.

Phogat, V.K., Aylmore, L.A.G. & Schuller, R.D. 1991. Simultaneous measurement of the spatial distribution of soil water content and bulk density. *Soil Science Society of America Journal* 55: 908-915.

Pralle, N., Bahner, M.L. & Benkler, J. 2001. Computer tomographic analysis of undisturbed samples of loose sands. *Canadian Geotechnical Journal* 38: 770-781.

Rachmanm, A., Anderson, S.H. & Gantzer, C.J. 2005. Computed-tomographic measurement of soil macroporosity parameters as affected by stiff-stemmed grass hedges. *Soil Science Society of America Journal* 69: 1609-1616.

Rogasik, H., Crawford, J.W., Wendroth, O., Young, I.M., Joschko, M. & Ritz, K. 1999. Discrimination of soil phases by dual energy x-ray tomography. *Soil Science Society of America Journal* 63: 741-751.

Sharp, M., Jouzel, J., Hubbard, B. & Lawson, W. 1994. The character, structure and origin of the basal ice layer of a surge-type glacier. *Journal of Glaciology* 40: 327-340.

Torrance, J.K., Elliot, T., Martin, R. & Heck, R.J. In Press. X-ray computed tomography of frozen soil. *Cold Regions Science and Technology*.

New Patterns of Permafrost Occurrence in a Mountain Environment, Based on an Example from the Tatra Mountains, Poland, and Abisko Area, Sweden

Wojciech Dobinski
University of Silesia, Faculty of Earth Sciences, Department of Geomorphology, ul. Będzińska 60, 41-200 Sosnowiec, Poland

Abstract

At present, research into the occurrence of mountain permafrost concentrates on its relationship to the currently changing climate. Modern research shows that in northern Scandinavia the permafrost extent is much wider than it has been believed so far. Comparative studies on the occurrence of permafrost in the Tatra Mountains and in the Abisko area concern both active and fossil permafrost. A set of geophysical research into permafrost of the Tatra Mountains and the Abisko area conducted in similar geological and climatic conditions reveals that two similar high-resistivity anomalies can be distinguished in both places. Shallower anomalies were interpreted as permafrost which is connected with current climate (contemporary permafrost). Deeper ones were interpreted in two ways: in the Tatra Mountains, as a layer of dry, much older, probably fossil permafrost, whereas in the Abisko area, as thermal differentiation within the permafrost layer occurring there, which probably indicates climate variability in the Holocene.

Keywords: Abisko; electroresistivity; fossil permafrost; geophysics; permafrost occurrence; tomography; Tatra Mountains.

Introduction

Recent decades show an increased interest in issues related to permafrost occurrence in mountain environment (Harris 2001, Gorbunov 2003, Haeberli 2003). The main research concentrates on the most current problem in earth sciences, which is climate warming and its impact on the components of earth surface. The frozen lithosphere (cryolithosphere), including seasonal snow cover, permafrost, glaciers and continental glaciers, as well as floating ice (Dobinski 2006), is the most sensitive to climate change. The predicted consequences of climate warming and their social aspect result in research being predominantly focused on the active layer and subsurface layer of permafrost.

Research into mountain permafrost in the Tatras and in Abisko is conducted in areas where permafrost occurrence is relatively poorly recognized (Svensson 1986). As a result, the main aim of this project is to determine permafrost extent and its forms of occurrence, its geophysical properties, probable origin and evolution and its relationships to the warming climate.

The first results of the research conducted in the Abisko area were presented last year (Dobinski 2007). Here a new hypothesis of permafrost occurrence in mountainous areas will be presented, based on geophysical data collected by the author and published last year.

Location

The survey areas—the Abisko Mountains (A) and the Tatra Mountains (B)—are located far away from each other, at a distance of 2100 km (Fig.1). Despite a relatively big latitude gradient, both areas of detailed surveys have properties that suggest the necessity of comparing one to the other. Two meteorological stations operating in the Tatras indicate a mean annual air temperature (MAAT) similar to the one in the survey area. The MAAT of Kasprowy Wierch stands at -0.8°C at the altitude of 1986 m a.s.l. and of Łomnicki Szczyt at -3.8°C at the altitude of 2632 m a.s.l. (Dobinski 1997, Niedzwiedz 1992) In the Abisko area, close to the research station ANS at the altitude of 388 m a.s.l., MAAT stands at -0.8°C and in the mountainous areas nearby, it drops to -4.0°C (Ridefelt & Boelhouwers 2006, Jonasson 1991). Nearby Tarfala Research Station (1151 m a.s.l.) has MAAT of -3.9°C, which is similar to the one measured on Łomnicki Szczyt.

Figure 1. Location of the research areas within the map of mountain permafrost in Europe (modified from Dobinski 2005).

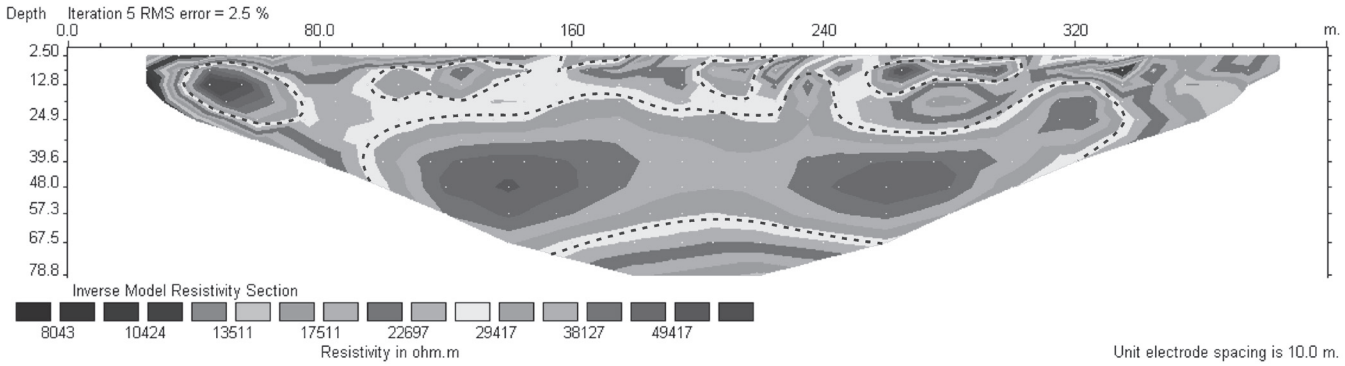

Figure 2. ERT profile performed on the mouton in the Abisko area. High-resistivity anomalies surrounded by the dashed line. Note high-resistive area at a depth of 25–65 m.

Nearby Tarfala Research Station (1151 m a.s.l.) has a MAAT of -3.9°C, which is similar to the one measured on Łomnicki Szczyt.

Both of these mountain regions underwent glaciation several times in the Pleistocene. It finished about 10,000 years BP in the Tatra Mountains (Baumgart-Kotarba & Kotarba 1995) and about 9,000 years BP in the Abisko area (Karlen 1979). Glaciation significantly altered the relief of the areas; in the final stage of evolution they were affected by periglacial processes, which ultimately shaped their relief. A considerable difference between the two areas observed in their topography lies mainly in the difference in relative altitude. In the Tatras, relative altitudes are much higher and due to this fact the mountains are steeper than the ones in the Abisko area. Such a topography results in lower dynamics, compared to the Tatras, of geomorphological processes occurring in the Abisko Mountains at present. Steep slopes in the Tatra Mountains, dominating above the permanent snow line, prevent formation of glaciers.

Geophysical surveys in northern Sweden were conducted on a granite mouton—a tor-like bare rock polished by the glacier—(ca. 450 m a.s.l.) located about 20 km west of Abisko, ca. 200 m north of the Kiruna–Narvik Road, near the Bjorkstugans station, beyond the exact mountain area. This mouton, not very high and with a bit fractured surface, was chosen as a particularly suitable area to be compared with the granite dome of Kasprowy Wierch, the Tatras, Poland, where electroresistivity and electromagnetic profiling was also performed. The mouton is slightly covered with glacial blocky deposits which accompany a slightly weathered *in situ* granite. It is partly overgrown with moss and grass, and wherever there are more deposits, a process of frost sorting can be observed. In Poland, the surveys were carried out on the dome summit of Kasprowy Wierch, which is also built of granite and has a 4 m thick cover weathered *in situ* in periglacial conditions and which is mostly overgrown with grass.

Methods

The following geophysical methods were applied in the surveys on the occurrence of mountain permafrost in the Abisko area and the Tatras: one-dimensional (1D) DC resistivity soundings (e.g., Vonder Mühll 1993), two-dimensional (2D) resistivity tomography (e.g., Kneisel 2006), shallow and deep electromagnetic soundings (EM) (Hauck et al. 2001), and measurement of bottom temperature of the winter snow cover (BTS) (Haeberli 1973). Such methods are quite commonly used in geophysical surveys on detection and mapping of permafrost in a mountain environment and can be said to be standard at present (Vonder Mühll et al. 2001, Hauck 2001).

Abisko area, Sweden

Two intersecting electrical resistivity profiles were carried out in the NS and WE directions. The WE profile was 200 m in length and had electrodes spaced at 2.5 m intervals. Suitable terrain conditions and the assumptions underlying the survey, which aimed at detection of permafrost at a considerable depth, resulted in the second profile being carried on the distance of 400 m, with electrode spacing of 10 m (Fig. 2). The electromagnetic method was chosen under similar assumptions. In the surveys, a EM-34 conductivity meter with a variable transmitter-receiver spacing was used, which allowed reaching the depth of about 80 m below the ground surface.

Kasprowy Wierch, Tatra Mountains, Poland

On Kasprowy Wierch, two 200 m 2D electroresistivity tomography with electrodes spaced at 2.5 m intervals and shallow electromagnetic sounding surveys were carried out. One of the ERT profiles was located above the tourist path and ran along it, while the other descended from the summit. Additionally, BTS temperature measurements were made on the summit dome and in the surrounding area.

Results

Mouton in the Biorkstugans area, Abisko.

The interpretation of the second profile, running N-S, reaches the depth of almost 80 m, and it presents a significant variation in resistivity values, but they all occur in a high value range. Note that the interpretation of the research in the second ERT profile probably did not include the active layer, the thickness of which in such an environment varies

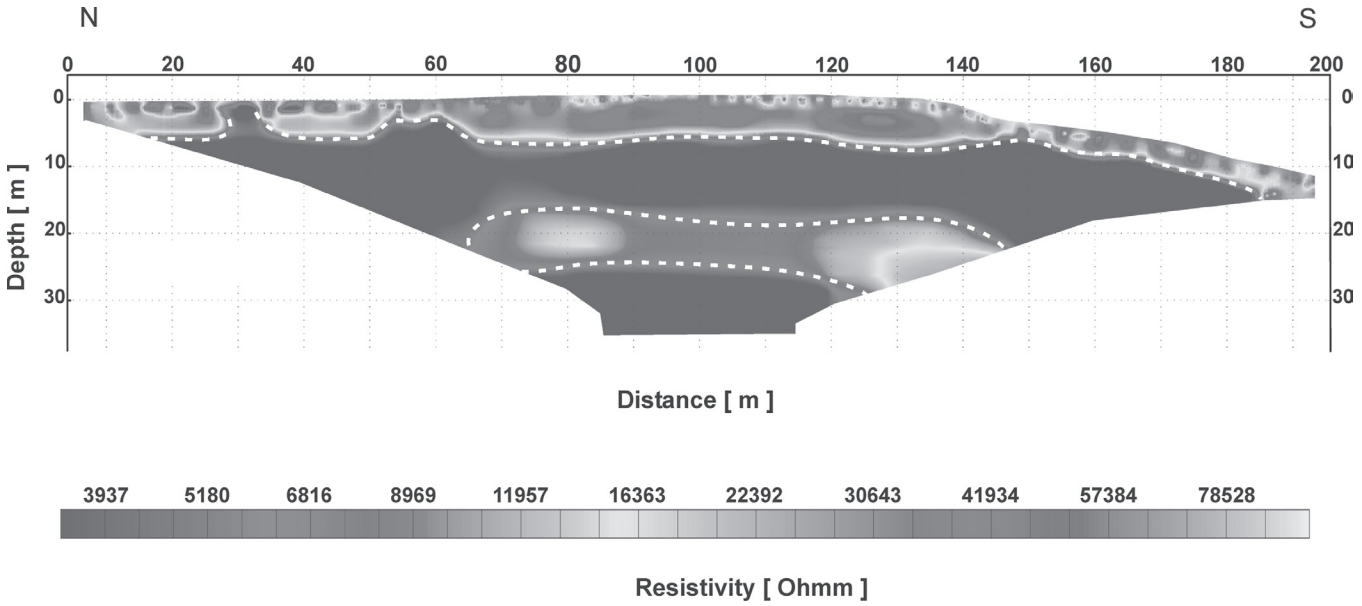

Figure 3. ERT profile performed on Kasprowy Wierch. High-resistivity anomalies surrounded by the dashed line. Note high-resistive area at the depth 15–25 m, and different vertical scale. (Due to appear in Hauck, C. & Kneisel, C. (in press), *Applied Geophysics in Periglacial Environments*. Cambridge University Press, reproduced with permission.)

between 1.5–2.5 m (Knutsson 1980) or more. At a depth of 3–15 m, a series of high-resistivity anomalies can be observed; their resistivity values range between 30 and 50 kOhmm, and they form an unclear layer. Below the depth of 25 m resistivity drops to around 20–30 kOhmm and it increases again to 30–50 kOhmm at the depth between 30 m and 60 m. In deeper places, resistivity falls again to stand at about 17 kOhmm or more. Lower resistivity values, below 10–13 kOhmm, are registered exclusively on the edges of the survey site; that is, in the places where the area could have been locally watered, as there is a river flowing nearby and the terrain there is wet. The profile does not show any anomalies characteristic of deep fractures. The image of the two high-resistivity anomalies, especially the deeper one, has a characteristic, more or less horizontal course.

The results are supported by deep electromagnetic soundings made by means of EM-34 conductivity meter. The findings of these surveys reveal variation in electromagnetic conductivity in various depths. The map of electromagnetic conductivity created for the depth of 15 m shows very little variation in values within the 3.2–4.0 mSm range. At the depth of 30 m, conductivity falls to 1.7–2.1 to rise again to 8.4–11.0 mSm at the depth of 60 m.

Kasprowy Wierch, Tatra Mountains, Poland

In the 2D resistivity tomography (Fig. 3) made on Kasprowy Wierch, two distinct high-resistivity anomalies can be distinguished. The first one, of a horizontal course, is discontinuous, and its fragments come over the surface. Electrical resistivity interpreted in it indicates the values from 30–90 kΩm. Such high electrical resistivity is characteristic of both: coarse blocky cover with numerous air voids and of places of permafrost occurrence (Dobinski et al. 2006, Vonder Mühll 2001).The layer is 3–4 m thick and its upper end is at a depth of 1–2 m. The horizontal arrangement of anomalies can be regarded as permafrost, whereas single, small, high-resistivity anomalies which come over the surface are probably air voids in blocky-cover. The layers below the delineated limit can be treated as a homogenous granodiorite massif with characteristic resistivity of approximately 4 kΩm. In its upper sections there can be fractures. In the massif, at the depth of 15–25 m, another high-resistivity anomaly, of 15–60 kΩm resistivity can be identified.

BTS temperatures measured on the summit dome of Kasprowy Wierch range from -2.7°C in the place of southern exposure, to -3°C on the summit, to -3.2°C in the place of slight northwest aspect (Dobiński 2004). In both places**,** high-resistivity anomalies running near the surface and much more deeply are observed. The shallow ones can be interpreted as active permafrost**;** the one connected with contemporary climate, where ice may occur. If we accept a highly probable assumption that geological structure in the survey sites, which are built of granite, is uniform, the change in resistivity and electromagnetic conductivity values should be mainly attributed to physical factors other than petrographic variety of rocks. A deep fracture would be accompanied by the infiltration of water of meteoric origin (Kasprowy Wierch) and of water coming from the stream and small water reservoirs near the mouton (Abisko). Such a change would rather lead to a decrease in resistivity values due to permafrost degradation and higher conductivity of water.

Discussion

Resistivity values and those of electromagnetic conductivity which occur on the mouton in the Abisko area, as well as resistivity values and BTS temperatures in the

Tatra Mountains, indicate that in both places high-resistivity anomalies should most likely be interpreted as permafrost occurrence, which would comply with the recent findings on permafrost occurrence in the Abisko area (Johansson et al. 2006) and in the Tatras (Dobinski et al. 2006). The results of surveys conducted both on Kasprowy Wierch and on the mouton in the Björkstugans area reveal that permafrost occurrence in both areas is probably not always accompanied by the occurrence of ground ice. Thus, the most likely interpretation of the obtained results is that these deep high-resistivity anomalies should also be regarded as occurrence of dry permafrost, older than permafrost present above it, which has relic character. This is the most probable hypothesis as it is commonly known that permafrost occurrence in the world is mostly the effect of Pleistocene cooling and such is its age (French 1996).

The thesis is supported in publications of other authors who have conducted surveys in this area. Ekman (1957) confirms the presence of at least 70 m thick permafrost near the Låkktajåkka tourist station at the altitude of 1220 m a.s.l.; that is a few kilometers away from the survey site. A borehole directly documenting this fact was drilled there in 1941. Another place where 20 m thick permafrost occurs is the Moskogaisa mine near Lyngen in Norway, at the altitude of 750 m a.s.l. (Ekman 1957). Relic and active permafrost is also distinguished in Scandinavian mountains by King (1984, Table 6, p. 36), who states that an active layer of relic permafrost is 4 m deep. He estimates the thickness of relic permafrost at 50–100 m and of active one at 40–140 m. A similar regularity is also registered in the Tatras (Dobinski et al. 2006), where under a layer of active permafrost there is probably fossil permafrost at the depth of about 15–25 m.

Fossil permafrost presence is documented in other places as well. The 100 m deep borehole drilled in March 2000 near the Tarfala Research Station (MAAT between -6 and -7°C) showed a temperature of -2.8°C in 100 m depth. Linear extrapolation of the borehole temperatures suggests permafrost thickness of 350 m (Isaksen et al. 2001). It is not possible for permafrost of such thickness to be solely an effect of contemporary climate influence (Lunardini 1995).

In the Alps (Zermatt) and in southern Scandinavia (Jotunheimen), a regularity similar to the one occurring in the Tatras (Kasprowy Wierch) and in the Abisko area can be observed. In 2D resistivity tomography performed near Stockhorn, one can distinguish two distinct high-resistivity anomalies, the first one in the 1–7 m depth and the second at the depth of about 20 m and more (Hauck 2001). Permafrost thickness in this place is estimated at about 160 m (King 2001), so both anomalies that occur there probably indicate its presence. A similar situation is on Jotunheimen (Fig. 6a) (Hauck et al. 2004), where a high-resistivity anomaly is visible in the lower part of the profile. Permafrost thickness for the borehole drilled in this area is estimated to be 380 m (Isaksen et al. 2001), which indicates that this high-resistivity anomaly might be interpreted as probable fossil permafrost. The possibility of its presence in this area is acknowledged by other researchers as well. (Ødegård et al. 1996). Nevertheless, as the resolution of the 2D resistivity tomography model decreases near the model boundary, the possibility of an inversion artifact must also be taken into account in the deeper part of both sections

The above assumptions are supported by an analysis of climate evolution in northern Scandinavia after glaciation. Long-term climatic history, deglaciation, and tree limit changes in the Holocene have been described mainly by Karlén (1976, 1979). The deglaciation of the Tornetrsk area took place around 9000^{14}C years BP (Karlen 1979). This information leads to the conclusion that in the mountain region of Abisko, in the entire Holocene period, temperature did not rise enough to reach MAAT >0°C, whereas in lower places the warming period was too short. During the Holocene there was not a period of time long enough to allow for a complete degradation of permafrost in the survey area. Rough estimates show that such an evolution took place in the Tatras too (Dobinski 2004).

Conclusions

Geophysical surveys carried out in the Abisko area indicate that active permafrost occurrence in this region is not solely limited to mountain and hill areas above 800 m a.s.l. (Jeckel 1988), and to muirs and palsa, but is also possible in other, lower places which are not covered with vegetation but constitute exposed convex forms (moutons) (Johansson et al. 2006). Thus, the occurrence of altitudinal and latitudinal permafrost probably overlaps.

Surveys on permafrost in Scandinavia and published results show that mountain permafrost, just like permafrost in western Siberia, reflects climatic fluctuations dating from at least postglacial period and that it occurs in both active and fossil forms. This allows for a more synthetic view on permafrost occurrence in the world. The published data indicate that such a hypothesis could also be applied in other mountain areas. Although it can be put forward at the present stage of research, it requires verification. It is impossible to prove the existence of permafrost by using the geophysical methods alone.

Acknowledgments

Geophysicists K. Wzietek and B. Zogala supported the field measurement and its interpretation. The constructive and helpful comments of two anonymous referees are gratefully acknowledged. Sincere acknowledgments go to Mira Jach for her work in translating the text into English. The work was financed from the funds of the University of Silesia, Research Project MNiSW: N306 052 32/3405 and EU ATANS Grant (Fp6 506004).

References

Baumgart-Kotarba, M. & Kotarba, A. 1995. High-mountain environment of the Tatras in the period of Pleistocene and Holocene transition. *Biuletyn Peryglacjalny* 34: 37-51.

Dobinski, W. 2007. First results of the geophysical research of the lower border of permafrost occurrence in the Abisko area, Lappland, Sweden. *Geophysical Research Abstracts* 9, 03075, 2007 SRef-ID:1607-7962/gra/EGU2007-A-03075.

Dobinski, W. 2006. Ice and environment: A terminological discussion. *Earth-Science Reviews* 79(3-4): 229-240.

Dobinski, W. 2005. Permafrost of the Carpathian and Balcan Mountains, Eastern and Southeastern Europe. *Permafrost and Periglacial Processes* 16(4): 395-398.

Dobinski, W. 2004. Wieloletnia zmarzlina w Tatrach: geneza, cechy, ewolucja. *Przegląd Geograficzny* 76(3): 327-343.

Dobiński, W. 1997. Distribution of mountain permafrost in the High Tatras based on Freezing and thawing indices. *Biuletyn Peryglacjalny* 36: 29-37.

Dobinski, W., Żogała, B. & Wziętek, K. 2006. Geophysical investigation of the contemporary and Pleistocene permafrost in the Kasprowy Wierch, Tatra Mountains, Poland. *Przegląd Geofizyczny* 51(1): 71-82.

Ekman, S. 1957. Die Gewasser des Abisko–Gebietes und ihre Bedinungen. *Kungl. Svenska Vetenskapsakademiens Handlingar* 6 (6): 172 pp.

French, H.M. 1996. *The Periglacial Environment*. Longman, 341 pp.

Gorbunov, A.P. 2003. *Vietchnaya merzlota gor ot ekvatora do poljarhyh shirot* (Permafrost of the mountains from equator up to polar latitudes), Almaty, 124 pp. (in Russian).

Haeberli, W. 1973. Die Basis-Temperatur der winterlichen Schneedecke als moglicher indikator für die Verbreitung von permafrost in den Alpen. *Zeitschrift für Gletscherkunde und Glazialgeologie* 9(1–2): 221-227.

Haeberli, W. 2003. Report of the Eight International Conference on Permafrost. *Frozen Ground* 27: 3-5.

Hauck, C. 2001. *Geophysical methods for detecting permafrost in high mountains.* PhD thesis, Laboratory for Hydraulics, Hydrology and Glaciology (VAW), ETH Zurich, Switzerland. *VAW-Mitteilung* 171: 215 pp.

Hauck, C., Gugielmin, M., Isaksen, K. & Vonder Mühll, D. 2001. Applicability of frequency-domain and time-domain electromagnetic methods for mountain permafrost studies. *Permafrost and Periglacial Processes* 12: 39-52.

Hauck, C., Isaksen, K., Vonder Mühll, D. & Sollid, J.L. 2004. Geophysical surveys designed to delineate the altitudinal limit of mountain permafrost: An example from Jotunheimen, Norway. *Permafrost and Periglacial Processes* 15: 191-205.

Harris, C. 2001. Editorial. *Permafrost and Periglacial Processes* 12: 1.

Isaksen, K., Holmlund, P. & Sollid, J.L., 2001. Three deep alpine permafrost boreholes in Svalbard and Scandinavia. *Permafrost and Periglacial Processes* 12: 13-25.

Jeckel, P., P. 1988. Permafrost and its Altitudinal zonation in northern Lappland. *Proceedings of the Fifth International Conference on Permafrost, Trondheim, Norway, 2–5 August 1988*: 170-175.

Johansson, M., Christensen, T.R., Akerman, H.J. & Callaghan, T.V. 2006. What determines the current presence or absence of permafrost in the Torneträsk Region, a sub-arctic landscape in northern Sweden? *Ambio* 35(4): 190-197.

Jonasson, C. 1991. Holocene Slope Processes of Periglacial Mountain Areas in Scandinavia and Poland. *UNGI Rapport 79*. Uppsala University, Department of Physical Geography.

Karlén, W. 1976. Lacustrine sediments and tree-limit variations as indicators of Holocene climatic fluctuations in Lappland, northern Sweden. *Geografiska Annaler* 58A(1–2): 1-33.

Karlén, W. 1979. Deglaciation dates from northern Swedish Lappland. *Geografiska Annaler* 61A(3–4): 203-210.

King, L. 1984. Permafrost in Skandinavien–Untersuchungsergebnisse aus Lappland, Jotunheimen und Dovre/Rondane. *Heidelberger Geographische Arbeiten* 76: 125 pp.

King L. 2001. News from members, Germany. *Frozen ground* 25: 25-26.

Kneisel, C. 2006. Assessment of subsurface lithology in mountain environments using 2D resistivity imaging. *Geomorphology* 80: 32-44.

Knutsson, S. 1980. Permafrost i Norgevägen. *Byggmästaren* 10: 8-11.

Lunardini V.J. 1995. Permafrost formation time. *CRREL Report 95-8*: 44 pp.

Niedźwiedź T. 1992. Climate of the Tatra Mountains. *Mountain Research and Development*, 12(2): 131-146.

Ødegård, R.S., Hoelzle, M., Johansen, K.V. & Sollid, J.L. 1996. Permafrost Mapping and Prospecting in Southern Norway. *Norsk Geografisk Tidsskrift* 50: 41-54.

Ridefelt, H. & Boelhouwers, J. 2006. Observations on regional variation in solifluction landform morphology and environment in the Abisko region, northern Sweden. *Permafrost and Periglacial Processes* 17: 253-266.

Svensson, H. 1986. Permafrost. Some morphoclimatic aspects of periglacial features of Northern Scandinavia. *Geografiska Annaler* 68A(3): 123-130.

Vonder Mühll, D. 1993. Geophysikalische Untersuchen im Permafrost des Oberengadins. *Mitteilungen der Versuchsanstalt für Wasserbau, Hydrologie und Glaziologie* 122: 222 pp.

Vonder Mühll, D., Hauck C., Gubler H., McDonald R. & Russill, N. 2001. New geophysical methods of investigating the nature and distribution of mountain permafrost with special reference to radiometry techniques. *Permafrost and Periglacial Processes* 12: 27-38.

Permafrost Dynamics at the Fairbanks Permafrost Experimental Station Near Fairbanks, Alaska

T.A. Douglas
Cold Regions Research and Engineering Laboratory Fairbanks, AK
M. Torre Jorgenson
Alaska Biological Resources, Fairbanks, AK
M.Z. Kanevskiy, V.E. Romanovsky, Y. Shur, K. Yoshikawa
University of Alaska Fairbanks, Fairbanks, AK

Abstract

The Fairbanks Permafrost Experimental Station was established in 1945 near Fairbanks, Alaska. In 1946 vegetation was removed from two plots (the Linell plots) to investigate the impacts of vegetation disturbance on permafrost degradation. We revisited the sites in 2007 to evaluate the permafrost table using probes and direct current electrical resistivity. The permafrost table has expanded downward to 9.8 m at a site where all surface vegetation and organic material was removed. The permafrost surface has remained at 4.7 m depth since 1972 at a second site where vegetation was removed but organic material was left intact. In 2005 a Circumpolar Active Layer Monitoring Network (CALM) site was established at an undisturbed plot nearby to provide a baseline assessment of the permafrost. The response of permafrost at the site to the hypothesized future climatic warming of the Alaskan Interior can be assessed, once a long-term record is available.

Keywords: boreal forest; electrical resistivity; monitoring; permafrost degradation; vegetation disturbance.

Introduction

Permafrost in thermal equilibrium can be drastically affected by disturbances such as clearing vegetation (Linell 1973, Nicholas & Hinkel 1996), forest fires (Viereck 1982, Burn 1998, Hinzman et al. 2003), or climatic change (Shur & Jorgenson 2007). The Fairbanks Permafrost Experiment Station near Fairbanks, Alaska (64.877°N, 147.670°W) was established by the U.S. Army in 1945 as a location where geotechnical, geophysical, and engineering studies could be performed on permafrost. The site has a rich history and was designated as a National Geotechnical Experimentation Site in 2003. In 1946 vegetation was removed from two plots at the site (the Linell plots) to investigate the impacts of vegetation disturbance on permafrost degradation. This paper summarizes the results of recent investigations focused on measuring the current state of permafrost at the site. Our results provide information on permafrost degradation where vegetation disturbance has lead to a change in the thermal regime either through engineering activities, fire, or climatic change. Permafrost at the study site is considered "warm" (the mean annual air temperature is -3.3°C) and mean annual temperatures in the area are increasing. As a consequence, future degradation of permafrost during climate warming can be assessed once a long-term record is available from the site.

Results

Linell plots and Circumpolar Active Layer Monitoring site

In 1946 three square plots 61 m on a side (3721 m^2) were identified at the Fairbanks Permafrost Experiment Station to investigate the influence of vegetation removal on permafrost (Linell 1973). Herein these plots are referred to as the *Linell plots*. One of the Linell plots was left undisturbed to preserve the subarctic taiga forest with dense white and black spruce. Vegetation was removed from the other two plots. One plot was stripped of trees by hand but the roots and organic mat were left intact (Fig. 1) while at the other plot all of the vegetation and surface organic material were removed (Fig. 2). Linell (1973) described permafrost degradation at the two disturbed sites 26 years later. In the completely disturbed site the thaw depth reached 6.7 m after 26 years while at the partially disturbed site the melting expanded to a depth of

Figure 1. The Linell plot where trees and shrubs were removed, but the organic mat and roots were left intact. From the U.S. Army Corps of Engineers, Permafrost Division, 1950.

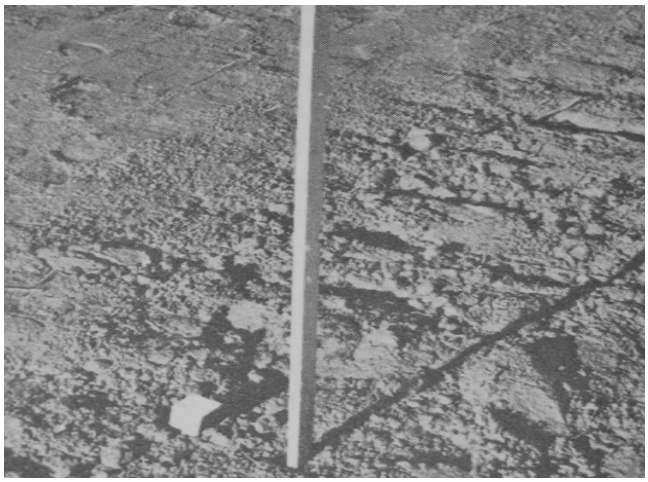

Figure 2. The completely disturbed Linell plot where trees, shrubs, the organic mat and roots were removed. From the U.S. Army Corps of Engineers, Permafrost Division, 1950.

Figure 3. The CALM site at the undisturbed plot in August 2006.

4.7 m. The results showed that permafrost degradation is linked to surface vegetation disturbance and that in warm permafrost random, mixed, low vegetation will not provide a stable thermal regime for permafrost.

In 2005 a Circumpolar Active Layer Monitoring Network (CALM) site was established in the undisturbed Linell plot. Thaw depths have been measured yearly in early October at 121 locations on an 11 by 11 cell grid with 3 m spacing. This provides thaw depth measurements over a 33 by 33 m (1089 m^2 area). Moss thickness and total thaw depth were measured and recorded at each probe location. In the fall of 2007 direct current electrical resistivity measurements were made along an 85 m long line at both of the disturbed Linell plots to quantify the state of permafrost 61 years after modification. A borehole was installed at the completely disturbed plot in 2007 to measure the current thaw depth and to ground truth the geophysical measurements.

Climate, soils, vegetation and permafrost in Interior Alaska

Fairbanks, located in Interior Alaska, has a continental climate with a mean annual temperature of -3.3°C and

Figure 4. A photograph in August 2007 of the Linell plot where in 1946 the surface vegetation was removed but the organic material was left intact.

typical monthly average temperatures of 20.2°C in the summer (July) and -31.7°C in the winter (January). Absolute extremes range from -51°C to 38°C (Jorgenson et al. 2001). The average annual wet precipitation is 407 mm and the typical average annual snowfall is 1.7 m. The Fairbanks Permafrost Experimental Station site sits on a gently sloping southward facing hill 6 km north of Fairbanks, Alaska.

Soils in the study area consist of tan silt and wind blown loess near the surface and grey silt at depths below 1.4 m. Permafrost gravimetric percent moisture contents range from 26% to 41% for the frozen silts which makes this relatively low moisture content permafrost (Linell 1973). The thin (2 to 32 cm thick) surface peaty organic mat has a gravimetric moisture content as high as 258% (Linell 1973). Organic rich silt and peat layers are common as are layers and inclusions of charcoal.

Vegetation at the Fairbanks Permafrost Experimental Station (Fig. 3) is typical of the Alaskan Interior- subarctic taiga forest with white and black spruce towering above a thick moss layer interspersed with low-bush cranberry and Labrador tea. Feather and sphagnum moss and woody debris cover the terrain surface (Hamilton et al. 1983).

Forest succession following disturbance is evident at both Linell plots. At the two disturbed plots dead or dying shrubs covered in moss are being replaced by white and black spruce and birch trees. The trees are taller at the less disturbed site where the surface vegetation was removed but the organic material was left intact (Fig. 4).

Permafrost in Interior Alaska is discontinuous, generally underlying north facing slopes and valley bottoms (Jorgenson et al. 2001). A detailed description of the types of permafrost in the Alaskan Interior is provided in Osterkamp et al. 2000). The thickest permafrost at the Fairbanks Permafrost Experimental Station, 60 m, is near Farmers Loop Road and the thickness decreases with increasing elevation. The mean annual temperature at 10 m depth from 1946 to 1972 was -0.5°C (Linell 1983).

Circumpolar Active Layer Monitoring site measurements

Thaw depths at the CALM site from 2005 to 2007 are generally between 20 and 80 cm (excluding moss) in early October (Table 1). Moss thickness ranges from 0 to 32 cm (Fig. 5). Linell (1973) presents consistent thaw depth readings of ~85 cm at the undisturbed plot from 1946 to 1972. This suggests recent climatic warming in the Alaskan Interior (1.5°C warmer at Fairbanks from the 1960s to the 1990s (Osterkamp & Romanovsky 1999)) may not be greatly affecting thaw depths at the Fairbanks Permafrost Experiment Station. In all three years of measurements the shallower moss cover is associated with deeper thaw depths.

Geophysical measurements at the Linell plots

Direct current (DC) electrical resistivity measurements have been used to quantify the presence of permafrost at many locations worldwide (e.g., Gilmore & Clayton 1995, Hauck et al. 2003, Hauck & Kneisel 2006). The electrical resistivity of a soil is controlled by its mineralogy, porosity, moisture content, cation/anion concentration of moisture, temperature, and whether the pore water is frozen or thawed. The resistivity (ρ) values of frozen soil are generally 10- to 1000 times greater than those of unfrozen or brine-rich soils (Harada & Yoshikawa 1996).

Direct current electrical resistivity measurements were run across the two disturbed Linell plots in September 2007 to quantify current thaw depths. We used two-dimensional resistivity profiling (IRIS instruments; Syscal pro R1 48-72 channel) for this investigation using a Wenner electrode configuration. The DC resistivity sounding employed four electrodes for measurement whereby a current (I) was delivered and received between the outer two electrodes and the resulting potential difference (V) was measured between the inner two electrodes. For this array on the ground surface, an apparent resistivity (ρ_a) between electrodes separated by distance (a) is:

$$\rho_a = 2\pi a(V/I) \quad (1)$$

The inversion analysis was performed with changing values of resistivity and layer thickness by using the linear filter method for a one-dimensional investigation (Das & Verma 1980). We do not have measurements of pore water salinity or moisture content across the resistivity lines and this limits the confidence of our interpretation of the resistivity measurements. However, based on the data presented in Linell (1973), the soil moisture contents, the soil temperature, and our probing and borehole measurements we are confident the resistivity markers we interpret as the upper boundary of the permafrost table are accurate.

For the acquisition of the two-dimensional apparent resistivity data we used multi-channel, equally spaced electrodes at 1.5 m for the minimally disturbed Linell plot and 2 m for the completely disturbed Linell plot. Each measurement was repeated up to 16 times, depending on the variance of the results. Two-dimensional model interpretation was performed using RES2DINV (Geotomo software) which performs smoothing and constrained inversion using finite difference forward modeling and quasi-Newton techniques (Loke & Barker 1996).

Resistivity profiles across the disturbed Linell plots show that in one case the permafrost continues to degrade while in another a small zone of potentially refrozen material has been recreated since 1973 (Linell 1973). Figure 6 includes a DC resistivity cross section of the plot where surface vegetation was cleared by hand but the surface organic material was left intact. Undisturbed permafrost is present at 0 m on the line (x-axis). The dark mass to the right center of the plot corresponds with a low lying grassy area along the DC resistivity line with standing water and minimal shrubs or trees. This wet soil affects DC resistivity measurements and yields an apparent highly resistive mass at a depth of 3 m that is not present based on frost probing. This is signified by the bulbous mass with resistivities >200 Ω-m from 34 to 47 m along the section. To the left (east) the resistivities that are >200 Ω-m likely signify permafrost at 9 m depth. This depth to permafrost was confirmed at two locations with an expandable frost probe. Figure 7 includes a DC resistivity cross section of the plot where surface vegetation and organic material were removed in 1946. Undisturbed permafrost is present from 0 to 25 m on the line (x-axis). A borehole encountered permafrost at 9.8 m (Fig. 8) which corresponds with the tabular region (black) consistently yielding a resistivity of >450 Ω-m.

Table 1. A summary of the summer average temperatures, active layer depth, and moss thickness from 121 points at the undisturbed Linell plot (CALM site) for 2005–2007.

Year	May-October mean air temperature (°C)[1]	Mean thaw depth without moss (cm)	Mean moss thickness (cm)
2005	13.7	44.5	13.0
2006	12.6	40.1	13.5
2007	12.9	43.7	13.6

[1]Alaska Climate Research Center.

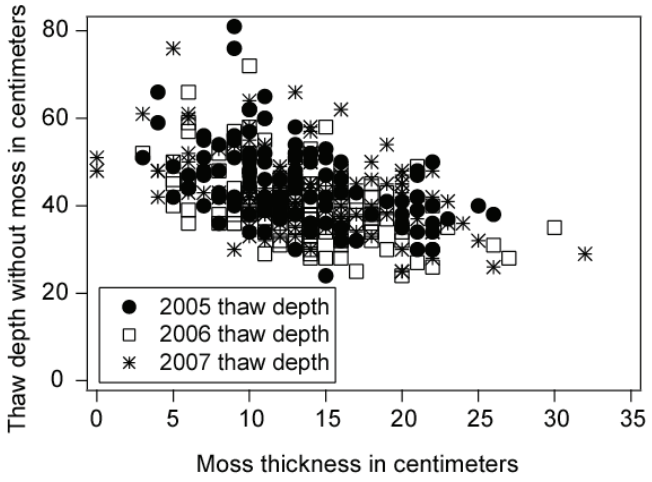

Figure 5. The relationship between moss thickness and thaw depth at the pristine Linell plot (CALM site) for 2005 to 2007.

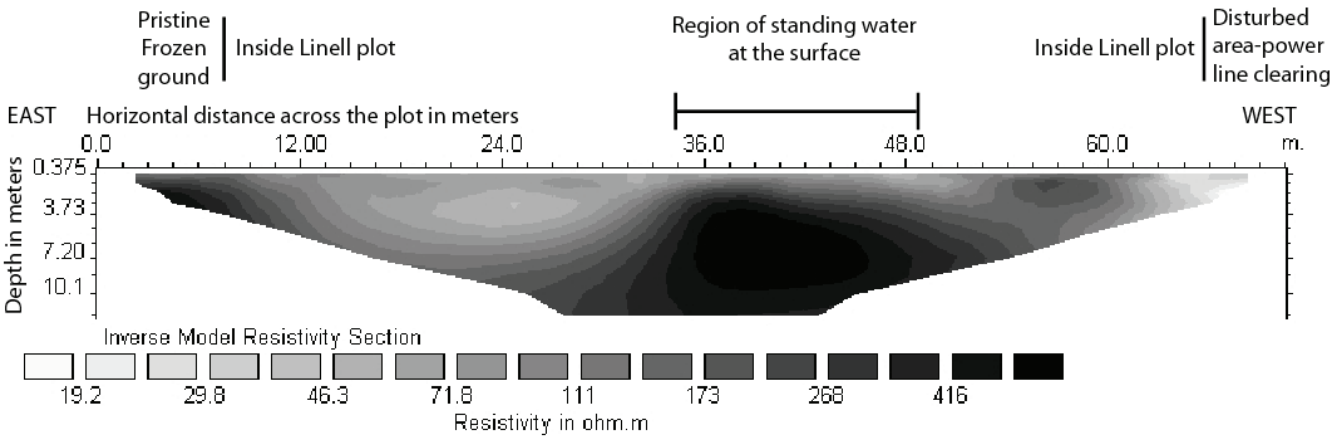

Figure 6. A direct current resistivity profile across the Linell plot where, in 1946, the surface vegetation was removed but roots and organic material were left intact. The unit electrode spacing is 1.5 m.

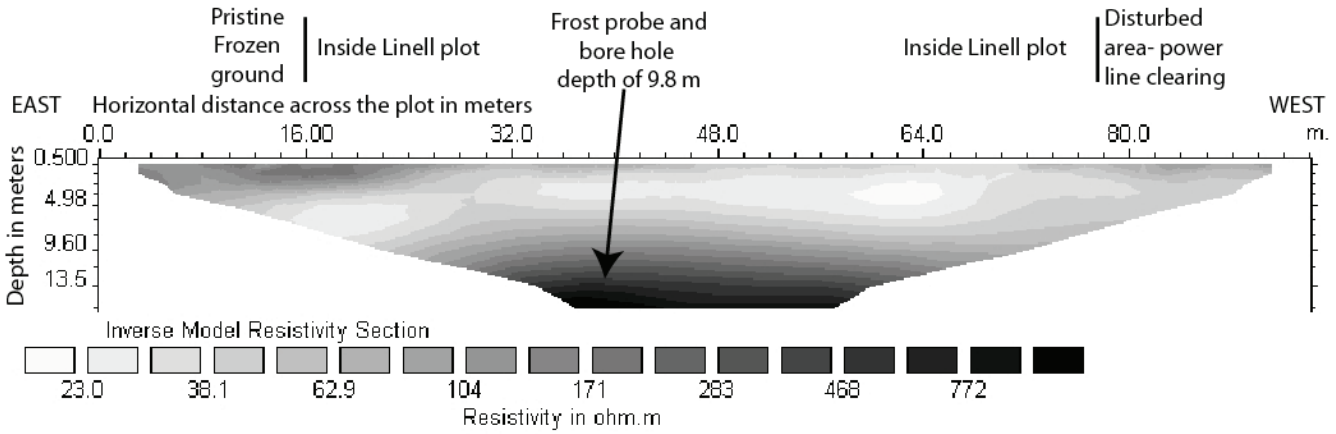

Figure 7. A direct current resistivity profile across the Linell plot where, in 1946, the surface vegetation, roots, and organic material were removed. The unit electrode spacing is 2 m. The arrow denotes where a borehole encounters permafrost at 9.8 m depth (Fig. 8).

The DC resistivity values here are ~450 to 800 Ω-m when permafrost is encountered. This is on the low end for studies reporting resistivity values for permafrost. Hoekstra and McNeill (1973) report values of 300 to 7000 Ω-m for "Fairbanks silt" with the values approaching 800 Ω-m for "Fairbanks silt" at -5°C. This is within the range of values we measured for soils that are similar to Fairbanks silt. Harada et al (2000) report values of 2100 and 12,000 Ω-m for permafrost at the Caribou-Poker Creek Research Watershed (CPCRW) located 20 km north of our study site. Yoshikawa et al. (2006) report values of 1000 to 14,000 Ω-m for permafrost at the top of a pingo at the CPCRW and 600 to 10,000 Ω-m for frozen ground at a pingo located 4 km west of the Fairbanks Permafrost Experimental Station. Permafrost in northern Quebec (Seguin and Frydecki 1994) yields values between 1000 and 5000 Ω-m. DC resistivity values are strongly controlled by the moisture content and the salinity (or conductivity) of the permafrost. In the Fairbanks area the mean annual temperature is -3.3°C. The permafrost is roughly 0.5°C to 1°C (Fig. 8) which is considered warm for permafrost. As a consequence, there is likely unfrozen water in the pore spaces of silt rich sediment at the top of the permafrost table. This could result in lower resistivity values than are measured at locations where colder temperatures and less unfrozen water are present.

A summary of our measurements combined with the data reported by Linell (1973) is provided as Figure 9. Permafrost destruction at the site where surface vegetation was removed but organic material was left intact appears to have ceased since 1973. While probing along the DC resistivity line at the site we identified a thin (50 cm) frozen layer between 1 and 1.5 m depth. This likely signifies a zone of aggrading permafrost. At the site where all vegetation and surface organic material were removed the depth to permafrost has increased to 9.8 m depth (based on frost probing and a bore hole installed at this location in the fall of 2007 that yielded temperatures below freezing at 9.8 m depth in October 2007 and January 2008 (Fig. 8).

If one assumes a maximum volumetric ice content of ~30%, the loss of 9.8 m of ice at the disturbed site and 4.7 m of ice at the partially disturbed site would lead to subsidence of ~2.9 m and ~1.4 m, respectively. This assumes all the ice was lost (as melt water) through evapotranspiration or subsurface flow which is not likely. The ground surface appears visibly

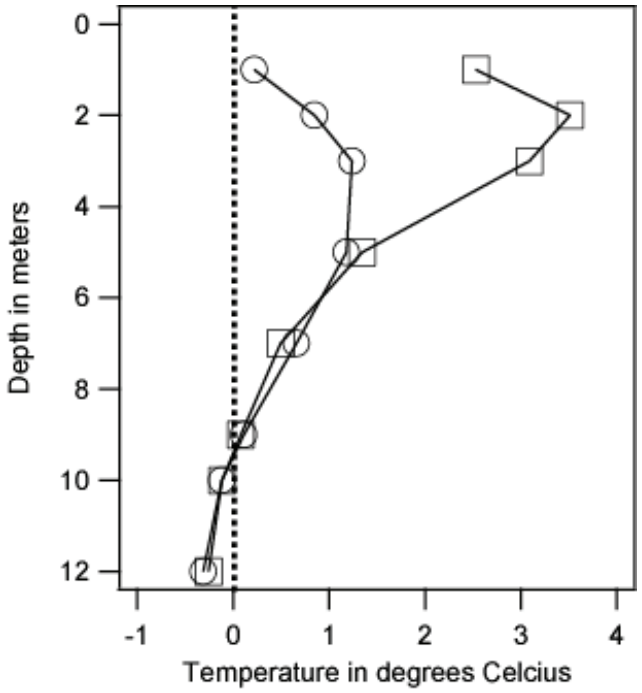

Figure 8. Borehole temperatures on October 19, 2007 (open boxes) and January 20, 2008 (open circles) at the Linell plot where surface vegetation, roots, and organic material were removed.

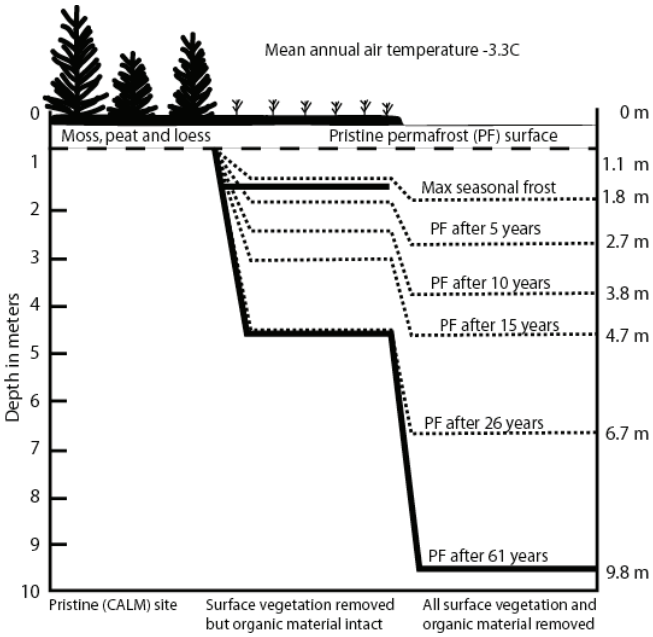

Figure 9. A cross section based on Linell, 1973. Vegetation removal from the two disturbed sites occurred in 1946. The bold line denotes the measurements collected in the fall of 2007, representing 61 years since disturbance.

depressed at the two disturbed Linell plots compared to the edges of the plots and to the control plot. However, the degree of subsidence cannot be ascertained beyond a visual estimation due to a lack of high resolution elevation measurements at the site prior to disturbance in 1946.

Discussion

Comparing the results from this investigation with that of Linell (1973) it is apparent that at both of the plots where vegetation was removed the permafrost expanded downward for the first 26 years while the permafrost table eventually stabilized at the partially disturbed site. This is likely due to the reestablishment of a boreal forest at the site within 25 years. This forest succession did not lead to the upward migration of the permafrost table, most likely due to the fact that ambient temperatures in the area are relatively warm. However, the small frozen layer at roughly 1.5 m depth at this site may signify that an epigenetic (downward freezing) regime is currently in place.

At the site where all the surface vegetation and organic material were removed the permafrost surface has migrated downward for the past 35 years. Vegetation is continuing to evolve and is currently transitioning from a shrub, birch, and willow forest to one with a higher density of spruce trees and moss. The downward migration of the permafrost surface has not been linear in nature (Fig. 10). In fact, the rate of permafrost degradation at both of the disturbed sites is best represented by a second order polynomial.

Since the climate of Interior Alaska has warmed slightly over the past three decades it is possible some of the

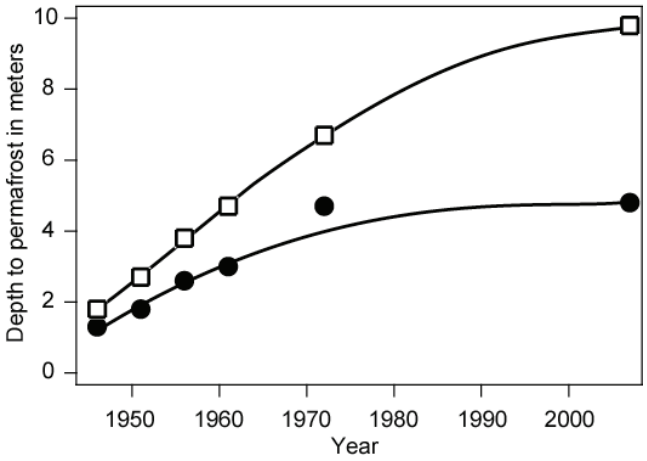

Figure 10. Permafrost degradation at the disturbed Linell plots. Boxes denote the site where surface vegetation and organic material were removed, and circles denote the site where surface vegetation was removed but organic material was left intact.

permafrost degradation at the Linell plots is attributable to climatic change. The downward migration of the permafrost surface may be augmented by warming temperatures in addition to the changing thermal regime caused by vegetation disturbance. Thaw depths at the pristine Linell plot (the CALM site) are ~80 cm and are within the range of values presented by Linell (1973) for the period from 1946 to 1972. The recent establishment of a Circumpolar Active Layer Monitoring Network (CALM) site at the undisturbed Linell plot will provide a baseline of the current and future state of permafrost which can be assessed once a long-term record (>10 years) has been measured.

Conclusions

Based on the results from this and previous studies, it is evident that the downward degradation of permafrost is highly dependent on the type of surface degradation and time. This has ramifications for forest succession following fire or human-caused disturbances to vegetation in permafrost terrains.

This study supports previous work showing that vegetation disturbance greatly affects permafrost stability. The regrowth of boreal forest vegetation at the partially disturbed Linell plot has lead to the cessation of permafrost degradation. In fact, a thin layer of frozen ground slightly below the typical thaw depth may be evidence of the reestablishment of permafrost. The site with greater vegetation disturbance has exhibited permafrost degradation since 1946, but the rate of degradation is not linear and is decreasing as the re-establishment of boreal forest continues. Resistivity values we measured for permafrost (~450 to 800 Ω-m) are relatively low compared to measurements in ice-rich permafrost. However, our site is characterized by low-moisture-content silts. Further studies of the thermal state and moisture content of the frozen silt at the site are warranted. Finally, ambient air temperatures have increased over the past few decades in the study area, and they are expected to continue to increase in the future. Though thaw depths in the permafrost at the CALM site appear to be somewhat stable since 1946, we will only be able to determine how future warming will continue to affect permafrost at the site with continued monitoring.

Acknowledgments

Many people donated time, equipment, and information to support this collaborative study. Site history was provided from Charles Collins and Karen Henry of CRREL. Field assistance from Stephanie Saari, Art Gelvin, Allan Delaney, Charles Collins, and Tohru Saito has been invaluable. Beth Astley shared her geophysical information for Birch Hill and Farmers Loop. Comments from two anonymous reviewers and Editor D. Kane strengthened the manuscript.

References

Burn, C.R. 1998. The response (1958–1997) of permafrost and near-surface ground temperatures to forest fire, Takhini River valley, southern Yukon Territory. *Canadian Journal of Earth Science* 35: 184-199.

Das, U.C. & Verma, S.K. 1980. Digital linear filter for computing type curves for the two-electrode system of resistivity sounding. *Geophysical Prospecting* 28: 610-619.

Gilmore, T.J. & Clayton, E.A. 1995. Mapping the top of the permafrost using surface direct current resistivity survey. *Environmental Geology* 30(1/2): 29-33.

Hamilton, T.D., Ager, T.A. & Robinson, S.W. 1983. Late Holocene ice wedges near Fairbanks, Alaska, U.S.A.: Environmental setting and history of growth. *Arctic and Alpine Research* 15(2): 157-168.

Harada, K. & Yoshikawa, K. 1996. Permafrost age and thickness near Adventfjorden, Spitsbergen. *Polar Geography* 20: 4, 267-281.

Harada, K., Wada, K. & Fukuda, M. 2000. Permafrost mapping by transient electromagnetic method. *Permafrost and Periglacial Processes* 11: 71-84.

Hauck, C., Mühll, D.V. & Maurer, H. 2003. Using DC resistivity tomography to detect and characterize mountain permafrost. *Geophysical Prospecting* 51(4): 273-284.

Hauck, C. & Kneisel, C. 2006. Application of capacitively-coupled and DC electrical resistivity for mountain permafrost studies. *Permafrost and Periglacial Processes* 17: 169-177.

Hinzman, L.D., Fukuda, M., Sandberg, D.V., Chapin III, F.S. & Dash, D. 2003. FROSTFIRE: An experimental approach to predicting the climate feedbacks from the changing boreal fire regime. *Journal of Geophysical Research* 108(D1): 8153.

Hoekstra, P. & McNeill, D. 1973. Electromagnetic probing of permafrost. National Academy of Sciences, National Research Council. *Proceedings of Permafrost: North American contribution to the Second International Conference:* 517-526.

Jorgenson, M.T., Racine, C.H., Walters, J.C. & Osterkamp, T.E. 2001. Permafrost degradation and ecological changes associated with a warming climate in central Alaska. *Climatic Change* 48: 551-579.

Linell, K.A. 1973. Long-term effects of vegetative cover on permafrost stability in an area of discontinuous permafrost. National Academy of Sciences, National Research Council. *Proceedings of Permafrost: North American contribution to the Second International Conference:* 688-693.

Loke, M.H. & Barker, R. D. 1996. Rapid least-squares inversion of apparent resistivity pseudosections by a quasi-Newton method. *Geophysical Prospecting* 44(1): 131-152.

Nicholas, J.R.J. & Hinkel, K.M. 1996. Concurrent permafrost aggradation and degradation induced by forest clearing, central Alaska, U.S.A. *Arctic and Alpine Research* 28(3): 294-299.

Osterkamp, T.E. & Romanovsky, V.E. 1999. Evidence for warming and thawing of discontinuous permafrost in Alaska. *Permafrost and Periglacial Processes* 10: 17-37.

Osterkamp, T.E., Vierick, L., Shur, Y., Jorgenson, M.T., Racine, C., Doyle, A. & Boone, R.D. 2000. Observations of thermokarst and its impact on boreal forests in Alaska, U.S.A. *Arctic, Antarctic and Alpine Research* 32(3): 303-315.

Seguin, M.-K. & Frydecki, J. 1994. Semi-quantitative geophysical investigations of permafrost in northern Quebec. *Journal of Applied Geophysics* 32: 73-84.

Shur, Y.L. & Jorgenson, M.T. 2007. Patterns of permafrost formation and degradation in relation to climate and ecosystems. *Permafrost and Periglacial Processes* 18: 7-19.

U.S. Army Corps of Engineers, Permafrost Division. 1950. *Investigation of Military Construction in Arctic and Subarctic Regions, Comprehensive Report 1945-48; Main Report and Appendix III - Design and Construction Studies at Fairbanks Research Area.* ACFEL Technical Report 28.

Viereck, L.A. 1982. Effects of fire and firelines on active layer thickness and soil temperatures in interior Alaska. *Proceedings of the Fourth Canadian Permafrost Conference. National Research Council of Canada Calgary: Ottawa, Ontario:* 123-135.

Yoshikawa, K. & eight others. 2006. Comparison of geophysical investigations for detection of massive ground ice (pingo ice). *Journal of Geophysical Research* 111(E06S19): 10 pp.

Recent Advances in Russian Geocryological Research: A Contribution to the International Polar Year

D.S. Drozdov, G.V. Malkova, V.P. Melnikov
Earth Cryosphere Institute, Russian Academy of Sciences, Siberian Branch, Tyumen, Russia

Abstract

Fifty years have passed since the previous Polar Year (1957–1959). After the relatively cold climatic period of 1950–1960, the abrupt warming of air and ground temperatures was evident for the north of Russia. The geocryological observations suggest that the rise in ground temperature slowed down in the early 1990s; the recent trend of changes in geocryological conditions is uncertain. Ongoing and future permafrost research and modeling of permafrost evolution under the impact of climate change and man-induced development should be based on wide-ranging scenarios. Generally, the permafrost and climatic trends show that there will be no significant changes in geocryological conditions in the upcoming 20 to 25 years. The decreasing continentality of the climate can increase the extent of destructive cryogenic processes on the continent and in the coastal zone, especially in the case of significant impact caused by development. Cryogenic structure of permafrost will control significantly the activity of external processes.

Keywords: air and ground temperatures; cryogenic processes; GIS; geocryological monitoring; geosystem; permafrost change.

Introduction

The International Polar Year (IPY) provides one of the most significant events for geocryologists. Fifty years have passed since the previous Polar Year (also International Geophysical Year, 1957–1959). Some of its participating Russian geocryologists are still active (G.F. Gravis, A.V. Pavlov, M.M. Koreisha, and others). The end of the 1950's was a time of rather cold climate and the main investigations in the permafrost zone concerned cryogenic structure of the upper permafrost layers. At present, due to the concerns for global warming, the main attention is focused on the problem of permafrost degradation and destructive external processes, especially in case of man-made impacts. The basic problem is the study of seasonal and annual changes in climate and permafrost conditions and their interaction. Our contemporary investigations are coordinated with numerous international IPY programs: Arctic Circumpolar Coastal Observatory Network (ACCO-Net) and our Coastal Cryolithozone of the Russian Arctic (COCRA); Thermal State of Permafrost and our International Network of Permafrost Observatories (INPO); Greening of the Arctic: Circumpolar Biomass (GOA) and, also, various Russian Integrative and Regional Programs to assess permafrost changes. Collecting and processing of climatic and geocryological data are performed using GIS-techniques applied to models at global, regional, and localscales.

The IPY research in the Eurasian polar region concerns the following general items (Melnikov et al. 2007):

- Contemporary changes in climate and sea hydrodynamics in Arctic regions;
- Geocryological structure and cryogenic features;
- Continental and subsea permafrost formation and evolution;
- Natural and man-made cryogenic physical and geological processes;
- Permafrost monitoring (including coastal permafrost);
- Development of GIS databases and maps as conceptual and graphical models;
- Development of the new techniques for permafrost research.

This report highlights some of the recent results from these investigations with a focus on Western Siberia.

Geosystem Approach and Processing of Geocryological Data

Geocryological studies, mapping, and monitoring of the northern territories affected by climate change and intensive development are aided by global, regional, and local GIS applications. Digital maps of onshore and offshore areas with attribute databases of geomorphology, landscapes, lithology, soil properties, geocryological conditions, bathymetry, etc. are efficient tools for the analysis of available data and for assessing the environment (Melnikov & Minkin, 1998). A wide-ranging generalization of information from databases, and the compilation and redrafting of thematic digital maps, makes it possible to reflect the present-day state, trends and dynamics of coastal processes (Drozdov et al. 2005).

The landscape (geosystem) approach is used to pass from the low hierarchical level to the higher level (and vice versa) while processing the data. This is necessary for the collection and generalization of primary data with the development of general small-scale maps, on the one hand, and for displaying general regional regularities on the large-scale maps, on the other hand. The landscape maps display geomorphology, lithology, geocryology, vegetation and their longitudinal and altitudinal zonality. Thus, it reflects the main features and properties of the modern environment. The overlay of the landscape and climatic maps allows one to generate spatial geocryological forecast as an element of general environmental forecast.

Climate-Permafrost Relationships: General Regularities

Global and regional modes are used to predict the evolution of permafrost as related to the climatic and economic conditions. Extrapolation of contemporary permafrost and climate trends indicates that there will be no significant changes in geocryological conditions in the upcoming 20 to 25 years. But the decreasing climatic continentality (Fig. 1) can accelerate the development of the destructive cryogenic processes, causing permafrost degradation. In the areas with significant summer warming (e.g., in Western Siberia), the active layer thickness should increase, and thermokarst, thermal erosion, and cryogenic landslides should be more intense. In the areas with prevailing winter warming, intensification of frost heave, cryogenic cracking, and ground-ice formation are predicted. Global and regional GIS and databases are used to reveal and describe these phenomena.

The most negative tendency for the permafrost stability is expected for the regions where climate warming is accompanied by continued economic development. The potential decrease in the permafrost stability in this case is not related to climatic feedback effects caused by development, as there are no direct evidences for this process (Pavlov & Malkova 2005).

The long-term prognosis (20 to 50 years) is developed from the assessment of Russian permafrost sensitivity to the short-term climatic change (one year). This assessment is based on temperature and precipitation calculations. The basic argument for the short-term prognosis is the changing of the active layer thickness and moisture. Thus, according to a short-term prognosis of the geocryological processes, no catastrophic events were expected in 2006 and this forecast proved to be correct (Gravis & Konchenko 2007). In 2007, cryogenic processes were expected to be more active in the eastern regions of Russia, and to result in disturbance of the natural landscapes. This forecast is yet to be verified.

It is established for the offshore Arctic areas that changes of coastal destruction are rhythmical and have no meaningful trend. All temporal anomalies in the coastal destruction rate are synchronous with the climatic fluctuations, including characteristics of sea hydrodynamics and the state of ice in the Arctic seas. The smoothed hydrodynamic forecast makes it possible to assume a subsequent stable rate of coastal destruction that would not exceed contemporary rates by more than 10%–20%. If all other conditions are equal, the dominant role in coastal processes is related to the spatial

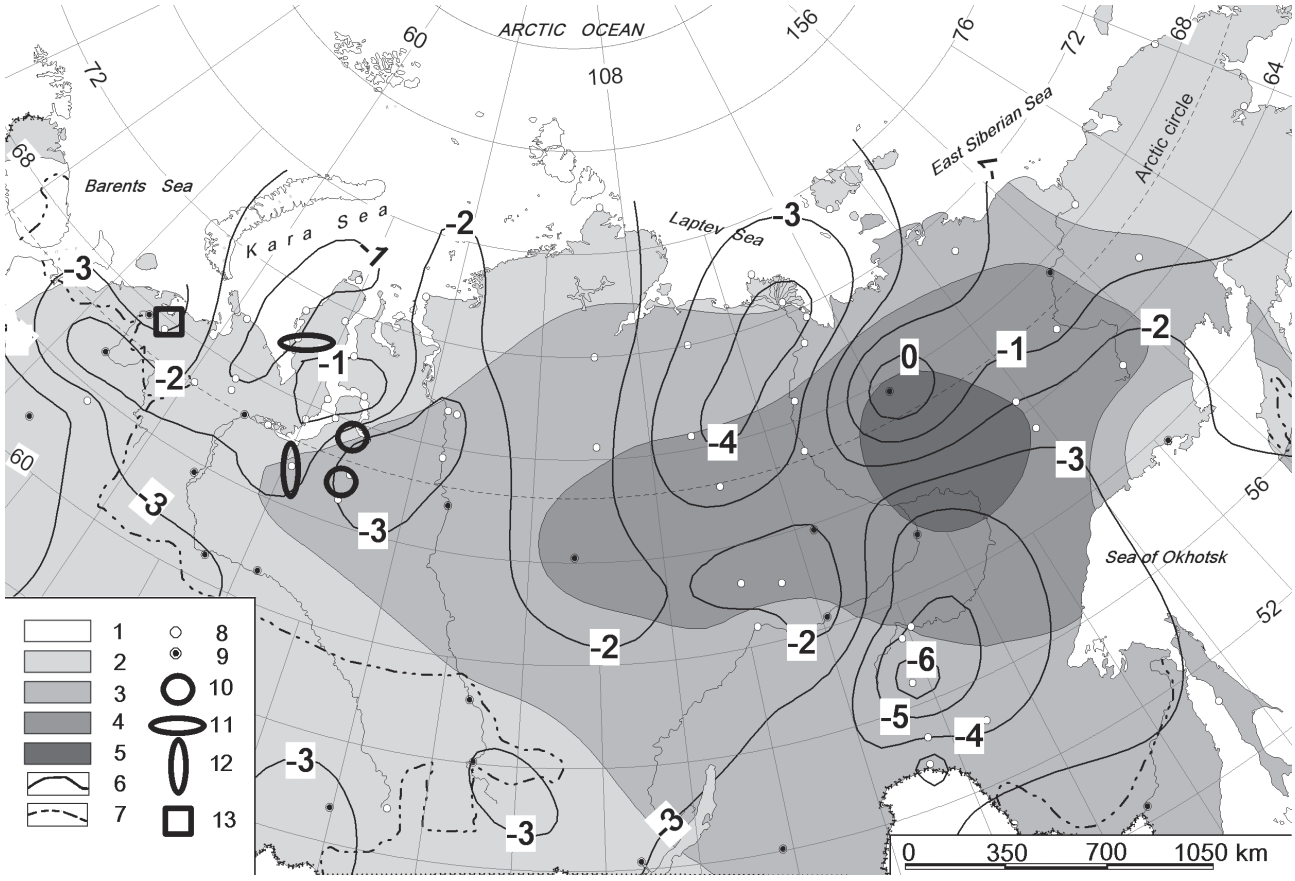

Figure 1. Map of climate continentality change owing to climate warming (amplitude contraction map). *1 – 5 – Annual amplitude of air temperature, °C: 1 – 20-30; 2 – 30-40; 3– 40-50; 4 –50-60; 5 – 60-70. 6 – change of annual amplitude since 1970, °C; 7 – southern limits of cryolithozone; 7 – 8 – weather stations with weather record: 7 – less then 100 years, 8 – more then 100 years; 10 – 13 – ECI SB RAS geocryological key-sites at: 10 – Urengoy gas-field, 11 – Yamal (Marre-Sale), 12 – Nadym, 13 – Pechora River mouth (cape Bolvanskii).*

variability of the cryogenic structure of permafrost (Vasiliev et al. 2005). The thermal erosion of the seacoast is considered to be the most destructive process, particularly in the case of ice-rich permafrost. Some anomalies are evident during the last decade, such as the correlation with fluctuations in the coverage of sea ice.

Monitoring of Unique Regions and Territories

Mapping and monitoring of unique territories are based on the regional and local landscape maps as the graphical tools. GIS techniques are used for the multivariate generalization of the experimental field data and for developing maps of the different conditions. Repeated geocryological surveys (for example, for the territory of Urengoy gas field, Western Siberia) show there have been no statistically significant changes in the permafrost temperature during the last several years. Compilation of these repeated maps is based on the reprocessing of existing data and on geocryological parameters aided by the new annual observations. Unfortunately, these regime data do not characterize all types of the geosystems. This limits the comprehensiveness of the repeated mapping.

Our experience in using insufficient data sets for compiling prognostic geocryological and environmental maps in the regions of new economic development is of particular interest. These maps are extremely important for feasibility studies and for the potential environmental impact assessment.

The medium-scale maps (1:100,000 to 1:200,000) of the natural and disturbed ecosystems, engineering-geocryological conditions, external geological processes, and permafrost stability were developed using GIS modeling (Drozdov et al. 2007). Expected gas and oil pipeline corridors cover about 3000 km^2. These are wide swaths of land ranging from 20 to 70 km as in: a) the Vankor oilfield to the north and to the south in Western Siberia; b) the Bovanenkovo deposit to the south in Western Siberia; and c) the northern branch of VSTO pipeline in East Siberia to the Pacific Ocean (Ust-Kut–Lensk–Aldan–Tynda). New geocryological information of limited extent made it possible to display up-to-date ground temperature and cryogenic processes in these regions.

Geo-Indicators of Cryogenic Processes

New data necessary for the reconstruction of Pleistocene-Holocene evolution and assessment of cryogenic stability of Russian Arctic are developed from offshore, on-shore and coastal expeditions. Geocryological structure, geocryological conditions, ice-content, ice-complex distribution, and external processes were examined in the European and Siberian North and in the coastal zone of Barents, Kara and Laptev seas. Some new conclusions can be made.

The investigations in Yenisey Bay (Kara Sea coastal zone) showed that polygenetic Pleistocene plains have very different geological and cryological characteristics. The sites with displaced sandy and loamy sediments and low ice content can be found in close proximity to the territories with horizontal sediment bedding and the presence of the ice complex. Sometimes, the ice-complexes occur in several layers. The alternation of ice-rich and ice-poor sites is observed along the coast; they are characterized by different rates of thermal abrasion and thermal erosion. Numerous slopes subjected to strong thermal erosion is indicative of the presence of ice-complexes even in the case when the latter cannot be diagnosed by either standard landscape surveys and remote sensing in this northernmost region of the Yenisey River (Streletskaya et al. 2007).

The traditional on-shore and coastal regime investigations that have been carried over a long time at the Bolvanskii key-site in the mouth of Pechora River (Barents Sea) were accompanied by seismic surveys. Geophysical seismic research and monitoring were conducted to analyze slope stability. This special seismic technique is based on theoretical relationships and experimental correlation between seismic characteristics of the soil and stress-strain condition of the soil massif. A very important feature of this technique is the opportunity to monitor and predict initial changes of the slope stability before significant change occurs. The length of forecasts range from months to several years. The error in expected spatial discontinuity does not exceed several meters (Skvortsov & Drozdov 2003). Repeated investigations during 2002–2006 showed that the relaxation of the stress-strain conditions took place, and slope stability increased. This micro-landscape mapping indicated that an existing crack on the surface, indicative of a weakened zone, became less noticeable from year to year. The seismic research, extended to the offshore zone, showed that the permafrost table is found at a depth of 8 m under the beach and descends to about 20 m at a distance of 200 m offshore (Skvortsov et al. 2007).

The theory of "landslide plains" explains how the changing of soil-biota conditions causes the new cryogenic landslides and how the new brine laden horizons are entrained into the active layer within the period of about 300 years (Leibman & Kizyakov 2007).

Frost heave and permafrost degradation are the main cryogenic processes in central part of Western Siberia. Complex monitoring near the town of Nadym revealed natural and anthropomorphic changes of landscape. The old peat mounds resulting from heaving are growing and new mounds continue to appear. The growth of the peat mounds is most active in the coldest winters; in milder winters, it is less intense. In contrast there are other processes like the increase in the active layer thickness and the rise of ground temperature. Temperature rise was very pronounced at the end of the 20th century. Locally it caused significant degradation of the permafrost. This tendency is moderated now, and geocryological conditions have become more stable. Man-made development increase permafrost degradation (Moskalenko & Ponomapeva 2006).

The micromorphological indicators of cryogenic conditions and processes during the early Cenozoic have been studied. The so-called cryogenic type of microstructure of sub-aerial sediments has been described. It is widespread and very stable. It can be traced in polygenetic syn-cryogenic and epi-

cryogenic soils presently frozen or thawed. The established differences in the microstructure of Quaternary and Late-Cenozoic sediments make it possible to reconstruct features of paleo-cryogenic origin and the sequence of permafrost aggradation and degradation cycles for the past 3,000,000 years (Slagoda 2003).

Geocryological Monitoring in the Important Economic Regions

The important economic regions in the permafrost zone are influenced by substantial development that, together with the natural climate fluctuations, change landscapes and geocryological conditions. The studies of ecological and geocryological regimes concern both spatial and temporal description and forecast changes to the properties of the geological environments. Several key sites are located in Western Siberia and the European North in different natural settings and under different cryological conditions: for example, at Urengoy gas field, near the town of Nadym, on the Yamal peninsula, and on the mouth of Pechora River (Fig. 1). The landscapes, external processes, cryolithology, active layer, and ground temperature are studied there. These studies are important both for the ecological and geological estimation of current state of the territories and for detection of general regularities governing the observed changes.

Changes of average annual ground temperature are smoothed in comparison to external changes (e.g., in air temperature). They make it possible to observe general cryological trends not hidden by the highly variable fluctuations and extremes. At Urengoy gas field, the ground temperature measurements were made in 1974, 1975, 1977, 1978, 1992, 1993, 1994, 1997, 1999, 2005, 2006, and 2007.. According to these data, the temperature of the permafrost increased approximately 1°C during the period 1975–1993 owing to the natural climatic warming. Land use changes added an extra 1°C to 2.5°C, but this ground temperature rise is located close to human constructions. Changes in the ground temperature are not identical at the different landscapes (geosystem rank). They vary over wide limits. In the southern forest-tundra the ground temperature increase ranges from 0.6°C to 2.1°C. In northern forest-tundra and southern tundra, its increase is somewhat lower (0.1°C to 1.6°C, Drozdov 2002). The continuous temperature observations of 1994–1999 testify to the retardation in the increase of the frozen ground temperature. In the next five years, a decrease in ground temperature was registered at some sites. The pattern of ground temperature change in the southern forest-tundra landscape zone is shown in Figure 2.

For areas with high shrubs, where much snow is accumulated during winter and where the frozen ground temperature at the beginning of the warming cycle was close to 0°C, the degradation of permafrost was observed. The top of the degrading permafrost can be found at a depth of approximately 10 m. Analogous processes occur at the forested sites. The thawing of ground has not ceased. At some tundra and boggy sites, the warming of permafrost was followed by significant

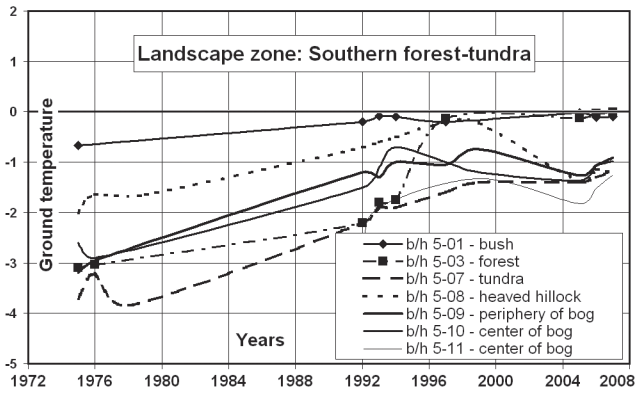

Figure 2. Ground temperature changes in southern forest-tundra at ~10 m depth (Urengoy gas field, Western Siberia) *b/h – borehole number and type of landscape site.*

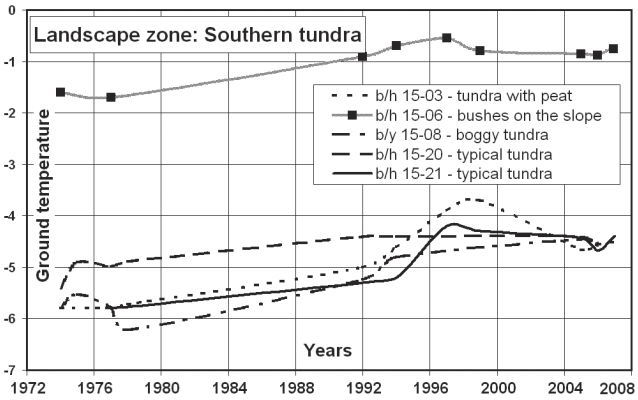

Figure 3. Ground temperature changes in southern tundra at ~10 m depth (Urengoy gas field, Western Siberia); *b/h – borehole number and type of landscape site.*

cooling in the mid 1990's. The more significant freezing can be found on hillocks. It is interesting that the temperature conditions in different geosystems become closer to one another under the impact of recent temperature changes; in the areas with degrading permafrost, the ground temperature is close to 0°C; in the areas with stable permafrost, it varies from -1°C to -1.4°C.

The same processes can be observed in the southern tundra landscape zone, but they occur generally under conditions of lower mean temperatures (Fig. 3).

All the geosystems are characterized by some temperature maximum in the mid-1990s. In most of the boreholes, temperatures at the depth of 10 m were very similar and rather cold: from -4°C to -5°C for the typical conditions.

A common feature for the northern part of Western Siberia is the rise in the ground temperature in the last three years (2005–2007). In the previous years, a decrease in the ground temperature took place. Thus, it is difficult to judge the real temperature trend in this region

The spatial and temporal distribution of permafrost temperatures are displayed on a series of temperature maps of Urengoy gasfield area, Western Siberia (Fig. 4). The first temperature map (B) is compiled on the basis of the results of the geocryological surveys in the period 1972 to 1977;

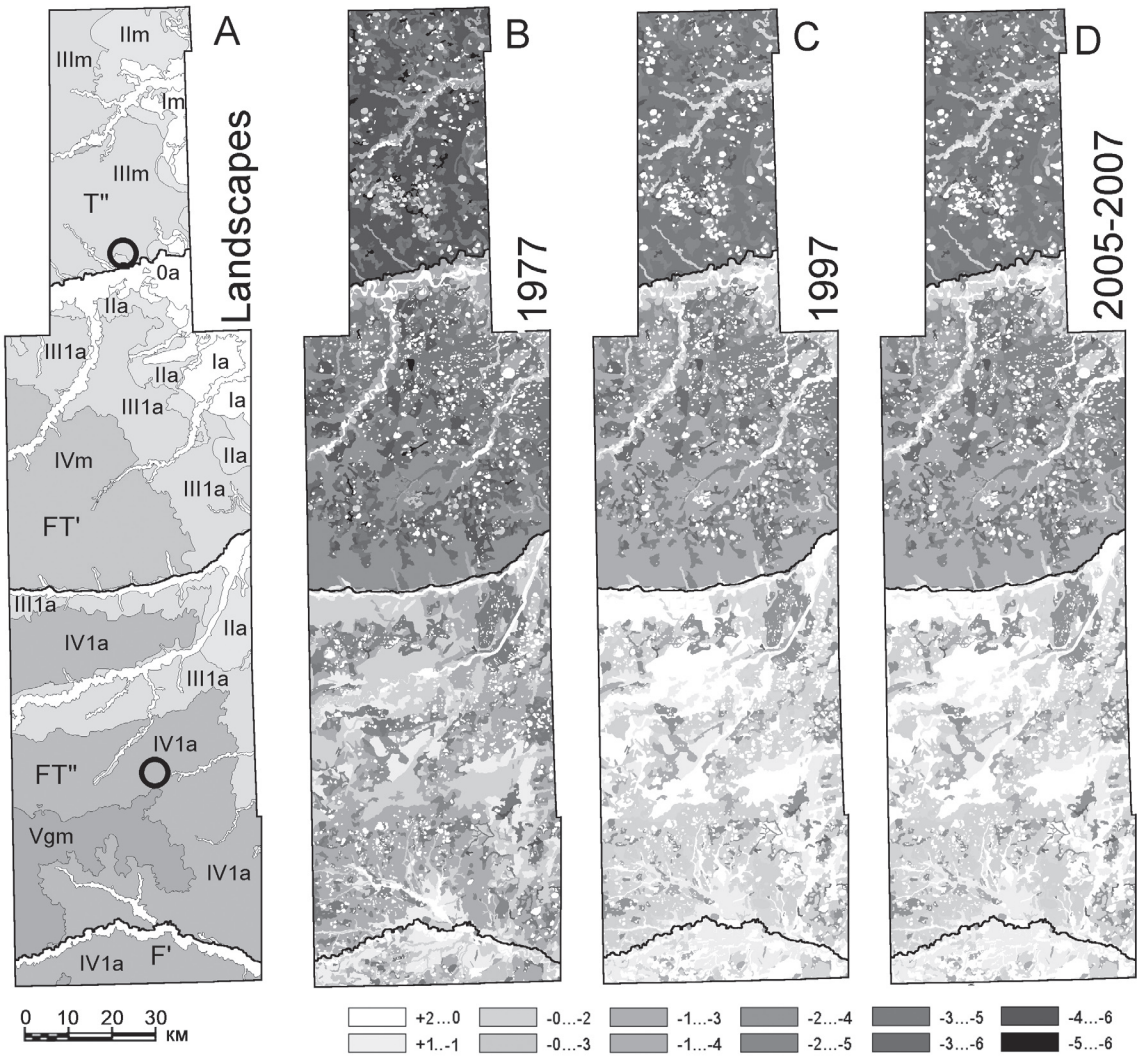

Figure 4. Natural dynamics of permafrost temperatures at the territory of Urengoy gas field (Western Siberia). *A – geosystem types (the larger letters – indexes of landscape zones; the smaller letters – landscape type index – number of geomorphologic level and genesis; black circle – geocryological regime key-site); B, C, D – ground temperature at 1977 (B), at 1997 (C) and at 2005-2007 (D).*

the second map (C) is drawn according to the data of the repeated simplified survey and thermal observations (1992 to 1997); the third map (D) is created on the basis of new thermal observations (1999, 2005 to 2007). Examining the gray-scale saturation of these maps, one can see that maps B and C reflect an average increase in the ground temperature of approximately ~1°C over a span of 20 years. Maps C and D indicate the absence of considerable temperature change during the last decade.

Conclusions

After the relatively cold period of the late 1950s, the decades of the 1970s and 1980s were characterized by the sharp warming of air and ground in the north of Russia. According to geocryological observations, the rise in ground temperatures slowed down and practically stopped since the middle 1990s. This invites us to assume that the warming tendency can be replaced by a cooling tendency. However, the recent short period of 2005–2007 showed an increase in ground temperatures. Thus, the real trend of modern geocryological condition is not factually clear. The modeling of permafrost evolution concerning the climatic and industrial influences should be performed for an ensemble of the scenarios. Extrapolation of contemporary permafrost climatic trends shows that there will be no significant changing of geocryological conditions in the coming 20 to 25 years, but the reduction of climatic continentality can increase the development of the negative cryogenic processes related to the increase in the active layer thickness, permafrost degradation, thermokarst, thermal erosion, and landslide activation in regions of summer warming. The most hazardous changes are expected in the regions, where climatic warming is accompanied by active land use change caused by development. The long-term prognosis (20 to 50 years) can provide an assessment of permafrost sensitivity to

the short-term climatic changes that differ from year to year in the Russian North.

The seacoast thermal erosion is considered to be stable and rhythmic and shows no significant trend. Some anomalies are observed during the last decade and are associated with fluctuations in sea ice coverage. The activity of coastal processes relies on the spatial variability of the coastal cryogenic structure. The theory of "landslide plains" explains how the changing soil-biota conditions cause the new cryogenic landslides and the inclusion of new brine laden horizons into the active layer.

The knowledge of recent geocryological regularities allows the development of the medium-scale map-models of natural and man-influencedt geosystems, engineering-geocryological conditions, geo-environmental situation and permafrost stability, even in case of insufficient data.

GIS-techniques, geosystem methods, new meteorological and geocryological data, different landscape-geocryological field experiments, geophysics, and lab analyses allow us to extend our knowledge about permafrost and its interactions with other environments within programs of IPY.

Acknowledgments

We express our deep gratitude for scientific and financial support to the Russian Foundation of Basic Research, the Russian Academy of Sciences (grant 05-05-64215), the Tyumen Governor, the U.S. National Science Foundation (ARC-0632400, ARC-0520578), the "Okeangeologiya" Scientific Research Institute, "Urengoygazprom" Company, and Yenisey Shipping.

References

Drozdov D.S., Korostelev Yu.V., Malkova G.V., Melnikov E.S., Soromotin A.V., Ukraintseva E.A. & Chekrygina S.N. 2007. Preliminary geocryological and environmental mapping of the areas of perspective economic activity. *Cryogenic resources of polar regions: Int. conf., Vol. II. Salekhard, June 2007*: 264-266.

Drozdov D.S. 2002. GIS investigations at geocryological monitoring of Urengoy oil-gas field (the northern part of Western Siberia). *Ecology of northern territories of Russia: Conf., Vol. 1, Archangelsk, June, 2002*, 89-94 (in Russian).

Drozdov D.S., Rivkin F.M., Rachold V., Ananjeva-Malkova G.V., Ivanova N.V., Chehina I.V., Koreisha M.M., Korostelev Yu.V. & Melnikov E.S. 2005. Electronic Atlas of the Russian Arctic Coastal Zone. *Geo-Marine Letters* 25(2-3): 81-88.

Gravis G.F. & Konchenko L.A. 2007. Cryogenic geological processes: problems of the short-term forecast. *Cryogenic resources of polar regions: Int. Conf., Vol. I. Salekhard, June 2007:* 131-133.

Leibman M.O. & Kizyakov A.I. 2007. Cryogenic landslides of the Yamal and Yugorsky peninsular. *Moscow: Earth Cryosphere Institute SB RAS,* 206 pp.

Melnikov E.S. & Minkin M.A. 1998. About strategy of development of electronic geoinformation systems (GIS) and databases in geocryology. *Earth Cryosphere* II(3): 70-76 (in Russian).

Melnikov V.P., Vasilyev A.A., Gravis G.F., Drozdov D.S., Leibman M.O., Malkova G.V., Melnikov E.S., Moskalenko N.G., Pavlov A.V., Ponomareva O.E., Skvortsov A.G., Slagoda E.A. & Smetanin N.N. 2007. Contemporary state, stability and dynamics of permafrost zone: international polar year, first decisions. *Cryogenic resources of polar regions: Int. Conf., Vol. I. Salekhard, June 2007*: 21-25.

Moskalenko N.G. & Ponomareva O.E. The temperature of the permafrost at largely hilly peat bogs in the northern taiga of Western Siberia and the forecast of its change. *Earth Cryosphere Assessment: Theory, Applications and Prognosis of Alterations.: Proceedings of the International Conference. Tyumen, 2006, Vol. 1*: 90-93.

Pavlov A.V. & Malkova G.V. 2005. Contemporary climate changes in the northern Russia: Album of general maps. *Novosibirsk, Academic publishing house "Geo",* 54 pp. (in Russian).

Pavlov A.V., Malkova G.V. & Skachkov Yu.B. 2007. Model Tendencies in the Evolution of Thermal state of cryolithozone under the climate changes. *Cryogenic resources of polar regions: Int. Conf., Vol. I. Salekhard, June 2007*: 34-38.

Skachkov Yu.B., Skryabin P.N. & Varlamov S.P. 25 years long monitoring of cryolithozone at Chabyda Station in Central Yukutia. *Cryogenic resources of polar regions: Int. Conf., Vol. I. Salekhard, June 2007*: 167-170.

Skvortsov A.G. & Drozdov D.S. 2003. Stress-strain conditions and stability of the Arctic coastal slopes: assessment using seismic surveys. *Permafrost: 8th International conference on permafrost: Extended abstracts. Zurich, ICOP, 2003*: 149-150.

Skvortsov A.G., Malkova G.V., Sadurtdinov. M.R. & Tsarev A.M. 2007. Geocryological conditions of the coastal part of the Pechora bay shelf in the region of Bolvansky-permanent-state-station according to the prospecting seismology data. *Cryogenic resources of polar regions: Int. conf., Vol. I. Salekhard, June 2007*: 170-173.

Slagoda E.A. Cryogenic deformations of the Cenozoic sediments at Baikal flexure. 2003. *Reports to the Academy of Sciences,* Vol. 393, No 8, part 1: 1105-1109 (in Russian).

Streletskaya I.D., Vasiliev A.A., Drozdov D.S. & Kanevskiy M.Z. 2007. Ice complex of Western Taymyr *Cryogenic resources of polar regions: Int. Conf., Vol. I. Salekhard, June 2007*: 99-102.

Vasiliev A.A., Ostroumov V., Rachold V. & Sorokovikov V.A. 2005. An Application of a Markov-chain model of shore erosion for describing the dynamics of sediment flux. *Geo-Marine Letters* 25(2-3): 196-203.

High-Resolution Numerical Modeling of Climate Change Impacts to Permafrost in the Vicinities of Inuvik, Norman Wells, and Fort Simpson, NT, Canada

C. Duchesne
Geological Survey of Canada, Ottawa, Ontario, Canada
J.F. Wright
Geological Survey of Canada, Sidney, British Columbia, Canada
M. Ednie
Geological Survey of Canada, Ottawa, Ontario, Canada

Abstract

Transient numerical ground temperature modeling conducted within an ARC-GIS-resident spatial analysis system was employed to predict the current and future distribution and character of permafrost in three study areas of the Mackenzie River Valley. Future impacts of progressive climate warming to 2055 were also predicted. Modeling results illustrate the variability in the evolution of permafrost characteristics, such as active layer and talik development, for representative terrain types. A clear north-to-south trend towards higher ground temperature was confirmed, paralleled by a north-to-south decrease in the areal extent and thickness of permafrost. Predicted ground thermal conditions for 2055 show minor changes at the base of permafrost, with the most substantive permafrost degradation being realized through the deepening of the active layer and the development of taliks in the top few to several meters below the ground surface.

Keywords: active layer; climate warming; Mackenzie River; numerical model; talik.

Introduction

The Mackenzie River Valley is characterized by widespread permafrost terrain of thickness ranging from more than 600 m in areas of the Mackenzie and Beaufort coastal plain, to only a few tens of metres or less in the southern extent of the valley (Judge 1973, Taylor et al. 1998). Heginbottom et al. (1995) mapped the continuous, discontinuous, and sporadic zones of permafrost in Canada, but at finer scales the distribution and character of permafrost are not well known. Numerical ground temperature models integrated within a geographic information system (GIS) provide a means for estimating the current distribution and character of permafrost across extensive geographic regions, and for generating time-series predictions of future impacts to permafrost under a progressively warming climate. This paper presents modeling results for three study areas in the Mackenzie River Valley (Fig. 1): Fort Simpson located in the discontinuous zone (15,405 km^2), Norman Wells overlapping the discontinuous and continuous zone (12,117 km^2) and Inuvik in the continuous zone (9089 km^2).

Numerical Models

Smith and Riseborough (1996) have proposed a simple analytical relation (TTOP) demonstrating direct linkages between key climate and terrain factors influencing ground temperatures. Under assumed thermal equilibrium, the model estimates the mean annual temperature at the top of permafrost (TTOP) or, when permafrost is not present, the mean annual temperature at the base of the annual freeze-thaw layer (TBAL). The model was applied to regional mapping of permafrost distribution in Norway's mountainous regions (Juliussen & Humlum 2007), and in the Mackenzie River Valley (Wright et al. 2003). For investigations of the transient impacts of climate change, the T-ONE one-dimensional, finite-element, heat conduction model provides reliable solutions to ground thermal problems in both natural and engineered environments (Goodrich 1982).

Both the TTOP and T-ONE models utilize similar model parameters representing the dominant climate and terrain factors

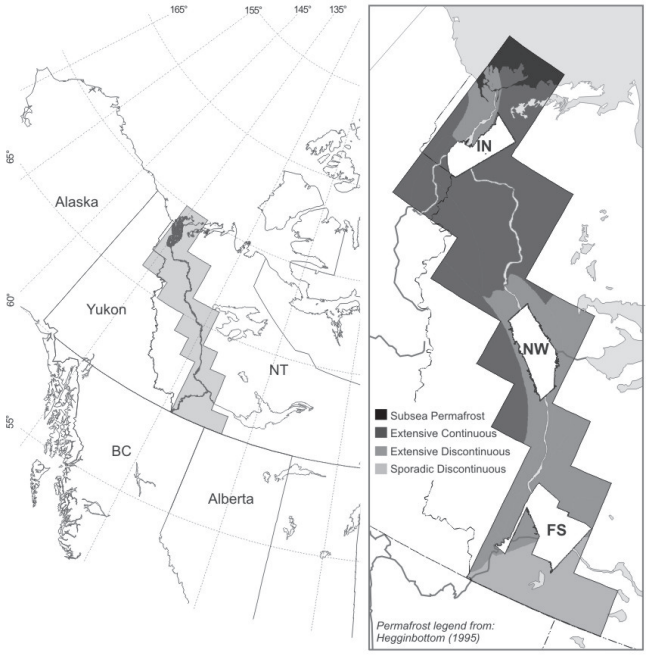

Figure 1. General and detailed location of the study areas modeled, northwestern Canada. IN: Inuvik, NW: Norman Wells, FS: Fort Simpson.

influencing the ground thermal state. The two models have been integrated within an ARC-GIS platform, enabling a quasi 3-dimensional grid space for generating predictions of permafrost occurrence, distribution, and temperature at local and regional scales, over selected time frames of interest.

Methods

Modeling parameters

To successfully apply the models to regional-scale mapping of permafrost, it is necessary to specify model parameter values which adequately reflect prevailing terrain and climate conditions within the study regions. The influence of atmospheric climate on the ground thermal regime is assumed to be primarily a function of air temperature as represented by thawing and freezing degree-day indices, and assumes that heat transfer in permafrost terrain is dominated by conductive processes (Outcalt et al. 1990). Thus, heat transfer through convective transport of water vapour and air within soil pore spaces, and the transient influences of rainfall infiltration and surface runoff (mass fluxes) are not considered. The use of seasonal n-factors links atmospheric temperatures to the ground thermal regime (Lunardini 1981) and provides a simplified representation of the influence of the buffer layer in modulating heat flow between the atmosphere and the ground surface. The summer vegetation cover is represented as a thawing n-factor, while the influence of snow cover is assumed to be implicit in the freezing n-factor (Wright et al. 2003, Jorgensen & Kreig 1988). Local topographic influences (as represented by a potential insolation index Ip), were not considered in this work in order to limit the number of unique terrain conditions modeled.

The general distribution of earth materials was obtained from available regional surficial geology maps (Hughes et al. 1972, Hanley et al. 1973, Rutter et al. 1980) supporting the assignment of model parameter values representing soil bulk density, soil mineralogy, and soil texture (Wright et al. 2003). These values are subsequently used for estimating the frozen/ unfrozen thermal conductivity (Johansen 1975) and specific heat capacity of surficial materials.

Information about the nature and extent of surface vegetation cover was obtained from conventional polygon maps based on regional surveys, and from multi-spectral classifications of Landsat TM satellite imagery at 30 m spatial resolution (GNWT Forest Management Division 2002). Integration of these data sources provided a basis for the assignment of seasonal n-factor values and soil moisture levels (Wright et al. 2003).

Calibration and validation

The GIS coupled T-ONE model was initially calibrated and validated using the TTOP analytical solution (Wright et al. 2003; Wright et al. 2001, unpubl.). Under conditions of thermal equilibrium, TTOP and T-ONE predictions of the temperature at the top of permafrost are virtually identical, meaning that although the model calibration was conducted using the computationally simple TTOP model, identical results regarding the presence/ absence of permafrost within the borehole dataset would have been obtained using the computationally more complex T-ONE finite element model. The model is capable of adequately reproducing observed trends in the regional distribution of permafrost occurrence and thickness within these regions, as documented in records from 154 geotechnical boreholes located in undisturbed, natural terrain (IPL 1982). Overall, the calibrated model correctly predicted the presence/ absence of permafrost in 134 of 154 cases (87%), and reasonably predicts the thickness of permafrost as compared to regional observations and limited borehole data (Wright et al. 2003). Also, the north-south distribution of ground temperatures data as estimated by TTOP agrees favourably with limited ground temperature data for the Mackenzie Valley presented by Judge (1973).

Climate and model equilibrium

The TTOP equilibrium ground temperature model was used to conduct an initial assessment of the likely range of ground temperatures expected within the individual study areas and supported the specification of initial equilibrium ground temperature profiles. Although true thermal equilibrium is never achieved between atmospheric climate and the ground thermal regime, initial conditions for forward modeling (including assumed equilibrium ground temperature profiles) were established circa 1730 AD (Ednie et al. 2008). This provided a basis for estimating current (year 2000) ground temperature profiles in support of transient ground thermal modeling through to 2025 and 2055, (although, due to space constraints, only results for 2000 and 2055 are presented in this paper). This approach was motivated by the observation that ground temperatures at numerous sites within the more southerly extents of permafrost terrain in the Mackenzie Valley appear to be near-isothermal close to 0°C (Smith et al. 2005), which we interpret as an indication that ground temperatures have been warming for an extended period of time. Measured and proxy records also suggest that there has been no extended period of stable climate in the northern hemisphere during the past few hundred years (Ednie et al. 2008). Figure 2 illustrates the initial equilibrium temperature and reconstructed paleo-climate trends used by the forward model to generate estimates of the current (year 2000) ground thermal state.

Burn et al. (2004) ranked scenarios from seven Global Climate Models (GCMs) and presents a series of plausible projections of climate warming in the Mackenzie Valley over the next 55 years. The median warming scenario with a temperature increase (over 1961–90 normals) of 1.3°C and 2.9°C for 2025 and 2055, respectively, was used to specify rates of regional climate warming in the Fort Simpson and Norman Wells study area. Since 1980, the recorded data for the Inuvik area indicate a steady increase in mean annual air temperature (Environment Canada 2002). Imposing a best-fit line through the data record suggests an increase in MAATs by 2000 which is well beyond the median warming scenario presented by Burn et al. (2004). Hence, for the Inuvik study area only, we have opted to extend the trend in recorded MAAT though to 2055, as this describes a more realistic scenario of future climate warming for this area (Fig. 3). With this trend, the MAAT for 2055 falls just below the projection for maximum warming as proposed by Burn (2004). For comparison purposes, modeling was also

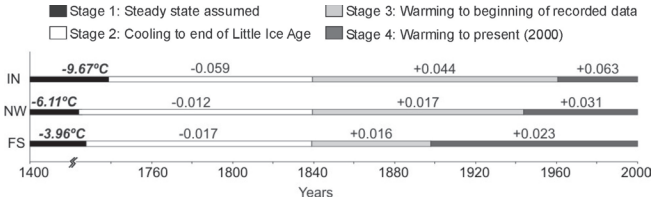

Figure 2. Paleo-climate trend used in the modeling. Stage 1: equilibrium temperature; Stage 2 to 4: subsequent ramps applied in °C/year.

conducted following an extension of the trend in recorded MAATs through to 2025, followed by a slight warming to 2055 based on the median warming ramp of +0.006ºC per year as specified by Burn et al (2004).

Configuration of the problem space

The T-ONE model was initiated using a single-layer geological substrate for all terrain types except in organic terrain, for which a two-layer substrate was modeled. In both cases, simulations were run at 6 hour time steps with grid spacing of 0.01 m at the ground surface exponentially increasing to a maximum of 8 m at greater depths. The depth of the grid was optimize according to TTOP estimation of the base of permafrost and was set at a minimum of 45 m in the Fort Simpson study area to 167 m in the Fort Good Hope region. A lower boundary heat flux of -40 mWm^{-2} was assumed. Within each 30 m grid element, ground temperatures were calculated at the specified depths below ground surface and iterated at successive time steps extending over the specified time intervals of interest (2000, 2025, and 2055). Model outputs are provided as a mean annual ground temperature.

T-ONE Modeling Results

Transient ground temperature modeling enables prediction of the incremental impacts to permafrost in response to a changing climate, and provides estimates of the timing of those changes. Typical model outputs include mean annual ground temperature profiles, permafrost distribution and thickness, active layer development and talik formation. A talik in this context is defined as the thawed layer between the seasonal active layer and the top of permafrost.

Inuvik

In general, moraine deposits cover ~45% of the Inuvik study area, with glaciofluvial/alluvial deposits occupying ~33%. Vegetation is dominated by shrubs (31%) followed by open black spruce (24%) and mixed forest (14%). Modeling using the extended trend in recoded MAATs predicts that 100% of the Inuvik area is underlain by permafrost at both 2000 and 2055. Mean ground temperatures at year 2000 range between -1.7°C in barren lichen cover underlain by glaciofluvial/alluvial deposits to -0.08°C in deciduous forest underlain by moraine deposits, increasing to -0.38°C and -0.01°C, respectively, by 2055 (Table 1).

Overall permafrost thickness ranges from ~40 m to over 150 m for white spruce on coarse-grained sediments. Modeling of present-day (2000) conditions predicts the absence of taliks overlying permafrost in the Inuvik area. Representative cases in Table 2 highlight the presence of thick permafrost in open and closed black spruce forests through to 2055 with increases in thaw depth of less than 1 m. Permafrost in shrub- and deciduous-dominated terrain is marginally thinner, with thaw depths of between 0.5 m and 3 m in 2000, with the development by 2055 of substantial taliks of up to 4.5 m for shrubs and 9 m for deciduous forest. Figure 4 shows the changes in permafrost thickness, thaw depth, and talik development for representative terrain units. The results for the median warming scenario presented by Burn et al. (2004) predicts slightly thinner seasonal active layers and more subdued talik development.

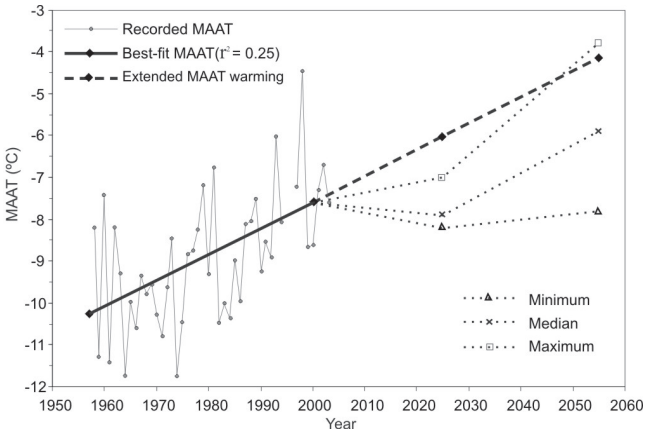

Figure 3. Minimum, mean, and maximum climate scenarios (Burn 2004) and extended trend of the 1970–2000 MAAT data for Inuvik.

Table 1. Predicted areal extent of permafrost and range of mean annual ground temperature (TTOP) in terrain modeled (excluding water bodies and bedrock) for each study area.

		Current conditions (2000)			Warming to 2055		
	% of study area modeled	% Frozen	Ground Temp. Min. (ºC)	Ground Temp. Max. (ºC)	% Frozen	Ground Temp. Min. (ºC)	Ground Temp. Max. (ºC)
IN	85.5	100	-1.65	-0.08	100	-0.38	-0.01
NW	79.6	96.0	-0.60	+2.13	85.9	-0.25	+2.90
FS	94.9	22.3	-0.24	+2.93	17.2	-0.02	+3.72

Norman Wells

About 50% of the Norman Wells study area is underlain by moraine deposits, followed by eolian/lacustrine deposits (18%) and glaciofluvial/alluvial deposits (12%). The dominant vegetation class is open black spruce forest (37%), followed by open white spruce (10%) and mixed forest (10%). The model predicts permafrost underlying 96% and 86% of the Norman Wells study area in 2000 and 2055, respectively (Table 1). Present-day (2000) ground temperatures range from -0.6°C to 2.1°C, with taliks over permafrost present in 13% of the study area). Continuous permafrost underlies

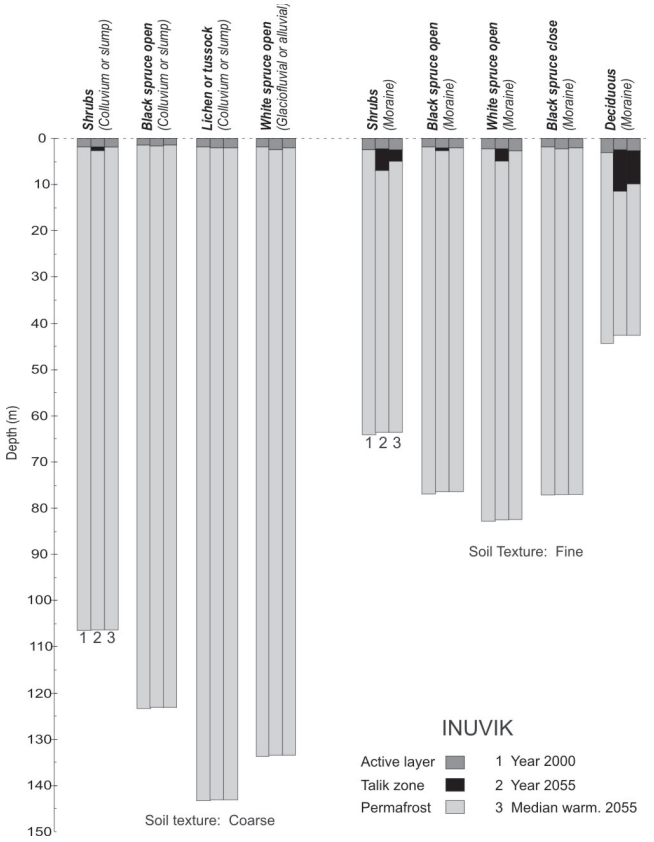

Figure 3. Summary of predicted active layer, talik and permafrost for representative terrain units in the Inuvik study area, 2000 and 2055; and 2055 median warming model of Burn (2004).

the majority of vegetation classes with the exception of deciduous forest (90% unfrozen), and fens and graminoids (100% unfrozen). Permafrost thickness ranges from 2.4 m under some deciduous forests to greater than 60 m beneath undifferentiated spruce, with a predicted thaw depth range from 0.6 m to 6.3 m. By 2055, relatively thin permafrost underlying deciduous forests, shrubs, and mixed forest is predicted to thaw completely, and for most representative terrain units, substantial taliks up to 8 m in thickness are predicted to develop under open white spruce on moraine. Table 2 and Figure 5 indicate changes in thaw depth ranging from a few centimetres to several meters, with complete permafrost thaw in the case of shrubs on moraine deposits. Only minimal permafrost thaw is predicted for open black spruce forest underlain by coarse-grained glaciofluvial/ alluvial deposits.

Fort Simpson

Moraine deposits underlie ~65% of the Fort Simpson area, followed by eolian/lacustrine and glaciofluvial/alluvial deposits, which underly about 24% and 8% of terrain, respectively. Closed black spruce and open black spruce forests each cover ~24% of the study area, with closed white spruce occupying ~12%. Modeling predicts that approximately 22% of the Fort Simpson study area is underlain by permafrost, decreasing to about 17% by 2055 (Table 1). Estimated current

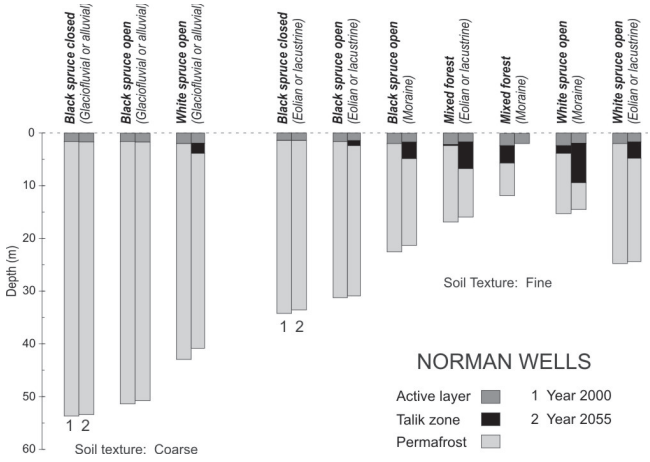

Figure 4. Summary of modeling results for representative terrain units in the Norman Wells study area.

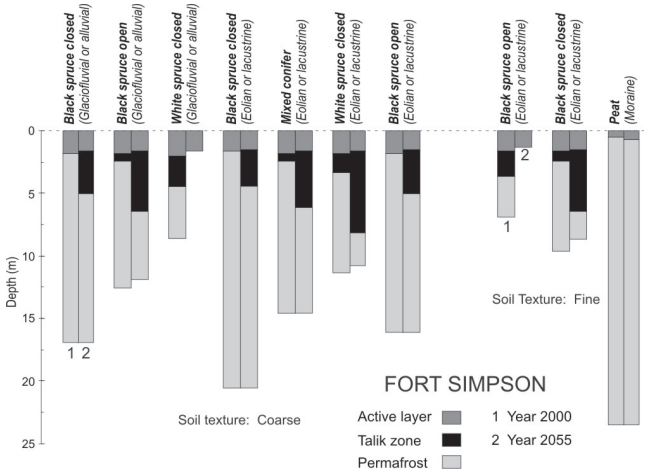

Figure 5. Summary of modeling results for representative terrain units in the Fort Simpson study area.

(2000) ground temperatures range from about -0.24°C in peat bogs to almost 3°C in graminoids underlain by till. In 2000, taliks are predicted to overlie 54% of permafrost (11% of the study area). Overall, permafrost thickness ranges from just a few meters to 20 m or more in peat bogs. Relatively thick permafrost will persist in peat bogs and closed black spruce forests through 2055 (Table 2). Permafrost thaw during this period varies significantly between vegetation classes, ranging from less than 1 m in peat plateaus to 5–6 m beneath white spruce forests. Under current conditions, the model estimates that permafrost temperatures in the Fort Simpson region are only slightly below freezing, and that most permafrost-bearing terrain will remain marginally frozen (near-isothermal close to 0°C) through to 2055. However, permafrost beneath some black and white spruce forests is predicted to disappear by 2055. The thickness of the thaw layer above permafrost is predicted to increase by 3–5 m by 2055, with the exception of peat bogs that will see only small changes in thaw depth and permafrost thickness (Fig. 5).

Table 2. Modeling results of representative terrain types.

Study area	Vegetation cover	Surficial geology	% area cover	Ground[1] Temperature (°C)		Active[2] layer depth (m)		Thaw depth[3] (m)			Permafrost thickness (m)		
				2000	2055	2000	2055	2000	2055	Chg	2000	2055	Chg
IN	Open B.Sp.	Moraine *(fine)*	22.6	-0.84	-0.01	1.80	2.00	1.80	2.74	**0.94**	75.08	73.78	**-1.3**
Modeled area: 9089 km^2	Shrubland	Moraine *(fine)*	27.6	-0.50	-0.01	2.42	2.20	2.42	6.98	**4.56**	61.76	56.53	**-5.23**
	Closed B.Sp.	Moraine *(fine)*	0.83	-0.95	-0.02	1.79	2.29	1.79	2.29	**0.5**	75.42	74.71	**-0.71**
	Closed	Moraine *(fine)*	0.67	-0.08	-0.01	3.05	2.41	3.05	11.41	**8.36**	41.23	31.25	**-9.98**
	Open W.Sp.	Glacioflu. or allu. *(coarse)*	0.09	-1.19	-0.01	1.87	2.43	1.87	2.43	**0.56**	131.9	131.5	**-0.4**
NW	Open B.Sp.	Moraine *(fine)*	23.5	-0.05	-0.01	2.16	1.81	2.16	5.37	**3.21**	20.5	16.69	**-3.81**
Modeled area: 12117 km^2	Open B.Sp.	Lacustrine or eoli. *(fine)*	6.7	-0.26	-0.01	1.67	1.62	1.67	2.71	**1.04**	30.54	29.29	**-1.25**
	Open B.Sp.	Glacioflu. or allu. *(coarse)*	3.3	-0.38	-0.01	1.75	2.22	1.75	2.22	**0.47**	50.30	49.74	**-0.56**
	Closed B.Sp.	Moraine *(fine)*	3.2	-0.14	-0.01	2.12	2.00	2.12	2.22	**0.10**	24.64	21.83	**-2.81**
	Shrubland	Moraine *(fine)*	2.4	-0.01	1.89	2.41	2.00	7.13	np[6]	-	3.08	0.00	**-3.08**
FS	Closed B.Sp.	Lacustrine or eoli. *(fine)*	3.6	-0.01	-0.01	1.62	1.44	2.55	6.82	**4.27**	7.19	2.09	**-5.10**
Modeled area: 15405 km^2	Shrubland	Moraine *(fine)*	4.5	1.89	3.03	2.00	1.62	np	np	-	np	np	-
	Closed B.Sp.	Lacustrine or eoli. *(coarse)*	2.8	-0.05	-0.01	1.76	1.44	1.76	4.48	**2.72**	19.30	16.34	**-2.96**
	Bog	Moraine *(fine)*	2.9	-0.24	-0.02	0.65	0.76	0.65	0.76	**0.11**	23.94	23.57	**-0.37**
	Closed B.Sp.	Glacioflu. or allu. *(coarse)*	1.4	-0.01	1.75	2.00	1.62	4.68	np	-	4.38	0.00	**np**

[1] TTOP if permafrost is present, otherwise temperature at base of seasonal freeze/thaw layer.
[2] Thickness of ground surface layer that thaws and refreezes seasonally.
[3] Cumulative depth of thaw over permafrost including the active layer and underlying talik where present.
np – no permafrost; chg. – change; B.Sp. – *Picea mariana*; W.Sp. – *Picea glauca*; Glacioflu. – glaciofluvial; allu. – alluvial; eoli. – eolian

Discussion

Our modeling results illustrate the variability in permafrost evolution for different terrain conditions (i.e., combinations of surficial materials and vegetation cover), under a continued climate warming. Where not already the case circa year 2000, ground temperatures are predicted to progressively warm towards isothermal, followed by the development and deepening of talik zones above permafrost. The formation of taliks has also been predicted by Kane et al. (1991). At the same time, the base of permafrost will slowly degrade upward towards the deepening talik zone. Latent heat effects are implied by the general increase in warming rates once ground temperatures increase above 0°C. For peat bogs characterized by relatively high heat capacities, active layer thickening and permafrost degradation is minimal within the time frames modeled. The model suggests that for much of Norman Wells and Inuvik terrain, only modest changes in permafrost thickness will be realized during this period, although increases in thaw penetration will be substantial for certain terrain types. The results may be summarized using the permafrost classification system of Shur & Jorgenson (2007). MAAT in the Inuvik area (“‘climate driven,’” even with a warming trend) would still be cold enough to sustain permafrost. In contrast, in the Fort Simpson area much of the terrain would be underlain by “‘climate-driven, ecosystem-protected’” permafrost where disturbance (e.g., change in the insulation layer) can cause the complete degradation of the permafrost with no re-establishment of initial permafrost conditions.

Numerical modeling affords a systematic and rigorous means for assessing ground thermal characteristics across extensive geographic areas. In the case of the TTOP and T-ONE models employed in this study, limited ground truthing and statistical validation of modeling outputs have established a reasonable level of confidence in model performance within the broader

Mackenzie Valley. While the T-ONE model generates apparently precise predictions (to multiple decimal points) of permafrost attributes such as temperature and thickness, it would be prudent to apply appropriate caution when evaluating model predictions, given that a -0.1°C change in ground temperature is equivalent to ~5 m of permafrost in typical surficial sediments. Also, we have noted that in the Inuvik area particularly, the model appears to overestimate active layer thickness and therefore possibly future rates of thaw penetration (Nixon, pers. com.). This may be related to our use of a one-layer system in which latent effects of excess ice and/or organic veneer are not adequately simulated.

Conclusion

Modeling of present-day (2000) ground thermal conditions confirms a clear north-to-south trend towards warmer ground temperatures, paralleled by a north-south decrease in areal extent and thickness of permafrost. The results also illustrate a north-to-south increase in thaw depth and development of taliks above the permafrost table. Predicted ground thermal conditions for 2055 (with a warming climate) confirms minor degradation at the base of permafrost with the greatest permafrost degradation occurring in the top few to several meters below the ground surface.

References

Burn, C.R., Barrow, E. & Bonsal, B. 2004. Climate change scenarios for Mackenzie River valley. *57th Canadian Geotechnical Conference, Québec,* 7A, Vol. 2: 2-8.

Ednie, M., Wright, J.F. & Duchesne, C. 2008. A Paleo-climatic reconstruction for transient ground thermal modeling in the Mackenzie River valley. *Proceedings of the Ninth International Permafrost Conference, Fairbanks, Alaska, June 28–July 3, 2008* (this proceedings).

Environment Canada. 2002. *Canadian Climate Normals: Canadian Monthly Climate Data and 1943–2000 Normals*. Environment Canada: Ottawa, CD-ROM.

GNWT Forest Management Division. 2002. *Northwest Territories Land Cover Classification.* Raster digital data, unpublished.

Goodrich, L.E. (1982). *An introductory review of numerical methods for ground thermal regime calculations*. National Research Council of Canada, DBR Paper 106, 133 pp.

Hanley, P.T., Hodgson, D.A., Hughes, O.L., Kurfurst, P.K., Lawrence, D.E., Zoltai, S.C., Pettapiece, W.W. & Pilon, J. 1973. *Surficial Geology and Geomorphology Maps of Fort Norman, Carcajou Canyon, Norman Wells and Sans Sault Rapids Map Areas, Mackenzie Valley.* Geological Survey of Canada, Open File 155.

Hegginbottom, J.A., Dubreuil, M.A. & Harker, P.T. 1995. Canada, Permafrost. In: *National Atlas of Canada. 5th ed*., Natural Resources Canada, MCR 4177.

Hughes, O.L., Hodgson, D.A. & Pilon, J. 1972. *Surficial Geology, Fort Good Hope, Arctic Red River, Fort McPherson, District of Mackenzie, Maps and Legend.* Geological Survey of Canada, Open File 97.

Interprovincial Pipe Lines (NW) Ltd. 1982. *Norman Wells Pipeline Project - Delineation of Permafrost Distribution by Geophysical Survey.* Summary Report KMP 0 to 868.3 to the National Energy Board, December 1982.

Johansen, O. 1975. *Thermal Conductivity of Soils*. Ph.D. Thesis. Trondheim, Norway. (CRREL Draft Translation 637, 1977, Ad 044002).

Jorgenson, M.T. & Kreig, R.A. 1988. A model for mapping permafrost distribution based on landscape component maps and climatic variables. *Proceedings of the Fifth International Conference on Permafrost, Trondheim, Norway,* 1*:* 176-82.

Judge, A.S. 1973. *Thermal Regime of the Mackenzie Valley: Observations of the Natural State.* Report 37-38, Environmental Social Committee, Northern Pipelines, Task Force on Northern Oil Development, Government of Canada, 177 pp.

Juliussen, H. & Humlum, O. 2007. Towards a TTOP ground temperature model for mountainous terrain in central-eastern Norway. *Permafrost and Periglacial Processes* 18: 161-184.

Kane, D.L., Hinzman, L.D. & Zarling, J.P. 1991. Thermal response of the active layer to climatic warming in a permafrost environment. *Cold Regions Science and Technology* 19:111-122.

Lunardini, V.J. 1981. *Heat Transfer in Cold Climates*. Toronto: Van Nostrand Reinhold Company, 731 pp.

Outcalt, S.I., Nelson, F.E. & Hinkle, K.E. 1990. The zero curtain effect: heat and mass transfer across an isothermal region in freezing soil. *Water Resources Research* 26: 1509-1516.

Rutter, N.W., Minning, G.V. & Netterville, J.A. 1980. Surficial Geology and Geomorphology, Fort Simpson, District of Mackenzie. *Geological Survey of Canada, Preliminary Map 3-1978*.

Shur Y.L. & Jorgenson, M.T. 2007. Patterns of permafrost formation and degradation in relation to climate and ecosystems. *Permafrost and Periglacial Processes* 18: 7-19.

Smith, S.L., Burgess, M.M., Chartrand, J. & Lawrence, D.E. 2005. *Digital Borehole Geothechnical Database for the Mackenzie Valley/Delta Region.* Geological Survey of Canada, Open File 4924, 30 pp.

Smith, M.W. & Riseborough, D.W. 1996. Permafrost Monitoring and Detection of Climate Change. *Permafrost and Periglacial Processes* 7: 301-309.

Taylor, A., Burgess, M., Judge, A., Allen, V. & Wilkinson, A. 1998. Canadian Geothermal Data Collection - Deep permafrost temperatures and thickness of permafrost. In: *International Permafrost Association, Data and Information Working Group, comp. Circumpolar Active-Layer Permafrost System (CAPS).* Boulder, Colorado: NSIDC.

Wright, J.F., Duchesne, C., Nixon, F.M. & Côté, M.M. 2001. *Ground Thermal Modeling in Support of Terrain Evaluation and Route Selection in the Mackenzie River Valley.* Summary Report, CCAF Project A073, Natural Resources Canada, 53 pp.

Wright, J.F., Duchesne, C. & Côté, M.M. 2003. Regional-scale permafrost mapping using the TTOP ground temperature model. *Proceedings of the Eighth International Conference on Permafrost, Zurich, Switzerland, 2003*: 1241-1246.

Variable Rate Modeling of Fluvial Thermal Erosion

L. Dupeyrat
UMR8148-IDES, CNRS-UPS, bât 509, Université Paris-Sud-11, 91405 Orsay, France
R. Randriamazaoro
Labo.P.M.T.M. Bat : L2, Institut Galilée Université Paris 13, Av. J. B. Clément 93430 Villetaneuse, France
F. Costard
UMR8148-IDES, CNRS-UPS, bât 509, Université Paris-Sud-11, 91405 Orsay, France
E. Carey Gailhardis
UMR8148-IDES, CNRS-UPS, bât 509, Université Paris-Sud-11, 91405 Orsay, France

Abstract

In periglacial regions, frozen river banks are affected by thermal and mechanical erosion. In Siberia, bank retreat of up to 40 m per year is observed. This thermal erosion occurs during a few weeks, at springtime, with high enough water temperatures and river discharges. Until now, models of thermal erosion have been based on the assumption of a constant melting rate. We have developed a more general model at variable rate, whose solution is calculated with the integral method. Results of this model are compared with experiments, carried out in a cold room. The model has contributed to better understanding of the roles of each parameter during the thermal erosion process. The duration of such an acceleration phase is systematically studied.

Keywords: ablation; heat balance integral method; periglacial river; permafrost; phase change; thermal erosion.

Introduction

Most periglacial rivers exhibit a breakup period and a flood season associated with high discharge rates and high water temperatures. The Lena River in Siberia and its tributaries can be divided into two classes (1) the Lena basin outlet and (2) the southern sub-basins (Aldan, upper Lena, Vilui valley). A relatively low stream temperature variation and a high discharge variation characterize the Lena basin outlet. The stream temperature varies from 0°C to 14°C, and the discharges can reach 100,000 m^3/s in early June (Gautier et al. 2003, Liu et al. 2005, Yang et al. 2002). In the second case, the southern sub-basins are characterized by relatively high stream temperature and low discharge. For these rivers, stream temperatures are up to 4°C higher than those of the Lena outlet (Liu et al. 2005) and can reach 18°C; the discharges are about ten times smaller than those in the Lena basin outlet (Liu et al. 2005, Yang et al. 2002). During the break-up and flood seasons the water flow in permanent contact with frozen river banks induces both a fluvial thermal and mechanical erosion. This problem is non-linear because it involves a moving boundary (an interface between solid and liquid) whose location is unknown. Until now, models of thermal erosion based on the assumption of a constant melting rate for a constant convective flux at the interface have been used to study thermal erosion of ice and permafrost (Costard et al. 1999). The objective of this study is to propose a model of thermal erosion of permafrost without the simplified assumption of a constant melt rate. Once validated by the comparison with laboratory experiments, the model will be applied to the Siberian rivers case.

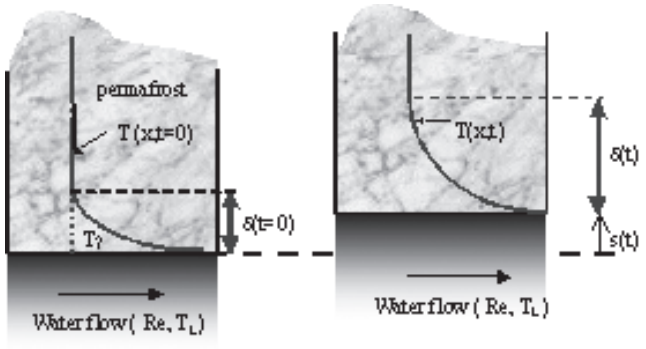

Figure 1. (a) The initially isothermal permafrost (T_∞) is suddenly heated by a permanent water flow (Re, T_L). After a rapid transient phase, the interface reaches the melting temperature (T_m=0°C). Then the thermal erosion initiates, and the interface starts to move. (b) The interface progressively moves. Its instantaneous position and erosion rate are given by s(t) and ds/dt. The instantaneous thickness of the thermal boundary layer is δ(t).

The Ablation Model at Variable Rate

Mathematical model

A semi-infinite permafrost sample initially at a uniform negative temperature (T_∞) is suddenly heated by a turbulent water flow of permanent temperature (T_L) and discharge (Q_L) (Fig. 1).

We suppose that all the sediment is immediately swept away by mechanical action of the water flow. The heat transfer occurs by conduction inside the permafrost (Eq. 1). At the permafrost-water interface, the convective heat flux from the water flow must balance the latent heat absorbed by melting, added to the conductive heat flux in the solid (Eq. 2).

$$\frac{\partial T}{\partial t} = \left(\frac{k}{\rho . c_p}\right)\frac{\partial}{\partial x}\left(\frac{\partial T}{\partial x}\right) \qquad x \geq s(t) \tag{1}$$

$$h\left(T_L - T_m\right) = \rho L \frac{\partial s}{\partial t} - k\left(\frac{\partial T}{\partial x}\right)_{x=s} \qquad x = s(t) \tag{2}$$

where k [W m^{-1} K^{-1}], ρ [kg m^{-3}], cp [J kg^{-1} K^{-1}] and L [J/kg] are the thermal conductivity, the density, the specific heat, and the latent heat of melting of the permafrost, and h [W m^{-2} s^{-1}] is the heat transfer coefficient between turbulent water and permafrost.

Resolution by the heat balance integral method

The heat-balance integral method consists of integrating the heat conduction equation (Eq. 3) over the thermal layer $\delta(t)$. It is based on the assumption of a quadratic boundary layer temperature (Eq. 4).

$$\frac{\partial}{\partial t}\int_s^{\delta} T dx = \left(\frac{k}{\rho . c_p}\right)\left[\left.\frac{\partial T(x,t)}{\partial x}\right|_{x=\delta} - \left.\frac{\partial T(x,t)}{\partial x}\right|_{x=s}\right] \tag{3}$$

$$T(x,t) = T_{\infty}\left[-2\left(\frac{x-s}{\delta - s}\right) + \left(\frac{x-s}{\delta - s}\right)^2\right] \quad s(t) < x < \delta(t), \tag{4}$$

The temperature distribution (Eq. 4) is substituted in Equation 1 and the heat equation is integrated (Eq. 3), applying boundary and initial conditions. Then, solutions in a-dimensional form are obtained (Goodman 1958). The system of Goodman (1958) is solved for every time t during the thermal erosion process in order to get the instantaneous thermal boundary layer $\delta(t)$ and eroded thickness $s(t)$ (Randriamazaoro et al. 2007).

Results

Both the thermal boundary layer and the ablation rate increase (acceleration phase) and stabilize (stationary phase) towards asymptotic values (Eqs. 5, 6), which correspond to the solutions of the constant rate-melting model (Aguirre et al. 1994, Costard et al. 2003).

$$\delta_{lim} = \frac{2.k.L}{c_{p.} \cdot q_{conv}} \tag{5}$$

$$\left(\frac{ds(t)}{dt}\right)_{lim} = \frac{q_{conv}}{\rho L + \rho . c_{p.}(T_{\infty} - T_m)} \tag{6}$$

where q_{conv} is the heat flux exchanged by convection at the interface between the water flow and the permafrost and includes both the effects of water temperature and discharge (Eq. 7).

$$q_{conv} = h.\left(T_L - T_f\right) \tag{7}$$

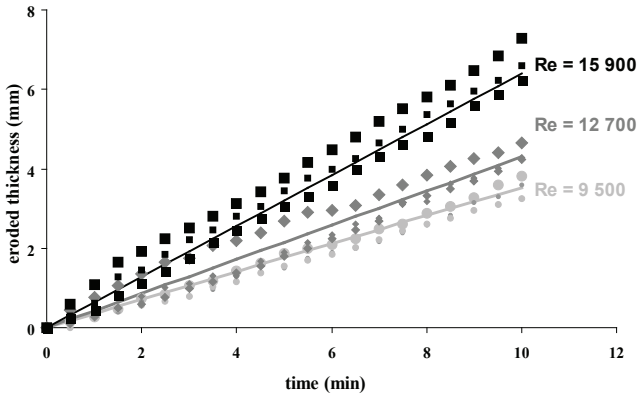

Figure 2. Measurements of eroded thickness of pure ice initially at –7.5°C, heated by a turbulent water flow at 5.5°C. In 10 minutes, the measured eroded thickness of the ice sample is 3.5 mm, 4.5 mm, 6.5 mm for Re=9500, 12,700, and 15,900 respectively.

Our model is validated by measurements of instantaneous eroded thickness of ice and permafrost samples in contact with a turbulent water flow in a cold room (Costard et al. 2003). One set of experiments is done on ice samples at an initial temperature equal to -7.5°C and the water temperature remains at 5.5°C during the experiments. Different Reynolds numbers are investigated. The ablation rate increases with the Reynolds number (Fig. 2).

Experiments suggest that the eroded thickness increases linearly with time (Fig. 2). Considering a stationary erosion rate, the measured erosion rate of ice is equal to 0.35 mm/min, 0.45 mm/min, and 0.65 mm/min for Re = 9500, 12,700, and 15,900 respectively. We tested our model to these particular experimental conditions (Fig. 3). The model predicts a first phase of acceleration during which both the thermal boundary layer and the erosion rate increase (Fig. 3). This first phase lasts a few minutes. The asymptotic values of the calculated ablation rate (Fig. 3) are consistent with the measured values (Fig. 2).

Other experiments are done on frozen ice sand samples (initially at –7.5°C) with different massic ice contents (ω=20%, 80%) and are compared with pure ice (Fig. 4). The turbulent water flow remains at 5.5°C and the Reynolds number is equal to 15,900.

The model is applied to these particular conditions, and again the experiments and the model are consistent (Figs. 4, 5).

The effects of the water temperature and the ice temperature are also investigated. The effects of the water temperature are predominant, whereas the effects of the ice temperature are very weak. The erosion rate increases with water temperature, ice temperature, and Reynolds number and decreases with the ice content. The model at variable rate predicts a first acceleration phase whose duration is typically greater for smaller erosion rates.

Then the model is applied to the Lena River. The convective heat flux is calculated (Eq. 7) for water temperature between 0°C and 20°C and for water discharges between 0 m^3/s and 120,000 m^3/s. The heat transfer coefficient h is estimated,

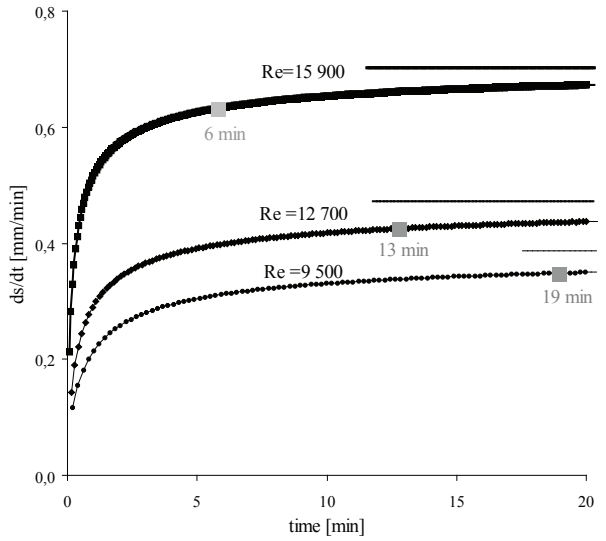

Figure 3. Theoretical erosion rate as a function of time for a water temperature equal to 5.5°C, an ice temperature equal to 7.5°C and different Reynolds numbers (Re=9500, 12,700, and 15,900) applied to the geometry of our hydraulic channel. The erosion rate increases rapidly (acceleration phase) and stabilises (stationary phase). The duration of the acceleration phase is calculated from the time necessary to reach 90% of the asymptotic value. The greater the Reynolds number, the greater the erosion rate and the smaller the duration of the acceleration phase. Measured values (Fig. 2) are consistent with the asymptotic calculated values.

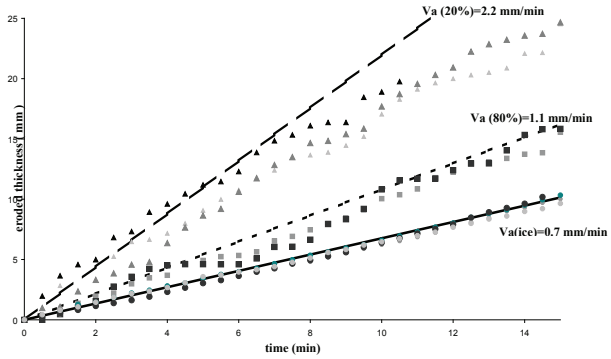

Figure 4. Measurements of eroded thickness of pure ice and sandy permafrost with different ice contents, initially at –7.5°C, heated by a turbulent water flow (5.5°C and Re=15,900). In 10 minutes, the measured eroded thickness is about 6 mm, 11 mm, 18 mm for pure ice, permafrost with ω=80%, and ω=20% respectively. Linear fit gives measured erosion rates equal to 0.7 mm/min, 1.1 mm/min and 2.2 mm/min for pure ice, permafrost with ω=80% and ω=20% respectively.

using the empirical law of Lunardini (1986) (A=0.0078, α=0.3333, β=0.9270) and the Manning equation applied to the geometry of the channel (Eqn. 8) (Costard et al. 2003).

$$h = A\left[\left(\frac{\sqrt{s}}{n}\right)^{3/5} l^{\,3/5-\beta}\right]\left[Pr^{\,\alpha}\left(\frac{k_w}{\upsilon_w}\right)^{\beta}\right] Q^{\,\beta-3/5} \qquad (8)$$

where $S = 0.0001$ m/m, $n = 0.1$, $l = 10$ km, k_w, v_w, Pr are the

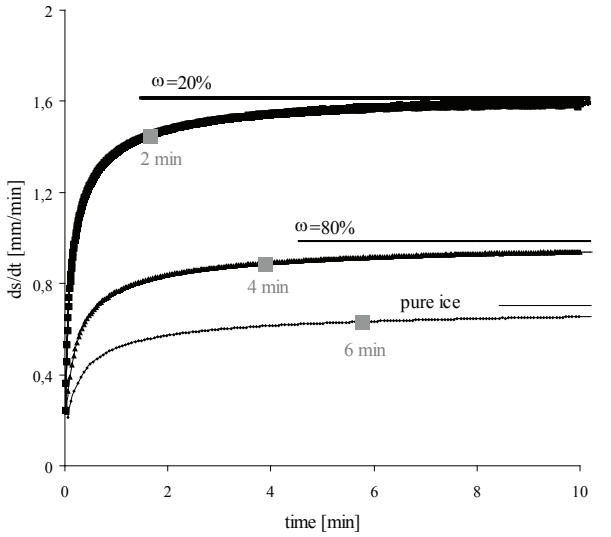

Figure 5. Theoretical erosion rate as a function of time for a water temperature equal to 5.5°C, an ice temperature equal to 7.5°C a Reynolds number equal to 15,900, applied to the geometry of our hydraulic channel. The erosion rate increases rapidly (acceleration phase) and stabilizes (stationary phase). The smaller the ice content, the greater the erosion rate and the smaller the duration of the acceleration phase. Measured values are consistent with the asymptotic values.

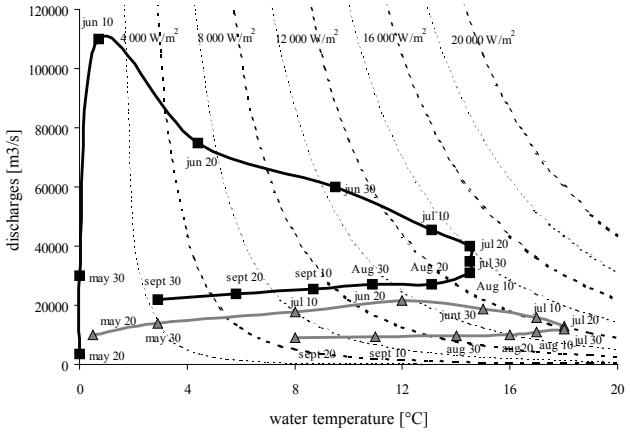

Figure 6. Diagram of heat flux versus discharge and water temperature.

---------- Isoflux lines (2 000 – 20 000 W/m^2)

■ Water mean temperatures and discharges in the Lena basin outlet (Yang et al. 2002, Liu et al. 2005)

Δ Water mean temperatures and discharges in the Lena sub-basins (Aldan, Upper Lena, Vilui basin (Liu et al. 2005)).

longitudinal slope, the Manning roughness coefficient, the width of the river, the thermal conductivity of water [W m^{-1} K^{-1}], the cinematic viscosity of water [m^2 s^{-1}], and the Prandtl number, respectively.

Isoflux lines are plotted from the calculated values of the convective heat flux (Fig. 6). On this diagram, simultaneous measurements of water temperatures and discharges in the Lena basin outlet and the southern Lena sub-basins (Yang et al. 2002, Liu et al. 2005) every 10 days during the flood season are reported.

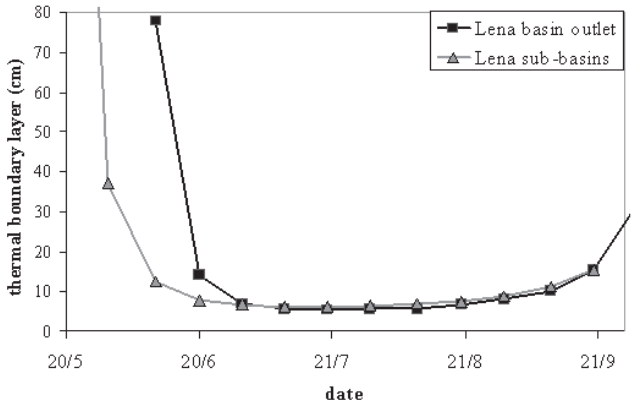

Figure 7. Evolution of the calculated thermal boundary layer thickness for the Lena basin outlet and the Lena sub-basins.

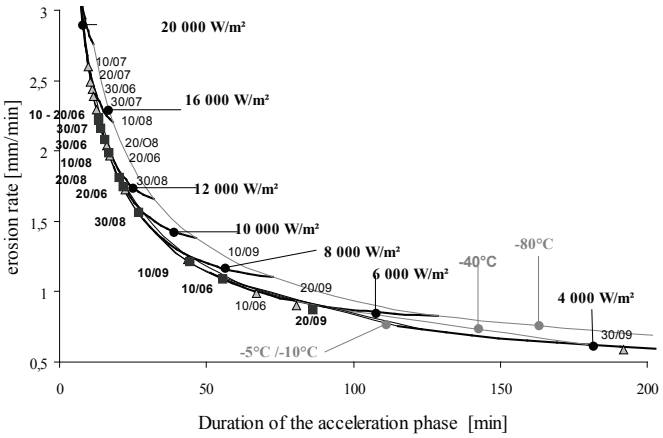

Figure 8. Diagram of ablation rate and duration of acceleration phase for various convective heat flux and ice temperature) – Isoflux lines (4000–20,000 W/m²)
——— Isothermal lines (-10°C to -80°C)
□ Ablation rate and duration of the acceleration phase in the Lena basin outlet
Δ Ablation rate and duration of the acceleration phase in the Lena tributaries (Aldan, Upper Lena, Vilui basin).

As expected, the heat flux increases when the water temperature and the discharge increase simultaneously from May to mid-June. By contrast, from June to July the water temperature is still increasing, while the discharge decreases by about 50%, and a positive trend of the heat flux is still observed. The maximum (12,000 W/m² and 14,000 W/m² for the southern Lena sub basin and for the Lena basin outlet, respectively) of the heat flux occurs during July when water reaches its maximum temperature. It appears that the convective heat flux evolution mainly depends on the water temperature evolution for Siberian rivers during the flood season. The heat flux variation for the Aldan, Upper Lena, and Vilui Rivers is similar to the one of the Lena basin outlet. The relative higher values of water temperatures for the southern Lena sub-basin are compensated by the relative higher values of the discharges for the Lena basin outlet.

With regards to specific heat flow, the application of the model of variable rate on pure ice or permafrost should allow determination of the thermal boundary layer thickness (Fig. 7), the ablation rate, and the duration of the acceleration phase (Fig. 8).

The greater the convective heat flux, the greater the erosion rate and the smaller the duration of the acceleration phase. The most favorable conditions to get the longer acceleration phase are obtained for the smaller values of the erosion rate at the beginning (early May) or at the end (October) of the flood season. For example, considering a small thermal erosion rate 0.06 mm/min (early May), the acceleration phase should last about 14 days.

Conclusions

A model of the fluvial thermal erosion has been formulated at variable rate. This mathematical model has been applied to a typical frozen river bank in permanent contact with a turbulent water flow. The expressions of the instantaneous melting thickness, ablation rate, and thermal boundary layer have been obtained by integral method and validated by experiments on ice samples. An acceleration phase occurs at the beginning of the process. The duration of this acceleration phase is quantified. Typically, the acceleration phase lasts longer for a low ablation rate. The ablation rate increases with water temperature and discharge and decreases with ice content. The effects of stream temperature and discharge can be represented by the convective heat flux. The heat flux along the river banks are identical for the Lena basin outlet and for the southern Lena basin because relative higher values of stream temperatures for the southern Lena sub-basin are compensated by the relative higher values of the discharges for the Lena basin outlet. From our studies, the stream temperature is an important parameter which controls the evolution of the erosion rate during the flood season. Further studies will take into account the possible effect of global warming on the thermal erosion rate.

Acknowledgments

Hydrological data were obtained from the Hydro-Meteorological Center under the auspices of the Permafrost Institute at Yakutsk. This program is supported by "Programme Reliefs de la Terre" INSU, CNRS, France, and GDR «mutations polaires: société et environnement».

References

Aguirre-Puente, J., Costard, F. & Posado-Cano, R. 1994. Contribution to the study of thermal erosion on mars. *Journal of Geophysical Research* 99: 5657-5667.

Costard, F. & Aguirre-Puente, J. 1999. Martian fluvial-thermal erosion: laboratory simulation. *Journal of Geophysical Research* 104: 14.091-14.098.

Costard, F., Dupeyrat, L., Gautier, E. & Carry-Gailhardis, E. 2003. Fluvial thermal erosion investigation along a rapid eroding river bank: application to the Lena river (central Siberia). *Earth Surface Processes and Landforms* 29: 1349-1359.

Gautier, E., Brunstein, D., Costard, F. & Lodina, R. 2003. Fluvial dynamics in a deep permafrost zone: the case of the middle Lena river (Central Yakutia). *Proceedings of the eighth International Permafrost Conference, Switzerland, Zurich, July 21-25, 2003:* 271-275.

Goodman, T.R. 1958. The heat-balance integral and its applications to problems involving a change phase. *Transaction ASME* 80: 335-342.

Liu, B., Yang, B. Ye & Berezovskaya, S. 2005. Long-term open-water season stream temperature variations and changes over Lena River Basin in Siberia. *Global and Planetary Change* 48: 96-111.

Lunardini, V.L., Zisson, J.R. & Yen, Y.C. 1986. *Experimental Determination of Heat Transfer Coefficients in Water Flowing Over Horizontal Ice Sheet.* CREEL Report 86-3. US Army Cold Regions Research and Engineering Laboratory.

Randriamazaoro, R., Dupeyrat, L., Costard, L. & Carey-Gailhardis, E. 2007. Fluvial thermal erosion: heat balance integral method. *Earth Surface Processes and Landforms* 32: 1828-1840.

Yang, D., Douglas, L.K., Hinzman, L., Zhang, T. & Ye, H. 2002. Siberian Lena River hydrologic regime and recent change. *Journal of Geophysical Research* 107: 4694. DOI : 10.1029/2002JD002542.

Modeling Mountain Permafrost Distribution: A New Permafrost Map of Austria

Barbara Ebohon
Department of Geography and Geology, University of Salzburg, Austria
Lothar Schrott
Department of Geography and Geology, University of Salzburg, Austria

Abstract

Alpine permafrost response is very sensitive to climate change. Thus, it is of great interest to estimate and assess permafrost distribution in high mountain areas. In this study, the permafrost distribution of the Austrian Alps was modeled by using commands of the programs PERMAKART (for steep slopes) and PERM (for footslope-positions) which were applied in a DTM with a resolution of 50 m. Possible and probable permafrost areas of the Austrian Alps comprise approximately 1600 km². The potential permafrost area has been compared with BTS, spring temperature measurements, alpine meadows, and isotherms of the MAAT (mean annual air temperature). The results of the validation show that the map still needs some improvement on a local scale, but simulates the possible and probable permafrost distribution of the Austrian Alps as a good general overview.

Keywords: alpine permafrost; Austrian Alps; simulation; validation.

Introduction

Several studies carried out in the Austrian Alps have shown permafrost distribution above approximately 2500 m a.s.l. (Lieb 1998). Current global warming already causes a degradation of permafrost in some mountain regions.

Of particular interest are areas with discontinuous permafrost on steep talus slopes and rock walls. Due to the absence of a blocky layer, rock faces react quickly to climate change compared with debris-covered slopes (Gruber et al. 2004, Mittaz et al. 2000). In densely populated and developed mountain areas (e.g., ski resorts, etc.), where a degradation of permafrost, in particular at its lower limit could cause enhanced debris flow and rockfall activity, mapping and modeling of permafrost distribution is an important prerequisite to prevent natural hazards and risks.

In Switzerland, Haeberli has already started to publish profound knowledge about permafrost distribution in the year 1975. Afterwards a lot of empirical models were developed (e.g., PERMAKART: Keller 1992, PERMAMAP: Hoelzle 1994, PERM: Imhof 1996, PERMAMOD: Frauenfelder 1998). Now, also complex process-oriented models (e.g., PERMEBAL: Stocker-Mittaz et al. 2002), which are based on the particular understanding of the energy fluxes between permafrost and the atmosphere (Hoelzle et al. 2001, Etzelmueller et al. 2001), are already available. However, until recently, the possible and probable permafrost distribution in Austria has been mapped and modeled for only a few local regions (e.g., parts of the High and Low Tauern range) (Lieb 1996, Lieb 1998, Kellerer-Pirklbauer 2005).

Compared to Switzerland, Austria has much less direct (e.g., BTS, geophysics) and indirect data of permafrost occurrence; therefore, modeling of permafrost distribution is just slightly developing.

The aim of this study is to model the permafrost distribution for the entire Austrian Alps by adjusted lower limits for possible and probable permafrost with a simple model considering the relation between slope, altitude, aspect, and permafrost occurrence. In this approach, the often-used trisection of sporadic (<30%), discontinuous (30–80%) and continuous (>80%) permafrost (Nyenhuis 2006) is applied, where sporadic equals possible and discontinuous equals probable permafrost.

Table 1. Values used for the simulation.

	Permafrost possible (sporadic)		Permafrost probable (discontinuous)	
	Steep Slopes	Foot-slope positions	Steep Slopes	Foot-slope positions
N	2300 m a.s.l.	1690 m a.s.l.	2500 m a.s.l.	2410m a.s.l.
NE	2450 m a.s.l.	2100 m a.s.l.	2600 m a.s.l.	2500m a.s.l.
E	2575 m a.s.l.	2220 m a.s.l.	2720 m a.s.l.	2520m a.s.l.
SE	2700 m a.s.l.	2230 m a.s.l.	2850 m a.s.l.	2630m a.s.l.
S	2900 m a.s.l.	2340 m a.s.l.	2900 m a.s.l.	2690m a.s.l.
SW	2650 m a.s.l.	2230 m a.s.l.	2850 m a.s.l.	2630m a.s.l.
W	2600 m a.s.l.	2160 m a.s.l.	2700 m a.s.l.	2510m a.s.l.
NW	2530 m a.s.l.	2120 m a.s.l.	2580 m a.s.l.	2470m a.s.l.
Flat areas	Permafrost possible (sporadic)		Permafrost probable (discontinuous)	
Wind-exposed	2590m a.s.l.		2710m a.s.l.	
Sheltered from wind	2640m a.s.l.		2900m a.s.l.	

Although such a map has, inherently, a limited accuracy, it allows approximations of the permafrost distribution on a national scale and enables comparisons with other Alpine provinces and countries (Frauenfelder et al. 1998).

Austria is positioned at the edge of the eastern margin of the Alps. The absolute heights of mountain ranges decline from west to east in Austria, so that the permafrost areas have their maximum extension in the western federal states.

Methods

The first well-known permafrost model in Central Europe, known as PERMAKART, has been introduced by Keller (1992). PERMAKART is implemented into the GIS-software ARC INFO. On the basis of the topo-climatic key from Heaberli (1975), which analyses the relation between slope, altitude, aspect, and permafrost occurrence, the model is able to distinguish between probable, possible, and no permafrost.

The model PERM (Imhof 1996) is also mostly based on the topo-climatic key from Heaberli (1975), but has been implemented into the raster-GIS-system IDRISI. For the calculation of the foot-slope positions, the differentiating GIS-System didn't offer the same possibilities as ARC VIEW. Therefore, foot-slope positions are generated manually through a smoothing of the DTM.

To work in detectible paces, every step was reproduced in ArcGIS9. Since the empirical values for the simulation (limits of possible and probable permafrost distribution related to altitude, aspect, slope- and footslope-positions) were originally deduced and calibrated for the Upper Engadine in the eastern Swiss Alps (Haeberli 1975), it was necessary to adjust them to the eastern Alps. Values of the lower limits of discontinuous permafrost in the central Alps of Austria were used after Lieb (1998) to model the probable permafrost distribution. Since values for the lower limit of possible permafrost were not available, they have been deduced from the relation between lower limits of possible to probable permafrost in Switzerland.

For the calculation of the lower limit of permafrost for wind-exposed areas, mean elevation values of steep slopes are generated for probable and possible permafrost. Concerning regions of possible permafrost, the lower limit for wind-sheltered areas lays 50 m above the one for wind exposed regions. For wind-sheltered areas, the highest value (2900 m a.s.l.) is used to determine the lower boundary of probable permafrost.

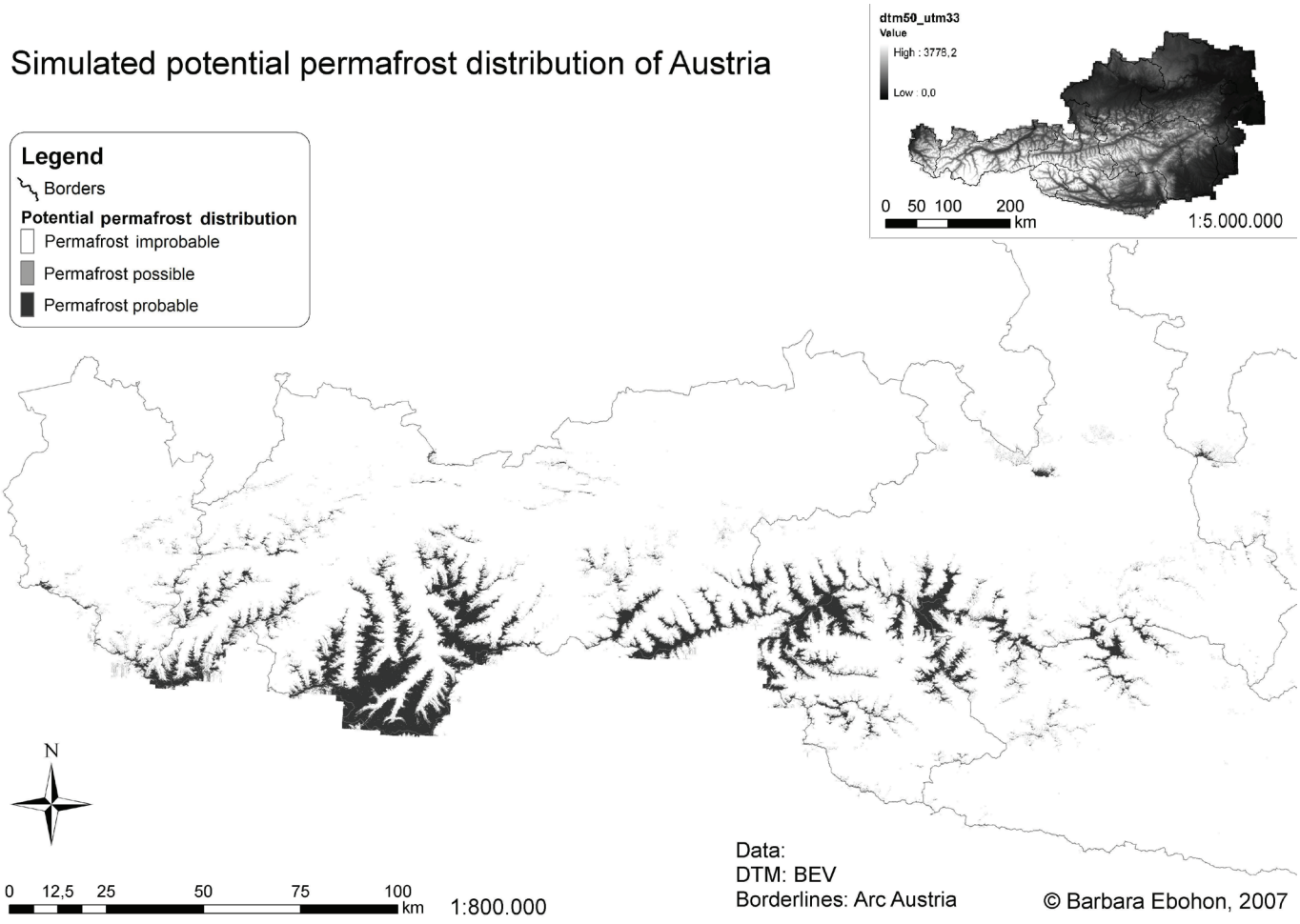

Figure 1. Map of the permafrost distribution of Austria showing the total permafrost territory of about 1600 km² (The difference between possible and probable permafrost can not be seen in this resolution: for higher resolution please see Figs. 5 and 6.).

Previous studies using PERMAKART and PERM show that this application of permafrost modeling, utilized on a nationwide scale, allows good approximations of permafrost distribution.

In a first approach, queries similar to the model PERMAKART (Keller 1994) were used to simulate permafrost of steep slopes. A map of inclination was produced and utilized to highlight all areas above the limits of possible and probable permafrost steeper than 10°, subdivided into different aspects.

The footslope-positions were worked out through a calculation of the curvature similar to the model PERM (Imhof 1992): First the DTM was smoothed, and then the original DTM was subtracted from the smoothed DTM. Areas which show values above zero are supposed to be convex regions, while all values below zero show concavities. In a next step, a map which pointed out all regions flatter than 10° was produced. This step allowed determining all flat and concave areas.

Afterwards all areas steeper than 10° were extracted and hemmed with a 150 m buffer. Following those queries, areas could be extracted which are concave, flat, and not more than 150 m away from steep slopes. On these footslope-positions the values for possible and probable permafrost were applied.

In this context, Haeberli (1975) and Etzelmueller (2001) stated that, in flat areas, the influence of air temperature is much more important than differences in radiation. Following that, flat, concave (troughs), and convex (domes) areas with less than 10° inclination above the lower limit of possible and probable permafrost were pictured.

All queries were summed and applied on a DTM with a resolution of 50 m using the UTM-coordinate system.

Table 2. Comparison of the results from the model starting to calculate steep slopes at 5° and at 10° inclination.

	5°model	10° model
Permafrost possible	711 km²	721 km²
Permafrost probable	899 km²	873 km²
Permafrost distribution (total)	1610 km²	1594 km²

Table 3: Relative permafrost areas of Austria (%) by federal states.

	Permafrost total	Permafrost possible	Permafrost probable
Burgenland	0.00	0.00	0.00
Carinthia	1.65	0.87	0.78
Lower Austria	0.00	0.00	0.00
Upper Austria	0.04	0.03	0.01
Salzburg	2.76	1.48	1.28
Styria	0.05	0.05	0.00
Tirol	9.28	3.84	5.44
Vorarlberg	1.90	1.28	0.61
Vienna	0.00	0.00	0.00
Austria	1.90	0.86	1.04

Results and Validation

Results

The permafrost map displays areas with improbable (equals no permafrost), possible, and probable permafrost and gives an overview of regional differences. At first sight, there is a strong dominance of permafrost occurrence in the western higher part of Austria, whereas the eastern part shows a somewhat patchy distribution.

To pay attention to different inclination thresholds discussed in the literature (5°/10°), two models with different conditions were applied. It is surprising that there are hardly differences in the calculated permafrost areas between the model which started calculating steep slopes at 5° inclination and the second one taking 10° into consideration. In the calculations that follow, the results of the 10° model were used.

Modeling results show that 1.9% of the territory of Austria can be assigned to mountain permafrost. This corresponds to an area of approximately 1600 km².

In Tyrol, 9.3% of the area is underlain by permafrost. This is a significant proportion compared to values for Switzerland (between 4 and 6%). Estimates for Salzburg, Vorarlberg, and Carinthia vary between 2 and 3%.

Validation

Validation was primarily a comparing of the modeling results with data from basal snow temperature measurements (BTS) and spring water temperatures.

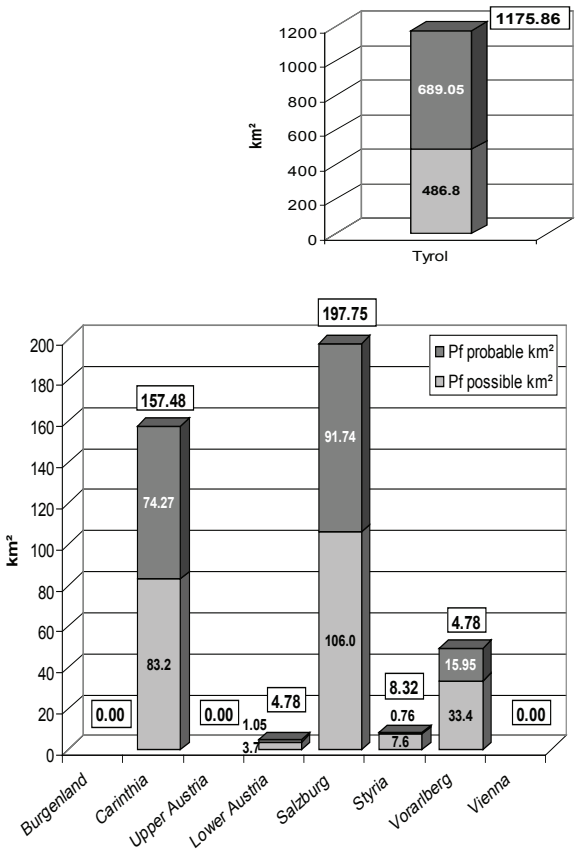

Figure 2a, 2b. Potential permafrost distribution of Austria in km².

Summarizing all measurements from local study sites such as Kaisergratspitz, Oelgrube, Sulzkar, Goessnitzvalley/ Langvalley, Hoher Sonnblick, Doesener Valley, Reisseck, and Hafergruppe, data from 300 point measurements allow a quick and reasonably good approximation of regional permafrost distribution.

Following the comparison between the simulated area with the measuring points, 48.7% of the measurements (BTS, spring water temperatures) match the three simulated categories (no PF, possible PF, probable PF). However, it should be noted that many points are just slightly outside the simulated permafrost area and probably a problem of DTM resolution or imprecise information of the point measurements which were mostly analogue and subsequently digitized for the validation. Combining the two categories, "PF possible" and "PF probable," into one entire zone, already 71.1% of the point measurements (BTS and spring water temperature data) used for validation accord with this calculation. Zoning the area of simulated permafrost after different exposures, it should be stated that N, NE, and SE are mapped well, and E, S, and SW are relatively well-presented. W and NW need further investigation on a local scale.

It can also be mentioned, that areas of rockslopes without vegetation, extracted from CORINE-Data 2000 (Aubrecht 1998), often match the modeled areas of permafrost.

Comparing the simulated permafrost area with the distribution of alpine meadows (CORINE 2000), only about 3% (44.5 km²) of simulated potential permafrost distribution intersects with them (Fig. 5). It has to be considered that permafrost and vegetation exclude each other often, but not always. It is notable that most intersections are northerly exposures. Therefore, northern aspects should be investigated more precisely on a local scale (e.g., grain size analyses, lithology, etc.).

It is well known that permafrost probably exists above certain threshold values concerning the MAAT (mean annual air temperature). Following this approach, another adjustment is made through the comparison of simulated permafrost areas with calculated isotherms based on MAAT from 1961–1990 and a total of 117 measurement stations and contour lines. The calculated isotherms mostly lay some few meters above the contour lines applied by Lieb (1996), who used the threshold of 2250 m a.s.l. for discontinuous permafrost and 3250 m a.s.l. for continuous permafrost. Comparatively, areas above the -2°C isotherm refer to discontinuous permafrost, while areas above the -6°C isotherm point to continuous permafrost. It must be stated, that only a small zone of continuous permafrost can be expected in Austria because most of the areas above -6°C MAAT are occupied by glaciers. In the N, NW, and NE aspects, the borderlines of discontinuous permafrost match the modeled area quite well, while in the SW, S, and SE aspects, borderlines are much lower than the limit of simulated permafrost.

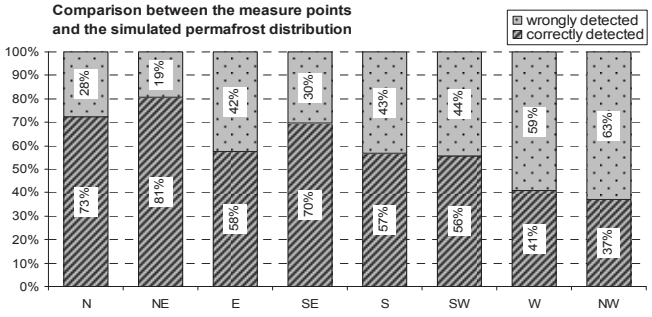

Figure 3. Comparison between measurement points (BTS, spring water temperatures) and permafrost occurrence (simulated permafrost distribution), differentiated in aspects.

Discussion

In summary, the simulation gives a useful overview of possible and probable permafrost distribution in the Austrian Alps. There are, however, still some unsolved problems and inaccuracies. As Keller & Hoelzle (1996) stated, one big issue is the appointment of the critical inclination, which differentiates between steep and moderate slopes. The approach presented has shown that there are minor differences between the permafrost areas calculated with the two models (5 and 10° inclination), but it remains unclear whether a threshold above 10° would show better results.

Also, the distinction between western and eastern Austria should be analyzed in more detail according to well-known temperature differences.

Improvements to this study would also be achieved by including more data on rock glaciers and higher resolution DTM data to better represent the strongly differentiated relief of the Austrian Alps.

Moreover, the distinction between the two categories—"permafrost possible" and "permafrost probable"—is still problematic because the data used on existing permafrost occurrences are based on point measurements (BTS and spring temperatures) only. The interpolation of these data produces simulated lower boundaries of permafrost distribution with limited accuracy. A further problem is related to the semantic differentiation of possible and probable permafrost, and to the unknown quantitative proportion of permafrost in these categories (Heginbottom 2002).

There are also problems with the values used themselves: they represent only mean values derived from one region in the Upper Tauern. Because of a lack of values for other areas, they were used to model the permafrost distribution for the entire area of Austria.

To improve the accuracy of the regional permafrost distribution map, more validation data from BTS measurements and field geophysics are needed. Furthermore, data should be more uniformly distributed over the Austrian territory.

It would then be possible to rework the empirical approach and to derive values for permafrost distribution. The more empirical data available, the better the adjustment to regional and local conditions would be.

Lieb (1996) stated that the difference between N and S orientation concerning intact rock glaciers is about 273 m (mean value for entire Austria). Whether the accuracy can be raised by adjusting the permafrost boundaries to this value is still an open question.

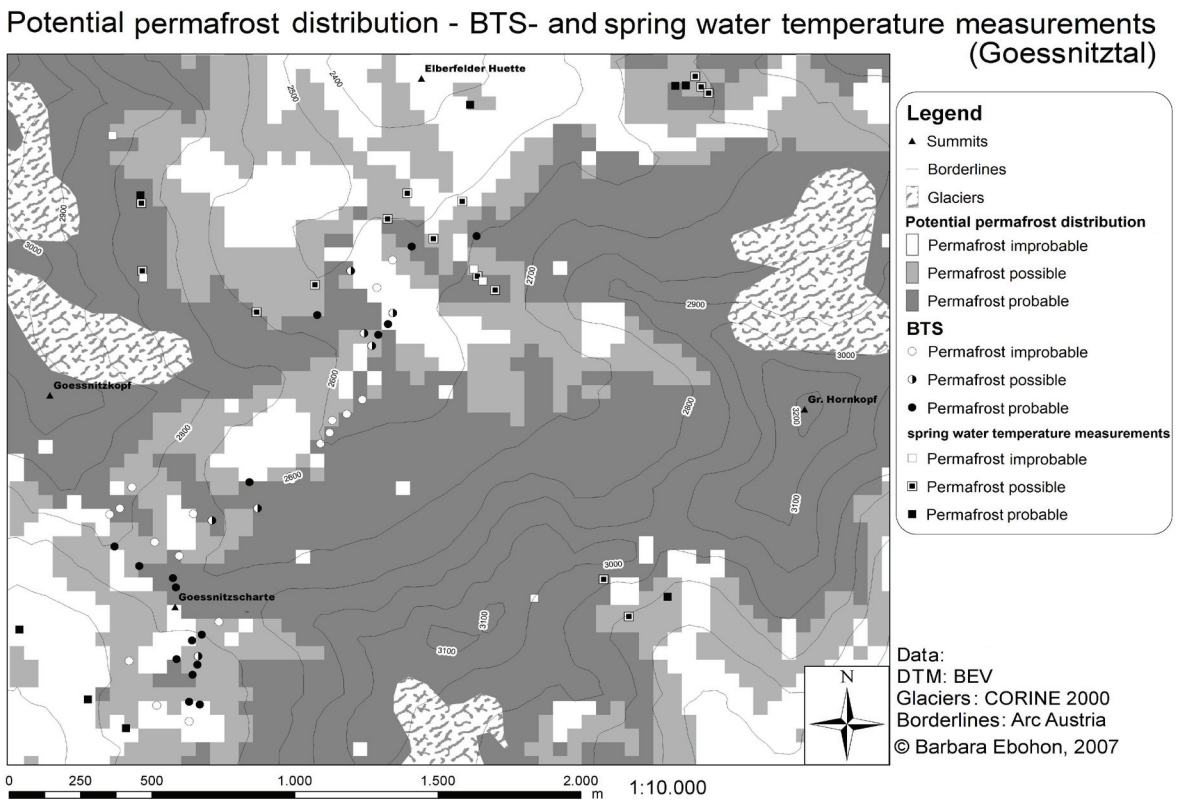

Figure 4. Permafrost distribution compared with BTS data and spring temperature measurements (data: G.K. Lieb, pers.com.).

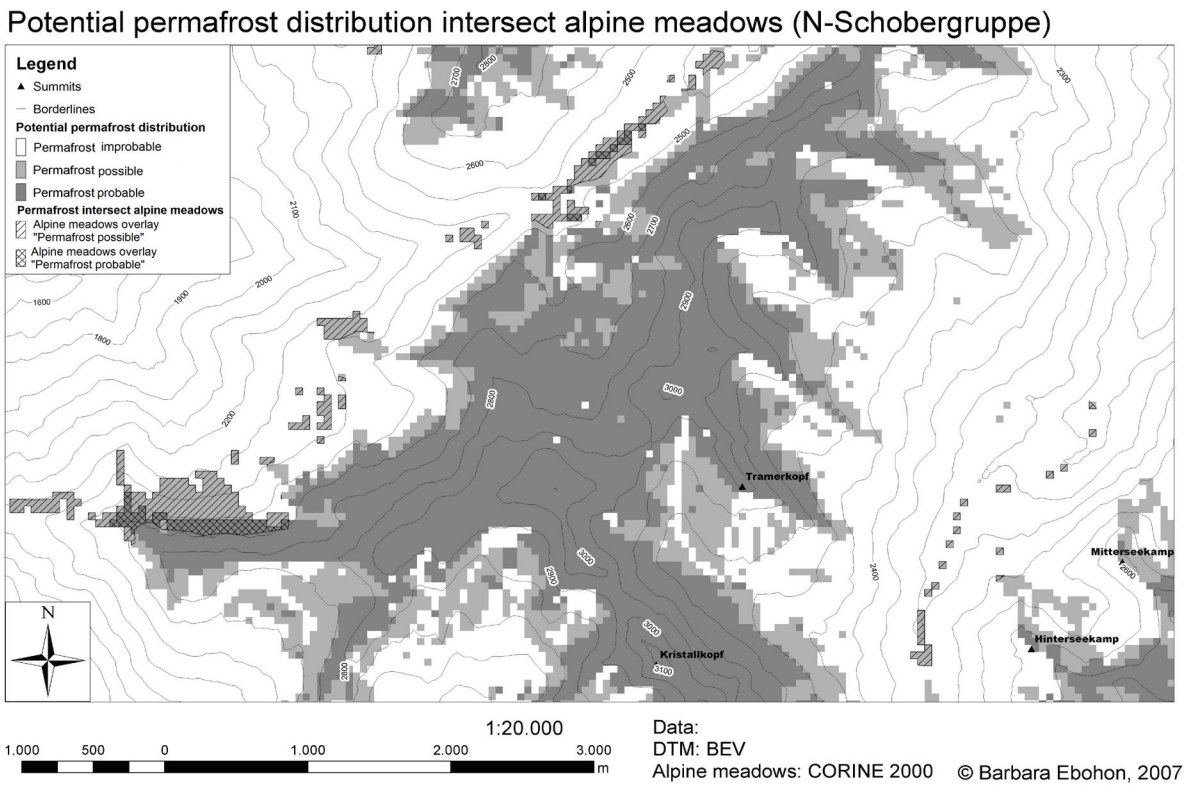

Figure 5. Comparison of simulated permafrost distribution with vegetation (alpine meadows).

Another important issue is the indication of permafrost areas at lower altitudes than expected, which is probably only possible to be pictured through a physically based model. This kind of model is able to reproduce the energy balance, and therefore, can record those areas and should be further developed in future.

Acknowledgments

We gratefully acknowledge the valuable comments by two anonymous reviewers.

Data were kindly provided by:

- Karl Krainer (University of Innsbruck): data from basal snow temperature measurements (BTS).
- Gerhard Karl Lieb (University of Graz): data from basal snow temperature measurements (BTS) and spring water temperature measurements.
- Wolfgang Schöner (ZAMG): Project PERSON (Permafrost-monitoring Sonnblick) GZ BMLFUW-UW.1.3.2/0528-V/5/2005 by order of Lebensministerium.
- Herbert Formayer (University of Natural resources and Applied Life Sciences, Vienna, Austria): Calculated Isotherms.
- Michael Avian (Graz, University of Technology).
- BEV: DTM.

References

Aubrecht, P. 1998. *CORINE Landcover Österreich. Vom Sattelitenbild zum digitalen Bodenbedeckungssatz*. Wien: Umweltbundesamt Monographien, 93: 59 pp.

Etzelmueller, B., Hoelzle, M., Heggem, E.S.F., Isaksen, K., Mittaz, C., Vonder Muehll, D., Ødegård, R.S., Haeberli, W. & Sollid, J.L. 2001. Mapping and modelling the occurrence and distribution of mountain permafrost. *Norwegian Journal of Geography* 55(4): 186-194.

Frauenfelder, R., Allgöwer, B., Haeberli, W. & Hoelzle, M. 1998. Permafrost investigations with GIS – a case study in the Fletschhorn area, Wallis, Swiss Alps. *Proceedings of the 7th International Conference on Permafrost, Yellowknife, Canada, June 23–27, 1998*: 291-295.

Gruber, S., Hoelzle, M. & Haeberli, W. 2004. Rock wall temperatures in the Alps: Modelling their topographic distribution and regional differences. *Permafrost and Periglacial Processes* 15(3): 299-307.

Haeberli, W. 1975. *Untersuchungen zur Verbreitung von Permafrost zwischen Flüelapass und Piz Grialetsch (Graubünden)*. Zürich: Mitteilung der Versuchsanstalt für Wasserbau, Hydrologie und Glaziologie der ETH Zürich, 17: 182 pp.

Heginbottom, J.A. 2002. Permafrost mapping: a review. *Progress in Physical Geography* 26(4): 623-642.

Hoelzle, M. 1994. *Permafrost und Gletscher im Oberengadin—Grundlagen und Anwendungsbeispiele für automatisierte Schätzverfahren*, Zürich: VAW Mitteilung der Versuchsanstalt für Wasserbau, Hydrologie und Glaziologie der ETH Zürich, 132: 121 pp.

Hoelzle, M., Mittaz, C., Etzelmller, B. & Haeberli, W. 2001. Surface energy fluxes and distribution models of permafrost in European mountain areas: an overview of current developments. *Permafrost and Periglacial Processes* 12(1): 53-68.

Imhof, M. 1996. PERM – ein Programm für die automatische Kartierung von Permafrost in den Schweizer Alpen. In: W. Haeberli, M. Hölzle, J.P. Dousse, J.M. Gardaz, M. Imhof, F. Keller, P. Kunz, R. Lugon & E. Reynard, *Simulation der Permafrostverbreitung in den Alpen mit geographischen Informationssystemen. Arbeitsbericht NFP 31*. Zürich: vdf Hochschulverlag, 15-34.

Keller, F. 1992. Automated mapping of mountain permafrost using the program PERMAKART within the geographical information system ARC/INFO. *Permafrost and Periglacial Processes* 3(2): 133-138.

Keller, F. 1994. *Interaktionen zwischen Schnee und Permafrost. Eine Grundlagenstudie im Oberengadin*. Zürich: Mitteilungen der Versuchsanstalt für Wasserbau, Hydrologie und Glaziologie der ETH Zürich, 127: 145 pp.

Keller, F & Hölzle, M. 1996. PERMAKART und PERMAMAP. In: W. Haeberli, M. Hölzle, J.P. Dousse, J.M. Gardaz, M. Imhof, F. Keller, P. Kunz R. Lugon, & E. Reynard, *Simulation der Permafrostverbreitung in den Alpen mit geographischen Informationssystemen, Arbeitsbericht NFP 31*. Zürich: vdf Hochschulverlag, 35-46.

Kellerer-Pirklbauer, A. 2005. Alpine permafrost occurrence at its spatial limits: First results from the eastern margin of the European Alps. *Norwegian Journal of Geography* 59: 184-193.

Lieb, G.K. 2007. personal comment (29.1.2007).

Lieb, G.K. 1996. *Beiträge zur Permafrostforschung in Österreich*. Arbeiten aus dem Institut für Geographie der Karl-Franzens-Universität Graz, 33: 223 pp.

Lieb, G.K. 1998. High-Mountain permafrost in the Austrian Alps (Europe). *Proceedings of the 7th International Conference on Permafrost, Yellowknife, Canada, June 23–27, 1998*: 663-668.

Mittaz, C., Hoelzle, M. & Haeberli, W. 2000. First results and interpretation of energy flux measurements over alpine permafrost. *Annals of Glaciology* 31: 275-280.

Nyenhuis, M. 2006. *Permafrost und Sedimenthaushalt in einem alpinen Geosystem.* Bonn: Bonner Geographische Abhandlungen 116: 142 pp.

Stocker-Mittaz, C., Hoelze, M. & Haeberli, W. 2002. Modelling alpine permafrost distribution based on energy-balance data: a first step. *Permafrost and Periglacial Processes* 13(4): 271-282.

Establishing Initial Conditions for Transient Ground Thermal Modeling in the Mackenzie Valley: A Paleo-Climatic Reconstruction Approach

M. Ednie
Geological Survey of Canada, Ottawa, Ontario, Canada
J.F. Wright
Geological Survey of Canada, Sidney, British Columbia, Canada
C. Duchesne
Geological Survey of Canada, Ottawa, Ontario, Canada

Abstract

The Geological Survey of Canada has implemented a GIS-coupled, finite-element ground thermal model for simulating the response of permafrost in the Mackenzie Valley to progressive climate change. Near-isothermal ground temperature profiles observed in southern portions of the Valley indicate that ground temperatures are presently in disequilibrium with the current climate, and have likely been warming for many decades or centuries. Finite-element methods require specification of initial conditions from which forward modeling can proceed. However, due to the lack of detailed information about current ground temperatures in the region, initial ground temperature profiles for forward modeling must be estimated based on available proxy data. In this work, climate trends observed in the paleo-climatic record are used to reconstruct regional air temperature trends over the past several hundred years. Numerical simulations using this paleo-climate reconstruction successfully reproduce the essential characteristics of the ground temperature regime as observed in borehole records.

Keywords: climate change; numerical model; permafrost; Mackenzie Valley.

Introduction

The Geological Survey of Canada has implemented the T-ONE one-dimensional finite-element ground thermal model (Goodrich 1982) into an ArcGIS platform to simulate the response of permafrost in the Mackenzie valley to progressive climate change. The purpose of the model is to facilitate rigorous and systematic study of the climate-driven evolution of regional ground temperatures as expressed in the present and future distribution and thickness of permafrost (Duchesne et al. 2008). Finite-element models require specification of initial conditions from which forward modeling can proceed, including an initial ground temperature profile for each geographic grid location modeled. Given the limited availability of actual data from instrumented boreholes, present-day ground temperature profiles can be estimated based on transient modeling from an assumed earlier period of quasi-equilibrium to the present. Apart from an initial ground temperature profile, our configuration of the T-ONE model requires specification of rates of change in atmospheric temperature (upper boundary condition) to drive the model according to past and/or future scenarios of climate change, and specification of the regional geothermal heat flux (lower boundary condition). For modeling near-surface ground temperatures, initial profiles can be equilibrated to the atmosphere and ramped using short meteorological data sets (Möldes & Romanovski 2006). However, the deeper ground thermal regime will continue to reflect aspects of the initial climate (such as the presence of deep permafrost) during the equilibrium period even when the ground surface is exposed to sustained atmospheric warming. The specification of initial ground temperature profiles and the time frame selected for modeling from past to present can potentially exert a strong influence on model predictions of the current ground thermal state. Available borehole observations in the discontinuous permafrost zone of the Mackenzie Valley frequently identify near-isothermal conditions close to 0ºC, implying that present day permafrost is in disequilibrium with the current atmospheric temperature regime. This notion is consistent with the observed progressive increase in mean annual air temperatures throughout the Mackenzie Valley during the past century. Taking into account this historic warming trend, we are unlikely to establish a reasonable representation of current ground thermal conditions by employing present-day, or even 20th century climate conditions as a starting point for forward modeling.

This paper describes the reconstruction of mean annual air temperature (MAAT) trends for the Fort Simpson region, NWT, using available climate records and proxy reconstructions of paleo-climatic data to (1) identify a suitable period of quasi-stable regional climate for estimating initial equilibrium ground temperature profiles, and (2) establish an appropriate scenario of climate change from past to present to facilitate prediction of present and future permafrost conditions. We have also compared the results of both equilibrium modeling (driven by contemporary climate data) and transient modeling (from past to present) to ground temperature profiles from selected boreholes in the Mackenzie Valley to illustrate the importance of initial conditions and specification of an appropriate start date for forward modeling.

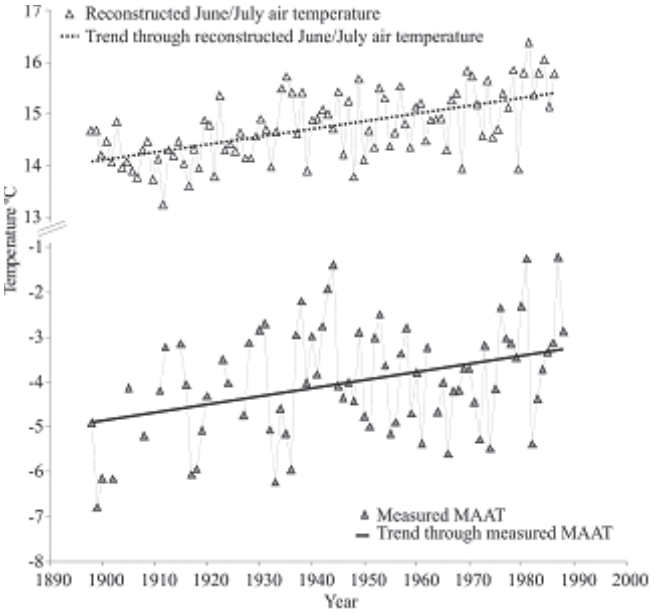

Figure 1. Best-fit lines through MAAT of measured June/July for Fort Simpson and of summer temperature reconstructions (Szeicz & MacDonald 1995) for the period 1898–1988.

Climate Data

Mean annual air temperatures from climate records

We have consolidated available climate data for the study area, consisting of two daily mean air temperature series. (Environment Canada 2002). The most recent data (for the period 1963–2002) were combined with older data (1898–1963) to produce a single continuous temperature series of daily averages. MAAT was calculated from the daily mean values from January 1 through December 31.

Proxy data for reconstructing paleo-climatic trends

A variety of different proxy records can be used to reconstruct past climatic conditions (Gajewski & Atkinson 2003), such as tree rings, lake sediments, ice cores, etc. Proxy data requirements for this study include: acceptable temporal resolution, ready availability, and suitable spatial extent of the reconstruction (site specific, regional, hemispherical, or global). Of these proxy types, tree rings satisfy the majority of the requirements. A limitation of the temperature reconstructions from tree rings is that they are specific to summer temperatures only and lack the contribution of winter months on the MAAT (Jones et al. 2003). A summer air temperature (June/July) reconstruction by Szeicz and MacDonald (1995) was selected out of a group of available data sets. The authors used age-dependent tree ring modeling to derive estimates of average summer air temperatures from AD 1638–1988. Their study provides important information on climate change trends over a relatively long time period for a region that is geographically consistent with the Fort Simpson study area. The data used for the climate reconstruction are available from the NOAA paleoclimatology web site (http://www.nc dc.noaa.gov/paleo/recons.html.)

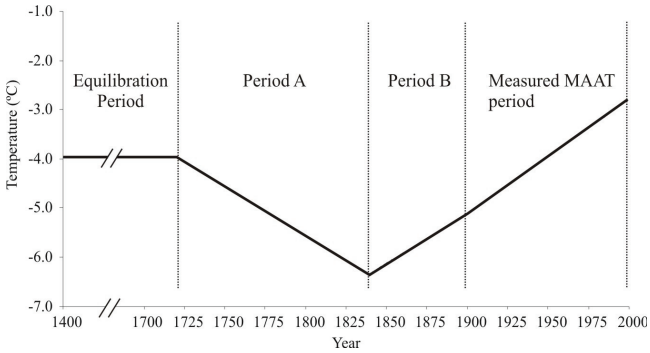

Figure 2. Reconstructed MAATs from 1720–1897 following trends in Group A and Group B, and measured MAAT from 1898–2000 with best fit line for Fort Simpson.

Mann et al. (1999) documented mean annual air temperature anomalies specific to the northern hemisphere for the period 1000–1998, based on tree ring and ice-core data. The reconstructed climate data are presented as MAAT anomalies relative to the 1961–1990 northern hemispherical mean. We used data for the period 1400–1746 to estimate a long-term MAAT representative of an extended period of quasi-stable climate assumed to exist prior to 1750. In this work, the hemispheric temperature anomalies provided by Mann et al. (1999) were examined for general climate trends in order to establish a long term deviation from the 1961–1990 air temperature normal (-3.72ºC) for Fort Simpson. Although not ideal for our purposes, the lack of available data alternatives has dictated that we rely on hemispheric rather than regional proxies to establish regional paleo-climatic trends prior to 1900.

Methods

Available temperature records and proxy climate data (Begin et al. 2000) indicate that Canada's western Arctic has experienced significant variations in mean annual air temperature over the past 250 years, with a modest cooling during the Little Ice Age followed by a progressive warming of climate from the early 1800s to present. As such it would be inappropriate to attempt to reproduce current permafrost conditions in the Mackenzie Valley by relying only on an equilibrium model of the ground thermal state. Neither would it be appropriate to initiate transient numeric modeling at any time during the past century or so without having initial ground temperature profiles specific to the time of initiation of the transient model.

Model initialization at quasi-equilibrium

In order to implement the transient numeric model, we specify a time at which a state of quasi-equilibrium was assumed to exist between atmospheric temperatures and the ground thermal state, from which forward modeling is initiated. For modeling purposes we assume the existence of an extended period of quasi-equilibrium prior to about 1750 AD, characterized by a long-term mean annual air temperature for Fort Simpson of about -4°C, based on the work of Mann

et al. (1999). These equilibrium ground temperature profiles serve as the starting point for forward modeling from past to present (i.e. AD 2000), through incorporation of the paleo-climatic trends described below.

Identification of paleo-climatic trends

We examined the relations between measured and reconstructed summer air temperatures and measured MAAT using simple linear regression. A low correlation (R2 = 0.14) for measured summer temperature regressed against measured MAAT indicates that summer temperatures are ideal predictors of MAAT for the Fort Simpson study area, although other studies have used summer temperatures in such a context (Juliussen & Humlum 2007).

A higher R2 value was obtained for winter air temperatures (December/January/February) regressed against measured MAAT. However, given the lack of reliable proxy data representative of regional winter temperatures, summer temperature reconstructions from tree-ring data were employed in this work. Linear regression of available data described trends in measured MAAT for Fort Simpson and the reconstructed June/July tree-ring temperatures for the period 1898–1988 (Fig. 1).

As mentioned above, the weak correlation between measured June/July air temperature and MAATs from climate records inhibits the direct use of predictive models for estimating past MAATs from proxy indicators of mean summer temperature. Alternatively, the slopes of the best fit lines through recorded MAATs and reconstructed June/July temperatures are very similar, being 0.018ºC/year and 0.015ºC/year, respectively. According to the general trends, MAAT has increased by about 1.8ºC over the past 100 years, and reconstructed June/July temperatures have increased by a similar amount (1.5ºC). Based on this similarity, it is feasible to use the reconstructed summer temperature trends as an indicator of general trends in regional MAAT. Therefore, the recorded MAAT for the year 1898 for Fort Simpson is used as an anchor point from which to transform the temperature trends observed within the summer proxy data to estimate MAAT for the entire proxy period. This transformation must be used with caution as previous studies, together with the relation mentioned above, suggest that summer temperatures explain less yearly variance than winter temperatures and can lead to potentially flawed indications of past climate if summer values alone are used to reconstruct yearly temperatures (Jones et al. 2003). Linear regression was also used to characterize the general trends in summer temperature data for discrete time intervals prior to 1898 (i.e. the beginning of recorded temperature data).

A three-year running average was applied to the tree-ring temperature reconstruction of Szeicz and MacDonald (1995) to clarify general trends in the data (Fig. 2). According to the smoothed data, a general cooling trend from quasi-equilibrium at 1746 reached a minimum temperature around 1838. This cooling period was followed by a general warming trend through to the present.

Based on the general trends observed, the reconstructed summer temperature data were partitioned at AD 1838, corresponding to the apparent minimum temperature of the contemporary Little Ice Age. The paleo-climate record was separated into two periods: period A from 1746–1838 and period B from 1839–1897 (Fig. 2). Period A is characterized by a pronounced cooling trend. A best fit line through the data ($r^2 = 0.41$) indicates a cooling rate of 0.0171ºC/year over 92 years with a total change in temperature of 1.57Cº. Period B is characterized by a warming trend from 1838 to the start of the modern temperature record in 1898. Based on a best-fit line through the data, mean annual air temperatures warmed by 0.98Cº during this 58 year period at a rate of 0.0169ºC/year.

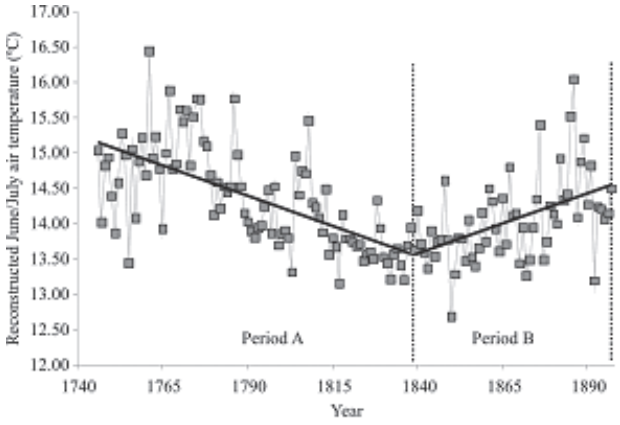

Figure 3. Reconstructed summer air temperatures from Szeicz & MacDonald (1995) smoothed wit h a 3-year running mean.

A best-fit line through the modern MAAT record for Fort Simpson ($r^2 = 0.27$) was used to specify an anchor point from which the trends identified in Figure 1 were used to estimate MAAT previous to the modern record. At the beginning of period A, the observed trend was forced backward by 25 years to 1721, intersecting with the assumed long-term equilibrium MAAT of -3.96ºC. This allowed for a smooth transition from the assumed long-term MAAT to the cooling trend characteristic of period A. Figure 3 shows the equilibration period using an average value from 1400–1720, reconstructed MAATs between 1721 and 1898 and the MAAT trend at Fort Simpson determined from the modern temperature record, which together comprise the paleo-climate scenario employed in transient ground thermal modeling from 1721 to present.

Comparison of modeled vs. recorded ground temperature

To facilitate evaluation of the influence of initial conditions and start date on model predictions, six measured ground temperature profiles from the Fort Simpson area are compared to results of transient numerical modeling, using the temperature reconstruction and an equilibrium solution based on the 1971–2000 normal. The boreholes are a part of a Geological Survey of Canada network for observing permafrost conditions throughout the Mackenzie Valley. The physical parameters assumed for each borehole site and corresponding modeling run are presented in Table 1. At this point it would prove useful to give a simple description

Table 1. Parameters recorded at each borehole and associated modeling properties.

Borehole properties				Modeled properties				
Borehole	Vegetation	Surficial geology	Material	Saturation (Sr)	NT	NF	Bulk density (Kg/m^3)	Texture
94TC1	Closed bs.	Glacio-lacustrine	Sand	0.80	0.55	0.24	1500	Coarse
97TC1	Aspen	Glacio-lacustrine	Silt	0.55	0.30	0.90	1500	Fine
97TC2	Closed bs.	Glacio-lacustrine	Sand	0.80	0.24	0.55	1500	Coarse
97TC4	Open bs.	Glacio-lacustrine	Fine sand	0.85	0.24	0.60	1500	Fine
99TC1	Open bs	Glacio-lacustrine	1.5 of organic over silt	1.0	0.14	0.50	300/ 1500	1.5 organic over fine
99TC2	Fen	Glacio-lacustrine	7 m organic over clay	1.0	0.12	0.70	300/ 1500	7 m Organics over fine

Note: Sr refers to soil water content in terms of the degree of pore saturation; bs. refers to Black spruce (*Picea mariana*).

of the mechanics of the T-ONE model. A more complete description of model parameters can be found in Duchesne et al. (2008) and Wright et al. (2003, 2001). Annual air temperature trends are incorporated in the model through seasonal thawing and freezing degree days. N-factors reflect the thermal off-set between ground surface and atmospheric temperatures. The thawing (summer) n-factor incorporates effects of vegetation on the ground thermal regime, while the effect of winter snow pack is assumed to be implicit in the freezing (winter) n-factor.

Moisture content is described in terms of the degree of pore saturation, based on porosity values derived from specifications of dry bulk density of earth materials. The model assumes a purely conductive heat flow, following the assumption that conduction is the dominant heat transfer process in permafrost landscapes (Hinkle & Outcalt 1994, Outcalt et al. 1990). The effect of latent heat due to the freezing of water or the thawing of ice is incorporated in the model. In the cases present in this paper, the one-dimensional modeling space was set at depth of 45 m with grid spacing ranging from 0.01 m at the surface to 2.0 m at depth. The lower boundary condition is defined in terms of geothermal heat flow, set at a regional value of -0.40 Wm^{-2} (Judge 1975).

The transient model was equilibrated using a -3.96ºC MAAT, with forward modeling initiated at 1721, following the generalized climate change scenario described in Figure 3 to the year 2000. For comparison purposes, a separate equilibrium solution was obtained for each borehole case using a MAAT of -3.01ºC, which is representative of the 1971–2000 climate normal at Fort Simpson.

Results and Discussion

The results of two modeling solutions (transient and equilibrium) were compared with measured ground temperature profiles from six boreholes located in the vicinity of Fort Simpson, NWT (Fig. 4). The largest discrepancy between modeled and measured ground temperatures occurs at borehole 97TC1, a deciduous forest site on glacio-lacustrine silt. Both transient and equilibrium modeling confirm the absence of permafrost at this site, but modeled ground temperatures are about 1ºC warmer than recorded values. This result may indicate an error in the specification of n-factor values for this vegetation category, as comparatively few deciduous cases were included in the initial parameter calibration process (Wright et al. 2003). For cases where borehole data show the presence of permafrost, both transient and equilibrium modeling predict ground temperatures slightly warmer than those observed in the borehole record. In general, the transient model captures the near-isothermal character of ground temperatures in boreholes 94TC1, 97TC2, 97TC4, and 99TC2, although transient model predictions for the latter are somewhat warmer than measured values, and equilibrium predictions even more so. In all cases except 99TC1 equilibrium modeling predicts ground temperatures at depth that are significantly warmer than those indicated by borehole data.

A close agreement of ground temperatures between measured values and those predicted by T-One transient modeling is observed at borehole 97TC4, with the prediction of 8 m of permafrost being close to that indicated in the borehole (~9 m), although a somewhat deeper thaw zone is indicated by the transient model in the upper few metres of the profile. In contrast, equilibrium modeling predicts substantively warmer ground temperatures with unfrozen conditions throughout the profile.

At borehole 97TC2, measured permafrost temperatures tend towards colder values at depths below about 5 m. This again confirms the notion that permafrost is progressively warming from the surface downward in response to climate warming during the past century or so. Transient modeling predicts the isothermal tendencies apparent in this borehole data, but predicts significantly warmer ground temperatures at depth. Actual permafrost thickness at this site is not known, but based on the temperature at the bottom of the profile, the transient model prediction of 22 m of permafrost is likely a reasonable estimate. In contrast, the equilibrium modeling based on the 1971–2000 normal significantly over-predicts ground temperatures at depth and grossly under-predicts permafrost thickness at this site.

Boreholes 99TC1 and 99TC2 are located in strikingly different settings, although they are separated by a distance of only about 10 m. Site 99TC1 is located on a raised peat plateau, while 99TC2 is situated in a wet collapse feature

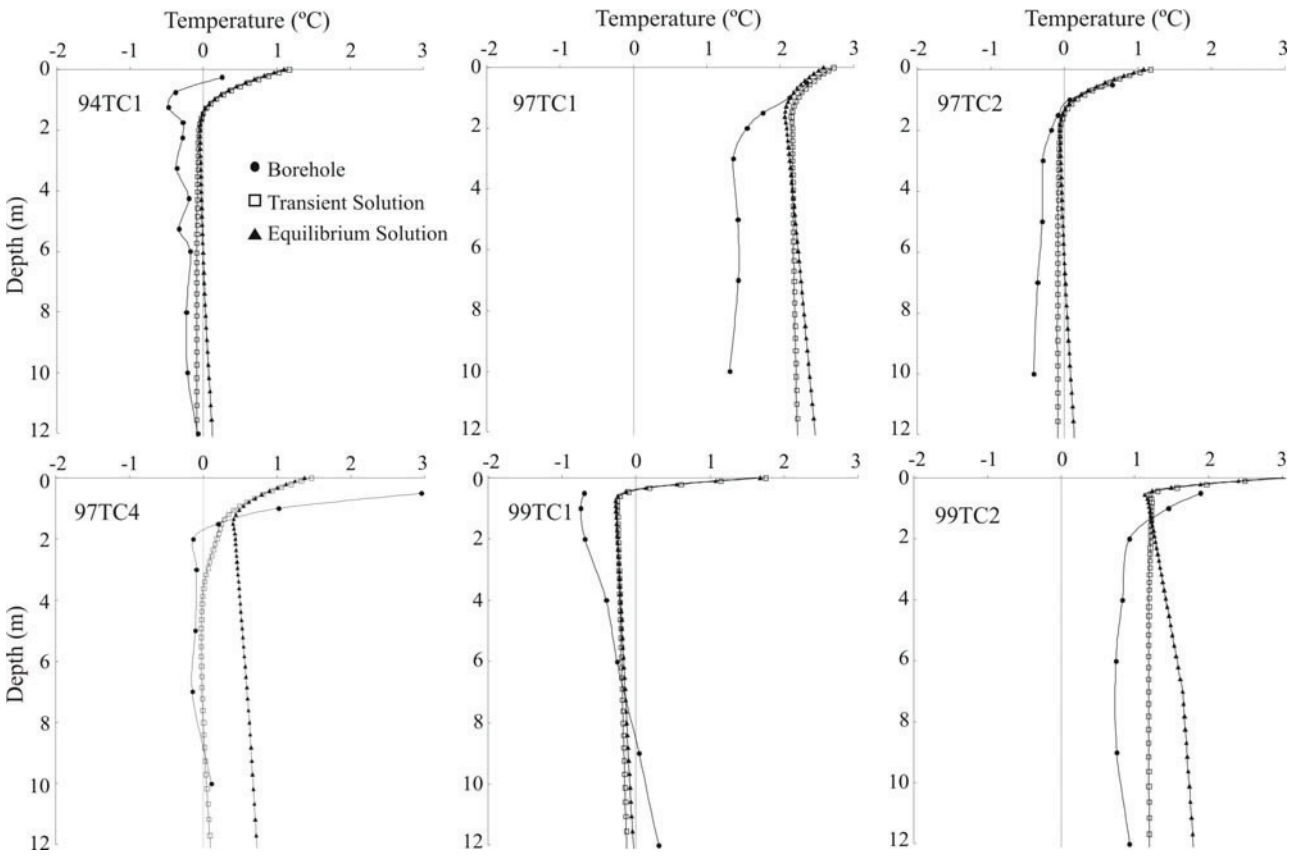

Figure 4. Measured ground thermal profiles from boreholes and results from a transient model using the climate reconstruction and an equilibrium solution based on 1971–2000 climate normal for the Fort Simpson area.

immediately adjacent to the peat plateau. Both sites are separated from an extensive fenland by a low ridge only a few metres wide. Recorded temperatures indicate that 99TC2 is unfrozen as correctly predicted by both transient and equilibrium modeling. The transient solution over-predicts ground temperatures at depth by about 0.5°C, while the equilibrium model over-predicts by about twice that amount. Borehole 99TC1 is characterized by a steep temperature gradient with uncharacteristically cold temperatures (~-0.8°C) at the near-surface, with unfrozen conditions below about 9 m depth. When examining this profile it is useful to consider that the raised peat plateau is about 2 m higher than the surrounding terrain. It is potentially exposed on its western face to winds from an extensive fen immediately adjacent to the site. Consequently, this site may experience reduced snow accumulation and therefore more direct exposure to cold winter temperatures at the ground surface. The presence of a 1.5 m layer of peat also insulates the ground during the summer months, promoting potentially colder near-surface ground temperatures. On the other hand, given the perhaps anomalously cold permafrost temperatures at 99TC1, the relatively shallow depth of permafrost at this site may reflect the influence of the adjacent fenland and/or its close proximity to the collapsed bog feature. Indeed, neither model adequately reproduces the ground thermal characteristics at this site, possibly due to the role of non-conductive and/or significant lateral heat fluxes in this environment.

In general, both the transient and equilibrium models tend to over-predict ground temperatures to some degree, relative to the borehole measurements. While near-surface ground temperature predictions are similar, the equilibrium model tends towards warmer temperatures at the base of the profiles. This difference can be explained by two factors: (1) the transient model was equilibrated at a slightly colder MAAT leading to a greater initial depth of permafrost circa 1721, and (2) transient modeling simulated approximately 100 years of cooling through to the end of the Little Ice Age (circa 1840) before warming to present-day conditions. It is also possible that the assumed thermal equilibrium between the atmosphere and ground circa 1700 is invalid, with either colder temperatures prevailing at that time or during some period earlier in the proxy record.

The differences between recorded borehole temperatures and the predictions of equilibrium modeling (as shown in Figure 4) illustrate that current ground temperature profiles are not in equilibrium with the modern climate regime, and that current ground temperatures at depth are colder than would be expected based on late 20th century climate. Furthermore, the near-isothermal character of ground temperatures observed in the majority of boreholes is not reflected in the equilibrium modeling, but is characteristic of the transient modeling from circa 1721, in spite of the 100 years or more of cooling prior to 1840. The results of

equilibrium modeling based on a late 20th century climate are likely to underestimate permafrost occurrence and thickness and to overestimate ground temperatures at depth. Although the transient modeling predicts somewhat warmer ground temperatures in comparison to available measured ground temperature profiles, the general characteristics of the ground thermal regime in permafrost environments are reasonably well replicated.

Conclusion

Using available proxy records to identify general trends in the paleo-climatic record, a reasonable estimation of regional trends in MAAT was reconstructed from an assumed quasi-stable climate prior to the mid-1700s through to present day. Trends in summer air temperature deviation determined from proxy data (1740–1890) were transformed into estimates of annual temperature trends in MAAT for the Fort Simpson region and intersected with the centurial trend identified in the modern temperature record (1900–2000). Transient numeric ground thermal modeling driven by this reconstructed climate scenario captures the general characteristics of the current ground thermal regime in the southern extent of permafrost terrain, as indicated by the congruency between model predictions and borehole measurements. Differences between recorded borehole temperatures and the results of equilibrium modeling (based on the 1971–2000 climate normal) indicate that ground temperatures in the Fort Simpson region are not in thermal equilibrium with the current climatic regime. Our results suggest that permafrost models incorporating present day or even 20th century climate will not adequately reproduce the essential characteristics of the current permafrost regime, and so are unlikely to produce reliable predictions of the future evolution of permafrost when standard scenarios of climate warming are applied. The results also indicate that there is considerable opportunity for improvement of our transient ground thermal modeling capability, including refinement of the paleo-climate trends established for forward modeling from past to present. A detailed analysis of modeling outputs from this work, together with additional comparisons of modeling results with more widely distributed borehole temperature records, will support refinement of model parameter assignments and increase confidence in model performance for regional and local-scale applications.

References

Begin, C., Michaud, Y. & Archambault, S. 2000. Tree-ring evidence of recent climate changes in the Mackenzie Basin, Northwest Territories. In: L.D. Dyke and G.R. Brooks (eds), *The Physical Environment of the Mackenzie Valley, Northwest Territories: a base line for the Assessment of Environmental Change*. Ottawa: Geological Survey of Canada, Bulletin 547: 65-77.

Duchesne, C., Wright, J.F. & Ednie, M. 2008. High resolution numerical modeling of climate change impacts to permafrost in the vicinities of Inuvik, Norman Wells, and Fort Simpson, NWT, Canada *Proceedings of the Ninth International Permafrost Conference, Fairbanks, Alaska, June 29–July 2, 2008* (this proceeding).

Environment Canada. 2002. Canadian Climate Normal: Canadian Monthly Climate Data and 1943–2000 Normal. Environment Canada: Ottawa. CD-ROM.

Gajewski, K. & Atkinson, D.A. 2003. Climatic change in northern Canada. *Environmental Reviews* 11(2): 69-102.

Goodrich, L.E. 1982. An introductory review of numerical methods for ground thermal regime calculations. Division of Building Research, National Research Council of Canada. *DBR Paper* No. 106, 133 pp.

Hinkle, K.E. & Outcalt, S.I. 1994. Identification of heat transfer processes during soil cooling, freezing, and thawing in Central Alaska. *Permafrost and Periglacial Processes* 5: 217-235.

Jones, P.D., Briffa, K.R. & Osborn, T.J. 2003. Changes in the Northern Hemisphere annual cycle: Implications for paleoclimatology. *Journal of Geophysical Research* 108(D18): 13-1-13-7.

Judge, A.S. 1975. Geothermal studies in the Mackenzie Valley by the Earth Physics Branch. In: Geothermal Service of Canada, *Geothermal Series No.2*. Ottawa: Energy Mines and Resources Canada, 12pp.

Juliussen, H. & Humlum, O. 2007. Towards a TTOP ground temperature model for mountainous terrain in Central-Eastern Norway. *Permafrost and Periglacial Processes* 18: 161-184.

Mann, M.E., Bradley, R.S. & Hughes, M.K. 1999. Northern hemisphere temperatures during the past millennium: Inferences, uncertainties, and limitations. *Geophysical Research Letters* 26(6): 759-762.

Möldes, N. & Romanovski, V.E. 2006. Long-term evaluation of the hydro-thermodynamics soil-vegetation scheme's frozen ground/permafrost component using observations at Barrow, Alaska. *Journal of Geophysical Research* 111: D04105.

Outcalt, S.I., Nelson, F.E. & Hinklel, K.E.. 1990. The zero curtain effect: heat and mass transfer across an isothermal region in freezing soil. *Water Resources Research* 26: 1509-1516.

Szeicz, J.M. & MacDonald, G.M. 1995: Dendroclimatic reconstruction of summer temperatures in Northwestern Canada since A.D. 1638 based on age-dependent modeling. *Quaternary Research* 44: 257-266.

Wright, J.F., Duchesne, C. & Côté, M.M. 2003. Regional-scale permafrost mapping using TTOP ground temperatures model. *Proceedings of the Eight International Permafrost Conference, Zurich, Switzerland, July 21-25, 2003*: 1241-1246.

Wright, J.F., Duchesne, C., Nixon, F.M. & Côté, M.M. 2001. Ground thermal modeling in support of terrain evaluation and route selection in the Mackenzie River valley, *CCAF Project A073. Summary Report*. Ottawa: Natural Resources Canada, 53 pp.

Seasonal Variations of Surface Radiowave Impedance of Frozen Ground

V.N. Efremov
Melnikov Permafrost Institute, SB RAS, Yakutsk, Russia

Abstract

The depth of superficial seasonal thawing observed in permafrost bodies with a thickness of hundreds of meters results in substantial seasonal variations in radiowave impedance for radio frequencies. This report outlines the results of an investigation of seasonal variations of radiowave impedance in Central Yakutia at a frequency range of 10–1000 kHz. The peculiarities of seasonal variations in the region include a significant influence of thawed layer conductivity on wave impedance magnitude and phase angle at the freezing of the seasonally thawed layer. This report reveals and analyzes the diverse nature and degree of seasonal variations of wave impedance magnitude, phase angle, and apparent resistivity in different frequencies during seasonal ground freezing and thawing at two sites of differing landscape but identical geological structure. Subsurface conductivity structure models were suggested, reflecting results of radiowave impedance sounding on the sites. Stabilization of apparent resistivity level change was registered in the period from August to October.

Keywords: frozen ground; seasonal variations; seasonally thawed layer; surface radiowave impedance.

Introduction

Our work during past years (Efremov 2007) was aimed at assessing physical properties of frozen ground, based on surface wave impedance (Wait 1962) or input impedance (Berdichevsky 1966) measurements.

$$Z = \frac{E_x}{H_y} = |Z|e^{-i\varphi} \quad (1)$$

The results of mathematical simulation demonstrated that radiowave sounding, used to study the structure and properties of permafrost, must involve measurement of surface wave impedance at a frequency range of 10–1000 kHz (Efremov 1995). The range of frequencies includes very-low-frequency (VLF from 10 kHz to 30 kHz), low-frequency (LF from 30 kHz to 300 kHz), and, partially, medium-frequency (MF from 300 kHz to 1000 kHz) belonging to the radio-frequency spectrum, propagating above the ground surface. For frozen ground, VLF sounding conduction currents prevail, which make it possible to assess frozen rocks resisitivity. At frequencies of 30–1000 kHz (LF-MF) the influence of displacement currents increases, but does not dominate. At these frequencies, there is a possibility of assessing resistivity and other physical properties of frozen ground, as a result of processing and interpretation of surface wave impedance measurement data.

To interpret the measured data, we use two components of wave impedance: |Z| magnitude and φ phase angle, as well as apparent resistivity that is determined using these components, taking into account the displacement currents (Veshev, Egorov 1966).

$$\rho = \frac{|Z|^2}{2\pi f\mu \cdot \sin 2\varphi} \quad (2)$$

Nevertheless, measurements of surface wave impedance within LF and MF bands, could be considerably affected by the conductive layer, formed in an active layer on the frozen ground surface as a result of seasonal thawing. The freeze-thaw cycle of the seasonally thawed layer is the reason for seasonal variations in components of surface radiowave impedance.

Results and Discussion

Some regional results

The results of surface radiowave impedance measurements in Central Yakutia and in numerical simulations demonstrate that the seasonal variations are significant and have some regional peculiarities. The region is characterized by a relatively deep seasonal thawing of permafrost, making 1.5–2 m, while its thickness is 300–400 m. With freezing of the seasonally thawed layer, its resistivity increases, and the phase angle grows at all frequencies. At frequencies of f >300 kHz at freezing we observe a significant increase of phase angle, and wave impedance magnitude grows, due to upper layer longitudinal conductivity reduction. At frequencies of f <300 kHz the wave impedance magnitude increase is less significant due to the effect of the formation of a cumulative non-conductive layer of frozen unconsolidated deposit above a more conductive layer composed of frozen rocks, in accordance with a two-layer model. At thawing of the seasonally-thawed layer, phase angle decreases as well as the wave impedance magnitude, which is more significant at f >300 kHz. The phase angle reduction, since some size of magnitude of longitudinal conductivity, is dependent on resistance permafrost (for example 0.05 $\Omega^{-1}\cdot$m for ρ=1000 Ω·m), accepts an asymptotic value. The decrease of wave impedance magnitude is proportional to the increase of longitudinal conductivity of such layers. We observed a sufficient convergence of apparent resistivities within MF range and seasonally thawed layer resistivity at

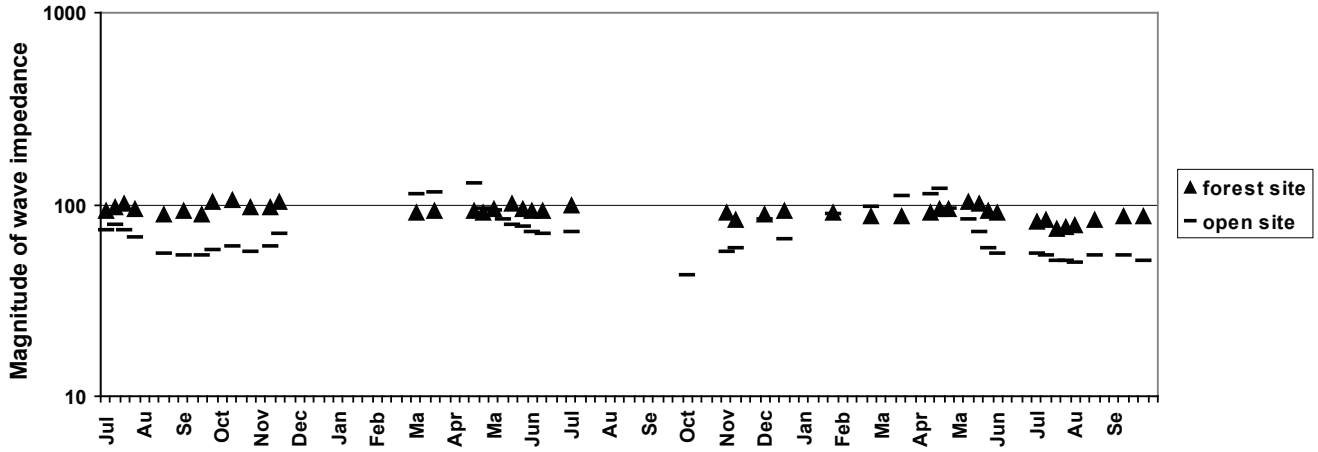

Figure 1. Seasonal variations of magnitude of wave impedance in MF (549 kHz) in test sites from July 2005 to September 2007.

constant current, which speaks to a significant influence of the seasonally thawed layer on wave impedance magnitude within the given range, as shown in the following.

According to experimental data obtained along the 200 km-long highway at the same sites (first in August, then in April of the following year), the fluctuation at LF, caused by the seasonally thawed layer (STL) freezing, gave on average: for wave impedance +18%, for phase angle +19°. At higher frequencies, in MF range, the fluctuation of wave impedance reached +40%, and phase angle fluctuation made +16° on average.

The increase of wave impedance magnitude at STL freezing, as well as the increase of this fluctuation at higher frequencies of the field were expected and totally fit into the results of numerical simulation (Efremov 1995). The increase of phase angle with freezing of the seasonally-thawing layer indicates that there is a thin conductive layer within the permafrost, and that the effect produced by this layer during the warm period is partially mitigated by the presence of a conductive seasonally thawed layer. This suggestion is proven by the results of numerical simulation for the frequency dependence of surface wave impedance for permafrost including a thin conductive layer.

Other factors than thawing, resulting in seasonal variations of surface impedance, may be abundant rainfall, or long absence of precipitation. In the first case, resistivity decreases and permittivity of the seasonally thawed layer increases as a result of the moistening; in the second case we see an inverse effect as a result of dehydration of the upper layer, evaporation, and gravitational moisture transfer to the bottom of the permafrost.

Results in test sites

Over the last years, observations of surface impedance seasonal variation were carried out in Central Yakutia at two test sites located 200 m away from each other in the same geological conditions, but in different landscapes – in forest with thawing of the ground down to 1.3 m, and in open space with thawing down to a depth of 1.9 m. The area where the sites are located is composed of sandy-loamy deposits with a total thickness of 30 m, overlying frozen rocks up to 300 m deep. Geological and geocryological profiles of both sites are typical for Central Yakutia.

The surface impedance measurements were carried out using reception of horizontal electric-field component E_x on a symmetric ungrounded receiver circuit, and of horizontal magnetic component of the field H_y - on a frame magnetic antenna. The measurements were carried out at the same sites with periodicity of 1–2 weeks during the warm period and on occasional days of thaw during winter. A surface impedance indicator IPI-1000 (Parfentyev & Pertel 1991) was used as a measuring instrument. The instrument represents a selective microvoltmeter, phase-angle meter, operating within a frequency range of 10–1000 kHz and measuring the magnitude of wave impedance accurate within 5%, and a phase angle inaccuracy rate of 1°.

The results of observations showed that the profiles of seasonal variations of complex wave impedance components for forest- and open sites do not have distinctions of kind (Figs. 1, 2).

At the forest site, the variations of surface radiowave impedance magnitude were not as significant, as variations of phase angle, with a range of deviation reaching 35°. At the open site, on the contrary, there was not as substantial a variation in phase angle as there was in surface radiowave impedance magnitude, reaching 58%. This difference can be explained by the presence of a thin conductive layer at different depths and by distinctions in cryogenic structure of the ground at the sites, resulting in different subsurface conductivity structures. According to the sounding data interpretation, at the forest site a conductive layer is indicated at the bottom of unconsolidated deposits, and in the open site at the bottom of a seasonally thawed layer. This presumes different subsurface conductivity structures, different depth of sounding on the sites, and consequently a different level of influence of conductive layers constituting the ground. The range of seasonal variations of apparent resistivity is wider at the open site than at the forest one. This can be explained by higher ice content in the ground and a thicker seasonally thawed layer at the open site.

At each of the sites, the components of wave impedance and the apparent resistivity seasonal variations profiles

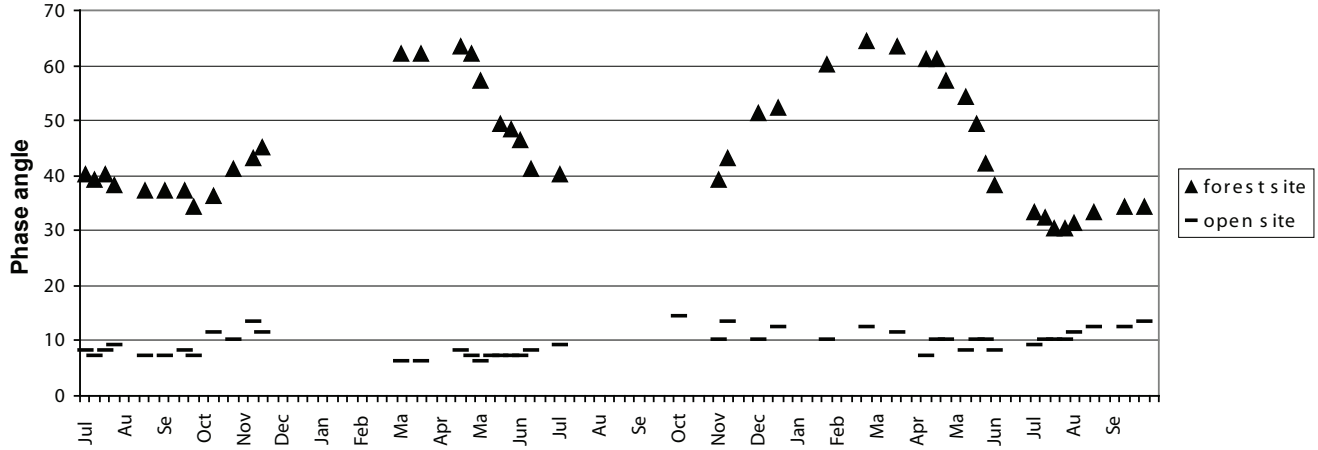

Figure 2. Seasonal variations of phase angle in MF (549 kHz) in test sites at period from July 2005 to September 2007.

substantially differ for different frequencies (Figs. 3, 4).

At the forest site, a sudden increase of phase angle within LF and MF (VLF remaining almost unchanged) was observed since the freezing of the seasonally thawed layer started in October and finished in April of the next year (Fig. 2). Here, the wave impedance magnitude decreased to VLF by the end of April and did not significantly change in higher frequencies (below than 800 kHz). Decrease of wave impedance magnitude reaching 56% occurs here in higher frequencies (higher then 800 kHz) during the period of intensive STL thawing from April until July. During the same period, at the forest site, we observed a rapid decrease of phase angle in LF-MF range, reaching 34°, apparent resistivity increasing within VLF and decreasing within MF (Fig. 4).

At the open site, the growth of wave impedance magnitude and of apparent resistivity occurs in LF-MF range, at freezing of the STL during the period from November until April of the following year and is accompanied by a slight decrease of impedance magnitude in VLF. At STL thawing during the period from April until June, wave impedance magnitude and apparent resistivity decrease within LF-MF and increase within VLF (Fig. 3). During the same period, the phase angle decreases within the range of frequencies lower than 400 kHz. During the period from May until July, the phase angle increases at high frequencies (higher than 800 kHz). It is essential to note that in 2007, STL thawing led to a more abrupt decrease of wave impedance magnitude within LF-MF than in the previous years.

Based on the analyses of our experimental data, we suggest four-layer and five-layer models of subsurface conductivity structure of the sites for warm and cold periods of the year, shown in Tables 1 and 2.

Besides STL freezing and thawing, seasonal variations of the surface radiowave impedance in Central Yakutia, a region of high temperature permafrost, are substantially influenced by temperature variations in the layer of annual temperature fluctuations (to a depth of 3 m). These temperature variations can result in changes of the resistivity. This part of the ground is freezing, and consequently, resistivity increases during the period from November until April. From May until July, while ground temperature rises, a decrease of resistivity is recorded in this part of the ground; and from August until October the resistivity change stabilizes. In the open site, the stabilization of wave impedance magnitude changes, phase angle, and correspondingly of apparent resistivity is indicated within the LF-MF band during the period from June until September. This is the result of compensation of the effect of a non-conductive layer made of frozen unconsolidated deposits, by the effect of the conductive STL (Fig. 4). Based on the results of numerical simulation, full compensation can be achieved under the condition given by (Efremov 1995):

$$\frac{h_1}{\rho_1} = \frac{h_2}{\rho_3} \tag{3}$$

where h_1/ρ_1 is the longitudinal conductivity of seasonally thawed layer; h_2 is the thickness of frozen unconsolidated deposits; ρ_3 is the resistivity of frozen rocks. It is significant to note that the levels of stabilization of wave impedance magnitude changes and apparent resistivity are lower in 2007 than in 2005 and 2006.

Over the last years, both open and forest sites have depicted a trend towards decrease of ground resistivity variations amplitude, correlated with decrease of freezing degree and increase of thawing degree (Fig. 4). These changes can be explained by increased snow cover thickness and warming of the climate. The increase of thawing depth is evidenced by measurements of thawing at sites with the help of a test prod. All this indicates a connection between seasonal variations of surface radiowave impedance and climatic changes.

Conclusions

Regional peculiarities of surface radiowave impedance seasonal variations for frequencies ranging between 10 – 1000 kHz have a significant influence on the thawed layer conductivity magnitude and the increase of phase angle at

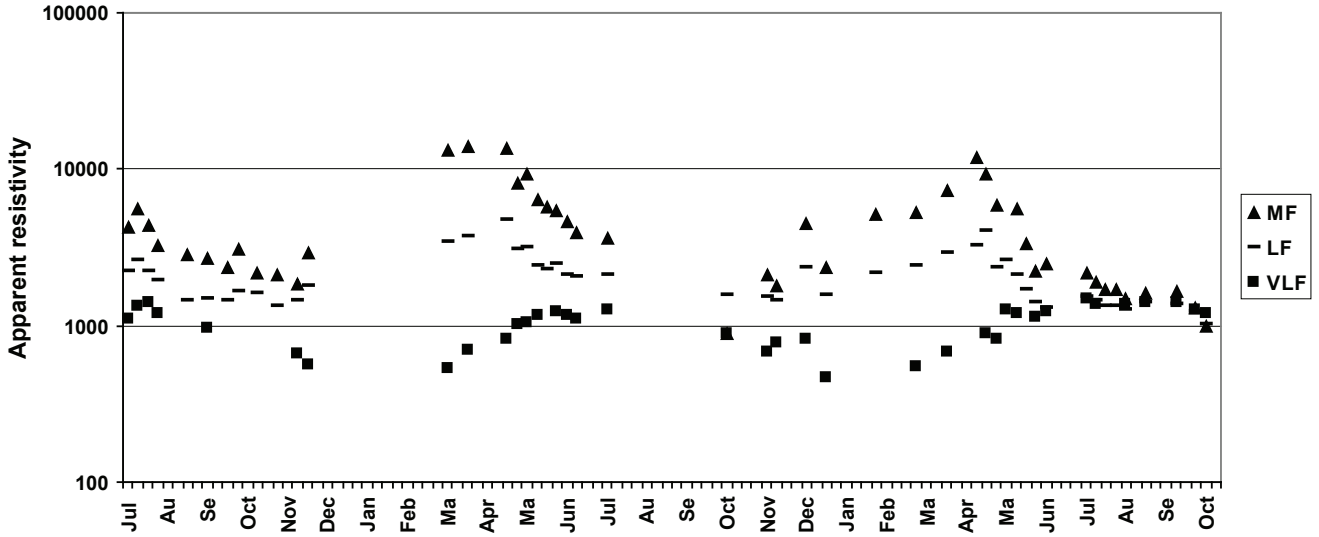

Figure 3. Seasonal variations of apparent resistivity (Ω·m) in MF-LF-VLF in the open site from July 2005 to October 2007.

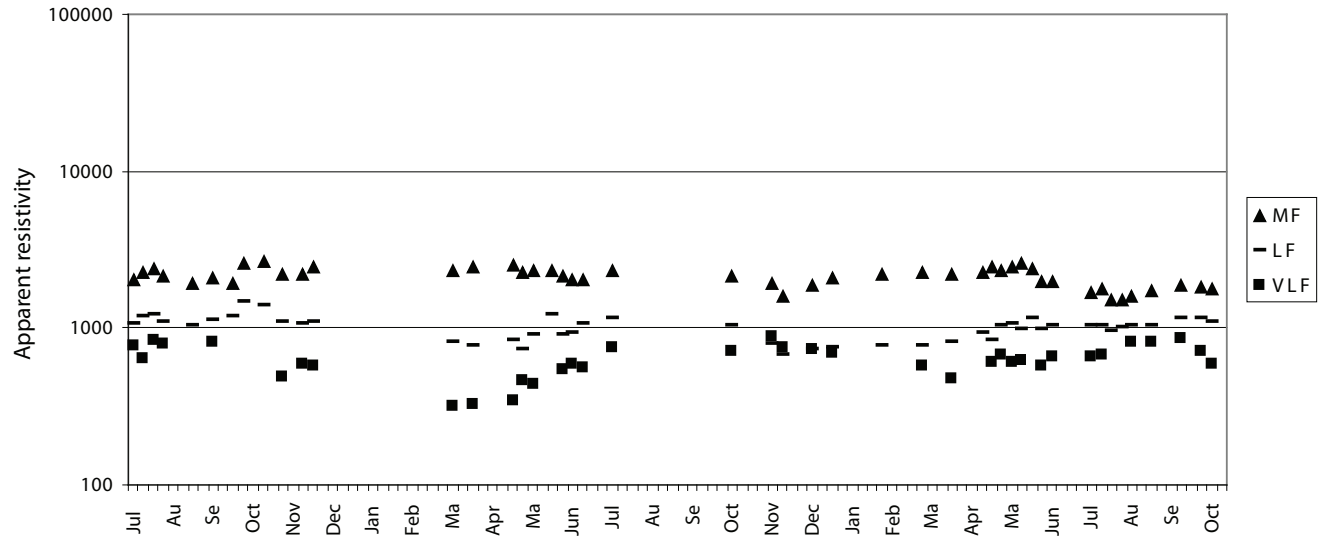

Figure 4. Seasonal variations of apparent resistivity (Ω·m) in MF-LF-VLF in the forest site from July 2005 to October 2007.

freezing of the seasonally thawed layer. This fact proves that within permafrost there is a thin conductive layer of cryolithological nature.

Seasonal variations in surface radiowave impedance components differ dramatically by character and degree of change in sites with differing landscapes, resulting from different geocryologic profiles. Besides, there is a difference in character and degree of change for different frequencies of 10–1000 kHz range at one and the same site. It results in the necessity to consider seasonal changes in frozen ground research by radiowave methods. On the other hand, the analysis given about seasonal variations of the surface radiowave impedance at various frequencies will allow gaining more specific information on the geocryological structure of the ground and the dynamics of seasonal changes occurring in it.

Freezing and thawing of the upper layer, to a considerable extent, change the subsurface conductivity structure of permafrost and the ratio of conductive and non-conductive layers within it. This consequently changes the ratio of conduction and displacement currents for the given frequency, which in its turn determines the phase angle. Therefore seasonal changes in the upper layer at thawing can hide (and at freezing intensify) the anomalies caused by conductive bodies within permafrost.

Stabilization of components of wave impedance and apparent resistivity during the period from August until October, caused by the compensation of influence from frozen unconsolidated deposits by conductivity of the seasonally thawed layer, gives us a chance to assess the resistivity of frozen rocks according to measured apparent resistivity. The period from August until October is the

Table 1. Models of the subsurface conductivity structure of the frozen ground in the forest site.

	April-November	December-March
1	Conductive layer	Medium resistivity layer
2	Variable high-resistivity layer	Variable high-resistivity layer
3	Very-high-resistivity layer	Very-high-resistivity layer
4	High-resistivity layer	High-resistivity layer

Table 2. Models of the subsurface conductivity structure of the frozen ground in the open site.

	April-November	December-March
1	Conductive layer	Medium-resistivity layer
2	Thin conductive layer	Variable high-resistivity layer
3	Variable high-resistivity layer	Very-high-resistivity layer
4	Very-high-resistivity layer	High-resistivity layer
5	High-resistivity layer	

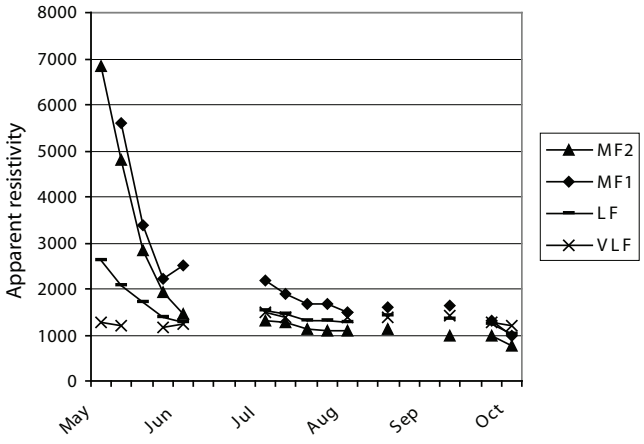

Figure 5. Seasonal variations of apparent resistivity (Ω·m) in MF-LF-VLF in open site at period from May 2007 to October 2007.

most practical for research of frozen rocks using radiowave methods in Central Yakutia and other regions, similar by climatic and geocryologic profiles.

Correlation of the seasonal variations of the surface radiowave impedance magnitude and phase angle with the degree of ground freezing and depth of thawing, allows us to assume the possibility of monitoring of changes in frozen ground caused by climatic changes.

References

Berdichevsky, M.N. 1968. *Electrical Exploration by Magnetotelluric Sounding Method (Elektricheskaya razvedka metodom magnitotellurichеskogo profilirovania)*. Moscow: Nedra, 255 pp (in Russian).

Efremov, V.N. 1995. Surface impedance in permafrost at radio frequencies. In: *Geophysical Investigations in Yakutia (Geofizicheskie issledovania v Yakutii)*. Yakutsk: Izd-vo Yakutskogo Universiteta, 70-80 (in Russian).

Efremov, V.N. 2007. On the real time tentative estimation of physical properties of frozen soils during radio impedance express-sounding. In: *Cryogenic Resources of Polar Regions. Proceedings of the International Conference in Salekhard City, West Siberia, June, 2007*. Pushchino 2: 311-313 (in Russian).

Parfentiev, P.A. & Pertel', M.I. 1991. A device for measuring VLF and LF surface impedance. In: *The Earth-Ionosphere Low-Frequency Waveguide (Nizkochastotnyi volnovod Zemlya-ionosfera)*. Alma-Ata: Golym, 133-135 (in Russian).

Veshev, A.V. & Egorov, V.A. 1966. *On Methodology for Observing and Interpreting the Results of Studies on the Fields of Radio Broadcast Stations*. Voprosy Geofiziki: Uchenye zapiski LGU, 329(16): 172-189 (in Russian).

Wait, J.R. 1962. *Electromagnetic Waves in Stratified Media. International Series of Monografs in Electromagnetics Waves.* Pergamon, Toronto, 3: 372 pp.

Using Indigenous Knowledge to Assess Environmental Impacts of Overland Travel Routes, Arctic Coastal Plain of Alaska

Wendy R. Eisner
Department of Geography and Environmental Studies Program, University of Cincinnati, Cincinnati, OH 45221-0131 USA
Kenneth M. Hinkel
Department of Geography, University of Cincinnati, Cincinnati, OH 45221-0131 USA
Benjamin M. Jones
Alaska Science Center, U.S. Geological Survey, Anchorage, AK 99508-4664 USA
Christine J. Cuomo
Institute for Women's Studies and Dept. of Philosophy, University of Georgia, Athens, GA 30602-2305 USA

Abstract

The overland travel routes from Barrow, Alaska, to inland regions are assessed using indigenous knowledge of Iñupiaq elders and hunters, as well as historic documents, aerial photos, and satellite imagery. Route information is superimposed on a satellite image within a geographic information system to identify areas of observed impact. The overall pattern for summer travel routes has not changed significantly over the past 50 years, despite the change from travel by foot and river boats to motorized vehicles, predominantly all-terrain vehicles. Route elements have altered, however: whereas traditional routes depended on conveyance by boat and included waterways, modern traffic detours around lakes and streams, are increasing the impact on tundra vegetation, soil, and permafrost.

Keywords: Alaska; GIS; indigenous knowledge; off-road vehicles; permafrost; thermokarst; trails.

Introduction

The traditional travel routes of the Iñupiaq people are an important and useful area of study for cultural geographers and anthropologists. Ethnographic studies have recognized so-called traveling landscapes as a rich repository of information about hunting and fishing resources, trading relations and kinship ties, and survival mechanisms. Our current research in northern Alaska utilizes indigenous knowledge (IK) of elders and hunters, who have primary and secondary information on natural and anthropogenic landscape changes. During the course of interviews with Iñupiaq elders from Barrow, Atqasuk, and Wainwright, informants repeatedly called attention to their present and past travel routes for both summer and winter travel. We consequently began to examine this information to determine how and why inland travel routes have changed, and to assess the impact of routes on the landscape.

We have collected and georeferenced relevant Iñupiaq summer inland travel information in a Geographic Information System (GIS) database. This includes overland trails on the tundra and river routes that utilize watercraft. Our informants have indicated on maps and satellite images the routes currently in use, as well as traditional routes that have been abandoned due to changes in ground-cover, hydrology, transportation technology, and viability (that is, the route no longer leads to useful sites). We are able to compare modern routes to those of the traditional Iñupiaq route system that existed in the 1950s (Spencer 1959), or before the proliferation of affordable snowmachines and All-Terrain Vehicles (ATVs). We also utilized some inland travel route information from the 1970s (Tremont 1987) and, more recently, trails that are visible on 1:50,000 color infrared (CIR) photography captured for the Barrow Peninsula in 2005.

The objective of this report is to identify the changes in travel routes on the Barrow Peninsula over the past half-century, assess the cause for route changes, and identify visible effects on the landscape. We will focus only on terrestrial travel in the summer period, when the potential for damage to the tundra is maximal. The use of snowmachines has, until recently, been restricted to winter and will not be considered here.

Background

The pre-motorized Iñupiat had a variety of reasons for traveling long distances inland, and food acquisition was just one of these. Spencer (1959) writes that the main interaction between the *nuunamiut* (inland Iñupiat) and the *tareumiut* (coastal Iñupiat) was based on organized trade. Trade was important for commodity exchange, but also vital for maintaining social ties and enabling groups to achieve economic stability. Trading generally commenced at specific times of the year, and often centered around traditional trading sites or areas. Other reasons to travel include accessing seasonal hunting and fishing areas, attendance at festivals, and travel to engage in warfare (Burch 2005).

The mode of transportation depended on the season of travel and the terrain along the specific route. The method of conveyance depended to a large degree on the season. Some portion of summer and early fall travel was simply done on foot. The traveling *umiaq*, a skin boat which is a smaller version of the whaling *umiaq*, was used to travel

the rivers and lakes between May and October. The loaded *umiaq* was difficult if not impossible to navigate in head- or cross-winds, and was often towed from the banks by dogs and family members (Spencer 1959, Burch 2005, Flossie Itta in Atqasuk August 2003 interview, Roy Nageak Sr. of Barrow in August 2006 interview). Rivers and streams were usually only deep enough for continuous travel in the spring; by summer gravel bars and boulders posed considerable obstacles. A sledge was often part of the boatload, and could be used when ice was encountered. In areas where the waterways were blocked or not connected, the travelers would portage. Overland travel was most intense during the summer and covered the maximum territory because people were accessing distant trading centers.

Several of our informants spoke of traditional travel by boat along inland waterways, and informants still use larger, motorized boats along the sea coast and bays. When feasible, they will enter larger, deeper rivers to navigate to their summer camps. Thus, boats still provide a viable alternative for moving large amounts of supplies to inland sites. The *umiaq* is no longer used for inland travel, having been effectively replaced by ATVs in the snow-free period. Similarly, snowmachines have entirely replaced dog teams for spring and winter travel. However, whereas a snowmachine can pull a large sledge with supplies, the ATV remains largely a single-person transport unit. One strategy is for inhabitants to haul their goods to summer camps while the snow cover is still in place. More recently, we have noticed a disturbing trend of snowmachine use on the tundra after snowmelt.

Dramatic change to summer tundra travel was triggered by the introduction of motorized vehicles for personal use. Commercially-manufactured, one-passenger ATVs for personal use became common in northern Alaska during the 1960s. Before that time, overland vehicles such as Caterpillar tractors were used exclusively by industry and government due to the excessive cost.

The introduction of the ATV has caused long-term effects not only on the environment, but on the traditional culture of the North Slope communities as well. Hunters are now able to make longer journeys inland after game. These are not expeditions, but short-term hunting forays based on expediency or opportunity, and can be made by an individual traveling with light gear. The Iñupiaq people are no longer dependent on waterways, but instead have to navigate along high, dry ground and are forced to avoid the wettest, marshiest areas. Streams, the former transportation arteries of inland travel routes, are now obstacles.

Study Area and Methodology

The Arctic Coastal Plain of northern Alaska is a flat, low-lying region of tundra vegetation with numerous thaw lakes developed in ice-rich permafrost**.** Approximately 22% of the land area on the Barrow Peninsula north of ~71° latitude (which constitutes the area of study for this article) is covered with thaw lakes, and at least 50% is scarred by basins formerly occupied by lakes (Hinkel et al. 2003). In this cold maritime climate, the seasonal thaw zone (active layer) is typically less than 50 cm deep.

Over the past four years, our team has conducted extensive interviews with over 40 Iñupiaq elders and hunters from Barrow, Atqasuk, and Wainwright. These interviews have focused primarily, but not exclusively, on thaw-lake dynamics. We integrated interview methods to include unstructured talks (Bernard 2002) as well as semi-directive interviews (Huntington 2000, Fox 2002), a format which encourages informants to speak freely about their observations and knowledge of environmental changes. During videotaped interviews, informants located sites on detailed 2002 Landsat 7+ satellite images and USGS topographic maps. Afterwards, the interviews were logged and all sites located on maps were geocoded and entered into an ArcGIS database.

We also utilized 1:63,360 and 1:50,000 scale CIR aerial photography captured for the Barrow Peninsula in 1979 and 2005, respectively.

Analysis

Comparison of modern and traditional summer routes

The modern summer travel routes on the Barrow Peninsula identified by the majority of IK holders are shown in Figure 1. These closely coincide with the traditional trade routes mapped by Spencer (1959), shown in Figure 2. Both show two main trails extending southward from the traditional village of Barrow, and generally heading toward the Inaru River and Admiralty Bay. However, there are substantial changes that occurred over the half-century period.

The first modern summer travel route (Fig. 1: Route A) begins at Isatquaq Lagoon near the eastern end of the Wiley-Post Airport runway. It runs in a southerly direction along the banks of an existent lake (Iksrugagvik: I; Note that all letters and numbers within parentheses refer to figure labels). The trail, which mainly follows the course of the Avak River, crosses Iksrugagvik Creek beyond the lake at Maloney Bridge (M) which was constructed by Roy Nageak Sr. about ten years ago to enable ATVs to cross. The route continues eastward along the Avak River, going past several recently drained lake basins (Sikiluk—K—is one named) and then toward Iko Bay and associated inlets.

The second modern summer travel route (Fig. 1: Route B) is an important link between Barrow and inland settlements. It originates near Imaiqsaun Lake (also called Fresh Water Lake) slightly south of Barrow, and runs along the margin of Pinguatchaiq Lake (P) towards the Sungugruak Lake (S) complex. It passes to the east of the now drained Ikkalgugruaq Lake (G) and then splits toward either eastward to Iviksuq (V) or continuing north toward Puluyaaq (U), both important historic settlements. This demarcates the limit of the routes as specified by our informants, although some indicated that the eventual goal was access to Admiralty Bay.

Both traditional routes (Fig. 2; digitized from Spencer's 1959 map) joined a larger network of trade routes across

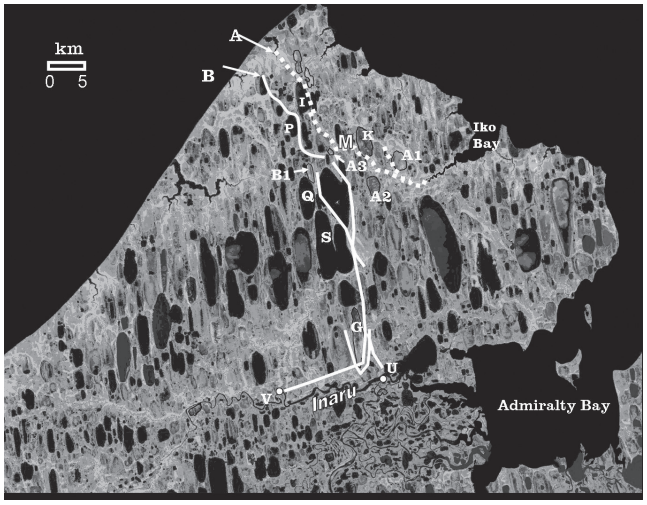

Figure 1. Modern summer travel routes A (dotted line) and B (solid line). Route information is superimposed on a 2002 Landsat 7+ satellite image within a GIS. Labels refer to place names and sites discussed in text.

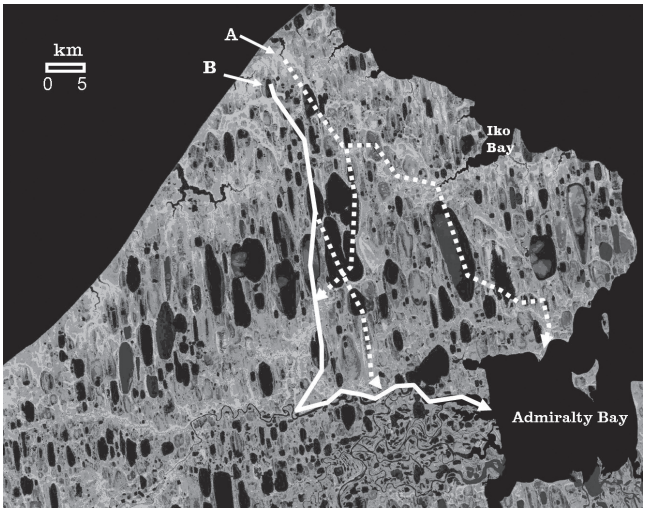

Figure 2. Traditional summer travel routes digitized from Spencer (1959).

northern Alaska and northwestern Canada. Beginning near Barrow, they utilize different streams and water bodies to eventually reach Admiralty Bay. From there, they traveled eastward to Lake Teshekpuk, and finally to the mouth of the Colville River, where there was an important trading center. Spencer (1959) noted that the people from Barrow took the inland fresh-water routes because often during the trading periods—early spring or fall—the sea ice posed too great an obstacle for safe travel along the coast of the Beaufort Sea. By contrast, the inland route through the rivers and lakes eventually arrived at Admiralty Bay, which was usually relatively ice-free at these times.

It is striking that the traditional route and the modern route are so similar, given the drastically different methods of conveyance. Modern routes are mainly used by hunters on ATVs and skirt around the lakes, often following raised shorelines. By contrast, the map by Spencer (1959) demonstrates traditional routes A and B taking full advantage of the lakes and streams for water passage. Several of our informants indicated that, in some places near Barrow, streams were artificially extended across shallow drainage divides to connect with nearby streams and thus reduce the number of portages.

We also compared these routes to those identified in a Minerals Management Service (MMS) survey report from 1987 (Tremont 1987). On the Barrow Peninsula, these routes coincide neither with our map nor with Spencer's traditional trading routes. The MMS map appears to follow waterways, but there is no indication as to whether these are river routes for boat traffic, ATVs trails, or even snowmachine trails.

Both the traditional and modern Route A (Figs. 1, 2) pass along the shores of three drained lake basins (Sikiluk (K), A1 and A2) that are shown as extant lakes prior to 1955. Interviewed Iñupiat noted that these lakes drained recently, although they were unable to specify the timing of these events. Another small basin (A3) was identified from satellite imagery as having drained between 1955 and 2002 (Hinkel et al. 2007). Route B passes along the margin of another drained lake basin (B1), identified by our informants on satellite imagery as having drained in the past 50 years. The southerly basin was formerly Ikkalgugruaq Lake (G) which drained in 1985 based on IK and satellite imagery. Lake drainage or changes in lake level would almost certainly necessitate changes in the route. One of the most experienced modern hunters in the Barrow area, Roy Nageak Sr. explained that he often chose the dry, flat shore on one side of the lakes as optimal for ATV travel.

Satellite imagery and aerial photography

The extent of permanent damage to the tundra from vehicular traffic is evident from the scars caused by vegetation disruption that are visible in aerial photography and high-resolution satellite imagery. We have examined the impacts on the area around Imaiqsaun Lake by using aerial photographs from 1979 and 2005 (Fig. 3). Because this lake was for many years an important source of fresh water for the Barrow community, there is a gravel road approaching it from the north that is visible on both photos. A seismic trail, dating to earlier times, can be seen to the far east in both photos. However, a very distinct ATV trail is apparent in the 2005 image. It departs from the gravel road going southeast, traveling along the dryer and elevated shoreline of an old drained lake basin. Eventually it converges with the traditional route as it follows the modern route B. We can detect the seismic trails in both the 1979 and 2005 photos, indicating visible damage persisting over 25 years. The impact of ATV use in the 2005 photo suggests recent and ongoing damage.

Modern routes are not absolutely fixed in space, and even traditional routes show deviations. This is especially true in the vicinity of Sungugruak Lake (S), where the narrow land bridge between Sungugruak and Qimuksiq Lake (Q) was breached around 1992. This narrow stretch of land was traditionally used as a corridor to access the hunting

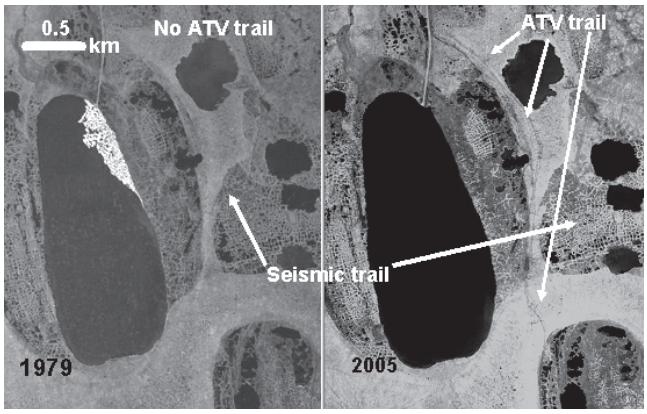

Figure 3. CIR aerial photography captured for the Barrow Peninsula showing ATV and seismic trails in 1979 (1:63,360) and 2005 (1:50,000).

and fishing cabins on the south side Sungugruak Lake. The Miller family of Barrow has a cabin on the south side of Lake Sungugruak; since the neck was breached in 1992, the family must travel a greater distance to reach their cabin (Donna Miller of Barrow in August, 2004 pers. comm.). The modern trails also diverge and converge as they approach cabins and popular hunting and fishing areas.

Discussion

The consequences of ATV usage on the culture and landscape of the Arctic Coastal Plain is profound. The inland regions have become increasingly accessible, but as more people travel the routes, they are subject to heavy vehicular traffic. This damages the vegetation, disrupts the protective organic mat, and destabilizes the underlying permafrost. Past researchers recognized and monitored the deleterious effects of motorized vehicles of all sorts on permafrost landscapes (Brown 1997, Lawson 1986, Nelson et al. 2003, Slaughter et al. 1990). They found that the long-term impacts depended to a large extent on the specific environmental setting: vegetation type and density, ice-content of permafrost, and soil type. The severity of impact also depended on the intensity of human use such as traffic frequency, vehicle weight and width, and even vehicle operation (Slaughter et al. 1990). A comprehensive study by Lawson (1986) emphasized that the ice content of the sediments, coupled with elevation and slope, were the most important factors in determining impact severity. Lawson (1986) also differentiated between the relative impacts of types of activities and their subsequent level of disturbance. Footpaths, even when they get heavy use, do not have the equivalent impact as off-road vehicles. Vehicle weight and the tearing effect of spinning, rough-studded tires are critical factors.

Repeated use by ATVs will eventually disrupt the surface vegetation to the extent that thermokarsting can occur. Depending on the topography of the landscape and the ice-content of the sediments, subsidence, melting wedge ice, slope instability, and lake drainage are a few of the possible outcomes.

Hunters that travel modern routes are cognizant of the environmental effects of ATVs and modern hunting practices, but feel they are caught in a double bind. In a recent interview, Roy Nageak Sr. (Barrow, August 2006 interview) said that the area around Maloney Bridge (Fig. 1, M) is getting swampier due to heavy traffic, and that he would soon be forced to move the bridge. Another hunter, Evelyn Donovan (Barrow, April 2006 interview) reported that the stream near the bridge is getting deeper, and expressed concern about the impact of increased traffic on the tundra. Roy explained that he sometimes "kicked himself" for building the bridge, since it facilitates ease of travel and focuses traffic along the route near the bridge, thus exacerbating damage to the tundra. He explained that the increased use was justified because of the rising cost of purchased food, giving the people of Barrow little choice but to depend to a greater extent on subsistence hunting. At the same time, the increase in gasoline prices has put pressure on hunters to economize by taking shorter routes. Whereas it used to take Roy more than half a day to get to the caribou hunting grounds on his ATV, by taking the bridge shortcut, he can reduce his travel time to an hour.

A recent study (Sonnenfeld 2002) showed an increase in disorientation and loss of geographic knowledge among the Iñupiat who travel on the North Slope. Although the study did not differentiate between summer and winter travel, nor did the author discuss the recent changes in transport mode as a factor in this disorientation, he did note how the loss of traditional knowledge has diluted the wayfinding ability of Iñupiat. During our own interviews, some informants were very outspoken in their concern that younger members of the community did not have the necessary skills to safely navigate in the tundra environment, especially in winter when the surface appears uniform (Thomas Itta Sr. Atqasuk, August 2004 interview). Further afield, Yup'ik Elders have voiced serious concerns about the inexperience of young people when it coincides with their increased travel through the tundra on ATVs and snowmachines (Bradley 2002). Again, during interviews in which we specifically asked about changes to the tundra, some informants expressed frustration at what they perceived as their own reduced knowledge of the landscape. They noted that, either they only went inland during the winter when the tundra was snow-covered and hence observed no changes, or else that they traveled through the landscape on their ATVs too quickly to notice any significant changes.

Concluding Remarks

There are a number of preventative and mitigation measures that have been recommended for addressing tundra disturbance due to ATV traffic. Residents and especially experienced hunters recognize that some terrain types are more resistant to disturbance, and therefore they may be interested in working with scientists to select routes which avoid sensitive areas (Slaughter et al. 1990). Regulation of ATV use may not be a realistic alternative, but the use of synthetic surface protection materials has been successful

in some areas. In a 2006 interview, Roy Nageak Sr. said that he recommended to the North Slope Borough that small portions of Route A be covered with a high-strength polymer ground stabilizing mesh. Use of this protective cover would have the dual advantage of directing traffic to a specific track, thus spatially restricting the damage, and stabilizing the vegetation and soil beneath the mesh. Ground stabilizing mesh is already being used in high-traffic areas within Barrow city limits, but is quite expensive.

The IK GIS enables us to compare earlier movements of peoples with current tundra usage and in assessing natural versus anthropogenic landscape change. By combining IK, information gathered from historic reports, and modern aerial photography, we are able to hypothesize causes for route modification or disappearance, and add a new perspective as to how human activities translate to the local landscape.

We can also observe how indigenous communities are adjusting to the impacts of landscape change and how they may be initiating or enhancing some of these changes themselves. Recently, we have noticed a somewhat alarming trend. Visible from the air are heavily traveled tracks across the tundra which extend from Barrow southward to near the Inaru River. The tracks are wide because the damage to the tundra causes local ponding, requiring users to shift to one side or the other. Further, conversations with local residents indicate that it is no longer uncommon for people to use snowmachines on the bare tundra in summer, especially in spring when heavy loads of goods are hauled to inland sites on attached sledges. The snowmachine track and sledge runners tear up the vegetation mat, and the large number of travelers exacerbates the damage. Concerned individuals have installed protective synthetic mats near traffic funneling points such as bridges, but this is a local and temporary solution. It is our hope that the information collected on routes and trail damage will enable community leaders to forecast how the landscape, travel routes, and access to resources will evolve in the future.

Acknowledgments

This work was supported by the National Science Foundation (NSF) under grants BCS-0548846, ARC-0539167, and OPP-0240174 to WRE. Any opinions, findings, conclusions, or recommendations expressed in this material are those of the authors and do not necessarily reflect the views of the NSF. Use of trade, product, or firm names is for descriptive purposes only and does not imply endorsement by the U.S. Government. We are grateful for logistical support from the Barrow Arctic Science Consortium and the Ukpeagvik Iñupiaq Corporation. We thank our Iñupiaq collaborators, especially Mr. Thomas Itta Sr. (deceased), Mrs. Flossie Itta, Mr. Roy Nageak Sr., Mr. Ron Brower Sr., and our translator and community liaison, Mrs. Lollie Hopson. The authors would like to thank Drs. Guido Grosse and William Manley for their very helpful reviews.

References

Bernard, H.R. 2002. *Research Methods in Anthropology*, 3rd Ed. Walnut Creek: Altimira Press.

Bradley, C. 2002. Traveling with Fred George: The Changing Ways of Yup'ik Star Navigation in Akiachak, Western Alaska. In: I. Krupnik & D. Jolly (Eds.), *The Earth is Faster Now: Indigenous Observations of Arctic Environmental Change*, Fairbanks, AK: Arctic Research Consortium of the United States, 241-264.

Brown, J. 1997. Disturbance and recovery of permafrost terrain. In: R.M. Crawford (Ed.), *Disturbance and Recovery in Arctic Lands: An Ecological Perspective*. Dordrecht: Kluwer Academic, 167-178.

Burch, E.S. Jr. 2005. Alliance and Conflict: The World System of the Iñupiaq Eskimos. Lincoln: University of Nebraska Press.

Fox, S. 2002. These things are really happening: Inuit perspectives on the evidence of climate change in Nunavut. In: I. Krupnik & D. Jolly (Eds.), *The Earth is Faster Now: Indigenous Observations of Arctic Environmental Change*, Fairbanks, AK: Arctic Research Consortium of the United States, 13-53.

Hinkel, K.M., Eisner, W.R., Bockheim, J.G., Nelson, F.E., Peterson, K.M. & Dia, X.Y. 2003. Spatial extent, age and carbon stocks of drained thaw lake basins on the Barrow Peninsula, Alaska. *Arctic, Antarctic, and Alpine Research* 35(3): 291-300.

Hinkel, K.M., Jones, B.M., Eisner, W.R , Cuomo, C.C, Beck, R.A. & Frohn, R. 2007. Methods to assess natural and anthropogenic thaw lake drainage on the western Arctic Coastal Plain of Northern Alaska. *Journal of Geophysical Research* 112: F02S16, doi:10.1029/2006JF000584.

Huntington, H.P. 2000. Using traditional ecological knowledge in science: Methods and applications. *Ecological Applications* 10: 1270-1274.

Lawson, D.E. 1986**.** Response of permafrost terrain to disturbance: A synthesis of observations from northern Alaska, USA**.** *Arctic and Alpine Research* 18: 1-17.

Nelson, F.E., Brigham, L., Hinkel, K.M., Parker, W., Romanovsky, V.E., Smith, O., Tucker, W. & Vinson, T. 2003. *Climate Change, Permafrost, and Impacts on Civil Infrastructure*. Special Report 01-03, Permafrost Task Force, U.S. Arctic Research Commission, Arlington, VA, 72 pp.

Slaughter, C.W., Racine, C.H., Walker, D.A., Johnson, L.A. & Abele, G. 1990. Use of off-road vehicles and mitigation of effects in Alaska permafrost environments: A review. *Environmental Management* 14(1): 63-72.

Sonnenfeld, J. 2002. Social dimensions of geographic disorientation in Arctic Alaska. *Etudes Inuit Studies* 26(2): 157-173

Spencer, R.F. 1959. *The North Alaskan Eskimo: A Study in Ecology and Society***.** Government Printing

Office, Smithsonian Institution, Bureau of American Ethnology, Bull. No. 171, 490 pp.

Tremont, J.D. 1987. *Surface Transportation Networks of the Alaskan North Slope*. OCS Report MMS 87-0010, Anchorage, Alaska: Minerals Management Service, 96 pp.

Permafrost in Iceland: Thermal State and Climate Change Impact

Bernd Etzelmüller
Department of Geosciences, University of Oslo
Thomas V. Schuler
Department of Geosciences, University of Oslo
Herman Farbrot
Department of Geosciences, University of Oslo
Águst Guðmundsson
Jardfrædistofan Geological Services, Reykjavik, Iceland

Abstract

This paper provides an overview of distribution and thermal characteristics of mountain permafrost in Iceland. Borehole temperature monitoring since summer 2004 and simple distribution modeling suggest widespread mountain permafrost in Iceland above 800 to 900 m a.s.l. The permafrost temperatures are close to 0ºC and some tens of meters thick in the elevation range of 800 to 1000 m a.s.l. At that elevation, the permafrost distribution is mainly governed by the distribution of snow, while above 1200 m a.s.l. smaller areas of continuous permafrost do exist. This presentation presents new borehole temperature data that have been collected until the summer 2007 and associated numerical modeling of snow influence on ground temperatures.

Keywords: ground temperatures; Iceland; modeling; permafrost.

Introduction

Within the context of climate-permafrost relationships in the North Atlantic region, Iceland represents a link between Scandinavia and Greenland. The regional distribution of permafrost in Iceland has been addressed by means of gridded mean annual air temperatures (MAAT) for the 1961–1990 period interpolated from point meteorological data (Etzelmüller et al. 2007) (Fig. 1). Etzelmüller et al. (2007) showed that MAAT~-3ºC gives an indication of the lower limit of widespread permafrost in Iceland, not regarding snow conditions or topographic aspect variability. Figure 1 suggests the presence of widespread mountain permafrost outside the already known sporadic permafrost zone in central Iceland. The lower limit increases in elevation towards the southeast, with elevations between 800 m a.s.l. in the north and more than 1000 a.s.l. in the southern part of Iceland. Permafrost is also predicted on the highest mountain peak areas along the southeastern coast above c. 900 m a.s.l. This paper presents new data series and modeling exercises to elaborate the influence of surface temperature and snow variation on permafrost temperatures in Iceland.

Setting

Iceland is located where the asthenospheric flow under the Mid-Atlantic Ridge interacts and mixes with a deep-seated mantle plume (Shen et al. 1998, Wolfe et al. 1997). This implies generally high geothermal heat fluxes due to heat conduction from the partly molten layer at approximately 10°-km depth (Flóvenz & Sæmundsson 1993). Iceland is characterized by maritime conditions with cool summers and mild winters. In the lowland areas, the MAAT for the 1961–1990 period was 4°–5°C in southern parts, 3°–4°C in the eastern and western parts, and 2°–3°C in northern, coastal parts of the country (Tveito et al. 2000). A large part of the precipitation falls with winds prevailing from eastern and southern directions (Einarsson 1984). Thus, mean annual precipitation increases from above 500 mm in the central and northern parts of the country to more than 3000 mm in the southeast.

In four boreholes, ground temperatures were monitored since 2004 (Farbrot et al. 2007) (Fig. 1). They are located in central and northeastern Iceland at ~890–930 m a.s.l. All boreholes are relatively shallow (12–22 m deep), penetrating through a shallow sediment cover into basaltic bedrock. All sites are on elevated plateaus, and significant slopes are more than 100 m away from the boreholes. The sites are not vegetated and are exposed to wind drift of snow.

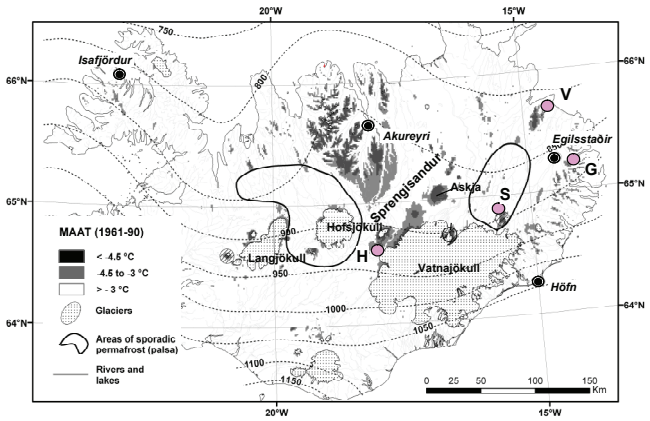

Figure 1: Key map and permafrost map of Iceland (based on Etzelmüller et al. 2007). G=Gagnheiði; S=Snæfell; V=Vopnafjörður; H=Hágöngur. The dotted contour lines indicate the lower limit of permafrost based on the distribution of MAAT~-3ºC.

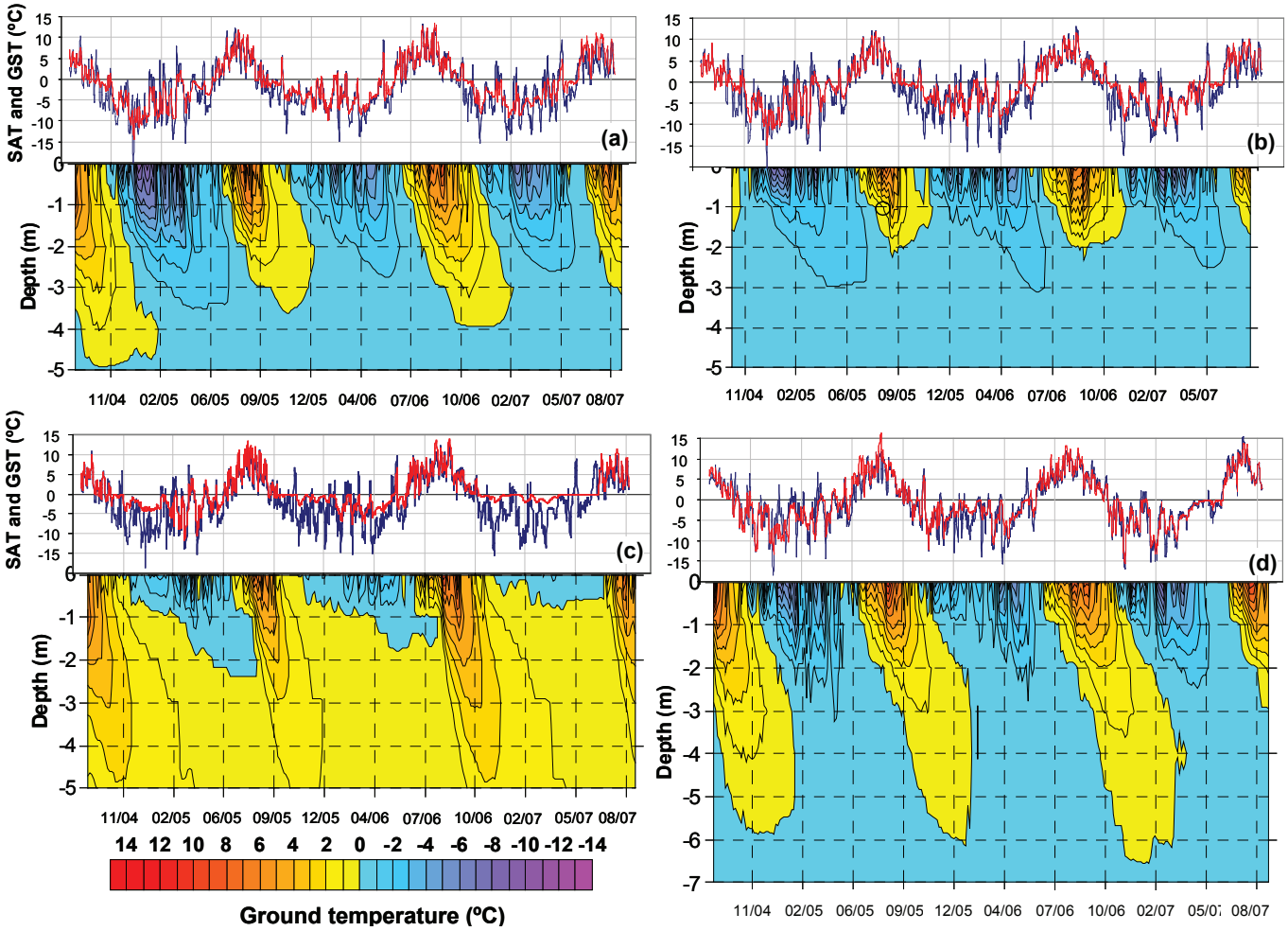

Figure 2: Depth-time series for air, surface, and ground temperatures at the four monitoring stations. The upper graph show SAT (surface air temperature) (blue) and GST (ground surface temperature) (Red) during the measurement period (August 2004 to August 2007). The lower diagram shows an interpolated depth-time series of ground temperatures. The contour interval is 1ºC, (**a**) Gagnheiði, (**b**) Snæfell, (**c**) Vopnafjörður, and (**d**) Hágöngur.

Methods and Results

Temperature monitoring and analysis

Instrumentation: All boreholes were initially equipped with UTL-1 miniature temperature dataloggers (MTDs) having an accuracy of ±0.27°C or better (cf., Hoelzle et al. 1999). In August 2005, the boreholes at Snæfell and Gagnheiði were equipped with thermistor chains consisting of 26 and 15 YSI S40006 thermistors, respectively. These thermistors have an absolute accuracy of ±0.05°C (Vonder Mühll 1992). Close to each borehole, single MTDs, measuring at intervals of 2 hours, were installed near the ground surface (i.e., at 1–5-cm depth) to record ground surface temperature (GST) and in radiation shields 1.5 m above ground to measure surface air temperatures (SAT). At Gagnheiði, the SAT from the meteorological station was used. Minor data gaps existed for air temperature measurements, which were filled in using linear regression to one of the other stations, usually with a $R^2>0.95$. More details of borehole location and characteristics are given in Farbrot et al. (2007).

Calculations: A set of parameters is calculated, representing an average over the three seasons reaching from September 1 to August 31 (Table 1). The frost number for air (F) and ground surface ($F+$) are calculated following Nelson and Outcalt (1987):

$$F = \sqrt{DDF_a} / \left(\sqrt{DDF_a} + \sqrt{DDT_a}\right) \quad (1)$$

and

$$F_+ = \sqrt{DDF_s} / \left(\sqrt{DDF_s} + \sqrt{DDT_s}\right) \quad (2)$$

where DDF are freezing degree days, DDT are thawing degree days and the indexes a and s refer to air and surface, respectively. The n-factors simply follow the equation

$n_T = DDT_s / DDT_a$ and $n_F = DDF_s / DDF_a$

for the freezing factor n_F and the thawing factor n_T, respectively, $TTOP$ (top of permafrost) temperatures are

estimated following, for example, Smith & Riseborough (2002):

$$TTOP = (r_K * n_T * DDT_a - n_F * DDF_a) / P \quad (3)$$

where P is the period (365 days) and r_K is the quotient between thermal conductivity of soil in thawed and frozen state, respectively. Values of thermal conductivity are taken from literature, with values varying between 1.7 and 1.9 $Wm^{-2}K^{-1}$ (Flóvenz & Sæmundsson 1993).

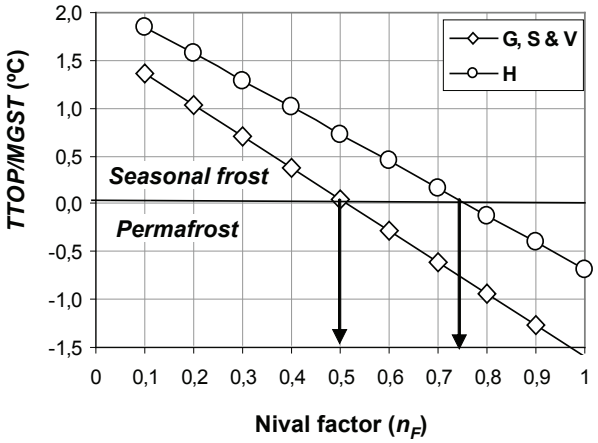

Figure 3: Modeled *TTOP* as a function of n_F, *G, S,* and *V* stands for Gagnheiði, Snæfell, and Vopnafjörður, respectively. For the three stations, it is assumed *DDF=1200* and *DDT=620* according to the last three seasons average (*MAT=-1.6ºC*), *H* stands for Hágöngur, assuming *DDF=1030* and *DD=780* (*MAT=-0.7ºC*), r_K*=1 and* n_T=1, as calculated from temperature measurements at the permafrost stations.

Results: The three records from Gagnheiði, Snæfell, and Vopnafjörður are highly correlated with respect to air temperatures with similar annual pattern, and have corresponding DDF_a and DDT_a values. Snæfell is slightly warmer than the two other stations (Table 1). However, ground temperatures are dissimilar (Fig. 2). The Vopnafjörður borehole has no permafrost and only shallow seasonal frost. The two others have permafrost, with *TTOP* temperatures above -0.5ºC. The active layer thickness was higher at Gagnheiði (3.5–4.5 m) than on Snæfell (~2 m), despite higher GST and SAT at the Snæfell station. This is due to higher water content at Snæfell, as discussed in Farbrot et al. (2007). The SAT at the Hágöngur station was slightly higher than the three others (0.7° to 0.8ºC); however, marginal permafrost is present, with an active layer thickness of ~5 m.

It is obvious that permafrost existence and temperatures are highly related to the snow cover at the stations. At the Vopnafjörður station the n_F-factor was at 0.5 or below, while all other stations showed n_F-values *>0.7*, up to *>0.9* (Hágöngur station). We have no recordings of snow cover thickness. All sites are wind-exposed, and thick snow accumulations are unlikely. According to Smith & Riseborough (2002) the obtained nival factors correspond to average snow depths of below 0.2 m, which is in accordance to winter observations at the field stations. No stations show persistent <0ºC winter temperatures, but numerous events of melting episodes throughout the season (Fig. 2). This has two effects: First, snow cover becomes isothermal even with low thicknesses because of latent heat release during refreezing, leading to lower n_F-factors. Second, snow cover decreases and occasionally disappears during these episodes, allowing

Table 1: Summary of temperature recordings at the four measurement stations calculated over three seasons. *SAT*= Mean surface air temperature. *GST* = mean ground surface temperature. *DDF* = freezing degree days. *DDT* = thawing degree days for air and surface (index *a* and *s*). n_T = thawing n-factor. n_F = freezing (nival) n-factor. *F* and *F+* are the frost number for air and surface. respectively. *TTOP* is *measured* mean temperature at the top of permafrost or the bottom of seasonal freezing.

Location	Period	SAT	GST	DDF_a	DDT_a	DDF_s	DDT_s	n_T	n_F	F	F+	TTOP
Vopna	2004/05	-1.7	0.1	1261.2	627.7	629.7	663.2	1.06	0.50	0.59	0.50	1.0
Vopna	2005/06	-1.6	0.4	1225.9	638.6	500.2	648.1	1.01	0.41	0.58	0.47	0.8
Vopna	2006/07	-1.4	1.1	1099.6	601.4	153.7	545.0	0.91	0.14	0.57	0.34	1.1
3-years average		***-1.6***	***0.5***	***1195.6***	***622.6***	***427.9***	***618.8***	***0.99***	***0.35***	***0.58***	***0.44***	***1.0***
Hágöng	2004/05	-0.6	-0.3	941.0	727.4	927.0	834.0	1.15	0.99	0.53	0.53	-0.2
Hágöng	2005/06	-1.1	-0.1	1109.5	706.4	784.0	751.9	1.06	0.71	0.56	0.51	-0.2
Hágöng	2006/07	-0.3	-0.1	1018.7	894.2	890.6	841.4	0.94	0.87	0.52	0.50	-0.1
3-years average		***-0.7***	***-0.2***	***1023.0***	***776.0***	***867.2***	***809.1***	***1.05***	***0.86***	***0.53***	***0.51***	***-0.2***
Gagn	2004/05	-1.6	-1.4	1164.9	601.8	1060.2	549.3	0.91	0.91	0.58	0.57	-0.15
Gagn	2005/06	-1.9	-0.9	1238.9	620.0	933.0	593.1	0.96	0.75	0.59	0.55	-0.15
Gagn	2006/07	-1.5	-0.5	1135.4	599.3	829.9	659.0	1.10	0.73	0.58	0.54	-0.1
3-years average		***-1.6***	***-0.9***	***1179.7***	***607.0***	***941.0***	***600.5***	***0.99***	***0.80***	***0.58***	***0.55***	***-0.1***
Snæfell	2004/05	-1.5	-0.9	1232.1	690.9	952.1	622.3	0.90	0.77	0.57	0.54	
Snæfell	2005/06	-1.6	-0.8	1252.9	655.9	870.7	570.5	0.87	0.69	0.58	0.54	-0.55
Snæfell	2006/07	-1.4	-0.5	1112.9	591.8	826.9	628.1	1.06	0.74	0.58	0.54	-0.55
3-years average		***-1.5***	***-0.8***	***1199.3***	***646.2***	***883.2***	***607.0***	***0.94***	***0.74***	***0.58***	***0.54***	***-0.55***

subsequent cold penetration, resulting in higher n_F-factors. This is especially obvious at the Vopnafjörður station, where deep seasonal frost could develop late in the 2004/05 season after a strong melting episode. The Hágöngur station showed less strong melting episodes. At the Vopnafjörður station, temperature decreases with depth with values <0.4ºC at -20 m. This indicates possibly relic permafrost below 25 m or so (cf. Etzelmüller et al. 2007, Farbrot et al. 2007).

Simple TTOP modeling following Equations (1) and (2) indicate that at the three stations of Vopnafjörður, Gagnheiði, and Snæfell, permafrost persists above a nival factor of n_F >0.5, while the Hágöngur station would produce positive "TTOP" with n_F-factors <0.75 (Fig. 3), showing virtually no snow during the winter season. Etzelmüller et al. (2007) proposed a limit of *MAAT=-3ºC* (normal period 1961–1990) for the lower limit of widespread permafrost in Iceland and Scandinavia. Theoretical considerations based on the TTOP model indicate a minimum n_F-factor of ~0.3 for TTOP <0 and MAAT=-3ºC. Since temperatures during the normal period 1961–1990 were about 1º to 2ºC lower than during our study (Farbrot et al. 2007), the Vopnafjörður station possibly had permafrost during at least the major part of the last century. Measured TTOP temperatures were lowest on Snæfell, which seems to have the most stable permafrost (Table 1). The two other permafrost stations show TTOP-temperatures very close to 0ºC, and seem to be in a stage of degrading. When modeling TTOP temperatures according to Equation (3), the r_K values are close to unity, indicating mostly similar TTOP than GST. This is possibly because of water advection and the influence of unfrozen water content close to 0ºC.

Modeling of ground temperatures

To investigate the sensitivity of ground temperatures to changes in snow coverage, we employ a numerical 1-D heat conduction model. We use an n-factor approach to derive GST from SAT and change the values of n to represent situations of different snow coverage. Based on the results, we discuss possible changes that may have led to the recent deterioration of permafrost at Vopnafjörður

Heat-conduction modeling principles: A numerical 1-D model of heat conduction is used, which accounts for latent heat and is forced by annual, monthly or daily GST input values (cf. Farbrot et al. 2007). The model solves the heat conduction equations following:

$$\rho\, c\frac{\partial T}{\partial t} = -k\frac{\partial^2 T}{\partial z^2} \tag{4}$$

(e.g., Williams & Smith 1989). As boundary conditions, we prescribe time series of GST and the geothermal heat flux

$$Q_{geo} = -k \cdot \partial T / \partial z \tag{5}$$

at depth, Q_{geo} was sat to 0 for shallow modeling domains below 30 m. Values for Q_{geo} were obtained from Flóvenz & Sæmundsson (1993), and must be regarded as regionally applicable values rather than local estimates. The thermal properties of the ground are described in terms of density ρ, thermal conductivity *k* and heat capacity *c*. Typical values for Icelandic basalt were derived from the literature (Flóvenz & Sæmundsson, 1993). In our model, we consider the change of latent heat *L* due to phase changes of the pore water by describing a temperature-dependent heat capacity $c_{(T)}$. In a small temperature interval between T_1 (-0.1ºC) and T_2 (0ºC) around the freezing temperature, we add the effect of latent heat release to the heat capacity of the substrate c_0 (e.g., Wegmann et al. 1998).

$$c_{(T)} = c_0 + \frac{L}{(T_2 - T_1)} \tag{6}$$

Any effects of heat advection related to groundwater flow are neglected in this study. The heat conduction equation (Equation [4]) was discretized along the borehole depth using finite differences, and subsequently solved by applying the method of lines (Schiesser 1991).

Calibration run: For this study, the study sites of Vopnafjörður (no permfrost) and Gagnheiði (warm and shallow permafrost) were selected. The model was calibrated using measured ground temperatures, and the values of *w* (volumetric water content) and *k* were adjusted to match modeled and measured temperature distributions, annual amplitudes at a given depth, and modeled and measured thicknesses of the active layer (Fig. 4). Generally, the fit revealed R^2-values of *>0.9*. The model performance was lower during spring and fall, most probably due to advective processes which are not accounted for, or deficits of the modeling approach because of lacking prescription of important processes. Values for material properties are taken from literature. The calibration indicates relatively dry

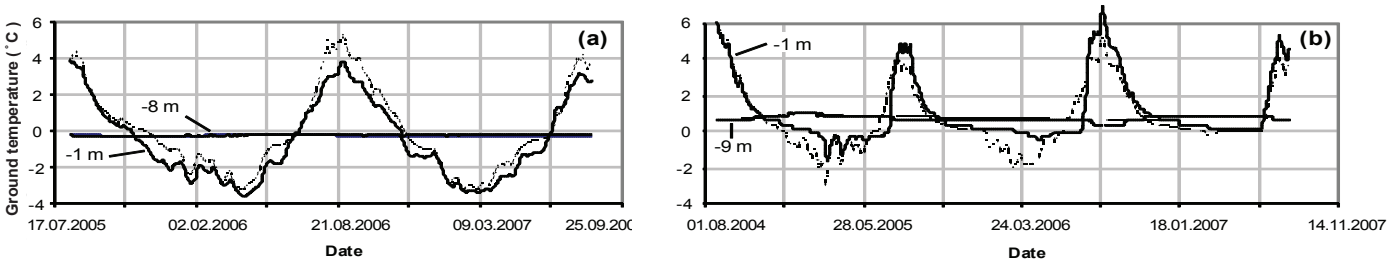

Figure 4: Examples of fit for modeled and measured ground temperatures in depth (8 and 9 m) and close to the surface (1 m). (a) Gagnheiði, (b) Vopnafjörður. Solid line is "modeled"; dashed line is "measured."

conditions at both sites, with volumetric water contents of below 5% (Farbrot et al. 2007).

Simulation run: To investigate the sensitivity of ground temperatures to changes in snow coverage, we use an n-factor linking GST to SAT and change the values of n_F to represent different situations. We prescribe SAT as a sinusoidal variation of specified amplitude around a specified annual mean temperature. Winter temperatures (defined as <0ºC) were damped using the n_F-factor.

Snow cover effect was simulated by changing n_F-factors, and SAT varies around a mean of *-1.6ºC* with amplitude of *9ºC* (Table 2). The n_F-factor was kept constant throughout the winter. For the Gagnheiði station, stable snow cover corresponding to n_F-factors <0.5 will lead to an almost instantaneous development of taliks. A smaller influence of snow coverage (n_F*>0.5)* is conserving the permafrost situation at Gagnheiði. This corresponds well with the TTOP analysis described previously, even if the TTOP approach produces errors especially close to 0ºC (Riseborough 2007). The same is valid for the Vopnafjörður station. Here, further warming of the ground is continued with n_F*<0.3,* while n_F*=0.4 to 0.6* results in a situation with no or very limited ground temperature trends, even after *40 years* of model run. This indicates that the measured n_F-factor (0.14) for the 2006/07 season at Vopnafjörður (Table 1) was exceptionally low. With n_F*=0.7* permafrost aggregates after 7 years of model run. This is also in rough correspondence to Figure 3

In a second simulation, we evaluated the impact of changing SAT on ground temperatures, assuming a constant snow cover like that observed during the three years of recent monitoring. We introduced a step change of ~1ºC warming for Gagnheiði (n_F*=0.7, MAT=-0.6ºC)* and cooling for Vopnafjörður station (n_F*=0.45, -2.8ºC)*. For the Gagnheiði station, a talik appears after c. 8 years, and permafrost is degraded within 50 years. This is roughly in accordance to the analysis shown in Farbrot et al. (2007). For the Vopnafjörður station the model produces permafrost after c. *15 a* with instant cooling to *-2.8 ºC* and a n_F*=0.45*. The air temperature value corresponds roughly to MAAT during the last normal period 1961–1990 in eastern Iceland close to 900 m a.s.l. After 50 years, permafrost is modeled to be approximately 10 m thick. This clearly demonstrates that permafrost at Vopnafjörður most probably has been degrading during the last decades, and that there might still be relic permafrost. It seems certain that the site had permafrost conditions during the Little Ice Age, since there is plenty of geomorphological evidence, such as rock-glaciers and well-developed patterned ground features.

Table 2: Simulation for varying snow conditions. The model was forced with a sinusoidal curve, with MAT of -1.6ºC and air temperature amplitude of 9ºC. AL=active layer depth; SF=seasonal frost depth after 20 years; GT=ground temperature; T=Tallilk, PF=permafrost. The initial ground temperatures were sat to the measured temperatures from 1.6.2007.

	Gagnheiði		**Vopnafjörður**			
n_F	GT response	AL (m)	GT response	SF (m)	AL (m)	PF thick after 20 a
0.1	T > 1 a		Warming	< 1.5		
0.2	T > 1 a		Warming	< 2		
0.3	T > 2 a		Warming	< 2.5		
0.4	T > 3 a		Stable (no PF)	< 3		
0.5	T > 12 a		Stable (no PF)	< 3.5		
0.6	Stable	> 5	Stable (no PF after 40 a)	< 4		
0.7	Stable	> 3.8	PF > 7 a		4.5	7 m
0.8	Stable	> 3.6	PF > 4 a		4	8 m
0.9	Stable	> 3.4	PF > 3 a		3.5	10 m

Summary and Conclusions

A three-year monitoring series of air and ground temperatures is presented for four permafrost stations in Iceland. Permafrost is warm, and in a degrading stage at two stations. At one, permafrost is absent, and this study indicates that permafrost may have existed at this station during some part of the last century. Snow is the decisive factor for permafrost distribution in elevation ranges between 800 m and 1000 m a.s.l. in Iceland, which corresponds to MAAT during the last normal (1961–1990) period of around *-3ºC*. A n_F *>0.6* seems necessary to keep permafrost stable in the elevation ranges below 1000 m a.s.l. in Iceland. The study demonstrates the sensitivity of ground temperatures to small changes in air temperatures and snow cover in the maritime mountains of Iceland. As ground temperatures are major decisive factors for understanding a suite of geomorphological processes, the understanding of the impact of expected climate warming on this environment is crucial.

Acknowledgments

This study was financed by the Norwegian Research Council (project 157837/V30). Jardfrædistofan Geological Services, Reykjavik, Iceland, and the Department of Geosciences, University of Oslo, Norway. The paper was certainly improved by the helpful comments by two anonymous reviewers. We want to thank all mentioned persons and institutions.

References

Einarsson, M.Á. 1984. Climate of Iceland. In: H. Van Loon (Editor), Climate of the oceans: World survey of climatology. Elsevier Science Publishers, pp. 673-698.

Etzelmüller, B. et al. 2007. The regional distribution of mountain permafrost in Iceland. *Permafrost and Periglacial Processes* 18(2): 185-199.

Farbrot, H. et al. 2007. Thermal characteristics and impact of climate change on mountain permafrost in Iceland. *Journal of Geophysical Research* 112: F03S90, doi:10.1029/2006JF000541.

Flóvenz, O.G. & Sæmundsson, K. 1993. Heat flow and geothermal processes in Iceland. *Tectonophysics* 225: 123-138.

Hoelzle, M., Wegmann, M. & Krummenacher, B. 1999. Miniature temperature dataloggers for mapping and monitoring of permafrost in high mountain areas: First experience from the Swiss Alps. *Permafrost and Periglacial Processes* 10(2): 113-124.

Nelson, F.E. & Outcalt, S.I. 1987. A Computational method for prediction and regionalization of permafrost. *Arctic and Alpine Research* 19(3): 279-288.

Riseborough, D. 2007. The effect of transient conditions on an equilibrium permafrost-climate model. *Permafrost and Periglacial Processes* 18(1): 21-32.

Schiesser, W.E. 1991. The numerical method of lines: integration of partial differential equations. Academic Press, San Diego, CA, USA, 326 pp.

Shen, Y., Solomon, S.C., Bjarnason, I.T. & Wolfe, C.J. 1998. Seismic evidence for a lower-mantle origin of the Iceland plume. *Nature* 395(6697): 62-65.

Smith, M.W. & Riseborough, D.W. 2002. Climate and the limits of permafrost: A zonal analysis. *Permafrost and Periglacial Processes* 13(1): 1-15.

Tveito, O.E. et al. 2000. Nordic temperature maps. Report No. 09/00, DNMI, Oslo.

Vonder Mühll, D. 1992. Evidence of intrapermafrost groundwater flow beneath an active rock glacier in the Swiss Alps. *Permafrost and Periglacial Processes* 3(2): 169-173.

Wegmann, M., Gudmundsson, G.H. & Haeberli, W. 1998. Permafrost changes in rock walls and the retreat of alpine glaciers: A thermal modelling approach. *Permafrost and Periglacial Processes* 9: 23-33.

Williams, P.J. & Smith, M.W. 1989. The frozen Earth: Fundamentals of geocryology. Cambridge University press, Cambridge, 300 pp.

Wolfe, C.J., Bjarnason, I.T., VanDecar, J.C. & Solomon, S.C. 1997. Seismic structure of the Iceland mantle plume. *Nature* 385(6613): 245-247.

Present and Past Distribution of Mountain Permafrost in the Gaissane Mountains, Northern Norway

Herman Farbrot
Department of Geosciences, University of Oslo and Norwegian Meteorological Institute, Norway
Ketil Isaksen
Norwegian Meteorological Institute, Norway
Bernd Etzelmüller
Department of Geosciences, University of Oslo, Norway

Abstract

The Gaissane Mountains, situated in northern Norway, reach elevations above 1000 m a.s.l. Our study area contains a range of active and relict periglacial features as well as numerous landforms related to the Pleistocene ice sheet. The distribution of permafrost in the mountains has been investigated through basal temperature of snow (BTS) measurements, continuous ground surface temperature (GST) measurements, and electrical resistivity tomography. Solar radiation and the presence or absence of coarse blocks are the two main factors controlling the thermal regime of regularly snow-covered ground. At fairly snow-free sites, the investigations indicate that mountain permafrost is common in the area above 350–450 m a.s.l. On the summits, about 1000 m a.s.l., geomorphic evidence combined with GST measurements suggest that the permafrost probably shows great antiquity, possibly prevailing since the last interglaciation.

Keywords: Gaissane Mountains; palaeopermafrost; permafrost mapping.

Introduction

In southern Norway, the lower regional altitudinal limit of mountain permafrost decreases eastwards with increasing continentality. The investigated sites in southern Norway have in common that the BTS variance to a great extent is explained by elevation, whereas the effect of solar radiation is secondary (Etzelmüller et al. 2003). Although Reusch (1901) a century ago recognized permafrost as a common phenomenon at high altitudes in northern Norway, few quantitative studies on mountain permafrost have been conducted in this area. Rather most investigations have focused on periglacial geomorphology and in particular palsas (Isaksen et al. 2008 and references therein). Gridded mean annual air temperature (MAAT) maps, however, indicate a similar altitudinal gradient for discontinuous permafrost limits also in northern Norway, decreasing from over 1000 m a.s.l. in coastal sites down to below 400 m a.s.l. in interior, more continental areas (Etzelmüller et al. 2008, Isaksen et al. 2008).

The aim of this study is to investigate occurrences of mountain permafrost in the Gaissane Mountains, northern Norway, by using measurements of ground surface temperature (BTS and Miniature Temperature Dataloggers [MTDs]) and electrical resistivity tomography (ERT). The factors controlling the distribution of permafrost are discussed. In addition, the distribution of paleopermafrost is briefly discussed based on geomorphic mapping.

Setting

The Gaissane Mountains are situated southwest of the Varanger Peninsula (70°N, 25°E) in the county of Finnmark, northern Norway (Fig. 1). The mountains reach elevations above 1000 m a.s.l. Western and southwestern parts of Norway are mostly influenced by western, Atlantic air flows bringing unstable weather patterns with high winter temperatures and moist air, whereas eastern parts of northern Norway are frequently dominated by Eurasian high-pressure systems involving stable air with high summer temperatures and low winter temperatures for long periods of time (Johannessen 1970). The official weather station closest to the field area is Banak (5 m a.s.l.), 20 km to the north. There, MAAT

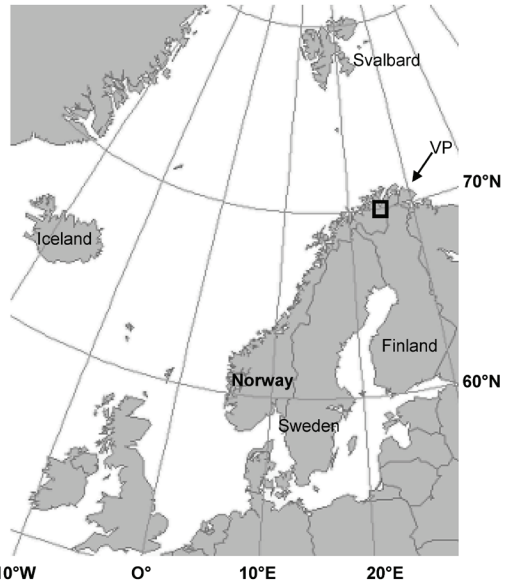

Figure 1. The Gaissane Mountains are situated in northern Norway, southwest of the Varanger Peninsula (VP).

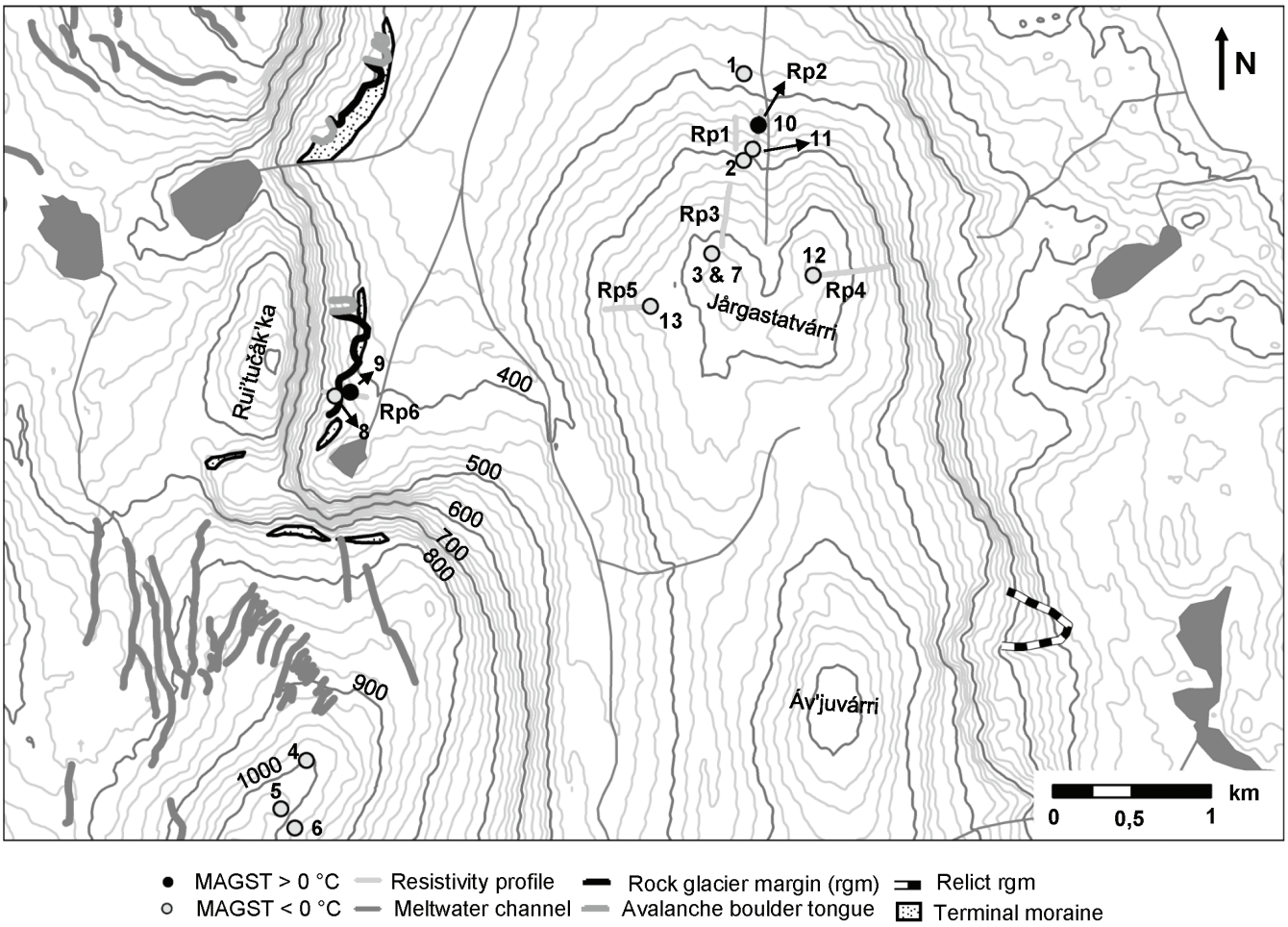

Figure 2. Map of the field area in Gaissane Mountains containing the positions of the ERT profiles (Rp1-6), MTDs and some geomorphic features. Letters refer to the MTDs in Table 1. The westernmost rock glaciers partly cover morainic ridges of presumable Preboreal age (Kellerer-Pirklbauer 2008).

(1961–1990) is 0.6°C and mean annual precipitation 345 mm. The winds are strong during winter, and above the forest line (250–300 m a.s.l.) extensive snow cover is commonly restricted to depressions.

The field area contains a range of active and relict periglacial features including rock glaciers, solifluction lobes, ploughing boulders, and patterned ground, as well as numerous landforms related to the Scandinavian ice sheet. The field area is situated well inside the glacial limit of the Younger Dryas ice; however, the summits were nunataks at that time (Marthinussen 1960).

Methods and Results

MTDs

13 UTL-1 MTDs were used during the period 2003–2006, 12 measuring ground surface temperatures and one measuring air temperature (Fig. 2, Table 1). The thermistors have a temperature range of −29° to +39°C, and the accuracy of the sensors are ±0.27°C (Hoelzle et al. 1999). The MTD data is probably not representative for long-term ground surface temperature conditions, since the observational period was characterized by considerably higher air temperatures than normal (1961–1990). By correlating the daily ground surface means with daily air temperature means from the weather station at Banak, a simple linear regression model was established. Using MAAT from Banak as independent variable, mean annual ground surface temperatures (MAGSTs) for the normal period 1961–1990 were estimated for the MTD sites. For these estimates to be reliable, we only used data from more or less snow-free sites, as indicated by the existence of high-frequency temperature fluctuations during winter (MTDs 1, 3-5, 8-13). The assumption is, thus, that these areas also remained snow free during the normal period 1961–1990 (cf., Farbrot et al. 2007). In general, a R^2 of > 0.70 (for all records: $p << 0.001$) was achieved in these analyses. Fitting a linear trend line through the estimated MAGST from the MTD sites indicate that the MAGST 0°C-isotherm of fairly snow-free sites is found at ~350 m a.s.l.

One year of air temperature measurements at an elevation of 614 m a.s.l. (MTD 7) combined with corresponding measurements from Banak weather station (5 m a.s.l.) reveal a mean altitudinal lapse rate of ~ -0.005°C m^{-1}. This fits well with investigations by Laaksonen (1976) indicating a similar mean vertical temperature gradient for Fennoscandia and in particular other investigations from northern Norway indicating comparable lapse rates (Isaksen et al., in prep.).

Table 1. Measured and estimated ground surface and air temperatures at the MTD sites in the Gaissane Mountains. MTD 10–13 were operating less than a year, but have been used for estimation of MAGST. MGST = Mean ground surface temperature, FDD = freezing degree days, TDD = Thawing degree days, MAAT = Mean annual air temperature, MAGST = Mean annual ground surface temperature, N = number of values in the statistical analyses, R^2 = Goodness-of-fit of a straight line fitted by least squares to the points.

	1	2	3	4	5	6	7 (Air)	8	9	10	11	12	13
Elevation (m a.s.l.)	389	508	614	1002	1034	982	614	471	428	433	487	643	593
MGST 03-04 (°C)	-	0.5	-1.1	-2.7	-2.8	-0.5	-	-	-	-	-	-	-
FDD 03-04	-	748	1379	1620	1692	783	-	-	-	-	-	-	-
TDD 03-04	-	942	977	634	683	597	-	-	-	-	-	-	-
MGST 04-05 (°C)	-	0.8	-0.9	-2.2	-2.4	-2.1	-0.9 (air)	0.3	1.3	-	-	-	-
FDD 04-05	-	679	1327	1501	1600	1211	1381	917	830	-	-	-	-
TDD 04-05	-	957	988	705	729	429	1048	1010	1291	-	-	-	-
MGST 05-06 (°C)	-	0.5	-0.8	-2.4	-2.4	-1.4	-	0.1	1.4	-	-	-	-
FDD 05-06	-	789	1254	1456	1439	1075	-	998	841	-	-	-	-
TDD 05-06	-	965	976	594	549	577	-	1051	1334	-	-	-	-
Est. MAGST (°C)	-0.4	-	-2.2	-3.5	-3.6	-	-	-0.8	0.2	0.4	-1.1	-1.6	-1.7
N	313	1039	1039	1039	1039	1039	398	725	725	336	336	333	335
R^2	0.853	-	0.887	0.812	0.788	-	0.895	0.804	0.884	0.705	0.887	0.913	0.892
Est. MAAT (°C)	-1.3	-1.9	-2.5	-4.1	-4.5	-4.3	-2.5	-1.8	-1.7	-1.5	-1.7	-2.6	-2.3
Est. surface offset (°C)	0.9	-	0.3	0.6	1.0	-	-	0.9	1.9	1.9	0.5	1.0	0.6

Hence, the measured mean lapse rate is assumed fairly representative for the 1961–1990 period, and, thus, MAATs for this period can be estimated for the MTD sites (Table 1), thereby enabling estimates of the surface offset (i.e., MAGST–MAAT). Surface offsets are mainly less than 1°C at dry sites without pronounced snow cover (Table 1). This fits with investigations from southern and northern Norway (Isaksen et al. 2007, 2008) and Iceland (Farbrot et al. 2007). From this approach, permafrost should
be common at locations with thin or no snow cover above the elevation of the –1°C-isotherm. Using the assumed mean altitudinal lapse rate of –0.005°C m^{-1}, the –1°C-isotherm is found at ~330 m a.s.l. in the field area.

BTS

Basal temperature of snow (BTS) measurements involve measuring temperatures at the bottom of the snow cover when the temperatures have stabilized before onset of melting. Under a thick, dry snow cover (>0.8–1.0 m) the ground surface temperature is mainly controlled by heat conduction from the subsurface, thereby reflecting the thermal regime of the ground. Permafrost is considered probable if BTS values <–3°C, possible if values are between –2° and –3 °C and improbable if values > –2°C (Haeberli 1973).

Table 2. Parametric (Pearsons r) correlation matrix for BTS as dependent variable and selected topographic attributes and presence and absence of coarse blocks at the ground surface expressed as a dummy variable. PR = Potential radiation, N = 163.

	Elevation	PR	Coarse blocks	Snow depth	Wetness index
BTS	-0.065	0.445*	-0.604*	0.289*	0.092

* Correlation is significant at the 0.01 level (2-tailed)

In March 2004, February 2005, and February 2006, a total of 334 BTS measurements were obtained. The measuring points' topographical characteristics such as elevation, slope, and aspect were estimated from a DEM with 25 m grid spacing (© Statens Kartverk). Further, the annual potential solar radiation (PR) was estimated based on the SRAD topographic model (Wilson & Gallant 2000). A potential topographic wetness index—defined as the quotient of the specific upstream area and the surface slope—was estimated based on Beven & Kirkby (1979). In addition, the surficial material type (presence or absence of coarse blocks) was recorded at each measuring

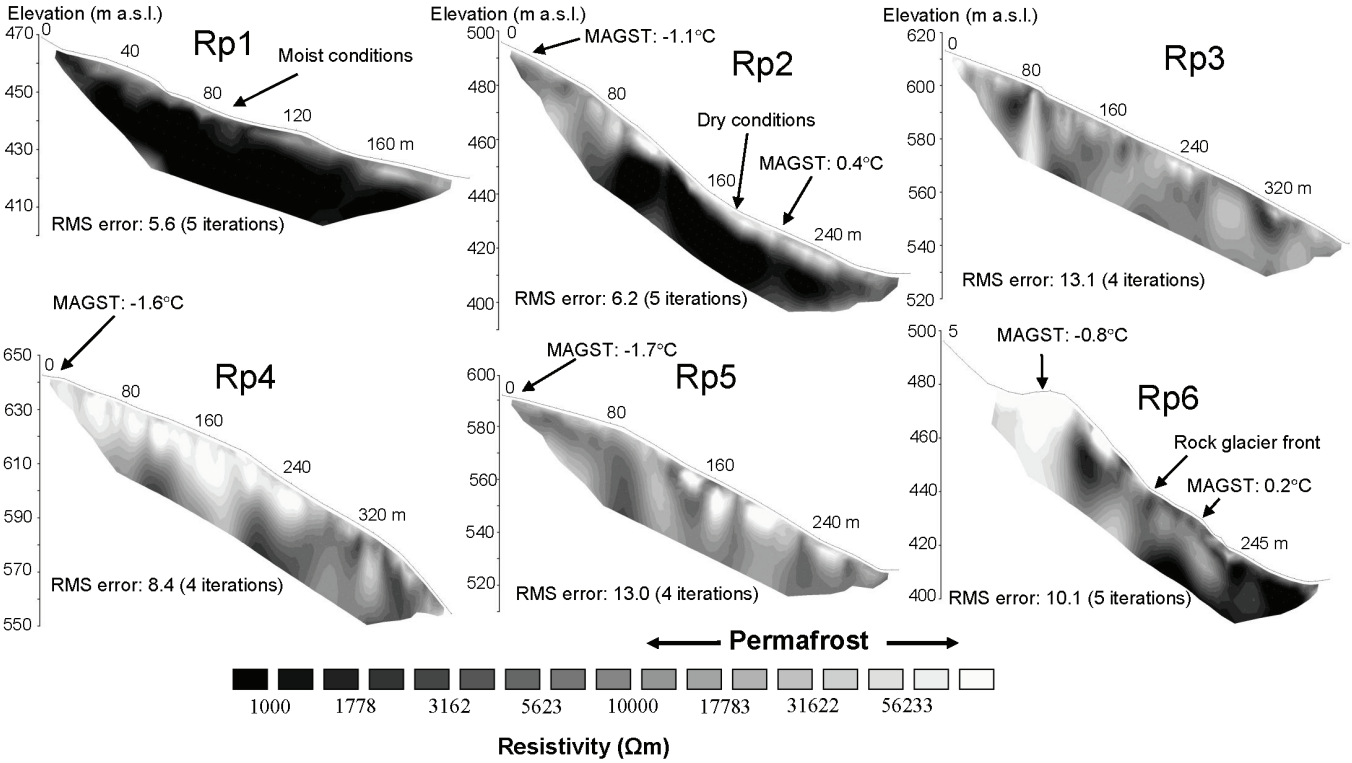

Figure 3. ERT profiles obtained in the Gaissane Mountains (for location, see Fig. 2). There is an overall increase in resistivity with elevation. The profiles indicate permafrost at elevations >450 m a.s.l., which corresponds well with estimated MAGSTs along the profiles.

site. Mean values were computed within diameters ≤10 m with consistent topographical and ground surface characteristics to try to overcome the problem of micro-scale variability and spatially clustered data (cf., Brenning et al. 2005), and these means (N=163) were used in the further analyses. From the correlation analysis, it is evident that PR and the presence or absence of coarse blocks, expressed as a dummy variable (1 means coarse material is present; 0 means coarse material is absent), are the major factors controlling BTS (Table 2). Mean BTS value for sites with coarse blocks is ~2.2°C lower than for sites without. However, the coarse-grained sites reveal less PR than the fine-grained sites. This effect is excluded by subtracting the assumed effect of lower PR on BTS values from the linear regression, thereby indicating that the effect of coarse blocks lowers the mean BTS value with 1.6°C. A linear regression model with the presence or absence of coarse blocks and PR as independent variables, explains 65% of the BTS variability. No significant correlation was found between BTS and elevation (at the 0.01 level [2-tailed]). Correlation between BTS and snow depth is significant but weak.

Electrical resistivity tomography

Electrical resistivity tomography (ERT) measurements are conducted by inserting an electrical current into the ground via two current electrodes. The resulting electrical potential between two other electrodes is measured, and from these measurements the true resistivity of the ground can be estimated. The existence of ice in the ground increases the resistivity markedly since the resistivity of ice is several orders of magnitude higher than water. Thus, resistivity measurements are highly valuable for detecting and characterizing ice-bearing permafrost (e.g,. Hauck & Vonder Mühll 2003). Six two-dimensional ERT profiles have been obtained in the field area (Fig. 3). Resistivity profile 1 (Rp1) is the lowermost profile (~400 m a.s.l.) across presumably permafrost free ground as indicated by BTS measurements. Hence, this profile presumably represents bedrock resistivities, thereby indicating that resistivity values >10 000 Ωm can serve as a conservative estimate for permafrost. This assumption corresponds well with the MTD measurements (Fig. 3). Generally, there is an overall increase in resistivity with elevation, and the profiles indicate permafrost above ~450 m a.s.l. Furthermore, Rp 6, a longitudinal profile along a rock glacier, indicates ice rich subsurface conditions within the rock glacier, although the possibility of air-filled cavities causing the high-resistive zone can not be excluded from the ERT measurements solely (cf., Hauck et al. 2004).

Discussion

BTS variability

The BTS measurements indicate that solar radiation and the presence or absence of coarse blocks are the two main factors controlling the thermal regime at snow covered sites (Table 2). The influence of PR is greater than what is found in southern Norway where ground thermal regime is highly correlated with elevation and to a lesser extent PR (Isaksen et al. 2002, Heggem et al. 2005). This difference seems plausible

as the solar height is lower in northern Norway.

The occurrence of openwork blocky debris in the field area is clearly a cooling factor for ground surface temperatures. Similar results have been found in a range of studies (e.g., Harris & Pedersen 1998), and recently in southeastern Norway (Juliussen & Humlum 2007). This is presumably due to air circulation within the voids, which was indicated by several observations of air ventilation funnels through the snow cover in wintertime.

The lack of significant correlation between BTS and elevation probably reflects that the BTS points are mainly scattered between 300 and 600 m a.s.l., and a greater elevation span would have increased the correlation (cf., Brenning et al. 2005), as obtained for the MTDs. The mentioned elevation range obviously shows large snow cover, soil moisture and vegetation cover variations, covering the elevation signal in the statistical analysis (cf., Isaksen et al. 2002).

Present permafrost distribution

No borehole temperature measurements are available within the field area, so identification of mountain permafrost relies on indirect methods. Below the forest line of about 250–300 m a.s.l., winter snow cover is fairly extensively developed, so permafrost is presumably absent there due to the insulating effect of snow (cf., Johansson et al. 2006). The lowermost presumably active rock glaciers in the area have their margins at ~430 m a.s.l., and both BTS and ERT measurements indicate that these features contain permafrost at present.

The consistency of the independent indirect methods (Table 3) leads to the conclusion that mountain permafrost is common above 350–450 m a.s.l. As all BTS measurements rely on point measurements with a stable snow cover of a least 80 cm, this should imply that these points represent warmer ground conditions compared to areas with limited snow cover, due to the isolating effect of snow (cf., Jeckel 1988). Developed snow covers are limited in the field area due to low precipitation and strong winds. Thus, the aerial extent of permafrost is presumably greater than indicated by BTS measurements (cf., Sollid et al. 2003). The permafrost distribution pattern indicated fits generally well with Johansson et al. (2006), stating that permafrost is common in the tundra zone above the forest line in the Torneträsk region, northern Sweden. The pattern also agrees with investigations by King & Seppälä (1987) in north-western Finland which indicate a lower limit of discontinuous permafrost of 300–500 m a.s.l. based on geoelectrical soundings.

Past permafrost conditions

Several relict periglacial landforms in the field area point to a cooler environment in the past than at present. Such landforms include a rock glacier, terminating in the birch forest, with its fronts at 180 m a.s.l., presumably relict tundra polygons, ploughing boulders found in the birch forest, and extensive areas of vegetated patterned ground. The low-elevation rock glacier witnesses a past lower limit of permafrost at least 200 m below the present.

The past lower limit of mountain permafrost in the field area were obviously variable during the Holocene climate fluctuations (cf., Kukkonen & Šafanda 2001). However, on the summits of about 1000 m a.s.l., a different picture emerges. The blockfields of the summit areas show no signs of Holocene modification. The lateral meltwater channels eroded into the blockfields together with the terminal moraines found on top (cf., Marthinussen 1960) indicate a pre-Late Glacial Maximum age of the blockfield and subsequent survival underneath cold-based, non-erosive ice. This interpretation is supported by investigations of blockfields on the Varanger Peninsula (Fjellanger et al. 2006). According to Heikkilä & Seppä (2003) maximum annual air temperatures in Fennoscandia were approximately 1.5–2.0°C higher during the mid-Holocene thermal optimum (HTO) than the reconstructed mean temperature of the last 200 years. Assuming a roughly equal coupling between air and ground surface temperatures, sub-zero MAGST probably still occurred in the summit areas of about 1000 m a.s.l. during HTO. This is based on the assumption that the summits have prevailed bare-blown, with limited influence of changes in the Holocene wind and precipitation patterns. Thus, although warm periods have occurred during the Holocene, affecting thermal regime and the permafrost thickness, permafrost conditions have presumably prevailed in the summit areas. This is supported by numerical modelling of permafrost in bedrock in northern Fennoscandia during the Holocene by Kukkonen & Šafanda (2001). Hence, assuming cold-based ice in the summit areas at least during the last glaciation, permafrost at these elevations probably is of considerable age, potentially spanning the Weichselian.

Table 3. Elevation of different environmental parameters and permafrost limits indicated by different indirect approaches. See text for details.

Environmental parameter/ permafrost limit	Elevation (m a.s.l.)
Tree line	250-300
Blockfield limit	~800
BTS	?
Estimated MAGST	350
ERT measurements	~450
-1°C isotherm	330
Active rock glacier	430

Conclusions

Based on these investigations the following conclusions concerning mountain permafrost in the Gaissane Mountains seem supported:

- At present permafrost is common above 350–450 m a.s.l.
- Coarse, openwork blocks tend to reduce ground surface temperatures significantly.
- The permafrost in the summit areas at about 1000 m a.s.l. is of considerable age, possibly prevailing since the last interglaciation.

Acknowledgments

This study was financed by the Norwegian Research Council (project no. 157837/V30) and the Department of

Geosciences, University of Oslo. We also want to thank M. Avian, M.K. Bagge-Lund, J. Fjellanger, R. Frauenfelder, H. Juliussen, A. Kellerer-Pirklbauer, B. Larsen, and L. Sørbel who participated in the field work. Andreas Kellerer-Pirklbauer and Rune S. Ødegård reviewed an earlier version of the manuscript. We thank all individuals and institutions for their contributions.

References

Beven, K.J. & Kirkby, M.J. 1979. A physically-based, variable contributing area model of basin hydrology. *Hydrological Sciences Bulletin* 24: 43-69.

Brenning, A., Gruber, S. & Hoelzle, M. 2005. Sampling and statistical analyses of BTS measurements. *Permafrost and Periglacial Processes* 16: 383-393.

Etzelmüller, B., Berthling, I. & Sollid, J.L. 2003. Aspects and concepts on the geomorphological significance of Holocene permafrost in Southern Norway. *Geomorphology* 52: 87-104.

Etzelmüller, B. et al. 2008. Mapping and modelling the distribution of permafrost in the Nordic countries. *Proceedings of the Ninth International Conference on Permafrost, Fairbanks, Alaska, June 29–July 3, 2008* (this proceedings).

Farbrot, H. et al. 2007. Thermal characteristics and climate change impact of mountain permafrost in Iceland. *Journal of Geophysical Research* 112, doi:10.1029/2006JF000541.

Fjellanger, J., Sørbel, L., Linge, H., Brook, E.J., Raisbeck, G.M. & Yiou, F. 2006. Glacial survival of blockfields on the Varanger peninsula, northern Norway. *Geomorphology* 82: 255-272.

Haeberli, W. 1973. Die Basis Temperatur der winterlichen Schneedecke als möglicher Indikator für die Verbreitung von Permafrost. *Zeitschrift für Gletscherkunde und Glazialgeologie* 9: 221-227.

Harris, S.A. & Pedersen, D.E. 1998. Thermal regimes beneath coarse blocky material. *Permafrost and Periglacial Processes* 9: 107-120.

Hauck, C., Isaksen, K., Vonder Mühll, D. & Sollid, J.L. 2004. Geophysical surveys designed to delineate the altitudinal limit of mountain permafrost; an example from Jotunheimen, Norway. *Permafrost and Periglacial Processes* 15: 191-205.

Hauck, C. & Vonder Mühll, D. 2003. Inversion and interpretation of two-dimensional geoelectrical measurements for detecting permafrost in mountainous regions. *Permafrost and Periglacial Processes* 14: 305-318.

Heggem, E.S.F., Juliussen, H. & Etzelmüller, B. 2005. Mountain permafrost in Central-Eastern Norway. *Norsk Geografisk Tidskrift-Norwegian Journal of Geography* 59: 94-108.

Heikkilä, M. & Seppä, H. 2003. A 11,000 yr palaeotemperature reconstruction from the southern boreal zone in Finland. *Quarternary science reviews* 22: 541-554.

Hoelzle, M., Wegmann, M. & Krummenacher, B. 1999. Miniature temperature dataloggers for mapping and monitoring of permafrost in high mountain areas: First experience from the Swiss Alps. *Permafrost and Periglacial Processes* 10: 113-124.

Isaksen, K., Farbrot, H., Blikra, L.H., Johansen, B. Sollid, J.L. & Eiken, T. 2008. Five year ground surface temperature measurements in Finnmark, Northern Norway. *Proceedings of the Ninth International Conference on Permafrost, Fairbanks, Alaska, June 29–July 3, 2008* (this proceeedings).

Isaksen, K., Hauck, C., Gudevang, E., Ødegård, R.S. & Sollid, J.L. 2002. Mountain permafrost distribution on Dovrefjell and Jotunheimen, southern Norway, based on BTS and DC resistivity tomography data. *Norsk Gografisk Tidsskrift-Norwegian Journal of Geography* 56: 122-136.

Isaksen, K., Sollid, J.L., Holmlund, P. & Harris, C. 2007. Recent warming of mountain permafrost in Svalbard and Scandinavia. *Journal of Geophysical Research* 112, doi:10.1029/2006JF000522.

Jeckel, P.P. 1988. Permafrost and its altitudinal zonation in N. Lapland. In: K. Senneset (ed.), *Proceedings of the Fifth International Conference on Permafrost, 1988*: 170-175.

Johannessen, T.W. 1970. The climate of Scandinavia. In: C. C. Wallén (ed.), *Climates of Northern and Western Europe.* Amsterdam: Elsevier Publishing company, 23-80.

Johansson, M., Christensen, T.R., Åkerman, J.H. & Callaghan, T.V. 2006. What determines the current presence or absence of permafrost in the Torneträsk region, a sub-arctic landscape in northern Sweden? *Ambio* 35: 190-197.

Juliussen, H. & Humlum, O. 2007. Towards a TTOP ground temperature model for mountainous terrain in central-eastern Norway. *Permafrost and Periglacial Processes* 18: 161-184.

Kellerer-Pirklbauer, A. 2008. The Schmidt-hammer as a Relative Age Dating Method for Rock glacier Surfaces: Examples from Northern and Central Europe. *Proceedings of the Ninth International Conference on Permafrost, Fairbanks, Alaska, June 29–July 3, 2008* (this proceedings).

King, L. & Seppälä, M. 1987. Permafrost thickness and distribution in Finnish Lapland; results of geoelectric soundings. *Polarforschung* 57: 127-147.

Kukkonen, I.T. & Šafanda, J. 2001. Numerical modelling of permafrost in bedrock in northern Fennoscandia during the Holocene. *Global and Planetary Change* 29: 259-273.

Laaksonen, K. 1976. The dependence of mean air temperatures upon latitude and altitude in Fennoscandia (1921–50). *Ann. Academ. Scient. Fennicae A III* 119, 19 pp.

Marthinussen, M. 1960. Marginal substages and drainage during deglaciation in the Repparfjord-Stabbursdal area, western Finnmark (in Norwegian). *Norges Geologiske Undersøkelse* 213: 118-169.

Reusch, H. 1901. Some contributions towards an understanding of the manner in which the valleys and mountains of Norway were formed (in Norwegian). In: *NGU Yearbook 1900*. Kristiania: Norwegian Geological Survey, 124-263.

Sollid, J.L., Isaksen, K., Eiken, T. & Ødegård, R.S. 2003. The transition zone of mountain permafrost on Dovrefjell, southern Norway. *Proceedings of the Eighth International Conference on Permafrost, Zurich, Switzerland*: 1085-1089.

Wilson, J.P. & Gallant, J.C. (eds). 2000. *Terrain analysis: Principles and applications*. New York: John Wiley & Sons, 512 pp.

Recent Changes in Ground Temperature and the Effect on Permafrost Landscapes in Central Yakutia

A.N. Fedorov
Melnikov Permafrost Institute SB RAS, Yakutsk, Russia
P.Y. Konstantinov
Melnikov Permafrost Institute SB RAS, Yakutsk, Russia

Abstract

The main objective of this paper is to determine the state of permafrost landscapes in Central Yakutia under recent climate change. Air and ground temperature data from monitoring sites of the Melnikov Permafrost Institute and records from weather stations at Yakutsk, Churapcha, and Pokrovsk are used. Analysis of the data indicates that the Pokrovsk records are most suitable for evaluating long-term ground temperature variations in Central Yakutia. A good correlation has been found between the data from monitoring sites and the Pokrovsk weather station. During the last several decades, major increases in ground temperature occurred in the early to mid 1980s and the early 1990s. At present, some cooling of ground temperature is observed, although air temperature shows an increasing trend. However, there is a high risk for active development of cryogenic processes in forest-free areas that can cause permafrost degradation and terrain disturbance. Thermokarst is actively developing in some areas of Central Yakutia. Disturbed landscapes, primarily the deforested anthropogenic complexes affected by agriculture, tree removal, or burning, are most sensitive under the current climate change.

Keywords: climate change; cryogenic process; ground temperature; permafrost landscape; thermokarst.

Introduction

Ground temperature is an important cryoecological characteristic of permafrost-affected landscapes. Its influence on the state and dynamics of permafrost landscape is difficult to overestimate. Analyses of the recent data from thermal monitoring sites in Central Yakutia are presented in the Russian permafrost literature (Skryabin et al. 1998, Varlamov et al. 2002, Pavlov 2003, Konstantinov et al. 2006, Pavlov & Malkova 2005, and others). These studies document ground temperature and thaw depth variability and indicate that ground temperatures show both an increasing and decreasing trend in the region where air temperatures are increasing. However, observations at monitoring sites are too short and do not provide sufficient information to evaluate long-term trends in natural processes. Direct field observations of the ground temperature regime in Central Yakutia are available only for the period since 1980.

Weather station records have to be used, therefore, in order to understand the long-term dynamics of ground temperatures. Vasiliev & Torgovkin (1996), Gilichinsky et al. (2000), and Romanovsky et al. (2007) analyzed ground temperature records from Yakutian weather stations for various depths and various periods and determined trends. Most weather stations in Central Yakutia demonstrate a strong increasing trend in ground temperature. Vasiliev & Torgovkin (1996) examined the period 1967-1992 when the largest increase in air temperature was observed in Central Yakutia. The period 1951-1996 was analyzed in Gilichinsky et al. (2000) and the value of this work is in comparing temperature trends in different regions of the Russian permafrost zone. Romanovsky et al. (2007) calculated trends in ground temperature at 1.6 m depth along the Tiksi-Yakutsk-Nagorny transect in Yakutia. The authors analyzed the spatial variability of ground temperatures and found that temperatures were increasing at some sites and decreasing at others during the period from 1956 to 1990.

The paper discusses the results of long-term observations on permafrost terrain dynamics at the Yukechi, Neleger, Spasskaya Pad, and Umaibyt sites near Yakutsk, and the variations in meteorological elements based on Yakutsk and Pokrovsk weather station records (Fig. 1).

The main objective of this paper is to determine the state of permafrost landscapes in Central Yakutia under recent climate change. Retrospective analysis of ground temperatures provides a basis for assessing changes in the thermal state of cryogenic landscapes. However many factors make such assessment difficult, such as the differences in soil conditions between weather stations, the inhomogeneities in data records due to relocation, and the indirect effects of anthropogenic disturbance of surrounding

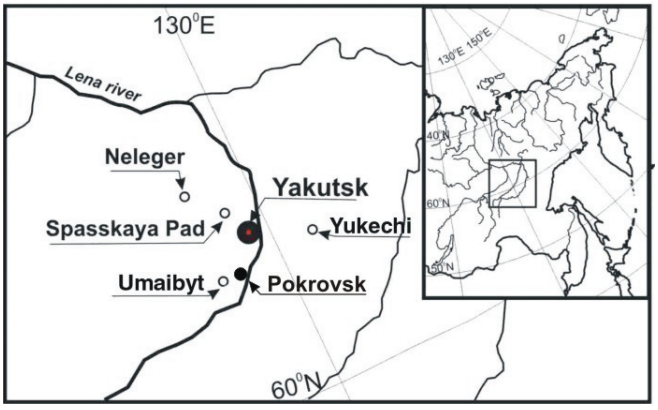

Figure 1. Location of Permafrost Institute's monitoring sites, and Yakutsk and Pokrovsk weather stations in Central Yakutia.

areas. Analysis of long-term ground temperature variations at weather stations during the entire period of instrumental observations will enable us to determine the development of cryoecological stresses in Central Yakutia, which is important for understanding the dynamics of cryogenic landscapes and for environmental protection planning.

Data Sources and Research Methods

Continuous ground temperature measurements in Central Yakutia have been made since 1931 (weather stations at Yakutsk and Pokrovsk). To determine representativeness of ground temperature records, data for depths of 1.6 and 3.2 m from the Yakutsk and Pokrovsk weather stations over the period 1931-2006 have been examined. The weather station data allow an assessment of both mean monthly and interannual variations in ground temperature. Based on the data analysis, Pokrovsk has been chosen as the most representative station for Central Yakutia. A measurement site at Pokrovsk was relocated in 1941. This move had little effect on the ground temperature record, because the new site was very similar to the older one in landscape and soil conditions. A site of the Yakutsk weather station was moved in 1964. The new and old sites differed greatly in landscape conditions, resulting in significant differences between the temperature series. Moreover, the Yakutsk data show virtually no variation after 1989 because of the change in the suprapermafrost water regime. This was a major reason for choosing the Pokrovsk records. Correlation coefficients between the mean annual ground temperatures at 1.6 and 3.2 m in Pokrovsk and Yakutsk are 0.85 and 0.88, respectively, at p=0.05 (during the period from 1965 to 1988 when the uniformity of measurement conditions was not disturbed by relocations or man-induced change in suprapermafrost water level).

Data obtained from the Yukechi, Umaibyt, Dyrgabai, and Tabaga monitoring sites, as well as the Neleger and Spasskaya Pad intensive observation sites, have been used to examine the effects of climate change on permafrost landscapes. These sites include measurements of ground temperature, thaw depth and active-layer moisture content, as well as observations of changes in microrelief and landscape at the facies level (Fedorov 1996, Fedorov et al. 1998, Konstantinov et al. 2001, Fedorov & Konstantinov 2003, Fedorov et al. 2003, Konstantinov et al. 2006). Ground temperatures at Spasskaya Pad and Neleger correlate well with the Pokrovsk weather station data. For example, the correlation coefficient of mean monthly temperatures at 3.2 m between Pokrovsk and the monitoring sites from October 2000 to September 2005 is 0.89 for Spasskaya Pad and 0.92 for Neleger. Such close relationship allows us to rely on the Pokrovsk records to analyze the long-term dynamics of ground temperatures and permafrost landscapes. We must also note that air temperature variations are relatively uniform across Central Yakutia. Correlation coefficients between locations are 0.89-0.98 (Skachkov 2001). In view of different record lengths and relocations of other weather stations, this fact allows us to use the Pokrovsk record as a basis for documenting long-term ground temperature variations (since 1931) in Central Yakutia.

Results

Interannual variations of ground temperature

A depth of 3.2 m was selected to analyze the long-term ground temperature variability, because materials at this level are perennially frozen. Temperature variations in the upper permafrost have a strong impact on the landscape and control degradation or recovery of the environmental conditions. An increase in temperature triggers cryogenic processes, while a decrease improves the stability of the upper permafrost.

The mean annual ground temperature at Pokrovsk for the period examined is -2.4°C and the standard deviation of the series is 0.44. The amplitude of annual means is 1.8°C, with a minimum of -3.3°C and a maximum of -1.5°C. The mean annual ground temperature has increased by 0.7°C over the period, with a trend of 0.1°C/decade (Fig. 2).

The time series of mean annual ground temperature shows a cyclic and progressive variation with an average period of 9.6 years. The maximum period is 12 years and the minimum is 8 years. Relatively high temperatures (the positive phase of the cycle) are observed in the mid 1930s, early 1940s, late 1940s-early 1950s, late 1950s-early 1960s, late 1960s-early 1970s, early 1980s-middle 1980s, early 1990s, and late 1990s-early 2000s. Two positive phases that occurred in the early 1940s and the late 1950s-early 1960s are less pronounced than the others. The temperatures series shows increasing values both for the positive and negative phases.

The most significant increases in ground temperature occurred in the early to mid 1980s and in the early 1990s, when the periods with maximum temperatures were longest and the periods with minimum temperatures were short. The temperature series before the 1980s can be characterized as stable, with alternating positive and negative phases.

Analysis of mean annual air temperature variations indicates that significant warming began in the late 1980s. Since then, the temperature series has changed from its normal pattern (Fig. 3). The mean annual air temperature at

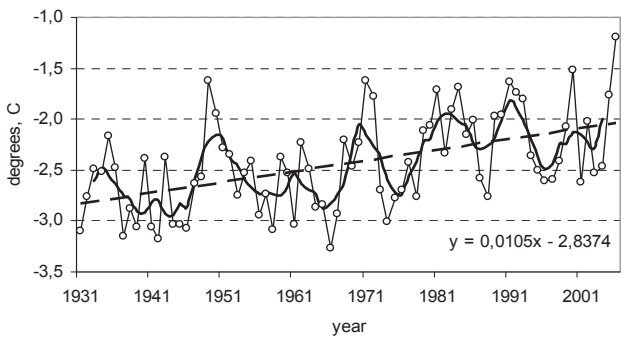

Figure 2. Interannual ground temperature variation at 3.2 m depth for the Pokrovsk weather station.

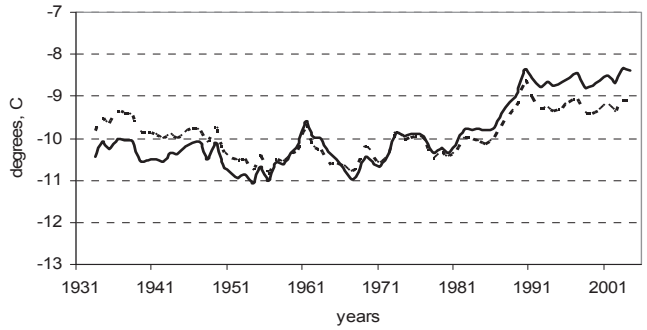

Figure 3. Variations in mean annual air temperature for Yakutsk (solid line) and Pokrovsk (dash line).

Yakutsk for the period from 1988–2005 was -8.5°C, while the long-term average had been -10.2°C (Handbook on the USSR Climate 1989). It is evident that the increase in ground temperatures from the early to mid 1980s was not due to a rise in air temperature. Being an integrating environmental parameter, ground temperature is not always consistent with variations of individual elements, such as mean annual air temperature or precipitation. We also note that air temperatures were higher at Pokrovsk than at Yakutsk until the mid 1950s, nearly identical between the mid 1950s and the mid 1970s, and colder since the mid 1970s to the present. This variation is likely due to circulation processes, since an anthropogenic factor has been ruled out by researchers (Skachkov 2001). However the increasing amplitudes of mean annual air temperature since the 1990s require a detailed analysis to determine the cause.

Of special interest is the change in ground temperature since 1980, with distinct cooling continuing to the present (Fig. 4a). Varlamov et al. (2002) attributed this cooling to the effect of snow cover. However the magnitude of the cooling is not so significant relative the entire series as to ameliorate the cryoecological stress (Fig. 2). There has been a steady increase in air temperature during this period in Central Yakutia (Fig. 4c), suggesting that Varlamov et al. are correct in relating the ground cooling to changes in snow cover. The variations in early winter (October, November and December) precipitation, which has an important effect on the permafrost temperature regime, provide some support to this view (Fig. 4b).

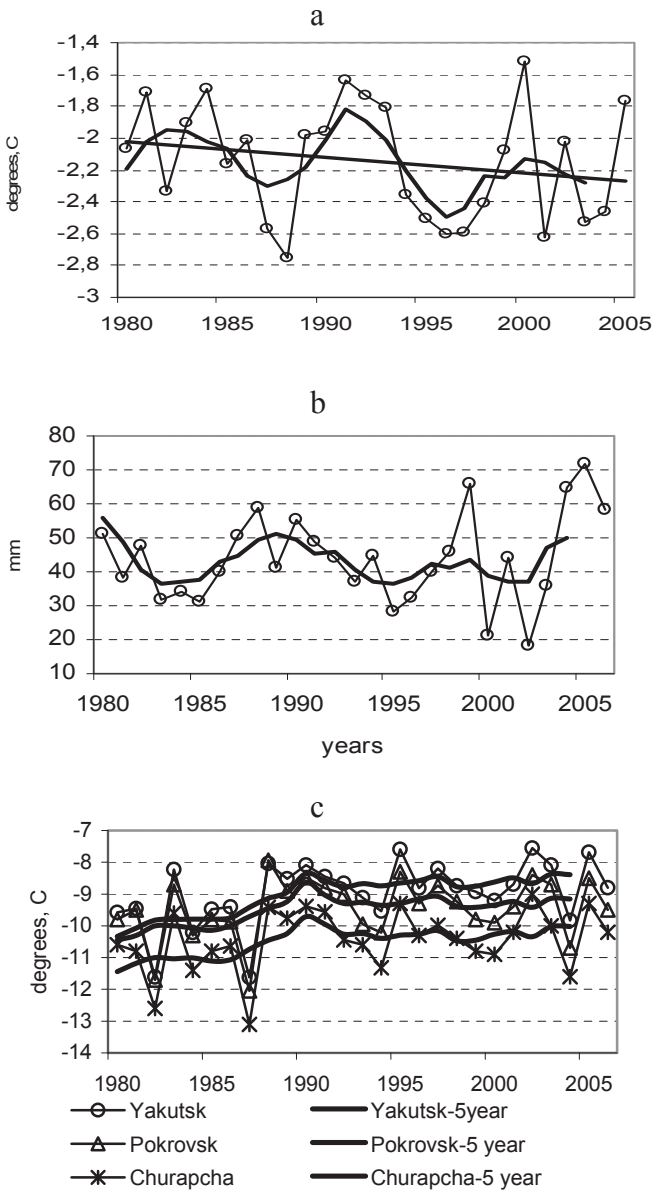

Figure 4. Ground temperature at 3.2 m for Pokrovsk (a) early winter precipitation for Yakutsk (b) and mean annual air temperature for Yakutsk, Pokrovsk and Churapcha (c) between 1980 and 2005. Thin lines – annual means, thick lines – 5-year running means.

Response of permafrost landscapes to impacts under present climatic conditions

Post-disturbance changes in permafrost and cryogenic landscapes have been studied during recent years as part of the Permafrost Institute's projects (Bosikov 1998, 2004, Fedorov et al. 1998, 2003, Gavriliev et al. 1999, 2005, Fedorov 2006). Thermokarst research is a major component in these investigations. Thermokarst studies are carried out at the Yukechi, Neleger, Spasskaya Pad and Umaibyt sites near Yakutsk.

The sites are heavily underlain by ground ice and contain numerous alases. Excess ice in permafrost is the main cause for thermokarst development. Central Yakutia, primarily between the Lena and Amga rivers, is dominated by ice-rich permafrost landscapes. The presence of wedge ice is readily identified by cemetery mounds on alas slopes and thaw depressions on the disturbed surfaces.

Generally, in Yakutia ice-rich permafrost landscapes are of limited distribution and occupy only near 10% of the region (Bosikov 1978), mainly within the densely populated areas such as the Lena-Amga watershed and the Viluy and Kolyma basins. However, thermokarst is not always active in ice-rich terrain. There are strong self-preservation forces in the landscapes that enable them to adjust and resist climate warming.

Climate plays a special role in thermokarst development. In Central Yakutia, thermokarst is actively developing in

the previously disturbed areas since the 1990s when air temperatures began increasing throughout the region. The landscapes disturbed by fire, forest harvesting and land clearing for agriculture have become an indicator of the impact of recent climate change on permafrost. Ground ice at these sites occurs at shallow depths, on average within 2 to 2.2 m of the surface. The long existence of the landscapes in an artificial state cannot but leave a trace. The active layer becomes heavily desiccated, requiring more heat for thawing compared to wet soils in forest. As a result, seasonal thaw reaches the tops of ice wedges in critical years, causing ice melting and ground subsidence.

Gavriliev et al. (2001) obtained original data on thermokarst activity at the Kerdyugen site located near the village of Tabaga in the vicinity of Yakutsk. They observed rapid development of initial thermokarst forms in an abandoned farm field. In the field, which was little affected by thermokarst in 1987, shallow thaw pits covered about half of the field surface by 1993; currently the entire 100 ha field is disturbed by thermokarst. Recent monitoring studies have shown that, during the periods of notable climatic stresses, the ecological state of anthropogenic landscapes significantly degrades. This causes abandonment of agricultural lands.

We conducted detailed thermokarst investigations at the Yukechi site which is situated on the right bank of the Lena River 50 km east of Yakutsk. The area is characterized by extensive development of thermokarst landforms. Recent climate warming has intensified thermokarst activity in the existing thaw depressions and accelerated the rates of ground subsidence (Fig. 5). In central portions of young water-filled thermokarst depressions 2 to 2.5 m in depth, an average rate of surface subsidence is 5–10 cm/yr.

Interesting data were obtained from the areas that had not been affected by cryogenic processes previously. These are flat treeless interalas areas with no visible indications of thermokarst such as thaw troughs over ice wedges. Such sites are experiencing subsidence in response to climatic stress.

Our investigations since 1992 show that this process has a distinctive trend. At many observation points, the ground surface has subsided 20–30 cm between 1992 and 2006 (Fig. 6). This subsidence can be attributed primarily to climate warming. The treeless landscapes with the desiccated active layer are most sensitive to climatic warming and most threatened by further disturbances.

Analysis of the obtained data indicates that subsidence at these sites develops impulsively, showing some rhythm. For example, significant subsidence occurred in 1995–1996, 2000–2001 and then in 2004 and 2006. These settlements are more directly related to variations in precipitation rather than to changes in ground or air temperatures. The years when settlement was initiated (1995, 2000 and 2004) were characterized by lower precipitation following the previous rainy season, while subsidence in 2006 was related to anomalously high rainfall. Initiation of deep subsidence is also related to moisture content of the active layer, starting in the seasons with high soil moisture contents (1995, 2000 and 2006).

Thus, the last two decades with maximum increases in air and ground temperatures are very sensitive to changes in meteorological conditions. Thawing of the top of ice wedges and subsidence of the ground surface occur in 2–3 year intervals. This is apparently related to the general increase in annual air temperature from the average by up to +1.4°C and annual ground temperature from the average by up to +0.6°C which creates instability in the state of permafrost. The activation of subsidence on existing thermokarst depressions and directed subsidence of well-drained, flat interalas meadows are a dramatic indicator of current climatic changes in Central Yakutia.

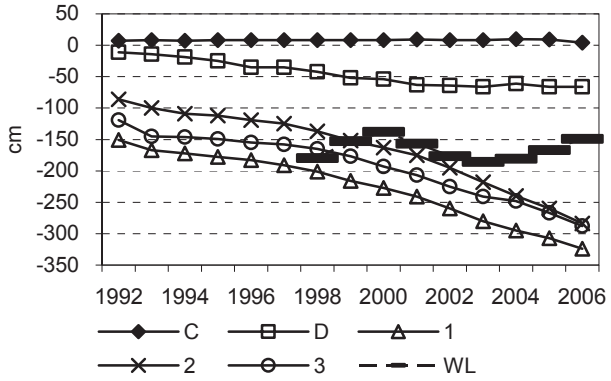

Figure 5. Surface subsidence at plot 2, Yukechi (well-drained inter-alas area). C – reference point, undisturbed inter-alas area, D – initial thaw depression, 1-3 – polygon centres within large thaw depressions, WL – water level.

The present response of disturbed areas underlain by ice-rich permafrost was investigated at the Neleger site in the vicinity of Yakutsk (Fig. 1).

It was found that cryogenic processes are most active during the first 5–6 years after disturbance, after which the processes stabilize and conditions develop for the recovery of permafrost terrain. If the forest cover is re-established over this period, the disturbed area is no longer the locus of ecological risk. At Kys-Alas (the Neleger site), which is underlain by ice-rich sediments, intensive thermokarst development with surface subsidence up to 10–15 cm began after the area was clear cut of trees in 1996. Subsidence continued to 2001, and then, between 2001 and 2004, the surface heaved due to refreezing of the thawed layer and exceeded the initial level. In 2004–2006, relative stability was observed (Fig. 7). The oversaturation of the active layer in the first few years after tree removal, as well as periodic strong cooling of the ground in early winter due to low snowfall in the winters of 2001/2002, 2002/2003 and 2003/2004, caused ground thawing to cease. An ice-rich layer formed at a depth of 110–180 cm which now acts as a protective layer.

The depth of thaw at this site has not exceeded 110 cm in recent years. Freezing of the oversaturated soils caused heaving and the relative surface levels have risen, on average, by 10–15 cm (Fig. 7). This mechanism of permafrost stabilization appears to be the main condition for recovery and optimization of the permafrost landscapes which are in a critical state.

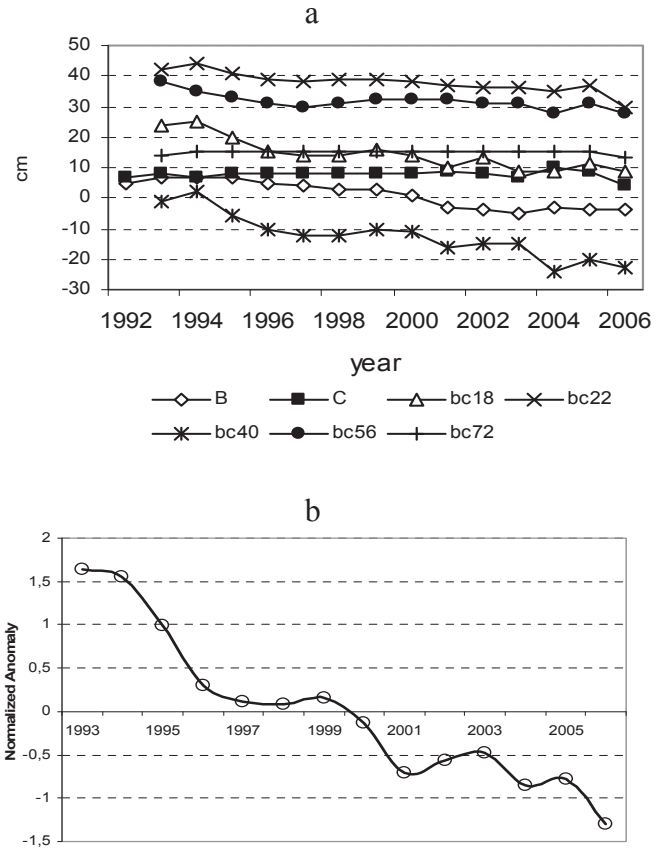

Figure 6. Surface subsidence in a well-drained inter-alas area, plot 2, Yukechi (a – observed values, b – averaged normalized anomalies) B and C – markers on stable flat surfaces; bc18, bc22, bc40, bc56 and bc72 – markers on relatively stable, flat surfaces near the slope of small thaw depressions. Normalized anomalies were calculated for each year as follows: $A = (i-i_{av})/\delta$ where i is the value for a given year; i_{av} is the long-term mean of a continuous series; δ is the root-mean-square deviation of a series.

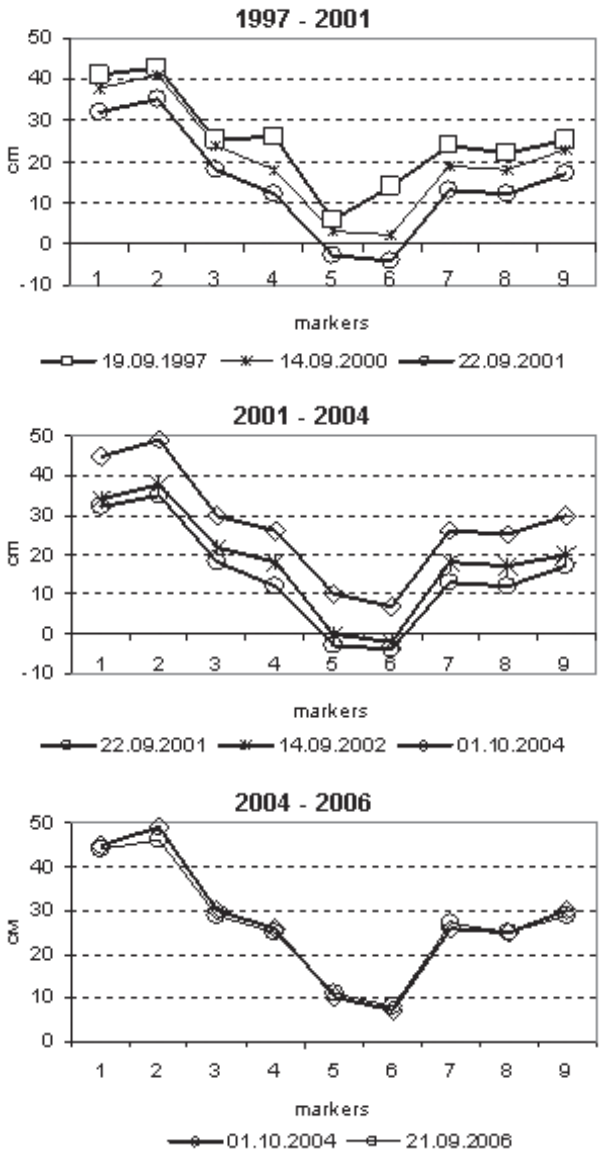

Figure 7. Changes in relative surface elevation at Kys-Alas, the Neleger site.

Conclusion

In conclusion, recent variations in air and ground temperatures are reflected in the change of permafrost landscapes in Central Yakutia. A good correlation between the mean monthly ground temperatures at Spasskaya Pad and Neleger and the Pokrovsk records has allowed construction of a reliable retrospective scheme for ground temperature variations in Central Yakutia. It should be noted that ground temperature data from most other stations are inhomogeneous due to instrument relocations and human impacts. The ground temperature diagram shows that relatively high temperatures from the 1980s to present have been stressful for permafrost landscapes, resulting in fairly active development of cryogenic processes. Disturbed areas are most sensitive, particularly where trees have been removed for land use (croplands and cuts). Such permafrost landscapes are more vulnerable and sensitive to meteorological variations under the current climate warming. On the other hand, our results also indicate that permafrost landscapes are capable of self-stabilization. This mechanism is relatively strong, so thermokarst development is as yet limited.

References

Bosikov, N.P. 1978. Alas coverage in Central Yakutia. In: *Geocryological Conditions in Mountains and Plains of Asia (Geokriologicheskie uslovia v gorakh I na ravninakh Asii)* (in Russian). Yakutsk: IMZ SO AN SSSR, 113-118.

Bosikov, N.P. 1998. Wetness variability and thermokarst dynamics in Central Yakutia. In: *Geocryological Problems (Problemy geokriologii)* (in Russian). Yakutsk: Izd-vo SO RAN, 123-127.

Bosikov, N.P. 2004. Man-caused thermokarst destruction of inter-alas landscapes in the Lena-Amga watershed (in Russian). *Kriosfera Zemli* VIII(4): 12-14.

Fedorov, A.N. 1996. Effects of recent climate change on permafrost landscapes in Central Sakha. *Polar Geography* 20(2): 99-108.

Fedorov, A. 2006. Present post-disturbance dynamics of permafrost in Central Yakutia. *Symptom of Environmental Change in Siberian Permafrost Region*. Sapporo: Hokkaido University Press, 225-231.

Fedorov, A.N., Gavriliev, P.P. & Konstantinov, P.Y. 2003. Study of the permafrost dynamics at Spasskaya Pad (in Russian). *Nauka i Obrazovanie* 3: 62-65.

Fedorov, A.N. & Konstantinov, P.Y. 2003. Observations of surface dynamics with thermokarst initiation, Yukechi site, Central Yakutia. *Proceedings of the 8th International Conference on Permafrost, Zurich, Switzerland, July 21-25, 2003*. Vol. 1: 239-243.

Fedorov, A.N., Konstantinov, P.Y., Vassiliev, I.S., Bosikov, N.P. Torgovkin, Y.I. & Samsonova, V.V. 1998. Observations of permafrost-landscape dynamics related to anthropogenic disturbances, Yukechi study site, Central Yakutia. *Proceedings of the Seventh International Conference on Permafrost, Yellowknife, Canada, June 23--27, 1998*: 259-263.

Gavriliev, P.P., Ugarov, I.S. & Efremov, P.V. 1999. The Permafrost-ecological monitoring of the agricultural lands in Central Yakutia (in Russian). *Kriosfera Zemli* 3: 92-99.

Gavriliev, P.P., Ugarov, I.S. & Efremov, P.V. 2001. *Permafrost and Ecology of Agricultural Landscapes in Taiga Areas, Central Yakutia (Merzlotno-ekologicheskie osobennosti taezhnykh agrolandshaftov Centralnoi Yakutii)* (in Russian). Yakutsk: Permafrost Institute Press, 195 pp.

Gavriliev, P.P., Ugarov, I.S. & Efremov, P.V. 2005. Cryogenic processes and ice-rich permafrost sensitivity to climate change and surface disturbance, Central Yakutia (in Russian). *Nauka i Obrazovanie* 4 (40): 84-87.

Gilichinsky, D.A., Bykhovets, S.S., Sorokovikov, V.A. et al. 2000. Use of the data of hydrometeorological survey for century history of soil temperature trends in the seasonally frozen and permafrost areas of Russia (in Russian). *Kriosfera Zemli* IV(3): 59-66.

Handbook on the USSR Climate, Vol. 24. Yakut ASSR 1989. (*Nauchno-prikladnoi spravochnik po klimatu SSSR. Vyp. 24. Yakutskaya ASSR)* (in Russian). Leningrad: Gidrometeoizdat, 608 pp.

Konstantinov, P.Y., Argunov, R.N., Gerasimov, E.Y. & Ugarov, I.S. 2006. On the relationship between seasonal thaw depth and interannual variation of mean annual ground temperature (in Russian). *Kriosfera Zemli* X(3): 15-22.

Konstantinov, P.Y., Rusakov, V.G. & Fukuda, M. 2001. Thermal regime of the upper permafrost layers in taiga landscapes, Yakutsk Area, 1996-2000. *Proceedings of the Ninth Symposium on the Joint Siberian Permafrost Studies between Japan and Russia in 2000, Sapporo, Japan, January 23-24, 2001*: 204-209.

Pavlov, A.V. & Malkova, G.V. 2005. *Recent Climatic Changes in Northern Russia (Sovremennye izmenenia klimata na severe Rossii)* (in Russian). Novosibirsk: Geo Publ., 54 pp.

Pavlov, A.V. 2003. Permafrost and climate changes in northern Russia: observations and forecasts (in Russian). Izvestia RAN. *Seria Geograficheskaya* 6: 39-50.

Romanovsky, V.E., Sazonova, T.S., Balobaev, V.T., Shender, N.I. & Sergueev, D.O. 2007. Past and recent changes in air and permafrost temperatures in eastern Siberia. *Global and Planetary Change* 56(3-4): 399-413.

Skachkov, Y.B. 2001. *Recent Climate Warming and Thermal Stability of Upper Permafrost in Central Yakutia.* Ph.D. Thesis Abstract (Termicheskaya ustoichivost' verkhnikh gorizontov kriolitozony Centralnoi Yakutii pri sovremennom potemplenii klimata. Avtoref. dis. kand. geogr. nauk) (in Russian). Yakutsk, 25 pp.

Skryabin, P.N., Varlamov, S.P. & Skachkov, Y.B. 1998. I*nterannual Variability of Ground Temperatures in the Yakutsk Area (Mezhgodovaya izmenchivost teplovogo rezhima gruntov rajona Yakutska)* (in Russian). Novosibirsk: SB RAS Press, 144 pp.

Varlamov, S.P., Skachkov, Y.B. & Skryabin, P.N. 2002. *Thermal Regime of Permafrost Landscapes in Central Yakutia (Temperaturnyi rezhim merzlotnykh landshaftov Centralnoi Yakutii)* (in Russian). Yakutsk: Permafrost Institute Press, 218 pp.

Vasiliev, I.S. & Torgovkin, Y.I. 1996. The influence of climate on temperature and thickness of the active layer. In: T*he Influence of Climate on Permafrost Landscapes in Central Yakutia (Vlianie klimata na merzlotnye landshafty Centralnoi Yakutii)* (in Russian). Yakutsk: Permafrost Institute Press, 37-45.

Methodical Design for Stability Assessments of Permafrost-Affected High-Mountain Rock Walls

Luzia Fischer
Glaciology, Geomorphodynamics & Geochronology, Department of Geography, University of Zurich
Christian Huggel
Glaciology, Geomorphodynamics & Geochronology, Department of Geography, University of Zurich

Abstract

Slope stability of steep rock walls in glacierised and permafrost-affected high-mountain regions is influenced by a number of different factors and processes. For an integral assessment of slope stability, a better understanding of the predisposing factors is particularly important, especially in view of rapid climate-related changes. This study introduces a methodical design that includes suitable methods and techniques for investigations of different predisposing factors in high-mountain rock walls. Current state-of-the-art techniques are reviewed, and their potential application for in situ and remote studies is assessed. A comprehensive array of analyses and modeling tools is presented, including data-acquisition methods and subsequent stability analyses. Based on two case studies of recent slope instabilities in the European Alps, the effective application and coupling of measurements, analyses, and modeling methods are shown.

Keywords: climatic change; high-mountain rock walls; investigation techniques; predisposing factors; slope stability.

Introduction

Hazards related to rockfall, rock avalanches and combined rock/ice avalanches from steep glacierised and permafrost-affected rock walls pose a significant threat to people and infrastructure in high mountain regions. Due to ongoing climatic change, a widespread reduction in stability of formerly glacierised and perennially frozen slopes might occur and result in a shift of hazard zones (Haeberli et al. 1997, Harris et al. 2001, Fischer et al. 2006). A major problem is the possible increase in magnitude and frequency of slope failures.

Slope stability of steep rock walls in glacierised and permafrost-affected high-mountain regions is influenced by a number of different factors such as topography, geological and geomechanical characteristics, hydrology as well as glaciation, permafrost distribution, and thermal condition. Gradual or abrupt changes in one or more of these factors may reduce the slope stability and eventually lead to a rockfall event. Among these factors, permafrost and glaciers are particularly prone to rapid changes in relation to ongoing climate change. Although these two factors are, together with the hydrological regime, assigned a likely important role in current and future slope destabilization, the effects are not clearly understood. A better understanding of the factors and mechanisms determining the slope stability of steep rock walls is thus a key factor and needs basic research.

The complexity of slope stability problems requires a number of different investigation and modeling techniques to consider the relevant physical processes and factors. However, high-mountain rock walls are an extremely challenging environment for currently existing technology and related investigations for a number of reasons. Often, the hazard source areas are situated in remote high-mountain regions and the on-site access to steep rock walls is mostly very difficult or prohibitively dangerous due to existing slope instabilities. Furthermore, the steepness complicates applications of airborne investigation techniques.

This article provides a review of current local-scale investigation techniques and introduces a multidisciplinary methodical design for comprehensive, stability-directed investigations of predisposing factors in steep, high-mountain rock walls which adequately considers the particular difficulties of steep and partly inaccessible ground conditions, based on a combination of on-site and remote methods. The design presented here does not claim to provide a complete approach; rather it bases itself on investigation techniques and analyses that were applied and tested within past and ongoing projects. Also, the rapidly advancing technology may require extension and adaptation of the design in the future.

Factors Influencing Slope Stability

Predisposing and triggering factors can be distinguished with respect to slope stability of rock walls. In the following, a short definition of the two different types of factors is given. Proposed methodical design for slope stability assessment is mainly focused on the investigation of predisposing factors; analyses of triggering factors usually require permanent monitoring methods.

Predisposing factors are physically measurable processes and parameters that permanently affect stress and strain fields in a flank, also in the stable state. They can be broadly categorized in topographical, geomorphological, geological, hydrological, and several other physically-based factors. In high-mountain areas, permafrost and glaciers are two additional important factors (Fig. 1).

Triggering factors can vary in time, space, and magnitude and eventually provoke slope failure. They include, for example, earthquakes, rainfall and snowmelt events that can result in increased water pressure, and rather seldom in high-mountain areas, human interactions.

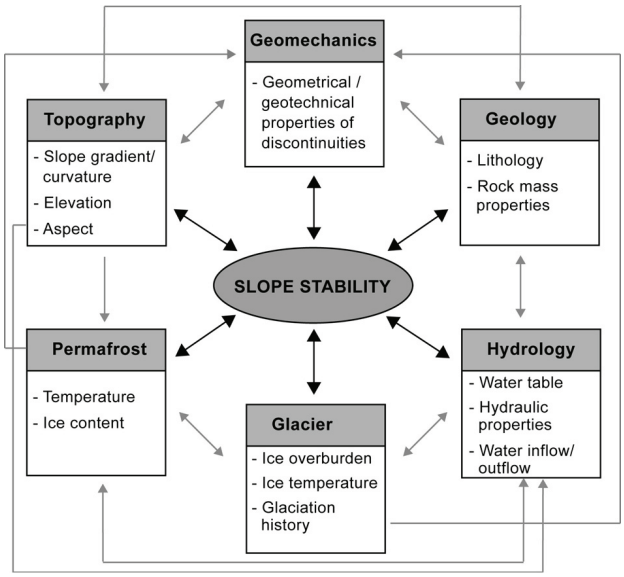

Figure 1. Predisposing factors influence the slope stability and have complex interactions among themselves which are represented by arrows.

Predisposing factors have complex interactions among themselves that influence slope stability (Fig. 1). Topography is a fundamental parameter for slope stability. Slope angle and morphology are important factors for the occurrence and spatial distribution of slope instabilities due to their strong influence on stress and strain fields within a flank. Topography is closely connected to the geological setting and the geomorphological history of a rock wall (erosion, glacial overburden), which, in turn, also effectively influence the geomechanical setting.

The geological setting is determined by the lithology and the geotechnical properties of the rock mass. The geological structures, i.e. discontinuities such as joints, bedding planes, schistosity, and fault zones are fundamental for slope stability, especially their geometrical and geotechnical characteristics. The shear strength as a major parameter for stability is directly related to the geotechnical properties such as cohesion, friction angle, aperture, infilling, and weathering.

Permafrost occurrence in a rock wall can strongly influence the geotechnical parameters of discontinuities, depending on ice content and temperature. The shear strength of ice-bonded discontinuities is strongly affected by the thermal regime in the sub-surface and may be reduced by a rise in temperature or finally the melting of ice-filled rock joints (Davies et al. 2001, Gruber & Haeberli 2007, Harris et al. 2001). This, in turn, also influences the hydrological regime, and may, for instance, result in an increase of the water pressure. The hydraulic setting in a steep rock wall is closely connected to the topography, geological setting, geomechanical characteristics, glaciation, and permafrost occurrence. Changes in water table and water pressure may significantly change the shear strength of the rock mass and therefore exert a strong influence on the slope stability.

Glacier ice may influence slopes differently. Hanging glaciers may have an impact on the thermal, hydraulic, and hydrologic regime in adjacent areas (Haeberli et al. 1997). The erosion by and retreat and down-waste of valley glaciers, in turn, may induce long-term change in the stress field inside the rock wall (Wegmann et al. 1998, Eberhardt et al. 2004).

Among the factors outlined in Figure 1, glaciation and permafrost are presently those subject to the most direct and rapid changes due to climatic change. Changes in these parameters can significantly influence other factors such as hydrology, geomechanical and geotechnical properties in particular. The response of steep high-mountain rock walls to changes in these predisposing factors is, at the same time, strongly conditioned by the topography and the geological setting, in particular by the geometrical and geotechnical characteristics of discontinuities (Ballantyne 2002).

Investigation Techniques and Methodology

Data acquisition

In this section, current state-of-the-art techniques for the investigation of the predisposing factors are illustrated, while in the following section subsequent analyses and processing methods are described (Fig. 2).

In situ field investigations are useful to obtain detailed data. Traditional geological in situ field studies are necessary to achieve data on geological and geomechanical characteristics of the rock mass. The lithological and geomorphological setting as well as geological structures can be mapped, and a preliminary assessment of the intact rock mass properties can be achieved, for example, using the Schmidt hammer method (Aydin & Basu 2005). The geomechanical and geotechnical properties of discontinuities can be assessed by measuring parameters such as orientation, frequency, spacing, aperture, and surface characteristics based on the application of rock mass classification systems (Hack 2002, Hoek & Brown 1997, Wyllie & Mah 2004). In case of inaccessible ground conditions, these types of investigations can also be conducted in the surrounding area with similar lithological and geomechanical settings. Limited observations of the hydrological regime can also be done in situ and from photographs; for instance, observations of water inflow or outflow in a mountain flank.

Point measurements of near-surface rock temperatures using temperature loggers installed a few cm to dm below the surface can constrain permafrost distribution and the prevailing thermal regime (Gruber et al. 2003). Nearby boreholes equipped with temperature loggers give an indication of temperature distribution at depth.

Geophysical techniques are powerful methods for the investigation of subsurface characteristics, but in steep rock walls difficult and complex in their application and therefore rarely exploited until now. Georadar, electrical resistivity tomography, and refraction seismic can be applied for the determination of subsurface structures and the distinction between frozen and thawing rock sections (Hauck et al. 2004, Heincke 2005, Krautblatter & Hauck 2007).

Remote sensing-based techniques are crucial due to the inaccessibility of wide areas of high-mountain walls.

Terrestrial and aerial imagery can be used for identifying

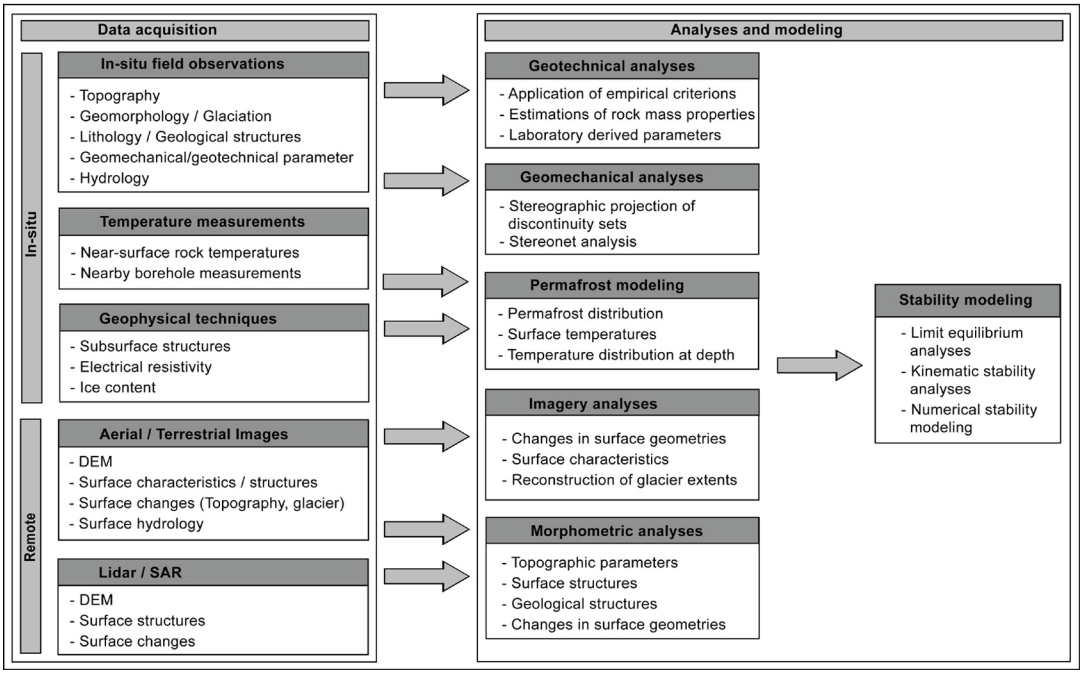

Figure 2. Methodical design for the assessment of slope stability in high-mountain areas containing different insitu and remote sensing-based methods. The upper part shows techniques for the data collection, the lower part processing and analyses of acquired data.

geological structures and surface changes with respect to ice cover and topography. Aerial photography can also be used for the generation of digital elevation models (DEMs), the measurement of terrain displacements and for detailed interpretations (Baltsavias et al. 2001). In some specific studies, terrestrial photography was used for identifying changes with respect to ice cover and slope instabilities on steep ice faces (Fischer et al. 2006, Kääb et al. 2005). These studies have shown the considerable potential of such image analyses which should be further exploited. Automatic cameras are a commonly applied tool for monitoring acute slope instabilities.

Airborne and terrestrial laser scanning (LiDAR) is a rapidly emerging and highly promising tool for acquiring very high-resolution DEMs for high-mountain areas, and thus for detecting small-scale topographic structures (Baltsavias et al. 2001, Janeras et al. 2004). Laser scanning applications from helicopter allow perpendicular recording of LiDAR data and simultaneous acquisition of digital photographs with little geometric distortion (Skaloud et al. 2005). Repeated measurements are the basis for deriving topographic changes. Ground-based synthetic aperture radar (SAR) technology is a capable tool for slope deformation studies (Atzeni et al. 2001, Singhroy & Molch 2004).

Analyses and modeling

Lithological and geomorphological data can be displayed on a map in a GIS for further applications or comparison with other parameters. The geomechanical and geotechnical data measured during fieldwork typically have to be processed to get required parameters for stability modeling by using empirical criteria and rock mass classification systems (Hack 2002, Hoek & Brown 1997) or with adequate laboratory tests. Geomechanical data such as the orientation of discontinuities can be displayed in stereographic projections and may be applied subsequently for kinematic analyses, limit equilibrium analyses, and numerical modeling (Stead et al. 2006).

For the modeling of permafrost distribution a number of models with varying levels of sophistication and at different spatio-temporal scales have been developed (Hoelzle et al. 2001, Gruber et al. 2003). The three-dimensional temperature distribution and its evolution with climatic change is an important component for rock slope stability considerations and has been assessed using numerical modeling by coupling a surface energy balance model with a subsurface heat conduction scheme (Noetzli et al. 2007). A modeling scheme that would directly include modeled permafrost distribution within slope stability models has yet to be developed, but it can be considered for the model assumptions.

Geophysical investigations can mainly be used as boundary conditions and reference values either for permafrost modeling or for analyses of the subsurface structures.

The most common application of remotely sensed image data consists of the interpretation and classification of the image content. Terrestrial and aerial imagery can be used for the identification and mapping of different surface features in steep rock walls and also their temporal changes. Digital aerial as well as terrestrial photos have considerable potential for quantitative analyses of geomorphic structures and changes in a rock wall by georeferencing or matching images based on a high-resolution DEM or photogrammetric techniques (Roncella et al. 2005).

DEMs represent the core of any morphometric investigation of predisposing factors. They can be obtained from stereo aerial and high-resolution terrestrial photos but also from LiDAR data (Kääb et al. 2005). From these DEMs, topographic parameters, large-scale morphotectonic features,

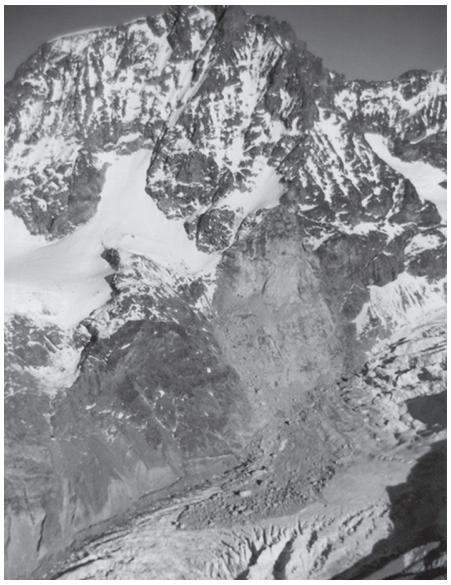

Figure 3. The western flank of the Piz Morteratsch with the Tschierva glacier in the foreground. Visible in the middle of the photo is the detachment zone of the 1988 rockfall and the deposits on the glacier (photo by A. Amstutz, 1988).

and geological structures can be extracted. A promising, yet not fully exploited method is the coupling of laser scanning data with photogrammetric analyses and terrestrial imagery analyses to extract important topographic and structural-geological parameters from DEMs. Main discontinuity sets can be distinguished and their geometrical pattern determined. Therefore, a preliminary assessment of potentially unstable areas may be performed based on geomechanical parameters with limit equilibrium and kinematic analyses using the data from in situ measurements or even only based on DEM analyses (Derron et al. 2005, Stead et al. 2001). Further structural and stability analysis with a DEM is made possible by the recent development of geologically oriented GIS tools (Günther 2003, Jaboyedoff et al. 2004).

For more complex slope stability assessments numerical methods are required. Numerical techniques used for rock slope analyses are generally divided into continuum and discontinuum approaches, or when combined, hybrid approaches (Barla & Barla 2001, Eberhardt et al. 2004, Stead et al. 2001, Stead et al. 2006). Numerical modeling is in fact a powerful tool for the assessment of failure mechanisms, but the level of topographic and geotechnical detail needed can limit the application.

Case Studies

Tschierva rock avalanche event

The Tschierva rock avalanche occurred on October 19, 1988, from the western flank of Piz Morteratsch (3751 m a.s.l., in the Engadin, Switzerland) on Tschierva glacier with an estimated volume of approximately 0.3×10^6 m^3 (Fig. 3).

For the re-analyses of the Tschierva rock avalanche, detailed numerical slope stability modeling was proposed. Therefore, in situ fieldwork and subsequent geotechnical and morphometric analyses have been done to obtain required accurate data (Fischer et al. 2007). The steps described here generally follow the scheme from Figure 2.

Figure 4. The Monte Rosa east face with the Belvedere glacier in the foreground (photo by L. Fischer, 2004). The detachment zone of the ice avalanche (2005) is marked with a black circle, the one of the rock avalanche (2007) in white.

The in situ field observations included:

- Preliminary analyses of rock mass properties (lithology, discontinuities, fault zones, water occurrence).
- Characterization of discontinuities (discontinuity sets, orientation, density, condition, aperture, filling).
- Surveying of detachment zone and adjacent area with manual rangefinder.

Subsequent complementary analyses included:

- Geotechnical and geomechanical analyses by using field data, stereographic plots, and empirical criterions.
- Photogrammetric analyses of aerial images for the evaluation of topographic changes.
- Analyses of aerial and terrestrial photos for detecting geological structures and water occurrence.
- Modeling of permafrost distribution.
- Reconstruction of glacier extents based on satellite images and historical topographic maps.

Numerical slope stability modeling was then performed with the 2-D distinct-element method model UDEC (by Itasca) to examine the possible failure mechanisms. Modeling of the unloading of the Pleistocene glacial overburden showed that subsequent redistribution of stress and strain fields in the flank had a strongly controlling influence on the geometry of the detachment zone. A sensitivity analysis of geotechnical parameters showed that the cohesion of the discontinuities was a fundamental parameter. The stability modeling for dry conditions also revealed that the failure mechanism was a combination of shear failure along preexisting discontinuities and development of brittle fractures propagation through the intact rock mass.

Coupled hydro-mechanical modeling demonstrated that slope stability was very sensitive to changes in water pressure. The existing fault zone crossing the rock slope induced an elevated water inflow due to the higher permeability and might therefore be, together with the long-lasting effects of ice unloading, a main factor for the slope instability.

Instabilities in the Monte Rosa east face

The Monte Rosa east face, Italian Alps, is one of the highest flanks in the Alps (2200–4600 m a.s.l.). Steep hanging glaciers and permafrost cover large parts of the wall (Fig. 4). Since the end of the Little Ice Age (~1850), hanging glaciers and firn fields have retreated continuously. During recent decades, the glaciers of the Monte Rosa east face experienced an accelerated and drastic loss. Some glaciers have completely disappeared. New slope instabilities and detachment zones developed and resulted in enhanced rockfall and debris flow activity (Kääb et al. 2004, Fischer et al. 2006). In August 2005, an ice avalanche with a volume of more than $1x10^6$ m^3 occurred, and in April 2007, a rock avalanche of about $0.3x10^6$ m^3 detached from the upper part of the flank.

The main focus of the investigations of the Monte Rosa east face was the assessment of the influence of glacier retreat and permafrost degradation on the current and possible future rockfall and ice avalanche activity (Fischer et al. 2006).

During field studies, the following data were compiled:

- Detailed geological and geomorphological mapping.
- Current glacier extents.
- Detailed map of the current detachment zones of mass movement activities.

Due to difficult and dangerous in situ access, this information was collected from distant ground-based and air-borne observations.

Further analyses included:

- Modeling of the permafrost distribution.
- Reconstruction of glacier extents since the early 20th century based on orthophotos and terrestrial photos.

The results were compiled in a GIS, and the overlay of each investigated factor revealed spatial as well as temporal linkages between investigated processes and their influence on the formation of new detachment zones.

The most important findings were that most detachment zones in the Monte Rosa east face are located in areas where surface ice has recently disappeared. In addition, many detachment zones are located at the altitude of the lower boundary of the estimated permafrost distribution, where presumably warm and degrading permafrost exists. A striking result is also that many detachment zones are situated in transition zones between orthogneiss and paragneiss. These findings demonstrate that the formation of detachment zones mostly seems to be caused by a combination of different factors.

Conclusion and Perspectives

The investigation of slope stability in steep, high-alpine rock walls is a major challenge, chiefly due to the difficulties in data acquisition and the complexity of the factors and processes influencing slope stability. In each case, the proceeding has to be adapted, and different methodologies have to be applied concerning the possibilities of data acquisition and the required stability modeling method.

The case study of the Tschierva rockfall shows that the appropriate method combination, including classic geological field investigation techniques, terrestrial and aerial image analyses, and permafrost modeling, allows the performance of detailed numerical slope stability modeling and the evaluation of possible failure mechanisms.

The much larger Monte Rosa east face, with surface and subsurface ice subject to extremely fast changes, represents the most challenging high-mountain conditions and required a more remote-based approach. However, local field surveys could be integrated for a comprehensive spatial and temporal analysis of predisposing factors and their interaction.

In the future, measurement, analytical, and modeling tools will be further advanced. For instance, ground-based SAR and helicopter-based LiDAR have only very recently been applied on large high-mountain walls and should be further developed. Advances are also expected with regard to a more comprehensive integration of high-technology data into slope stability assessment methods.

Acknowledgments

This project is funded by the Swiss National Science Foundation (project no. 200021-111967). We acknowledge constructive comments made by two reviewers and editors.

References

Aydin, A. & Basu, A. 2005. The Schmidt hammer in rock material characterization. *Engineering Geology* 81: 1-14.

Atzeni, C., Basso, M., Canuti, P., Casagli, N., Leva, D., Luzi, G., Moretti, S., PieraccinI, M., Sieber, A.J. & Tarchi, D. 2001. Ground-based radar interferometry for landslide monitoring and control. *Proceedings of the ISSMGE Field Workshop on Landslides and Natural/ Cultural Heritage Trabzon (Turkey), August 23–24, 2001*: 195-209.

Ballantyne, C.K. 2002. Paraglacial Geomorphology. *Quarternary Science Reviews* 21: 1935-2017.

Baltsavias, E.P., Favey, E., Bauder, A., Boesch, H. & Pateraki, M. 2001. Digital surface modelling by airborne laser scanning and digital photogrammetry for glacier monitoring. *Photogrammetric Record* 17(98): 243-273.

Barla, G. & Barla, M. 2001. Investigation and modelling of the Brenva Glacier rock avalanche on the Mount Blanc Range. *Proceedings of the ISRM Regional Symposium Eurock 2001, Espoo, Finlandia, 3-7 giugno, 2001*: 35-40.

Davies, M.C.R., Hamza, O. & Harris, C. 2001. The effect of rise in mean annual temperature on the stability of rock slopes containing ice-filled discontinuities. *Permafrost and Periglacial Processes* 12 (1): 137-144.

Derron, M.-H., Jaboyedoff, M. & Blikra, L. H. 2005. Preliminary assessment of rockslide and rockfall hazards using a DEM (Oppstadhornet, Norway). *Natural Hazards and Earth System Sciences* 5: 285-292.

Eberhardt, E., Stead, D. & Coggan, J.S. 2004. Numerical analysis of initiation and progressive failure in natural rock slopes - the 1991 Randa rockslide. *Int. J. Rock Mech. Min. Sci.* 41: 69-87.

Fischer, L., Kääb, A., Huggel, C. & Noetzli, J. 2006. Geology, glacier retreat and permafrost degradation as controlling factors of slope instabilities in a high-mountain rock wall: the Monte Rosa east face. *Natural Hazards and Earth System Sciences* 6: 761-772.

Fischer, L., Huggel, C. & Lemy, F. 2007. Investigation and modelling of periglacial rockfall events in the European Alps. *EGU - Geophysical research abstracts*.

Gruber, S. & Haeberli, W. 2007. Permafrost in steep bedrock and its temperature-related destabilization following climate change. *Journal of Geophysical Research* 112: F02S18.

Gruber, S., Peter, M., Hoelzle, M., Woodhatch, I. & Haeberli, W. 2003. Surface temperatures in steep alpine rock faces – A strategy for regional-scale measurement and modeling. *Proceedings of the 8th International Confernce on Permafrost 2003, Zurich, Switzerland*: 325-330.

Günther, A. 2003. SLOPEMAP: programs for automated mapping of geometrical and kinematical properties of hard rock hill slopes. *Computer and Geosciences* 29: 865-875.

Hack, R. 2002. An evaluation of slope stability classification. *Proceedings of ISRM EUROCK 2002, Portugal, Madeira, Funchal, Nov. 25-28, 2002*: 3-32.

Haeberli, W., Wegmann, M. & Vonder Mühll, D. 1997. Slope stability problems related to glacier shrinkage and permafrost degradation in the Alps. *Eclogae geologicae Helvetiae* 90, 407-414.

Harris, C., Davies, M.C.R. & Etzelmüller, B. 2001. The assessment of potential geotechnical hazards associated with mountain permafrost in a warming global climate. *Permafrost and Periglacial Processes* 12 (1): 145-156.

Hauck, C., Isaksen K., Vonder Mühll, D. & Sollid, J.L. 2004. Geophysical surveys designed to delineate the altitudinal limit of mountain permafrost: an example from Jotunheimen, Norway. *Permafrost and Periglacial Processes* 15: 191-205.

Heincke, B. 2005. Determination of 3-D fracture distribution on an unstable mountain slope using georadar and tomographic seismic refraction techniques. *Doctoral thesis*, ETH Zurich.

Hoek, E. & Brown, E. 1997. Practical estimates of rock mass strength. *Int. J. Rock. Mech. Min. Sci. Abstr*. 27 (3): 1165-1186.

Hoelzle, M., Mittaz, C., Etzelmüller, B. & Haeberli, W. 2001. Surface energy fluxes and distribution models relating to permafrost in European mountain permafrost areas. *Permafrost and Periglacial Processes* 12: 53-68.

Jaboyedoff, M., Baillifard, F., Philippossian, F. & Rouiller, J.-D. 2004. Assessing fracture occurrence using "weighted fracturing densit": a step towards estimating rock instability hazard. *Natural Hazards and Earth System Science* 4: 83-93.

Janeras, M., Navarro, M., Arnó, G., Ruiz, A., Kornus,W., Talaya, J., Barberá, M. & López, F. 2004. LIDAR applications to rock fall hazard assessment in Vall de N´uria. *Proceedings of the 4th ICA Mountain Cartography Workshop, Vall de Núria, Catalonia, Spain*.

Kääb, A., Huggel, C., Barbero, S., Chiarle, M., Cordola, M., Epinfani, F., Haeberli, W., Mortara, G., Semino, P. Tamburini, A. & Viazzo, G. 2004. Glacier hazards at Belvedere glacier and the Monte Rosa east face, Italian Alps: Processes and mitigation. *Proceedings of the Interpraevent 2004 – Riva/Trient*.

Kääb, A., Huggel, C., Fischer, L., Guex, S., Paul, F., Roer, I., Salzmann, N., Schlaefli, S., Schmutz, K., Schneider, D., Strozzi, T. & Weidmann, I. 2005. Remote sensing of glacier- and permafrost-related hazards in high mountains: an overview. *Natural Hazards and Earth System Sciences* 5: 527-554.

Krautblatter, M. & Hauck, C. 2007. Electrical resistivity tomography monitoring of permafrost in solid rock walls. *Journal of Geophysical Research* 112: F02S20.

Noetzli, J., Gruber, S., Kohl, T., Salzmann, N. & Haeberli, W. 2007. Three-dimensional distribution and evolution of permafrost temperatures in idealizes high-mountain topography. *Journal of Geophysical Research* 112: F02S13.

Roncella, R. Forlani, G. & Remondino, F. 2005. Photogrammetry for geological applications: automatic retrieval of discontinuity in rock slopes. *Proceedings of SPIE-IS&T Electronc Imaging, SPIE* 5665: 17-27.

Skaloud, J., Vallet, J., Keller, K., Veyssiere, G. & Kölbl, O. 2005. HELIMAP: Rapid large scale mapping using handheld LiDAR/CCD/GPS/INS sensors on helicopters. *Proceedings of ION GNSS 2005 Congress, Long Beach, California*.

Singhroy, V. & Molch, K. 2004. Characterizing and monitoring rockslides from SAR techniques. *Advances in Space Research* 33: 290-295.

Stead, D., Eberhardt, E., Coggan, J. & Benko, B. 2001. Advanced numerical techniques in rock slope stability analyses-applications and limitations. *Proceedings of the International Conference on Landslides-Causes, Impacts and Countermeasures, Davos 2001*: 615-624.

Stead, D., Eberhardt, T. & Coggan, J.S. 2006. Developments in the characterization of complex rock slope deformations and failure using numerical modeling techniques. *Engineering Geology* 83: 217-235.

Wegmann, M., Gudmundsson, G.H. & Haeberli, W. 1998. Permafrost changes in rock walls and the retreat of Alpine glaciers: a thermal modelling approach. *Permafrost and Periglacial Processes* 9: 23-33.

Wyllie, D.C. & Mah, C.W. 2004. *Rock Slope Engineering,* 4th ed. New York: Spon Press, 431 pp.

Permafrost in Marine Deposits at Ilulissat Airport in Greenland, Revisited

Niels Foged
Arctic Technology Centre, Department of Civil Engineering, Technical University of Denmark, DK-2800 Kgs. Lyngby, Denmark
Thomas Ingeman-Nielsen
Arctic Technology Centre, Department of Civil Engineering, Technical University of Denmark, DK-2800 Kgs. Lyngby, Denmark

Abstract

Ilulissat Airport was constructed in 1982 to 1984 after detailed geotechnical investigations as the construction site included up to 12 m thick basins of marine clay deposits. Despite soil temperatures of approximately -3°C the soil appeared unfrozen from 4 m to 5 m below ground surface due to a high residual salt content in the porewater. However, in the less saline top zone massive ice layers were found constituting up to 30% by volume. These formations, representing a typical example of saline permafrost, caused the planned position of the runway to be shifted towards the northwest and the layers to be removed and replaced with compacted blasted rock fill. However, a test fill of 2.5 m of rock fill and coarse gravel was constructed in the abandoned area in order to establish experiences for future constructions. Background, previous findings, and present activities are also topics in an accompanying paper, Ingeman-Nielsen et al. (2007).

Keywords: airport; construction; embankment; freezing point depression; saline permafrost; test fill.

Introduction

In Greenland it has been very difficult and costly to establish the traffic infrastructures necessary for the development of a modern society under the present physiographic and climatic conditions. The establishment of the airport in Ilulissat (Jakobshavn) was a milestone in a traffic project based on the aircraft type DASH-7, which could land on a short 700 m "Short Take Off and Landing" – STOL runway with an in-flight angle of 7.5° instead of the normal 3°. At present 7 airports of this type are operational and more will be established. Ilulissat Airport was the first to be constructed using rock fill on rock outcrops and marine clay under permafrost. Consequently, the geotechnical investigations started in 1978 were very detailed and led to new findings on saline clay permafrost published by Foged and Bæk-Madsen (1980).

Investigations in 1978–1982

Ilulissat Airport was constructed in 1980–1984 two km north of the town on a plain area with shallow rock outcrops surrounded by marine clay deposits. It is situated in discontinuous permafrost and project investigations from 1978 to 1985 focussed on the thermal state of these deposits and the geotechnical properties of frozen and unfrozen clay being the possible foundation for the runway embankment, taxiway, and terminal area. The soil investigations were carried out for Asiaq–Greenland Survey (Previously Grønlands Tekniske Organisation) by the Danish Geotechnical Institute with the senior author being responsible for special field and laboratory work.

Engineering geology

Ilulissat is located in the central bay of West Greenland, which was glaciated repeatedly during Quaternary but most soil formations relate to the last Weichselian-glaciation (Wisconsin) and to the late-glacial and Holocene deglaciation. Onshore, the most important deposits are local side moraines and glaciomarine clay and silt sediments overlain by Holocene solifluction deposits and topsoil in the form of only slightly decomposed peat. According to Bennike and Björck (2002) the innermost part of the bay near to Jakobshavn was not deglaciated before earliest 9600 years before present (BP). The glaciomarine sediments were deposited at a relative high sea level of >50 m above present. The saline pore water is maintained to a high degree as desalination due to freshwater percolation was not effective during the Holocene climatic optimum between 8000 and 5000 years BP (Weidick 1968, Foged 1979, and Foged & Bæk-Madsen 1980). After 5000 years BP it is assumed that the climate caused permafrost to develop as seen today.

Geotechnical investigations

The distribution of sediments, permafrost, and bedrock of gneiss was delineated using engineering geological field survey and aerial photos, Figure 1. This work was supplemented with geophysical investigation by means geoelectrical measurements using Wenner configurations for subsurface mapping of the marine clay basins and Schlumberger electrical soundings to delineate geological and permafrost boundaries. In connection with this more than 70 boreholes were carried out using a self-transportable rotary core drilling rig, indispensable in the very wet muskeg peat and solifluction soil top-layer. A number of boreholes were equipped with soil temperature PT-100 sensors sat down in PEL-tubes with an antifreeze liquid. The sensors were generally measured manually during the investigation and construction periods.

Figure 1. Orthophoto of the Ilulissat Airport. The test fill and the present research area is located at the southeastern corner on the solifluction slope. Equidistance is 2 m. ©Asiaq 2000.

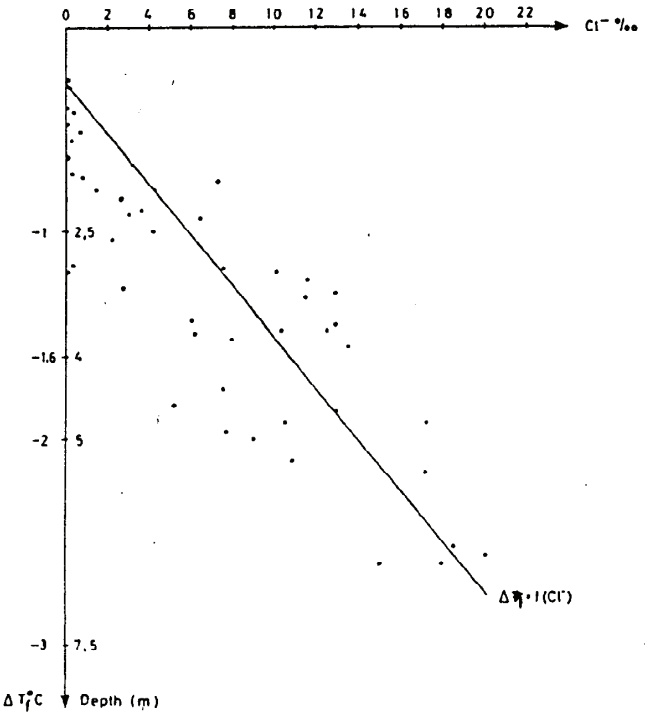

Figure 2. Salinity as function of depth in boreholes and the estimated minimum freezing point depression.

Table 1. Chemical composition of pore water (g/l).

Borehole No.	Depth (m)	w (%)	Ca^{+} (g/l)	Mg^{++} (g/l)	K^{+} (g/l)	Na^{+} (g/l)	Cl^{-} (g/l)
79005	3.1	30.3	0.66	0.44	0.22	5.45	11.72
79011	5.0	34.1	0.65	0.36	0.30	4.84	10.26
79012	3.6	46.4	0.35	0.18	0.23	2.59	6.03
79012	8.0	63.4	0.35	0.25	0.24	3.94	8.52
Seawater			0.40	1.35	0.38	10.50	19.00

Collected soil specimens were stored in their frozen state and transported to the laboratories in Denmark for geotechnical classification properties as water content w (%), bulk density ρ_b (g/cm^3) using the Archimedes principle of volume determination with buoyancy in chilled trichlorethene, void ratio and saturation degrees of water and ice, S_r and $S_{r,ice}$ (%), using the specific soil particles density of ρ_s = 2.75 g/cm^3 and ρ_{ice} = 0.917 g/cm^3. The salinity variations in the pore water were established as the chloride content Cl^- (grams per liter = g/l or ‰) using $AgNO_3$–titration on diluted samples. Some additional tests on the cation-distribution by means of specific electrodes are shown in Table 1. Consequently, it was considered that Cl^- might be a useful indicator of the total ion content in the pore water as also shown by Foged (1979).

On intact core samples from the borings the freezing point depression ΔT_f was found by means of controlled, very slow thawing from the storage temperature. The results are shown together with the measured chloride content and the estimated minimum freezing-point depression as function of Cl^- in Figure 2.

Generally, the thawing showed a general transition over a wide temperature range, which also was seen in a series of consolidation tests carried out with well-controlled temperature steps of 1°C from -9°C to 0°C and continuous deformation registrations and further ordinary loadings shown in Figure 3. The example relates to borehole 78020 Lab.No. 156 from the depth of 3.2 m on frozen clay with a water content of 31.5% and Cl^-=13.0 g/l. From a geotechnical viewpoint it was very interesting that the test specimen after the controlled drained thawing, which caused 7.8% of deformation, showed an apparent preconsolidation of 210 kPa much higher than the in situ stress level of σ_o<55 kPa, due to desiccation of the clay structure by ice lenses. The sample appeared in thawed condition as a fissured silty clay. Another finding was that the drainage process takes place under partially frozen conditions, as seen from the step function of deformation in Figure 3.

Permafrost

The investigations showed the presence of saline marine clays in most depressions in bedrock, with sediment thicknesses up to 12 m. From a theoretical viewpoint this is a permafrost formation as temperatures below a thin active layer (0.2 m to 0.8 m at the time of drilling) were between

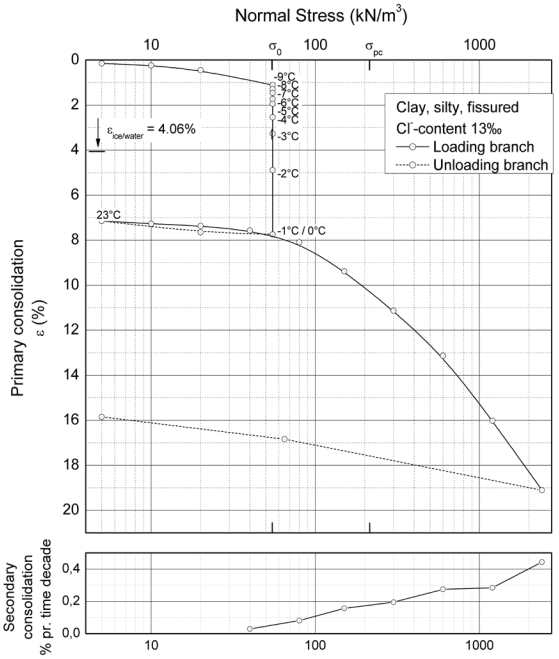

Figure 3. Sample deformation under controlled thawing followed by ordinary consolidation in a number of loading steps.

-1°C and -3.5°C. Technically however, it was obvious that the clay material was only partially frozen and often unfrozen below a depth of 4 m to 5 m b.g.s. The cause was also found by geoelectrical measurements showing extreme low electrical resistivity (<4 ohmm) and as previously shown by chemical analyses, which showed that the pore water changed gradually with depth from fresh water at the surface towards seawater at depths >5 m. The varying concentrations of pore water salinity give rise to various freezing-point depressions down through the deposits. Consequently, the thermal stability is very vulnerable to changes in the heat flux as the latent heat of soil layers may be limited. The clay formations showed variable freezing point depressions from -1°C to -3.5°C. Generally we found under 0.5 m active layer a 2 m to 4 m thick layer of frozen ice-rich clay was found underlain by unfrozen clay at soil temperatures of -3°C down to bedrock.

Furthermore, the geotechnical strength and deformation properties in such deposits must also vary with the thermal state from frozen deposits to unfrozen soil resulting in low shear and deformation properties. This would be of critical importance, when a runway is to be constructed on an embankment of up to 5 m of rock fill on top of such deposits.

Evaluations done related to the construction

Fine-grained deposits will always cause freezing point depression because of capillary tension in the pores, (Williams 1967, Pusch 1979, Tsytovich 1975) and parts of the water may remain unfrozen down to a temperature of -10°C. However, the combination with varying salinity in the pore water we found in literature only some results with the same tendency described by Young et al. (1979). It was

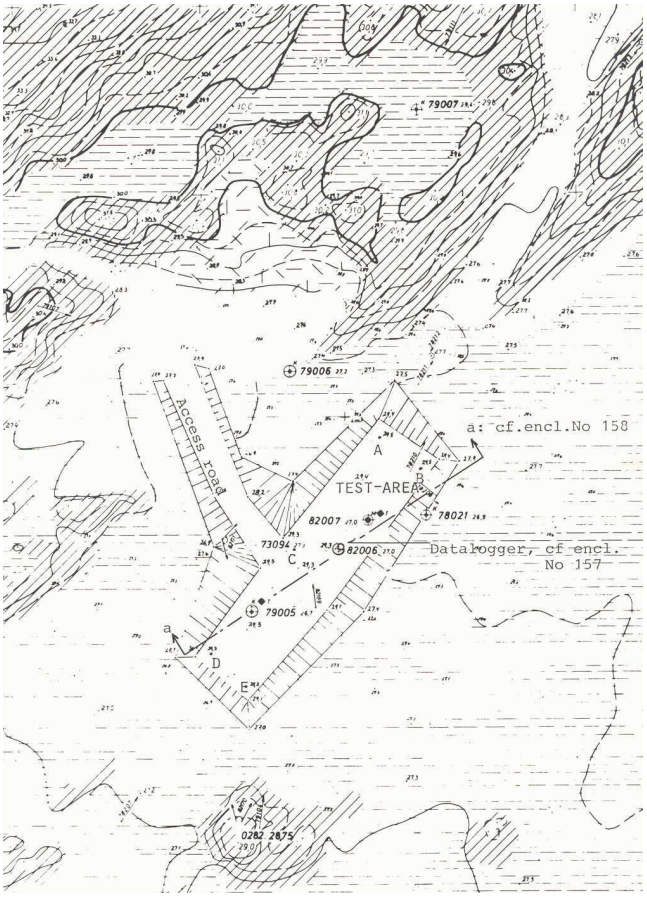

Figure 4. Test site at the south eastern corner of the present runway.

characteristic for the area and other locations in Ilulissat (Olesen 2003), that a considerable part of the pore water is frozen at a depth of 4 m to 5 m below ground surface. The soil exhibits properties of unfrozen material in spite of temperatures of -2°C to -4°C. Consequently, only a limited heat capacity is available when temperature conditions change in the area due to constructions (and as seen today climatic changes). At that time we could not find practical experiences from the Arctic that could be directly applied.

The initial program showed major problems with two basins situated in the southeastern part of the area. The partly frozen and unfrozen sediments up to 12 m in thickness gave rise to latent risk of settlements caused by thawing and ordinary consolidation due to applied load from the construction. These conditions motivated the final choice of location for the runway as shown on Figure 1. Even with this choice, critical soil conditions were met to a minor extent along the runway and it was decided to excavate these small basins and to substitute the clay with compacted rock fill.

Test fill

With a view to future road construction, terminal area, and extensions of the runway, investigations were initiated in a test fill being placed in the critical area in combination with continuous recording of temperature in representative borings under and outside the test fill. The results have been

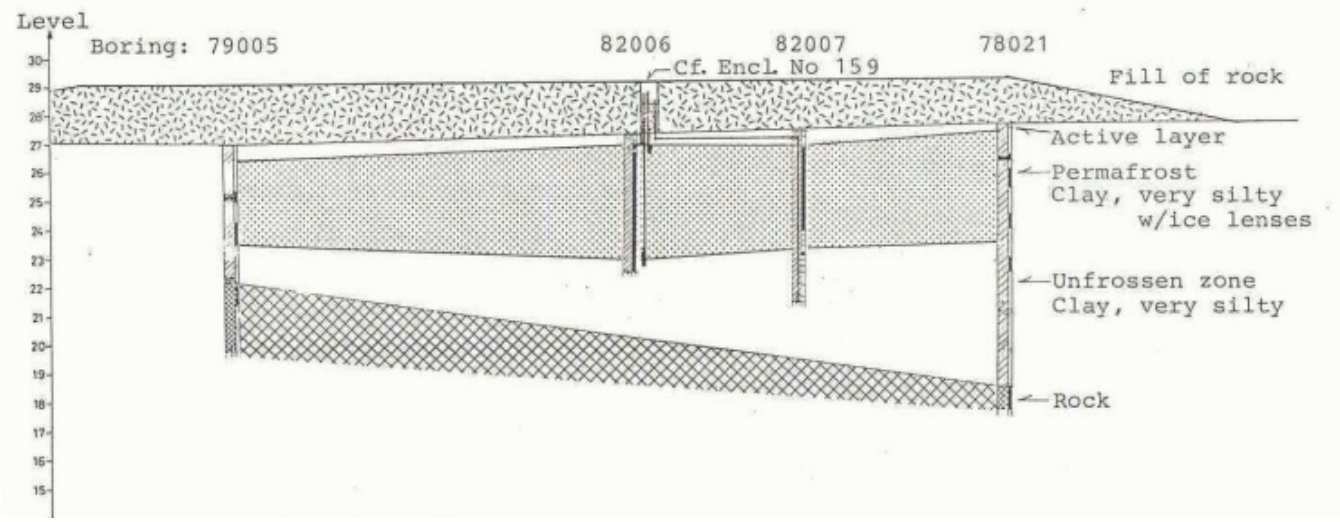

Figure 5. Cross section in the test fill along A-B.

the background for a M.S. project at the DTU Institute for Geology and Geotechnical Engineering in cooperation with the Danish Geotechnical Institute with the senior author as supervisor. The topic for the master thesis by Civil Engineer M.S. Søren Frederiksen (1993) was: "Foundation in Permafrozen Areas" reflecting construction methods of a fill area of compacted blasted rock fill. The technical details and the results through the initial observational period (approximately 5 years) and later on have never been published.

Ilulissat Airport and Test Fill

The test site was placed before construction of the runway as shown on Figure 4 and with a cross section as shown in Figure 5 in a typical basin of marine clay in the southeastern part of the airport area. The test fill was constructed along with some instrumented boreholes with deformation gauges and temperature sensors. The test fill was observed for 5 years during and after construction of the airport and in 2007 found intact and partly operational. The original technical findings are reported by the Danish Geotechnical Institute Geotechnical report No. 9 Jakobshavn Ilulissat. Temperaturmålinger. Prøvefelt. dated 1985-04-23 to Grønlands Tekniske Organisation (Asiaq-Greenland Survey).

The soil and permafrost conditions relate to boreholes 78021, 79005, 82006, and 82007 of which 78021 was selected for presentation in Figure 6. The soil formations consist of marine clay and silt deposits, being part of the marine Quaternary clay formation found up to approximately 50 m a.s.l. in Ilulissat. The profile shows diluted seawater content in the top zone and occurs presently partly permafrozen and unfrozen as previously discussed. The test site was established close to the present safety zone with a typical ca. 2.5 m thick layer of blasted rock fill overlain by some graded coarse gravel similar to the safety zone. For control of the changes in temperature in the test fill and the underlying marine clay a series of continuous temperature measurements were carried out in the boreholes 79005, 82006, and 82007. The deformation gauges were placed at the bottom and top of the real permafrost layer and at the original terrain surface under the test fill. Secured by a measuring well as seen in the cross section the settlement gauges were placed inside a lubricated tube to secure free motion. Furthermore 5 fixed measuring points were established on the top of the test fill in the graded gravel.

The boreholes outside the construction area show a slight tendency of temperature rise (1°C to 2°C) during the period until 1984. Below the test fill a yearly mean temperature of -4°C was found in 2 m depth rising to -3°C at 4 and 5.5 m of depth before filling up (1980 to 1982). After construction (1982 to 1984) values of -5.5°C to -3.5°C were found. The technical conclusion was that the 2.5 m rock fill and graded coarse gravel isolate against conductive heat during summer and allows enhanced convective heat transfer during winter resulting in approximately 1°C to 1.5°C lower yearly mean temperature. The settlement measurements show at all gauges and defined points less than 1 mm to 3 mm mainly reversible deformation, which are at the limit of the measuring resolution. Consequently, it must be stated that during the short control period the effect of filling up with 2.5 m of very coarse grained fill of blasted rock with a top layer of graded gravel must be considered positive.

In 1993 Søren Frederiksen visited the Ilulissat Airport area and downloaded from the data logger a full set of data from 1984 to 1987. He also collected a new series of measurements.

Below the test fill the original surface showed total settlements of 3 cm and the boundaries to top and bottom of originally permafrozen clay were unchanged. However, the top of the test fill showed continued settlements of up to 7 cm over the total period. The time series of the temperature sensors in boreholes B82006 and B82007 show that the upper limit of permafrost rises and a larger part of the original soil maintains permafrozen as expected.

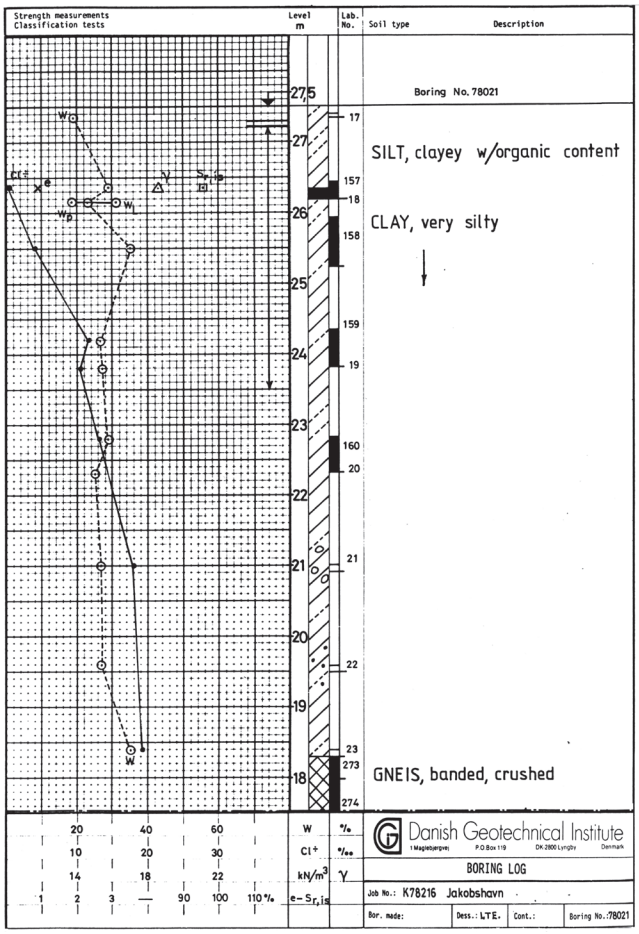

Figure 6. Typical original borehole diagram for borehole 78021 from the test fill showing the discussed soil classification parameters.

Figure 7. Photo of the tilt and heave of the fence pile due to a horizontal slide of the rock fill slope guided by deformation in the active layer.

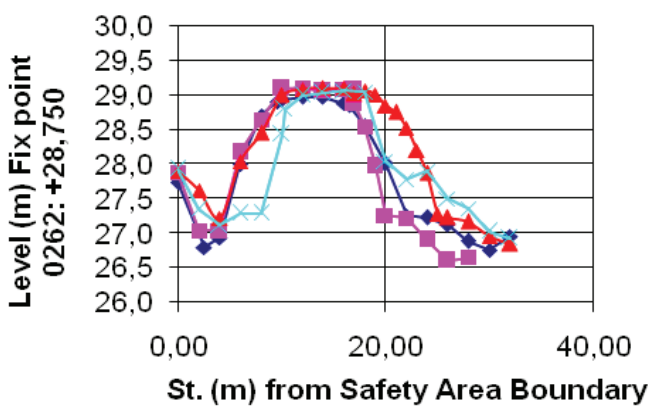

Figure 8. Results of a leveling of the test fill carried out in June 2007.

Ilulissat Airport and test fill, revisited in 2007

In the NSF ARC-0612533 project "Recent and future permafrost variability, retreat and degradation in Greenland and Alaska: An integrated approach" this area was chosen as a type locality for permafrost studies in saline clay related to infrastructures. In June and August 2007 we revisited the area after 25 years of operation and found the constructions in very fine condition with only minor failures and deformations at the boundary of the test fill as seen on Figure 7. The slope of the test fill has moved horizontally due to a failure in the active layer which also turns the airport fence approximately 30°C. Søren Frederiksen showed some vertical deformation due to frost heaving of the pile.

In 1993 Søren Frederiksen observed somewhat less heave of the fence piles, however he did not observe any sliding. Consequently, it must be concluded that the present climate since 1993, which had the lowest registered temperatures since the construction of the airport, might have caused changes in the shear strength or changed the thickness of the active layer allowing for a failure to take place. We performed a levelling of the test fill surface in June 2007. The results for 4 sections A-D with a distance of 10 m perpendicular to the fence with station 0 at the safety zone boundary are shown in Figure 8. The failure zone in the test fill is found between St. 17 and 19 and in front of the test fill the sloping side and the soil layers in front of it show obvious horizontal displacement approximately 0.5 m away from the constructed test fill boundary. The fence is deformed similarly. In comparison to the levelling performed in the period of 1982 to 1987 and in 1993 the central part of the test fill shows only very little deformation as the level is found to a value of approximately +29 comparable to the earlier levelling results of +29.15 to +29.30 in July 1993.

Conclusions

The present contribution and an accompanying contribution, Ingeman-Nielsen et al. (2007), to NICOP 2008 present the new findings together with an overview of the project investigations done during the period of 1978 to 1984.

The geotechnical deformation and strength properties were studied in detail and influenced the final design and construction very distinctly. It was decided to keep the runway away from the deep basins of marine clay for stability and settlements reasons. Under the runway and taxiway and in the terminal area frost susceptible soils were substituted by rock fill.

These decisions led to a generally very stable runway, taxiway, and terminal area. According to interviews with the technical personnel at the airport only one repair has been performed of the asphalt concrete layer in an area where settlements occurred due to some natural silt and clay being left under the bearing layer during construction of compacted rock fill and coarse gravel fill.

The behavior of the test fill slope shows the present climatic change might explain a boundary failure and horizontal deformation in front of the test fill causing the Airport fence to tilt and heave.

Consequently, the detailed studies carried out in 1978 to 1985 have led to safe construction with very little need for repair and maintenance. We will continue the permafrost studies in the coming period as part of the present NSF ARC-0612533 project "Recent and future permafrost variability, retreat and degradation in Greenland and Alaska: An integrated approach." The locality is a well documented example on saline permafrost under discontinuous permafrost condition.

Acknowledgments

The original investigations were performed by the Danish Geotechnical Institute for Grønland Tekniske Organisation (now ASIAQ) on behalf of Grønlands Luftshavns Væsen GLV (now Mittarfeqarfiit). During design and construction of Jakobshavn Airport the senior author had a very close cooperation with Civil Engineer Poul Væver-Petersen from the Danish/Greenlandish consultant Nielsen & Rauschen-berger (now NIRAS). Permission to publish and valuable discussions with lead members and employers of the mentioned institutions are gratefully acknowledged. Furthermore, the work done in the M.S. Thesis by Civil Engineer Søren Frederiksen, INUPLAN, Nuuk, Greenland has been of great value.

The later part of this research was funded by the Polar Earth Science Program, Office of Polar Programs, National Science Foundation (ARC-0612533).

References

Bennike, O. & Björck, S. 2002. Chronology of the last recessionof the Greenland Ice Sheet. *Journal of Quaternary Science* 17 (3): 211-219.

Christiansen H.H. & Humlum, O. 2000. Permafrost. In: B.H. Jakobsen, J. Böcher, N. Nielsen, R. Guttesen, O. Humlum & E. Jensen (eds.), *Topografisk Atlas Grønland*. Copenhagen: C.A. Reitzets Forlag, 32-35.

Danish Geotechnical Institute. *Geotechnical Reports related to K78216 Jacobshavn*. (Restricted, internal, unpublished).

Foged, N. 1979. *Engineering Geological Investigations of Quaternary Marine Clay Deposits on West Greenland*. Ph.D .Thesis. The Institute for Applied Geology. Technical University of Denmark,. (In Danish with English Overview).

Foged, N. & Bæk-Madsen, C. 1980. Jakobshavn Airport. thermal stability in marine deposits. *Proceedings of 2nd International Symposium on Ground freezing*, *Trondheim, Norway.* Reprint 1-10.

Frederiksen, S. 1993. *Foundation in Permafrozen Areas. A Blasted Rock Test Fill Influence on the Thermal Conditions*. M.S. Thesis. Institute for Geology and Geotechnical Eng.

Olesen, O.B. 2003. *Shallow Borehole Temperatures, Ilulissat, Greenland.* Greenlandic Geological Survey (GEUS). Distributed by National Snow and Ice Data Center/ World Data Center for Glaciology.Digital Media.

Pusch, R. 1979. Unfrozen water as a function of clay microstructure. *Engineering Geology* 13: 157-162.

Tsytovich, N.A. 1975. *The Mechanics of Frozen Ground.* New York: McGraw-Hill Book Company.

Weidick, A. 1968. *Observations on Some Holocene Glacier Fluctuations in West Greenland.* Meddelelser om Grønland, Bd. 165, Nr. 6, København.

Williams, P.J. 1967. *Properties and Behavior of Freezing Soils,* Norwegian Geotechnical Institute, Publ. No. 72, Oslo, Norway.

Young, R.N., Cheung, C.H. & Sheeran, D.E. 1979. Prediction of salt influence on unfrozen water content in frozen soils. *Engineering Geology* 13: 137-155.

Genesis of Reticulate-Chaotic Cryostructure in Permafrost

Daniel Fortier
University of Alaska Fairbanks, Institute of Northern Engineering, Fairbanks, U.S.A.
Mikhail Kanevskiy
University of Alaska Fairbanks, Institute of Northern Engineering, Fairbanks, U.S.A.
Yuri Shur
University of Alaska Fairbanks, Department of Civil and Environmental Engineering, Fairbanks, U.S.A.

Abstract

Cryostratigraphic studies in the CRREL permafrost tunnel in Alaska revealed the presence of multi-directional ice veins in the permafrost which was described as reticulate-chaotic cryostructure. Our hypothesis relates the formation of this cryostructure to inward freezing of saturated sediments trapped in underground channels cut in the permafrost by thermo-erosion. The multi-directional reticulate ice veins were formed in the sediments deposited in the underground channels after the cessation of the underground water flow. This hypothesis was confirmed by laboratory experiments which reproduced reticulate-chaotic cryostructures and thaw unconformities in the sediments similar to those observed in the CRREL permafrost tunnel.

Keywords: CRREL tunnel; freezing cell; ground ice; ice segregation; reticulate cryostructure; underground thermo-erosion.

Introduction

The CRREL permafrost tunnel (≈ 64°57′N, 147°37′W) is located near Fairbanks, Alaska. In the 1960s, a 110-m long tunnel and an inclined winze were excavated in the ice-rich silt and the underlying fluvial gravel that locally form the permafrost. The geology, the cryostratigraphy, the chronology of the tunnel, and the properties of the permafrost were described in many publications (Sellmann 1967, 1972, Pettibone & Waddell 1973, Huang et al. 1986, Hamilton et al. 1988, Long and Pewe 1996, Shur et al. 2004, Bray et al. 2006). The stratigraphy of the permafrost exposed in the tunnel and in the winze consists of an ice-saturated gravel deposit unconformably covering weathered schist bedrock. Fluvial sandy silts overlay the gravelly unit and are covered by partially reworked eolian silts. The latter are syngenetic in nature, ice-rich, and characterized by a micro-lenticular cryostructure and, to a lesser extent, by layered and lenticular-layered cryostructures (Shur et al. 2004; Bray et al. 2006, Kanevskiy et al. 2008).

This paper focuses on the genesis of reticulate-chaotic cryostructures firstly described in the CRREL permafrost tunnel by Shur et al. (2004). The reticulate-chaotic cryostructures are associated with stratified sediments or massive ice bodies enclosed in the frozen ground or cross-cutting ice wedges. A reticulate cryostructure develops when ice crystals oriented in the direction of freezing and growing into the still unfrozen sediments are intersected by crystals of other orientation (Shumskii 1964a). Mackay (1974) proposed that the preferred growth of reticulate ice veins was linked to the restriction of an upward flow of water which prevented the maintenance of a stationary freezing plane and the growth of horizontal ice lenses. Murton and French (1994) mentioned that it is unclear why some reticulate cryostructures are regular and others are irregular. Our hypothesis is that reticulate-chaotic cryostructures observed in the CRREL permafrost tunnel were formed in a closed-system by inward freezing of saturated sediments deposited in underground thermo-erosion channels or gullies. The objective of this study was to reproduce in the laboratory inward freezing of saturated sediments in underground channels analogs in order to support our interpretations of reticulate-chaotic cryostructures genesis.

Methods

Field methods

Cryostratigraphic studies, performed in the CRREL permafrost tunnel in 2004–2006 (Shur et al. 2004, Bray et al. 2006), revealed the occurrence of a cryostructure named reticulate-chaotic. We logged and sketched the permafrost stratigraphy of exposures with reticulate-chaotic cryostructures enclosed in syngenetic permafrost. Samples were retrieved, described, and analyzed for their ice content. The grain size distribution of the sediments was obtained using sieves and an hydrometer (ASTM D422 2008). We studied the morphology and the density of reticulate ice veins and ice lenses within the sediments. Special attention was paid to the contact between the sediments with reticulate-chaotic cryostructure and the enclosing original syngenetic permafrost.

Laboratory methods

To reproduce reticulate-chaotic cryostructures, we conducted 20 laboratory experiments. We used a temperature-controlled environmental chamber to freeze sediments in PVC cells at temperature between -20°C and -25°C for at least six hours. Saturated sand or silt at room temperature were poured

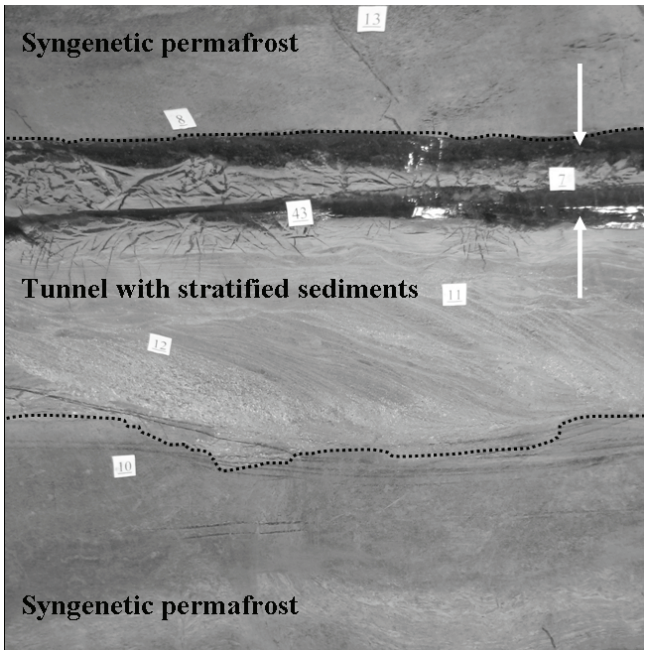

Figure 1. Underground channel filled with stratified sediments enclosed in syngenetic eolian silt. The erosion unconformities are outlined by dotted lines. The upper part of the underground channel contains layers of clear ice (arrows) underlain by stratified sediments dissected by reticulate-chaotic ice veins. The white paper scales are 2.5 x 2.5 cm.

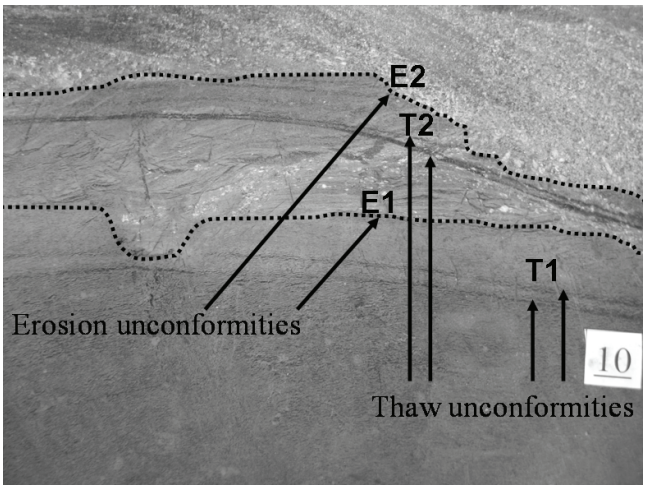

Figure 2. Close-up of erosion and thaw unconformities shown in Figure 1. The lowermost erosion unconformity (E1) is older and located at the bottom of the ice-poor stratified silts. Ice lenses located at the boundary with the underlying ice-rich syngenetic eolian silts mark the location of the thaw unconformity (T1) associated with E1. The uppermost erosion unconformity (E2) is younger and located at the bottom of the ice-poor stratified sand and gravel. The younger thaw unconformity T2 associated with this erosion boundary is marked by ice lenses located in the previously deposited sediments. The paper scale is 2.5 x 2.5 cm.

in the cells and allowed to freeze. After two days, a core was extracted from the central part of the frozen sediments to produce a cavity. A portable carbide and diamond crown drill was used for this procedure. The coring stopped at 5 cm to 10 cm above the bottom of the cells. The environmental chamber was then set to -5°C and kept at this temperature for one day to allow frozen soils to warm-up to this temperature. The cavity was used as an analog for underground thermo-erosion channels enclosed in permafrost. Cavities were filled with well-mixed supersaturated sediments previously kept at temperature between 1°C to 4°C. We used clay, silt, and sand sediments to test the effect of soil texture on the configuration of the cryostructures. We used soils with 80% and 150% gravimetric water content to test the effect of water content on the density of reticulate ice veins. Slices of frozen soil approximately 5 cm thick cut from the extracted cores and conditioned to -5°C were used as lids to close the underground channel analogs. The samples were allowed to freeze back in situ at a temperature of -5°C for 7 days to 14 days depending on the size of the freezing cells.

We used three different sizes of circular freezing cells to test the effect of underground channel size on the development of ground ice cryostructures. The first type of cell was 30 cm in diameter, 37 cm tall and covered by a 10 cm thick layer of mineral wool. The bottom and the top of the cell were covered by a 5 cm thick extruded polystyrene layer. The second type of cell was 17 cm in diameter, 75 cm tall and insulated by 5 cm thick extruded polystyrene rings. The third type of cell was 10 cm in diameter, 30 cm tall and covered by a 3 cm thick insulation layer. This cell was equipped with a consolidation device and cooled by thermal baths from the top and the bottom of the cell.

After the experiment, the frozen samples were extracted from the cells and cut into slices about 5 cm thick. The cryostructures were described. We analyzed the ice content of cores 2.5 cm in diameter extracted from the center and the side of the underground channel analogs slices. The geometric configuration of the ground ice formed and the contact with the enclosing sediments were described and compared to field observations in the CRREL permafrost tunnel.

Results

Field observations

Twenty ice wedge exposures can be observed in the adit of the CRREL permafrost tunnel. With the exception of one, all the observed ice wedges are showing signs of thermo-erosion. Remains of ice wedge with shapes atypical of syngenetic ice-wedge growth were observed at the erosion boundaries. Some ice wedges were cut by underground channels and gullies filled with sediments cutting across or enclosed in ice wedges. These underground channels are also enclosed in the syngenetic eolian silt surrounding the ice wedges (Fig. 1).

The syngenetic undisturbed permafrost comprises organic-rich fine eolian silts with abundant rootlets, oxydo-reduction stains, and millimeter-to-centimeter thick peat layers (Fig. 1). The permafrost is characterized by an ice-rich micro-lenticular cryostructure with gravimetric water contents usually above 100%.

Figure 3. Typical reticulate-chaotic cryostructure with multi-directional interconnected ice veins and ice lenses. The handle of the knife is about 6 cm long.

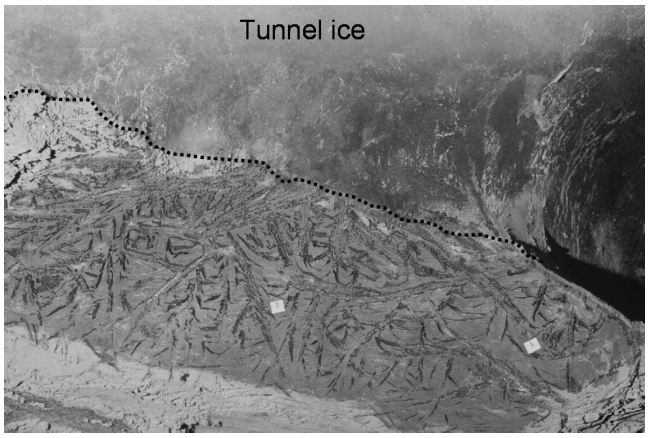

Figure 4. "Tunnel ice" underlain by sediments with high-density reticulate-chaotic cryostructure. The white paper scales are 2.5 x 2.5 cm.

The underground channels could often be traced over several meters. They had a slight inclination and flat to bowl-shape channel bottom. The channels were outlined by erosion unconformities at their contact with the syngenetic undisturbed permafrost (Fig. 2). In the underground channels, the sediments were mostly stratified and clearly different than the surrounding syngenetic eolian silt (Figs. 1, 2). For instance, in Figure 1, the underground channel is filled with ice and silty sands and gravels having oblique, cross, wavy, and horizontal stratifications (see also Fig. 2). The average gravimetric ice content of the cross-stratified sands in the underground channel is 44.6% (n = 8), whereas it is 107.7% (n =17) in the surrounding syngenetic permafrost.

In some cases the underground channels were only partially incised in the wedges and extended in the adjacent underground channels previously cut in the syngenetic permafrost. Among the observed channels, the grain-size fraction and the stratification patterns varied which suggests the occurrence of different sources of sediments and depositional modes, probably related to distinct thermo-erosion events along similar flow paths.

Along the boundaries of the underground channels, thaw unconformities were observed (Fig. 2). They were marked by a continuous ice lens a few millimeter-thick sub-parallel to the channel boundaries. The thaw unconformities were usually located a few millimeters to a few centimeters in the syngenetic permafrost surrounding the underground channels. The permafrost between the erosion boundary and the thaw unconformity did not have a micro-lenticular cryostructure. This indicates that after deposition of the saturated sediments, the release of heat from the water trapped in the underground channels melted the ground ice of the adjacent syngenetic permafrost. Freezeback of the thawed sediment created an ice lens marking the thaw unconformity. When underground channels were observed to cut through prior channels the thaw unconformities were located in the sediment of the eroded channels (Fig. 2). Thaw unconformities were also observed in the ice wedges cut by channels. Millimeter-thick ice lenses, often with elongated air bubbles aligned perpendicular to the thaw unconformity, were intercalated between the ice wedge and the sediments of the underground channels.

Usually, the sediments deposited in the underground channels were characterized by a reticulate-chaotic cryostructure made of multi-directional interconnected ice veins and ice lenses (Fig. 3).

Close to the underground channel boundaries, the ice veins were aligned perpendicular and the ice lenses parallel to the erosion unconformities. The concentration of ice veins and ice lenses were higher close to the channel boundaries, especially but non-exclusively at the bottom of the channels and decreased toward the center of the channel (Fig. 4). In the underground channels, the layers of sediments with reticulate-chaotic cryostructure were sometimes intercalated with centimeter-thick layers of clear ice with mineral or organic inclusions (Fig. 1).

About 60% of the underground channels cutting through the ice wedges and the enclosing syngenetic permafrost were partially or entirely filled by sub-horizontal non-foliated ice bodies (Fig. 4). The ice was clear to whitish, sometimes with orange to dark-brown bands in the central part and contained embedded organic matter. The ice had a columnar crystalline structure and bubble trains that suggested inward freezing. In the literature, this type of ice was previously called "thermokarst-cave ice" (Shumskii 1964b, Bray et al. 2006) or "pool ice" (Mackay 1988, 1997). We propose the term *tunnel ice* to describe massive ice bodies formed by inward refreezing of water trapped in underground thermo-erosion pipes, channels, and tunnels (Fortier et al. 2007). Usually at the bottom of these *tunnel ice* bodies we observed a sub-horizontal layer of sediment with a reticulate-chaotic cryostructure (Fig. 4).

Laboratory observations

The experiments in the laboratory reproduced reticulate-chaotic cryostructures similar to those observed in the field (Fig. 5). They were formed in the underground channel analogs during freezeback of the sediments.

The density of ice veins and ice lenses was always greater along the walls of the channel analogs than in the central part,

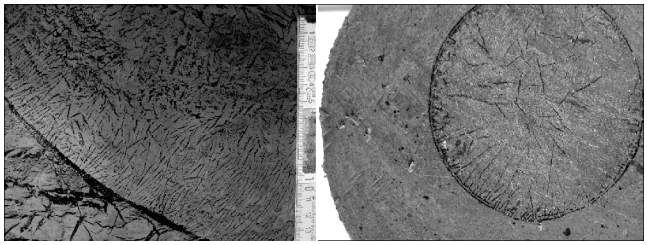

Figure 5. Comparison of field (A) and laboratory (B) observations. (A) Portion of an underground channel. The boundary (lower left corner) of the channel is outlined by a mm-thick ice lens. The sediments in the channel (right corner) are characterized by a reticulate-chaotic cryostructure (B) Channel analog 8 cm in diameter showing an ice lens at the channel boundary and reticulate-chaotic cryostructure similar to what was observed in the field (A).

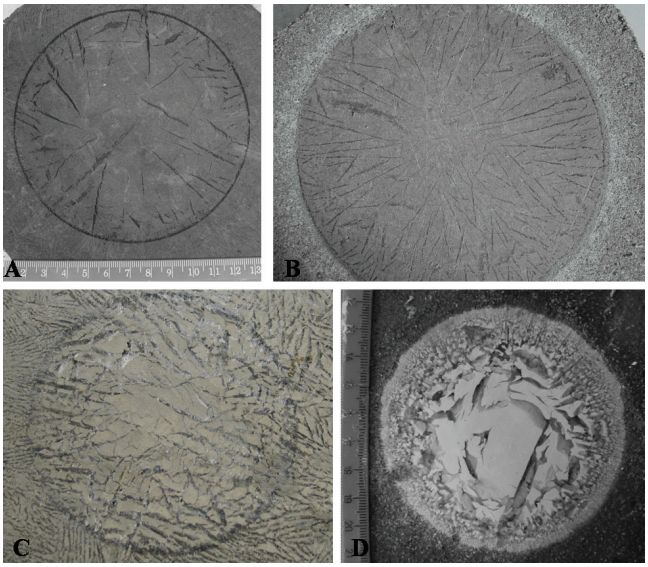

Figure 6. Cross-sections of channel analogs 8 cm in diameter with reticulate-chaotic cryostructures. (A) syngenetic eolian silt from the CRREL permafrost tunnel, 80% water content slurry; (B) fine silt <75µm, 80% water content, slurry; (C) fine silt <75µm and clay, 150% water content slurry; (D) clay, 150% water content slurry.

independent of grain-size and water content of the sediments (Fig. 6). Figures 6 and 7 show that the ice veins and ice lenses are often interconnected close to the boundary of the channel analog. In cross section, the ice veins were mostly aligned normal to the boundary. They extended toward the center with many ice lenses connected sub-perpendicular to them. The pattern of ice veins was more chaotic in the center of the channel analogs (Fig. 7). Consolidated sediments produced thin ice veins.

We observed thaw unconformities at the boundary of some underground channel analogs. On Figure 8, the ground ice in the frozen sediment enclosing the channel analog melted and secondary ice lenses were formed after freezeback.

Larger and thicker ice veins and ice lenses were formed in larger freezing cells. We used silt with a grain size fraction <75 µm and a water content of 150% for the slurry. Figure 9 shows that a thick ice lens was formed at the channel analog boundary. Large multi-directional ice veins were formed in the center of the channel analog.

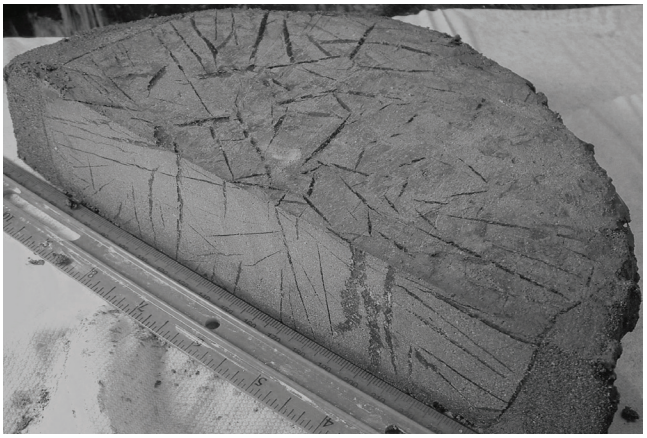

Figure 7. Cross-sections of a channel analog 25 cm in diameter (silt <75 µm, 150% water content slurry) with interconnected multi-directional ice veins and ice lenses. Note the similarity with reticulate ice veins of Figures 3 and 4.

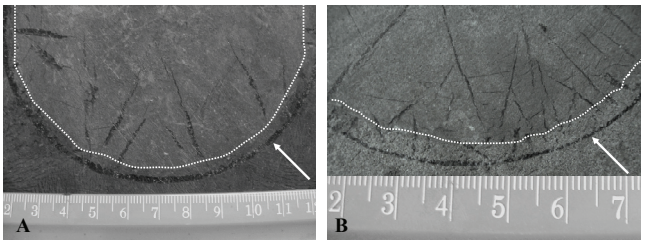

Figure 8. Cross-sections of channel analogs 8 cm in diameter showing thaw unconformities (arrows) located in the enclosing frozen ground. The dotted lines indicate the channel analog boundaries. (A) fine eolian silt from the CRREL permafrost tunnel with 80% water content. (B) coarse eolian silt from the CRREL permafrost tunnel with 80% water content.

We observed that fine-grained sediments produced more and larger ice veins and ice lenses than coarse-grained sediments. In Figures 6A and 6B, eolian silt from the CRREL tunnel was used for the experiment. In the experiment of Figure 6C, we used a mix of silt with a grain size fraction <75 µm and kaolinite clay. Experiments with clay soils are presented in Figures 6D and 10. The fine sediments produce a well-developed reticulate-chaotic cryostructure with a high density of ice veins and ice lenses. Figure 10 shows that the chaotic nature of the cryostructure and the formation of a thick ice lens at the channel analog boundary were better expressed in clay sediments.

In Figure 8A the gravimetric ice content of the sample after freezing was 122% at the channel boundary and 51% in the center whereas it was 58% at the channel boundary and 53% in the center in Figure 8B.

Discussion

Mechanism of reticulate-chaotic cryostructure formation

We observed in our experiments that saturated and super-saturated sediments trapped in frozen cavities (underground channel analogs) and submitted to slow inward freezing develop a reticulate-chaotic cryostructure. After deposition of the sediment, release of heat from water trapped in the

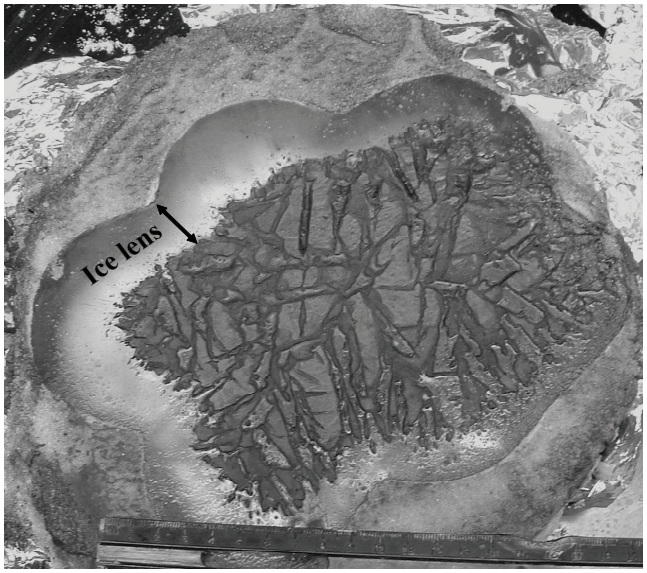

Figure 9. Cross section of a large channel analog formed in a large freezing-cell. A thick lens of pure ice was formed along the channel boundary between the coarse frozen sand and the fine silt (dark colored) in which large interconnected multidirectional reticulate ice veins were formed. The gravimetric ice content of the silt is 287%.

sediment can melt the ground ice in the adjacent frozen sediments (Fig. 7). Inward freezing of the sediment creates one or more ice lenses at or close to the channel boundary (Figs. 6, 7, 8, 9, 10). Thicker ice lenses and larger reticulate ice veins were developed in: (1) slow freezeback scenarios (large freezing cells), (2) sediments with high water content, and (3) fine-grained sediments (fine silt and clay) (Figs. 6C, 6D, 9, 10). Due to redistribution of water in a closed system, the periphery of the underground channels analogs contained more ground ice than the center. At the beginning of freezing the uniform propagation of the freezing front inward created similarly aligned reticulate ice vein along the channel boundary. The chaotic nature of the reticulate ice veins is better expressed towards the center of the channels due to the slowing down and uneven inward propagation of the freezing front in sediments with lower water contents.

Formation of reticulate-chaotic cryostructures in the CRREL permafrost tunnel

Our experiments support the idea that reticulate-chaotic cryostructures were formed in relation to thermo-erosional events in the CRREL permafrost tunnel. A widespread network of underground channels was developed and buried during the syngenetic aggradation of the permafrost. The channels enclosed in the syngenetic eolian silt and cutting through the ice wedges were formed by underground thermo-erosion (Péwé 1982, Fortier et al. 2007). The stratified sediments in the tunnel were deposited by water flowing into the underground channels and after the cessation of the underground flow, either due to blockage or after the surface run-off period. The multi-directional ice veins observed in the sediments filling up the channels and at the base of the non-

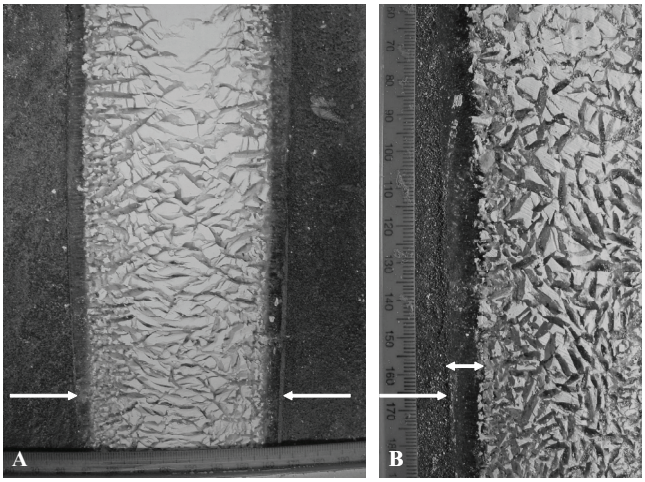

Figure 10. (A) longitudinal cross-section of a channel analog 8 cm in diameter. (B) Close-up of (A) showing a well-developed ice-rich reticulate-chaotic cryostructure in clay (150% water content slurry) with a thick ice lens (arrows) at the channel boundary.

foliated *tunnel ice* bodies were formed after inward freezing of the sediments. Slow freezeback of supersaturated fine-grained silt developed dense reticulate-chaotic cryostructure patterns with thick ice veins.

Conclusion

Freezing of sediments trapped in underground channels cut by thermo-erosion in the permafrost that are submitted to inward freezing develops a reticulate-chaotic cryostructure. Availability of water, its ability to move through the sediments, and the rate of freezing can create thick ice lenses at the channel boundary and large multi-directional reticulate ice veins in the sediments. The irregular nature of the reticulate-chaotic cryostructure is linked to the uneven propagation of the freezing front in a closed-system with limited water supply. The reticulate-chaotic cryostructure is often observed close to or in contact with *tunnel ice* bodies. This type of ice is formed by inward freezing of water trapped in the underground channels. Our results help to identify ground ice associated with the process of underground thermo-erosion in permafrost exposures.

Acknowledgments

Special thanks are owed to the Fairbanks Office of the Cold Regions Research and Engineering Laboratory for access to the CRREL permafrost tunnel. Margaret Cysewski, Matthew Dillon, and Eva Stephani provided great assistance in field and in the laboratory. The reviewers and the associate editor are gratefully acknowledged for their suggestions to improve the manuscript. This work was supported by the National Science Foundation by grants (EPS-0346770) to Daniel Fortier and Mikhail Kanevskiy and (ARC–0454939) to Yuri Shur. Any opinions and findings expressed in this material are those of the authors and do not necessarily reflect the views of the funding agencies.

References

American Society of Testing and Materials. 2008. ASTM D 422 (Reapproved 1998): Standard test method for particle-size analysis of soils. A*nnual Book of ASTM Standards*. West Conshohocken, Pennsylvania: ASTM, (accessed online).

Bray, M.T., French, H.M. & Shur, Y. 2006. Further cryostratigraphic observations in the CRREL permafrost tunnel, Fox, Alaska. *Permafrost and Periglacial Processes* 17: 233-243.

Fortier, D., Allard, M. & Shur, Y. 2007. Observation of rapid drainage system development by thermal erosion of ice wedges on Bylot Island, Canadian Arctic Archipelago. *Permafrost and Periglacial Processes* 18: 229-243.

Gell, W.A. 1978. Ice-wedge ice, MacKenzie Delta – Tuktoyaktuk peninsula area, N.W.T., Canada. *Journal of Glaciology* 20: 555-562.

Hamilton, T.D., Craig, J.L. & Sellmann, P.V. 1988. The Fox permafrost tunnel: a late Quateranry record in central Alaska. *Geological Society of America Bulletin* 100: 948-969.

Huang, S.L., Aughenbaugh, N.B. & Wu, M.-C. 1986. Stability study of CRREL permafrost tunnel. *Journal of Geotechnical Engineering* 112: 777-790.

Kanevskiy, M., Fortier, D., Shur, Y., Bray, M. & Jorgenson, T. 2008. Pleistocene syngenetic permafrost in the CRREL permafrost tunnel at Fox, Alaska. *Proceedings of the Ninth International Conference on Permafrost, Fairbanks, Alaska, June 29–July 3, 2008* (this proceedings).

Long, A. & Pewe, T.L. 1996. Radiocarbon dating by high-sensitivity liquid scintillation counting of wood from the Fox permafrost tunnel near Fairbanks, Alaska. *Permafrost and Periglacial Processes* 7: 281-285.

Mackay, J.R. 1988. Catastrophic lake drainage, Tuktoyaktuk Peninsula area, District of Mackenzie. In: *Current Research*, *Part D*. Geological Survey of Canada, Ottawa, Ontario, Paper 88-1D: 83-90.

Mackay, J.R. 1997. A full-scale field experiment (1978–1995) on the growth of permafrost by means of lake drainage, Western Arctic Coast: a discussion of the method and some results. *Canadian Journal of Earth Sciences* 34: 17-33.

Murton, J.B. & French, H.M. 1994. Cryostructures in permafrost, Tuktoyaktuk coastlands, western arctic Canada. *Canadian Journal of Earth Sciences* 31: 737-747.

Pettibone, H.C. & Waddell, G.G. 1973. Stability of an underground room in frozen gravel. *Proceedings, American Contribution, Second International Conference on Permafrost, Yakutsk, U.S.S.R., July 13-28, 1973*. Publication 2115. Washington, D.C.: National Academy of Sciences: 699-706.

Péwé, T.L. 1982. *Geologic Hazards of the Fairbanks Area, Alaska*. College, Alaska, Division of Geological and Geophysical Surveys. Special Report 15, 109 pp.

Sellmann, P.V. 1967. *Geology of the USA CRREL Permafrost Tunnel Fairbanks, Alaska*. Hanover, New Hampshire, Cold Regions Research and Engineering Laboratory. Technical Report 199, 22 pp.

Sellmann, P.V. 1972. *Geology and Properties of Materials Exposed in the USA CRREL Permafrost Tunnel*. Hanover, New Hampshire, Cold Regions Research and Engineering Laboratory. Report 177, 16 pp.

Shumskii, P.A. 1964a. Principal of Structural Glaciology. New York: Dover Publications, 497 pp.

Shumskii, P.A. 1964b. Chapter IX. Ground (subsurface) ice. In: P.F. Shvetsov, B.N. Dostovalov (eds.), *Principles of Geocryology (Permafrost Studies*). Academy of Sciences of the USSR, 1959. V.A. Obruchev Institute of Permafrost Studies: Moscow: 247-327 (in Russian). National Research Council of Canada, Ottawa, Technical Translation 1130, 118.

Shur, Y., French, H.M., Bray, M.T. & Anderson, D.A. 2004. Syngenetic permafrost growth: cryostratigraphic observations from the CRREL tunnel near Fairbanks, Alaska. *Permafrost and Periglacial Processes* 15: 339-347.

Fast Permafrost Degradation Near Umiujaq in Nunavik (Canada) Since 1957 Assessed from Time-Lapse Aerial and Satellite Photographs

Richard Fortier, Ph.D.
Centre d'études nordiques, Université Laval, Québec (QC), Canada G1V 0A6
Bernard Aubé-Maurice, M.Sc.
Département de géologie et de génie géologique, Université Laval, Québec (QC), Canada G1V 0A6

Abstract

The spatio-temporal evolution of lithalsas and thermokarst ponds near Umiujaq in Nunavik (Canada) was studied using time-lapse aerial photographs collected in 1957, 1983, and 2003, and IKONOS satellite images taken in 2005 to assess the permafrost degradation. Nine typical sectors located in valleys totalizing a survey area of 2.245 km^2 were selected. The areas occupied by the lithalsas and thermokarst ponds were respectively 0.421 and 0.024 km^2 in 1957 (18.8 and 1.1% of the survey area) and 0.251 and 0.066 km^2 in 2005 (11.2 and 3.0%). The permafrost extent decreased 40%, while the thermokarst one increased 175% in 48 years. According to the climate data from Environment Canada, the mean annual air temperature was quite variable over the study period but increased 3°C during the last 15 years. Climate warming is therefore the main driver of permafrost degradation, but other concurrent mechanisms affecting the thermal balance of permafrost exacerbate the observed degradation.

Keywords: climate warming; lithalsas; mapping; permafrost degradation; thermokarst ponds; time-lapse aerial photographs.

Introduction

Both palsas and lithalsas are cryogenic mounds formed in frost-susceptible marine sediments under a cold climate (Pissart 2002). They are important components of the periglacial landscape in the discontinuous permafrost zone in Nunavik (Canada). The tops of these periglacial features stand a few meters above the surrounding ground due to the accumulation of segregation ice; their mineral cores are ice-rich and they have a diameter of a few tens of meters making them easily recognizable on aerial photographs even at a scale as large as 1:40,000. They are an excellent indicator of the presence of ice-rich permafrost. While the palsas are covered by peat, the lithalsas are free of peat cover (Pissart 2002) and their surfaces are dotted with frost boils. Permafrost degradation due to climate warming and eventually the thawing of lithalsas leave ramparted thermokarst ponds (Luoto & Seppälä 2003, Pissart 2002).

Based on paleoecological studies of permafrost peatlands (Allard & Seguin 1987b), the inception of palsas occurred during cold periods of the Holocene with a maximum extent during the Little Ice Age (LIA), but they are now decaying in response to climate warming. The thawing of palsas and lithalsas located in the discontinuous permafrost zone along the east coast of Hudson Bay, Nunavik (Canada), was studied respectively by Payette et al. (2004) and Vallée & Payette (2007). Their results show continuous permafrost degradation during the 20th century. Between 1957 and the beginning of the 21st century the area occupied by ice-rich permafrost decreased by 84% and 23% respectively at the southern and northern limits of the discontinuous permafrost zone. Permafrost loss was compensated by a concurrent gain in thermokarst ponds. The subsidence of palsas surfaces due to the ground ice melting was of the order of 1 to 1.5 m from 1993 to 2003 (Payette et al. 2004). According to Payette et al. (2004), the main climatic driver for accelerated permafrost thawing was snow precipitation. The hydric conditions affect also the dynamics of lithalsas and control in part their decay (Vallée & Payette 2007).

The purpose of the present study is to map the spatial distribution of lithalsas and thermokarst ponds near Umiujaq in Nunavik (Canada) using time-lapse aerial photographs and satellite images to assess the permafrost degradation since 1957. The comparison of these photographs will allow the evaluation of the decrease of ice-rich permafrost extent. Since the thermal regime of the lithalsas is closely related to climate changes, the assumption of permafrost degradation due to climate warming recently observed in Nunavik (Chouinard et al. 2007) will be thus verified.

Study Area

The study area is located in the discontinuous permafrost zone close to the Inuit community of Umiujaq on the east coast of Hudson Bay, Nunavik, Canada (Figs. 1, 2). The deglaciation of the area took place 7600–7300 years ago. Marine sediments were then deposited in deep valleys. After emergence, the deposits were eroded and colonized by vegetation, and ice-rich permafrost aggraded. Large fields of lithalsas are found in the valleys.

Lithalsas and Thermokarst Ponds

An example of a recent collapse of a lithalsa due to climate warming and an expansion of a thermokarst pond to the detriment of the lithalsa is shown in Figure 3. According to field observations including deep temperature profiles

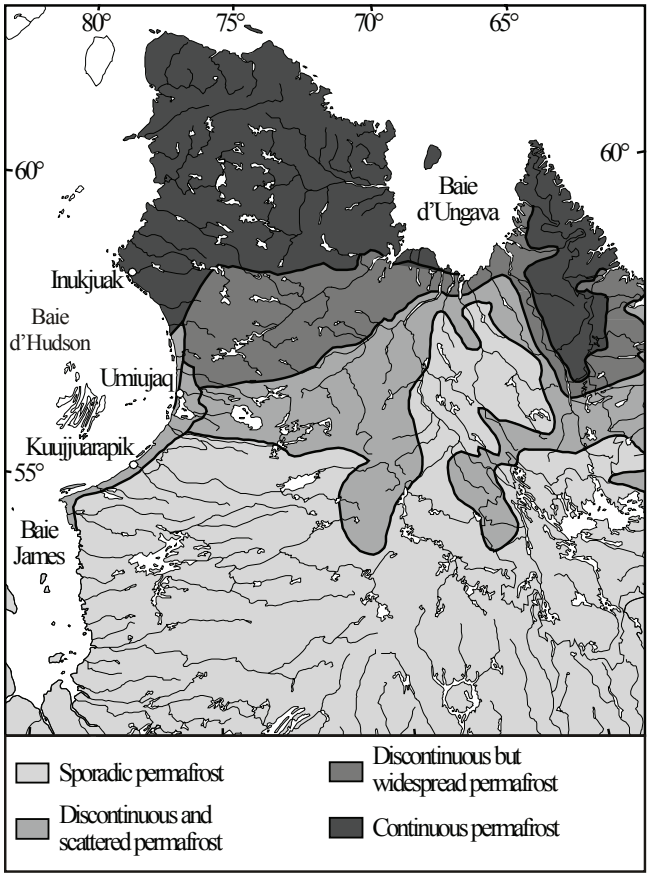

Figure 1. Map of permafrost distribution in Nunavik, Canada (modified from Allard & Seguin 1987a). Location of the Inuit communities of Kuujjuarapik, Umiujaq and Inukjuak along the east coast of Baie d'Hudson.

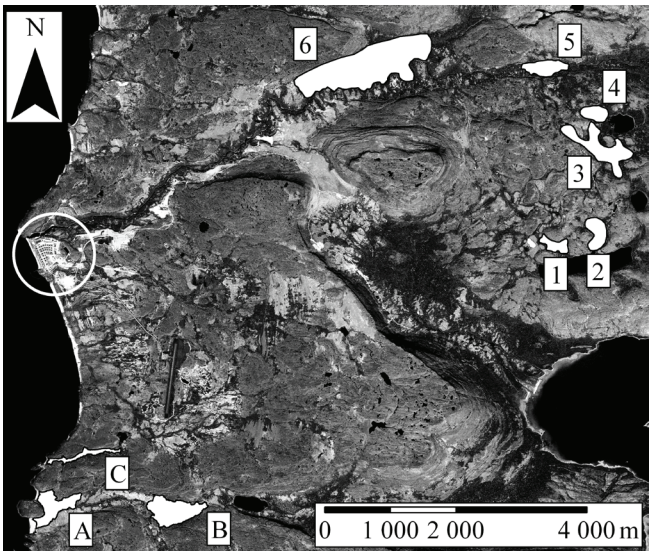

Figure 2. IKONOS satellite image of Umiujaq taken on July 26th 2005. Location of the Inuit community of Umiujaq (white circle) and the nine sectors (white areas identified with a number or a letter) mapped in the present study.

Figure 3. Example of permafrost degradation in 18 years from August 1989 to July 2007. The thermokarst pond on the left overruns progressively to the right the lithalsa. The arrow indicates the location of a thermistor cable. Note the man in the forefront near the small active layer detachment failure on August 18th 1989 for the scale. The road leading to the airport of Umiujaq in the background in 2007 was not yet built in 1989.

near Umiujaq, a typical lithalsa has a diameter of 40 m and a height of 2.5 m above the surrounding ground; the active layer is 1.5 m thick and the permafrost base is 12.5 m deep. The average volumetric ice content of the ice-rich core is 50%. For a permafrost thickness of 11 m, the total thickness of segregated ice lenses is then 5.5 m. The difference of 3 m between the frost heaving of the lithalsa surface and the ice accumulation is due to the irreversible over-consolidation of marine sediments occurring during freezing. These sediments were first deposited in a normally consolidated state before freezing. The formation of segregation ice fed by cryosuction can induce a decrease in void ratio as high as 30% of the saturated sediments in the freezing fringe (Konrad & Seto 1994). Therefore, after the permafrost thaws, a depression filled with water as deep as 3 m is left (2.5–5.5 m or 30% decrease in void ratio of a 10 m thick sediment layer). Due to solifluction on the lithalsa slopes there is an accumulation of materials on its sides explaining the remnant ring-shaped rampart left around the thermokarst pond (Fig. 3). Typically, a rampart is 3 m wide and 1 m high above the surrounding ground for an approximate volume of 350 m^3. This volume accounts for about 0.30 m (350 m^3 over a surface area of 1250 m^2) of the depression left. Following the water budget, drainage

system and sediments permeability, the thermokarst pond can be more or less filled with water (Yoshikawa & Hinzman 2003).

Methods

Three series of aerial photographs collected in 1957 (series A-15618, Natural Resources Canada), 1983 (series Q83857 and Q83858, Ministère des Ressources naturelles et de la Faune, Québec) and 2003 (series Q03201, Ministère des Ressources naturelles et de la Faune, Québec), and one IKONOS satellite image taken in 2005 (Fig. 2) were used to map the spatio-temporal evolution of the lithalsas and thermokarst ponds. The snow cover was not totally melted in the series of aerial photographs taken on June 18, 1957 (Fig. 4A) making difficult the delineation of the thermokarst ponds. The aerial photographs in 1983 and 2003 cover only the west part of the satellite image including the village and airport infrastructures (Fig. 2). The satellite image was provided in a digital format, already orthorectified according to a digital elevation model of the world, and georeferenced.

Nine sectors typical of the lithalsas fields found in the study area and totaling a survey area of 2.245 km^2 were selected (Fig. 2). The mapping of permafrost degradation was carried out using ArcMap from ESRI. The satellite image allowed not only the delineation of the limits of lithalsas and thermokarst ponds in 2005 but also the georeferencing and rectification of the aerial photographs before mapping these periglacial features in 1957 and 1983. Based on numerous tie points selected and identified on both satellite image and aerial photographs, the georeferencing and rectification of the digitized aerial photographs were performed for each sector. The stereoscopic view of the aerial photographs in 1957, 1983, and 2003 allowed the delineation of the limits of lithalsas and thermokarst ponds. The lithalsas and thermokarst ponds look like heaved forms and ramparted depressions filled with water respectively and can be easily identified and mapped on the aerial photographs. However, only the water surface was mapped. These limits were then reported on different layers in ArcMap. Because the aerial photographs in 2003 and the satellite image in 2005 were so close in time, there was no real change in permafrost extent. However, the stereoscopic view of the photographs in 2003 was quite useful for delineating the lithalsas and thermokarst ponds on the satellite image in ArcMap.

Results

Spatial distribution of lithalsas and thermokarst ponds

An example of permafrost degradation mapping between 1957 and 2005 for Sector 1 (Fig. 2) is given in Figure 4. Permafrost degradation was already occurring in 1957 under the form of small thermokarst ponds mainly located along the northern valley wall and east of Sector 1 (Fig. 4E). The decrease in permafrost extent is major in the 48 years from 1957 to 2005. Most of the permafrost degradation visible in 2005 has taken place principally along the northern valley wall where the thermokarst ponds have replaced the lithalsas (Figs. 4G, 4H, 5).

The statistics on the areas occupied by the lithalsas and thermokarst ponds in 1957 and 2005, and the difference in areas between 1957 and 2005 appear in Table 1 not only for Sector 1 but also for the other sectors. The numbers of lithalsas or thermokarst ponds mapped in each sector and the numbers of vanished lithalsas or appeared thermokarst ponds between 1957 and 2005 are also given in Table 1.

The permafrost and thermokarst extents were also mapped on the aerial photographs taken in 1983 only for Sectors A, B, and C covered by this series of aerial photographs (Table 1). The rate of permafrost degradation increased in recent years from an annual loss rate of 380 m^2 or 0.8% between 1957 and 1983, to 640 m^2 or 1.6% between 1983 and 2005.

Spatial accuracy of the mapped areas

The spatial accuracy of the areas occupied by the lithalsas and thermokarst ponds is evaluated to 20% and 60% respectively. It depends on the spatial resolution of the aerial photographs and satellite image and the capability of the cartographer to delineate accurately the limits of the lithalsas and ponds. According to statistics drawn from the mapping, the average areas occupied by a lithalsa and a pond are 1200 m^2 and 130 m^2 respectively. If these areas are assumed to be perfect circles, the average radius is 20 m for a lithalsa and 6 m for a pond. The pixel side of the aerial photographs and satellite image is about 0.8 m. If an accuracy of ±2 m for the radius is supposed to take into account the spatial resolution and the error on the limit delineation, respective accuracies of ±250 and ±80 m^2 are found for the areas occupied by a lithalsa and a pond. For the photographs taken in 1957, the spatial accuracy of the areas occupied by the ponds is likely higher than 60% due to the snow cover still present at that time in the depressions between the lithalsas hiding the ponds (Fig. 4A).

Discussion

Climate variability

According to Chouinard et al. (2007), the surface temperature at the end of the LIA in Nunavik was colder of 1°C in comparison to the reference period 1961–1990.

Climatic data are available for the Inuit communities of Kuujjuarapik and Inukjuak respectively 160 km south and 250 km north of Umiujaq (Figs. 1, 6). No trend in snowfall is obvious over the record period (Fig. 6A). However, a marked trend to climate warming of at least 3°C is observed since 1992 (Figs. 6B, 6C). The mean annual air temperature is well above the average air temperature found for the reference period 1961–1990 plus one standard deviation since 1998 except for 2004.

Permafrost degradation

The thermal regime of permafrost is closely related to climate changes, and the main mechanism of permafrost decay is climate warming. Permafrost thawing is a long-term process due to the latent heat of fusion of ice delaying the impacts of climate warming on permafrost. The permafrost degradation already observed in 1957 (Figs. 4A and 4E) was therefore inherited from climate warming of 1°C since the LIA (Chouinard et al. 2007). In 1957 the lithalsas were probably not yet in equilibrium with the climate and permafrost degradation was still in progress.

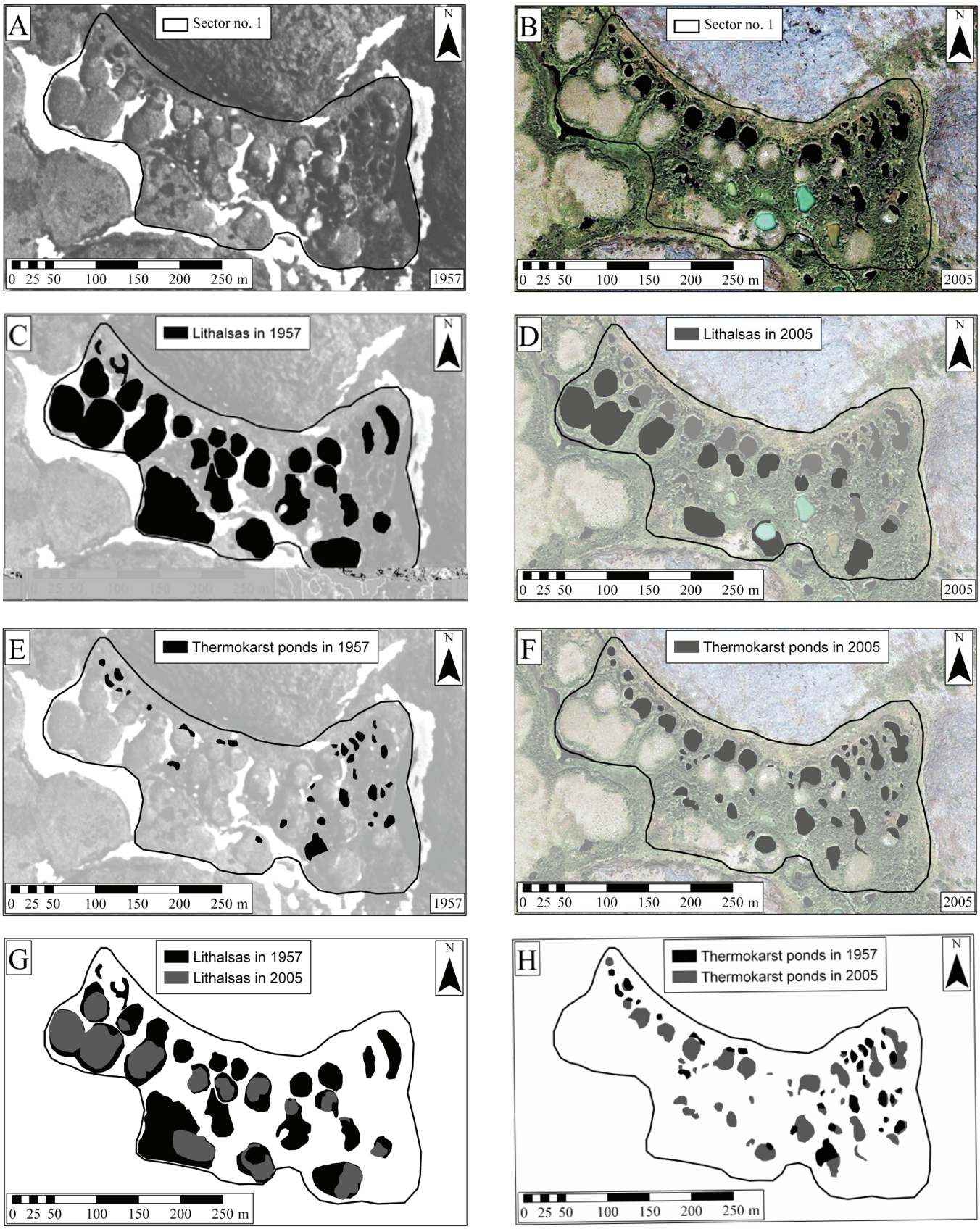

Figure 4. A) Study area no. 1 in 1957 (aerial photograph no. 39, series A-15618, reproduction authorized by the Minister of Public Works and Government Services of Canada 2007, courtesy of the National Air Photo Library, Mapping Services Branch, Natural Resources Canada). B) Study area no. 1 in 2005 (IKONOS satellite photograph). Spatial distributions of lithalsas in 1957 (C) and 2005 (D), and thermokarst ponds in 1957 (E) and 2005 (F). Superposition of spatial distributions of lithalsas (G) and thermokarst ponds (H) in 1957 and 2005.

Table 1. Areas occupied by lithalsas and thermokarst ponds in 1957, 1983 (sectors A, B, C) and 2005.

Lithalsas										
Sectors		Land occupation in 1957		Land occupation in 1983[5]		Land occupation in 2005		Difference in area between 1957 and 2005		
no.	(x 10^3 m^2)	(x 10^3 m^2)[1]	(%)	(x 10^3 m^2)[1]	(%)	(x 10^3 m^2)[1]	(%)	(x 10^3 m^2)[2]	(%)[3]	(%)[4]
1	71	29 (24)	40.8			11 (14)	15.5	-18 (-10)	-25	-62
2	118	11 (22)	9.3			4 (13)	3.4	-7 (-9)	-5.9	-64
3	297	61 (52)	20.5			35 (46)	11.8	-26 (-6)	-8.8	-43
4	83	18 (23)	21.7			7 (16)	8.4	-11 (-7)	-13.3	-61
5	129	21 (28)	16.3			6 (15)	4.7	-15 (-13)	-11.6	-71
6	1014	230 (103)	22.7			161 (97)	15.9	-69 (-6)	-6.8	-30
A	190	23 (16)	12.1	21 (14)	11.1	15 (13)	7.9	-8 (-3)	-4.2	-35
B	268	19 (21)	7.1	14 (16)	5.2	9 (11)	3.4	-10 (-10)	-3.7	-53
C	75	9 (10)	12.0	6 (6)	8.0	3 (3)	4.0	-6 (-7)	-8.0	-67
Subtotal (A+B+C)	533	51 (47)	9.6	41 (36)	7.7	27 (27)	5.1	-24 (-20)	-4.5	-47
Total	**2245**	**421 (299)**	**18.8**			**251 (228)**	**11.2**	**-170 (-71)**	**-7.6**	**-40**

Thermokarst ponds										
Sectors		Land occupation in 1957		Land occupation in 1983[5]		Land occupation in 2005		Difference in area between 1957 and 2005		
no.	(x 10^3 m^2)	(x 10^3 m^2)[1]	(%)	(x 10^3 m^2)[1]	(%)	(x 10^3 m^2)[1]	(%)	(x 10^3 m^2)[2]	(%)[3]	(%)[4]
1	71	3 (33)	4.2			8 (51)	11.3	5 (18)	7.0	167
2	118	1 (17)	1.7			5 (21)	4.2	4 (4)	2.5	150
3	297	1 (10)	0.3			9 (50)	3.0	8 (40)	2.7	800
4	83	1 (14)	1.2			7 (27)	8.4	6 (13)	7.2	600
5	129	1 (19)	0.8			8 (32)	6.2	7 (13)	5.4	700
6	1014	2 (12)	0.2			8 (46)	0.8	6 (34)	0.6	300
A	190	3 (22)	1.6	4 (18)	2.1	4 (19)	2.1	1 (-3)	0.5	33
B	268	7 (70)	2.6	9 (86)	3.4	11 (95)	4.1	4 (25)	1.5	57
C	75	4 (37)	5.3	6 (41)	8.0	6 (50)	8.0	2 (13)	2.7	50
Subtotal (A+B+C)	533	14 (129)	2.6	19 (145)	3.6	21 (164)	4.0	7 (35)	1.3	50
Total	**2245**	**24 (234)**	**1.1**			**66 (391)**	**3.0**	**42 (157)**	**1.9**	**175**

The data in parentheses are the numbers of lithalsas or thermokarst ponds mapped in each sector.
The data in parentheses are the numbers of vanished lithalsas or appeared thermokarst ponds between 1957 and 2005 in each sector.
Difference relative to the area of each sector.
Difference relative to the area occupied by the lithalsas or thermokarst ponds in each sector in 1957.
Only Sectors A, B and C are covered by the aerial photographs taken in 1983.

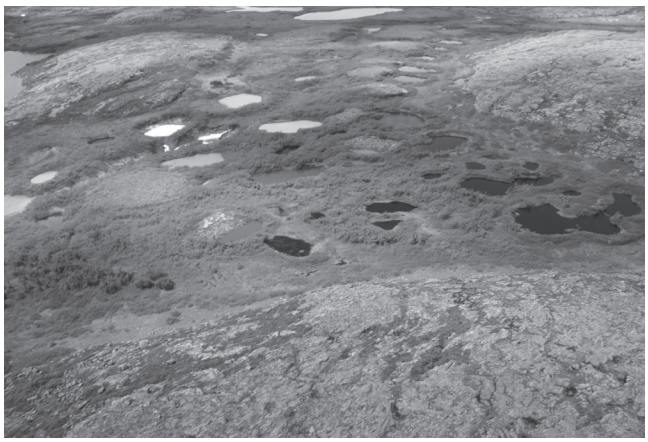

Figure 5. Aerial view of the sector no. 1 looking to the west taken on July 14, 2007. The presence of thermokarst ponds is more important close to the northern valley wall than in the middle of the sector.

From 1957 to 1983, the climate was more or less stable (Fig. 6), but the permafrost was still decaying at a loss rate of 0.8%/year for Sectors A, B, and C (Table 1). However, due to the trend of climate warming of 3°C over the last 15 years (Fig. 6), the rate of permafrost decay increased to a value of 1.6%/year between 1983 and 2005. The variability of annual snowfall without any trend (Fig. 6A) can be ruled out as a potential explanation of permafrost decay. Even if the actual climate stabilizes, permafrost decay will continue until a new thermal equilibrium is reached.

In addition to climate warming, other concurrent mechanisms affect the thermal balance of permafrost and exacerbate its degradation. The melting of ground ice in excess induces a differential thaw subsidence more important on the warmer sides of a lithalsa than its top. The subsidence is progressing from the sides to the top of the lithalsa (Fig. 3). Thaw subsidence allows the formation of a small thermokarst pond and the

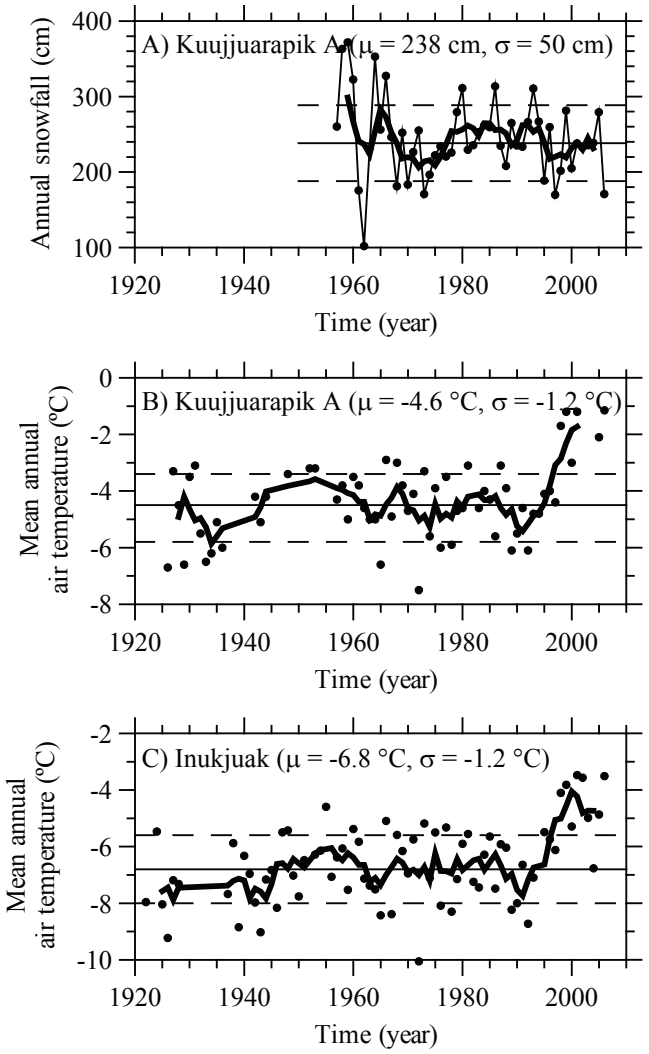

Figure 6. A) Annual snowfall at Kuujjuarapik A. Mean annual air temperature at Kuujjuarapik A (B) and Inukjuak (C). Climate data from Environment Canada. Thick lines correspond to a 5-year running average through mean annual snowfall or air temperature. Full and dotted horizontal lines are respectively the average and ±standard deviation (values in parentheses) of snowfall or air temperature over the reference period 1961-1990.

accumulation of snow. Freezing of the active layer underneath the thermokarst

pond is delayed the next winter due to the latent heat of freezing of water while the thermal insulation of thick snow cover also prevents further ground freezing. In addition, the vegetation growth under less severe climatic conditions favors the accumulation of snow in winter. These multiple degradation mechanisms have a snow ball effect. As soon as permafrost warming begins, these mechanisms operate and eventually can cause the lithalsa disappearance even if the climate is stabilized at some point. The warmest lithalsas, such as the ones close to the valley walls where the marine deposits are thinner and the heat flow is higher due to the high thermal conductivity of rock close to the surface are more susceptible to disappear first (Figs. 4A, 4B, and 5). The heat coming from running water on the valley walls can also contribute to permafrost warming.

Conclusions

Widespread and fast permafrost degradation is currently occurring at Umiujaq, Nunavik (Canada). These changes in the periglacial landscape were documented using time-lapse aerial photographs collected in 1957, 1983, and 2003, and satellite images taken in 2005. The rate of permafrost degradation increased over the last two decades due to a trend to climate warming of 3°C observed in Nunavik since 1992. At the annual loss rate of 1.6% found between 1983 and 2005, the disappearance of ice-rich permafrost will occur in this region through the next five to ten decades.

Acknowledgments

We would like to express our sincere gratitude to the Inuit community of Umiujaq for their hospitality and friendly support. The research presented herein was supported by the NSERC. Thanks are addressed to Nicolas Bélanger for his help in the mapping. The manuscript was substantially improved following the constructive comments from anonymous reviewers.

References

Allard, M. & Seguin, M.K. 1987a. Le pergélisol au Québec nordique: bilan et perspective. *Géographie physique et Quaternaire* 41: 141-152.

Allard, M. & Seguin, M.K. 1987b. The Holocene evolution of permafrost near the tree line, on the eastern coast of Hudson Bay (northern Quebec). *Canadian Journal of Earth Sciences* 24: 2206-2222.

Chouinard, C., Fortier, R. & Mareschal, J.-C. 2007. Recent climate variations in the subarctic inferred from three borehole temperature profiles in Northern Quebec, Canada. *Earth and Planetary Science Letters*, doi: 10.1016/j.epsl.2007.09.017.

Konrad, J.-M. & Seto, J.T.C. 1994. Frost heave characteristics of undisturbed sensitive Champlain Sea clay. *Canadian Geotechnical Journal* 31(2): 285-298.

Luoto, M. & Seppälä, M. 2003. Thermokarst ponds as indicators of the former distribution of palsas in Finish Lapland. *Permafrost and Periglacial Processes* 14: 19-27.

Payette, S., Delwaide, A., Caccianiga, M. & Beauchemin, M. 2004. Accelerated thawing of subarctic peatland permafrost over the last 50 years. *Geophysical Research Letters* 31(18): 1-4.

Pissart, A. 2002. Palsas, lithalsas and remnants of these periglacial mounds. A progress report. *Progress in Physical Geography*, 26(4): 605-621.

Vallée, S. & Payette, S. 2007. Collapse of permafrost mounds along a subarctic river over the last 100 years (northern Québec). *Geomorphology* 90(1-2): 162-170.

Yoshikawa, K. & Hinzman, L.D. 2003. Shrinking thermokarst ponds and groundwater dynamics in discontinuous permafrost near Council, Alaska. *Permafrost and Periglacial Processes* 14: 151-160.

An Integrative Observation of Kinematics and Geophysical Parameters of Gianda Grischa Rock Glacier, Upper Engadine, Swiss Alps

Regula Frauenfelder
Department of Geosciences, University of Oslo, Norway
now at Norwegian Geotechnical Institute, Oslo, Norway
Christian Hauck
Institute for Meteorology and Climate Research, Forschungszentrum Karlsruhe, University of Karlsruhe, Germany
Christin Hilbich
Department of Geography, University of Jena, Germany
Christof Kneisel
Department of Physical Geography, University of Würzburg, Germany
Martin Hoelzle
Department of Geography, University of Zurich, Switzerland

Abstract

An integrative analysis of rock glacier kinematics and ice content is presented using photogrammetric analyses and different geophysical techniques. The studied rock glacier system is situated in the eastern Swiss Alps, and comprises forms of different activity. Geophysical surveys (electrical resistivity measurements, refraction seismics) have been performed on one active rock glacier, an inactive one, as well as on a relict part underlying the active rock glacier. The highest resistivity values representing ice rich permafrost were obtained on the active rock glacier. The inactive and relict parts showed lower resistivity values. The results of the Electrical Resistivity Tomography (ERT) correspond well with the results of the seismic survey. Based on streamline interpolations, the active rock glacier is estimated to be min. 4 to 5 ka old, assuming a constant creep rate. Ground surface temperatures on this rock glacier vary strongly between years, mainly in response to the prevalent atmospheric conditions (air temperature, snow cover); this is also reflected in the year-to-year fluctuations of active layer thickness visible in the geophysical soundings.

Keywords: geophysics; ground surface temperatures; kinematics; photogrammetry; rock glaciers; Swiss Alps.

Introduction

Rock glaciers are complex morphological structures and can exhibit a large variability concerning kinematics, subsurface properties like ice content and porosity, and genesis. They are usually divided into three classes concerning their ice content and kinematics: (1) active (supersaturated with ice and creeping), (2) inactive (degrading ice and/or almost no creeping) and (3) relict (free of ice, no creeping).

In this contribution an integrative analysis of rock glacier kinematics and geophysical surveying is presented using photogrammetric analyses and different geophysical techniques. The study site is a complex, multi-unit rock glacier system in the eastern Swiss Alps. The objective of the study is (a) to link the kinematic behaviour to the subsurface properties and their temporal evolution, and (b) to get insights into the reaction of such a multi-unit rock glacier system to climate forcing. For this purpose, geophysical monitoring profiles have been installed for periodic measurements of electrical resistivity and seismic P-wave velocity in addition to ground surface temperature monitoring and kinematic velocity measurements. The presented rock glacier system is composed of active, inactive, and relict rock glacier bodies of similar nature and settings (e.g., headwall geology, cleavage, weathering conditions, slope angle, regional climate), thus enabling the simultaneous investigation of different forms that differ, most probably, mostly in their temporal history.

Geographic Setting

The Gianda Grischa rock glacier system is situated on the western slopes of Piz Julier (3384 m a.s.l.) in a side valley of Julier Pass, eastern Swiss Alps. The rock glacier system consists of three individual landforms (Fig. 1): (A) a W-exposed active rock glacier, overlaying (B) an older, possibly relict part, and (C) a W- to SW-oriented inactive rock glacier.

The active rock glacier (A) is c. 1000 m long and between 170 and 390 m wide and is situated between 2540 and 2800 m a.s.l. This rock glacier exhibits a flat root zone separated from its moderately inclined tongue by a steep slope. While the flatter areas show some ridges and furrows, such structures are absent in the steep slope. Of the possibly relict part (B), underlying the active rock glacier, only the tongue is visible, which is c. 100 m long and 100 m wide. The surface of this part is composed of small rocks and pebbles overgrown by vegetation (alpine grasses, dwarf willows, etc.). The inactive rock glacier (C) is 780 m long and 300 m wide; its surface consists of a very coarse top layer and shows a conspicuous ridge-and-furrow topography.

The area was covered by a small mountain glacier during the Egesen stage of the Younger Dryas cold phase. In the subsequent warming periods, this glacier decayed. During the Little Ice Age the catchment area of the currently active rock glacier (A) was already free of surface ice, while the

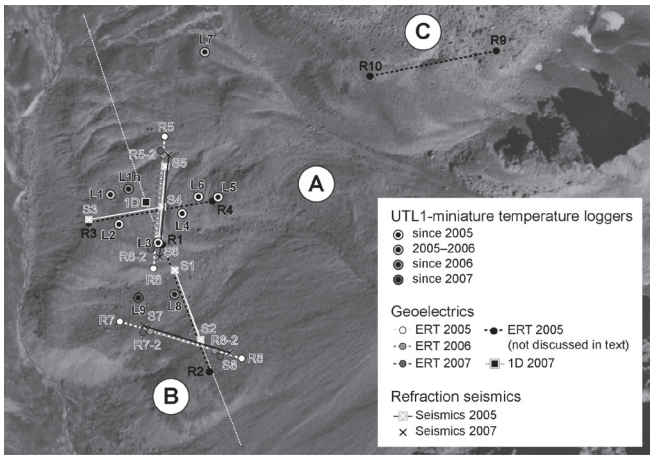

Figure 1. Aerial photograph of the Gianda Grischa rock glacier system with measurement locations: UTL1-miniature temperature loggers (dotted circles), electrical resistivity tomography (ERT) profiles (R1–R10, circles), one-dimensional sounding (rectangle), refraction seismics profiles (S1–S8, crosses). (A) active rock glacier, overlaying (B), an older, possibly relict part, (C) inactive rock glacier. Black-and-white aerial photograph from swisstopo, 11. 8. 1998, Flight-line 152, Image-No. 4647.

root zone of the presently inactive rock glacier (C) was still covered by a small cirque glacier. Today, both cirques are free of surface ice except for some small pluriannual ice patches.

Methods

Velocity measurements and streamline calculations

Using photogrammetrically derived digital elevation models and scanned aerial photography, ortho-images with 0.2 m resolution were computed digitally. From these digital ortho-images, horizontal surface displacements were derived using an image correlation technique described in detail in Kääb & Vollmer (2000). The age structure of the rock glacier surface was assessed from streamlines interpolated from the obtained surface velocity field. Assuming steady-state conditions, these streamlines represent the trajectories of specific particles on the surface and can thus be used to obtain rock glacier age estimates (for more details, cf. Kääb et al. 1998). The actual advance rate can be considerably smaller than the surface velocity, and therefore, surface ages obtained on the base of surface velocity streamline interpolations constitute a minimum age. Kääb (2005) derived empirical values of rock glacier advance rates and found that the total age of the considered rock glaciers is 2–5 times higher than the minimum age obtained for the surface.

Ground surface temperature measurements

Miniature temperature datalogger devices have been installed at six locations on rock glaciers (A) and (B) in summer 2005. One of these loggers had to be moved to a new location in 2006, and two additional loggers were installed in 2006 and 2007, respectively. Six of the loggers record the ground surface temperature (GST) at shallow depths, two loggers measure GST in air voids of the coarse blocky layer; all loggers measure in a 2h-interval. The thermistor used is a TMC-1T with a temperature range of -29°C to +39°C, with an accuracy given by the manufacturer of better than 0.25°C (cf. Hoelzle et al. 1999 for an in-depth discussion of the applied devices).

Geoelectrical techniques

Geoelectrical sounding techniques are based on the electrical resistivity differences between different subsurface materials. For a given frequency, resistivity depends mainly on the material type and the unfrozen water content of the sample (Hoekstra & McNeill 1973). Resistivity values for mountain permafrost targets can be very high and can vary over a wide range from 1–10 kOhm.m to a few MOhm.m (e.g., Haeberli & Vonder Mühll 1996). The method has been successfully applied to detect and characterize different permafrost structures in mountain terrain in various studies (e.g., Ishikawa et al. 2001, Isaksen et al. 2002, Hauck & Vonder Mühll 2003, Marescot et al. 2003).

Depending on the lateral heterogeneity and the target depth, one-dimensional (1D) vertical electrical soundings (VES) or two-dimensional (2D) electrical resistivity tomography (ERT) surveys can be conducted. For monitoring purposes, ERT measurements are repeated at certain time intervals using a permanently installed electrode array. This fixed-electrode array effectively filters resistivity variations due to variable electrode contacts or geological background variations, as mainly temporal resistivity changes are determined.

In our study, we used an "OYO McOhm" instrument for VES and a "SYSCAL Junior Switch system (IRIS)" as well as a "Geotom (Geolog)" instrument for ERT measurements. Electrode spacing of the initial surveys was 5 m, for the monitoring surveys 2 m spacing was employed in order to achieve a better resolution within the active layer. ERT data sets were inverted using the software package RES2DINV (Loke & Barker 1995). Further details on particularities of geoelectric applications in mountain permafrost are, for example, given in Kneisel & Hauck (2008).

Refraction seismics

Seismic investigations are based on different velocities of acoustic waves in subsurface materials. Energy from the seismic source is transported in waves and both reflected and refracted at interfaces. Refraction seismics concentrates on the first arrivals of the signal. The method is well suited to determine the presence or absence of ice, particularly in loose sediments. Differences in seismic velocities occur between frozen and non-frozen areas: permafrost is usually indicated by higher values, due to interstitial ice. Typical seismic velocity values for unfrozen loose sediments are lower than 1500 m s^{-1}, but can reach up to almost 4000 m s^{-1}, when icebound (Maurer & Hauck 2007).

In this study, a 12-channel "Geometrics Seismograph" equipment with a sledge-hammer as source was applied. Geophone spacing was 10 m, with six shot points.

Results and Discussion

Kinematics and age estimates

Horizontal average annual surface velocities were determined photogrammetrically between 1971 and 1998 (Fig. 2a). During the 27 years under observation, the active rock glacier crept downslope with an average velocity of approximately 0.4 to 0.5 ma^{-1}, reaching maximum velocities of up to 1 ma^{-1}. Compared to other rock glaciers in the region, Gianda Grischa is deforming at a considerable rate (e.g., Murtèl rock glacier: v_{max} = 0.2 ma^{-1}, Muragl rock glacier: v_{max} = 0.5 ma^{-1}, cf. Kääb 2005). Both the inactive rock glacier and the possibly relict part showed no statistically significant movement in the period 1971–1998.

More recent velocity measurements are not available yet, but are envisaged in the near future, in order to relate the kinematics to the results of the ongoing measurements of thermal and geophysical properties.

Rock glaciers are formed by the continuous deformation of ice-rich debris material, with the result that the age of the surface becomes greater along the flowlines from their root zone to their front. Minimum surface age estimates obtained from photogrammetric streamline interpolations are in the order of 4 to 5 ka (Fig. 2b). Both frontal lobes of the spatulate tongue seem to be of comparable age and lie on the overridden, older tongue which shows no movement.

Considering that such surface ages constitute a minimum age and that the total age of the rock glacier can be up to 2–5 times higher than the minimum age obtained for its surface (see above, section 'Methods') implies that this rock glacier presumably began to evolve during the early Holocene (for a more detailed discussion cf. Frauenfelder et al. 2005).

Ground surface temperature

Mean annual air temperature (MAAT) at the front of the rock glacier, at an altitude of 2540 m a.s.l., is approximately -1.1°C, as derived by Hoelzle & Gruber (2008). Ground surface temperature (GST) measurements are ongoing since autumn 2005 at different sites at altitudes between 2586 and 2640 m a.s.l. Mean annual GST on the active rock glacier was between -1.0 and -2.1°C at five out of seven sites during 2005–2006. During 2006–2007 MAGST was negative at one out of six sites (Table 1).

These year-to-year fluctuations are in good agreement with the prevalent atmospheric conditions (air temperature, snow cover) in the area. The MAAT measured at the nearby Murtèl-Corvatsch station showed a very cold winter 2005/2006, contrasted by a very warm winter 2006/2007 (Fig. 3).

Snow cover conditions (thickness and duration), both influencing the ground thermal regime, were normal during winter 2005/2006 as compared to the existing measurements since 1972. In contrast to this, snow cover thickness during winter 2006/2007 was the thinnest ever recorded in the last 35 years. Under normal conditions, winter 2006/2007 would have been one of the coldest recorded, due to the lacking isolation of the snow cover. However, winter 2006/2007 was characterized by a record warm period, lasting from September 2006 until May 2007. This fact is well represented in the MAGST measured on the rock glacier (Fig. 3).

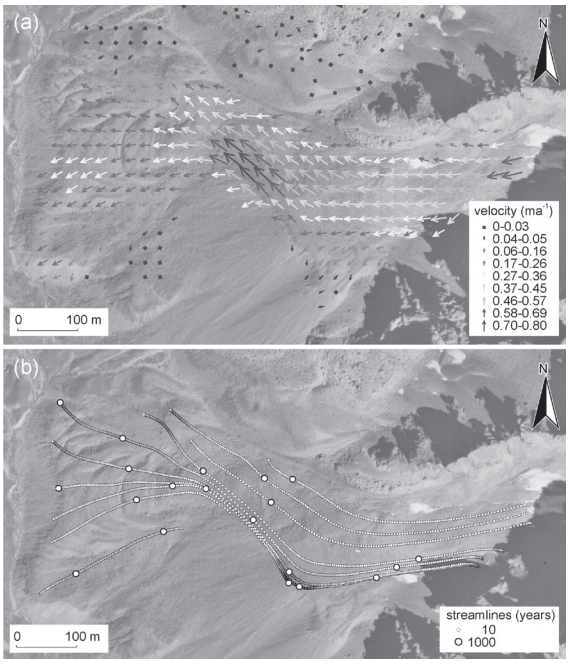

Figure 2. Photogrammetrical measurements on the Gianda Grischa rock glacier system: (a) Horizontal average annual surface velocities between 1971 and 1998; (b) Streamline calculations. Black-and-white aerial photograph from swisstopo, 11. 8. 1998, Flight-line 152, Image-No. 4647.

Table 1. Mean annual ground surface temperatures (MAGST), as measured at different sites on the active and the relict rock glacier from 2005 (resp. 2006) until 2007 (resp. 2006). Abbreviations: Instal. = Date of installation; De-instal. = Date of de-installation.

ID	Instal.	De-instal.	Altitude [m a.s.l.]	MAGST 05/06 [°C]	MAGST 06/07 [°C]
L1	31.8.2005	18.9.2006	2604	-2.102	--
L1n	18.9.2006	ongoing	2615	--	+2.028
L2	31.8.2005	ongoing	2608	+0.215	damaged
L3	31.8.2005	ongoing	2616	+0.508	+2.045
L4	31.8.2005	ongoing	2623	-2.029	-0.150
L5	31.8.2005	ongoing	2640	-1.936	+0.157
L6	31.8.2005	ongoing	2628	-0.970	+1.276
L7	31.8.2005	18.9.2006	2622	-1.507	--
L8	18.9.2006	ongoing	2603	--	+2.348

As the measurements show, winter 2006–2007 was characterised by warm air temperatures, combined with thin snow cover. Although the thin snow cover allowed a certain amount of ground cooling and thereby partly outbalanced the influence of the warm air temperatures, the overall result of these atmospheric conditions was considerably "warm" GSTs on the rock glacier.

Geophysical subsurface characterisation

ERT surveys have been performed on both the active (A) and the inactive (C) rock glacier, as well as on the possibly relict part (B) underlying the active rock glacier. As a complementary method, seismic surveys have been

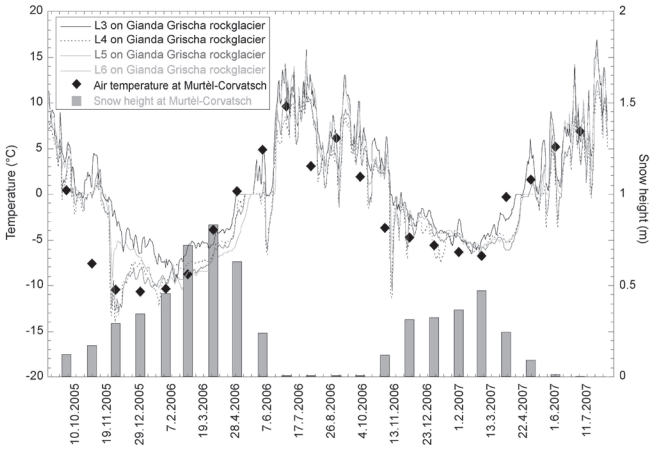

Figure 3. Ground surface temperatures (GSTs) in the period 2005–2007 as measured continuously at four locations on the active rock glacier, and air temperature and snow depth measurements from the nearby Murtèl-Corvatsch weather station.

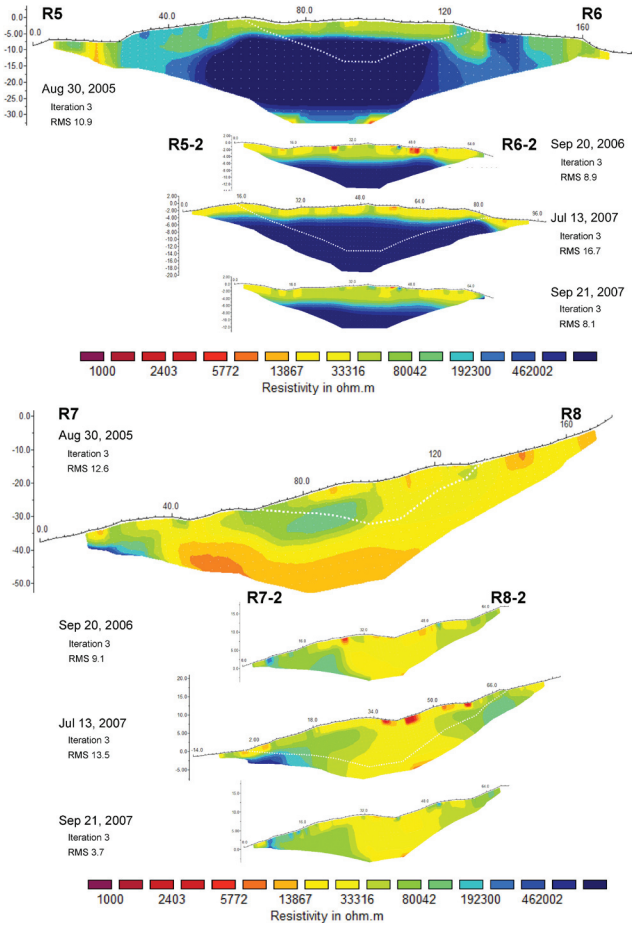

Figure 4. Results of the Electrical resistivity tomography (ERT) measurements: (top) Transversal profile on the active rock glacier (profile line R5–R6); (bottom) longitudinal profile over the edge of the active rock glacier onto the underlying, older (possibly relict) part (profile line R7–R8). R#-numbers refer to the measurements in 2005 (5 m spacing), R#-2-numbers refer to the monitoring profiles from 2006 and 2007 (2 m spacing).

conducted on the active and relict part. The aim was to confirm or contradict the geomorphological and kinematic evidence and to roughly estimate the ice content in the different rock glaciers.

On the active rock glacier (A) the active layer is comparably thick with about 4–5 m (in September, Fig. 4, top) and resistivity values between 30 and 50 kOhm.m. The maximum investigation depth is c. 30 m (obtained with a 5 m spacing profile in August 2005). From this profile a lense-shaped structure is visible with maximum values between c. 200 and >500 kOhm.m. The lateral extent of this high resistive anomaly coincides with the morphological and kinematic evidence for recent high activity. Beneath the maximum, resistivities decrease again indicating a decreasing ice content below 20–25 m depth. Even though this latter interpretation is supported by an additional ERT profile along the rock glaciers flowline (not shown here) and by the VES results (Fig. 5, Table 2), this result remains uncertain, as the reliability of the ERT profiles decreases with depth due to the high resistivity and the limited penetration depth (cf. Hauck & Vonder Mühll 2003, Marescot et al. 2003).

The corresponding seismic results show a similar active layer depth (August measurement) and a high velocity layer below the active layer, with maximum velocities between 2500–4000 ms^{-1} (Fig. 6), indicating the possibility of a significant ice layer, the velocity of ice being 3500 ms^{-1}. Both measurements are in good accordance with evidence from comparable blocky rock glaciers (e.g., rock glacier Murtèl, Maurer & Hauck 2007) and strongly suggest the presence of ice-rich permafrost or even massive ice cores. The depth of the bedrock could not be estimated conclusively.

Measurements on the inactive rock glacier (C, not shown here) and on the possibly relict part (B, Fig. 4, bottom) show significantly lower, but still comparably high resistivity values around c. 50 kOhm.m.

Although the inactive rock glacier showed no statistically significant movement in the period 1971–1998, the results of the ERT survey may indicate the presence of strongly degraded subsurface ice with higher amounts of unfrozen water which no longer has the appearance of one massive and supersaturated ice core. The resistivity values of this inactive rock glacier correspond well with the ERT results from other permafrost landforms with less (but still significant) ice content (cf. Hilbich et al. 2008b). The same is true for the older part, underlying the active rock glacier, which was mapped as relict due to its geomorphological habitus (lateral and frontal sides with low slope angles, collapsed inner structure, considerably dense vegetation cover) and the absence of measurable movement.

On the other hand, the lack of seasonal changes in most parts of the profile may indicate an absence of significant ground ice, as this would lead to, for example, a significant deepening of the surficial unfrozen layer between July and September.

Similarly, the observed seismic velocities are lower than in the active rock glacier, but still high enough to indicate possible ice occurrences. The depth of the relict part of the rock glacier is estimated around 25 m. At shallower depths, the comparatively small P-wave velocities suggest air-filled

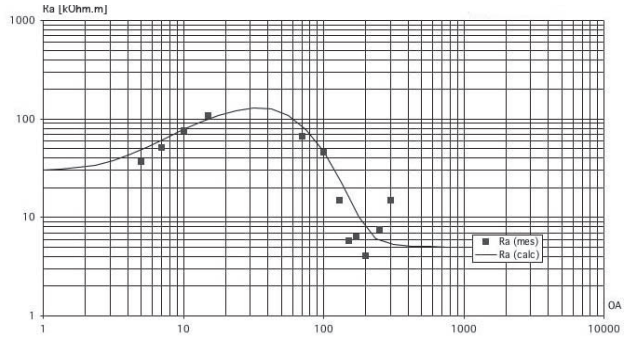

Figure 5. Sounding curve of the one-dimensional sounding (1D) on the active rock glacier (A in Fig. 1).

voids or cavities not only on the inactive and relict rock glacier, but also on the margins of the active one (Fig. 6). As these voids can cause equally high resistivities as massive ground ice, some heterogeneity concerning the ice content on the active rock glacier can, therefore, not be excluded.

The VES results confirm the general findings from the active rock glacier with a 4 m thick active layer (30–65 kOhm.m) and an approximately 20 m thick permafrost layer below (> 250 kOhm.m). Below this layer, the presence of two increasingly apparent resistivity measurements may indicate the bedrock layer or a possible further relict permafrost occurrence some 50–60 m below the surface, which was shielded from atmospheric conditions by the overlying, presently active rock glacier. Even though geomorphic evidence of a relict rock glacier below at least parts of the active rock glacier (cf. above) may argue for the latter, the geophysical evidence is too scarce to allow a reliable interpretation.

Geophysical monitoring

Two profiles were chosen as future monitoring profiles: R/S5–6 on the active rock glacier and R/S7–8 on the possibly relict part (cf. Fig. 1). To better resolve the active layer and the upper part of the permafrost, where seasonal and long-term changes will be largest, a reduced electrode spacing of 2 m was chosen. Up to now, measurements were conducted on September 20, 2006, July 13, 2007, and September 21, 2007. Due to the use of a different ERT instrument in July 2007, these measurements have slightly larger penetration depths.

For the active rock glacier profile the ERT monitoring results show a significant increase in the thickness of the unfrozen layer (low resistivity values) from July to September 2007. A similar thickening, but much smaller, can be seen from September 2006 to September 2007, indicating warmer subsurface conditions in 2007 than in 2006, which is also confirmed by the MAGST measurements (see above). In contrast to this, no such effects can be found on the possibly relict part. Differences can be seen in the lower part of the slope, where the profile nears the active rock glacier, but a clear seasonal increase of the unfrozen layer thickness as well as an interannual signal are missing. From this finding may be deduced that the ice content is low or absent in most of profile R7–8, as a significant ice content would lead to seasonal resistivity contrasts near the interface between

Table 2. Apparent resistivities and thickness of the layers in the 1D model, as shown in Figure 5.

Layer	Resistivity [kOhm.m]	Thickness [m]
1	30–65	3–5
2	>250	20 (–40)
3	5–10	∞

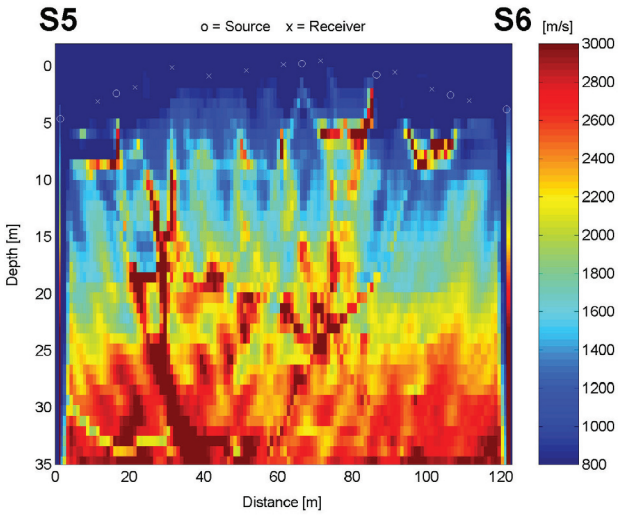

Figure 6. Results of the refraction seismics measurements on the active rock glacier (profile line S5–S6).

the active layer and the permafrost body (cf. Hauck 2002, Kneisel 2006, Hilbich et al. 2008a). This is further supported by the very small vertical resistivity gradient throughout most parts of the profile. An exception may be the lowest part of the profile, where the resistivity increases strongly with depth.

Conclusions and Perspectives

The present study shows that a sound combination of different photogrammetrical, geophysical, and meteorological methods can reveal new insights about individual rock glaciers or even complex rock glacier systems. Photo-grammetrical measurements (velocity, streamlines) help to identify moving and non-moving parts and allow age constraints to be derived. Geophysical surveys give insights into the composition and about the ice content of the studied features. Ground surface temperature measurements and additional meteorological data (such as air temperature, snow cover thickness and duration from nearby meteorological stations) give further information that helps to better understand observed kinematic behaviour, such as, short-term velocity changes as recently reported from many Alpine rock glaciers (e.g., Ikeda et al. 2003, Lambiel & Delaloye 2004, Roer et al. 2005).

In summary, our data show a connection between lower resistivities, larger unfrozen water content, and higher MAGST, with higher creep velocity and vice-versa. More extensive and repeated monitoring is necessary, however, to reliably link the kinematic behaviour to the thermal and subsurface properties.

Once longer time-series of such combined measurements are available, this data will help to explain climate forcing impacts on mountain permafrost, such as the above mentioned observed recent increase in rock glacier velocity. The presented monitoring approach will then enable the assessment of future changes of rock glacier dynamics and their causes in the atmosphere and the subsurface. These data can be used as much needed input and forcing variables in permafrost evolution models.

Acknowledgments

This study has been financially supported by the Swiss Academy of Sciences ("Reisestipendien in Botanik, Zoologie und Erdwissenschaften") and the Department of Geosciences, University of Oslo. We would also like to thank an anonymous reviewer for his constructive comments, which greatly helped to improve the manuscript.

References

Frauenfelder, R., Laustela, M. & Kääb, A. 2005. Relative age dating of Alpine rock glacier surfaces. *Zeitschrift für Geomorphologie N.F.* 49(2): 145-166.

Haeberli, W. & Vonder Mühll, D. 1996. On the characteristics and possible origins of ice in rock glacier permafrost. *Zeitschrift für Geomorphologie* 104: 43-57.

Hauck, C. 2002. Frozen ground monitoring using DC resistivity tomography. *Geophysical Research Letters* 29 (21): 2016, doi: 10.1029/2002GL014995.

Hauck, C. & Vonder Mühll, D. 2003. Inversion and interpretation of 2-dimensional geoelectrical measurements for detecting permafrost in mountainous regions. *Permafrost and Periglacial Processes* 14(4): 305-318.

Hilbich, C., Hauck, C., Hoelzle, M., Scherler, M., Schudel, L., Voelksch, I., Vonder Mühll, D. & Mäusbacher, R. 2008a. Monitoring mountain permafrost evolution using electrical resistivity tomography: A 7-year study of seasonal, annual, and long-term variations at Schilthorn, Swiss Alps. *Journal of Geophysical Research* 113: F01S90.

Hilbich, C., Hauck, C., Delaloye, R. & Hoelzle, M. 2008b. A geoelectric monitoring network and resistivity-temperature relationships of different mountain permafrost sites in the Swiss Alps. *Proceedings of the Ninth International Conference on Permafrost, Fairbanks, Alaska* (this proceedings).

Hoekstra, P. & Mc Neill, D. 1973. Electromagnetic probing of permafrost. In: F.J. Sanger & P.J. Hyde (eds.), *Proceedings of the Second International Conference on Permafrost*. National Academy of Sciences, Washington DC: 517-526.

Hoelzle, M., Wegmann, M. & Krummenacher, B. 1999. Miniature temperature dataloggers for mapping and monitoring of permafrost in high mountain areas: First experience from the Swiss Alps. *Permafrost and Periglacial Processes* 10(2): 113-124.

Hoelzle, M. & Gruber, S. 2008: Borehole and ground surface temperatures and their relation to meteorological conditions in the Swiss Alps. *Proceedings of the Ninth International Conference on Permafrost, Fairbanks, Alaska* (this proceedings).

Ikeda, A., Matsuoka, N. & Kääb, A. 2003. A rapidly moving small rock glacier at the lower limit of the mountain permafrost belt in the Swiss Alps. *Proceedings of the Eighth International Conference of Permafrost*, Zurich, Switzerland, Swets & Zeitlinger, Lisse: 455-460.

Isaksen, K., Hauck, C., Gudevang, E., Ødegård, R.S. & Sollid, J.L. 2002. Mountain permafrost distribution in Dovrefjell and Jotunheimen, southern Norway, based on BTS and DC resistivity tomography data, Norwegian Journal of Geography 56: 122–136.

Ishikawa, M, Watanabe, T. & Nakamura, N. 2001. Genetic difference of rock glaciers and the discontinuous mountain permafrost zone in Kanchanjunga Himal, Eastern Nepal. *Permafrost and Periglacial Processes* 12(3): 243-253.

Kääb, A. 2005. *Remote sensing of mountain glaciers and permafrost creep*. Zurich: University of Zurich, Switzerland, Physische Geographie 48, 264 pp. (ISBN 3 85543 244 9)

Kääb, A., Gudmundsson, G.H. & Hoelzle, M. 1998. Surface deformation of creeping mountain permafrost. Photogrammetric investigations on Murtèl rock glacier, Swiss Alps. *Proceedings of the Seventh International Permafrost Conference, Yellowknife, Collection Nordicana* 57, Centre d'Etudes Nordiques, Université Laval, Canada: 531-537.

Kääb, A. & Vollmer, M. 2000. Surface geometry, thickness changes and flow fields on creeping mountain permafrost: automatic extraction by digital image analysis. *Permafrost and Periglacial Processes* 11: 315-326.

Kneisel, C. & Hauck, C. 2008. Electric methods. In: Hauck, C. & Kneisel, C. (eds.), *Applied Geophysics in Periglacial Environments*. Cambridge: Cambridge University Press, in press.

Kneisel, C. 2006. Assessment of subsurface lithology in mountain environments using 2D resistivity imaging. *Geomorphology* 80: 32-44.

Lambiel, C. & Delaloye, R. 2004. Contribution of real-time kinematic GPS in the study of creeping mountain permafrost: examples from the Western Swiss Alps. *Permafrost and Periglacial Processes* 15: 229-241.

Loke, M.H. & Barker, R.D. 1995. Least-squares deconvolution of apparent resistivity. *Geophysics* 60: 1682-1690.

Marescot, L., Loke, M.H., Chapellier, D., Delaloye, R., Lambiel, C. & Reynard, E. 2003. Assessing reliability of 2D resistivity imaging in permafrost and rock glacier studies using the depth of investigation index method. *Near Surface Geophysics* 1(2): 57-67.

Maurer, H. & Hauck, C. 2007. Geophysical imaging of alpine rock glaciers. *Journal of Glaciology* 53(180): 110-120.

Roer, I., Kääb, A. & Dikau, R. 2005. Rock glacier acceleration in the Turtmann valley (Swiss Alps). *Norwegian Journal of Geography* 59(2): 157-163.

Deployment of a Deep Borehole Observatory at the High Lake Project Site, Nunavut, Canada

Barry M. Freifeld
Lawrence Berkeley National Laboratory, Berkeley, CA, USA
Eric Chan and Tullis C. Onstott
Princeton University, Princeton, NJ, USA
Lisa M. Pratt and Adam Johnson
Indiana University, Bloomington, IA, USA
Randy Stotler, Brian Holden and Shaun Frape
University of Waterloo, Waterloo, Ontario, Canada
Susan M. Pfiffner and Sarah DiFurio
University of Tennessee, Knoxville, TN, USA
Timo Ruskeeniemi
Geological Survey of Finland, Espoo, Finland
Ian Neill
Zinifex Canada Inc., Ontario, Canada

Abstract

We deployed a deep permafrost observatory in a borehole at the High Lake Project Site (67°22′N, 110°50′W), Nunavut, Canada with the aims of (1) investigating the physical and chemical limitations on microbial life within such environments, (2) developing life-detecting technologies for the exploration of life on Mars, and (3) constraining the hydrological and thermal parameters relevant to the evolution of permafrost and groundwater flow in these environments. The High Lake Project Site is located in an Archean mafic volcanic belt, with permafrost extending down to 458±5 m depth. The borehole, drilled to a total depth of 480 m, provides multifunctional monitoring capability: subpermafrost geochemical sampling, thermal profile, and estimation of hydraulic and thermal formation properties. The primary sampling objectives are delineating salinity gradients, gas concentration, pH, pe, microbial abundance, community structure, and activity, as well as isolating pristine subpermafrost brine for future studies. A multimode fiber-optic cable, along with a heat-trace cable, was installed to perform distributed temperature-perturbation sensor (DTPS) measurements along the entire length of the borehole. Following successful installation of the borehole observatory, we acquired a thermal perturbation dataset and obtained estimates for formation thermal conductivity and heat flux.

Keywords: borehole observatory; climate change; geothermal profile; microbial sampling; permafrost instrumentation; permafrost thickness.

Introduction

Given that global climate models predict the greatest increases in temperature at arctic latitudes, permafrost is increasingly looked upon as a harbinger of climate change (Anisimov et al. 2007). Borehole thermal profiles provide information on past ground-surface temperature histories (GSTH) not available from atmospheric temperature records collected prior to the twentieth century (Lachenbruch & Marshall 1986, Harris & Chapman 1997). To invert thermal profile data for estimating GSTH, thermal properties need to be constrained. Prior studies have either used laboratory measurements performed on drill cores or cutting fragments, or have used estimates based on lithologic descriptions (Taylor et al. 2006, Majorowicz & Safanda 2001).

Understanding a permafrost site's hydrogeological and thermal conditions is important for predicting the destabilization of permafrost by construction activities, assessing mine inflows, contaminant transport risks, and for the design of tailing and waste rock impoundments (Harris 1986). Given that the economic activities in arctic Canada are predominantly (diamond and metal) mining, as well as oil and gas exploration and production, engineering the necessary infrastructure and assessing the impact that infrastructure has on the natural environment requires understanding both present site conditions and evolving climatic conditions.

In the summer of 2007 we installed a multifunctional borehole observatory at the High Lake Project Site (67°22′N, 110°50′W), in Nunavut Territories, Canada, with the aim of acquiring a broad spectrum of environmental data. Within the permafrost, a distributed thermal perturbation sensor (DTPS) was used to measure the thermal profile; based on these temperature data, we can estimate formation thermal conductivity. Beneath a pneumatic packer located above the base of the permafrost, a U-tube geochemical sampling system acquired fluid samples for delineating gas concentration, pH, pe, microbial abundance, and community structure and

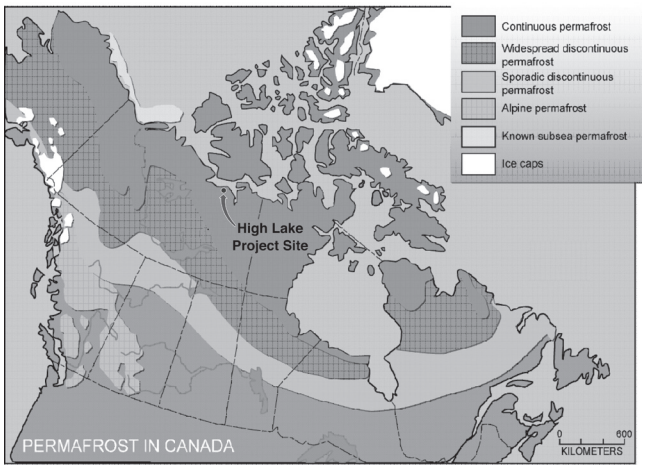

Figure 1. High Lake Project Site Location in Nunavut Territories, Canada. Permafrost base map from NRC Atlas Website, http://atlas.nrcan.gc.ca/.

activity, as well as isolating pristine subpermafrost brine for future studies (Freifeld et al. 2005). A pressure-temperature sensor collocated with the U-tube sampling inlet facilitated estimation of hydraulic conductivity.

This paper presents the thermal and hydrologic data collected following installation of the U-tube and DTPS and contains a preliminary interpretation of these data. One of the unique results of our field program was our method of using *in situ* data to estimate formation thermal conductivity with high spatial resolution. This approach—resulting in better estimates of formation thermal conductivity, as contrasted to using laboratory derived values—can reduce uncertainty in prediction of GSTH when inverting borehole temperature measurements.

High Lake Site and Observatory Description

Site description

The High Lake Project Site, shown in Figure 1, is located in an Archaen Mafic volcanic belt, with permafrost extending down to 460 m on a mining exploratory lease originally purchased by Wolden Resources and currently operated by Zinifex Canada Inc. All of the work was conducted within a 75 mm diameter borehole, designated HL03-28. HL03-28 was initially drilled in 2003 to a length of 335 m (depth 304 m) as part of Wolfden Resource's characterization of base metals for potential economic extraction from the High Lake volcanogenic massive sulfide deposit. In July 2006, our project team cored continuously to lengthen HL03-28 to 535 m. After removing an ice blockage that formed in the borehole during the previous season, we installed a permanent borehole observatory.

Borehole observatory

The High Lake borehole observatory targeted both the permafrost region for geothermal investigation and the subpermafrost formation for estimation of hydrologic properties and collection of fluid samples. The

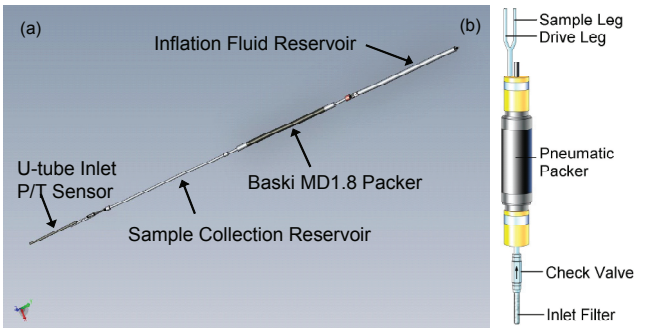

Figure 2. (a) High Lake bottom hole assembly showing the sequence of components from bottom to top (left to right on the schematic). (b) Conceptual layout of a U-tube sampler. The Sample Collection Reservoir formed the "U" portion of the U-tube at High Lake.

instrumentation at the bottom of the borehole, consisting of a pneumatic packer, a U-tube sampling system with a sample fluid reservoir, and a pressure-temperature sensor, are collectively referred to as the bottom hole assembly (BHA). The fluid, electrical, and fiber-optic lines running between the BHA and the surface are referred to as the deployment string.

Figure 2(a) shows a schematic of the High Lake BHA. With an overall length of 14.9 m, the BHA is composed of (from top to bottom) a fluid reservoir for packer inflation, a pneumatic packer (Baski Model MD18, Denver, CO, USA), a sample fluid collection reservoir, a pressure-temperature sensor (In-situ Level Troll 500, Fort Collins, CO, USA) and a U-tube inlet composed of a 40 μm sintered stainless steel filter and a check valve.

Prior to deployment of the BHA, the fluid reservoir was filled with 3 lL of propylene glycol. Propylene glycol was chosen because of its low freezing point and its inability to permeate through the rubber packer gland. To inflate the packer, we applied a N_2 head to the reservoir (using a 6.4 mm stainless steel tube), forcing the fluid into the packer and inflating the packer gland. The central mandrel of the packer served as a conduit for transport of sampled fluid and electrical signals between the surface and the BHA.

A traditional U-tube sampler, as shown in Figure 2(b), is composed of a looped tube, forming a "U" that is open to the formation via a check valve. To recover a sample, compressed N_2 gas, applied to the drive leg, forces the check valve to close, and fluid is transported up the sample leg to the surface. At High Lake, the inlet filter and check valve were both located beneath a 7 lL sample collection reservoir. Using a small, 6.4 mm-diameter inner tube terminating 10 cm from the bottom of the sample collection reservoir (to form a sample leg), the outer large diameter cylinder served the function of the traditional U-tube drive

independent sample lines that ran up to the surface.

The DTPS deployed at High Lake consisted of an HDPE jacketed multimode fiber-optic cable that runs from the top of the packer fluid reservoir up to a Distributed Temperature Sensor (DTS; Agilent Technologies Manufacturing GmbH & Co. KG, Model N4385A, Böblingen, Germany) located at

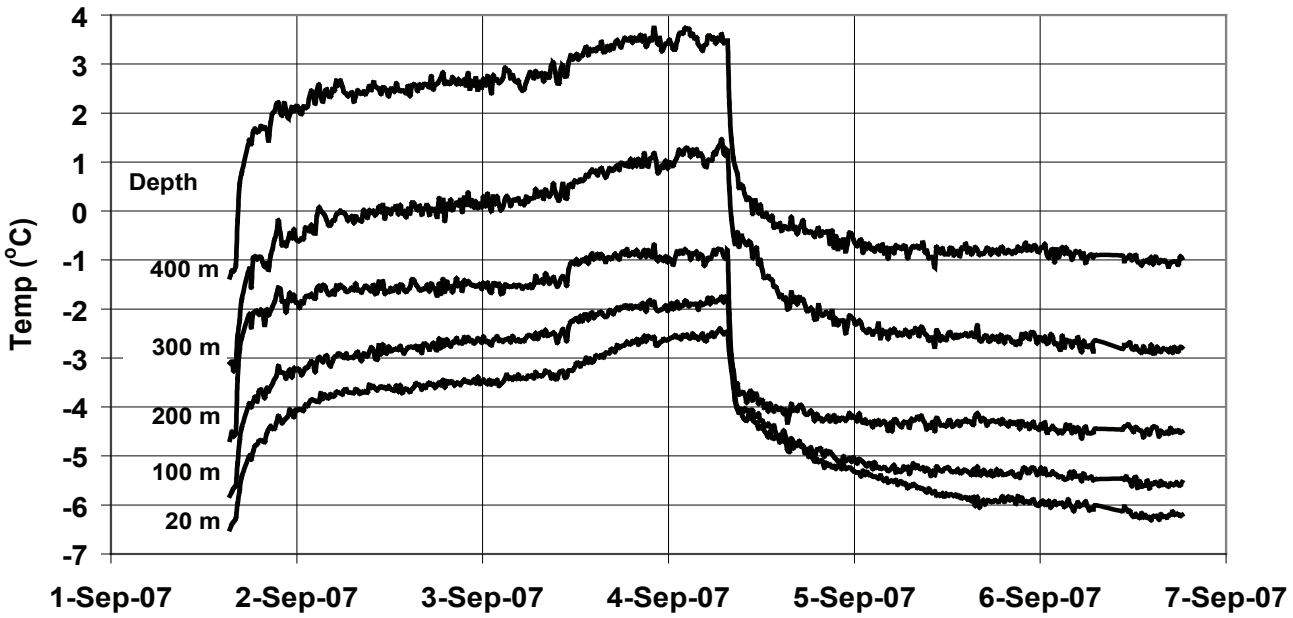

Figure 3. High Lake thermal profiles acquired using a distributed temperature sensor. Heating was initially conducted at a rate of 16.8 W/m for 43 hours, followed by heating at 20.5 W/m for 21 hours. Following the geothermal gradient, the thermal profiles go from coolest (shallowest) to warmest (deepest).

the surface. The DTS uses a laser backscattering technique to measure temperature with a 1 m spatial resolution along the length of the fiber. An overview of the DTS technology as applied to environmental monitoring can be found in Selker et al. (2006). Parallel to the fiber-optic cable is a two-conductor 14 AWG direct burial (outdoor) cable shorted at the bottom, which provides uniform heating along the length of the well when current is applied.

Following the wellbore completion process, the temperature was allowed to equilibrate for 1 month before thermal data were collected. To conduct the DTPS measurement, we first acquired a baseline thermal profile. While energizing the heater cable, additional thermal profiles were obtained at 15-minute intervals to record the thermal transient during heating. After 64 hours of monitoring the heating, the generator was turned off, and cooling was monitored for an additional 58 hours. Figure 3 shows a limited subset of the hundreds of thermal transients recorded.

Results

Fluid sampling

Immediately after deployment of the borehole observatory, the U-tube was operated five times over a span of three days, recovering a total of approximately 60 lL. Although samples were still contaminated with $CaCl_2$ saturated drilling fluids used during the removal of the ice plug a few days earlier, the salinity declined five-fold with the purging of wellbore fluids. The sampling lines eventually froze, despite the fact that heat was being applied at a rate of 20 W/m in an attempt to keep the sample lines flowing. The thermal data (discussed later in detail) show borehole temperatures approaching –7°C and moderate to high formation thermal conductivity, indicating the potential for rapid heat loss of the sampling system. In retrospect, an insulated hose encompassing both the sampling lines and the heat-trace cable would have ensured the continued operation of the sampling system.

Hydraulic conductivity

During operation of the U-tube sampling system, the bottomhole pressure was continuously recorded using a pressure/temperature sensor located near the inlet of the U-tube sampling system (Fig. 4). The U-tube sampling event corresponds to a sharp increase in pressure (over several minutes) immediately followed by a rapid decrease in pressure, as the compressed gas is vented from the sampling tubing. As fluid reenters the borehole, the downhole pressure rebounds. As shown in Figure 4(b), the increase in pressure occurs in two distinct phases: (1) a slow pressure increase immediately after sampling and venting of the sample lines, which corresponds to filling of the downhole sample reservoir, and (2) a quicker increase, which corresponds to filling of the small-diameter sampling lines that run up to the surface.

To estimate the hydraulic conductivity of the formation beneath the packer, we apply Thiem's Equation. Assuming a homogeneous confined radial aquifer, the hydraulic conductivity is:

$$K = \frac{Q}{2\pi\left(h(r) - H\right)L} \ln\frac{r}{R} \quad (1)$$

where Q is the volumetric flux into the borehole, L the length of the packed-off interval, r the radius of the well, R the radius to a fictitious constant head boundary (assumed to be 2 m), and $h(r)$ (determined in the next section to be 349 m H_2O) and H are the heads at these two locations.

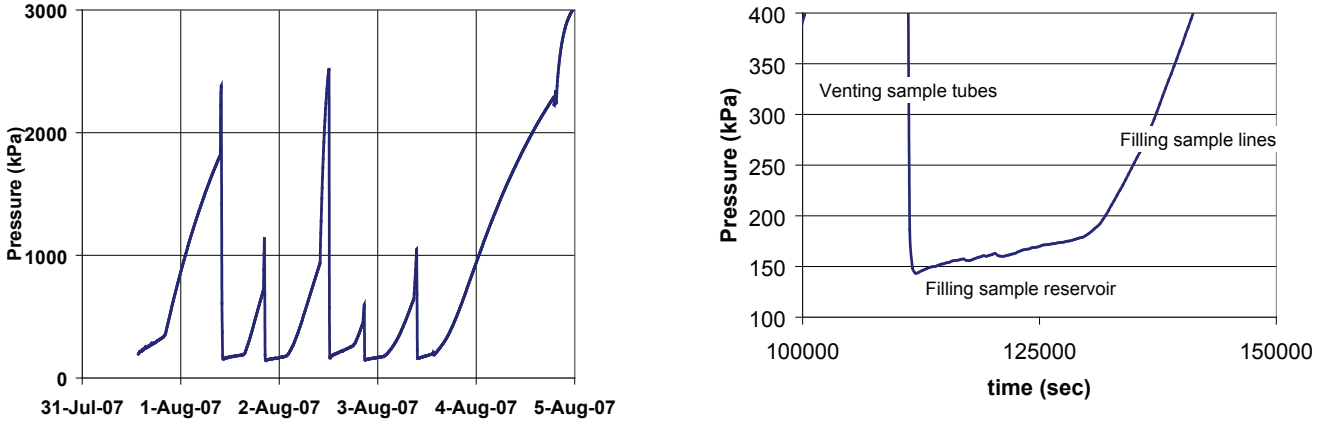

Figure 4. (a) Pressure response during U-tube sampling events as measured near the U-tube inlet. (b) Following acquisition of a U-tube sample and sample line N_2 gas venting, the pressure rebounds slowly as the sample reservoir fills, followed by a quicker rebound during filling of the small diameter sample lines.

To apply Thiem's equation, which requires steady-state conditions, we assume that the head *H* within the sample reservoir represents a pseudo-steady head of 18 m (Figure 4b)—justified because the change in head (3 m over several hours) is small compared to *h(r)–H*. *Q*, is assumed equal to the flux into the sample reservoir, determined as the product of the change in the fluid height within the sample reservoir (per unit time) and the reservoir's cross-sectional area.

Given the geometry of the High Lake borehole, the hydraulic conductivity *K* is estimated to be 2.3×10^{-11} m/s. This exceptionally small conductivity is typical of unfractured igneous rocks.

Permafrost thickness and hydrostatic head

Our results provide the best measured thickness of permafrost in this region, as other nearby estimates by the Geological Survey of Canada are from much shallower boreholes (e.g., Taylor et al. 1998). A linear extrapolation through the lower 120 m of fiber-optic temperature sensor data, with the addition of the discrete data point measured by the Level Troll pressure-temperature sensor (Figure 5), indicates that the base of the permafrost is at 458±5 m, where the depth uncertainty is based upon propagating a temperature error of ±0.1°C into the depth estimate. A small correction (+0.025°C) has been applied to account for the thermal perturbation created near the base of the well during the wellbore completion process, following the method suggested by Lachenbruch & Brewer (1958). By plotting the temperatures measured after wellbore completion as a function of $Log_e(t/(t-s))$, where *t* is the time elapsed since wellbore completion and *s* is the duration of the thermal perturbation (assumed to be 1.25 days), we correct for the effect of cooler water being introduced deeper in the borehole during the completion process (Figure 6).

The steady-state subpermafrost hydrostatic pressure can also be estimated by plotting pressure as a function of $Log_e(t/(t-s))$—referred to as a Horner Plot in well test literature. Using the pressure data from the Level Troll pressure-temperature sensor, we determined the hydrostatic pressure at a depth of 430 mbgs to be 3420 kPa. This is equivalent to a freshwater head of 349 m or a water table at 81 mbgs.

Thermal perturbation measurements

The DTPS experiment was conducted over a span of five days, with 63 hours of heating and 58 hours of cooling (Figs. 3, 5). To interpret the acquired thermal transients, we used a one-dimensional radial model explicitly incorporating the fluid-filled borehole and steel casing, surrounded by rock with homogeneous thermal properties, to invert cooling data. The formation of ice, which was observed to occur at depths shallower than 30 mbgs during cooling (as indicated by the thermal transients remaining stable near the freezing point of the borehole fluid [–4.5°C] for several hours), was not explicitly incorporated, but will be in future analyses. Heating data are not used, because small variations in spatial distance between the fiber-optic cable and the heating cable create large differences in temperatures. During cooling, however, conduction of heat tends to homogenize temperatures near the wellbore, making the simulations insensitive to the exact separation between the heating cable and monitoring fiber.

Figure 7 shows modeled cooling transients as a function of rock thermal conductivity, with data shown for selected depths. The model data are shown as lines and the measurements are shown as points. Using the one-dimensional radial model to invert the DTPS data, thermal conductivity is estimated along the wellbore with a spatial resolution equivalent to the 1 m resolution of the DTS (Fig. 8). The results shown in Figure 8 are consistent with the borehole lithology and literature values (Clauser & Huenges 1995), in which lower thermal conductivity felsic metavolcanic strata overly mafic metavolcanic strata. The exceedingly high thermal conductivities are attributed to zones in which the core was observed to consist of at least 50% pyrite.

Heat flux

Using the baseline temperature profile (Fig. 5) and the thermal conductivity profile (Fig. 8), the vertical heat flux

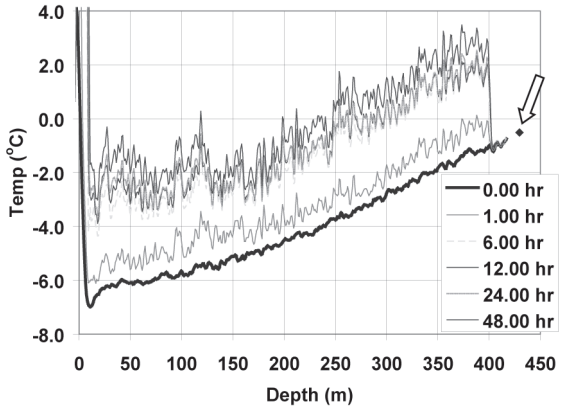

Figure 5. Thermal profiles acquired using a DTS. The lowest profile is the baseline prior to heating and cooling. The arrow points to a temperature measurement provided by the downhole Level Troll pressure-temperature sensor.

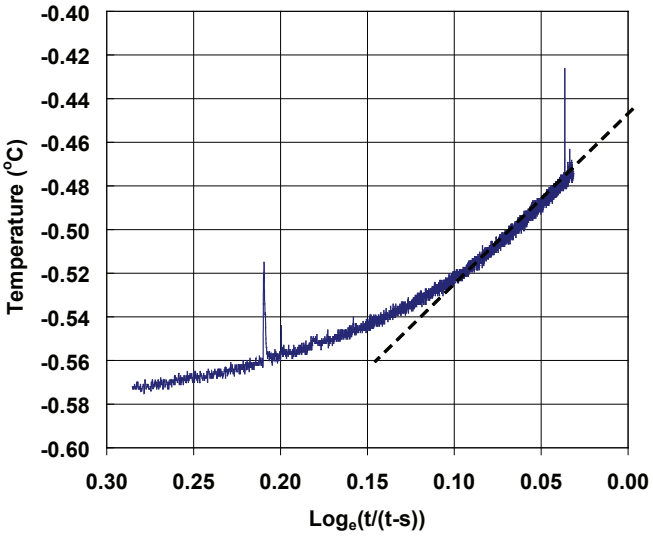

Figure 6. Temperatures measured in HL03-28 at a depth of 430 m following the wellbore completion process, as suggested by Lachenbruch & Brewer (1959) to determine undisturbed conditions. The temperatures extrapolated along the dotted line indicate the well is still 0.025°C cooler than at equilibrium.

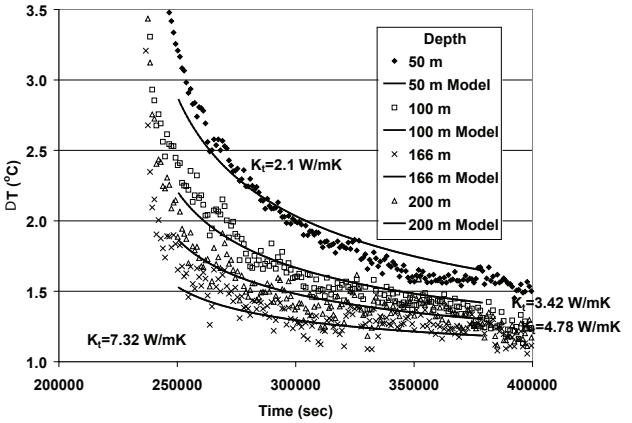

Figure 7. One-dimensional thermal simulations of DTPS testing showing modeled cooling transients along with select measurements. Time is measured from start of heating.

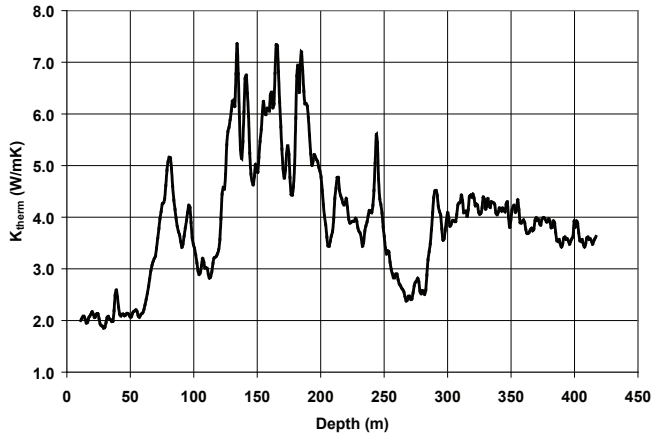

Figure 8. Thermal conductivity as a function of depth using a 1-D model to invert DTPS data. The results are consistent with lithology, in which shallow tuffs are underlain by ore-bearing mafic intrusives.

can be estimated in the vicinity of the wellbore. Using averaged values for thermal conductivity within the felsic metavolcanic units at a depth of 50 to 100 m, we estimate a heat flux of 30 mW/m^2, whereas at a depth between 300 and 400 m, the heat flux is much greater, 70 mW/m^2. The value of 70 mW/m^2 is considerably greater than the average value of 46±6 mW/m^2 reported for two wells 320 km south of High Lake by Mareschal et al. (2004) at Lac du Gras, Nunuvut, Canada. It is also greater than the value of 54.1 mW/m^2 estimated by inversion of thermobarometric data by Russell & Kopylova (1999) at the Jericho Kimberlite Pipes located 230 km southwest of High Lake. The much higher heat flow at High Lake can probably be attributed to the effect of the massive volcaniclastic sulphide deposit that can act as a conduit for conduction of heat to the surface.

The reduction in the estimated heat flux observed at the shallower depths (50 m to 100 m) at HL03-28 is consistent with other studies investigating GSTH. This change in heat flux is apparent in Superior Province temperature logs (Shen & Beck 1992), temperature logs from three borehole in northern Québec (Chouinard et al. 2007), and also in temperature profiles reported in the Canadian Arctic Archipelago (Taylor et al. 2006). However, without more detailed information on the three-dimensional shape of the High Lake ore body, which could influence lateral heat flux, and/or the regional history of snow cover, which would impact vertical heat flux (Stieglitz et al. 2003), it is impossible to know how much of the observed warming can be attributed solely to changes in GSTH.

Conclusions

We have deployed a multifunctional borehole observatory at the High Lake Project Site, which includes a bottomhole assembly for subpermafrost geochemical sampling using a

U-tube sampler located beneath a packer, and a pressure/temperature sensor for monitoring hydrologic conditions. The deployment lines contained a distributed thermal perturbation measurement system, consisting of a fiber-optic cable for distributed temperature measurements, and a heat trace cable to uniformly heat the wellbore.

Given the interest in using borehole temperature profiles as an indicator of paleoclimate, we have demonstrated a methodology for using the DTPS data for estimating formation thermal conductivity as a function of depth with meter-scale resolution. Having *in situ* estimates for thermal properties can reduce uncertainty in inverting borehole temperature profiles, leading to more accurate delineations of ground surface temperature history (GSTH). Future work using the High Lake data set will estimate the GSTH using the detailed thermal conductivity profile and the measured baseline temperature profile.

Acknowledgments

This work was supported by a grant from the NASA Astrobiology Institute (NASA NNA04CC03A). Additional support was provided through the Geological Survey of Finland, Espoo, Finland, POSIVA Oy, Finland, SKB, Sweden, and the Nuclear Waste Management Organization, Ontario, Canada. The authors wish to recognize the invaluable assistance and logistic support provided by Zinifex Canada Inc. in giving access to the High Lake Project Site. We thank Stefan Finsterle, Jacek A. Majorowicz and Alan E. Taylor, who provided numerous constructive comments on this manuscript. We also wish to acknowledge the generous loan of the Agilent DTS by Agilent Technologies.

References

Anisimov, O.A., Vaughan, D.G., Callaghan, T.V., Furgal, C., Marchant, H., Prowse, T.D., Vilhjálmsson, H. & Walsh, J.E. 2007. Polar regions (Arctic and Antarctic). In: M.L. Parry, O.F. Canziani, J.P. Palutikof, P.J. van der Linden & C.E. Hanson (eds.), *Climate Change 2007: Impacts, Adaptation and Vulnerability. Contribution of Working Group II to the Fourth Assessment Report of the Intergovernmental Panel on Climate Change*, Cambridge: Cambridge University Press, 653–685.

Clauser, C. & Huenges, E. 1995. Thermal conductivity of rocks and minerals. In: T.J. Ahrens (ed.), *Rock Physics and Phase Relations: A Handbook of Physical Constants*. American Geophysical Union.

Freifeld, B.M., Trautz, R.C., Yousif K.K., Phelps, T.J., Myer, L.R., Hovorka, S.D. & Collins, D. 2005. The U-Tube: A novel system for acquiring borehole fluid samples from a deep geologic CO_2 sequestration experiment. *J. Geophys. Res.* 110: B10203, doi:10.1029/2005JB003735.

Harris, R.N. & Chapman, D.S. 1997. Borehole temperatures and a baseline for 20th-Century global warming estimates. *Science* 275: 1618–1621.

Harris, S.A. 1986. *The Permafrost Environment*. London, England: Biddles Ltd., Guildford and King's Lynn. 276 pp.

Lachenbruch, A.H. & Brewer, M. 1959. Dissipation of the temperature effect in drilling a well in arctic Alaska, United States Geological Survey Bulletin 1083-C, 73–109.

Lachenbruch, A.H. & Marshall, B.V. 1986. Changing climate: geothermal evidence from permafrost in the Alaskan Arctic. *Science* 234: 689–696.

Mareschal, J.C., Nyblade, A., Perry, H.K.C., Jaupart, C. & Bienfait, G. 2004. Heat flow and deep lithospheric thermal structure at Lac de Gras, Slave Province, Canada. *Geophys. Res. Lett*. 31: L12611, doi:10.1029/2004GL020133.

Majorowicz, J.A. & Safanda, J. 2001, Composite surface temperature history from simultaneous inversion of borehole temperatures in western Canadian plains. *Global and Planetary Change* 29: 231–239.

Russell, J.K. & Kopylova, M.G. 1999. A steady state conductive geotherm for the north central Slave, Canada: Inversion of petrological data from the Jericho Kimberlite pipe. *J. Geophys. Res.* 104: 7089–7101.

Selker, J.S., Thévenaz, L., Huwald, H., Mallet, A., Luxemburg, W. van de Giesen, N., Stejskal, M., Zeman, J., Westhoff, M. & Parlange M.B. 2006. Distributed fiber-optic temperature sensing for hydrologic systems. *Water Resour. Res.* 42: W12202, doi:10.1029/2006WR005326.

Shen, P.Y. & Beck, A.E. 1992. Paleoclimate change and heat flow density inferred from temperature data in the Superior Province of the Canadian Shield. *Palaeogeogr., Palaeoclimatol., Palaeoecol. (Global Planet. Change Sect.)* 98: 143–165.

Stieglitz, M., Déry, S.J., Romanovsky, V.E. & Osterkamp, T.E. 2003. The role of snow cover in the warming of arctic permafrost. *Geophys. Res. Lett.* 30(13): 1721, doi:10.1029/2003GL017337.

Taylor, A.E., Burgess, M.M., Judge, A.S., Allen, V.S. & Wilkinson, A. 1998. Canadian Geothermal Data Collection—Deep permafrost temperatures and thickness of permafrost. In:*Circumpolar Active Layer Permafrost System (CAPS), Version 1.0*. Compiled by International Permafrost Association, Data and Information Working Group, National Snow and Ice Data Center, University of Colorado, Boulder, CO. CD-ROM.

Taylor, A.E., Wang, K., Smith, S.L., Burgess, M.M. & Judge, A.S. 2006. Canadian Arctic permafrost observatories: detecting contemporary climate change through inversion of subsurface temperature time series. *J. Geophys. Res.* 111: B02411, doi:10.1029/2004JB003208.

The Permafrost Legacy of Siemon W. Muller

Hugh M French
10945 Marti Lane, North Saanich, British Columbia, Canada
Frederick E. Nelson
Department of Geography, University of Delaware, USA

Abstract

Siemon W. Muller's contribution to permafrost engineering in North America is widely recognized. His status in this field derives from a 1943 US Army engineering manual, compiled from translated Soviet literature and prepared to alleviate problems experienced during construction of the Alcan (Alaska) Highway. Muller's status in permafrost science is derived from the same source, but in this context his contribution is less well defined. A previously unpublished manuscript by Muller, drafted prior to 1963, could have made a contribution to permafrost *science* as significant as his earlier effort was to permafrost *engineering*. It would also have encouraged development of a holistic approach to geocryology in North America, similar to that developed in Russia and China, as opposed to the dualism that evolved between permafrost science and permafrost engineering in the mid-century North American literature.

Keywords: geocryology; history of science; North America; permafrost engineering; permafrost science.

Introduction

Siemon W. Muller is generally regarded as the "father" of permafrost studies in North America. Muller used the term *permafrost*, which he apparently calqued from Russian (Kabakchi & Butters 1989, French & Nelson 2008), to describe the perennially frozen and often ice-rich terrain encountered during construction of the Alcan (Alaska) Highway in 1942–43. He documented the engineering problems associated with construction in ice-rich permafrost terrain in a US Army handbook, first printed in 1943 and subsequently declassified and printed in book form in 1947 (Muller 1943, 1947). This book formed the framework for North American permafrost engineering over the next two decades.

Less clear is Muller's legacy as regards permafrost science in North America. A monograph by Stephen Taber (1943), published virtually simultaneously, provided a more thorough discussion of the genesis and evolution of perennially frozen ground in Alaska. The present paper draws upon a previously unpublished manuscript completed by 1963 (French & Nelson 2008) and speculates about how Muller's contribution to permafrost science might have been enhanced if this manuscript had been published at that time. The near-complete manuscript was found in 1996 in his files.

The Man

Of critical significance to Muller's permafrost legacy was his Russian heritage. He was born in Blagoveshchensk, eastern Russia, near the border of Manchuria. He left Russia shortly after the Russian revolution and moved to the US in 1921. His fluency in Russian allowed him to introduce Russian permafrost knowledge into North America at a time when few North American scientists were fluent in Russian and there were few contacts between Soviet and North American scientists.

Contrary to what one might expect, permafrost was a distinctly subsidiary interest for Muller, and he never contributed to its primary literature. The central focus of his research was the Triassic paleontology and stratigraphy of western Nevada. His teaching responsibilities at Stanford University, where he studied and worked for more than 40 years, included courses in historical geology, paleontology, stratigraphy, and the geology of California.

During the 1930s, Muller developed a close collaboration with the USGS geologist Henry Ferguson. They worked together on the geology of western Nevada, and Muller assumed a part-time affiliation with the USGS. Muller's knowledge of stratigraphy, structural geology, and field methods, combined with his knowledge of Russian, explains why he was approached by the US Army in 1942 to give geological advice during construction of the Alcan Highway. The outstanding merit of the 1943 US Army handbook was its accurate, well-organized summary of early Russian permafrost literature. This allowed others to solve the many permafrost engineering problems encountered in wartime projects in Alaska and northern Canada.

Upon his return to academia in 1945, Muller resumed his teaching responsibilities and collaborative research with Henry Ferguson. He also began teaching a course on permafrost. His only graduate student to concentrate on permafrost was Troy Péwé (PhD Stanford, 1953) but others, such as Lou deGoes and some USGS staff at Menlo Park, probably attended his classes. Muller published virtually nothing on permafrost during the remainder of his career. The unpublished book manuscript referred to above appears to have been his only attempt to add to the permafrost literature. We can only speculate about the reasons why he did not bring the book to publication (see French & Nelson 2008).

The Growth of Geocryology in the USSR

The occurrence of perennially frozen ground in northern North America had been known in general terms for more than a century by the time of Muller's 1943 report (e.g., Leffingwell 1919; see French 2003, 29–34). By the early 1930s the extent of frozen ground in both Alaska and northern Canada was reasonably well known. However, a detailed understanding of the permafrost terrain of central Alaska was still lacking.

By contrast, the Russian experience with frozen ground was far more extensive (see Shiklomanov 2005). This was because an Institute of Permafrost had been established in Yakutsk by the USSR Academy of Sciences in 1939. Also, the movement of population, often penal in nature, to the more remote parts of Siberia had begun. The boreal forest was being removed and agriculture started. Russian-language texts soon summarized extensive knowledge about permafrost (e.g., Sumgin 1927, 1937), and the first edition of what was to become the standard Russian text on permafrost for the next 25 years, *Obshcheye Merzlotovedeniya (General Permafrostology*), was published in 1940 (Sumgin et. al. 1940). By the late 1950s, a major publication by the V.A. Obruchev Institute of Permafrost Studies, Moscow, entitled *Osnovy geokriologii (merzlotevedeniya) (Principles of Geocryology*) (Shvetsov & Dostovalov 1959) had appeared. This text was divided into two volumes: Part I – General Geocryology and Part II – Engineering Geocryology. The science and engineering aspects of permafrost were explicitly linked in one discipline: geocryology. A similar approach to geocryology developed later in China (Academia Sinica 1975, Zhou et al. 2000).

The Emergence of Permafrost Science and Permafrost Engineering in North America

In North America, the most significant early advances in understanding permafrost phenomena were made in a series of laboratory experiments by Stephen Taber, an American engineer. In a number of papers published between 1916 and 1930, he examined the mechanics of frost action and the process by which ice segregates in freezing soil (Taber 1929, 1930). These were seminal contributions, soon followed by Swedish studies of frost heaving, especially as they applied to roads and buildings, and then by Japanese military engineers in Manchuria during the Second World War (see Sugaya 1956). It was in a similar context that Muller became involved, in 1942–43, in construction of the Alcan Highway (Fig. 1).

In the same year that Muller's US Army handbook appeared, Stephen Taber published a monograph-length paper summarizing available knowledge on perennially frozen ground in Alaska (Taber 1943). This paper describes the climatic and vegetation conditions associated with perennially frozen ground and related geomorphological processes, including freezing and thawing, frost heaving, and mass wasting. It also discusses the Quaternary-age gravels and silts that overlie bedrock in Alaska, their frozen nature, and the occurrence of ground ice, both in bedrock and surficial sediments. Finally, a sequence of Pleistocene events is set out, involving successive periods of sediment deposition, deep freezing, deep thawing and erosion, and refreezing.

Taber's 1943 monograph, rather than Muller's, might more properly be regarded as the beginning of modern permafrost science in North America. Not only does it discuss the conditions associated with permafrost occurrence (as does Muller's), but also it considers the Pleistocene history and origin of permafrost and ground ice as mentioned above. These became central themes in permafrost science in North America in the second half of the 20th century. Examples are T.L. Péwé's Pleistocene and Quaternary geology work in Alaska, J.R. Mackay's permafrost and ground-ice-related studies in the western Canadian Arctic, and A.L. Washburn's concern for solifluction and mass-wasting processes. It is significant that Taber used the term "perennially frozen ground" and made no mention of either "permanently frozen ground" or "permafrost." The latter were the two terms used by Muller in his 1943 manual. Permafrost is now, of course, generally referred to as being "perennially" rather than "permanently" frozen ground.

Muller's primary concerns in his 1943 manual were the geotechnical and engineering problems associated with ice-rich permafrost terrain. His admirably explicit treatment

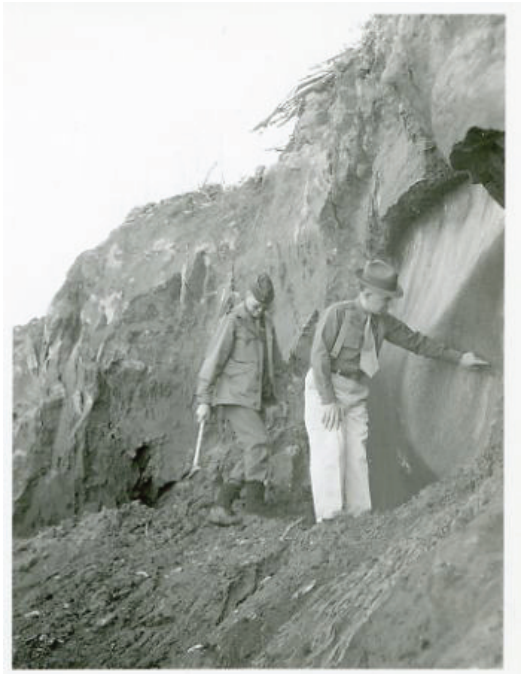

Figure 1. Photo of Siemon Muller in 1944, near Fairbanks, Alaska, with Roy Earling, President of the U.S. Smelting, Refining, and Mining Company, and Fairbanks Exploration Company. Muller is wearing the clothes of a US Army officer, but with no insignia or rank; he was a civilian. The sediments that enclose the ice wedges are part of the Goldstream Formation of Wisconsinan age (~120,000 to 10,000 years ago). The upper 1.5 m (above the ice wedges) is Holocene-age sediment (Ready Bullion Formation). Caption details supplied by T.L. Péwé, December 1996. Source of photo: unknown.

of these issues promoted the formation of governmental research agencies involved with cold regions geotechnical engineering in both the US and Canada (e.g., the Snow, Ice and Permafrost Research Establishment [SIPRE], later to become the Cold Regions Research and Engineering Laboratory [CRREL], in Hanover, New Hampshire, and the Division of Building Research [DBR], National Research Council of Canada [NRCC], in Ottawa, Ontario); and the emergence of professional groups such as the Technical Committee on Cold Regions Engineering (TCCRE) of the American Society of Civil Engineers (ASCE), the Cold Regions Engineering Division of the Canadian Society of Civil Engineering (CSCE), and the Cold Regions Geotechnology Division of the Canadian Geotechnical Society (CGS).

The Muller and Taber publications of 1943 are complementary. Symbolically, they mark the beginning of a dualism that continues in North America between the literature of permafrost science and permafrost engineering. Attempts were initially made to bridge the divide, as personified by the close collaboration between Roger Brown and Hank Johnston at the NRCC (e.g., Brown & Johnston 1964, Johnston et al. 1963), and various USGS reports on permafrost terrain problems in Alaska (e.g., Hopkins et al. 1955, Lachenbruch 1962, Ferrians et al. 1969). However, it is fair to conclude that cold regions engineering soon developed as a separate discipline, only to be reunited with permafrost science every five or ten years at the international permafrost conferences.

"Frozen in Time" – The 1963 Manuscript

Muller's previously unpublished manuscript (French & Nelson 2008) indicates that he was acutely aware of the imbalance between permafrost science and permafrost engineering in his 1943 monograph. It is clear that in the 15 years following his return to academia in 1945, he closely followed the permafrost literature in both North America and the USSR. Not only did he attempt to update the North American engineering practices described in his 1943 manual, but also he attempted to incorporate Russian understanding of permafrost science. Several examples can be offered.

First, Muller was aware of the importance of the unusual permafrost conditions that characterize the base of the active layer and the top of permafrost. This is why he used the term *active zone* rather than the more conventional term *active layer* that dominated the North American literature. The evolution of his ideas concerning near-surface permafrost terrain is illustrated in Figures 2 and 3, where Muller's 1943 diagram is compared with a reworked version in the later manuscript. In Figure 3b Muller indicates that the active zone is composed of two layers: a near-surface layer that freezes and thaws annually and a lower layer ("pereletok") that might remain frozen in certain years of cooler summers and thawed in others of warmer summers. This reflected the Russian permafrost literature. Nearly 30 years were to pass

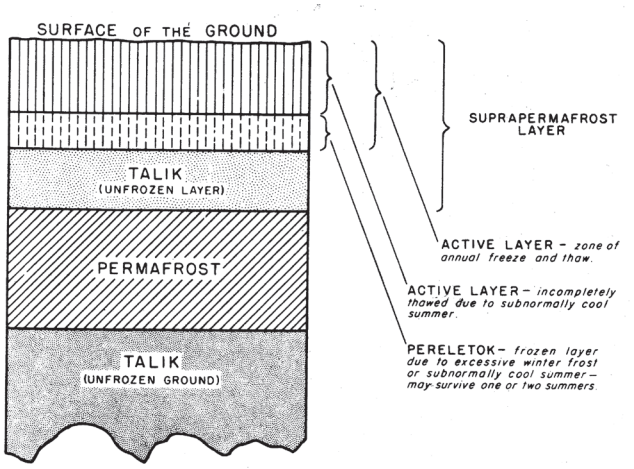

Figure 2. Muller's 1943 Figure 5, entitled "Diagram showing the different layers in the permafrost area."

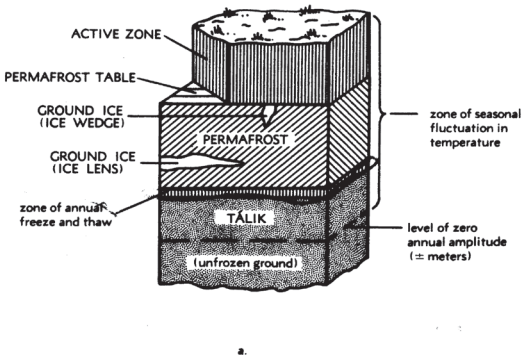

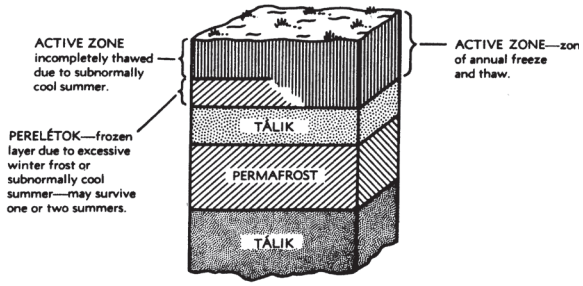

Figure 3. The 1963 manuscript's Figure 1, entitled "Diagrams of profiles with permafrost."

before a three-layer concept of the active layer-permafrost interface was formally introduced into the North American literature (Shur 1988, Shur et al. 2005). This ice-rich zone has been termed the *transient layer.*

It is now clear that the depth of the active layer fluctuates on both yearly and decadal time scales. It promotes an ice-rich layer (or "zone") at the active layer-permafrost interface. Current global warming concerns also focus attention upon this ice-rich layer; for example, it is central to the second phase of the Circumpolar Active Layer Monitoring (CALM II) program (Nelson et al. 2004).

Second, Muller understood the complex role played by vegetation over permafrost distribution and nature. Even before 1943, there was a large Russian literature available on

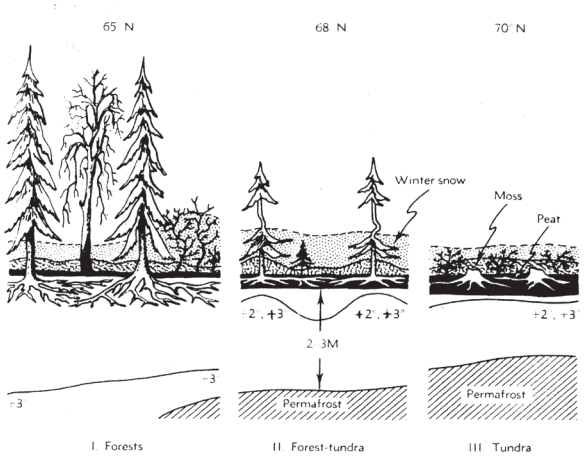

Figure 4. The 1963 manuscript's Figure 47, entitled "The combined effect of moss, peat, and snow on the distribution of roots and on the summer ground temperatures in forests, forest-tundra, and tundra, at latitudes of 65ºN, 68ºN and 70ºN."

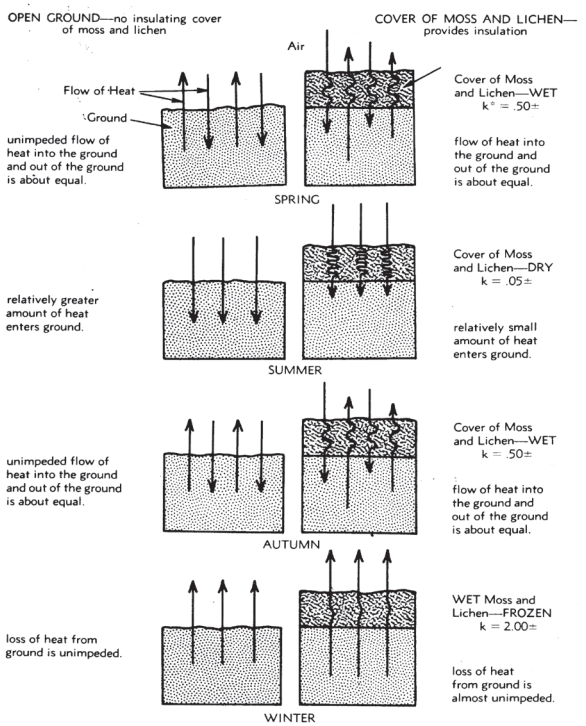

Figure 5. The 1963 manuscript's Figure 4, entitled "Flow of heat between air and ground in tundra country."

this topic (e.g., Sumgin et al. 1940, Tyrtikov 1956). Muller relied heavily on a text by A.A. Grigor'yev (1956) describing the vegetation of the Russian subarctic and tundra. For example, an elegant figure summarizes the effects of moss, peat, and snow on vegetation in the forest, forest-tundra, and tundra at latitudes of 65°, 68°, and 70°N (Fig. 4). It was not until after Muller had drafted his manuscript, and translations of the 1959 *Principles of Geocryology* had appeared, that North American permafrost scientists began to appreciate the importance of vegetation (e.g., Brown 1966, 1970).

The importance ascribed by Muller to the influence of vegetation was also a precursor to modern studies of permafrost, ground climate, and the "n-factor" (e.g., Lunardini 1978, Klene et al. 2001). For example, Figure 5 summarizes his discussion of the effects of soil thermal conductivity (k) upon heat flow in "open ground" (i.e., tundra with no insulating cover of moss and lichen) and in terrain where a cover of moss and lichen provides insulation.

Third, Muller expanded the treatment of ground ice in his 1943 manual by discussing ground ice in the context of cryostructures and cryotextures. This Russian approach (Vtyurin 1965) was far more advanced than the descriptive classification used in North America at the time (e.g., Pihlainen & Johnston 1963), since it inferred genesis and implied permafrost history. The cryostratigraphic approach to permafrost history only developed in North America three decades later (e.g., Mackay 1974, Burn et al. 1986, Murton & French 1993).

In other ways, too, Muller was ahead of his time. For example, he used some of the "cryo" terminology of K. Bryan (1946). At the time, this was largely rejected by the academic community. He thereby avoided the semantic pitfalls associated with the terms *frozen* and *unfrozen*, an ambiguity that continued into the 1990s (Burn 1998). Also, in his discussion of "cryogenic" weathering, he relied on Soviet literature that preceded later research, demonstrating the existence of microbiological processes at sub-zero temperatures (e.g., Gilichinsky et al. 1995).

Finally, many engineering concepts in the earlier text were upgraded to incorporate advances in the 1950s. For example, the manuscript reveals that Muller clearly understood the significance of moisture migration in freezing soils and its relevance to frost heave and ice segregation. Following recent Soviet work (Bozhenova 1957), Muller illustrated how moisture migrates in freezing soils (Fig. 6). Although this was confirmed by the subsequent work of E. Penner (1959), it was not until 20 years later that its geomorphological significance was recognized (e.g., Cheng 1983, Mackay 1983).

One of the last meetings Muller attended before his death in 1970 was a USGS seminar dealing with the Alaska North Slope. When Muller raised a concern about the engineering planning of the proposed pipeline, the USGS scientist A.H. Lachenbruch (1970, J5) responded that "substantial unsolved problems have received remarkably little attention." One is tempted to speculate about the impact Muller's then-unpublished text might have had on the subsequent construction of the TAPS Pipeline later in that decade.

Conclusions

Muller's pioneering status in North American permafrost engineering is well deserved. Viewed from the privileged position of hindsight, however, one can argue that his 1943 monograph neglected permafrost science. Undoubtedly, the realities of wartime explain this.

Muller's "lost" manuscript was an attempt to rectify this deficiency, but unfortunately and for unknown reasons, he abandoned his nearly completed project, never to return to it.

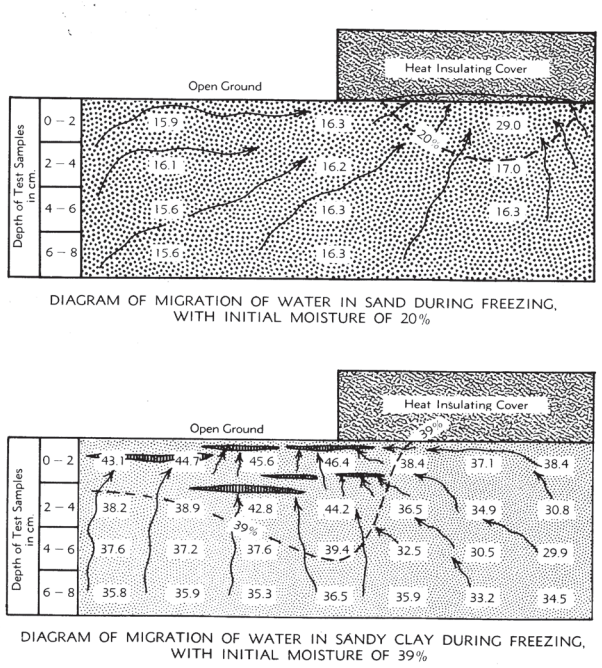

Figure 6. The lower two diagrams of the 1963 manuscript's Figure 13, entitled "Diagrams of migration of water in sand (sandy clay) during freezing with initial moisture contents of 13%, 20%, and 39%."

Muller's manuscript, if published in 1963 at the time of the First International Conference on Permafrost, would have advanced permafrost science in North America in the same way that his 1943 US Army handbook became a benchmark for permafrost engineering in North America. It contained concepts and information that would have advanced permafrost science in North America by at least two decades. But even more important, by integrating permafrost science with permafrost engineering, Muller would have promoted a holistic approach to geocryology in North America. This would have made the study of permafrost in North American more similar to the discipline of geocryology that developed in both Russia and China.

Acknowledgments

HMF acknowledges the late Troy L. Péwé, who instilled in him an appreciation of the legacy of Siemon Muller and who passed to him, in 1995, many of Muller's books, papers and photographs. Jerry Brown and an anonymous reviewer provided helpful comments on the manuscript

References

Academia Sinica. 1975. *Permafrost*. Lanzhou: Research Institute of Glaciology, Cryopedology and Desert Research, China, 124 pp. (in Chinese). (National Research Council of Canada, Ottawa, Technical Translation, 2006 (1981), 224 pp.).

Bozhenova, A.P. 1957. Physical phenomena and processes in freezing and frozen grounds. *Merzylykh Gruntov, Institut Merzlotevedeniya*, Akad. Nauk SSSR, 3: 23-27 (in Russian).

Brown, R.J.E. 1966. Influence of vegetation upon permafrost. In: *Proceedings, Permafrost International Conference, Washington, D.C.*, National Academy of Science – National Research Council, Publication 1287, 20-25.

Brown, R.J.E. & Johnston, G.H. 1964. Permafrost and related engineering problems. *Endeavour* XXIII(89): 66-72.

Bryan, K. 1946. Cryopedology – the study of frozen ground and intensive frost action with suggestions on nomenclature. *American Journal of Science* 244: 622-42.

Burn, C.R. 1998. The active layer: two contrasting definitions. *Permafrost and Periglacial Processes* 9: 411-416.

Burn, C.R., Michel, F.A. & Smith, M.W. 1986. Stratigraphic, isotopic and mineralogical evidence for an early Holocene thaw unconformity at Mayo, Yukon Territory. *Canadian Journal of Earth Sciences* 23: 794-803.

Cheng, G. 1983. The mechanism of repeated-segregation for the formation of thick layered ground ice. *Cold Regions Science and Technology* 8: 57-66.

Ferrians, O.J., Jr., Kachadoorian, R. & Greene, G.W. 1969. Permafrost and related engineering problems in Alaska. *United States Geological Survey Professional Paper* 678, 37 pp.

French, H.M. 2003. The development of periglacial geomorphology: 1-up to 1965. *Permafrost and Periglacial Processes* 14: 29-60.

French, H.M. & Nelson, F.E. (eds.) 2008. *Frozen in Time: a Manual on "Permafrost and Engineering Problems" by S. W. Muller.* New York: American Society of Civil Engineers, Technical Committee on Cold Regions Engineering, in press.

Gilichinsky, D., Wagener, S. & Vishnevetskaya, T.A. 1995. Permafrost microbiology. *Permafrost and Periglacial Processes* 6: 281-291.

Grigor'yev, A.A. 1956. *The Subarctic*. Moscow: Institute of Geography, USSR Academy of Sciences, 223 pp. (in Russian).

Hopkins, D.M., Karlstom, T.D. & others. 1955. Permafrost and groundwater in Alaska. *United States Geological Survey Professional Paper* 264-F, 113-146.

Johnston, G.H., Brown, R.J.E. & Pickersgill, D.N. 1963. *Permafrost Investigations at Thompson, Manitoba: Terrain studies*. Ottawa: Division of Building Research, National Research Council, Technical Paper 158, 51 pp.

Klene, A.E., Nelson, F.E., Shiklomanov, N.I. & Hinkel, K.M. 2001. The N-Factor in natural landscapes; variability of air and soil-surface temperatures, Kuparuk River Basin, Alaska, USA. *Arctic, Antarctic and Alpine Research* 33: 140-148.

Lachenbruch, A.H. 1962. Mechanics of thermal-contraction cracks and ice-wedge polygons in permafrost. *Geological Society of America, Special Paper* 70, 69 pp.

Lachenbruch, A.H. 1970. Themal considerations in permafrost. In: W.L. Adkison & M.M. Brosgé (eds.), *Proceedings of the Geological Seminar on the North Slope of Alaska*. Pacific Section, American Association of Petroleum Geologists, Los Angeles, J1-J5.

Leffingwell, E. de K. 1919. The Canning River region, northern Alaska. *United States Geological Survey Professional Paper* 109, 251 pp.

Lunardini, V. 1978. Theory of n-factors and correlation of data. *Proceedings of the Third International Conference on Permafrost, Edmonton, Alberta, Canada 10–13 July 1978:* 40-46.

Mackay, J.R. 1974. Reticulate ice veins in permafrost, Northern Canada. *Canadian Geotechnical Journal* 11: 230-237.

Mackay, J.R. 1983. Downward water movement into frozen ground, western arctic coast. *Canadian Journal of Earth Sciences* 20: 120-134.

Muller, S.W. 1943. *Permafrost or Permanently Frozen Ground and Related Engineering Problems*. United States Geological Survey, Strategic Engineering Study, Special Report No 62, Intelligence Branch Office, Chief of Engineers, U.S. Army, 136 pp.

Muller, S.W. 1947. *Permafrost or Permanently Frozen Ground and Related Engineering Problems.* Ann Arbor, MI: J. W. Edwards, 231 pp.

Murton, J.B. & French, H.M. 1994. Cryostructures in permafrost, Tuktoyaktuk coastlands, western Arctic, Canada. *Canadian Journal of Earth Sciences* 31: 737-747.

Nelson, F.E., Shiklomanov, N.I., Hinkel, K.M. & Christiansen, H.H. 2004. Introduction: the Circumpolar Active Layer Monitoring (CALM) Workshop and the CALM II Program. *Polar Geography* 28: 253-266.

Penner, E. 1959. The mechanism of frost heaving in soils. *Highway Research Board, Bulletin* 225: 1-13.

Péwé, T.L., 1953. *Geomorphology of the Fairbanks Area, Alaska*. Ph.D. Dissertation, Stanford University, 308 pp.

Pihlainen, J.A. & Johnston, G.H. 1963. *Guide to a Field Description of Permafrost*. Ottawa: National Research Council, Associate Committee on Soil and Snow Mechanics, Technical Memorandum 79, 23 pp.

Shiklomanov, N.I., 2005. From exploration to systematic investigation: development of geocryology in 19th- and early-20th-Century Russia. *Physical Geography* 26: 249-263.

Shur, Y. 1988. The upper horizon of permafrost soils. *Proceedings of the Fifth International Conference on Permafrost, Trondheim, Norway, 2–5 August, 1988:* 867-871.

Shur, Y., Hinkel, K.M. & Nelson, F.E. 2000. The transient layer: implications for geocryology and climate-change science. *Permafrost and Periglacial Processes* 16: 5-18.

Shvetsov, P.F. & Dostovalov, B.N. (eds.) 1959. *Osnovy geokriologii (merzlotovedeniya) (Fundamentals of geocryology)*. Moscow: Collected publications by staff members of the USSR Academy of Sciences, Institute of Permafrost, Parts I and II, USSR Academy of Sciences Press (in Russian).

Sugaya, J. 1956. *Congelation-structure and frost-heaving ratio at Assan, Manchuria*. Ottawa: Canada Defence Research Board, Translation T 54 J (from unpublished manuscript) by E. R. Hope, 18 pp.

Sumgin, M.I. 1927, 1937. *Soil Permafrost within the USSR.* Vladivostok: 1st edition; Moscow – Leningrad: 2nd edition, Academii Nauk USSR, 372 pp. (in Russian).

Sumgin, M.I., Kachurin, S.P., Tolstikhin, N.I. & Tumel, V.F. 1940. *Obshche merzlotovedeniya (General Permafrostology).* Moscow – Leningrad: USSR Academy of Sciences, 340 pp. (in Russian).

Taber, S. 1929. Frost heaving. *Journal of Geology* 37: 428-461.

Taber, S. 1930. The mechanics of frost heaving. *Journal of Geology* 38: 303-317.

Taber, S. 1943. Perennially frozen ground in Alaska; its origin and history. *Geological Society of America Bulletin* 54: 1433-1548.

Tyrtikov, A.P. 1956. The effect of vegetation on perennially frozen soil. In: *Data on the principles of the study of frozen zones in the earth's crust*, Issue III, Institute of Permafrost Studies, USSR Academy of Sciences, Moscow. (in Russian). (National Research Council of Canada, Ottawa, Technical Translation 1088 (1964), 69-90).

Vtyurin, B.I. 1965. *Cryogenic Structure of Quaternary sediments*. Moscow: Nauka, Academy of Sciences USSR, 151 pp. (in Russian).

Zhou, Y., Gou, D., Cheng, G. & Li, S. 2000. *Geocryology in China*. Lanzhou: Cold and Arid Regions Environmental and Engineering Research Institute (CAREERI), Chinese Academy of Sciences, 450 pp. (in Chinese).

Seasonal Thaw of Soils in the North Yakutian Ecosystems

D.G. Fyodorov-Davydov, A.L. Kholodov,V.E. Ostroumov, G.N. Kraev, & V.A. Sorokovikov
Institute of Physicochemical and Biological Problems in Soil Science, Russian Academy of Sciences, Pushchino, Moscow
S.P. Davydov
Northeast Science Station, Pacific Institute of Geography, Far East Branch, RAS, Chersky, Sakha (Yakutia) Republic, Russia
A.A. Merekalova
Geographical Faculty, Lomonosov State University, Moscow, Russia

Abstract

The active layer thickness **(**ALT) in tundra ecosystems of North Yakutia is controlled by soil texture. Normal thaw depth in zonal soils of sandy tundra are about 50–105 cm, while in soils of loamy tundra it is 35–70 cm. In the intrazonal ecosystems, the seasonal thaw depth is smaller than in complementary zonal ecosystems. Studies in the Kolyma Lowland show that the ALT pattern is subject to climatic zonality. ALT reaches 27–37 cm in the Arctic tundra subzone; in the Typical tundra it is 41–42 cm, and 43–49 cm in the Southern tundra. In the Northern taiga, the thaw depth under positive microrelief elements varies between 43 and 90 cm in loamy soils and between 65 and 120 cm in sandy soils. According to our data, the active layer in Yana-Indigirka and Kolyma Lowlands experienced a progressive thickening over the 2000–2006 period.

Keywords: active layer; climate; permafrost; Russia; soils.

Introduction

The monitoring of the active layer thickness (ALT) plays an important role in global permafrost observation efforts. During the 1996–2006 period, extensive active-layer field observations were conducted in North Yakutia under the auspices of the international Circumpolar Active Layer Monitoring (CALM) program (Brown et al. 2000). An analysis of empirical data and previously published information (e.g., Karavaeva 1969, Garagulya et al. 1970, Savvinov 1976, Soloviev 1978, Elovskaya et al. 1979, Perfilieva et al. 1991) have revealed spatial and temporal patterns of seasonal thaw for one of the least investigated regions. Special emphasis was placed on analysis of the active layer response to changing air temperature attributable to climate variability and change.

Analysis, conducted in permafrost regions of West Siberia, indicates pronounced deepening of seasonal thaw over the decades (Moskalenko 2001, Melnikov et al. 2004, Pavlov et al. 2004). No long-term measurements of the active layer depth are known from North Yakutia. In this paper we investigate the spatial and temporal ALT trends for North Yakutia and its relation to landscape and climatic variables. Due to the lack of adequate long-term empirical information, this study is focused primarily on recent changes in the active-layer thickness.

Study Area

The study was conducted primarily in the tundra zone of North Yakutia and Northern taiga subzone of the Lowlands (Fig. 1). The observational sites were selected to represent characteristic landscapes of both bioclimatic zones.

The tundra zone of Yakutia occupies the coast and islands of East-Siberian and Laptev seas and extends to 250–300 km inland. Based on climatological and geobotanical criterion, it is subdivided into Arctic, Typical, and Southern tundra subzones. The territory is largely underlain by ice-rich loamy sediments of the Late Pleistocene yedoma formation, which was subject to extensive thermokarst and thermoerosion processes since the Holocene optimum. The topography is represented by alternating yedoma uplands and thermokarst depressions (alases). Upland surfaces are covered by low shrub/sedge/green moss, sedge/green moss/dryas, or green moss/osier associations, and characterized by zonal Cryozem or Gleyzem (*Glacic Haploturbels, Typic Haploturbels,* and *Typic Umbriturbels*) soils. The microrelief is represented by frost mounds. Alases are predominantly occupied by polygonized bogs. A few areas in the tundra zone are underlain by well-drained sand deposits covered by low shrub/lichen and green moss/low shrub/lichen associations with Podbur (*Spodic Psammoturbels*) soil representing a zonal soil type. The microrelief is characterized by frost mounds and hummocks.

The sites representative of the Northern taiga are underlain by loam and sands. Vegetation is characterized by larch forest with the low shrub/lichen, lichen/green moss, and low shrub/green moss/lichen associations often growing under shrub storey. Cryogenic microrelief is less expressed in Northern taiga than in tundra. Flood-plain landscapes are spotty and include drained river banks and different types of bogs. Sedge/green moss/willow and *calamagrostis* associations are found near the river channels. Frost mounds are abundant and pronounced, and they are associated with the Alluvial soddy gleyic (*Typic Umbriturbels*) soils. There is a huge variety of flood-plain bogs.

The climate of Yakutia's tundra zone is severe and strongly continental. The mean annual air temperature in tundra zone varies between -11.5°C and -15.0°C. The mean

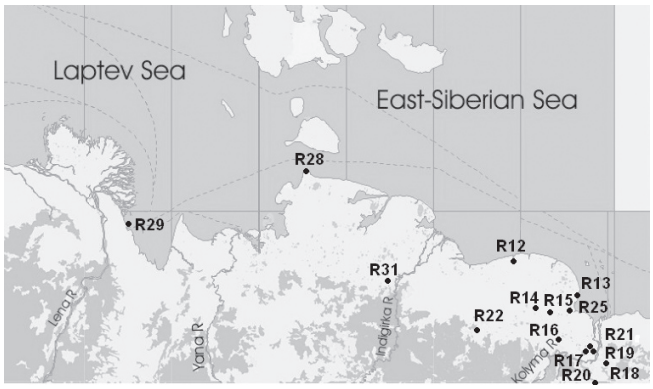

Figure 1. Map of the North Yakutia lowland with the CALM-site locations: R12 - Bolshaya Kuropatochya River (plakor and slope); R13 - Malyi Chukochiy Cape (plakor and alas); R14 - Bolshaya Chukochya River; R15 - Malaya Konkovaya River (plakor and alas); R16 - Segodnya Pingo; R17 - Akhmelo Channel; R18 - Mountain Rodinka; R19 - Glukhoe Lake; R20 - Malchikovskaya Channel; R21 - Akhmelo Lake; R22 - Alazeya River; R25 - Yakutskoe Lake; R28 - Svyatoy Nos Cape; R29 - Bykovsky Cape (plakor and alas); R31 - Allaiha River.

air temperature in January is -29.0°C to -37.5°C. The mean July air temperature varies between 2.5°C and 5.0°C in Arctic tundra and between 6.5°C and 11.5°C in Typical and Southern tundra.

The area is underlain by continuous low-temperature permafrost that is 500–650 m thick. The coldest permafrost (-10°C to -12°C) is found in the yedoma uplands of the tundra zone. Alases and areas underlain by sand are characterized by higher permafrost temperatures (-8°C to -10°C). The permafrost temperature of the Northern taiga varies within a -5°C to -8°C range and can be warmer near large streams.

Observational Program

An array of 19 active layer monitoring sites was established following standardized CALM procedure (Brown et al. 2000) in the following North Yakutian subregions: Bykovskii Peninsula, Yana-Indigirka Lowland, and Kolyma Lowland (Fig. 1). Sixteen sites are located in tundra, while the remaining three sites are situated in the Northern taiga zone. Each site consists of a regular 1 ha grid. ALT observations are carried out by graduated metal rode at 10 m interval, yielding 121 point measurements per each site. The points were arrayed with 10 m spacing in aligned rows. A set of supplementary sites of variable sizes was established in landscapes under-represented by the primary CALM sites. A detailed description of sites and observation methodology is provided in Fyodorov-Davydov et al. (2004).

Spatial Controls of Active Layer Thickness at Different Scales

The thickest active-layer of 110–125 cm was found in sandy dunes, while minimum ALT (15–30 cm) was observed at sphagnum- and/or grass/green moss-covered polygonized bogs and palsas, underlain by peat soils.

In zonal tundra, ALT usually corresponds well to soil texture. Mean multi-year ALT values for sandy Podbur soils are about 50–105 cm, with maximum recorded thaw depth reaching 120–150 cm. Loamy Cryozem and Gleyzem soils are characterized by 35–70 cm ALT with the maximum reaching 75–80 cm (Table 1).

Observations in the Kolyma Lowland, the region with the highest number of sites, showed that ALT generally corresponds to climatic zonality. For similar yedoma watersheds with zonal tundra vegetation, frost mound microrelief, and Cryozem soils, the mean multi-year ALT values increase from north to the south (Table 2). The typical ALT value for northern-most Arctic tundra is about 27–37 cm, followed by 41–42 cm in Typical tundra and 43–49 cm in southern most Southern tundra. Microtopographically, the zonal ALT pattern is better expressed for frost mounds than intermound depressions. The overall ALT difference between Northern and Southern tundra locations is about 12–22 cm. ALT difference within frost mounds increases to 30 cm, and decreases to 10–13 cm for intermound depressions (Table 3).

Sandy tundra soils are located predominantly in the northeast of the Kolyma Lowland (so called Khallerchinskaya tundra) and distributed in a narrow latitude belt within the Southern tundra subzone. Due to meridian distribution of the sandy soil, the ALT there differs more than in loamy soils characteristic of yedoma landscapes (Table 4). For instance, on the sandy sites with zonal vegetation, the ALT within the mounds increased to 35–53 cm from north to the south (1.7–2.0 times), and to 18–41 cm (1.4–1.8 times) for intermound depressions. ALT in polygonal crack areas does not express any latitudinal zonality.

The mean ALT generally increases along the tundra-taiga direction (Table 2). However, the spatial heterogeneity of landscapes also increases from north to south as the timber stand, soil and vegetation types, slope angles, and exposure play a more pronounced role. Within the Northern taiga subzone, the ALT for loamy soils ranges between 43 and 91 cm (Table 3) and between 65 and 119 cm for sandy soils (Table 4). At the same time, at the zonal boundary, the ALT in the forests is thinner than in tundra. Trees (larch) decrease the soil temperature by (a) shading ground surface; (b) creating a shielding effect through their horizontal root systems; (c) creating an additional organic soil horizon (forest litter); (d) promoting the wide occurrence of mosses; and (e) significantly delaying snow melt. As a result, in the northeast of Kolyma Lowland, the mean ALT in sandy soils of Northern taiga (R19) was up to 5–15 cm less than in its tundra analogue (R21).

The differences of seasonal thaw depth between intrazonal landscapes are determined by soil moisture and the presence and thickness of peat horizons in the soil profile. Along streams, alluvial soddy gleyic soils of riverbanks thaw to 35–90 cm, alluvial peat-gley soils of the central part of the floodplain active layer extend to 20–50 cm. In thermokarst depressions (alases), Gleyzem soils of well drained sites thaw to 25–55 cm, and the ALT at polygonized bogs with Peat-Gleyzem soils is 10–35 cm. Since the bogs are more

Table 1. The active layer thickness in different sites of observation.

Region	Subzone	Site number	Site name	Lat.	Long.	Landscape	Texture of soils parent material	Obser-vation years	Active layer thickness, cm		
									mean values (different years)	min values (different years)	max values (different years)
Yana-Indigirka Lowland	Arctic tundra	R28	Svjatoy Nos cape	72°52′	141°01′	zonal site, plakor	loam	2001	38	16	60
	Typical tundra	R31	Allaiha River	70°33′	147°26′	zonal site, plakor	loam	2004-2006	41.5	2-28	64-65
Bykovskiy Peninsula	Arctic tundra	R29	Bykovskiy Cape	71°47′	129°25′	zonal site, plakor	loam	2003-2006	32	6-22	45-50
						alas	loam	2004-2006	30	13-20	44-53
Kolyma Lowland	Arctic tundra	R12	B.Kuropatochya River	70°55′	156°38′	zonal site, plakor	loam	1996	37	18	58
						zonal site, slope	loam	1996	27	8	48
	Typical tundra	R13	Cape M.Chukochiy	70°05′	159°55′	zonal site, slope	loam	1999-2006	42	14-37	43-64
						alas	loam	2000-2006	39	8-24	46-80
		R25	Yakutskoe Lake	69°51′	159°30′	zonal site, slope	loam	1999-2006	41	0-29	40-73
	Southern tundra	R14	B.Chukochya River	69°29′	156°59′	zonal site, slope	loam	1996-2006	42.5	3-20	54-66
		R15	M.Konkovaya River	69°23′	158°28′	zonal site, plakor	loam	1999-2006	39	14-18	50-65
						alas	loam	1996-2006	32	3-11	45-65
		R22	Alazeya River	69°19′	154°59′	zonal site, plakor	loam	1998-2005	49	1-31	70-80
		R16	Segodnya Pingo	69°05′	158°54′	polygonized bog	sand	1996-2006	41	10-25	58-100
		R21	Akhmelo Lake	68°50′	161°02′	zonal site	sand	1996-2006	92	7-56	107-145
		R17	Akhmelo Channel	68°49′	161°26′	flood-plain	loam	1996-2006	49	13-33	67-97
	Northern taiga	R19	Glukhoe Lake	68°48′	160°58′	zonal site, plakor	sand	1996-2006	81	5-51	107-148
		R18	Mountain Rodinka	68°45′	161°30′	zonal site, slope	loam	1998-2006	78.5	25-31	107-135
		R20	Malchikovskaya Channel	68°31′	161°26′	flood-plain	loam	1996-2006	52	2-32	77-108

Table 2. The active-layer thickness for zonal series of loamy soils.

Subzone	Latitude	Site number	Site name	Active layer thickness in different year (cm)										Mean multiyear values
				1996	1998	1999	2000	2001	2002	2003	2004	2005	2006	
Arctic tundra	70°55′	R12	B.Kuropatochya River	27-37	-	-	-	-	-	-	-	-	-	-
Typical tundra	70°05′	R13	Cape M.Chukochiy	-	-	37	33	38	44	49	-	50	43	42
	69°51′	R25	Yakutskoe Lake	-	-	23	37	38	47	-	-	55	45	41
Southern tundra	69°29′	R14	B.Chukochya River	43	41	38	41	-	-	-	-	48	44	42.5
	69°19′	R22	Alazeya River	-	46	46	-	-	50	-	51	53	-	49
Northern taiga	68°45′	R18	Mountain Rodinka	-	72	74	75	75	76	81.5	85	85	83	78.5

frequent and extensive in flood plains and alases than in well-drained areas, the mean ALT values are significantly lower compared to adjacent zonal ecosystems. In the sandy Khallerchinskaya tundra, the ALT depends on the thickness and composition of soil organic horizons. In polygonized bogs this corresponds to different stages of bog formation. For younger bogs, ALT varies from 47–55 cm, 18–27 cm in later stages of bog development and peat formation, and 33–60 cm in bogs characterized by the peat degradation stage. Mean ALT at the standard 100x100 m R16 site, covering the different stages of polygonized bogs, was about 1.5 times less than in the microplakor with zonal sandy soil, and about 2.2 times less than at the analogous R21 site characterized by a zonal landscape of sandy tundra.

Table 3. The mean values of active-layer thickness for zonal series of loamy soils under different microrelief elements.

Subzone	Latitude	Site name	ALT under different microrelief elements (cm)	
			mounds	depressions
Arctic tundra	70°55′	B.Kuropatochya River	38	26
Typical tundra	70°05′	Cape M.Chukochiy	46	31
	70°02′	B.Chukochya River (lower stream)	45	23
Southern tundra	69°33′	B.Chukochya River (middle stream)	56.5	28
	69°19′	Alazeya Rive	68	36
Northern taiga	68°51′	Arbyn Lake	43-44	32
	68°44′	Mountain Rodinka	60-90	45-60
	68°44′	Komarok Brook	54-91	39
	68°33′	Duvany Yar	57-60	44.5
	68°30′	Malchikovskaya Channel	64-70	-

Temporal Active Layer Dynamics

Annual ALT observations indicate a pronounced thickening of the active layer over 2000-2005 for both zonal and intrazonal soils of the Kolyma Lowland. This period was characterized by high summer temperatures. Based on observations at the Chersky Meteorological Station, the mean summer air temperatures over the 2000–2005 period were 11.3°C-13.7°C, a significant increase compared to the 1998–1999 minimum of 8.3°C-9.8°C. Due to warming, 10 of 12 sites demonstrated an ALT increase (r=0.67-0.96, n=10). In 2003, the thickening of the active layer became evident at all tundra (R13, R14, R21, R22, and R25) and Northern taiga (R18 and R19) zonal ecosystems, as well as at the majority of intrazonal landscapes including flood plains (R17), alases (R13A), and polygonized bogs (R16).

The maximum increase in ALT was observed in sandy Podbur soils and varies from 32 cm (40% from the multi-year mean) in taiga (R19, Fig. 2A), up to 40 cm (44%) in tundra (R21, Fig. 2B). An extremely high increase of 26 cm (65%) was found in the polygonized bogs of the Khallerchinskaya tundra (R16, Fig. 2C), where the relative increase of ALT was higher than at the zonal sites. The greatest ALT sensitivity to the increase of summer temperatures was realized at sites characterized by more advanced stages of bog development and covered by green moss and green moss/lichen/sedges. For these sites, a comparison with ALT data from the mid-1990s indicates an ALT increase of 11–18 cm, or 27%–51%, from the multi-year mean. By contrast, at the younger bogs covered with sedge/sphagnum, the ALT increase did not exceed 3%.

For loamy cryosol soils within the tundra zone, the relative ALT increase is reduced from north (Typical tundra) to south (Southern tundra).

At the upland site of the East Siberian Sea coast (R13), the ALT has increased by 13 cm (33%) (Fig. 2D), in the mid-stream of Bolshaya Chukochya River (R14) by 10 cm (24%) (Fig. 2E), and in the similar landscape at the tundra/taiga boundary (R22) by only 7 cm (14%) (Fig. 2F). In the

Table 4. The values of active layer thickness for zonal series of sandy soils on different nanorelief elements.

Subzone	Latitude	Site name	Active layer thickness in different nanorelief elements (ñm)			
			hummocks of mounds	mounds	depressions	polygonal cracks
Southern tundra	69°35'	Stanovaya	-	51	-	-
	69°23'	Laiydoskoe Lake	-	59	50	-
	69°23'	B.Konkovaya River	78	71	62,5	-
	69°10'	B.Pokhodskoe Lake	-	65	52	46
	69°08'	Golyavino Lake	-	50	-	-
	69°05'	Segodnya Pingo	71	63	61	51
	68°54'	Vankhotveem River	93	89	82	66.5
	68°51'	Arbyn Lake	77-88	70-83	63-75	56
	68°50'	Akhmelo Lake	102-105	98-104	89-91	-
	68°48'	Stadukhinskaya Channel	-	86	68	36
Northern taiga	69°12'	Kray Lesa	-	70	-	-
	68°48'	Glukhoe Lake	-	65-119	-	-

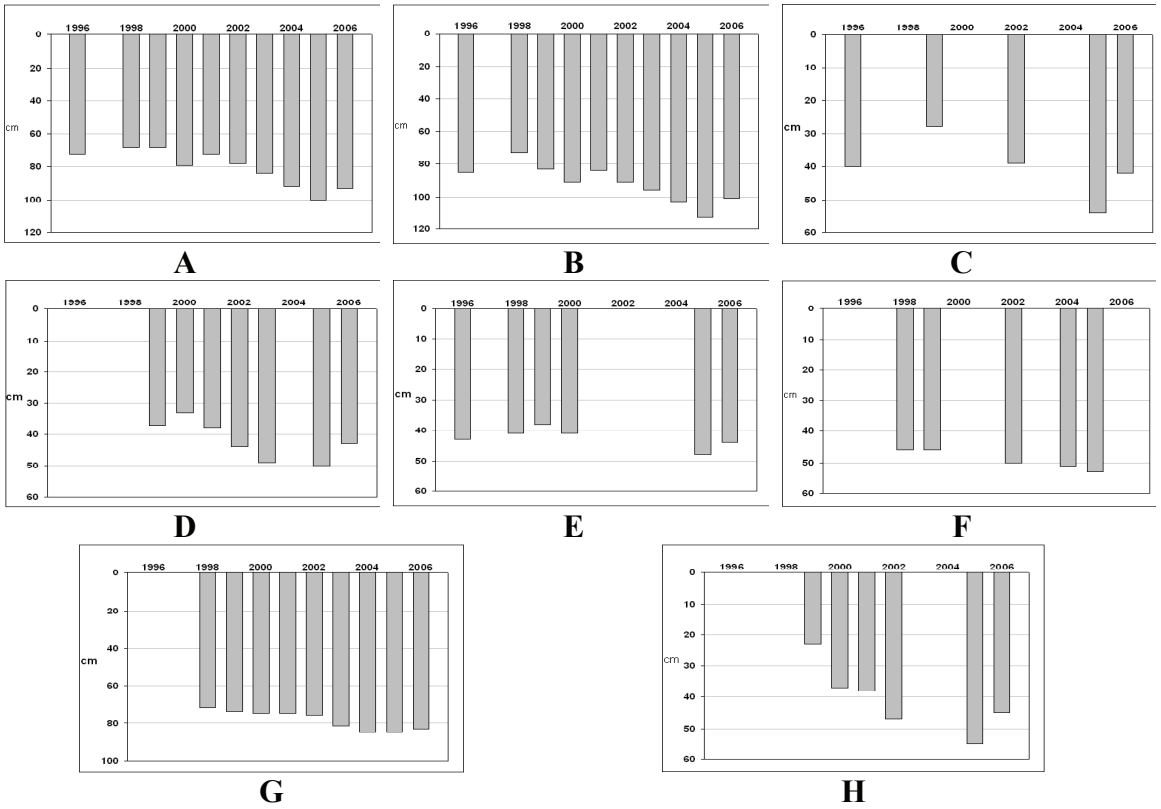

Figure 2. The annual dynamics of active layer thickness in different sites of the Kolyma lowland: A - Glukhoe Lake, R19; B - Akhmelo Lake, R21; C - Segodnya Pingo, R16; D - Malyi Chukochii Cape, R13; E - Bolshaya Chukochya River, R14; F - Alazeya River, R22; G - Mountain Rodinka, R18; H - Yakutskoe Lake, R25.

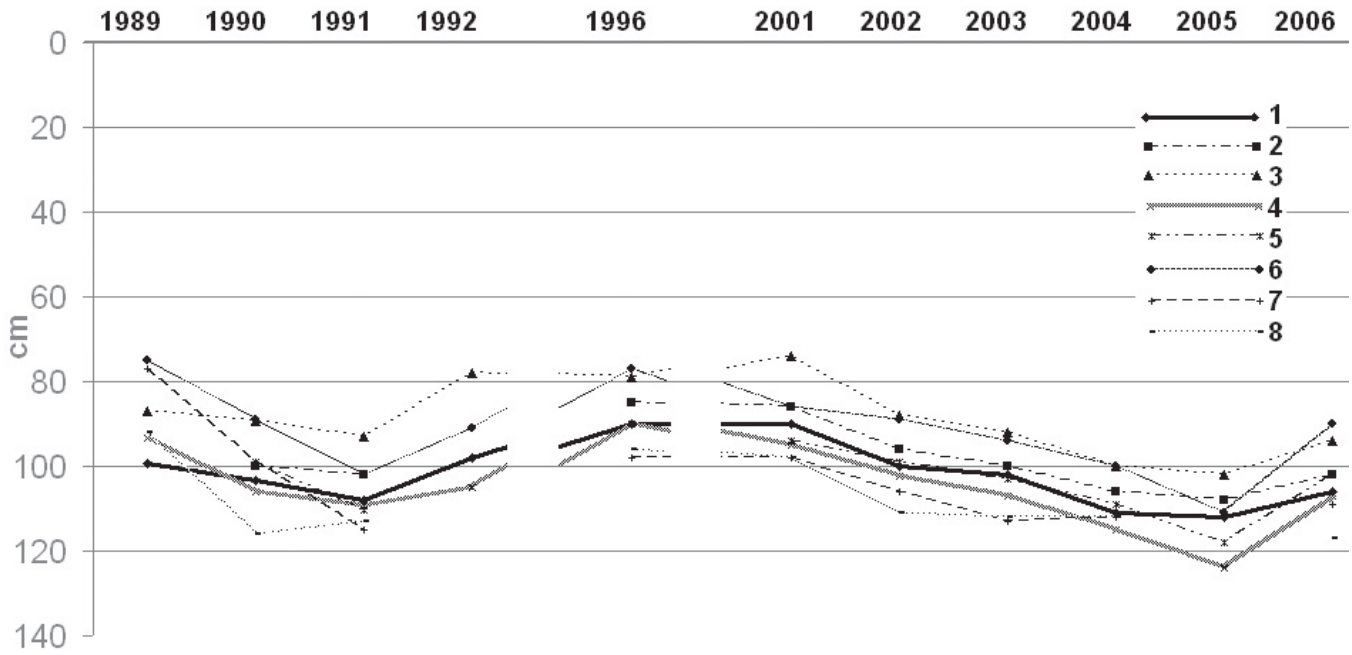

Figure 3. Annual dynamics of active-layer thickness under different micro- and microrelief elements at a tundra site near Akhmelo Lake. Legend: 1 - top of a hillock (microplakor), hummocks on the surface of mounds; 2 - top of a hillock, between hummocks in the limits of mounds; 3 - top of a hillock, between mounds; 4 - slope of a hillock (microslope), hummocks on the surface of mounds; 5 - slope of a hillock, between hummocks in the limits of mounds; 6 - slope of a hillock, between mounds; 7 - microdepression, bare spot medallions; 8 - microdepression, ridges surrounding spot medallions.

Northern taiga subzone (R18), ALT increased by 13 cm (17%) (Fig. 2G).

An even greater thaw increase of 32 cm (80%) (Fig. 2H) was observed at the other northern site (R25), located on a steep (20°–25°) southeast slope, where the ice-rich layer common to yedoma is absent.

Low summer temperatures in 2006 (10.5°C) led to a relative decrease in ALT (3%–36%) from the multi-year mean. However, ALT has never reached the level of cold of the 1998–1999 years (Fig. 2).

An increase of ALT during the investigation period was also observed at the nearby Yana-Indigirka Lowland. In 2004–2006, the mean ALT increased from 38 to 44 cm at the upland site of Typical tundra subzone (R31). On the Bykovskiy Peninsula site (R29), no significant ALT changes were obtained in either upland yedoma or alas landscapes.

The longest ALT record is available for a site established near Akhmelo Lake. Figure 3 shows temporal ALT variability at the Akhmelo site for different landscape elements over the 1989–2006 period. In 1991, the ALT reached 93–115 cm under different landscape elements in response to a high mean summer air temperature of 14.9°C.

In the mid-1990s, the active layer thinned to 74–98 cm, and beginning in 2002, ALT began to increase. In 2004–2005, the majority of the landscape elements exceeded the 1991 ALT level by 4 to 14 cm. Based on the long-term record presented in Figure 3, we can assume that the progressive increase in ALT observed over the Kolyma and Yana-Indigirka Lowlands is not attributable to irreversible global change processes, but rather show a thermal maximum of a century-scale cycle of unknown period.

Conclusions

1. The ALT in the tundra zone of North Yakutia varies significantly depending on soil texture. The mean multi-year ALT values within the positive microrelief elements are 50–105 cm for sandy Podbur soils and 35–70 cm for loamy Cryozem and Gleyzem soils.

2. The distribution of ALT in yedoma uplands and slopes is strongly influenced by climatic zonality (subzonality), which is more pronounced within positive microrelief elements than within depressions.

3. In general, the soils of flood plains, thermokarst depressions (alases), and polygonized bogs have thinner ALT than soils of corresponding zonal ecosystems. The difference in ALT between intrazonal landscapes is determined by soil moisture and thickness of peat horizons in the soil profiles.

4. The majority of soils at Northeast of Yakutia (Kolyma and Yana-Indigirka Lowlands) experienced a pronounced (14%–80%) increase in ALT over the 2000–2006 period.

Acknowledgments

This research in supported by the U.S National Science Foundation (grant OPP-9732051). We are also grateful to the Civil Research and Development Fund (GAP project RUS2-1468) in assisting us in logistical organization of the field campaign.

References

Brown, J., Hinkel, K.M. & Nelson, F.E. 2000. The circumpolar active layer monitoring (CALM) program: research designs and initial results. *Polar Geography* 24(3): 165-258.

Elovskaya, L.G., Petrova, E.I. & Teterina, L.V. 1979. *Soils of North Yakutia.* Novosibirsk: Nauka, 303 pp (in Russian).

Fyodorov-Davydov, D.G., Sorokovikov, V.A., Ostroumov, V.E., Kholodov, A.L., Mitroshin, I.A., Mergelov, N.S., Davydov, S.P., Zimov, S.A. & Davydova, A.I. 2004. Spatial and temporal observations of seasonal thaw in the Northern Kolyma Lowland. *Polar Geography* 28(4): 308-325.

Garagulya, L.S., Kudryavtsev, V.A., Kondratieva, K.A. & Maksimova, L.N. 1970. Influence of geological-geographical factors on the temperature regime of active layer grounds in the north part of Yana-Indigirka basin. *Permafrost Researchings X*, Moscow: Moscow University Publishing, 59-79 (in Russian).

Karavaeva, N.A. 1969. *Tundra Soils of North Yakutia*. Moscow: Nauka, 205 pp (in Russian).

Melnikov, E.S., Leibman, M.O., Moskalenko, N.G. & Vasiliev, A.A. 2004. Active-layer monitoring in the cryolithozone of West Siberia. *Polar Geography V* 28(4): 267-285.

Moskalenko, N.G. 2001. The seasonal soil thawing in natural and disturbed ecosystems of West Siberian northern taiga. *Abs. of the Third International Conference on Cryopedology: Dynamics and Challenges of Cryosols, Copenhagen, August 20-24, 2001*.

Pavlov, A.V., Skachkov, Yu.B. & Kakunov, N.B. 2004. An interaction between the active layer depth changing and meteorological factors. *Earth Cryosphere* VIII (4): 3-11 (in Russian).

Perfilieva, V.I., Teterina, L.V. & Karpov, N.S. 1991. *Vegetation Cover of Yakutia Tundra Zone*. Yakutsk, 192 pp (in Russian).

Savvinov, D.D. 1976. *Hydrothermic Regime of Soils within the Permafrost Zone*. Novosibirsk: Nauka, 254 pp.(in Russian).

Soloviev, P.A. 1978. Thickness of surface seasonally frozen ground on the territory of Yakutia. *Geocryological and Hydrogeological Researching in Yakutia*. Yakutsk: 3-12 (in Russian).

Emplacement of Lobate Rock-Glacier Landforms and Landscape Modification, Mareotis Fossae, Mars

S. van Gasselt
Freie Universitaet Berlin, Planetary Sciences and Remote Sensing, Malteserstr. 74-100, D-12249 Berlin, Germany
E. Hauber
German Aerospace Center (DLR), Institute of Planetary Research, D-12489 Berlin, Germany
A.P. Rossi
RSSD of ESA. ESTEC, NL 2200 AG, Noordwijk, The Netherlands
G. Neukum
Freie Universitaet Berlin, Planetary Sciences and Remote Sensing, Malteserstr. 74-100, D-12249 Berlin, Germany

Abstract

The so-called fretted terrain at the Martian dichotomy boundary exhibits a variety of creep-related morphologies generally known as lobate debris aprons and lineated valley fills. These features usually occur along troughs and circumferentially to remnant massifs. We here report on investigations of debris aprons and adjacent terrain in the Tempe Terra/Mareotis Fossae region and provide observational evidence for several phases and mechanisms of debris supply at remnant massifs comprising rock fall and large-scale landsliding and terminating with deposition and disintegration of a widespread surficial mantling deposit. The mantling deposit disintegrates by processes similar to thermokarstic degradation as indicated by heavily dissected areas and characteristic shallow and aligned circular depressions. Comparisons of theoretically derived cross-section profiles to topographic measurements along and across lineated-valley fill units, as well as lobate debris aprons, provide additional clues that such creep-related landforms are currently degrading,. It is also shown that a considerable volume of debris/ice is transported along the intra-highland valleys. Such processes might even be active today, as geomorphologic features appear pristine, and crater-size frequency measurements yield ages in the range of 50–100 Ma only. Such observations confirm modeling results of the stability of ground ice on Mars. Various phases of emplacement and degradation confirm theories about cyclic re-deposition of volatiles caused by the changes of the configuration of orbital parameters of Mars.

Keywords: climate; Mars; periglacial; planetary permafrost; rock glaciers.

Introduction

A variety of landforms indicates the possible existence of past or present ice in the near subsurface of Mars (Sharp 1973, Carr 1977 Rossbacher & Judson 1981, Lucchitta 1981). Among the most prominent ice-related features are lobate debris aprons. They have been interpreted to be a mixture of rock particles and ice (Squyres 1978, 1979) analogous to terrestrial rock glaciers, i.e., debris transport systems comprising a mixture of rock fragments and segregational and/or interstitial ice (Barsch 1996). The analogy between terrestrial rock glaciers and Martian lobate debris aprons is mainly based on (a) their lobate shape, (b) the cross-sectional convex-upward profile, (c) characteristic sets of ridges and furrows, and (d) their relationship to adjacent regions indicative of permafrost-related morphologies. Lobate debris aprons have been observed primarily along steep escarpments near the dichotomy boundary (Squyres 1978, 1979, Mangold 2001) and the large impact basin of Hellas Planitia (Squyres 1979, Crown et al. 2002). Rock glaciers are sensitive indicators for the climatic environment during their formation and are thought to be possible large and accessible water reservoirs (Whalley & Azizi 2003). Morphologies of lobate debris aprons in Tempe Terra are similar to terrestrial talus rock glaciers (Whalley 1992, Barsch 1996) which are usually derived from footslope debris situated underneath steep wall-rock of mountainous permafrost environments.

Settings and Observations

The Tempe Terra/Mareotis Fossae region (Fig. 1) is located between 270°E–294°E and 46°N–54°N and is characterized by the steep dichotomy escarpment and the so-called fretted terrain (Sharp 1973) which separates the study area into the southern highland assemblages and a region known as the northern lowland plains. Young surficial deposits interpreted as features related to creep of ice and debris (Squyres 1978, 1979) and mapped as Amazonian surficial units by Scott & Tanaka (1986) fill broad fretted channels of the heavily deformed Noachian highlands, extend from the dichotomy escarpment in northern direction, and are located circumferentially to knobs and remnants of the Noachian basement. The north-south extent of the fretted terrain in our study area varies between 60 km to 170 km. The undissected upland has an elevation of -2700 m at 294°E and about 0 m at 280°E. The lowland has its highest elevations also in the western part of the study area and slopes gently (~0.1°) towards NE, reaching minimum elevations of -4500 m at the eastern border of the study area. Elevation difference between uplands and lowlands decreases from 3000 m to 1500 m.

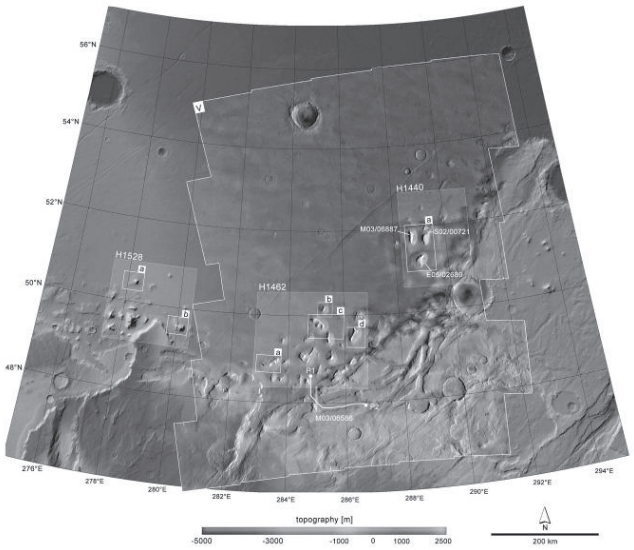

Figure 1. Study area in the Tempe Terra/Mareotis Fossae region as represented by the Viking global image mosaic (MDIM-2.1) superimposed on MOLA (MEGDR) topographic data and location of image scenes discussed in the text; [V] manually processed medium-resolution Viking image mosaic; H1528, H1462, H1440 refer to HRSC image numbers discussed in the text; lettered boxes and white outlines refer to sub-scenes depicted from HRSC image data; individual MOC scenes used in this study are labeled accordingly; P1-P2: topographic profile discussed in the text.

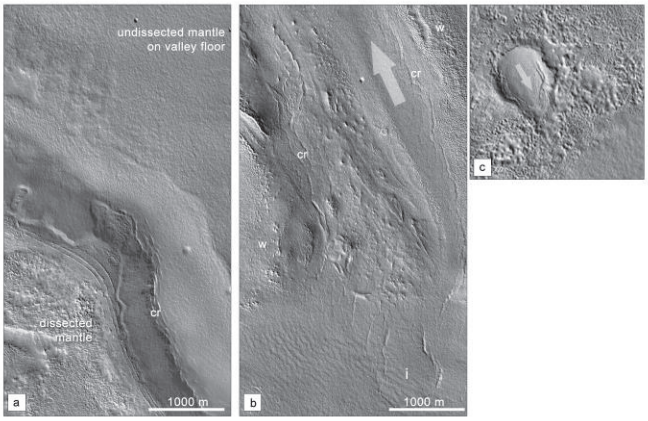

Figure 2. MOC sample scenes of the dichotomy boundary. (a) fretted channel floor (right) and wall (lower left). A mantling deposit is intact on the valley floor, but heavily degraded on the uplands. Crevasses [cr] on the floor of the fretted channels are characteristic of creep and flow of ice and debris. Parallel thin ridges 15–20 m wide run at constant elevations along the upper channel wall. (b) Floor of a fretted channel is covered by a mantling deposit. Crevasses [cr] are situated near the channel walls [w]. They also outline an impact crater completely buried by the mantle [i]. (c) Impact crater filled by mantling deposit. The mantle seems to have flowed out of the crater, scale is 1000 m across.

This difference is slightly less than that reported from the dichotomy boundary on the eastern hemisphere of Mars, i.e., Deuteronilus, Protonilus and Nilosyrtis Mensae, with 2-6 km. Highlands have a generally flat surface, sloping at an angle of less than 0.1° when measured perpendicular to the dichotomy boundary. The surfaces of very large upland segments bounded by fretted channel have larger slopes toward the lowlands (1–2°) and might be tilted as blocks. Such fretted channels have steep walls and flat floors (Squyres 1978), the latter of which are often characterized by so-called "lineated valley fill" (Squyres 1978, 1979}, which is interpreted as material comparable to that of lobate debris aprons but confined to the valley extent. In the study area, fretted valleys have uniform widths of 5–10 km and constant depths of a few hundred meters. The morphologic boundary between highland and lowland areas is characterized by two and sometimes three distinct components: (a) a steep upper slope, i.e., the wall-rock, (b) an intermediate shallow-sloped unit with downslope facing striae, and (c) the highly textured apron (Carr 2001). An intermediate unit is only rarely observed at isolated remnants. At a few sample locations we measured the angles of intermediate units (6°–8°) and angles of debris aprons (2°–4°).

Mantling deposit

A mantling deposit can be observed at scarps and channels near the dichotomy boundary (Fig. 2) as well as around isolated remnant massifs and aprons (Fig. 3) that are located in the lowlands. The deposit does not show any preference to geographical or topographic location, thus, covering all parts of the study area. This observation is based on high-resolution image data (1.5–12 m/pixel) taken with the Mars Orbiter Camera (MOC) that clearly show surfaces at the dichotomy boundary that are covered by that deposit. The mantling deposit is often degraded by erosion, resulting in surfaces whose texture are highly variable, ranging from smooth over stippled, pitted, or knobby to heavily etched. In some places the mantling is completely removed. The disintegration process seems to be controlled by slope aspect, the southern (sun-lit) slopes being more affected than northern slopes.

On the floors of some fretted channels we identify crevasse-like features (Fig. 2). Their specific geometry resembles that of terrestrial chevron crevasses in glaciers, (e.g., Benn & Evans 2003, Menzies 2002). Lineations correspond to longitudinal or transversal lineations and are frequently observed at terrestrial features indicative of creep of ice and debris. Such lineations can be observed at small scales as illustrated in Figure 2. Other lineations are formed by ridges that are thin (15–20 m wide) and extend at approximate constant elevations along upper channel walls; they seem to be genetically connected to the mantling deposit (Fig. 2a). A thick mantling is also observed in a number of image scenes covering the remnant massifs of the Tempe Terra lowland: as seen in Figure 3a, the surface of three debris aprons (A-C) appears relatively smooth although different sets of transversal ridges on the apron can still be observed. The crest of remnant A is characterized by a scalloped and fretted depression (d) and sets of elliptical and aligned shallow depressions on the eastern slope which have a dimension of few tens of meters. Both the crest depression as well as the slope depressions are located in a mantling deposit and

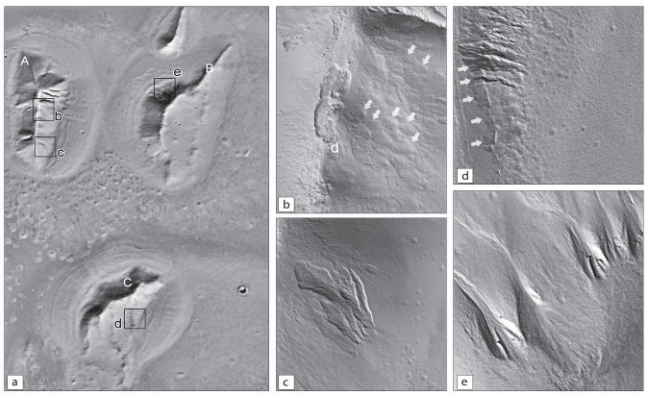

Figure 3. Sample scenes of HRSC in orbit 1440 covering the easternmost study area. Labeled black boxes in (a) refer to MOC sample scenes (b-e). All scenes show indications for the disintegration of a thick mantling deposit. (b) Unusual scalloped depression at remnant crest and elliptical depressions at eastern wall (arrows). (c) Overlapping gullied slide flows. (d) Small slide flows incised into the footslope talus of remnant C. All incision start at the boundary (arrows) between talus and debris apron and are located in a mantling deposit. (e) Slide flows incised into surficial mantling deposit of remnant B.

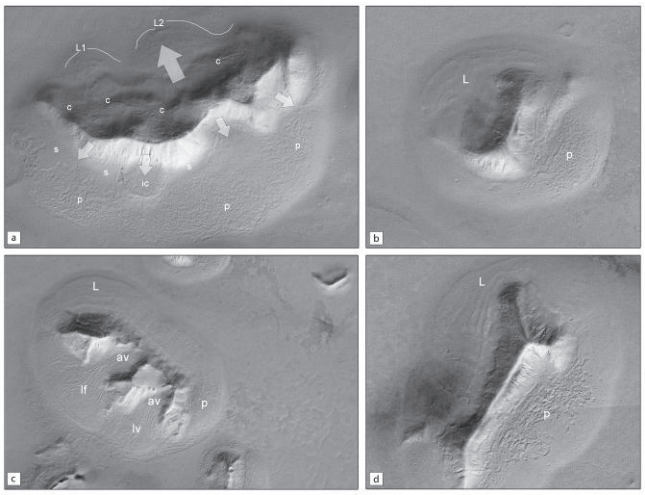

Figure 4. Sample scenes of HRSC in orbit 1462 covering the central lowlands of Tempe Terra. (a) Arcuate remnant massif characterized by an inclined surface tilting towards northern direction; two main directions of transport are observed: large lobes form in northern direction [L1-L2], large coherent debris masses with a pitted surface [p] advance in southern direction. An impact crater [ic] has been completely filled by erosional debris. The talus shows a generally smooth surface texture [s]. Arcuate and sub-parallel furrows on remnant indicate extensional flow [c]. (b) Small isolated remnant knob located northeast of remnant shown in (c); northern apron texture is characterized by ridges and furrows [L], southern apron has a pitted appearance [p]. (c) Alcoves [ac] are incised into remnant massif forming Accumulation zones of debris that is subsequently transported downslope as seen in longitudinal surface lineations. (d) Elongated remnant massif with well-defined crest exhibits transversal ridges and furrows [L] on northern apron and a pitted surface [p] on southern apron. Note also, all aprons are comparable in size when related to the remnant massif.

are indicative of material removal. Mantling-related mass-wasting features are shown in 3c–e where gullied slide flows initiate instantaneously somewhere at the mid-slope, overlap partly and produce faint terminal depositional fans (Fig. 3c, d) that are indicative of dry mass-wasting processes.

As seen in Figure 3d, gullied slide flows can be related to a boundary where the remnant talus abuts the mantling deposit. While the northern sets of slide flows are deeply incised and well expressed, the southern are shallower (Fig 3e).

Disintegration texture

Many debris aprons in Tempe Terra are characterized by surface textures indicative of disintegration of either the surficial mantling deposit or the main debris/ice body. As shown in Figure 4, a slightly northwards inclined and elongated remnant shows a well-pronounced debris apron emerging near the foot of a remnant. While the northern debris apron is characterized by at least two large lobes with transversal ridges (L1–L2), the southern apron is more homogeneously developed with a highly pitted surface texture (p). Below the southern scarp, talus forms as expressed by a relatively smooth texture (s). Eroded remnant material has filled an old impact crater (ic). The southern scarp of the remnant is relatively steep when compared to the northern remnant slope. Flow ridges (c) indicate that material is eroded as coherent sheet and thus contributes to the development of the northern apron. Arrangements of transversal ridges and furrows located on a northern apron and a pitted surface texture located on the southern apron is observed in the scenes depicted in Figures 4b, d. In Figure 4b, the shapes of the remnant massif and debris apron are more circular and the remnant slope angles are approximately comparable in the north and south. However, the northern remnant slopes is composed of a single large bowl-shaped depression in which material is collected from the wall-rock and subsequently transported downslope towards the plains. In Figure 4d, the pitted surface in the south has not reached the terminal area of the apron but is restricted to the remnant footslope. Figure 4c shows well-expressed alcoves (av) at the southwestern remnant slopes and longitudinal sets of furrows and ridges (lf, lv) in the direction of maximum slope gradient. The pitted surface texture seen in Figures 4a, b and d is here restricted to a small area of the southeastern debris apron (p) while lobes (L) are again restricted to the northern apron. In the westernmost region of the Tempe Terra study area, remnants and aprons are developed slightly differently when compared to those in the central and easternmost areas. Northern apron slopes show a ridge-and-furrow texture but it extends asymmetrically farther away from its source. Contrasting to this, the remnant in Figures 5b–b′ is heavily dissected by alcoves and cirque-like features. Towards the north, longitudinal and transversal ridges and furrows prevail while towards the south aprons merge with the apron of the dichotomy escarpment and show sets of depressions at various sizes. For few aprons crater-size measurements could be obtained to derive ages (Fig. 6). Elliptical depressions indicate deformation of impact craters after apron emplacement. In order to obtain the last

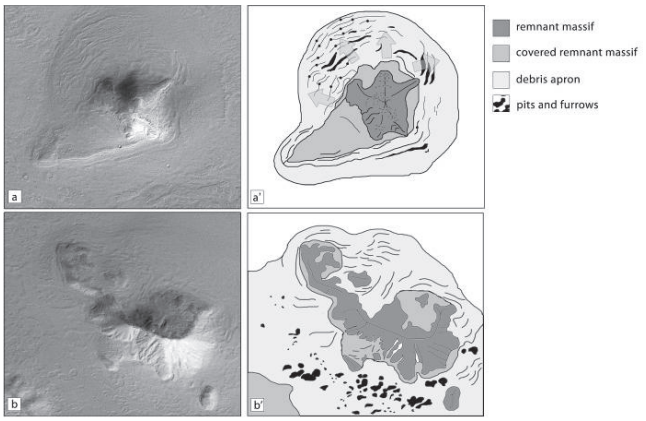

Figure 5. Sample scenes of HRSC in orbit 1528 and schematic maps covering lobate debris aprons of the westernmost study area. Labeled boxes refer to labels in Figure 1; [a–a′] isolated small remnant massif with circumferential lobate debris apron, northern apron shows pattern of ridges and valleys characteristic of compressional flow (ridges) and extensional flow (furrows); [b–b′] flow lineations at debris apron are in longitudinal configuration below alcove depression facing northeast and in transversal configuration under remnant scarp. Southern apron is characterized by pitted texture indicative of degradation.

resurfacing period only fresh-appearing craters have been mapped. Measurements provided ages in the range of 0.01 to 0.05 Ga which is consistent with data obtained from other debris apron (Squyres 1978, Mangold 2003, Berman et al. 2003, Head 2005, Li 2005, van Gasselt 2007).

Geomorphometry

Lobate debris aprons were digitized using a common GIS environment (Fig. 7). We derived geographic coordinates, topographic elevations, lengths, areas and volumes and made simplifications with respect to the (a) base of the debris apron, which was assumed to be horizontal and flat (Barsch 1996), and (b) to the volume of that part of the remnant massif located below its visible extent, i.e., covered by apron debris. In plan view, the remnants north of the dichotomy boundary in Tempe Terra have a more or less irregular polygonal shape and a rugged top, in contrast to the more flat-topped mesas of the type locations in Elysium or Arabia Terra (Mangold & Allemand 2001). The cross-sectional shapes of the aprons are convex upward and steepening towards the terminus of the apron (Fig. 8). The length of debris aprons varies between 1.4 km to 6.3 km averaging at ~4.0 km in northern direction and ~3.5 km in southern direction. The average lengths of aprons are significantly less than values provided by Mangold (2001) with 10.8 to 33 km, and also less than those given by Carr (2001) and Colaprete & Jakosky (1998) with 15 km. Thicknesses of (upper) remnant massifs in Tempe Terra range from ~20 m to ~1100 m. The thickness of aprons varies between ~70 m and ~600 m under the assumption of a flat base. Minimum thickness values are lower than those given by Mangold (2001) (276 m) for the Deuteronilus area, maximum values are about the same. Volumes of debris aprons at Tempe Terra range from <10 km³ to ~300 km³ with a mean surface

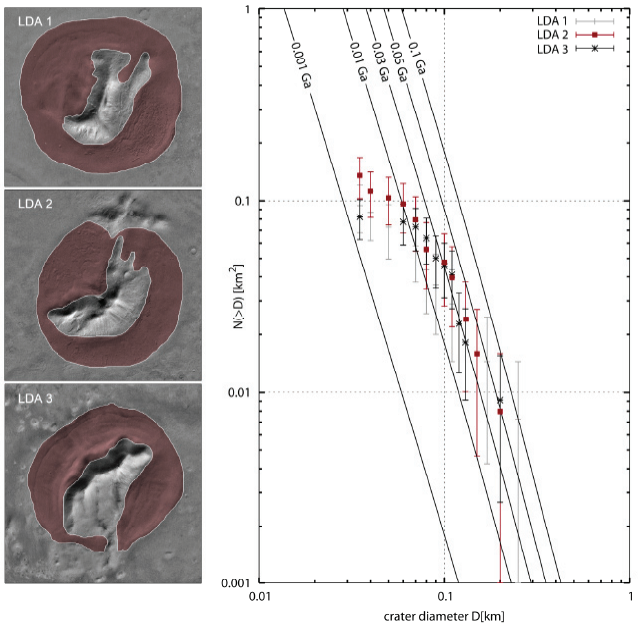

Figure 6. Ages derived for debris-apron surfaces of the central and eastern part of the study area. Stair-stepped distribution indicates multiple episodes of erosional activity, derivation of isochrones (in Ga) are based on Hartmann and Neukum (2001) with the polynomial production function coefficients by Ivanov (2001); for a discussion on errors, see Neukum et al. (2004).

area of ~282 km² (Fig. 7). The remnants have a mean size of ~115 km² (15 to >1000 km²) and a mean volume of ~21 km³ (<5 to 200 km³). As Barsch (1996) summarizes, there might be a close relationship between the source area of debris production and the surface area of a (terrestrial) rock glacier at the footslope with values between 1:1.36 to 1:4.4 (Wahrhaftig & Cox 1959, Barsch 1977, Gorbunov 1983). From 27 observations at Tempe Terra we obtain a factor of 2 for the remnant size when compared to the area occupied by the debris apron. Mangold (2001) calculated the basal shear stress and obtained values in the range of $\sigma = 34–108$ kPa for the Deuteronilus/Protonilus Mensae areas. These values are lower than photoclinometrically derived values by Squyres (1978). For the Tempe Terra region we obtain values between 6.7–82.4 kPa for average apron lengths, with an average of ~38 kPa. The calculated values are not consistent with basal shear stresses given for terrestrial rock glaciers by Whalley (1992) with 100–300 kPa. This may indicate an ice content which is higher (Hauber et al. 2007) than typically considered for rock glaciers or very low strain rates due to a low shear stress. Inactive rock glaciers tend to have generally lower slopes as either debris material was eroded or volatiles were removed, subsequently causing thermokarstic degradation of the rock-glacier surface (Barsch 1996, Ikeda & Matsuoka 2002, Berthling et al. 1998).

Discussion and Conclusions

Image data provide observational evidence for the existence of a widespread mantling deposit in the Tempe Terra/Mareotis Fossae region which covers not only debris

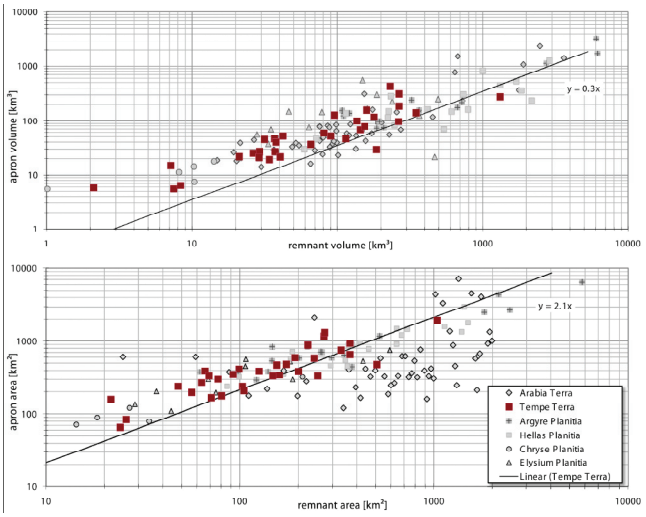

Figure 7. Plot of derived ratios between volumes (a) and areas (b) of remnant massifs and debris aprons as indicator for the degradational state. Values of Tempe Terra massifs and debris aprons (dark squares) are approximated by linear fit.

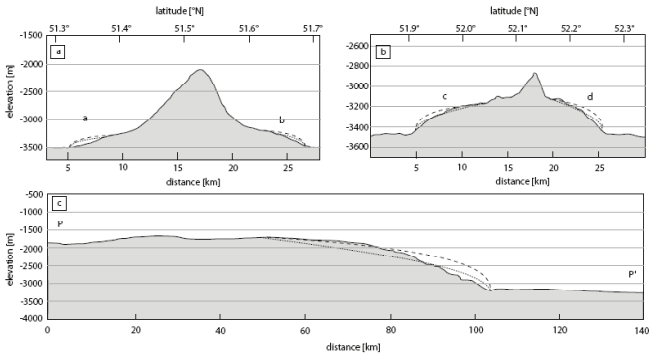

Figure 8. MOLA-based topographic profiles across debris aprons (a, b) and along fretted channel (c) and theoretic profiles of debris aprons obtained from equation derived by Paterson (2001).

aprons of the lowlands but also the escarpment of the Martian dichotomy boundary. At the dichotomy escarpment this mantling deposit shows several characteristics of creep and deformation as well as for processes of disintegration similar to thermokarstic degradation of ice-rich surface materials. Indicators for the mobility of that mantling deposit are found at various locations.

We confirm the presence of a mantle at latitudes higher than ~30–50° as inferred from global-scale roughness maps (Kreslavsky 2000) and directly observed in MOC images (Carr 2001, Malin 2001). Flow lineations on debris aprons resemble closely features known from terrestrial rock glaciers comprising various sets of transversal and longitudinal ridges and furrows indicative of differential movements controlled by subsurface topography. At several locations in Tempe Terra, southward-facing debris aprons show a pitted surface texture that is interpreted as indicators for thermokarstic degeneration and loss of volatiles subsequently leading to collapse and formation of shallow depressions or pits. Their restricted extent suggests control by sun-irradiation (Rossi et al. 2008). Shallow depressions form primarily in mantling material covering remnant massifs whereas pits and furrows are more often observed on the debris-apron surface. Degradation of surfaces is also confirmed by observations of theoretically derived cross-profiles of debris aprons and lineated valley fill units. Both creep-related landforms show an unsatisfactory fit to the model curve. The convex-upward shape of lineated valley fill at the entrance of fretted channels shows not only debris transport perpendicular to valleys walls but also in parallel direction. This furthermore indicates that flow lineations seen in lineated valley fill deposits are not only caused by compression but also by the downslope movement along the valley. It is suggested that the main processes of landsliding and rockfall had come to an end and that subsequent deposition of a mantling deposit caused smoothing of the underlying topography and allowed formation of such slides and gullied flows. Resurfacing ages of 0.01 to 0.05 Ga are consistent with ages obtained from other debris apron locations on Mars. Geomorphometrically derived area ratios of the depositional zone and source area show values that are comparable to estimates given in Barsch (1996) for terrestrial rock glaciers, indicating that the genetic configuration is comparable. Geologically recent degradational and thermokarstic processes are in good agreement with modeling work of obliquity variations of the planet's rotational axis and variations of the planet's eccentricity and precession (Murray et al. 1973, Pollack 1979, Toon et al. 1980, Jakosky et al. 1995). It was shown that prolonged periods of higher obliquity lead to mobilization of volatiles at the poles and to precipitation at lower latitudes (Levrard et al. 2004). This process (a) might have lead to saturation of remnant-related talus deposits with ice causing subsequently creep of debris, and (b) also contributed to a mid-latitudinal mantling deposit (Rossi et al. 2008).

References

Barsch, D. 1977. Eine Abschätzung von Schuttproduktion und Schutttransport im Bereich aktiver Blockgletscher der Schweizer Alpen, Z. *Geomorph. Supp.* 28: 148-–160.

Barsch, D. 1996. *Rockglaciers: indicators for the present and former geoecology on high mountain environments.* Berlin, Germany: Springer, 331 pp.

Benn, D.I. & Evans, D.J.A. 2003. *Glaciers and glaciation*. London, England: Arnold, x+734 pp.

Berman, D.C., Hartmann, W.K. & Crown, D.A. 2003. Debris aprons, channels, and volcanoes in the Reull Vallis region of Mars. In: *Lun. Planet. Sci. Conf. Abs., XXXIV, #1879, 12-17 March.* CD-ROM. League City, Tex., USA: Lun. Planet. Inst.

Berthling, I., Etzelmüller, B., Eiken, T. & Sollid, J.L. 1998. Rock glaciers on Prins Karls Forland, Svalbard. I: internal structure, flow velocity and morphology. *Permafrost Perigl. Proc.* 9(2): 135-145.

Carr, M.H. & Schaber, G.G. 1977. Martian permafrost features. *J. Geophys. Res.* 82(11): 4039-4054.

Colaprete, A. & Jakosky, B.M. 1998. Ice flow and rock glaciers on Mars. *J. Geophys. Res.* 103(E3): 5897-5909.

Crown, D.A., Pierce, T.L., McElfresh, S.B.Z. & Mest, S.C. 2002. Debris aprons in the eastern hellas region of mars: Implications for styles and rates of highland degradation. In: *Lun. Planet. Sci. Conf. Abs., XXXIII, #1642*. CD-ROM. League City, Tex, USA.

Gasselt, van S., Hauber, E. & Neukum, G. 2007. Cold-climate modification of Martian landscapes: A case study of a spatulate debris landform in the Hellas Montes region, Mars. *J. Geophys. Res.* 112 (E09006).

Gorbunov, A. 1983. Rock glaciers of the mountains of middle Asia. *Proceedings of the Fourth International Conference on Permafrost, Fairbanks, Alaska*: 359-362.

Hartmann, W.K. & Neukum, G. 2001. Cratering chronology and the evolution of Mars. *Space Sci. Rev.* 96(1-4): 165-194(30).

Hauber, E., van Gasselt, S., Chapman, M.G. & Neukum, G. 2007. Geomorphic evidence for former lobate debris aprons at low latitudes on Mars: indicators of the Martian paleoclimate. *J. Geophys. Res.* 112: E09006, doi:10.1029/2006JE002842.

Head, J.W., Neukum, G., Jaumann, R. et al. 2005. Tropical to mid-latitude snow and ice accumulation, flow and glaciation on Mars. *Nature* 434: 346-351.

Ikeda, A. & Matsuoka, N. 2002. Degradation of talus-derived rock glaciers in the Upper Engadin, Swiss Alps. *Permafrost Perigl. Proc.*13(2): 145-161.

Ivanov, B.A. 2001. Mars/Moon cratering rate ratio estimates. *Space Sci. Rev.* 96(1-4): 87-104(18).

Jakosky, B.M., Henderson, B.G. & Mellon, M.T. 1995. Chaotic obliquity and the nature of the Martian climate. *J. Geophys. Res.* 100(E1): 1579-1584.

Kreslavsky, M. & Head, J.W. 2000. Kilometer-scale roughness of Mars: results from MOLA data analysis. *J. Geophys. Res.* 105: 26,695-26,712.

Laskar, J., Correia, A.C.M., Gastineau, M., Joutel, F., Levrard, B. & Robutel, P. 2004. Long term evolution and chaotic diffusion of the insolation quantities of Mars. *Icarus* 170(2): 343-364.

Levrard, B., Forget, F., Montmessin, F. & Laskar, J. 2004. Recent ice-rich deposits formed at high latitudes on Mars by sublimation of unstable equatorial ice during low obliquity. *Nature* 431: 1072-1075.

Li, H., Robinson, M.S., & Jurdy, D.M. 2005. Origin of Martian northern hemisphere mid-latitude lobate debris aprons. *Icarus* 176(2): 382-394.

Lucchitta, B.K. 1981. Mars and Earth–comparison of cold-climate features. *Icarus* 45(2): 264-303.

Lucchitta, B.K. 1984. Ice and debris in the fretted terrain, Mars. *J. Geophys. Res.,* Supp. 89(B1): B409-B419.

Mangold, N. 2001. Lobate debris aprons as potential targets for ground ice detection analogs to terrestrial rock glaciers. In: *Conf. Geophys. Detect. Subsurf. Water Mars, #7009.* Houston, Tex., USA: Lun. Planet. Inst.

Mangold, N. & Allemand, P. 2001. Topographic analysis of features related to ice on Mars. *Geophys. Res. Lett.* 28(3): 407-410.

Mangold, N. 2003. Geomorphic analysis of lobate debris aprons on Mars at Mars Orbiter Camera scale: evidence for ice sublimation initiated by fractures. *J. Geophys. Res.* 108(E4): 8021.

Menzies, J. (ed.) 2002. *Modern and Past Glacial Environments.* Oxford, England: Butterworth-Heinemann, xxii+5543 pp.

Milliken, R.E., Mustard, J.F. & Goldsby, D.L. 2003. Viscous flow features on the surface of Mars: observations from high-resolution Mars Orbiter Camera (MOC) images. *J. Geophys. Res.* 108(E6): 5057.

Murray, B.C., Ward, W.R. & Yeung, S.C. 1973. Periodic insolation variations on Mars. *Science* 180(4086): 638-640.

Mustard, J.F., Cooper, C.D. & Rifkin, M.K. 2001. Evidence for recent climate change on Mars from the identification of youthful near-surface ground ice. *Nature* 412: 411–414.

Neukum, G., Jaumann, R., Hoffmann, H. et al. 2004. Recent and episodic volcanic and glacial activity on Mars revealed by the High Resolution Stereo Camera. *Nature*. 432: 971-979.

Paterson, W.B. 2001. *The Physics of Glaciers*, 3rd ed. London, England: Butterworth-Heinemann, ix+496 pp.

Pollack, J.B. 1979. Climatic change on the terrestrial planets Icarus 37(3): 479-553.

Rossbacher, L.A., & Judson, S. 1981. Ground ice on Mars—inventory, distribution, and resulting landforms. *Icarus* 45(1): 39-59.

Rossi, A.P., van Gasselt, S., Pondrelli, M., Zegers, T., Hauber, E. & Neukum, G. 2008. Periglacial landscape evolution at Lower Mid-Latitudes on Mars: The Thaumasia Highlands, *Proceedings of the Ninth International Conference on Permafrost, Fairbanks, Alaska, June 29–July 3, 2008* (this proceedings).

Scott, D.H. & Tanaka, K.L. 1986. *Geologic map of the western equatorial region of Mars*. 1:15,000,000. Map I-1802-A. U.S. Geol. Surv. Misc. Inv. Ser.

Squyres, S.W. 1978. Martian fretted terrain: flow of erosional debris. *Icarus* 34(3). 600-613.

Squyres, S.W. 1979. The distribution of lobate debris aprons and similar flows on Mars. *J. Geophys. Res.* 84(B14): 8087-8096.

Sharp, R.P. 1973. Mars: fretted and chaotic terrains. *J. Geophys. Res.* 78: 4073-4083.

Toon, O.B., Pollack, J.B., Ward, W., Burns, J.A. & Bilski, K. 1980. The astronomical theory of climatic change on Mars. *Icarus* 44(3): 552-607.

Wahrhaftig, A.L. & Cox, A. 1959. Rock glaciers in the Alaska Range. *Bull. Geol. Soc. Am.* 70: 383-436.

Whalley, W. 1992. A rock glacier in South Ellendalen, Lyngen Alps. *Norsk Geografisk Tidsskrift* 46: 29-31.

Whalley, W.B. & Azizi, F. 2003. Rock glaciers and protalus landforms: analogous forms and ice sources on Earth and Mars. *J. Geophys. Res.* 108(E4): 8032.

Climatic Change and Fluvial Dynamics of the Lena River (Siberia)

Emmanuèle Gautier
University Paris 8, CNRS UMR 8591 Laboratory of Physical Geography, F-92195 Meudon Cedex, France
François Costard
CNRS UMR 8148 IDES Interactions et Dynamique des Environnements de Surface, Université Paris 11, F-91405 ORSAY Cedex, France
Daniel Brunstein
CNRS UMR 8591 Laboratory of Physical Geography, F-92195 Meudon, France
Julien Hammadi
University Paris 8, Dep. Geography, F-93526 Saint-Denis Cedex, France
Alexander Fedorov
Melnikov Permafrost Institut, Siberian Branch Russian Academy of Science, Yakutsk, Republic of Sakha, 677010, Russia
Daqing Yang
Water and Environmental Research Center, University of Alaska Fairbanks, AK 99775, USA

Abstract

It has been recently reported that climatic change greatly influences Arctic rivers. The Yakutia region is a particularly interesting area for its spectacular floods, for its lowest temperature records, as well as for its maximum thickness of permafrost. The hydrology of the Lena and its tributaries is characterized by an extremely episodic flow regime. In spring during the break up period, the joined increase of the water discharge and stream temperature contributes to an active thermal erosion along the frozen river banks. Here we report recent climatic change in Central Siberia, and its impact on the thermal erosion. We first point out three major evolutions since the 1990s: a reduction of the river ice thickness in winter, a pronounced increase of the stream temperature in the spring, and a slight increase of the discharge during the break up period (May–June). A GIS analysis based on aerial pictures and satellite images highlights the impact of the water-warming on the frozen banks. The vegetated islands appear to be very sensitive to the water temperature increase, showing an acceleration of head retreat (+21%–29 %).

Keywords: climatic change; fluvial dynamics; fluvial islands; GIS analysis; Lena River; thermal erosion.

Introduction

The Lena River is one of the largest Arctic rivers located in a permafrost environment. With its huge basin (2.49 million km²) and its south-north orientation (exceeding 4000 km) the Lena crosses several latitudinal belts (Fig. 1). Central Siberia is one of the coldest and driest zones (with mean temperature of 9°C and mean precipitation of 190 mm yr^{-1}) and has very thick and continuous permafrost (1500 m). For these reasons, the hydrology of the Lena and its tributaries is characterized by an excessive fluvial regime and exhibits a spectacular flood mostly controlled by periglacial dynamics. This study examines current climatic change and its impacts on the middle Lena River dynamics, from the Tabaga gauging site (located upstream of Yakutsk) to the junction of the Aldan River (Fig. 1). From the beginning of November to May, a continuous ice cover can be observed as thick as 2 m in Central Siberia; the discharge of the Lena River is low, 900–1500 $m^3.s^{-1}$ (Tabaga gauging site). The break up starts around May 15 for the Lena, corresponding to an increase of the stream temperature up to 18°C from May to July and to a rise of the water level up to 8–10 m, which inundates flood plain and islands. Highest floods occur generally in June and can be 50,000 $m^3.s^{-1}$ at Tabaga. Then, in July, the discharge rapidly decreases. The fluvial landforms consist of a large number of shallow, wide channels that are between several hundred meters and three kilometers wide. These multiple channels are separated by sandy bars and large forested islands. Downstream of Yakutsk, the flood plain width can be up to 25 km and exhibits various thermokarstic landforms due to the local melting of the continuous permafrost.

During the annual fluvial outburst (May–June), the joined increase of river water temperature and discharge induces the propagation of a thawing line within the frozen riverbank. The interaction between thermal erosion and fluvial erosion during the flood creates specific forms on the banks ('thermo erosive niches') and locally causes important bank retreat (Are 1983, Jahn 1975, Walker & Hudson 2003). Our previous studies highlighted the spatial and temporal variability of the thermal and mechanical erosion on banks of the middle Lena River. We showed that the island heads are particularly subjected to this erosion process, with mean values of 15 m year and maximal values of 20 m, and an exceptional rate up to 40 m was measured locally (Gautier et al. 2003, Costard & Gautier 2007).

Arctic regions respond disproportionately to global warming. In Yakutia, a mean air temperature increase of 1.2°C was registered since the end of the 1980s; this impacts directly the permafrost temperature (Fedorov & Konstantinov 2003,

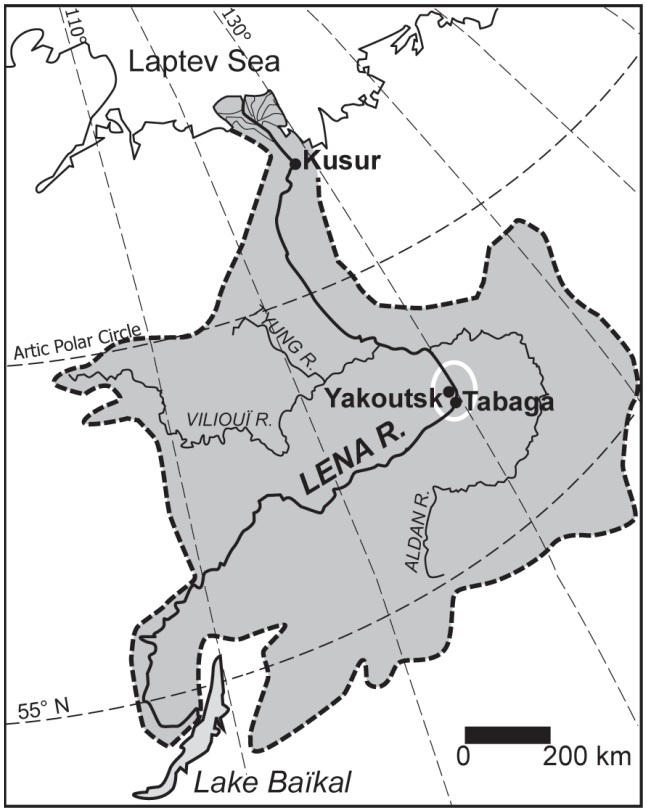

Figure 1. The Lena Basin and the study zone.

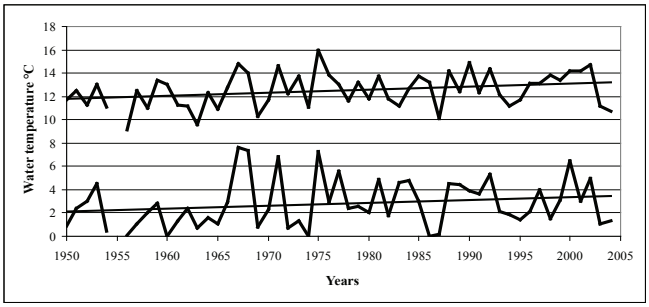

Figure 2. Water temperature of the Lena River since 1950 (May: below and June: above).

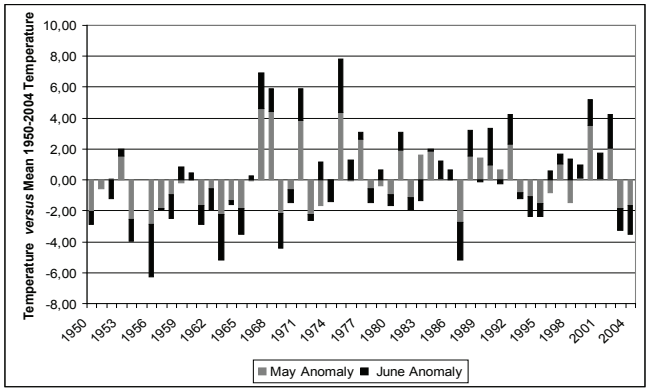

Figure 3. Anomaly of stream temperature in May and June (1950–2004, in °C).

Pavlov 1994). The thickening of the active layer reinforced by the increasing precipitation related to cyclone activity in the North Atlantic provokes a marked rise of the Arctic rivers discharge (Peterson et al. 2002, Serreze et al. 2000, Yang et al. 2002). Therefore, the objective of the present study is (1) to characterize precisely the hydro-climatic change in Central Siberia (water, air, permafrost temperatures, and river discharge) and (2) to quantify the impact of the change on erosion and sedimentation processes on the Lena River near Yakutsk.

Data and Methods

Firstly, the study is based on different sources of environmental data such as climatic data (air, permafrost, and river water temperatures) since the 1950s. We especially examined the water temperature because of its impact on thermal erosion (Costard et al. 2003). Parameters concerning the river were also detailed: discharge, water level, thickness of river ice during the winter, and date of the beginning of the outburst since 1936 at the Tabaga gauging site.

Secondly, we conducted a 35 years diachronic GIS analysis (1967–2002) of 300 km of the fluvial landforms on the Lena River upstream and downstream of Yakutsk in order to evaluate the effects of recent global warming on the mobility of the fluvial units. On aerial pictures (Corona declassified pictures, 1967 and 1980) and satellite images (Landsat 4–7: 1992, 1999, and 2002), landforms were precisely analyzed. The delineation (1) of the channel banks and (2) of the vegetated island banks allows us to quantify their erosion rates since 1967. The position of the islands in the channel, their area, and their form were also determined. Finally, we examined the correlation between the erosion rate variations and the various hydrometeorological variables (discharge, stream temperature, river ice thickness).

Hydro-Climatic Change and Morphodynamics Disruption

Influence of current climatic change on hydrology

All studies concerning Siberia clearly identify the signs of climatic change in the 1980s or at the beginning of the 1990s. On the right bank of the Lena River, 50 km southeast of Yakutsk, A. Fedorov & P. Konstantinov (2003) clearly underline a strong air temperature change, the mean temperature since 1992 being 1.2°C higher than for the whole period (1931–2002). Furthermore, the period 1992–2002 was marked by a pronounced raise of the summer temperature. Correlatively, since the beginning of the 1980s, the soil temperature at 3.2 m depth is also characterized by positive anomalies (Fedorov & Konstantinov 2003). This observation agrees with D. Yang et al. (2002), who show a strong warming in winter and spring over the Lena basin.

On the middle Lena River, the stream temperature has undergone an important change since 1950, that is characterized by positive trends during the flood season (May and June) up to 2°C (Fig. 2). More precisely, the river temperature increase has been particularly pronounced since

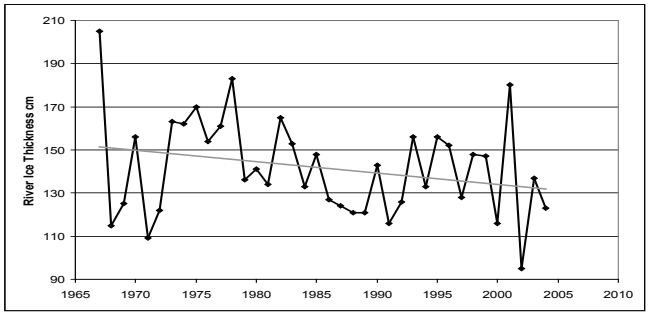

Figure 4. River ice thickness of the Lena River at the Tabaga gauging station since 1967.

1990: +0.73°C (May) and +0.97°C (June) (Costard et al. 2007).

On Figure 3 two periods can be seen: the first 25 years are characterized by an important variability, whereas water temperature since 1975 is more regular and generally marked by positive anomalies. The frequency of temperature anomaly is particularly significant; between 1950 and 1975, positive anomalies of water temperature occurred every 4 years in May and every 2.66 years in June; during the period 1976–2004, they were registered every 1.87 year in May and 1.71 in June (Fig. 3).

The ice cover of the river is the third factor showing a marked evolution. From the beginning of November, a continuous ice cover can be observed as thick as 2 m. Even if the ice cover varies greatly each winter, Figure 4 clearly shows its thinning since 1967. Before 1987, the river ice thickness was 1.48 m on average during winter and exceeded 1.5 m every two years. From 1987 to 2004, the mean thickness was 1.34 m and exceeded 1.5 m every 4.25 years.

The water discharge of the Lena River shows a strong interannual irregularity. Because of this irregularity, it is difficult to detect easily a possible hydrologic change. However, two signs seem to reveal a recent evolution. First, a very moderate increase of 3% of the discharge can be noticed at Tabaga since the 1980s. The winter undergoes greater water discharge since the 1980s, particularly at the end of the cold season (March–April: +22%-23%, Fig. 5). The break up period (May–June) is characterized by a slight but progressive increase: +4% for 1980–1992 and +7% since 1992.

Second, the frequency of abundant discharge has clearly increased during the last 25 years. In April, the frequency of the highest discharge doubled: discharge exceeding 1000 $m^3.s^{-1}$ (the mean discharge) was registered nine times between 1936 and 1980 (i.e. every 4.88 years), and it has occurred ten times since 1980 (every 2.4 years). In May, the frequency of discharge higher than 15,000 $m^3.s^{-1}$ also doubled (frequency of 7.33 years before 1980, frequency of 3.42 after). Furthermore, the evolution of the discharge in May is particularly marked for the period 1996–2004, that underwent repeated high water discharge exceeding by 22%–57% the mean value. The evolution is less clear for June and July. June discharge is characterized by the strongest interannual variability; the highest water levels were registered between 1956 and 1963,

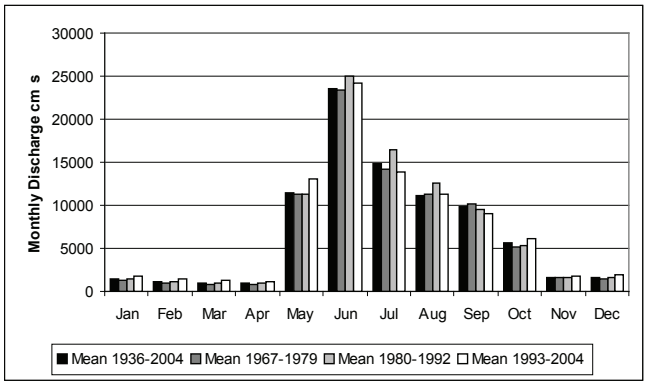

Figure 5. Evolution of water discharge of the Lena River since 1936 (Tabaga gauging station).

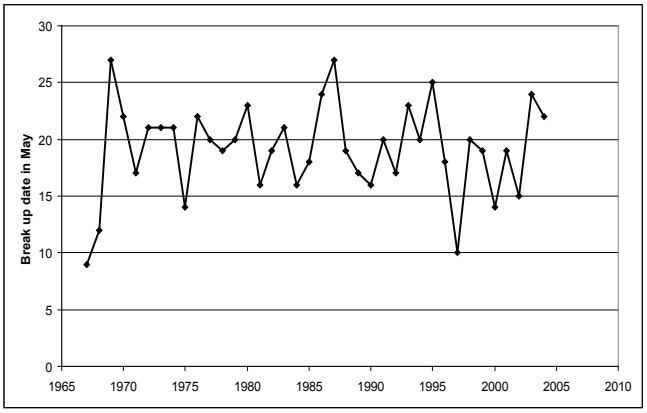

Figure 6. Break up date in May on the Lena River at Tabaga since 1967.

corresponding to a period of low water temperature (Fig. 2). However, an increase of high discharge was also observed since 1980; discharge exceeding 30,000 $m^3.s^{-1}$ was registered six times between 1936 and 1980 (i.e. frequency of 7.33 years), and this value was reached five times for the period 1981–2004 (every 4.8 years). May and June discharges are inversely correlated; it must be remembered that the local inundation is controlled by the flood wave coming from the south and the water provided by the thawing active layer and by the snowmelt. No important rainfall or groundwater supply sustains the river discharge in Central Siberia during summer.

Therefore, the relative abundance of water discharge in May and June must be examined with regards to the break up date. The date of the beginning of the break up is highly variable in May; at Tabaga, it occurs generally around May 15–20, rarely before May 10 or after May 25 (Fig. 6). No important change can be seen nowadays concerning the date of break up. An early break up generally induces an important discharge in May; on the contrary a late break up favors a higher discharge in June.

Impact of hydro-climatic change on fluvial landforms

The middle Lena River develops a multiple-channel pattern. Two types of channels can be distinguished: (1) wide active channels (some of them are dewatered at the end

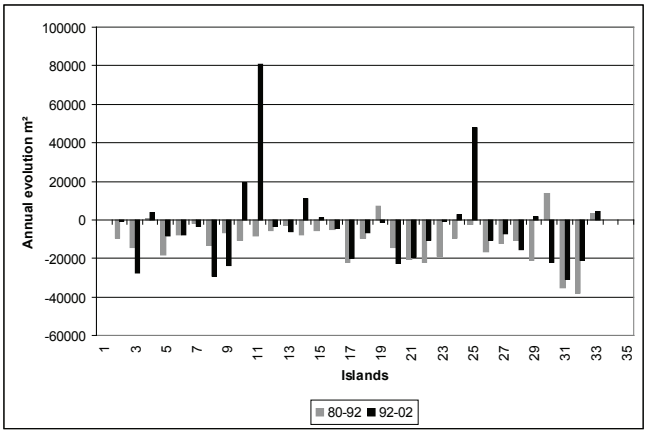

Figure 7. Area evolution of 35 islands since 1980.

of summer and during winter); (2) small sinuous and narrow branches crossing islands and flood plain (these channels are inundated only during the flood peak). A previous study based on satellite image analysis documented the erosion rates on main channels banks (Costard et al. 2007, Costard & Gautier 2007). Actually, for the 1967–2002 period, the mean retreat of the channel banks was low or moderate, with an average value of 2 m per year; maximal values of 14–18 m per year were registered locally. These values must be considered with regard to the active channel width; the bank retreat represents only 0.05%–0.1% of the main channel width. For this reason, active channels remained relatively stable during the study period; no migration or avulsion was observed on the middle Lena River.

The large, forested islands represent important mesoforms of the hydrosystem. Just upstream of Yakutsk, because of the widening of the flood plain, the Lena River forms huge islands. Several km long, these islands are densely vegetated. We could classify these islands in three types: (1) T1: islands located in the central part of the channel; (2) T2: islands located near the river bank and (3) T3: islands located downstream of an unvegetated bar (Costard et al. 2007). We noticed that island heads undergo a stronger erosion than channel banks, with mean value of 15 m per year. The erosion is located on the head of the island; therefore, the island migrates progressively downstream, keeping its general shape. Most interesting is the variability of the island head retreat depending on its type. T1 and T2 islands are subjected to a higher erosion rate, with mean bank retreat of 20 m per year and maximal retreats exceeding 40 m. Because of the position of these islands, the river water is in permanent contact with the frozen banks during the flood, and the thawed sediments are swept away by the current; thus thermal and mechanical erosion are jointly at work, explaining the rapid migration of the form. For the third type, the upstream bar protects the island head from rapid erosion (7 m per year).

The diachronic study of the fluvial landforms since 1967 (date of the first picture) reveals a disruption of the river morphodynamics, that is expressed by the island mobility. For the three types of islands, a marked acceleration of

Figure 8. Evolution of an island located upstream of Yakutsk (1980–2002). Lines: limit of the perennial vegetation; points: island head; background image: Corona 1980 (adapted from Hammadi 2007).

erosion was measured since 1992. Actually, the mean erosion rate of T1 islands increased by 29% (reaching 23 m per year) and by 22% for T2 islands (21 m per year). T3 Islands also undergo a rapider migration (+21%).

The erosion of the island heads could have just implied a progressive reduction of the island areas. In fact, the evolution of islands is relatively complex.

The comparison of the total area of 35 islands located just upstream of Yakutsk between 1967 and 2002 reveals two main models of evolution (Fig. 7). The first model is a progressive decrease of the island area; this evolution is noticeable especially for small islands that are disappearing. On the contrary, eight islands undergo a greater sedimentation on their downstream part, that compensates for the head retreat. An important aggradation on bars located downstream of these islands is observed (Fig. 8). This evolution model is generally observed on very large islands. This accelerated deposition is accompanied by vegetation colonization on the middle part and tail of the island.

Discussion

The hydro-climatic change on the middle Lena River is complex. The discharge increase (+3%) at Tabaga is less pronounced than on the low Lena River at Kusur. B.J. Peterson et al. (2002) calculated for six large Eurasian Arctic rivers (including the low Lena River at Kusur) a mean annual rate of discharge increase of 7%. At Kusur, the spring discharge increases strongly (Yang et al. 2002). But, the dam regulation on the Viliou river (an important tributary of the Lena River, Fig. 1) has a strong influence on the water temperature and discharge on the low Lena River (Liu et al. 2005, Ye et al. 2003). On the contrary, we can consider that the hydrological change of the middle Lena River mainly depends on climatic change, because of the lack of large dams in the upper Lena basin. In this part of the valley, the most significant sign of a possible hydrologic change is the increasing frequency of high discharge, especially in May.

The accelerated erosion on island heads induces an increase of sediment supply in the channel. But, the progressive growth of several islands lets us suppose that the greatest part of the sediment load (mainly sand) provided by the thermal and mechanical erosion process does not migrate over long distances downstream and accumulates on wide bars and long islands. One of our projects is to evaluate precisely in the field this erosion and sedimentation rhythm.

Two hypotheses can be proposed to explain the accelerated erosion of island heads. The first is the increase of the discharge during May and June. The increasing frequency of high discharge in May and June is certainly an important factor of fluvial bed erosion. It has been demonstrated that the duration of efficient discharge determines the bank retreat. But the observed hydrological change alone seems too weak to explain such an aggravation of erosion rates. The second hypothesis is the impact of the water temperature during the flood season by up to 2°C. Actually, the ablation model developed by F. Costard et al. (2003) and R. Randriamazaoro et al. (2007) helped to determine the role of different factors (mainly discharge, permafrost, air and water temperatures, and Reynolds Number) on thermal erosion. Relative effects of water temperature and discharge have been studied separately. The model demonstrates that water temperature is four times more important than Reynolds Number. The measured increase up to 2°C of the stream temperature alone could increase the erosion rate respectively by 26% and 16% in May and June. The laboratory simulation experiment and the physical approach (Costard et al. 2003) demonstrated that exceptional erosion rates can be best explained together with a high water temperature, and mechanical erosion in association with some particular geometry of the channel. In the near future, a more precise numerical modeling will take into account the impact of global warming on the erosion rate for fluvial systems in a periglacial environment.

A last but very important factor must also be taken into account: the vegetation. The islands are densely vegetated with pioneer bushes on freshly dewatered areas and mature forests on stable and higher zones. This vegetation cover seems not to protect efficiently the island heads against the erosion: the thermal process during the flood destabilizes the thawed and non-cohesive deposits. But, the progressive colonization by pioneer sequences (mainly composed by *Salix*) on the middle and downstream section of the island exerts a great control on the sedimentation. The sediment trapping effect of the vegetation is well known (Gautier & Grivel 2006, Hickin 1984, Steiger & Gurnell 2003). For this reason, one of our future objectives is to examine precisely interactions between river and vegetation dynamics.

Conclusion

In the case of the Lena River, fluvial islands are indicative of ongoing dynamic change; the islands express the readjustment of the fluvial system to physical factors (increasing water temperature and secondly, increasing discharge). This study clearly highlights the first sign of destabilization of the fluvial bed directly related to global warming and it appears that climatic change has a strong impact on fluvial forms of this Arctic river. The increasing water temperature directly impacts the erosion rate of the islands, and a greater instability of these fluvial forms is clearly observed. Furthermore, we previously demonstrated that the middle Lena River is a low-energy fluvial system in spite of its great floods, because of its very gentle slope and the brevity of the morphogenic discharge (Gautier & Costard 2000). Thus, the rapidity of the fluvial form readjustment is indicative of the very deep impact created by the present climatic change. It can be supposed that continuation of the recent global warming will induce an increasing destabilization of the river banks and amplify the sediment supply in the riverbed. For society, the increasing mobility of the fluvial bed and the increasing flooding represent very important risks: the great majority of towns and industrial infrastructures are installed on the river banks. The Lena River represents also a major transportation axis in winter and summer. The precise quantification and location of erosion will participate to the prevention of the risk.

Acknowledgments

Hydrological data were provided by the Hydrometeorological Center of Yakutia, under the auspices of the Permafrost Institute at Yakutsk. This program is supported by "Programme Reliefs de la Terre" INSU, CNRS, France, and GDR «Mutations Polaires: Société et Environnement».

References

Are, F.E. 1983. Thermal abrasion on coasts, *Proceedings, Fourth International Conference on Permafrost, Fairbanks, Alaska*. Washington DC: National Academy Press, 24-28.

Costard, F., Dupeyrat, L. Gautier, E. & Carey-Gailhardis, E. 2003. Fluvial thermal erosion investigations along a rapidly eroding river bank: application to the Lena River (central Yakutia). *Earth Surface Processes and Landforms* 28: 1349-1359.

Costard, F. Gautier, E., Brunstein, D. Hammadi, J. Fedorov, A. Yang, D. & Dupeyrat, L. 2007. Impact of the global warming on the fluvial thermal erosion over the Lena River in Central Siberia. *Geophys. Res. Lett*. 34(14): Art. No. L14501 JUL 18 2007.

Costard, F. & Gautier, E. 2007. The Lena River: main hydromorphodynamic features in a deep permafrost zone. In: A. Gupta (ed.), *Large Rivers: Geomorphology and Management*. John Wiley, 225-232.

Fedorov, A. & Konstantinov, P. 2003. Observations of surface dynamics with thermokarst initiation, Yukechi site, Central Yakutia. In: M. Philips, S. Springman & L.U. Arenson (eds.), *Proceedings of International Permafrost Conference, Zurich*: 239-243.

Gautier, E. & Costard, F. 2000. Les systèmes fluviaux à chenaux anastomosés en milieu périglaciaire: la Léna et ses principaux affluents en Sibérie Centrale. *Géographie Physique et Quaternaire* 54(3): 327-342.

Gautier, E. Brunstein, D. Costard, F. & Lodina, R. 2003. Fluvial dynamics in a deep permafrost zone: the case of the middle Lena River (Central Yakutia). In: M. Philips, S. Springman & L.U. Arenson (eds.), *Proceedings of International Permafrost Conference, Zurich*: 271-275.

Gautier, E. & Grivel, S. 2006. Multi-scale analysis of island formation and development in the Middle Loire River, France. In: J.S. Rowan, R.W. Duck & A. Werrity (eds.), *Sediment Dynamics and the Hydromorphology of Fluvial Systems*. IAHS Pub. 306: 179-187.

Hammadi, J. 2007. *Impact du Changement Climatique sur l'érosion Thermo-Dynamique des Berges de la Léna (Sibérie Centrale)*. Geography Master Research, Univ. Paris 8, 150 pp.

Hickin, E. 1984. Vegetation and river channel dynamics. *Canadian Geographer* 28: 111-126.

Jahn, A. 1975. *Problems of the Periglacial Zone*, Washington DC: Warzawa, 223 pp.

Liu, B. Yang, D. Ye, B. & Berezovskaya, S. 2005. Long-term open-water season stream temperature variations and changes over Lena River Basin in Siberia. *Global and Planetary Change* 48(1-3): 96-111.

Pavlov, A.V. 1994. Current change of climate and permafrost in the Arctic and Subarctic of Russia, *Permafrost Periglacial Processes* 5: 101-110.

Peterson, B.J., Holmes, R.M,. McClelland, J.W., Vörösmarty, C.J., Lammers, R.B., Shiklomanov, A.I., Shiklomanov, I.A. & Rahmstorf, S. 2002. Increasing river discharge to the Arctic Ocean. *Nature* 298: 2171-2173.

Randriamazaoro, R. Dupeyrat, L. Costard, F. & Carey-Gailhardis, E. in press. Fluvial thermal erosion: heat balance integral method. *Earth Surface Processes and Landforms*.

Steiger, J. & Gurnell, A.M. 2003. Spatial hydrogeomorphological influences on sediment and nutriment deposition in riparian zones: observations from the Garonne River, France. *Geomorphology* 49: 1-23.

Walker, H.J. & Hudson, P.F. 2003. Hydrologic and Geomorphic Processes in the Colville Delta, Alaska. *Geomorphology*, 56: 291-304.

Yang, D., Kane, D., Hinzman, L., Zhang, X,. Zhang, T. & Ye, H. 2002. Siberian Lena River hydrologic regime and recent change. *J. of Geophys. Res.* 107(D23): 4694-4703.

Ye, B., Yang, D. & Kane, D. 2003. Changes in Lena River streamflow hydrology: human impacts vs. natural variations, *Water Resources Research*, 39(8): 1200, doi: 10.1029/2003WR001991.

Inter-Alas Agricultural Landscapes and Active Layer Trends and Dynamics in Response to a Warming Climate in Central Yakutia

P.P. Gavriliev
Melnikov Permafrost Institute, SB RAS, Yakutsk, Russia

Abstract

This report presents the new long-term (1989–2006) data on monitoring of diverse reaction of active layer, permafrost table, and agricultural landscapes to the climate warming. We have investigated the genuine patterns in the dynamics of progressive development of anomalous cryogenic processes and phenomena, such as intensive degradation of the ice complex up 0.5–0.9 m during sporadic anomalously warm summer-autumn seasons, rich in precipitation; 2.9 times increase in the depth to the permafrost table; sudden activation of different stages of thermokarst, from barely visible *bylar* to young lake thermokarst within 15–18 years, in conditions of rapid climate warming (about 0.09°C/year) and diverse agricultural land use.

Keywords: agricultural landscape; climate warming; ice complex; permafrost process; thermokarst.

Introduction

The peculiarities of formation, stages, and activations of cryogenic processes and phenomena, which cause fundamental changes in thermal condition of permafrost, active layer, and cryogenic relief of geosystems, are permanently in the focus of interest of renowned scientific centres, and their significance needs to be periodically defined more precisely because new data permanently occur. Since the 1950s a great number of works exploring these issues was published and much progress achieved in understanding anthropogenic and natural cryogenic processes and phenomena in northern regions and countries of the world (Russia, Yakutia, western Siberia, Alaska, northern Canada, etc.) (Soloviev 1959, Kachurin 1961, Grechishchev et al.1980, Feldman 1984, Shur 1988, Pewe 1954, Washburn 1988, Osterkamp & Romanovsky 1998, Osterkamp et al. 2000, Gilichinsky & Kimble 1997, Racine et al. 1998, Gavriliev 2001).

Many works, summarizing the available data, state that in context of global climate changes and intensive natural resource development, different regions differ in pace and scale of changes in geocryologic conditions and development of cryogenic processes.

Huge agricultural land resources of Yakutia occupy 67,435.6 thousand ha or 22.2% of its total area. From 20 to 60% of large masses of taiga, valley, and shallow valley soils are underlain by shallow (1–2.5 m) permafrost with wedge ice (ice complex). Considerable areas of territory of the north and the subarctic are characterized by low resistivity to anthropogenic impact (Grechishchev et al. 1980, Gavriliev 2001). Melioration and agricultural development of the permafrost-covered area result in both, advantages, and, in some cases, irreversible negative cryogenic processes and their consequences for the northern nature and ecosystems (Gavriliev 2001). In permafrost area and, especially, in the areas of ice complex distribution, cryogenic (cryogeological) processes activation and the way they influence stability and transformation processes of agricultural and natural permafrost landscapes is very specific and still needs to be thoroughly investigated, taking into account the rapid climate warming (about 0.09°C/y) and existence of a variety of ways of agricultural land use.

This work aims at revealing patterns of permafrost processes dynamics, specifically patterns of activation of initial stages of thermokarst in agriculture-affected lands with ice complex sediments at present day.

This study is a continuation of our earlier work (Gavriliev & Efremov 2003).

Research Methods

In 1989–2006 Melnikov Permafrost Institute, SB RAS, carried out monitoring of active layer, frost phenomena, and permafrost and wedge ice tables (up to 10–15 m deep) in taiga, alas, and valley landscapes, both natural and agricultural, in different physical-geographical regions of Yakutia (Fig. 1). This monitoring network, being multipurpose, includes 6 test sites and 36 experimental plots.

In 1989–2006 we have implemented monitoring observations of dynamics of seasonal thawing-freezing depth, water-saturation and temperature of soil; identified their hydrophysical properties and plasticity; studied the peculiarities of grain-size classification and cryogenic structure of close-to-surface tables of permafrost and ice wedge (ice complex sediments), development of cryogenic and post-cryogenic processes and phenomena, as well as parameters of soil cover (snow, moss layer, forest floor, etc.). In investigating the regularities of permafrost processes and phenomena dynamics, we used detailed permafrost and landscape methods and topographic shoots(at scale range 1:100–1:5,000), and photointerpretation, used in geocryology. The methods for cryogenic processes investigation are specified in works (Grechishchev et al. 1979, 1980, Shur 1988, Pavlov 1997, Gavriliev & Efremov 2003).

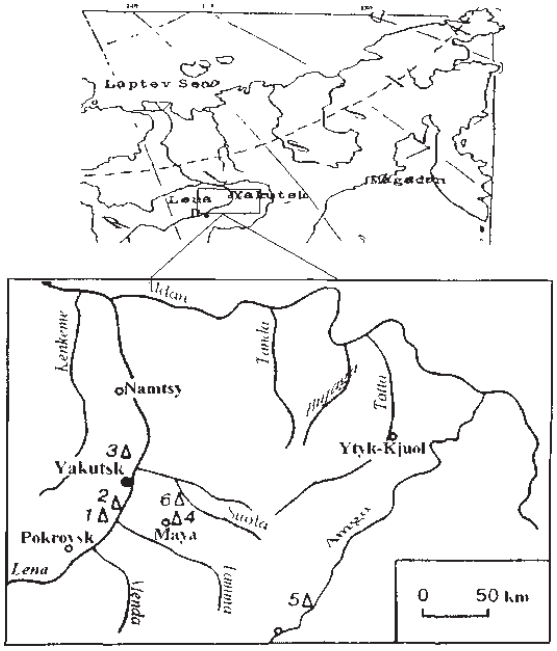

Figure 1. Location of monitoring sites. Sites indicated by triangles: 1–Kerdyugen, 2–Khatassy, 3–Spasskaya Pad', 4–Maia (Dyrgebai), 5–Amga, 6–Khorobut.

Results and Discussion

Diverse reaction of ice complex soils, active layer, and agricultural landscapes to the climate warming and agricultural development

Central Yakutia is among the regions in the north of Russia with maximal effect of global climate warming, reaching 2–2.5°C (Pavlov 2000). According to the data from weather stations of the region, dramatic changes of climate elements were registered during the past 25 years, including: 14 warm winters and 6 anomalously warm winters with air temperatures exceeding the normal by 3–4°C, and during some months by 5–8°C. There was not one cold winter (Skachkov 2000 et al.).

The amount of precipitation ranged during warm period ±1.5–3 times of the regular one, this included anomalously warm and dry summer of 1998 and mean annual air temperature higher than the normal by 4.5°C, as well as increase of snow cover height in some years by 1.5–3 times of the background value, and in subsidence by 1.4–3 times higher than background standard, according to the data of snow survey.

It was determined that during past 15–20 years in central Yakutia at high rate of climate warming and ice complex landscape surface disturbance, a trend towards permafrost degradation is indicated. Thus, in inter-alas areas, depending on landscape-anthropogenic conditions, at forest stubbing, and agricultural development, mean annual temperatures of perennially frozen ground rose to 1.5–2.5°C.

At sporadic inter-alas areas of agricultural landscapes of sixth-seventh terraces of the River Lena, an unprecedented high thawing rate of ice-rich permafrost was indicated,

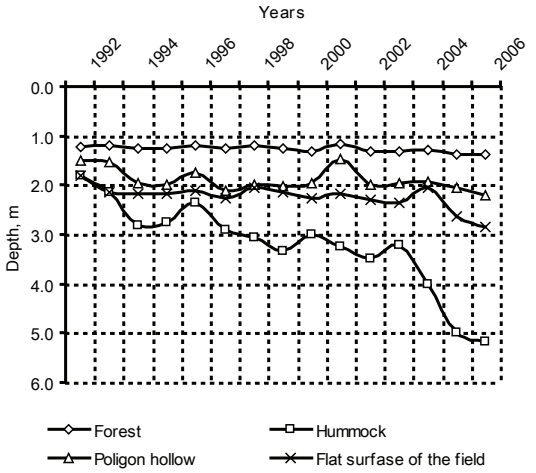

Figure 2. Dynamics of thaw depth at Dyrgebai site on the right bank of the River Lena, 1992–2006.

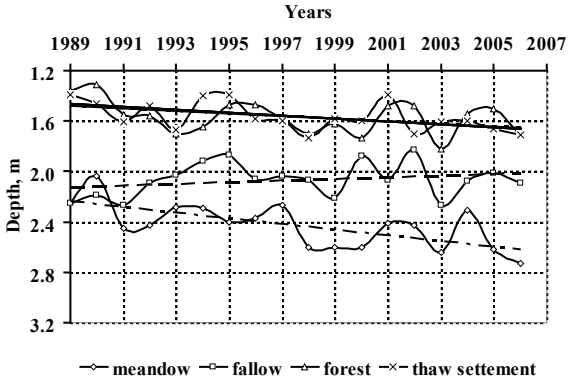

Figure 3. Dynamics of seasonal thaw depth at Kerdyugen site on the left bank of the Lena River, 1989–2006.

reaching 0.5–0.9 m during some excessively rainy, relatively warm summer-autumn seasons (1994, 1997, 2004–2006), preceded by anomalously warm winters. In 1989–2006 the trend of ice complex soils thawing in inter-alas areas of agricultural landscapes averaged from 0.03 to 0.27 m/y, and in the natural (undisturbed) landscapes, it is considerably lower: from 0.007 to 0.01 m/y (Figs. 2, 3).

During the period of 1993 to 2006 anomalously intensive increase of perennially frozen ground occurrence depth was registered, making 2.9 times, at permafrost and wedge ice thawing starting from 1.8 to 5.17 m. At the same time the thickness of thawed zone in the upper layer of the ice complex ground (Δh_i) in Dyrgebai site at Abalakh (sixth) terrace of the Lena River made, correspondingly, from 0.3–0.5 m to 1.5–3.7 m, which resulted in intensive development of thermokarst subsidence, deformation, and surface degradation in various types of cryogenic relief: from hardly-visible thermal subsidence (undeveloped *bylar*) to undeveloped lake thermokarst (see further).

According to the degree of dangerousness and non-dangerousness of the results of reaction–development of undesirable geocryologic and soil processes caused

by surface disturbance, different types of agricultural landscapes form the following consequences (in descending order): inter-alas fallows, used as pastures, in case of wedge ice immediately beneath the seasonally thawed layer (STL); inter-alas irrigated farming areas (fallows, sowed grasslands) at presence of wedge ice in the zone of potential seasonal thawing; inter-alas fallows where wedge ice occurs out of STL; irrigated valley lands; irrigated alas lands; shallow valley haylands; and natural alas lands (alas landscapes).

Along with an overall positive trend of permafrost degradation (thawing), we can note some short-term fluctuations (rhythms, reflecting cycles ranging between 3–4 and 9–11 years), activations and fadings of negative and positive nature (i.e., permafrost table descending and ascending). These fluctuations of seasonal thawing depth reduce, to considerable extent, the danger of fundamental disturbance of frozen-complex ground stability eventually resulting in occurrence of low-grade anthropogenic landscapes and lake thermokarst, but not inevitably.

Activation of natural-anthropogenic cryogenic processes and phenomena in inter-alas agricultural landscapes

New spatial-temporal patterns were revealed in cryogenic processes and phenomena dynamics in inter-alas lands of permafrost agricultural landscape complexes in nowadays conditions.

The analysis of results of long-term research work (1989–2006) on agricultural landscapes condition in Central Yakutia revealed, within the mentioned above landscapes, the activation of destructive cryogenic processes, related with the general 1.5–2.5°C increase of mean annual air temperature in the region and increasing anthropogenic stress.

Yu.L. Shur, a well-known permafrost scientist, has noticed: "There are few thermokarst observations and they refer to initial stages of the process. Such observations applied to areas with ice complex sediments include two or at the most three stages of thermokarst relief development: undeveloped bylar, mature bylar, iyo" (1988, 106).

Our field observations conducted in 1989–2006 in the agricultural areas, which are situated on the V–VII medium-height terraces of the middle Lena River on its left (Kerdyugen site) and right (Maia site) banks and are underlain by ice-rich permafrost, identified and assessed 8 and 12 manifestations of anomalous natural-anthropogenic cryogenic processes and phenomena, respectively. These include:

1) inter-alas surfaces unaffected by cryogenic processes (thaw subsidence, thermal erosion, frost fracture, etc.);
2) polygonally fractured areas;
3) undeveloped bylar, i.e., flat area, affected by separate micro-subsidential crater 0.3 m depth above ice wedges;
4) destabilized (weakened) areas in active layer and disruption of sensitivity of ice complex grounds with subsurface voids, loose sediments, i.e., with drastic changes in permafrost soil composition, construction and in all properties;
5) anomalously rapid surface deformations and active layer destruction by thermokarst subsidences of various forms and sizes (up to 1.8 m and more);
6) bylar, i.e,. deformated area with subsidences and polygonal shallow gullies network above ice wedges (at 0.3–0.5 m depth);
7) iyo, i.e., feeble shallow gully with water within bylar limits;
8) thermokarst mound, i.e., deformated area with bumpy-hollow microrelief;
9) hollow-like subsidence (subsidence hollow gullies, extended in one direction (e.g., in direction of dyodya);
10) subsidence thermoerosion formations (focuses of thermoerosion draft);
11) initial thermokarst depression (or primary areal thermokarst) without lake, but still watering in some particular rainy periods (2005–2007). These thermokarst phenomena often cause permafrost bogging.
12) undeveloped (young) thermokarst lake (dyodya).

These results improve and significantly enlarge already-known patterns of thermokarst formation development stages (Soloviev 1959, Shur 1988, Gavriliev & Efremov 2003, and others). Besides, they evidence an anomalously rapid progressive development of thermokarst stages, not sufficiently studied before.

Activation of primal thermokarst (or primal areal thermokarst)

Five thermokarst stages are observed *in situ* at Dyrgebai test site. For rather short period (1991–2006) clearly-defined primal thermokarst depression with polygonal bumpy-hollow microrelief without lake, but watering in particularly rainy periods (2005 and 2006) formed in one of the key areas of Dyrgebai. For the last 15 years, the longitudinal profile of the primal thermokarst depression (or primal areal thermokarst) increased from 6.2 m in 1994 up to 101.3 m in 2006 (or by 16.3 times), its width—from 40–50 m (by 12.5 times), and its depth increased from 0.35–2.1 m (by 6 times).

The most rapid surface subsidences (14–24 cm/y) above the thawing ice wedge occurred in central watered areas of developing thermokarst depression (primal areal thermokarst). Thus interpolygonal surface hollow gully deformation is 2.02 m, and in polygonal block, which replaces ice wedge, deformation is 0.95 m (*vide* Figs. 2, 3). No significant surface level depression of permafrost agricultural landscapes was noticed in the droughty basin-like subsidences in inter-alas arable lands, grassland, and long-fallow soils.

Other test sites Dyrgebai and Kerdyugen saw correspondingly 11 and 6 similar primal thermokarst depressions develop with the same polygonal microrelief. Three of them in inter-alas agricultural landscape Dyrgebai revealed a tendency of passing onto undeveloped thermokarst lake stage.

Activation of undeveloped thermokarst lake

Here and there in the agricultural lands, small thermokarst lakes form (dyodya, tympy) in taiga inter-alas areas at upper

relatively flat and concave meso-relief areas of fifth-seventh terraces in the middle Lena river. For development of these natural-anthropogenic lakes at least 10 factors and criteria are needed:

1) ice complex within the potential (maximum) depth of the seasonal thawing;

2) climatic conditions: humid and warm years;

3) permafrost-hydrological conditions and criteria for thermokarst lake development, including:

- assemblage of effect of several water delivery sources (types): atmospheric (P_{os} = precipitation), hillside (deluvial) ($S_n > S_{om}$ = the recharge from surface-water exceeds their discharge), permafrost (W_m and $W_{лв}$ = water amount from structure-formative permafrost ices thawing and from ice wedge thawing to depths h_m accordingly), suprapermafrost water input ($S_{мв}$) of active layer to subsidence (or basin) from outer spillway, and water does not drain from closed subsidence and thermokarst basins $W_{лв}$ and $S_{ом}$;
- drastic increase of permafrost water source fraction $W_{лв}$, $W_{тв}$ and $S_{мв}$ during the undeveloped or young lake formation as a result of intensive permafrost and wedge ice thawing;

4) geological and geomorphological conditions: undrained area with slopes of less than 0.5°;

5) positive subsidence water balance formation;

6) ice content of ice complex grounds of more than 50-60% of their volume;

7) water cover appearing in subsidence or thermokarst depression having width exceeding the critical value: from 0.7–1.0 up to 1.5–1.8 m (Feldman 1984);

8) area of thermokarst depression should be rather large for spontaneous thermokarst;

9) activation of mechanisms of self-enhancement of permafrost processes and phenomena;

10) irrational land use.

Undeveloped (young) thermokarst lakes are developed and evolve mostly at fallows and along the arable lands edges, sometimes at very various territories. For example, four lakes formed at test site Dyrgebai, two lakes at Kerdyugen site, and at other inter-alas masses such as Khaya-Yurdya, Urasalakh, etc. All dyodyas have rounded shape, with the diameter from 25–80 m, basin depth from 1.5–6 m, and sides are abrupt. These dyodya formed about 35–60 or more years ago as a result of forest clearance, soil cover removal and thawing of large ice aggregation etc. Thermokarst lake (dyodya) #4 at Dyrgebai test site is the youngest one; it formed only 20 years ago after agricultural development of the area.

Conclusions

1. Rather realistic reaction (weak, moderate, strong) of the soils active layer, permafrost processes and ice complex table of inter-alas agricultural landscapes up to 10 m deep to discontinuous climate warming and various ways of agricultural land use.

2. Results and data obtained during 18 years of integrated monitoring observations (1989–2006) helped to reveal spatial-temporal patterns in progressive development of anomalous natural-anthropogenic permafrost processes and phenomena, which were not sufficiently studied before. That includes the research of 6 thermokarst stages from bylar to young lake thermokarst at rapid climate warming (about 0.09° C/y) and various ways of land use.

3. Rhythmical and trend patterns of dynamics of seasonal thawing depth, permafrost processes and table fluctuation of ice complex grounds of inter-alas agricultural areas, which were not sufficiently studied before are nowadays revealed.

4. If the present tendency of climatic warming in central Yakutia with air temperature trend around 0.09°C/y and agricultural land use ratio increase keep on, the possibility of activation (manifestation) of permafrost processes and especially that of thermokarst remains very high.

References

Feldman, G.M. 1984. *Thermokarst and permafrost (Termokarst i vechnaia merzlota)* (in Russian). Novosibirsk:Nauka, 260 pp.

Gavriliev, P.P. 2001. Dangerous natural and anthropogenic processes and difficult ecological situations (geographical, geocryological and soil aspects). In: *Permafrost and ecological peculiarities of taiga landscapes in Central Yakutia (Merzlotno-ecologicheskie osobennosti taezhnykh agrolandshaftov Tsentralnoi Yakutii)* (in Russian). Yakutsk: Izd-vo Instituta Merzlotovedenia SO RAN, 113-148.

Gavriliev, P.P. & Efremov, P.V. 2003. Effects of cryogenic processes on Yakutian landscapes under climate warming. *Proceedings of the Eighth International Conference on Permafrost, Zurich, Switzerland, July 21–25, 2003*: 277-282.

Gilichinsky, D. & Kimble, J. (eds.) 1997. *Cryosols in classification hierarchy. Advances on fundamental research of the Earth cryosphere in Arctic and Subarctic; Proc. intern, conf., Pushchino, 22–26 April, 1996 (Special issue)*. Novosibirsk: Nauka, 3-6.

Grechishchev, S.E., Chistotinov, L.V. & Shur, Yu.L. 1980. *Cryogenic physical and geological processes and their prediction (Kriogennye fiziko-geologicheskie protsessy i ikh prognoz)* (in Russian). Moscow: Hedra, 380 pp.

Kachurin, S.P. 1961. *Thermokarst in the USSR area (Termokarst na territorii SSSR)* (in Russian). Moscow: Izd-vo AN USSR, 291 pp.

Osterkamp, T.E. & Romanovsky, V.E. 1998. Recent changes in permafrost and active layer conditions in Alaska. *Proceedings of 49th Arctic Science Conference/lARC Inauguration American Association, 25–28 October, 1998,* Fairbanks: University of Alaska, 61-62.

Osterkamp, T.E., Viereck, L., Shur, Y. et al. 2000. Observations of thermokarst and its impact on boreal forests in Alaska, U.S.A. *Arctic, Antarctic, and Alpine Research,* 32(3): 303-315.

Pavlov, A.V. 1997. Permafrost-climatic monitoring of Russia: methods, observation results, prediction (in Russian, abstract in English). In: *Earth Cryosphere (Kriosfera Zemli)* 1(1): 47-58.

Pavlov, A.V. 2000. Results of the International Conference "Monitoring of cryosphere", Pushchino, 1999 (in Russian, abstract in English). In: *Earth Cryosphere (Kriosfera Zemli)* 4(1): 44-51.

Pewe, T.L. 1954. *Effect of permafrost on cultivated fields, Fairbanks Area Alaska*. Geol. Surv. Bull. 989-F. Washington,164-186.

Racine, C.H., Jorgenson, T.M. & Walters J.C. 1998. Widespread and rapid permafrost degradation on the Tanana Flats in Central Alaska. *Proceedings of 49th Arctic Science Conference/lARC Inauguration American Association, 25-28 October, 1998.* Fairbanks: University of Alaska, 186-187.

Shur, Yu.L. 1988. *Upper layer of permafrost and thermokarst (Verkhniy gorizont tolschi merzlykh porod i termokarst)* (in Russian). Novosibirsk: Nauka, 213 pp.

Skachkov Yu.B. 2000. Present-day climate changes in Central Yakutia. In: *Climate and Permafrost: complex research in Yakutia (Klimat i merzlota: kompleksnye issledovanie v Yakutii)* (in Russian). Yakutsk: Izd-vo Instituta Merzlotovedenia SO RAN, 113-148.

Soloviev, P. A. 1959. *Cryolithozone of the northern part of the interfluve Lena and Amga interfluve (Kriolitozona severnoi chasti Leno-Amginskogo mezhdurechia)* (in Russian). Moscow: Izd-vo AN USSR, 144 pp.

Washburrn, A.L. 1988. *The world of cold. Geocryological research (Mir kholoda. Geokriologicheskie issledovania)*(in Russian). Moscow: Progress, 384 pp.